Universidade do Minho
Escola de Engenharia

Pedro Miguel Gonçalves Martinho

Mechanical design of hybrid moulds - Mechanical and thermal performance implications

Tese de Doutoramento
Ciência e Engenharia de Polímeros

Trabalho efectuado sob a orientação do
Professor Doutor António Sérgio Pouzada
Professor Doutor Paulo Jorge da Silva Bártolo

Março de 2010

ABSTRACT

The design and manufacture of injection moulds are the most time-consuming phases in the development of new plastics products. In the last two decades the advances in rapid prototyping and manufacturing technologies made possible the use of materials alternative to steel in some mould components. The integration of these components with conventional mould structures originated to the concept of hybrid mould. This alternative design solution aimed at satisfying the need for deployment of short series of new products more quickly and at competitive prices.

This research work investigates the influence of materials used in moulding blocks of hybrid moulds in the mould performance, namely, reproducibility, operation regimes, thermal and mechanical issues. Furthermore it was analysed the effect on the definition of the more adequate processing conditions and the moulding properties.

The study was based on tri-dimensional objects: a tubular cylindrical part and a more geometrically complex support box. The tube was produced in an existing simple instrumented hybrid mould and the support box was produced in a reusable and flexible hybrid mould. The latter was designed and manufactured in the context of this research work.

The performance of the hybrid moulds was evaluated by comparing various combinations of moulding blocks (cavity and core) produced in alternative materials with the standard steel solution when injection moulding polypropylene. The comparison was based on the observation of the morphology structure of the mouldings, the thermal performance, the moulding shrinkage and the structural performance of the mould. The moulds were instrumented with pressure and temperature sensors and a load cell for monitoring the ejection force needed on a moulding pin incorporated in the lateral movement of the support box.

The prediction of the moulding performance of the moulds was done using the injection moulding software Moldex3D. The mechanical performance of the components in alternative materials was done with the structural analysis software ANSYS *Workbench*.

The results show the importance of predicting the mould regime temperature when establishing the appropriate processing conditions when softer materials are used in the moulding blocks. It was concluded that in the design of hybrid moulds it is necessary to consider the deformation of the moulding blocks that are caused by the pressure field during injection. This is critical to predict the shrinkage and the final dimensions of the mouldings.

RESUMO

O projecto e o fabrico de moldes de injecção para plásticos ocupam um longo período de tempo no desenvolvimento de novos produtos. Nas duas últimas décadas os avanços das tecnologias de prototipagem e de fabrico rápido tornaram possível o uso de materiais metálicos alternativos e de resinas sintéticas em alguns componentes do molde. A inserção destes em estruturas convencionais deu origem ao conceito de molde híbrido. Esta solução alternativa procurou satisfazer a necessidade de colocar pequenas séries de novos produtos no mercado mais rapidamente e com preços competitivos.

Este trabalho de investigação explora, essencialmente, a influência dos materiais usados nos blocos moldantes de moldes híbridos no desempenho do molde (ex. reprodutibilidade, regimes de funcionamento, aspectos térmicos e mecânicos). Também se estudou a sua influência no estabelecimento das condições processamento mais adequadas e nas propriedades das peças moldadas.

Estudaram-se duas peças de geometria tridimensional: uma peça tubular e uma caixa-suporte com detalhes complexos. O tubo circular foi produzido num molde híbrido simples e já existente e a caixa-suporte num molde híbrido flexível e reutilizável. O segundo molde foi especificamente projectado e fabricado no âmbito deste trabalho de investigação.

O desempenho dos moldes híbridos foi avaliado comparando o efeito de várias combinações de materiais alternativos nos blocos moldantes (bucha e cavidade) com a sua versão convencional em aço, na moldação de polipropileno. A comparação contemplou a observação da estrutura morfológica, o desempenho térmico, a contracção das moldações e o desempenho estrutural do molde. Os moldes foram instrumentados com sensores de pressão e temperatura e com uma célula de carga para medir a força de extracção de um pino moldante incorporado num movimento lateral da caixa-suporte.

Utilizaram-se softwares de simulação do processo de moldação por injecção (Moldex3D) e estrutural (ANSYS Workbench) na previsão do desempenho dos componentes moldantes dos moldes híbridos.

Os resultados mostram a importância da previsão do regime de temperatura de funcionamento do molde híbrido no estabelecimento das condições apropriadas ao processamento quando são utilizados materiais menos rígidos nos elementos moldantes. Foi constatado, ainda, que no projecto de moldes híbridos se devem considerar as deformações dos blocos moldantes causadas pelas pressões durante o ciclo para prever a contracção e as dimensões finais das peças moldadas.

ACKNOWLEDGEMENTS

This work would not be possible without the valuable support and help provided by several individuals, institutions and industrial companies. I want to express my gratitude to and refer those whose contributions were of major importance.

First and foremost I would like to thank my supervisor, Professor António Sérgio Pouzada, for the continuous support and availability, for his valuables suggestions and encouragements during all of this work. His rigorous sense of things and outmost scientific skills were of great help, regarding the scope, organisation and the even in reviewing the writing of all the work involved in this thesis. I can never value too much all the experience and teachings that he provided me during all the time I spent with him. *Obrigado Professor!*

I also thank Professor Paulo Bártolo, co-supervisor of this research work, for the suggestions and help with English in some writings, and on the logistics at the Polytechnic Institute of Leiria.

Also, I would like to thank the Mechanical Engineering Department (DEM) of the Polytechnic Institute of Leiria, where part of this work was performed, for all the possible conditions provided, including the facilities, the equipment and the time granted to conclude this work.

Many thanks to the Polymer Engineering Department (DEP) and Polymer and Composites Institute at University of Minho, for the facilities and equipment provided and for supporting this research program.

I thank the Foundation for Science and Technology, for the research grant SFRH/BD/28113/2006.

To Coretech for all the help provided in the simulation work, particularly to Eng.ª Teresa Neves and Eng.ª Marisa Mendes.

To Professor Jovita Oliveira of the DEP at University of Minho for the scientific and technical guidance on the mouldings morphology analysis.

To Professor Marques Pinho and Mr. Araújo of the DEM at University of Minho for the help in load cell instrumentation and calibration.

To the technicians of the DEP at University of Minho, especially to Mr. Serafim Sampaio for the help and valuable suggestions in injection moulding experiments.

To the Federal University of Santa Catarina, Brazil, for the support provided, friendship and kind hospitality during my work at Florianópolis.

TABLE OF CONTENTS

LIST OF SYMBOLS, ACRONYMS AND ABBREVIATIONS

2.5D	2 ½ Dimensional system
3D	3 Dimensional system
3DP	3 Dimensional Printing
Ac	Contact area
As	Surface area
ABS	Acrylonitrile-Butadiene Styrene
ACES	Accurate Clear Epoxy Solid
AIM	ACES Injection Mould
ASTM	American Society of Testing Materials
CAD	Computer Aided Design
CAM	Computer Aided Manufacturing
CAE	Computer Aided Engineering
c_p	Specific heat
D	Diameter
$d_{postcure}$	Final dimension in the part
d_{CAD}	Dimension set in the original drawing
$D_{imp(i)}$	Impression dimension in *i* direction
$D_{part(i)}$	part dimension in *i* direction
DIN	Deutsches Institut für Normung (*in English*: German Institute for Standardization)
DMA	Dynamic Mechanical Analysis
DMLS	Direct Metal Laser Sintering
DOE	Design of experiments
E	Modulus of elasticity
E_{st}	Stored thermal and mechanical energy
E_g	Thermal energy generation
E_{in}, E_{out}	In-flow and out-flow terms of the thermal and mechanical energy transport across the control surfaces
F	Force
F_{eject}	Ejection force
F_{guide}	Force on pillar guide
F_a^{max}	Recorded friction force
F_n	Normal contact force applied by the pneumatic cylinder in the apparatus
FDM	Fused Deposition Modelling
g	Gravitational constant
h	Heat transfer coefficient

HDPE	High Density Polyethylene
HM-1	Hybrid Mould 1
HM-2	Hybrid Mould 2
HSC	High Speed Cutting
HSM	High Speed Machining
ISO	International Standards Organization
k	Thermal conductivity
k_{polym}	Thermal conductivity of the polymer
k_{resin}	Thermal conductivity of the resin
k_{steel}	Thermal conductivity of the steel
L_i	Linear dimension in direction i
LOM	Laminated Object Manufacturing
m	Subscript used to designate the x location of discrete nodal points
n	Subscript used to designate the y location of discrete nodal points
p	pressure
p_{ap}	Contact pressure applied by the pneumatic cylinder
p_c	Contact pressure
P_i	Pressure data registered by the pressure sensor i
PA	Polyamide
PACVD	Plasma Assisted Chemical Vapour Deposition
PC	Polycarbonate
PE	Polyethylene
PP	Polypropylene
ProM	ProMetal
PS	Polystyrene
PVD	Physical Vapour Deposition
$\dot{q}$	Heat flux
$\dot{Q}$	Heat flow
R	Thermal resistance of the body
RM	Rapid Manufacturing
RP	Rapid Prototyping
RPT	Rapid Prototyping and Tooling
RR	Resin/Resin materials in the core and cavity respectively
RS	Resin/Steel materials in the core and cavity respectively
R_1S	Epoxy resin (Biresin® L74) filled with 60% (weight) aluminium powder in the core and steel in the cavity
R_2S	SL resin (DSM Somos® 11120/2) in core and steel in cavity

R_3S	Epoxy resin (Biresin® L74) filled with 15% (volume) short steel fibres in core and steel in cavity
RT	Rapid Tooling
s	Plastic part thickness
Sh_i	Shrinkage in *i* direction
SLS	Selective Laser Sintering
SLS_m	Selective Laser Sintering of metallic powder
SL	Stereolithography
SLA	Stereolithography Apparatus
SS	Steel/Steel materials in the core and cavity respectively
SSF	Short Steel Fibres
STDV	Standard Deviation
STL	Structured Triangular Language
Ti	Temperature data registered by the temperature sensor *i*
$\overline{T}$	Cycle average mould temperature
T_{eject}	Temperature at ejection
T_{cold}	Local temperature on the cold surface
T_g	Glass transition temperature
T_{hot}	Local temperature at the hot surface
$T_{m,n}$	Temperature at *m* (x-location) and *n* (y-location) nodal points
$T_{m,n}^p$	Temperature at *m* (x-location) and *n* (y-location) nodal points and *p* time dependence of *T*
T_{room}	Room temperature
T_w	Temperature at wall
T_{inj}	Injection temperature
T_{int}	Melt temperature at the interface
T_m	Melt temperature of polymer
T_{mould}	Mould temperature
T_M^-	Moulding zone temperature on the cavity side (negative side)
T_M^+	Moulding zone temperature on the core side (positive side)
T_s	Surface temperature
t	Time
t_c	Cooling time
TCC	Thermal contact conductance
TCR	Thermal Contact Resistance
V	Volume
X_m	Mass average
α	Coefficient of thermal expansion

δ	Deformation
δ_{pol}	Polymer deformation
$\delta_{pressure}$	Deformation caused on the core and cavity by the moulding pressures
ε	Elastic strain
$\varepsilon_{pressure}$	Elastic strain of the deformable moulding element
μ_e	Static coefficient of friction
ρ	Density
ξ	Hildebrand parameter

1 INTRODUCTION

In the last two decades, the search for solutions that allow the production of new products through a rapid and economic way motivated the development of a large number of new technologies. The employment of new fabrication techniques, the development and the utilization of computational tools for design analysis are some aspects that were associated to this transformation.

The use of plastics components in engineering applications has grown quickly. Nevertheless the development of a new plastic component by conventional routes can be a long process. Consequently, it is necessary the use of techniques and methodologies to reduce the duration of this process and to assure the quality of new products. Technologies like Rapid Prototyping (RP), Rapid Tooling (RT) and Computer Aided Engineering analyses (CAE) are seen as indispensable to guarantee the rapid success and quality for these products. Thus, the use of rapid prototyping and tooling (RPT) techniques is important in the areas of the conception and design of plastics products. Contributing to this reality, the increasing need of reducing development and production time while guaranteeing reliability and cost reduction of the project are also demanding designer constraints. The introduction of RPT techniques in the product development cycle and in an iterative form (*i.e.* verification/optimization) provides better results. These techniques appeared at the end of the eighties when layer by layer material addition processes were developed (*e.g.* [1-3]). The basis of these techniques is the planning of the part using CAD (Computer Aided Design) systems and its precise geometrical information. The generated information is sent directly to the RP machine without user intervention. This Rapid Prototyping (RP) process was initially applied in the production of parts aiming at the materialization of prototypes without many requirements in terms of resistance and precision. In contrast to traditional machining methods, the majority of RP systems tend to produce parts using an additive process [4, 5]. It also provides an accurate model for design verification. Currently, RP systems use three-dimension CAD solid models to build physical models. One of the current applications of RP technologies is in injection

moulding giving rise to a new generation of tool-making techniques commonly referred to as Rapid Tooling (RT) processes. The techniques for the fast production of injection moulding tools are not used for all components of injection moulds. The structure is machined by conventional processes, and RPT techniques are used for the moulding blocks. The moulding blocks can be manufactured either in alternative metallic materials or synthetic materials. These moulds were branded as hybrid moulds [6] and are generally considered for production of small batches of products. The alternative of hybrid moulds for short injection moulding runs is seen as one of the ways for technological innovation with great potential of application in the plastics industry. New market conditions require faster product development and reduced time to market which at the same time demand higher quality, greater efficiency, and at lower cost. Furthermore, the ability to meet the technical requirements of the manufactured products is also mandatory. As mentioned by other researchers (*e.g.* [7, 8]), developing the tools for prototype and production components represents some of the most time-consuming and costly phases in new product development. This is particularly problematic for low-volume products or rapidly changing high volume products. Many RT solutions were used for various applications as RT brings significant benefits to the industry [9, 10].

The integration of mould design and RP/RT technologies has already shown the potential to produce complex mould cores and cavities [11]. This trend confirmed the objectives of fast toolmaking and reduction of the time-to-market of short runs of plastics parts. Therefore, switching to an engineering design process based on RP/RT techniques and CAE design tools, in the development of injection moulds, makes the mouldmaking industry to be able to compete cost effectively in the new market environment [12]. This change will reduce costs and time in the production of the mould, and guarantees high quality products.

As mentioned recently by Pouzada, all the manufacturing routes analysed for hybrid moulds have as a common goal reducing costs and time in the production of injection moulding components and tools [13].

1.1   Research context

The research in injection moulding of thermoplastics materials addresses aspects associated with the technologies used in the manufacturing of the moulds, specifically in the case of smaller batch sizes. Some of these aspects include the influence of the tool

manufacturing method and materials on the tool wear and life. In particular, the product shape, the mould structure and the mechanical design should be integrated to ensure that it will be feasible to keep the wear and the structural integrity during the mould life [14-16]. Furthermore, hybrid tools must allow a moulding cycle time as short as possible. An emerging issue being addressed in the context of designing injection moulds is their reutilisation. A strategy must be designed for the mouldmaking industry to get some advantage from reutilisation in view of further cost reduction and savings in tool development and manufacturing time [8, 17].

In the case of hybrid moulds it is necessary to integrate design and manufacturing methods, foreseeing their reutilisation instead of straight scrapping/recycling. Moreover, the environmental impacts of RPT techniques must be considered [18, 19]. One possible reutilisation strategy implies the reuse of existing mould structures. However, this alternative has difficulties, since mould structures were already designed according to the specifications of the plastics parts.

Finally, the idea of building moulds with moulding inserts manufactured in alternative metallic or synthetic materials can have a significant impact in the mouldmaking industry, as it is: *Efficiency,* reducing waste and energy consumption; *Agility*, enabling adaptability for customization; *Flexibility*, enabling the rapid modification and fabrication of design concepts and *Value chain enhancement* [8]. However, using hybrid moulds poses several challenges that need to be addressed:

- New cost effective materials with improved strength, thermal performance, hardness and mouldability;

- Exploitation of RPT possibilities: limitations regarding accuracy, repeatability and detailing;

- New design methodologies as designers and engineers need to change their ways of thinking;

- Systematic integration of computer simulation tools in the design workflow to guarantee that hybrid moulds perform "first time right".

In this context, this research programme had two main goals: the investigation of design solutions specific for hybrid moulds and the assessment of the reliability of RPT moulding blocks. Additionally, aspects related to the reusability of hybrid moulds for short production runs and design solutions for reutilisation were considered.

1.2   Global objectives

The main goal of this research is the investigation of the reliability of moulding blocks obtained with rapid prototyping techniques. Additionally, thermal aspects, structural integrity and dimension accuracy is considered.

Furthermore, this research intends to study and analyse the mechanical and thermal implications on the performance of tools with RP moulding blocks. The performance of hybrid mould inserts for short and long lateral movements, namely their mechanical behaviour in comparison with conventional solutions and thermal performance associated to the design of the cooling and ejection systems of the mould are considered in this study.

1.3   Thesis structure

This thesis is organized in 5 chapters before the Conclusions and the Recommendations for further work. The Introduction chapter describes the approach to the research work focused on the use of hybrid moulds in plastics injection moulding. A brief introduction is made to the concept of hybrid mould, their problems, the demands and challenges for their use.

The second chapter reviews the state-of-the-art on topics such as: rapid prototyping and tooling techniques; hybrid mould design and manufacturing; hybrid mould block materials, injection moulding process parameters, and tribological and wear behaviour of the moulding blocks obtained by RPT. A review is also made on the hybrid mould lifecycle approaches and costing. This chapter concludes with the consequent description of the main objectives of the research work.

Chapter 3 reviews theoretical aspects associated to the hybrid mould design and their implications on the thermal and mechanical behaviour. The main governing equations and numerical solutions used for the injection moulding process simulation are also described in this chapter. The injection moulding simulation tools are used to predict thermal and flow behaviour and moulding shrinkage. A new approach is developed for the calculus of the shrinkage of parts obtained in injection moulds with *soft* moulding blocks. This approach is validated further ahead in Chapter 5 when experimental results are discussed.

In the Chapter 4 it is detailed the mould designed for testing and assessment of the various moulding elements (blocks and insert pins) and the ejection force on the moulding pins in real processing conditions. The mould instrumentation for assessment of pressure in the impression and temperature of the moulding surface during its processing is also described

in detail. The characterisation methods are also presented in this chapter. These include: i) morphological structure and shrinkage associated to the injected parts and ii) tribological analysis based on the experimental ejection forces and those predicted using actual coefficient of friction.

The discussion of the experimental results and numerical simulations is thoroughly developed in the Chapter 5. This chapter also includes a briefly description of the main objectives of the simulation techniques used for the hybrid moulds. The software Moldex3D was used to simulate the injection moulding process. The regime mould temperature, the thermal and flow behaviour and the part shrinkage were the main simulations carried out. The software ANSYS *Workbench* was used for structural simulations. Analyses were made to predict the deformation and structural integrity of the core moulding blocks and pins. The recorded pressure and temperature profiles during processing are analysed and compared with simulations using Moldex3D. The shrinkage around the moulding pins was measured after ejection and calculated at room temperature. The results are analysed and compared with simulations.

Finally, the main conclusions are drawn and some recommendations for further work are proposed.

2 STATE OF THE ART

Novel fabrication strategies have been proposed as an alternative to conventional methods for the production of injection moulds for short series of plastics parts. The additive technologies were seen as more adequate to injection moulds. These technologies induced a new generation of tool-making techniques commonly referred to as rapid tooling (RT) processes. Various authors have different perceptions of what is RT. Some, as Chua and co-workers consider that RT is RP applied to the manufacture of injection moulds [20]. Others state that RT may also include machining processes as HSC (High Speed Cutting) [21]. According to Williams, RT is enabling artists to produce quality parts and accelerating time to market by concentrating on the tool rather than the part [22]. King and Tansey mentioned that RT is the ability to build prototype tools directly as opposed to prototype products directly from the CAD model resulting in compressed time to market solutions [23]. Rosochovski *et al.* see RT as a natural extension of RP [24].

Since the universe of RT techniques is continuously increasing, there is a tendency to classify them into groups. Several classifications have been proposed. Chua and co-workers suggest a classification of RT techniques, as shown in Figure 2.1, based on the RP technologies used in production [20]. In this classification, tooling is classified on the basis of the stiffness of the tool materials, and also fabrication strategies direct or indirect tooling. Tooling for short manufacturing runs is often known as soft tooling, which are easier to work with than tooling steels. Tooling for longer manufacturing runs is known as hard tooling and usually uses tool steels.
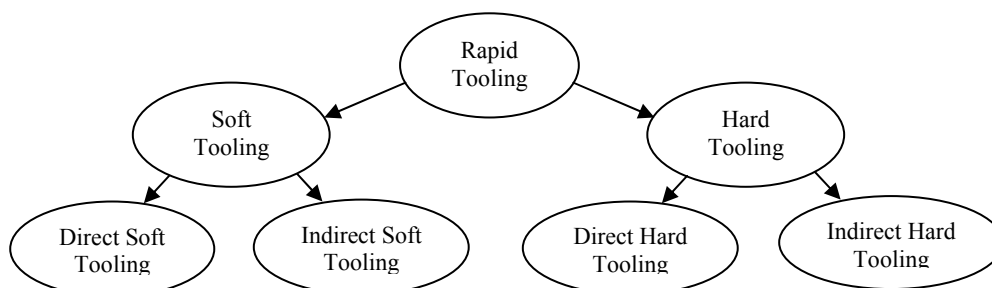

Figure 2.1- Classification of Rapid Tooling (source: Chua *et al.* [20])

In direct tooling the tool is obtained directly in the RP process. Some of the direct soft tooling processes include direct AIM and SL composite tooling. The indirect soft tooling includes the silicone moulds, the epoxy tooling and the spray metal tooling [25]

The use of RP techniques for hard tooling has the advantage of building highly complex shapes to create the tools that could not be made using conventional machining and polishing methods [26]. Another quoted advantage is the quick production of those tools. Examples of direct hard tooling include the process of Laminated Metal Tooling [27, 28] and of indirect hard tooling includes the 3D Keltool method [20].

2.1   Rapid tooling processes

RT is known to be a fast and rather inexpensive method for the production of short and medium run injection moulds. Usually it implies a direct and an indirect process. The direct process produces components of the mould (usually moulding elements) directly without the requirement of using a pattern (or master) whereas indirect processes involve always the fabrication of a master by a rapid prototyping process, adequate to the specifications of the final product, and appropriate techniques to produce the moulding elements. This section describes the direct and the indirect processes used herein.

2.1.1   Indirect Processes

Indirect processes start with a physical pattern (or master) from which the part shape is copied into the mould. The fabrication of injection moulds using RT became more relevant after the possibility of making the masters through RP technologies [29, 30]. Silicone moulds, epoxy moulds and moulds produced by spraying metallic powders (or spray tooling), patented by Beck *et al.*, Curfman and Palma respectively [31-33] have been associated to the production of the injection moulds by RT indirect processes [25, 34].

In this research study only silicone moulds and epoxy composite moulds were used in the experimental work. The spray metal tooling was not considered in this research study, essentially, due the long manufacturing time associated to the technique.

The silicone moulds and the epoxy-based composite mould components are produced by vacuum casting. The resins are poured (in vacuum) around the pattern to produce the respective mould components. The physical model of the part, the *master*, is the reference for the creation the mould impression [35]. The main function of the master is to reproduce

the part or the mould component with precision and the surface texture [36]. The moulding blocks constructed with silicone rubber can be used to mould a variety of materials at relatively low temperature, low volume and low pressure production processes [30, 37, 38]. One application of the silicone moulds is the production of plastics parts in polyurethane [20]. It allows an excellent reproduction of part details and surface textures [37, 39]. Nowadays silicone moulds are also used for casting epoxy composites to produce moulding elements for hybrid moulds (e.g. [40, 41]). The life of a silicone mould depends largely on the surface finish of the prototype pattern. In most instances it will reproduce up to 20 parts with a gradual deterioration of surface quality [24, 42]. The biggest advantage of silicone moulds is their flexibility that facilitates demoulding from the mould no matter how complex the geometry is [30, 38]. Silicone moulds are being used alongside RP technologies that make the prototype model of the part. The main advantage of the casting process is on the short time required to obtain freeform moulding geometries compared with conventional cutting processes [42, 43].

With the epoxy-based composite material, two distinct ways can be used to produce the moulding elements (blocks or other inserts): 1) by vacuum casting in a silicone mould (usually producing the moulding element of an only time) or 2) by vacuum casting in a frame prepared with the master, the cooling channels and the sprue. This procedure has a drawback arising from defects generated by the handling of materials before casting [34, 37, 44]. The epoxy resin is usually filled with metallic powder (commonly aluminium) to improve the heat transfer and reduce the wear of the tool (*e.g.*[45, 46]). Sabino-Netto *et al.* investigated the development of a metal-polymer composite using short steel fibres (SSF) and epoxy-based resin [47]. The main advantages of adding the metallic fillers are associated to the improvements on material strength and thermal properties like thermal conductivity [13, 48, 49].

This indirect process consists of casting an epoxy composite around the master pattern to form the mould (Figure 2.2).
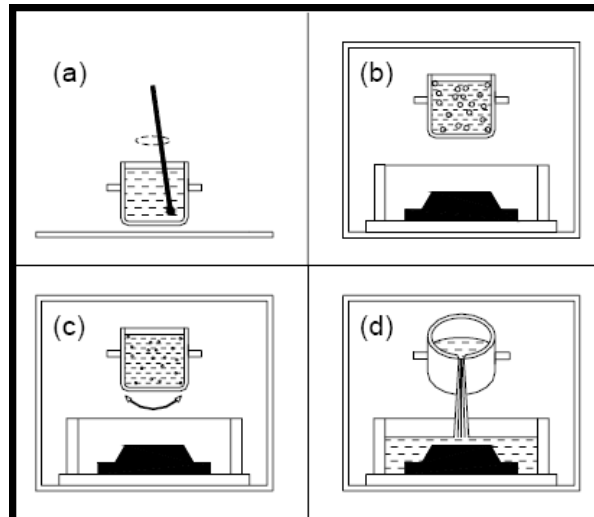
Figure 2.2.- Diagram of the resin processing method using vacuum pouring: (a) manual component mixture, (b) first degassing, (c) second degassing with agitation, (d) pouring (source: Vasconcelos *et al.*[43])

Using epoxy moulds is often the fastest way to complete short runs of functional parts manufactured by injection moulding. These moulds must be used with low injection and packing pressures [43, 50].

2.1.2   Direct Processes

Direct processes start with a 3D CAD model, which is usually translated into some intermediate file format and used by the machine tool controller. Machine tools can be additive or subtractive [51]. In this group of processes, RP technologies such as Stereolithography (SL), Selective Laser Sintering (SLS), Laminated Object Manufacturing (LOM), Fused Deposition Modelling (FDM) and 3D Printing, are used to produce moulding elements for injection moulding. Some of the direct processes are also commonly used to produce masters to be used in indirect processes. Usually, direct processes specific names are attributed by the RP equipment manufacturer.

Stereolithography

The stereolithography (SL) process, as an original concept, was put forward by Kodama as an automatic method for fabricating a three-dimensional plastic model with photo-hardening polymer [52]. Based on Kodama's idea, in 1986, Hull conceived the SL method and filed one of the most important patents in rapid prototyping [2]. This patent describes a method and apparatus for generating solid objects, by forming successive cross-sectional layers (Figure 2.3).
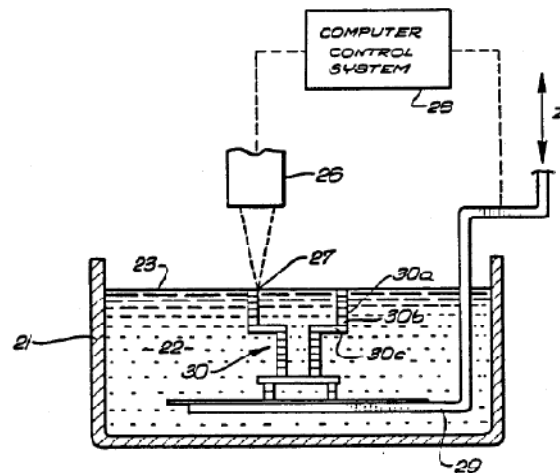
Figure 2.3 - Stereolithographic process of descendent fabrication (source: Hull [2])

This process builds three-dimensional models from a photosensitive liquid polymers that polymerises when exposed to ultraviolet (UV) light. Other source of light, such as Infrared Radiation (IR) or even visible radiation can also be used [53-55]. The model is built on a movable platform situated just below the surface in a container of liquid resin (epoxy or acrylate), as shown in Figure 2.4. A UV laser traces out the first layer, materialising the model cross section [55]. The surface layer of the resin is cured selectively by the laser beam following the path defined in the slicing model. After this layer has been created, and the movable platform is lowered into the container, a new thin layer of liquid monomer floods the model and the process is repeated [24].
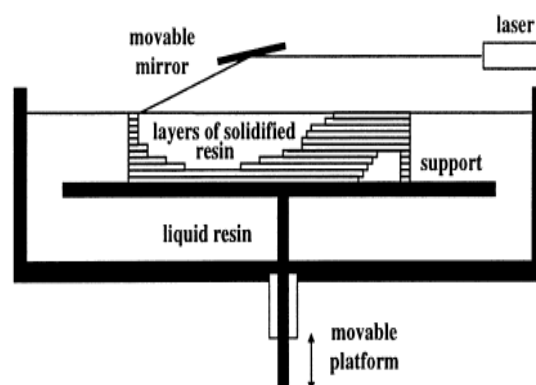
Figure 2.4 - Stereolithography principle (source: Rosochowski *et al.* [24])

Due to its dimensional accuracy and material properties SL process has been used for both direct and indirect tooling applications. In the case of indirect tooling SL masters have been mainly used to produce silicone moulds and epoxy tooling (*e.g.* [30]). The use of the SL directly in the RT manufacturing can be possible using solid inserts (ACES - Accurate Clear Epoxy Solid) or shell inserts (Direct AIM) [37, 56, 57].

The SL resins available for use in the stereolithography process are essentially variants of epoxy and acrylic [58]. The degree of curing of the part obtained by SL process depends on the resin photosensitivity and building parameters [59]. Due to difficulties in optimizing these parameters, a post-curing process by ultraviolet radiation or by thermal treatment is required to increase the degree of cure improving thermal, mechanical and chemical properties [60]. The SL process has been commercialized by 3D Systems (Rock Hill, USA) since 1987 [61].

Another possible material possibility to use in moulding blocks using stereolithography is the Nanoform^{TM} 15120. The resin NanoForm^{TM} 15120 from DSM Somos (Hoek van Holland, The Netherlands) is an epoxy resin filled with ceramic nanoparticles that produces strong and stiff parts, enabling its use for functional purposes such as testing for assembly or fluid motion testing within ducts. The use of this specific type of resins for injection moulding was already tested and proved their feasibility on short to medium run production [62]. The mechanical and thermal properties of these materials are improved when post-cure treatments are considered. However no significant variation on hardness is verified allowing finishing operations even after the thermal treatment. Koster *et al.* compared these materials as shown in Table 2.1, taking Watershed as a reference RP material [62].

Table 2.1 – Properties of RP materials (source: Koster *et al.* [62])

material	Tensile strength (MPa)	E modulus (MPa)	HDT (°C) @1,81MPa
Watershed (transparent)	50	2750	49.3
Prototool (white)	75	10650	88
Nanoform (grey)	48	5000	52.9

Laser Sintering/melting

Selective Laser Sintering

The sintering process, usually called Selective Laser Sintering (SLS), was developed in the Texas University by Deckard and Bourell and patented in 1989 [63]. The process consists in the use of infrared radiation to bond particles of specific powder materials [64]. A powerful laser beam promotes the selective sintering of a powder material in successive

construction layers. It uses a high-power laser to selectively heat powder material just beyond its melting point. The laser traces the shape of each cross-section of the model to be built, sintering powder in a thin layer. It also supplies energy that not only fuses neighbouring powder particles, but bonds each new layer to those previously sintered. The laser energy is directed onto the powder via a scanning system where it causes the powder to sinter to become a solid. The sintering takes place in a sealed heated chamber at a temperature near the powder melting point and is filled with an inert gas to reduce oxidation of the powder being sintered. After each new layer is solidified, the working platform is lowered, a new covering of powder layer is spread and the scanning is repeated [65, 66]. The powder that remains unaffected by the laser acts as a natural support for the model and remains in place until the model is complete. After all the layers are defined, the non-sintered powder is discarded to reveal the solid object formed inside [4, 24].

There are two types of Laser Sintering processes: the indirect and the direct one. In the indirect Laser Sintering process low temperature polymers are used as binders [67]. The polymer binders are either mixed with the primary powder (*i.e.*, separate binder and structural powder particles) or coated on the surface of the primary powder (*i.e.*, using coated particles where the binder material is applied as a coating around the structural material) [68]. The direct Laser Sintering process involves the direct melting and consolidation of selected regions of the powder bed. For example, direct SLS enables to produce high or full density parts [69, 70].

As a consequence of building objects with powdered materials, models produced through indirect SLS are porous. The porosity can lead to failure because of low mechanical resistance, and also affects the surface quality. Porosity is mainly dependent on the size of the powder particles. Larger powder particles produce models with high porosity and rough surface quality, while small powder particles produce models with lower porosity and smooth surface quality [68, 71]. The main advantages associated to the SLS technology are the good part stability, the wide range of processing materials, no part supports and little post-processing required. Another important advantage of SLS over other techniques is the freedom of form fabrication [72]. Any geometry can be built without restrictions of geometric complexity like negative angles, undercuts or hard-to-program features. Additionally, this technique allows building rapid tools with conformal cooling channels [23, 73].

Many types of materials, such as polyamide (PA), polystyrene (PS), polycarbonate (PC), acrylonitrile butadiene styrene (ABS), metals, ceramics and composites can be used in SLS applications. The objects produced through the SLS process have small and medium dimensions (from 10 to 800 mm, major dimensions) and high geometrical complexity. The moulds produced with SLS commercial available materials can produce on average of 50.000 to 100.000 parts in the more common thermoplastics [51].

SLS was initially commercialized by DTM (Washington, USA) till 2001, when it was acquired by 3D Systems. In the mid 1990's EOS (Munich, Germany) appeared with the concept of Direct Metal Laser Sintering (DMLS), which was later developed into the concept of Selective Laser Melting (SLM). Recently other companies such as MCP and Concept Laser appeared in the market with variants of the SLS and SLM processes [74].

Direct Metal Laser Sintering

A variation of the SLS process is the Direct Metal Laser Sintering (DMLS) process, developed by EOS GmbH of Munich, Germany, and available commercially as the EOSINT M 250 laser sintering machine since 1995 [75] until 2008. A scheme of the EOSINT M 250 machine can be seen in Figure 2.5 and the process used a laser that is directly exposed to the metal powder in liquid phase sintering. No preheating unit is required and no inert gas atmosphere is applied. The parts are built on the steel base plate that is specially coated with bronze. Hence, the first powder layer can be strongly bonded to the base plate during laser sintering [76]. A post-processing of further infiltration can be avoided for the offered steel powders, because nearly dense parts can be produced [77].
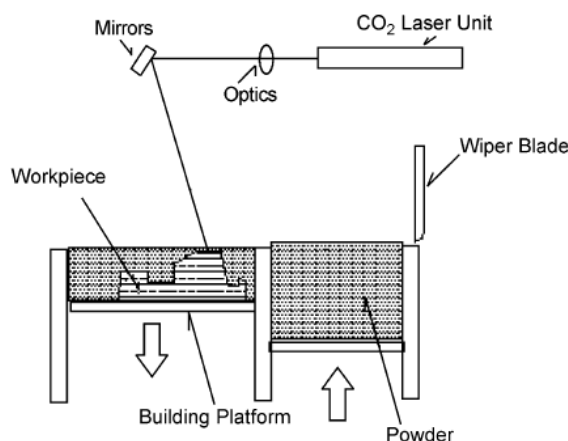

Figure 2.5 - Schematic diagram of the EOS machine (source: Khaing *et al.* [76])

The major problem with sintered tooling has been the poor surface which has required tool inserts to be subjected to high levels of hand finishing and even machining [78].

Three Dimensional Printing

The Three Dimensional Printing (3DP) is another sintering process resulting prototypes developed at Massachusetts Institute of Technology by Sachs and Cima [79].

The ProMetal is a 3D Printing metal process that enables to build directly the parts without casting [80]. ProMetal was patented in 1989 [81] and industrialized by Extrude Hone (USA). The principle is based on metal components built by selectively binding metal powder layer by layer but here the structural skeleton must be debinded, sintered and/or infiltrated with bronze to produce a finished part that is 60 % steel and 40% bronze. It is an accurate, flexible, and reliable process and enables to build directly the parts without casting. The geometrical complexity is nearly unlimited since this technology allows complex cooling channels or light structures. It is a very high building speed and large dimensions can be obtained [82].

The ProMetal parts look like a foundry part requiring only milling of some local areas to obtain a good finish [80]. The direct production of the ProMetal parts follows several steps. First of all the part is created in any standard CAD application. Next the part file is electronically sent and optimized for output to the RT machine. Then the powered metal is collected from the metal powder supply and spread onto the build piston. After that the print head applies a layer of binder to the powered metal to form the first "slice" of the part. Before the part is lowered to allow the next layer of metal to be spread, a new layer of powdered metal is collected while a driving lamp is applied to the built slice. The next layer of metal is spread across the build piston. Additional binder is applied to bond the metal powder together and to the previous slice. The process repeats until the entire part has been printed (Figure 2.6).
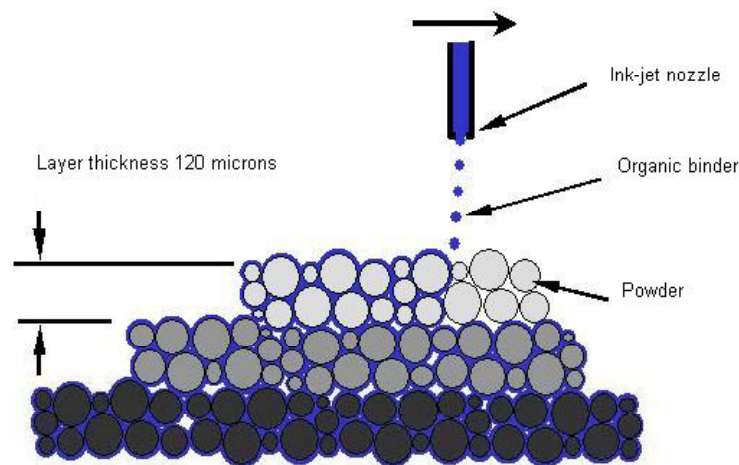

Figure 2.6 - Printing on the powder (source: Dormal [82])

After the printing step, the "green" part, approximately 60% of base powder, 30% of binder solvent and 10% of binder active solvent, is placed into a furnace. The metal powder commonly used is the stainless steel and the binder is bronze. The next step is a fast curing treatment (2 hours at 180ºC) to guarantee minimal properties of handling of this green part. The structural skeleton is then debinded and also pre-sintered [82]. The final mechanical properties are not excellent but good enough for many basic applications.

The other way is to fully sinter the part in the oven to reach 95-98% of the properties of the chosen material and also nearly the full density in the right material and not in a hybrid material. Some recent developments made at Fraunhofer IFAM (Bremen, Germany) show good results on 17-4PH powder with values for tensile strength and yield strength being much higher than the values obtained with bronze infiltration [83]. Finally, the part is ready for post processing (polishing, milling, surface grinding, etc.) to reduce the bad surface quality produced by a 3D printing process with 120 μm layers [82].

When compared with other technologies, the mechanical properties are better with ProMetal, except for the new EOS H20 which is a real tool steel (1100 MPa, 42 HRC). A common point of the ProMetal is that the thermal processing steps (debinding and sintering) are clearly similar although the binder is different. This is one of the main positive point for the DMLS since the EOS process is a real direct manufacturing process.

These additive technologies (SLS_m, ProMetal, SLM…) are still in evolution and new enhancements appear regularly but so far the layer thickness is better with EOS (20 μm) than with ProMetal (120-170 μm). This has an impact on the global surface quality of the parts [82]. The geometrical complexity is nearly unlimited since the ProMetal technology allows complex cooling channels or light structures. In unsupported zones this technology uses the powder as support during building that is removed afterwards. The building speed is much higher reaching up to 1100 cm^3/h using a printhead with 32 nozzles. DMLS is ranging between 5 and 20 cm^3/h depending on powder and build parameters. Real benchmarks on several case studies reported values between 15 and 100 times faster with ProMetal (thermal post processing not included). The superiority of DMLS is clear with a local precision around 0.05 mm. The other two stay below 0.2 mm [82].

Finally, the Selective Laser Melting (SLM) process is described in US Patent 6215093 as follows: "The method is characterised in that the metallic material in powder form is applied in the form of a metallic powder free of binders and fluxing agents, that it is heated

by the laser beam to melting temperature, that the energy of the laser beam is chosen in such a way that the layer of metallic powder is fully molten throughout at the point of impact of said laser beam" [84]. As shown also in Levy *et al.*, the equipment is similar to the SLS process. However, the material is completely melted by the laser beam guided by a scanner (Figure 2.7). It has similarities with welding techniques [85].
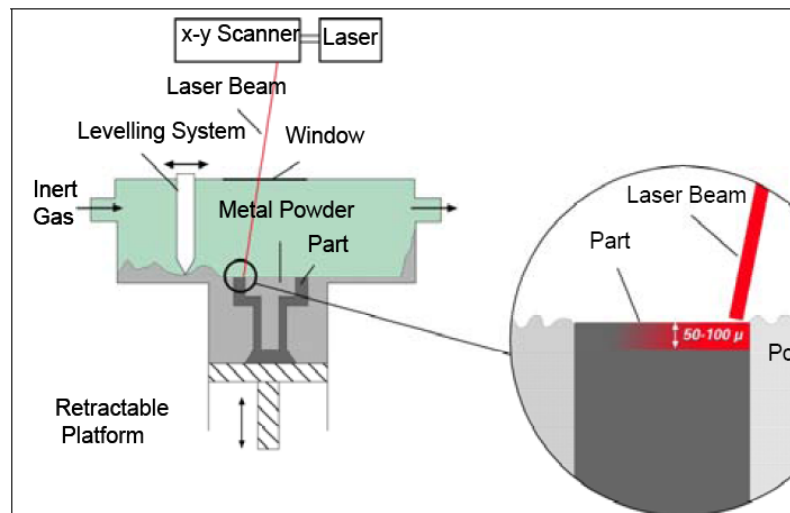

Figure 2.7 - The SLM system principle: layer thickness 0.05 – 0.1 mm ; Laser Nd:YAG wavelength 1064 nm (source: MCP [86])

Most available SLM systems use a Nd:YAG laser, in total congruence with the results of SLS modelling (*e.g.* [87]).

2.2   Hybrid moulds

The concept of hybrid mould is established as a mould with moulding inserts manufactured in alternative metallic materials or in synthetic materials [6, 88]. To produce this type of moulds (Figure 2.8) RPT techniques are used for the moulding blocks and standard conventional machining techniques for the mould structure [11, 44, 89].

This concept aims at producing moulding zones in alternative materials as fast as possible and with competitive mechanical, fabrication time and quality standards. In the case of non-metallic rapid tools, the material selection is of great importance because the number of successful shots depend on the material used [90]. Furthermore it is expected to reduce costs and time to production, and to produce parts with suitable aesthetical and performance properties [91].
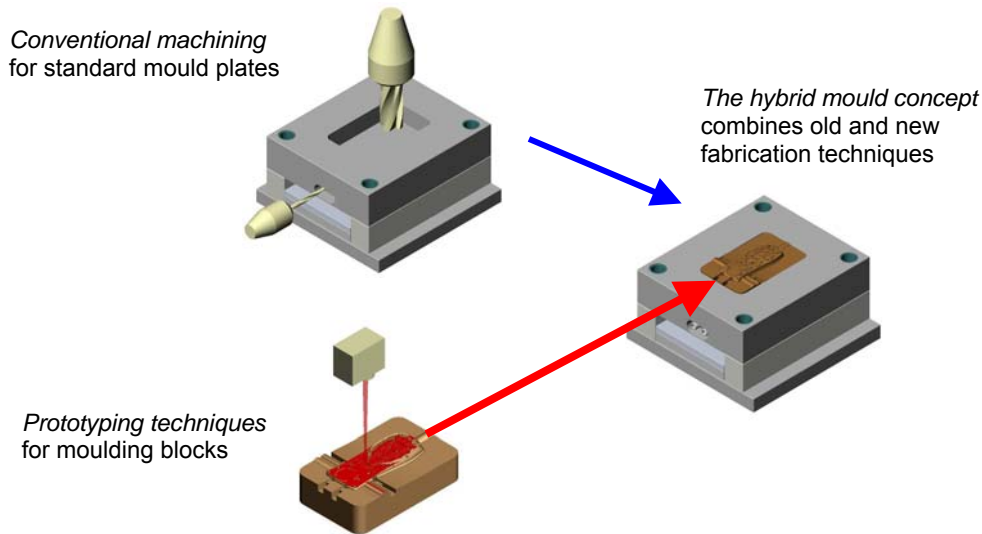
Figure 2.8 - The hybrid mould concept (source: Pontes *et al.* [11])

2.2.1   Hybrid mould specifications

The concept of hybrid mould implies specific engineering specifications. Several authors have been investigating various aspects related with the use of hybrid moulds in injection moulding. A recent research project [11] produced some design rules for hybrid moulds as, for example, radius for corners, draft angles for release, plastic flow restrictions easing, etc. Textbooks refer that when designing hybrid moulds for production, the rules for injection moulding tools must be followed (*e.g.* [21]). Some researchers mentioned the importance of considering the design for reutilisation of the existing structures (*e.g.* [8, 92]). From this point of view, specific requirements should be considered when designing hybrid moulds, namely:

- The possibility to fit as many part sizes as possible;

- An easy way to exchange the moulding blocks without the need to remove the entire mould from the injection machine;

- The possibility of using conformal cooling channels, *i.e.*, channels that follow the contour of the part;

- The freedom of positioning ejector pins according to the part geometry;

- The flexibility to adapt injection systems.

Of this way, product shape, mould structure and mechanical design should be carefully considered to ensure that it is feasible to keep the wear within acceptable values during the

mould life [16, 93]. Additionally, hybrid tools must guarantee an injection moulding cycle time as short as possible.

Another specification for these moulds is the adjustment of their lives to limited series of production. The hybrid moulds are produced in materials softer than tool steel. Thus the lower mechanical and thermal strength only make possible the production of short and medium series of plastics parts. On the other hand the soft materials allow easier manufacturing and shorter delivery time. However, the use of these materials also poses some concerns regarding the mould lifecycle and the influence on the properties of the mouldings [23].

2.2.2   Thermal and mechanical design aspects

To satisfy the hybrid mould specifications, mechanical and thermal design aspects have to be considered, namely, the injection and mould material shrinkage, the dimensions and layout of the cooling channels, the gating layout and the ejection system.

The reduced thermal conductivity of the epoxy composites used in hybrid moulds (as in Table 2.2) determines that the injection moulding cycles are much longer than in standard moulds due to the low cooling rate before ejection [13].

A study with a development hybrid mould producing 1.5 mm thick tubular parts when moulding polypropylene with a standard steel core and a epoxy composite core [94] showed clearly this effect (Figure 2.9).

Table 2.2 - Core material properties (source: Bareta *et al.* [95])

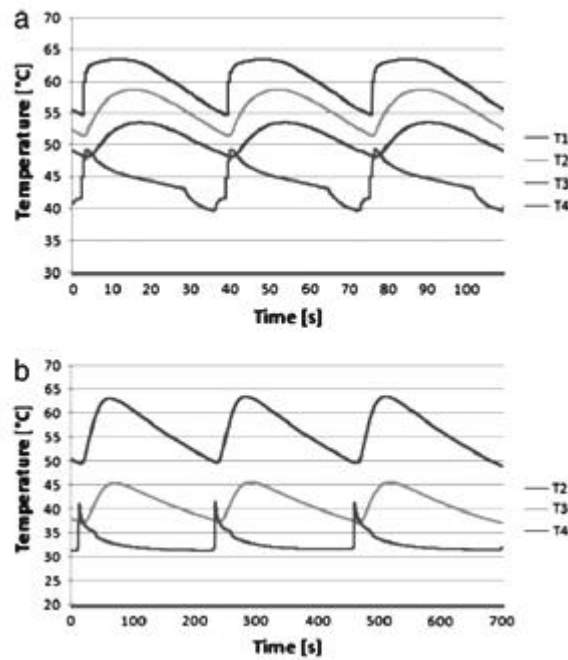| Property	P20	Aluminium	Zamak-5	Epoxy Resin
Density [$Mg.m^{-3}$]	7.80	2.71	6.76	1.75
Specific heat [$J.kg^{-1}.K^{-1}$]	460	782.3	420	1050
Thermal conductivity [$W.m^{-1}.K^{-1}$]	29	138	109	1
Coefficient of thermal expansion [K^{-1}]	12×10^{-6}	22.5×10^{-6}	27.4×10^{-5}	60×10^{-5}
Young modulus [GPa]	210	70	85	6.86

Figure 2.9 - Temperature evolution in (a) steel core and (b) epoxy/SSF core (source: Roobaert *et al.* [96])

Also, characteristics like glass transition temperature (T_g), thermal deflection temperature and the heat resistance are important to evaluate the mould material capacity [92]. Resin composites have lower thermal conductivity than metals, which significantly increase the injection cycle. The lower thermal conductivity of the resins contributes for higher regime mould temperatures. However, the temperature that a mould can tolerate must be lower than the resin glass transition temperature [97].

The cooling process is considered one key issue in the studies of hybrid moulds [44]. The targets that a correct cooling system has to follow are the uniformity of the wall temperature and a gradual reduction of the polymer temperature, in order to find a compromise between the necessities of reducing cycle time, allowing for the crystallization. According to the literature (*e.g.* [98, 99]), the layout of the cooling channels has a high importance in obtaining uniform cooling, because it controls the moulding surface temperature distribution and evolution during the cooling period. In the design of the cooling system it should be taken under considerations aspects as: the diameter of the cross-section (or the cross-section area if not circular), the distance between channels and the distance between the channel and wall of the mould (*e.g.* [100]). The main problems that arise when choosing these dimensions concerns to the pressure losses derived from the choice of the diameter and the layout of the channel. A heating/cooling relationship reported by Zollner gives a general guideline for the positioning of the channels. He

recommends that the value resulting from the relationship should stay between 2.5 and 5% for semicrystalline thermoplastics and between 5 and 10% for amorphous [101].

Conformal cooling channels (Figure 2.10) have been used for this purpose allowing for the uniformity of cooling and a significant cooling time reduction [44, 102, 103]. Xu, for instance, concluded in his studies that an efficient and uniform control of the mould temperature through conformal cooling is the first step toward the dynamic thermal management of the injection moulding process for quality and productivity [104]. The conformal channels can be easily produced during the production of the moulding block by RPT [102, 105, 106].
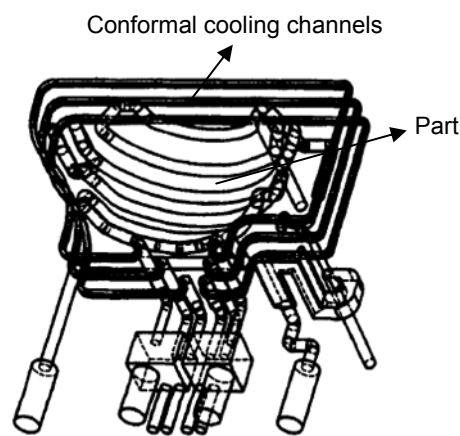

Figure 2.10 - Conformal cooling channels (source: Xu *et al.* [103])

The mould temperature is regulated by circulation of a fluid, usually water or oil that flows in the cooling channels. The flow rate determines the circulation fluid regime. Better cooling efficiency is achieved in turbulent regime (*e.g.* [105]). High flow rates are necessary for this regime. Voet *et al.* showed the influence on cooling with turbulent and laminar fluid regimes in three different injection moulds, including hybrid solutions [107]. They concluded that when the flow rate goes up, the cooling capacity will increase too. Their studies also showed that the use of parallel cooling channels is beneficial in terms of cooling effects, as there is a smaller pressure drop in the mould. The major drawback of this configuration is the limitation in connecting all cooling circuits in the mould [16, 107].

Another issue regarding hybrid moulds is the dilatation of the materials used in the cores. It causes difficulties in the ejection process, and therefore it is recommendable that it must be considered in the design phase of the mould [14]. In this study three 'soft' materials, aluminium, Zamak and an epoxy composite, were used to evaluate its potential interest to produce RT inserts.

The effect of using hybrid moulds on the properties of thin parts, using various RPT techniques, was also studied [108]. The feasibility of construction moulds by the casting process for the injection moulding of a thin wall plastic part was demonstrated, and minor damages reported near to the gate.

2.2.3   Moulding block materials

As mentioned recently by Pouzada, the more recent developments are the interest for the other materials conveying structural capability, thermal conductivity and enabling an easy and quick shaping [13]. The combination of aluminium and graphite in view of the high aspect ratio of the graphite was studied [109]. The tensile modulus and the yield stress of the various composites are shown in Figure 2.11. It was verified a synergistic effect of using 20% aluminium and 10% graphite when comparing these composites with a commercial material, Neukadur VG SP5 (Altropol, Germany).
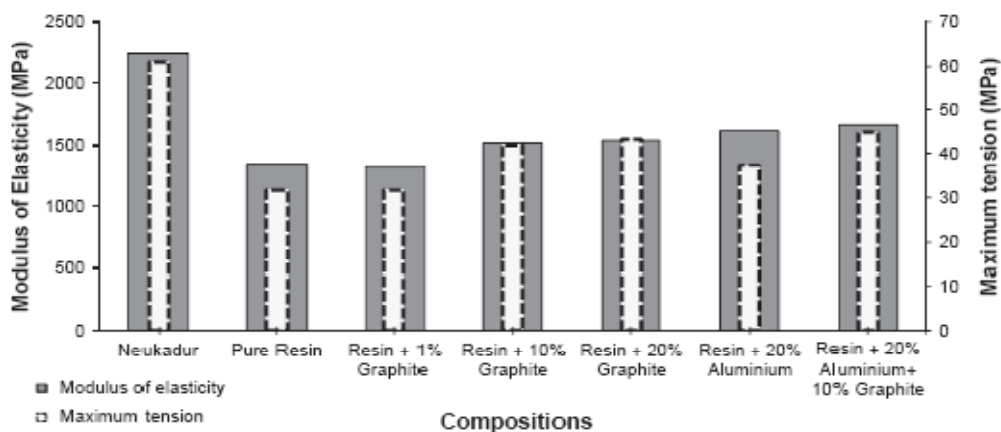

Figure 2.11 - Tensile modulus and yield stress for the various epoxy composites (source: Pontes *et al.* [109])

Polymer based materials

Although the need of improvements on strength and thermal properties of the resins used in moulding elements of hybrid moulds, it is possible to find thermosetting resins (usually epoxy), with or without fillers, to resist at thermo-mechanical environment involved in an injection moulding cycle. Ideally, the polymer or its composite should have the capacity to keep its hardness, tensile strength and compression strength over the injection moulding temperature cycle. The advantage of these composites is their easy processability [46].

Fillers

Metallic fillers are mostly used with epoxies to produce commercial composites for rapid mould-making. Problems may arise from the non-uniform mixing between the epoxy resin and the curing agent [110]. The difference between the density of the fillers and the density of the resin also imply non-uniform mixture. Vasconcelos *et al.*, also mentioned that high temperatures (160ºC) affect the mechanical properties of the composite, due to resin softening and reduction of the particle and fibre/matrix adhesion. Furthermore, temperature fluctuations also promote the coefficient of thermal expansion mismatches between the dispersed phases and the epoxy resin, leading to differential thermal stresses that can contribute to the degradation of the interface quality [46]. In their studies, they also concluded that the adhesion between the fillers and the resin matrix depends on the geometric relations and surface chemistry. The fibres tend to adhere more strongly to the resin matrix than the aluminium particles. These are easily removed when submitted to high pressures, while the fibres increase considerably the load carrying capacity, reducing the friction coefficient, and consequently the composite wear rate.

Metal-polymer composite using short steel fibres (SSF) and epoxy resin was studied recently [48]. It was observed that the composite filled with 40% of steel fibres had about 360% increase of elastic modulus. However, the same composite had a decrease of 44% on tensile strength. This composite also presents an increment on thermal conductivity of 250% in comparison of the epoxy resin [47, 49].

Manufacturing

Epoxy composites may be shaped by vacuum casting into a mould where the impression is defined using a "master" produced by Rapid Prototyping (*e.g.* [44]), or by machining a pre-cured resin block (*e.g.*[14]). In the case of pre-cured resin blocks the machining is critical to avoid failure or excessive roughness [111, 112].

Regarding the aluminium and Zamak materials, it is highlighted the easy of machining of these materials and their good properties such as resistance to corrosion and thermal conductivity. Other studies had shown that manufacturing using High Speed Cutting (HSC), the two materials usually applied are also aluminium and Zamak [113-116].

The main advantage of the casting process is the short time required to obtain freeform moulding geometries compared with conventional cutting processes. In the casting resin

processes, copper refrigeration tubing is usually used as cooling lines within the mould inserts (*e.g.*[106, 117]. After backfilling, mechanical fasteners are attached to the cooling lines.

Failure

Typically the moulding blocks produced in epoxy composites can fail by adhesion, breakage, or chipping of any part of the geometry. In the research project *Hibridmolde*, and as published by Queirós *et al.*, the performance of hybrid moulds using moulding blocks, produced by different RPT techniques, namely, epoxy tooling, SLSm and spray tooling, was studied [118]. As published by Queirós *et al.*, it was observed failure and faster degradation in the moulding blocks (Figure 2.12) made with the resin used in the epoxy tooling (Neukadur VG SP 5). The blocks produced through laser sintering of metals did not suffer failure in service, although conformal cooling channels were difficult to produce [119]. However, as mentioned by Kruth *et al.*, the objects built with powdered materials are porous, and porosity can lead to failure because of low mechanical resistance [68, 71].
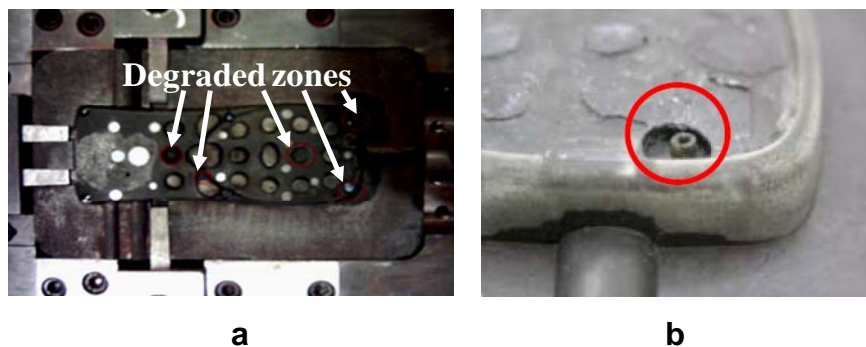

Figure 2.12– Failure in epoxy moulding block: a) after 14 cycles, b) prematurely (source: Hibridmolde [118])

Queirós and co-workers also stated that the Metal Spraying was not good, mainly, for parts with complex geometries. However, if the geometry is open and smooth, and if there are no difficulty in extracting patterns, this technique can be successively used. The thermal performance of the mould is much better than the Epoxy Resin insert mould [119].

Vasconcelos *et al.* verified a highest wear in aluminium filled epoxy and correlate this fact with the debris derived from the particle pullout [46]. They associated the decrease of the material integrity with the cohesion between the aluminium particles and resin due to its interface resistance. Furthermore, they also stated that the approximately equiaxial aluminium particle geometry and the chemical nature produce a relatively poor adhesion force to the epoxy matrix, as suggested before by Barthés-Labrousse *et al.* [120, 121].

Another kind of failure is the damage at the gate area of the aluminium filled epoxy core moulding block manufactured in an epoxy composite filled with aluminium (Figure 2.13), observed by Bareta [95]. He also verified the pitting effect on the surface moulding, as shown in Figure 2.14, and associated both types of failure to the erosion caused by the aluminium particles.
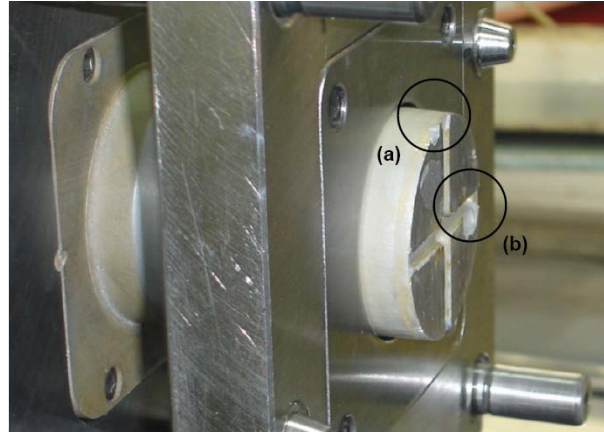

Figure 2.13 – Failure at the gate area of the core moulding block (source: Bareta [95])

Figure 2.14 – Failure of the epoxy/Al core moulding surface (source: Bareta [95])

The processing conditions also can influence the performance of the moulding blocks. For instance Cheah *et al.* reveal the existence of fine hairline cracks due to the higher operating pressure and temperature encountered during the moulding of PC material in a EP250 tooling resin (marketed by HEK-GMBH) comprised of 75% aluminium powder and 25% epoxy [34]. The higher pressures imposed during moulding cause a significant amount of stress to be generated within the mould, causing it to crack. Figure 2.15 shows the cracks observed on the cavity side mould half after a series of 400 moulding cycles.
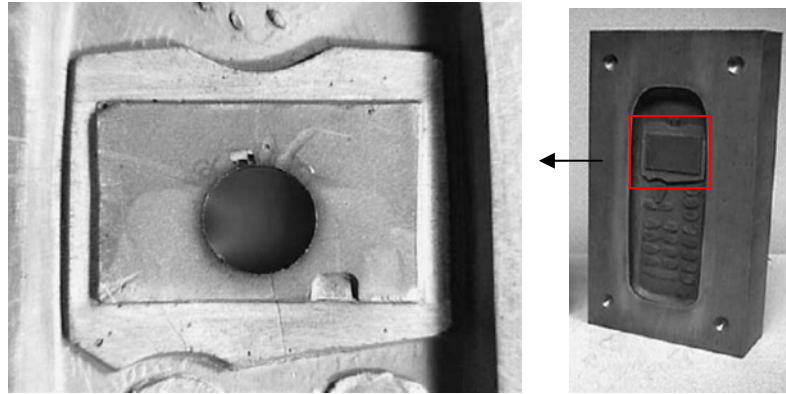
Figure 2.15 - Cracks appearing on the surface of a mould half (source: Cheah *et al.* [34])

The moulding blocks produced by SL have mechanical limitations. According to Gonçalves *et al.*, the choice of the best SL resin for the moulding blocks of a rapid tool, leads preferentially to a resin with high tensile strength and T_g, but with an intermediate elastic modulus, in order to enable the absorption of more energy. It is also important to check the chemical affinity with the polymer to be injected and the material selection for moulding blocks (core and cavity). The Hildebrand parameter (ξ), which reflects the material solubility, can also provide information about the material chemical affinity [122]. The SL process has been used in various studies for producing moulding blocks (*e.g.* [9, 57, 102, 123]). For instance, Ribeiro Jr observed premature failure in the SL moulds (Figure 2.16) and suggested that mould breakage is more likely to occur as a result of high temperatures incurred during moulding rather than by any detrimental changes to mechanical properties over time [57].
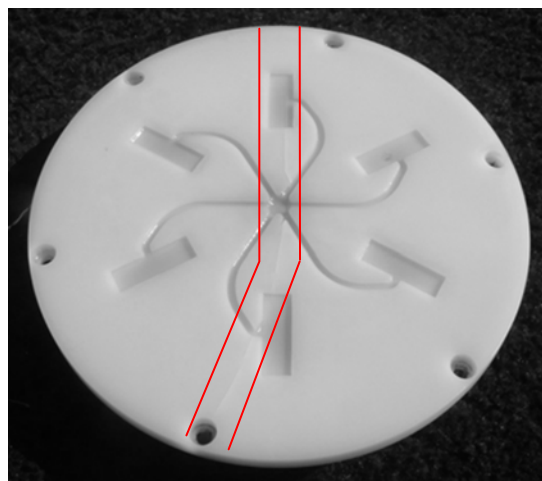

Figure 2.16 – Premature failure in SL mould (source: Ribeiro Jr *et al.* [57])

Westphal *et al.* observed wear of the core during ejection, *i.e.*, small particles of the SL core were found at the surface of the mouldings [123]. They associated this failure to the chemical adhesion between the two materials, during the injection phase. Palmer *et al.* also stated that the two major failure mechanisms for raised features in stereolithography tooling are due to injection flow and ejection pullout. Injection flow failure usually occurred in tall features (height ratio of 9 - referred to the height divided by the thickness, Figure 2.17a) with little resistance to bending and pullout failure usually occurred in features with a height ratio of three (Figure 2.17b). Another kind of failure, also mentioned by Palmer, is chipping: a fatigue-based failure mechanism similar to pullout failures, which occurs in longer lasting features [124].
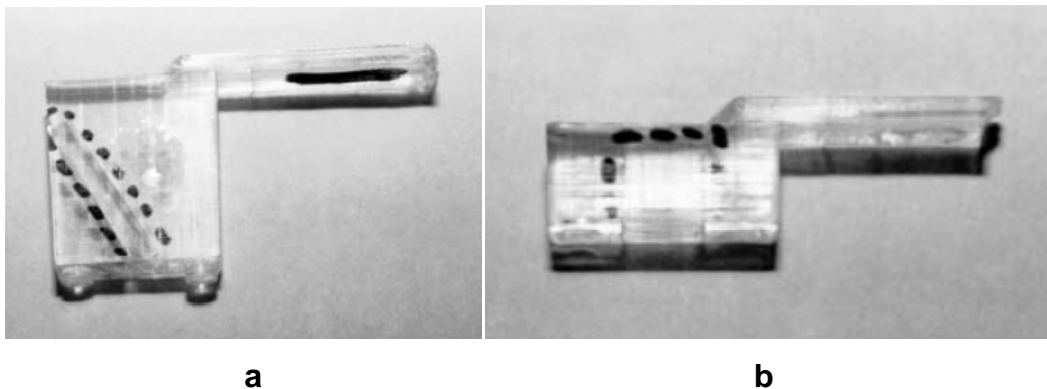

a   **b**

Figure 2.17 - Injection moulded part with: a) injection flow failure of mould feature (height ratio 9), b) an ejection pullout failure of a mould feature (height ratio 3). The dotted lines outline the mould feature broken off in the part (source: Palmer *et al.* [124])

As mentioned by Pouzada, in spite of the high dimensional accuracy of the SL parts there are structural integrity problems when they are directly used in the moulding blocks [13]. These problems arise either from thermal fatigue [57] or adhesion of the SL resin to the moulded polymer [123, 125].

The behaviour of hybrid moulds using moulding blocks made from SL Vantico 5260 resin was assessed by Gonçalves and co-workers. Four thermoplastics (iPP, ABS, PET and PA 6.6) were moulded, and their mechanical, thermal and chemical properties analysed and related to the performance of the moulding process. The geometry used (Figure 2.18) had the objective of highlighting some critical points already pointed out during the operation of hybrid moulds with SL inserts, namely, the draft angle of 10º that intensifies the stair-step effect caused by the SL construction method, making difficult the ejection of the injected parts [93].

Figure 2.18 - PET moulding perforated by the ejector pin (source: Gonçalves *et al.* [93])

They concluded that the injection materials with solubility parameters (or Hildebrand parameter) close to the SL resin are likely to cause wear on the moulding core, due to chemical adhesion between the two materials during the injection phase, as observed by overmoulding the thermoplastic on the SL block (Figure 2.18). However, their studies also mentioned that the moulding blocks made by SL for deep mouldings perform well when the moulded polymer is weaker (in terms of modulus and strength) than the SL resin. Furthermore the design of the ejection system requires careful consideration in the cases of materials of higher shrinkage (typically the semicrystalline materials) and polymers stiffer than the SL resin [93]. During the ejection phase, friction forces are generated between the part (plastic) and the core moulding block. The coefficient of friction between plastic/steel depends on the surface texture of the core and the ejection temperature [126]. Generally, the ejection force is considered as the result of the interaction between part geometry, mould geometry and material, moulding material and processing conditions [127]. In conventional injection moulds where metals are used to build the whole mould, the origin of the friction force during ejection mainly results from the roughness of the surfaces and the shrinkage of the thermoplastic material [125, 127]. However in hybrid moulds with resin moulding blocks, the contact between polymer-polymer and the chemical adhesion are relevant especially at high temperatures [128, 129].

Gonçalves *et al.* showed that to minimise adhesive wear it is important to inject polymers with Hildebrand solubility parameters different to the resin. It was also observed a significant elastic deformation of the cores, when resins with low Young modulus were used to produce the moulding blocks [125]. In these cases the effective ejection force is lower than expected. Similarly, Salmoria *et al.* (2005) who studied the use of stereolithography resins to produce moulding blocks, also shown that it is not possible to

inject polymers of both higher tensile modulus and strength than the resin, due to the generalised failure of the moulds when parts were pulled out from the core. These problems can be increased if the ejection system is incorrectly designed [130].

Stereolithography, due to its ability to produce quickly precision parts, is a frequent option for obtaining moulding blocks for small series of injection mouldings. When the production of a given number of parts using SL tools is considered, the knowledge of the mechanical and thermal properties of the SL resin used in the moulding blocks, and those of the thermoplastics to be injected are important for the success of the production. This arises from the low values of these properties when compared with metals [59].

Finishing

Based on experiences with laser sintered inserts, some authors (*e.g.* [73, 131]) concluded that the surface quality of SLS inserts is insufficient to be immediately used as moulding surface. Therefore the product needs an adequate finishing process. For instance, if an end user wants to bring the SLS mould into full production, one possibility is to apply a surface coating that will rise surface hardness of the mould and/or improve the release behaviour.

Studies on hybrid injection moulds refer that the SLS moulds can be delivered very fast. However, it is important to notice that, without an adequate finishing process, the mould will have an unsuitable surface roughness [97]. For this reason, it will suffer from wear sooner than a conventional mould, which limits the quantity of parts it can deliver [132]. To solve this problem, some surface coatings (mainly the carbon-based coatings such as Diamond Like Coating) can be used to improve the behaviour of the mould [133]. Chemical vapour deposition (CVD) diamond coatings can potentially play an important role in the plastic injection moulding industry. They have well established characteristics in what concerns their high hardness, low friction coefficient and inertness. Therefore they provide proper coating for specific micro-features on mould tools and significantly contribute to reduce mould tool intervention due to service and maintenance. Neto and co-workers concluded that moulded objects with the diamond-coated inserts present more homogeneous surfaces than the ones moulded by inserts without coating, indicating that overall mould-tool intervention may be reduced when using diamond-coated surfaces [133]. Additionally, Physical Vapour deposition (PVD) and Plasma Assisted Chemical Vapour Deposition (PACVD) of micro-layer coatings are a relatively fast and easy way to

improve the surface hardness of the SLS mould inserts. This reduces friction between mould and injected part reducing the wear on the mould [97, 134].

2.3   Injection moulding

2.3.1   General aspects

The mechanical performance of the injection moulds or, specially, the moulding elements, is dependent on the shrinkage, the ejection system, the injection point and the gate position. The shrinkage of the polymer to be injected needs to be taken into account in the hybrid mould design, mainly the moulding elements. Around 95% of the shrinkage happens inside the mould. This is compensated by incoming material. The remainder of the shrinkage takes place following the production of the part [135, 136]. Thus, mainly the established processing conditions and the cooling system have a high influence on the shrinkage and properties of the parts (*e.g.*[98, 137]). If the cooling system is well designed more uniform is the shrinkage and better quality parts are obtained. Moreover, if the water lines could be conformed to the shape of the part and their cross section changed to increase the heat conducting area, then a more efficient heat removal is achieved [44]. This may also help to reduce warpage when the part is ejected, as the plastic would be cooled more uniformly. Therefore, if the part is ejected with the same temperature at every point, the subsequent shrinkage is also uniform avoiding warpage of parts [138]. Besides the shrinkage of the polymer also the shrinkage of the resin used to produce the required moulding elements can influence the final dimensions of the part to be injected, and thus it must be taken into account on the hybrid mould design [13].

The gating option also affects the mechanical properties of the part, mainly due to welding lines [139, 140]. Additionally, the gate position can influence the injection time and the overall injection cycle time. Moreover, when the gate is located in the external surfaces can leave visible marks that can be unacceptable for production purposes, with important consequences in terms of pos-processing time.

The ejection system main function is to remove the moulding from the mould. This functional system may also cause visible marks and permanent deformations, or even the breakage of the part. To avoid these damaging or catastrophic effects it is necessary to optimize the number, location and dimensions of the ejector pins and air vents [141].

Therefore, the design of the ejection system has attracted special attention in some research studies (*e.g.* [21, 93, 127, 130, 141-143]). Typically they consider different layouts of the ejector pins to examine the effect of the number, location and size of the pins on the ejection.

The effect of processing parameters on the ejection force has been also researched (*e.g.* [132, 144-146]). Pontes *et al.* and Balsamo *et al.* demonstrated that the ejection force increases with the cooling time and roughness of the mould wall and showed that the coefficient of friction between the part and the mould core does have a significant influence on the ejection process [132, 146]. The effect of the core roughness and injection pressure on the ejection force was studied and found out that there is an optimal surface roughness when the ejection force is lower [144, 145]. Pontes and co-workers also concluded that both the testing temperature and the surface roughness are important in the control of the friction behaviour [127, 147].

2.3.2   Processing parameters

In the cycle time of injection moulding comprises mould closing time, filling time, packing time, cooling time and ejection time. Cooling time occupies the longest portion of time in the cycle and usually has a direct impact on the whole cycle and, therefore, on productivity.

When plastics are used in engineering components they must fulfil several product requirements as mechanical performance, dimensional tolerances, temperature resistance, life expectancy and others [148]. Many of these requirements and properties are dependent on the injection moulding setup, which can be described in terms of the moulding parameter setting and the properties of the materials used in the injection mould tool (*e.g.* [127]).

The injection parameters (moulding temperature, pressure, speed, etc.) play a relevant role in the mould life. The adjustment of the injection moulding parameters is particularly important for hybrid moulds [92]. In this case, product shape, mould structure and mechanical design should be carefully considered to ensure that it is feasible to keep the wear within acceptable values during the mould life [16, 93]. These are the main reasons for why the machine set-up for the injection process using prototype tooling should be carried out with extra care when compared to a traditional mould set-up. Additionally,

hybrid tools must guarantee an injection moulding cycle time as short as possible. The time for the melt to solidify is significantly longer than for metallic moulds, due to the much lower thermal conductivity of the moulding block materials.

Some attention has been paid to the effects of a particular tooling option on the cycle time. Long cycle times have been raised as an important issue mostly because of their detrimental effect on tool life [149]. Since SL resins weaken with increased temperature, it is important to avoid excessive heat by increasing the cycle time [150]. For SL tooling in particular, there is a need for compromise with regard to cooling time. It has been repeatedly noticed that SL tools require longer cooling times [151, 152].

2.3.3 Tribological issues

In the first decade of the 20th century, wear of moulds and tools was an issue for plastics processors. In order to avoid wear related failure of tools, tool makers have employed a series of approaches to reducing the rate of wear. It has long been understood that hardened surfaces with good lubricants tend to wear slower than unlubricated soft surfaces [153]. In general, wear of sliding mechanisms such as pins, sleeves, slides, and cams, is predictable with the body of knowledge amassed in the tribology of sliding and rotating metal components [154, 155].

Several areas of the mould in contact with the molten plastic exhibit wear. During injection moulding, the thermoplastic tends to replicate the mould surface [156, 157].

Engelmann and co-workers investigated the types of wear that occur in a mould. Three very distinct mechanisms exist: abrasive, erosive, and adhesive wear [15]. Characteristics of these three wear mechanisms have been isolated as they relate to injection moulds. Certain design features in a mould are linked to each of these mechanisms [158]. Understanding this relationship makes mould wear more predictable, avoidable, and correctable.

In the injection moulding cycle, the mechanical process of ejection of the parts may affect their quality; at this stage the parts are mechanically forced to separate from the moulds. This ejection force may be quite high if the parts are moulded over deep cores [159]. The design of the ejection system depends on factors such as the draft angles, the surface finish, and the properties of the moulding material at the ejection temperature [126]. The most

important factor for designing the ejection system is the ejection force that varies with materials and the processing conditions [160].

During the cooling of the moulding, the roughness of the polymer and the mould surfaces, the shrinkage undergone by the polymer and the adhesion between the two materials, originates a resistance to the ejection that must be overcome for removing the moulding from the mould [125, 132]. The optimisation of the injection mould systems requires that the frictional behaviour of the mouldings during ejection is known and predictable [126, 130, 160]. However, an additional problem may become in the case of chemical affinity between the moulding and mould materials, because it may originate adhesion that has to be overcome upon ejection [159]. It has been also mentioned that the mechanism of wear that would be occur when exist contact with materials which have similar affinity is the adhesive wear [153].

The mechanism of adhesive wear occurs when two solid surfaces slide over another one under pressure. Surface projections are plastically deformed and eventually weld together by the high local pressure. As sliding continues, these bonds are broken, producing pits on the surface, projections on the second surface, and frequently tiny, abrasive particles, all of which contribute to future wear of surfaces. Polymers having the same solubility parameters and cohesive energy parameters present important adhesive characteristics [125, 161].

Several strategies have been proposed to minimise the wear mechanisms for injection moulds. Engelmann *et al.* pointed out that the strategy for wear reduction involves polishing smooth surfaces to decrease the amount of mechanical interlock between the moulding part and the moulding surface or increasing the hardness of the mould surface [158].

Recently, Correia *et al.* also mentioned that the direction of polishing affects the ejection which is further enhanced by the replication effect [159]. Their studies suggest that the tribological mechanism related to the ejection of injection mouldings include aspects related to the mechanical interaction between the mould and the moulding materials, and also, in specific cases, chemical adhesion between the materials. They also stated that the mould surface roughness associated to the shear strength of the moulding material should be considered in the wear of the plastics moulding.

The position and shape of the cavity strongly influences the wear. It was observed significant wear mechanisms in the neighbourhood of the gate but almost no wear at the inserts . This confirmed that wear is mainly caused by friction between the mould and solidified product material and not by the flow of the melt in the impression. Earlier studies showed significant wear in the gate area on runner channels and the most pronounced wear occurred at the exit of the gate opening [15]. Moreover the injection parameters (moulding temperature, pressure, speed, etc.) required to process the polymers play a relevant role in the cavity life. The more severe the parameters are the more damage they are expected to cause in the cavity inserts, reducing their life.

The key to increase the mould life is the correct diagnosis of the wear mechanism(s) that is/are present for a given component. Correct identification of the wear signature, is just as important as correctly identifying a moulding fault in the part produced. Similarly, identification of the part and mould geometries that can contribute to wear in a tool is the first critical step in designing a solution to provide tool longevity [15].

2.3.4   Thermo-mechanical environment

During the injection moulding cycle the material is submitted to a complex thermo-mechanical environment. The flow of the polymer melt into a cold mould impression is a typical example of an unsteady, non-isothermal, three-dimensional flow of a compressible, viscoelastic fluids [138, 162]. During this process each particle in the material is subjected to a different mechanical and thermal history. When the melt flows through the gate into the impression, a frozen layer of solidified material is formed due to the cold mould walls. The shear rate is maximum near the interface between the frozen skin layer and the melt, and null at the centre. The cooling rate is high near the mould wall where the orientation caused by the stresses induced by the flow is not able to relax. The interior will cool down more slowly due to the insulation effect of the already solidified polymer [138]. The resulting high thermal gradient and the constrained shrinkage introduce residual stresses in the mouldings (*e.g.* [163]). All these variables, together with the pressure evolution inside the mould impression, define the thermo-mechanical environment that constrains the overall morphology development and affecting the final mechanical properties in the product (*e.g.* [162, 164, 165]). If the thermo-mechanical history variables (pressure, temperature, flow and cooling rate), can be monitored directly or indirectly in the impression, the moulded product properties can be accurately and consistently predicted

[166]. The Figure 2.19 shows a typical pressure evolution inside the mould impression and its main features [167].
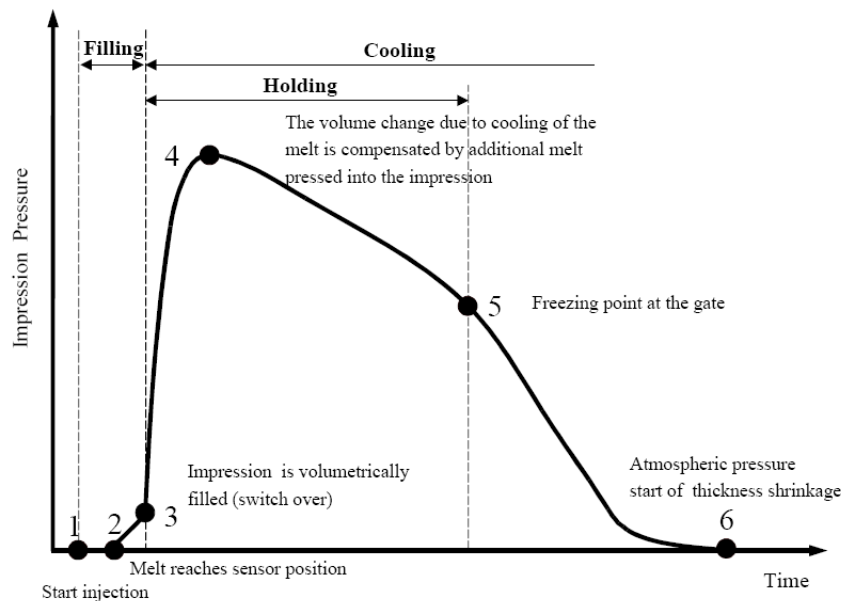

Figure 2.19 - Typical pressure evolution inside the mould impression (source: Pontes [138])

In injection moulding, the thermal and the mechanical phenomena are strongly coupled. This arises from the dependence of the viscosity on the temperature and on the shear rate. For semicrystalline polymers, the temperature and stress fields also determine the crystallization kinetics. The microstructural consequence is the formation of a typical layered-up pattern, normally known as the skin-core structure. The skin layers are highly oriented because of the stress fields and high cooling rates imposed upon the material. The core crystallizes in quasi-static conditions, and normally evidences a spherulitic structure [168]. The individual characteristics of each layer and their relative magnitude (*i.e.,* thickness) are determined by the specific thermomechanical environment imposed during processing [169].

2.3.5   Morphological structure

The morphology of the mouldings has been widely seen as a very useful way of interesting how processing affects the properties. Especially with semicrystalline materials, as it is the case of polypropylene, it is known that the change in processing conditions lead to important changes in the morphology of the moulded material that in turn influences the product properties (*e.g.* [165, 168, 170]). Other authors (*e.g.* [91]) also documented that the performance of parts obtained with hybrid moulds is an important issue. The injection

moulded thermoplastics keep a residual molecular orientation as a combined result of the chain alignment during the mould filling followed by a high cooling rate leading (*e.g.* [171]). This frozen-in orientation causes an anisotropic morphology whose pattern affects the in-service properties of the parts [165, 172]. These authors also refer that the behaviour of the mouldings depends on the morphology built up during processing. The characterization of the microstructure of the injected parts can be made by polarized light microscopy (*e.g.* [173, 174]). It may be correlated with the mechanical performance. The characterization of the microstructure of the injected parts may be correlated with the mechanical performance (*e.g.* [165, 168, 172]).

Usually, the characteristic laminated microstructure of injection moulded PP, features a layered structure across the thickness. The number of layers depends on the degree of discrimination of the micro-structural features (type of crystalline structures, degree of orientation, etc.). The definition of five layers is common: a spherulitic core, two intermediate crystalline and oriented layers and two highly oriented skins with a characteristic "shish kebab" type structure [175]. However, for engineering studies it is preferred the discrimination in only three layers: skin-core-skin [165, 171, 172, 176]. In these studies it is evident that the structure close to the mould walls (skin) is different from the inner region (core).

The differences found in the crystalline structures result from the thermo-mechanical conditions during the injection cycle. Several studies focused on the influence of changes of the morphological parameters on mechanical properties [168, 170, 172, 177-179]. When the same material is used in the moulding blocks a symmetrical structure with respect to their mid-plane tends to be developed. When heterogeneous moulding blocks are used asymmetric structures with respect to the mid-plane develop [148]. In these cases also the slower cooling at the resin-core side causes the development of a coarse structure with large spherulites.

2.4   Shrinkage

The dimensions of an injection moulded product are dependent on the change of dimensions with respect to those of the impression. This change results from the material properties, processing variables, mould and part design. The plastic product shows an as-moulded shrinkage defined as the reduction in the size of a moulded part in relation to the

impression. The shrinkage varies in the space and it is usually quoted at room temperature just after the part has been ejected from the mould:

$$Sh_i = \frac{D_{imp} - D_{part}}{D_{imp}}$$
2.1

where D_{imp} is the dimension in the impression in the *i* direction at a reference temperature and D_{part} is the corresponding part dimension [138].

Due to the importance in obtaining reliable final dimensions of the moulded product, extensive research was started in 1967 [180] to analyse the effect of processing variables, mould and part design on the as-moulded shrinkage in different thermoplastics. It is known that the shrinkage of injection mouldings is governed mainly by the thermal and pressure history during the moulding cycle. Some of the causes that contribute for shrinkage are the crystallinity (semicrystalline materials are more prone to thermal shrinkage than amorphous) and the thermal strain (caused by geometric effects such as thickness changes or sharp inside corners) and the moulding conditions [181]. Mould temperatures and holding pressure are the moulding conditions that mainly affect the final dimensions of the mouldings. Generally, as observed in the work by Pontes *et al.*, increasing the mould temperature or decreasing the holding pressure lead to higher shrinkage parts. In semicrystalline materials the expected shrinkage percentage can vary from 1% to 2.5% [127, 137].

2.5 CAE simulation tools

Rapid prototyping, rapid tooling and Computer Aided Engineering (CAE) technologies are important to rapidly produce quality thin wall plastics parts. However, one of the major limitations of current CAE tools is that it is not yet possible to get the appropriate material characteristics used in some rapid prototyping technologies [182]. For instance, Cardon also referred that the currently available flow simulation softwares, such as Moldflow or Moldex3D, do not accept temperature dependant heat characteristics [183].

The application of analysis tools that would enable the correct design of cooling systems in order to guarantee uniformity of cooling along the part would drive significant improvements in mould production and definition of process specifications. Peixoto *et al.*, used CAE and rapid tooling technologies for the design process of a thin wall plastic part with a simple geometry [108]. In their studies it can be seen that the conditions set on the machine were very close to the moulding conditions determined by the Moldflow software.

The control of the processing parameters in the stereolithography inserts is very important during the first productions for the durability of the moulds [184]. It is recommend that the process starts with incomplete mouldings produced at lower pressure and increase the pressure until the complete filling of the mould. Also the thermal behaviour of the stereolithography inserts implies long cycle times (about 3 minutes) due to the lower thermal conductivity of the resins used. They used the commercial software *Algor* to predict the thermal behaviour of stereolithography inserts. Studies on the effects of the thermal conditions associated with different materials on the injection mould on part shrinkage showed that the process conditions that affect more the shrinkage mechanism are the holding pressure, and the melt and mould temperatures [185]. Among these, the parameter that presents higher influence on the part shrinkage is the holding pressure, which decreases the shrinkage when it increases. It was also shown that the holding pressure has different effects along the flow length [185]. This effect is more evident for areas far from the gate [138].

2.6   Economical aspects

The usual way of producing injection moulded plastics parts is associated to errors that inflate the final cost, resulting in more expensive products when quality is required [186]. This is particularly problematic for low-volume products or rapidly changing high volume products [7, 187].

The cost of moulds for conventional and rapid tooling has been estimated using various models (*e.g.* [20, 92, 188, 189]). For example, the Nagahanumaiah model is based on the concept of cost drivers and modifiers. In conventional tooling, the cost drivers are estimated by mapping the mould features into machining features. For direct rapid tooling methods, the cost drivers are estimated using the rapid prototype build process parameters [190].

Peças and co-workers reported on two case studies to demonstrate the impact of RPT in mouldmaking [189]. The case studies were analysed using a comprehensive cost model able to calculate the costs incurred in each solution during the life cycle stages of the moulds. They applied a life cycle cost methodology to compare mould manufacturing options, on a life cycle approach.

The cost of tool development in indirect soft tooling, with the exception of arc spray metal tooling, is the lowest [20]. The cost of tool development for these technologies results not only from the RP master but also from the backing material. The direct soft tooling has the shortest development time as very little manual work is needed. If manual work is involved, this is usually for the finishing. The increasing cost of the raw materials, more obvious in recent years, the awareness of ecological impacts and the need for the reduction of the final cost of the products lead to the surge of recycled products. However, the final cost must be economically viable without compromising the final quality of the recycled product [8]. Other issues still remain associated to the design and operation of hybrid moulds, in so far the alternative materials influence the physical, geometrical and mechanical properties of the final mouldings [148]. Furthermore when hybrid moulds are used for production, the moulding block materials determine the injection cycle time [11]. This context has been motivating further research on hybrid moulds.

2.7   Lifecycle, reutilisation and recycling

Some of the current design strategies in the injection mould design include the redesigning of conventional injection moulds to increase their lifecycle, the reuse of existing mould structures and the use of recycled elements to produce moulding blocks [8, 92].

Usually, the lifecycle of an injection mould comprises five distinct stages: design, manufacturing, service, recycling and decommissioning [8, 191]. At every stage there are emissions and consumption of resources.

The Life Cycle Assessment (LCA) and the Life Cycle Management (LCM) concepts appear as management tools that allow the evaluation of environmental issues like air emissions, masses and energetic streams of a product or service in its entire life cycle. With this approach, managers will be able to predict the total cost of a product, the natural resources consumed, the energy spent and the environmental impact associated to a specific product [191].

The lifetime of the injection moulds, especially of hybrid moulds, is limited independently of the technology used to produce the moulding blocks [39]. The lower thermal conductivity of the current resins used is one of the main causes of that limitation, because it the heat exchange between the mould, the moulded part and the external environment is difficult. Another aspect that limits the hybrid moulds life is the lower mechanical

resistance of these resins. Studies proved that the material tensile stress and the elasticity modulus drops significantly with the increasing temperature [57, 192]. This fact originates the failure during the part ejection, when applied stresses exceed the mould material tensile strength.

Also during the injection moulding process, the injection parameters (moulding temperature, injection pressures and speed, etc.) play a relevant role in the mould life. The establishment for more severe parameters causes more damage in the moulding blocks reducing their life. The adjustment of the injection moulding parameters is particularly important for hybrid moulds [92]. In this case, product shape, mould structure and mechanical design should be carefully considered to ensure that it is feasible to keep the wear within acceptable values during the mould life [16, 93].

Usually, when injection moulds reach their production life, they are warehoused and destroyed. The reutilisation of these moulds represents an important strategy to be followed by producers of plastics parts but is usually neglected. The analysis of the reutilisation and recyclability of injection moulds is introduced as an innovative element on the life cycle of injection moulds. The introduction of this factor will affect all the other stages of the design and manufacturing process. Also there is the increasing demand for quality, the reduction of the developing periods and delivery of the products, the concurrence of new materials, the lower manpower costs of third world economies, the market globalisation, etc. All these imply strategic decisions towards: the concurrent fabrication, the knowledge as production factor, innovative products and processes, flexible enterprises, sustainable development, manpower qualification [8].

A proposal for obsolete injection moulds being not obligatorily destroyed and extending their life cycle is necessarily environment friendly. The reutilisation of the mould structure and the accessories lead to considerable reduction of the residues that must not be warehoused in expensive facilities that have a negative visual impact and lately should be recycled by remelting at a high energy cost. Thus, the reutilisation implies considerable savings and a cost reduction in the new product being developed on the basis of a reusable mould [8].

2.8   Objectives of the work

In this global scenery it was considered appropriate to define as main objectives of this research work the following:

i.   The mechanical design of hybrid moulds with the mechanical solutions for long and short side movements, especially in the context of minimising the mould structure and optimizing the ejection and cooling system design in view of further reutilisation;

ii.   Modelling of thermal and dimensional aspects of the performance of hybrid moulds;

iii.   Study of the properties of the products moulded with research hybrid moulds in terms of shrinkage, cycle time and dimensional accuracy;

iv.   Analysis of tribological issues associated to the hybrid mould performance;

v.   Application of CAE tools to the analyses of the performance of hybrid moulds;

vi.   Analyses of structural integrity of the components of hybrid moulds obtained with rapid manufacturing techniques.

3 THEORETICAL BACKGROUND

Aspects related to thermal and mechanical mould design, the use of simulation tools for predicting thermal and mechanical behaviours, and other simulation and injection moulding processing issues are described in this chapter. The first section, *Thermal and mechanical aspects in hybrid mould design*, is divided in three subsections: thermal analysis, dimensional analysis-shrinkage and strength analysis-ejection forces. The second section, *Numerical approach on the use of simulation tools*, is also divided in three subsections: dimensional simulations, interfaces between simulation tools and other simulation and processing aspects to be taken into account, mainly, with the use of hybrid moulds.

3.1 Thermal and mechanical aspects in hybrid mould design

Injection moulding is a cyclic process. The main phases of the moulding cycle are: filling, packing, cooling and ejection. The process starts with feeding the molten polymer from the hopper to the injection unit of the injection moulding machine. In the filling phase the impression is filled under pressure with the melt at injection temperature. After this phase, additional polymer melt is packed into the cavity to compensate the shrinkage as the polymer solidifies (packing phase). During the cooling phase the injected polymer is cooled until the part is sufficiently rigid to be ejected. The last step is the ejection phase in which the mould is opened and the part is ejected, after which the mould is closed again to begin the next cycle [113].

During the design of a plastic injection mould factors such as the mould size, the part geometry, the number of cavities, the runner and gating systems must be analyzed [21]. In technical parts the design and performance of the cooling system, which is very much dependent from thermal considerations, requires special attention.

3.1.1   Thermal analysis

During the moulding cycle the mould temperature raises while the plastic material is injected, and drops progressively until the next injection. Further to the polymer enthalpy variation, the mould temperature is dependant on the flow regime of the cooling fluid, the temperature and type of the cooling fluid, the architecture of the channels, and the mould material properties, namely its thermal conductivity. For an adequate performance of the mould it is expectable that the heat transfer rate is maximised and temperature distribution in the moulding surface is kept as uniform as possible.

The estimation of the relative thermal performances of injection moulds can be made by applying the lumped capacitance method [193]. This method assumes that the temperature in the interior of the solid body is uniform during the process.

The measure of the relative importance of the thermal resistance inside a solid body is given by the relation of the external and internal resistances. This relation can be expressed by the *Biot* number:

$$Bi = \frac{hL_c}{k} \qquad\qquad 3.1$$

where *h* is the convective coefficient, L_c the characteristic dimension of the wall and *k* the thermal conductivity of the respective materials. The Biot number gives information about the temperature variation along the thickness wall, depending on the external resistances (*i.e.*, the materials in contact with the injected polymer), as shown in the scheme of Figure 3.1.
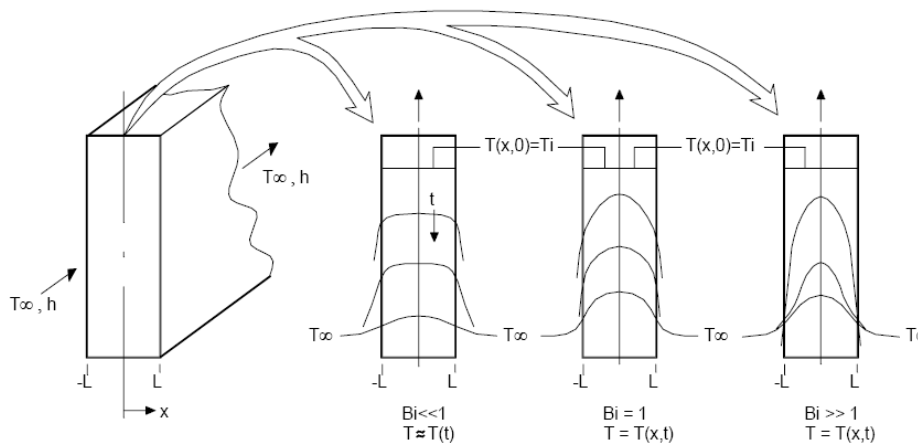
Figure 3.1 - Temperature distribution, in a wall cooled symmetrically by convection, for different Biot numbers, in transient regime (source: Incropera et al. [193])

The temperature analysis along the wall thickness is different depending on the Biot number in each interface.

Figure 3.2 schematically represents the heat transfer between the injected polymer and the moulding elements. In the context of this research work the core is in steel and the cavity is in resin. T_{wi} represents the temperature in the respective wall interface.
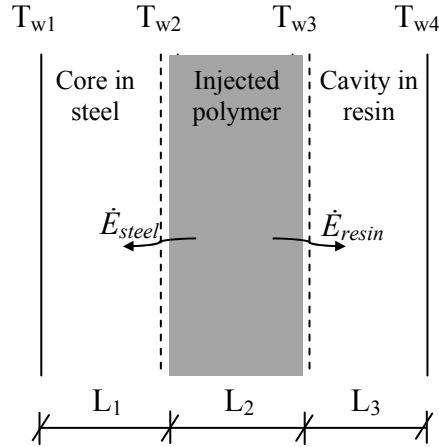

Figure 3.2– Heat transfer by conduction between the injected polymer and the moulding elements in contact

An overall energy balance applied to the domain composed by the injected polymers and the moulding elements, illustrated in Figure 3.2, is:

$$\dot{E}_{st} = \frac{dE_{st}}{dt} = \dot{E}_{in} - \dot{E}_{out} + \dot{E}_g \qquad 3.2$$

The energy terms of the equation include the stored thermal and mechanical energy (E_{st}), the thermal energy generation (E_g), and the thermal and mechanical energy transport across the control surfaces, that is, the inflow and outflow terms (E_{in} and E_{out}).

In Cartesian coordinates the heat diffusion equation is written as

$$\frac{\partial}{\partial x}\left(k\frac{\partial T}{\partial x}\right) + \frac{\partial}{\partial y}\left(k\frac{\partial T}{\partial y}\right) + \frac{\partial}{\partial z}\left(k\frac{\partial T}{\partial z}\right) + \dot{q} = \rho c_p \frac{\partial T}{\partial t} \qquad 3.3$$

where T is the temperature, t the time, x, y, and z the Cartesian coordinates, ρ the density, c_p the specific heat, and k the thermal conductivity. This equation, often referred to as the "heat equation", provides the basic tool for heat conduction analyses. From its solution, the temperature distribution $T(x,y,z)$ is obtained as a function of time.

Assuming that the terms $\dot{E}_{in}$ and $\dot{E}_g$ in equation 3.4 are very small, this equation becomes:

$$\dot{E}_{st} = -\dot{E}_{out} \qquad 3.4$$

The heat transfer in the polymer/mould interfaces is a process of transient conduction. Thus, applying equation 3.4 to the control volume of the two interfaces, one may obtain the equations 3.5 and 3.6:

$$\rho V c_p \frac{dT}{dt} = \frac{K_{steel} A_s (T_{w2} - T_{w1})}{L_1} \qquad\qquad 3.5$$

$$\rho V c_p \frac{dT}{dt} = \frac{K_{resin} A_s (T_{w4} - T_{w3})}{L_3} \qquad\qquad 3.6$$

where ρ is the density of the injected polymer, V the volume of the impression, c_p the heat capacity of the polymer, k the thermal conductivity, A_s the surface area, T the surface temperature, and L the wall thickness.

To calculate the effective *Biot* number in each control volume the heat transfer by conduction at each side of the interface must be considered. Referring to Figure 3.2 the following relations apply to the various heat flows, $\dot{Q}$,

$$\dot{Q}_{steel.conduction} = \dot{Q}_{pol.conduction} \qquad\qquad 3.7$$

and

$$\dot{Q}_{resin\ conduction} = \dot{Q}_{pol.conduction} \qquad\qquad 3.8$$

Therefore the effective Biot numbers for each case (interface polymer/steel and interface polymer/resin) are given by the following equations:

$$Bi_{pol.steel} = K_{steel} A_s \frac{T_{w2} - T_{w1}}{L_1} = K_{pol} A_s \frac{T_{w3} - T_{w2}}{L_2} \qquad\qquad 3.9$$

$$Bi_{pol.resin} = K_{resin} A_s \frac{T_{w4} - T_{w3}}{L_3} = K_{pol} A_s \frac{T_{w3} - T_{w2}}{L_2} \qquad\qquad 3.10$$

Considering typical values for the problem showed in Figure 3.2, as L_1=0.01 m; L_2=0.002 m; L_3=0.01 m; K_{steel}= 29 W/(m.K); K_{polym}=0.1507 W/(m.K); K_{resin}=0.6065W/(m.K), and the temperatures differences approximately the same, the respective *Biot* numbers are:

$$Bi_{pol.steel} \approx 38.5$$

$$Bi_{pol.resin} \approx 1$$

As shown in Figure 3.1, for the cases of *Biot* number equal or bigger than 1, the temperature variation inside the wall is different in each point along the time. To have the knowledge of the material temperature in each location x at an instant of time t $(T = f(x,t))$, in the wall thickness, it is necessary a numerical approach. For this analysis the medium must be considered as a set of *discrete* points defined by subdividing the medium in small

regions and assigning to each one a nodal reference point, or node. The nodal points are identified using a dual system associate to the array [*m, n*] as shown in the Figure 3.3.

a
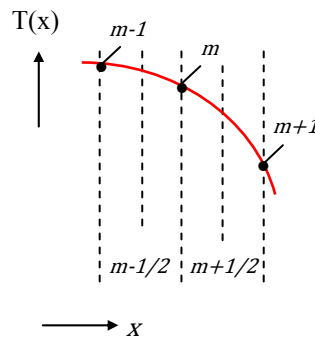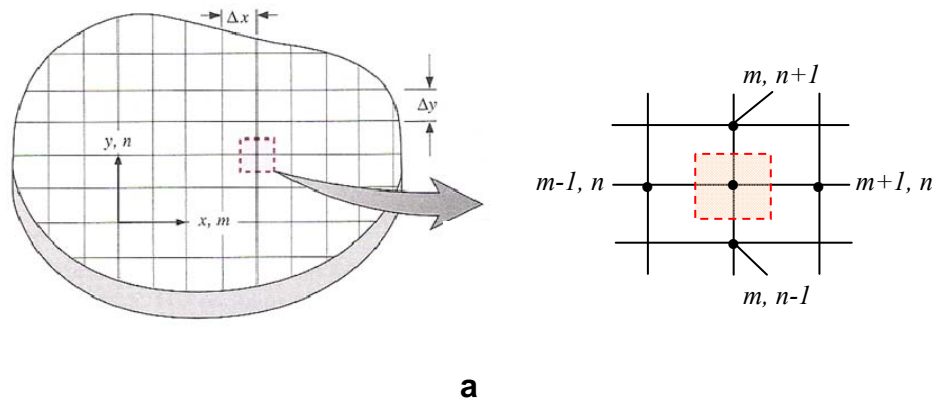
$$\left.\frac{\partial T}{\partial x}\right|_{m-1/2,n} \approx \frac{T_{m,n}-T_{m-1,n}}{\Delta x} \qquad\qquad 3.11$$

$$\left.\frac{\partial T}{\partial x}\right|_{m+1/2,n} \approx \frac{T_{m+1,n}-T_{m,n}}{\Delta x} \qquad\qquad 3.12$$

b

Figure 3.3 – Two-dimensional conduction: a) Nodal network, b) Finite-difference approximation
(source: Incropera *et al.* 2007)

Each node represents a region where the temperature is the average temperature at that region. For example, the temperature at the node (*m, n*) in Figure 2a) is the average temperature of the surrounding shaded area. The numerical accuracy of the calculation depends on the number of nodal points. For the two-dimensional system in Figure 3.3 and transient conditions, with constant properties and no internal generation [193, 194], the heat equation is:

$$\frac{1}{\alpha}\frac{\partial T}{\partial t} = \frac{\partial^2 T}{\partial x^2} + \frac{\partial^2 T}{\partial y^2} \qquad\qquad 3.13$$

The finite-difference form of this equation, using central differences is obtained considering the derivatives:

$$\frac{\partial^2 T}{\partial x^2} \approx \frac{T_{m+1,n} + T_{m-1,n} - 2T_{m,n}}{(\Delta x^2)} \qquad\qquad 3.14$$

$$\frac{\partial^2 T}{\partial y^2} \approx \frac{T_{m,n+1} + T_{m,n-1} - 2T_{m,n}}{(\Delta y^2)} \qquad\qquad 3.15$$

It is also necessary to discretize the problem in time. The integer *p* is introduced as

$$t = p \times \Delta t \qquad\qquad 3.16$$

Therefore the finite-difference approximation to the equation 3.13 becomes:

$$\left.\frac{\partial T}{\partial t}\right|_{m,n} \approx \frac{T_{m,n}^{p+1} + T_{m,n}^{p}}{(\Delta t)} \qquad\qquad 3.17$$

The superscript *p* is used to denote the time dependence of *T,* and the time derivative is expressed in terms of the difference in temperatures associated with the new *(p+1)*and previous *(p)* times.

The implementation of the *finite-difference method* to the transient conduction problems of the injection moulding cycle was made using the software *Mathcad* (Adept Scientific, UK). For writing the program the flowchart shown in Figure 3.4 was developed in view of its application to the mould HM-1 used in this research and introduced in Chapter 4. The full program considering cylindrical coordinates is listed in the Appendix 1.
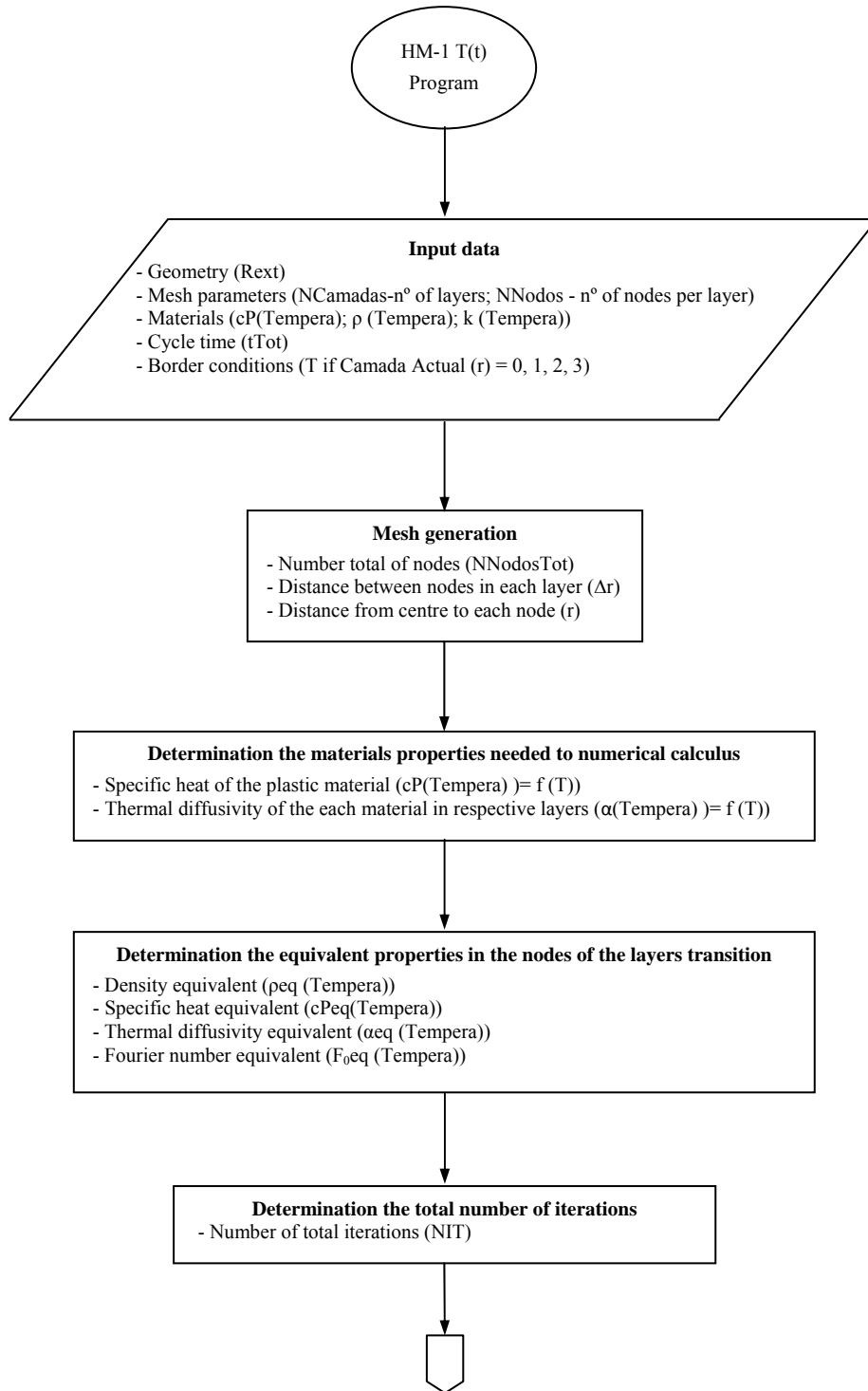
Figure 3.4 – Flowchart of the program to determine the temperature field in the mould HM-1
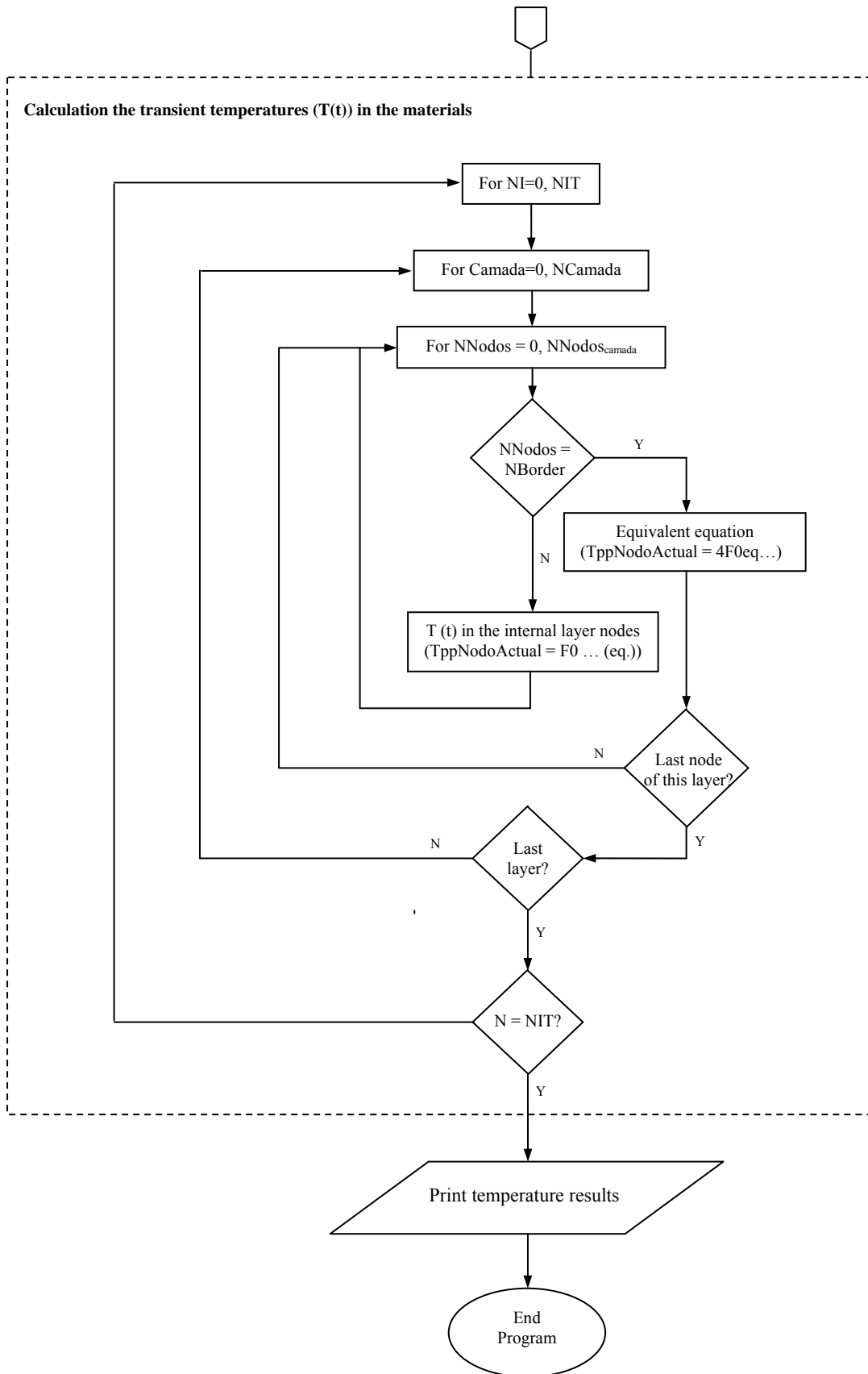
Figure 3.4 (continued) – Flowchart of the program to determine the temperature field in the mould HM-1

3.1.2 Dimensional analysis - Shrinkage

The shrinkage of injection mouldings, which is determinant in their final dimensions and dimensional accuracy, is governed by the thermal and pressure history during the moulding cycle. However, when resin moulding blocks are used in injection moulds the final dimensions of the mouldings are a consequence of the polymer shrinkage and the deformation by pressure of the non-metallic moulding blocks during processing. In this case the shrinkage of the part depends on the changes in the polymer specific volume arising from crystallisation and temperature variation, and on the core and cavity deformations caused by the moulding pressure. The pressure is imposed initially by the melt injection pressure and later by the part that shrinks onto the core. The shrinkage (Sh_i) in a moulded product is calculated in percentage as:

$$Sh_i = \frac{D_{imp} - D_{part}}{D_{imp}} \times 100 \hspace{3cm} 3.18$$

where D_{imp} is the impression dimension in the *i*-direction at a reference temperature, and D_{part} is the corresponding part dimension.

In the case of a moulding block likely to deform in the range of the moulding shrinkage, the final dimension in the part is the result from the dimension variation associated to the cooling of the polymer (resulting from thermal and crystallinity/solidifying effects) and to the deformation caused by the injection pressure on the moulding block:

$$D_{part} = D_{imp} - \delta_{pol} - \delta_{pressure} \hspace{3cm} 3.19$$

Thus the shrinkage of the part in these moulds, as a first approximation, will be the result of the two deformations, polymer deformation (δ_{pol}) and the deformation caused on the core and cavity by the moulding pressures ($\delta_{pressure}$):

$$Sh_i = \frac{\delta_{pol} + \delta_{pressure}}{D_{imp}} \hspace{3cm} 3.20$$

Or, in terms of the actual dimensions and impression deformation

$$Sh_i = \frac{D_{imp} - D_{part}}{D_{imp}} + \varepsilon_{pressure} \hspace{3cm} 3.21$$

where $\varepsilon_{pressure} = (\delta_{pressure}/D_{imp})$ introduces the effect of the deformation of the moulding block.

This argument was already introduced elsewhere [195] and is of practical interest when plastics precision parts are moulded with hybrid moulds with *soft* cores. In this case the

actual shrinkage of the mouldings depends also on the deformation of the deformable moulding blocks.

3.1.3   Strength analysis - Ejection forces

The ejection phase is considered in the design of moulds for deep core mouldings where problems may occur in the ejection system performance or even failure of the actual mouldings or the moulding pins.

The ejection force depends on the force exerted by the moulding onto the core and is a result of the shrinkage. The initial ejection force, *F_{eject}*, is required to overcome the static friction between the plastics and the mould core. It is a function of the contact pressure at the moment of ejection, the contact area and the static friction coefficient:

$$F_{eject} = \mu_e \times p_c \times A_c$$ 3.22

where p_c is the contact pressure of the plastics on the core, μ_e is the coefficient of friction at the moment of ejection, and A_c is the contact area.

The contact pressure depends on factors that determine the shrinkage at the moment of ejection, namely the degree of crystallinity and the temperature of ejection, as shown, for example, in reference [147]. The static friction coefficient at the moment of ejection depends not only on the pair 'moulded material–mould material' and moulding surface roughness, but also on the processing conditions, as demonstrated by Pouzada and Ferreira who also developed a method for its determination in as-processing conditions [126].

The main steps considered on calculating the ejection force are illustrated in the Figure 3.5.
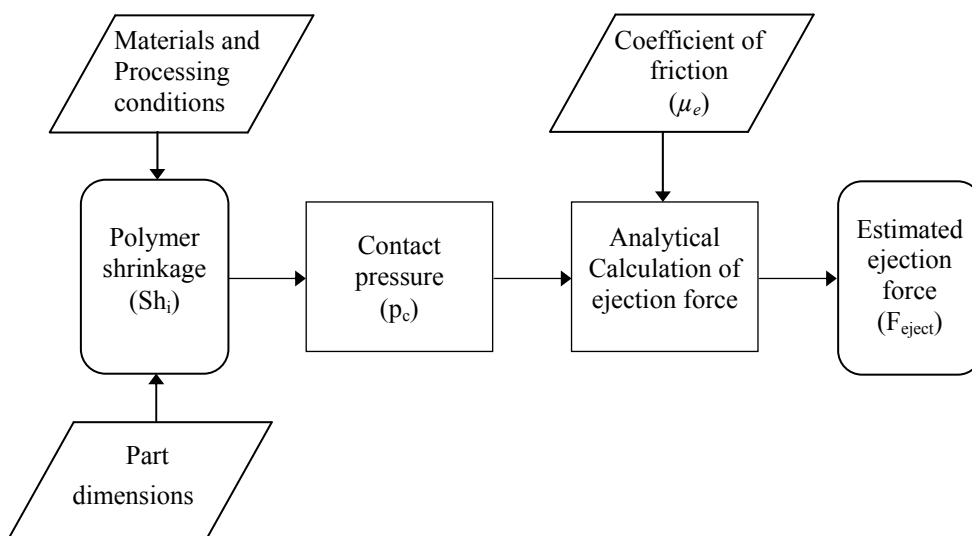
Figure 3.5 - Analytical procedure to calculate the ejection force

To determine the contact pressure on the moulding pin, besides the shrinkage of the injection polymer used, it is necessary to take into account the thermal expansion and the deformation of the material of the moulding pin or core. This pressure can be calculated as:

$$p_c = E_{pol}(T_{eject}) \times Sh_i \qquad 3.23$$

where E_{pol} (T_{eject}) is the modulus of elasticity at the ejection temperature and Sh_i is the shrinkage of the moulded material.

When metallic materials are used in the mould, Sh_i may be considered as depending only on the polymer shrinkage ($Sh_i = f(\delta_{pol})$) because the steel strain is some orders of magnitude lower than the polymer. If lower modulus materials are used in the mould their strain is of the order of magnitude of the moulded material; therefore the actual shrinkage of the moulding depends on the polymer itself and also on the moulding block deformation, *i.e.*, $Sh_i = f(\delta_{pol}, \delta_{pressure})$.

The coefficient of thermal expansion of epoxy matrix composites, α, is higher than metals. Thus, for the calculation of the contact pressure it may be necessary to calculate the resulting strain ($\varepsilon_{\Delta T}$) due to the temperature variation from ejection, T_{eject}, to ambient, T_{room}:

$$\varepsilon_{\Delta T} = \alpha \times (T_{eject} - T_{room}) \qquad 3.24$$

If this strain is significant, *i.e.*, of the same order of magnitude of Sh_i, it should be considered in the computation of F_{eject}. After these considerations, for the case of a cylindrical pin, the equation 3.22 becomes:

$$F_{eject} = \mu_e \times E(T_{eject})_{pol} \times \left(Sh_i + \alpha \times (T_{eject} - T_{room})\right) \times \pi \times D \times L \qquad 3.25$$

where D is the diameter of the moulding pin and L the length of the pin in the direction of ejection.

In the design of the ejection systems there is also the need to calculate the dimensions of their mechanical components. An example is the inclined guide pillar responsible for the side movements in moulds for geometrically complex mouldings.

The previous derivation of the ejection force is an input datum for the design of the components associated to the sliding group. A scheme is shown in Figure 3.6 where it is established the relation between the ejection force and the inclination of the guide promoting the lateral movement.
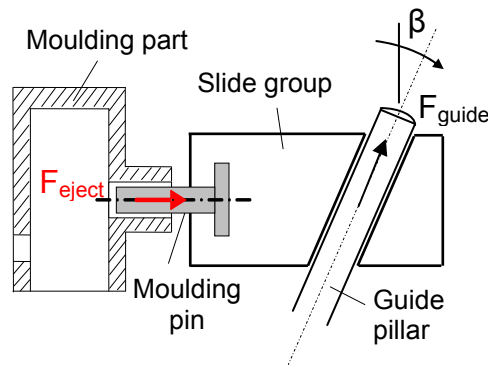
Figure 3.6 – Sliding group showing the movement of the moulding pin on the side of the part

The force in the inclined guide pillar required to start the lateral movement must be greater than:

$$F_{guide} = \frac{F_{eject}}{cos(90° - \beta)} \qquad\qquad 3.26$$

where F_{guide} is the force acting in the guide pillar to initiate the demoulding movement. This force depends on the ejection force and the angle of inclination, β. Thus, the force acting in the guide pillar is given by:

$$F_{guide} = \frac{\mu_e \times E(T_{eject})_{pol} \times \left(Sh_i + \alpha \times (T_{eject} - T_{room})\right) \times \pi \times D \times L}{cos(90° - \beta)} \qquad\qquad 3.27$$

3.2   Numerical simulation aspects

Since the early 1990s, numerical simulation is fundamental as a tool in product design in general and injection mould design in particular. The algorithms in the injection flow simulation tools are based on the Navier-Stokes equations [196]. These tools are used to predict and optimize typical injection moulding parameters such as gate location, runner balancing, flow fronts, cooling, or fibre orientation.

As already mentioned in Chapter 1, rheological and structural simulation tools were used in this research programme. The flow simulator Moldex3D release 9.1 (CoreTech, Taiwan) was used for the moulding process and the structural analyzer ANSYS Workbench release 11.0 (ANSYS, USA) for the stress analysis.

In this section the main differences between the 2.5D and 3D simulations, the type of elements usually used in mesh models, the possible interfaces and, finally, issues to be taken into account on simulation procedures are reviewed briefly.

3.2.1 Dimensional simulations (2.5D or 3D)

The full 3D simulation of injection moulding was introduced in the last nineties. Often a full 3D simulation code requires a large number of elements leading to long computation time. Before these the faster running 2.5D simulation codes based on the Hele-Shaw model [197] were used to simulate the injection moulding process [198, 199]. Commercial 2.5D codes provide satisfactory results with flat and thin injection mouldings. These 2.5D analyses are known as a mid-plane simulations and assume that the flow profiles are identical along the flow path. They are common in thin mouldings of constant wall thickness, *i.e.*, with a high aspect ratio, and when the optimized simulation requires a large number of iterations. There is a clear difference of the simulated flow front profiles at a low injection speed between the 2.5D and the 3D simulations [200]. Other authors (*e.g.* [199]) mentioned that 2.5D simulation is not appropriate in dealing with adjacent sections with very different thickness, an effect known as "step effect". In light of this, true 3D moulding simulation became increasingly popular in the recent years [201] also due to the increasing capacity of computer processing.

The 3D simulations are based on solid mesh objects composed of small solid elements namely, tetrahedron, pyramid, prism or hexahedron. The surface mesh objects, corresponding to 2.5D dimensional simulations, are a set of connected triangle or quadrilateral faces that, when well connected, represents the boundary of a model [202, 203].

The most common 3D mesh uses 3D tetrahedron elements. The mesh generator is not a real 3D methodology, as the mesh generator uses the Dual Domain skin mesh, and afterwards develops tetrahedral mesh elements between it. For complex geometries, hybrid non-structured meshes are also generated. However, when compared with structured ones, *i.e.*, composed with the same type of element ordered in space, they can lead to more processing capacity and computation time, and they also can lead to the increase of numerical errors [202].

A hybrid mesh is composed of different geometrical element types (*e.g.* tetrahedral, pyramidal). The bulk of the model is meshed with tetrahedral elements and the region just beneath the model surfaces is meshed with triangular prismatic elements (Figure 3.7). This type of mesh is used by the Moldex3D simulation software (CoreTech, Taiwan).
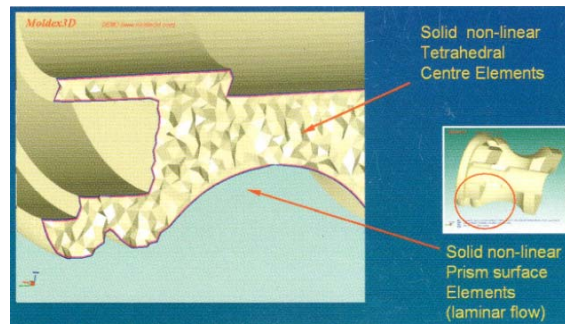
Figure 3.7 – Hybrid mesh (Source: British Plastics & Rubber [204])

In these cases the mesher generates both types of element and creates one to five layers of prismatic elements depending on the thickness of the part. Both elements support non-linear behaviour but the prismatic elements pre-suppose laminar flow. Usually the generation of the prismatic triangular mesh is applied to obtain temperatures and shear rates variation in the plastic part and branch runner systems [202].

A large number of layers of tetrahedral elements increase significantly the total number of elements. However it is important to have into account that with small number of elements the temperature, for example, is going to be underestimated and the pressure will be overestimated. Usually this problem is solved considering at least three layers.

Some problems in simulations can be solved considering a hybrid mesh. A thin mesh, with a higher resolution, includes a larger number of events inside the moulding, but also requires a longer computation time.

Simulation tools

Moldflow MPI (Autodesk – Moldflow, USA), Moldex3D (CoreTech, Taywan) and Cadmould (simcon, Germany) are some simulation tools used in injection moulding. Moldflow patented the *Dual Domain Mesh* principle, the so called *Fusion Mesh*. This methodology uses a skin mesh on the outside surfaces of the part, obtained from a common STL format [203, 205].

The distance between the mesh surfaces defines the part thicknesses. The mesh density plays a key role in determining the thickness of varying geometry such as draft ribs or living hinges. The same thickness ratio limitations that apply for 2.5D mesh models also apply to the *Dual Domain Mesh* models [203].

3D simulation is closer to real life but takes longer to compute [206, 207]. The use of 3D simulation is recommended for thick mouldings, when large thickness variation occurs,

and for those with low aspect ratio (say less than 10:1). The 3D simulation is also superior for fibre-reinforced mouldings, and for warping and shrinkage predictions [208].

3.2.2   Interfaces

Injection moulding simulators are capable of simulating the filling, packing and cooling phases, as well as the shrinkage and warpage after ejection. For hybrid moulds it is desirable that the software packages include the possibility of taking into account the effect of deformation and poor thermal behaviour of the non-metallic moulding blocks. Thus, it is fundamental the integration of the injection moulding and structural analysis simulators, to reflect the mechanical behaviour of the tool in the moulding process. This can be done automatically using an interfacing program, as Moldex3D-I2 for the case of Moldex3D.

Problems may arise in translating injection moulding data into structural analysers. The accuracy of finite element or finite volume analyses is dependent on the mesh density and quality. The mesh density indicates the size of the elements in relation to the size of the body being analysed. The mesh density need not be uniform all over the body. There may be areas of mesh refinement (more dense meshes) in some parts of the body to obtain better model definition and better accuracy on the simulation result. However, simulations on uniform density meshes, in which all elements have similar volume and are nearly equilateral, are accurate and stable, but slow, due to the high number of elements [206, 209].

The mesh requirements for injection moulding analyses are different from structural analyses. Structural analysis focuses on the area of stress concentration whereas for injection moulding higher element resolution across the thickness direction is required. Injection moulding analyses typically require more and denser elements than structural analyses.

3.2.3   Other simulation and processing aspects

Concept and process variables are examined during the design process on computer before the mould is actually manufactured. Thus, potential defects may be identified and corrected earlier in the design process.

The studies on hybrid moulds have shown the importance of using CAE technologies to speed up the production of quality plastics parts (*e.g.* [44, 210-213]). However, currently

available CAE databases are limited in terms of the material properties required for accurate design analysis.

Some aspects related with design for simulation have been described (*e.g.* [12, 211, 214]). The occurrence of air gaps resulting from the shrinkage of the polymer or insufficient venting may lead to a problem known as thermal contact resistance (TCR). These defects between the moulding surface and the moulded part, if not considered, may cause substantial errors in the simulations [215, 216]. Therefore it is recommendable that the air gap is considered in the simulation model as shown in Figure 3.8.
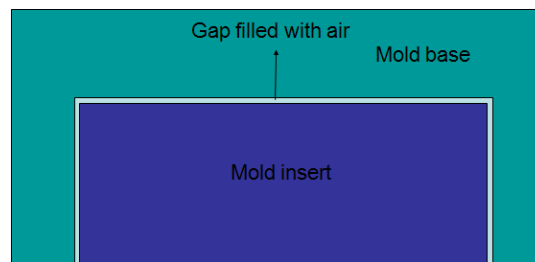
Figure 3.8 - Small gap between the mould insert and the mould base

In some finite element models TCR is either neglected or included only as an intrinsic characteristic of the system. A thermal system can be described by analogy to the Ohm's law considering the equation:

$$\overline{\Delta T} = \dot{Q} \times R \qquad\qquad 3.28$$

where $\overline{\Delta T}$ is the average temperature drop across the thermal body, $\dot{Q}$ is the heat flowing through that body, and R is the thermal resistance of the body [217]. When the temperature drop occurs at the interface between two bodies TCR takes place. It is a function of the surface geometry, properties of the interacting materials and air, applied mechanical loads, and thermal load. In the *ANSYS workbench* software TCR is included as a user supplied real constant value of thermal contact conductance (TCC) [W/m^{2}K]. The relationship between TCC, heat flux and temperature is given by:

$$\dot{q} = TCC \times \left(T_{hot} - T_{cold} \right) \qquad\qquad 3.29$$

where $\dot{q}$ is the heat flow per unit area, T_{hot} is the local temperature at the hot surface and T_{cold} is the local temperature at the cold surface. It is possible to predict appropriate and solution dependent values for TCR with ANSYS, using a multi-scale iterative approach. However, this requires the ability to accurately model microscale surface geometries and to calculate the gap dependent thermal conduction [218].

TCR in the polymer/mould interface affects the heat transmission coefficient, h_{int}. This coefficient is used for the simulation of heat resistance between the two materials. The typical equations used in simulation softwares (*e.g.* [219]) are:

$$h_{int} \times (T_{int} - T_M^-)_{x=-b} = -k \times \left(\frac{\partial T}{\partial n}\right)_{x=-b} \qquad\qquad 3.30$$

$$h_{int} \times (T_{int} - T_M^+)_{x=+b} = -k \times \left(\frac{\partial T}{\partial n}\right)_{x=+b} \qquad\qquad 3.31$$

where T_{int} is the melt temperature in the interface of the two materials; T_M^- and T_M^+ are the moulding zones temperatures, on the cavity side (negative side) and on the core side (positive side), respectively. The indices *–b* and *+b* indicate the positive and negative side of the distance relatively to the centre of the part (equivalent to half of its thickness) and *n* the direction to be considered. If the thermal conductivity is zero, (thermal isolated border), the exchanges between the two materials do not exist. If one assumes an extremely high value, then there is a perfect thermal contact between the materials. In this case the interface temperature is considered as equivalent to the mould wall temperature. Many times, the default value considered in commercial softwares is 25000 W/m² K.

During the mould filling, due to TCR the mould-melt interface temperature (T_{int}) is usually higher than the mould temperature (T_M). The difference between T_M and T_{int} depends on the thermal properties of the mould material, the polymer melt and the processing conditions (Figure 3.9).
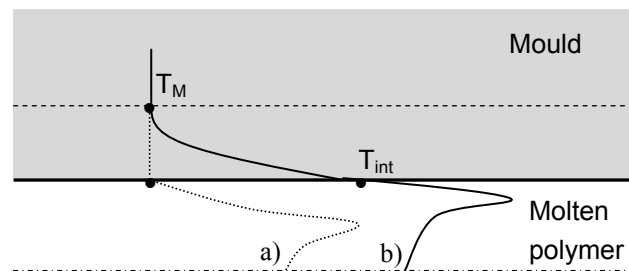
Figure 3.9 – Temperature on mould-melt interface: a) underestimated temperature by a constant mould temperature, b) temperature considering the heat transfer coefficient

For the usual cases T_{int} may not be so different from T_M. This means that T_M may be used instead of T_{int} in the simulation. However, for the thin walled part cases, high speed filling or melt with highly temperature-dependent viscosity, the use of T_M tends to underestimate the mould-melt interface temperature, leading to the overestimation of the injection pressure.

Thus, it is convenient to work with the heat transfer coefficient, which is defined by:

$$q_s^n = h \times (T_s - T_m) \qquad\qquad 3.32$$

where h is the local convection heat transfer coefficient, T_s the surface temperature and T_m the melt temperature [193].

4 EXPERIMENTAL

4.1 Specifications

The main specifications for the hybrid moulds for the production of short and medium injection moulding series of plastics parts to be developed in this study are:

- To produce parts with details that require lateral movements of various amplitudes (short and long);

- Use of alternative materials in the moulding elements;

- Interchangeability of the moulding blocks made in various materials in the standard structure;

- Design of the structure and bolsters that accommodate moulding blocks with dimensions indicated in the Table 4.1;

- The hybrid mould must be designed for reutilisation;

- Easy and rapid interchangeability of the moulding blocks without removing the mould from the injection moulding machine;

- Use of RPT processes for obtaining the moulding blocks.

Table 4.1 - Maximum dimensions for the moulding blocks

	Length [mm]	Width [mm]	Height [mm]
Maximum	60	32	75
Minimum	35	15	40

4.2 The plastics parts

This study was based on two geometries of plastics parts: a three dimensional tubular part that has been used in shrinkage and morphology studies on hybrid moulds [14, 185] and a more complex object with features implying the use of side cores. The latter will be referred to in the following as the "support box".

4.2.1 The tubular part

The geometry of the tubular part with a nominal thickness of 2 mm is shown in Figure 4.1. It has a volume of 24.7 cm^3 and was designed to produce a uniaxial flow in the cylindrical body.
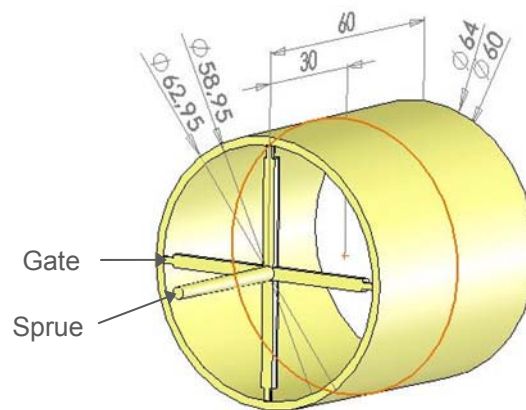
Figure 4.1 – Tubular part dimensions with spider gating system (4 gates) [185]

4.2.2 The support box

The shape and dimensions of the support box with a nominal thickness of 2 mm are shown in the Figure 4.2.The volume of the part is 15.4 cm^3.
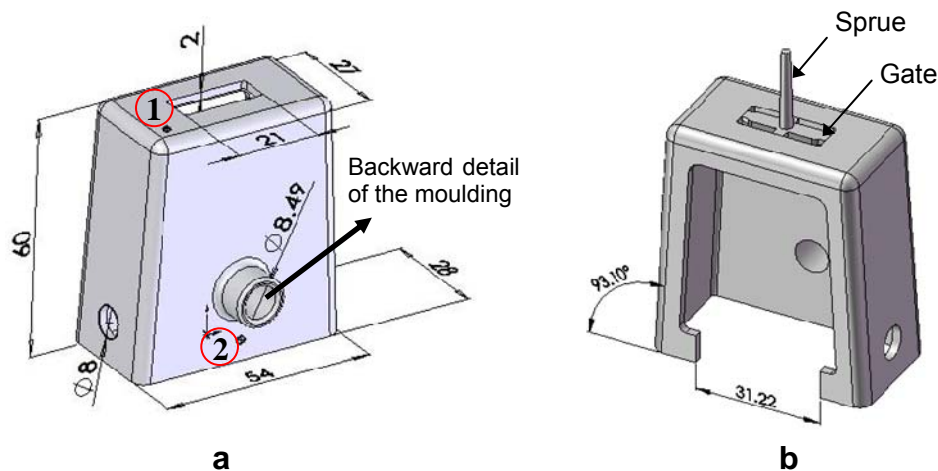
Figure 4.2 - Support box: a) main dimensions, b) part with the runner system

This part has a lateral circular hole on the left side, a fitting detail on the back and a cavity with an opening for enabling distortion studies. The draft angle considered for the side walls is 3º and the corners are rounded to allow manufacturing the whole core also by machining.

4.3   The hybrid moulds

The hybrid moulds used to produce the testing parts are identified as Hybrid Mould 1 (HM-1) for the tubular part, and Hybrid Mould 2 (HM-2) for the support box.

4.3.1   Hybrid Mould HM-1

Mould design

The HM-1 is a mould designed by Pouzada for studies on hybrid mould performance. There are two versions of this tool: one that was developed by Gomes *et al.* and is based on a standard steel structure with interchangeable moulding blocks (Figure 4.3) [185] and another by Bareta *et al.* [14]. In this work it was used the Gomes *et al.* version. The injection is made through a spider system with 4 gates. A stripper plate is used for ejection.
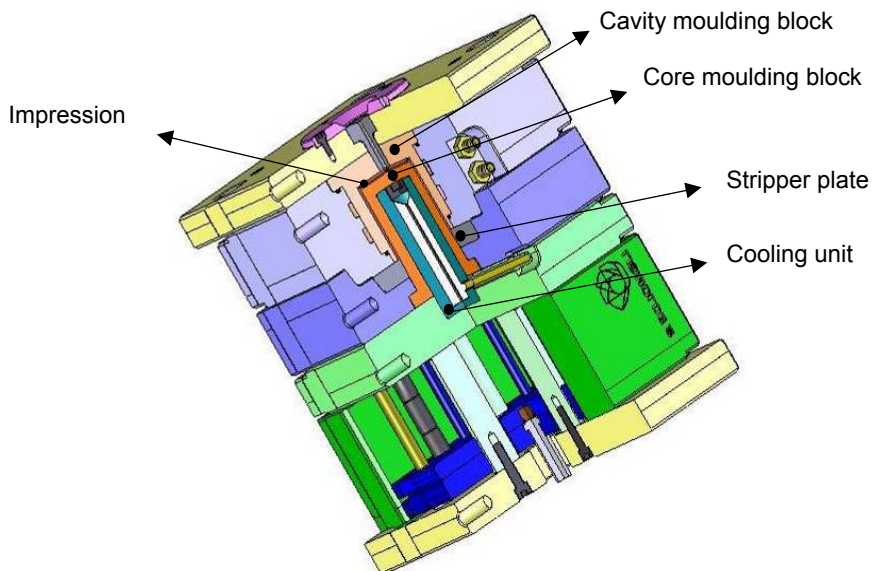
Figure 4.3 - HM-1 standard design

The interchangeable moulding blocks are shown in the Figure 4.4. They are easily assembled in the mould structure.
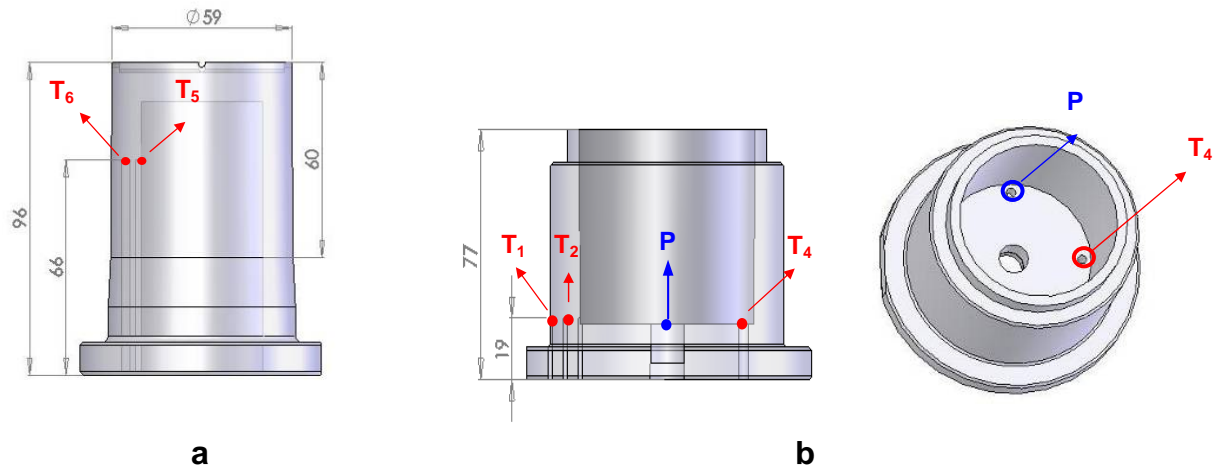
Figure 4.4 - HM-1 moulding blocks and sensors location: a) core, b) cavity

The moulding blocks in this study were made in tool steel DIN W Nr. 1.2311 and epoxy composite based filled with 60% (in weight) of aluminium powder.

Instrumentation

The instrumentation includes 6 sensors located as shown in Figure 4.4: four Type-K thermocouples (T_1, T_2, T_5 and T_6), one Hotset TEF 15 Type-K temperature sensor (Hotset, Germany) (T_4) and one Kistler 6157 BA pressure sensor (Kistler, Switzerland) (P). The steel moulding blocks were fitted with the T_4 and P sensors in the cavity and the T_5 and T_6 sensors in the core. The resin moulding blocks were fitted with the T_1, T_2 and T_4 sensors in the cavity and the T_5 sensor in the core.

A Priamus system was used to get pressure data (Priamus, Germany) and the temperature values were collected with a USB TC-08 thermocouple data logger system (Picotech, UK).

The pressure and temperature data were acquired in real time with the data acquisition system. An example of core and cavity temperature variation in continuous service is shown in Figure 4.5. Important instant times are identified in the cavity temperature profile.
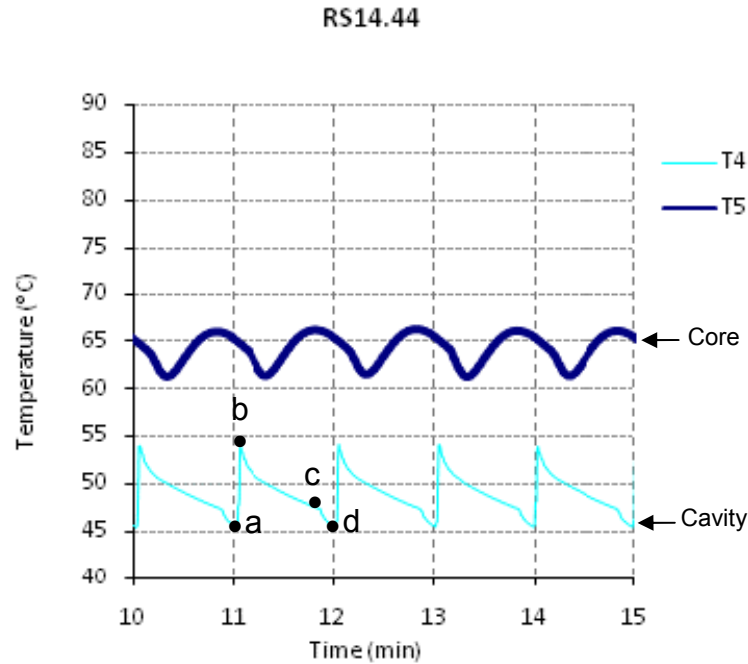
Figure 4.5 - Temperature vs. time (RS14.44 moulding conditions)

In Figure 4.5 it is also visible how the temperature varies during consecutive cycles, inside the core (sensor T_5) and at moulding surface of the cavity (sensor T_4). The repeatability between cycles is clear.

The temperature monitoring at the cavity with the sensor T_4 clearly shows the steep rise during injection, from a up to the maximum point b, the steady cooling during the cooling phase (b-c) and the quicker cooling after the opening of the mould (point c) down to the start temperature, point d. The thermal amplitude (b-a) is monitored at one of the gates.

The parts were obtained with the following moulding conditions:

- Injection temperature of 230ºC;
- Mould temperature of 40ºC;
- Injection pressure of 42 MPa;
- Holding pressure of 14 MPa;
- Holding time of 5 s;
- Cooling time of 44 s.

Only the moulding blocks combination was changed (RS-Resin core and Steel cavity; RR-Resin core and Resin cavity; SS-Steel core and Steel cavity).

Typical pressure data for some moulding block combinations and processing conditions are shown in Figure 4.6 where data variation is recorded over the injection cycle.
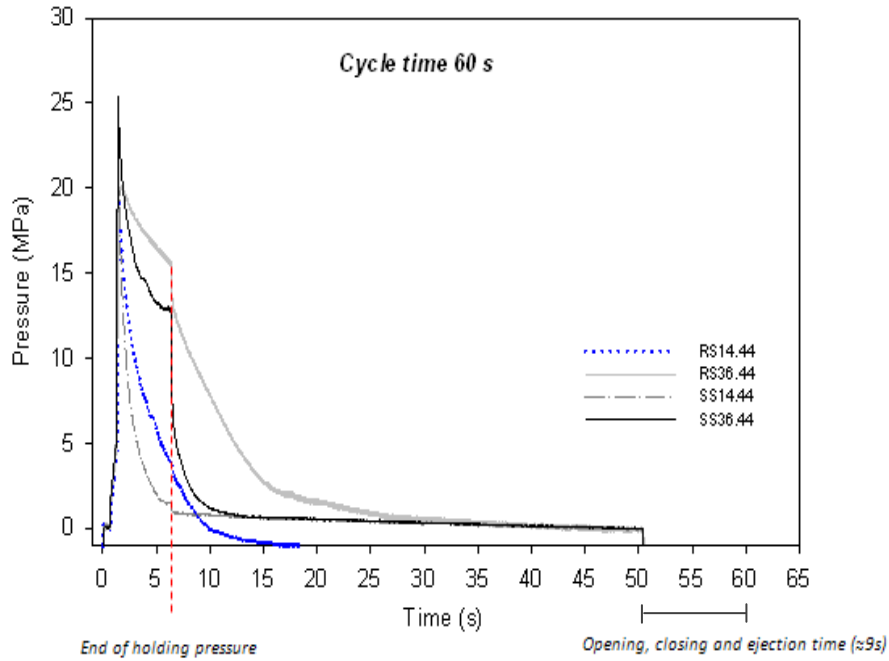
Figure 4.6 - Pressure vs. time (including RS14.44 moulding conditions)

4.3.2   Hybrid Mould HM-2

Mould design

The hybrid mould for the support box was designed considering reutilisation and maximum flexibility in operation (Figure 4.7). This solution was already presented elsewhere [220] and attached in appendix 2. The ejection side of the mould includes the core fitted in the core plate, the ejection system, the cooling system and the movable elements. The injection side contains the cavity block fitted in the cavity plate, the injection system and the cooling system.
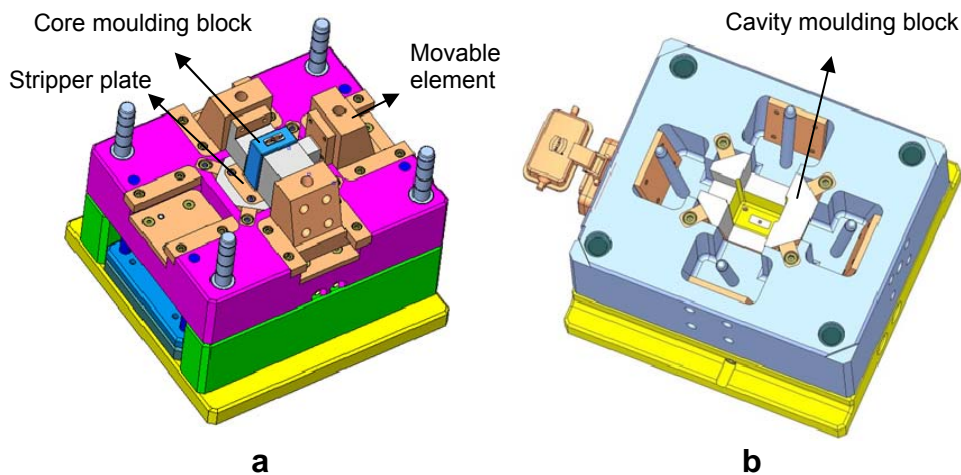
Figure 4.7 - HM-2 standard design: a) ejection side, b) injection side

The details of the moulding blocks are shown in Figure 4.8.

a   **b**
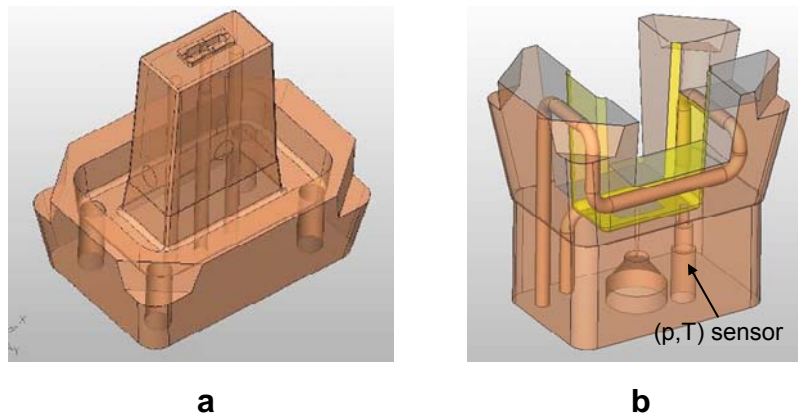
Figure 4.8 - Moulding blocks: a) core b) cavity

These blocks are assembled in the mould structure. The detailed design of the mould is included in appendix 3.

The structure of the mould was designed to allow the installation of four lateral or side movements (Figure 4.9) to define lateral details on the moulding. The shorter side movement come a displacement of 3 mm and the longer one a displacement of 11 mm.
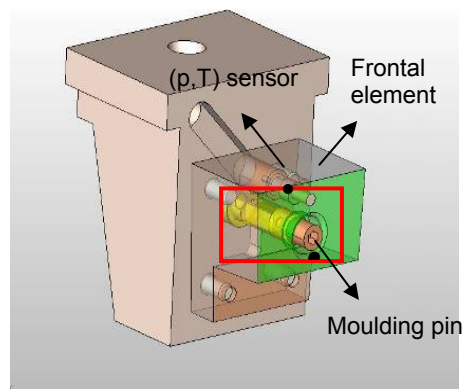
Figure 4.9 - HM-2 slide group that define the back detail of the moulding

Instrumentation

The instrumentation implemented in the HM-2 mould enabled the monitoring of the thermal and flow behaviours and the assessment of the ejection force in the back detail of the moulding. The instrumentation included two Kistler integrated temperature and pressure sensors (Types 6190BA and 6190CA) and a specifically designed and developed load cell. The integrated sensors were placed in the cavity block and in the back slide group where the load cell was also fitted (Figures 4.8b and 4.9). The pressure and

temperature integrated sensors enabled the collection of data close to the gate location ((1) - begin of flow) and welding line ((2) - end of flow) of the part, as shown in Figure 4.2. These locations make it possible to determine the required injection pressure, the temperature difference on the part during the injection cycle and the fill time. Furthermore the sensors can be used to monitor the reproducibility of the mouldings and the mould performance.
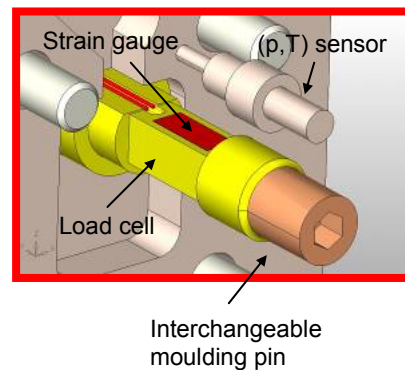
Figure 4.10 - Load cell design

Data acquisition system

A National Instruments Compact DAQ USB data acquisition system (National Instruments, Portugal) was used to collect strain data from the load cell during the injection cycle. The pressure and temperature data were gathered from the integrated sensors connected to another data acquisition system, Kistler SCP-Compact (Kistler, Switzerland). An example of data during moulding is depicted in Figure 4.11 for points identified in the Figure 4.2.
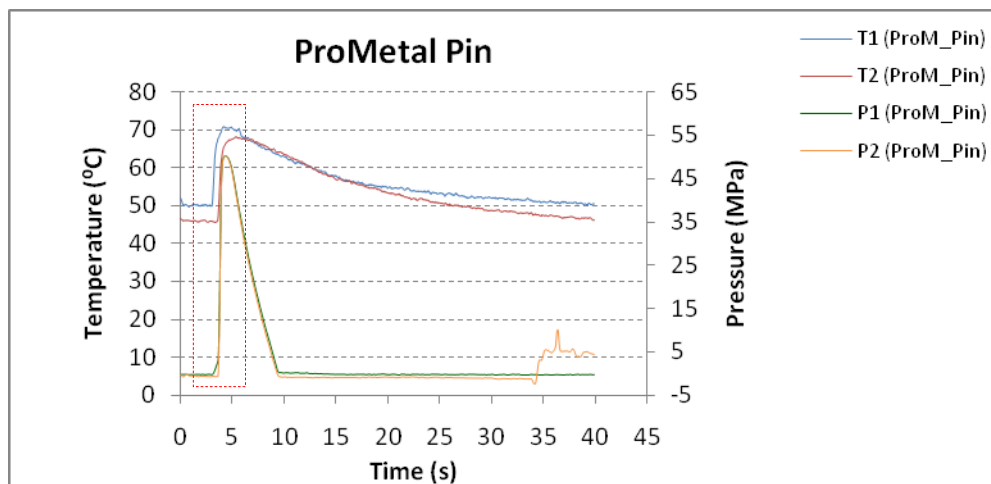
Figure 4.11 – Pressure and temperature data from HM-2 with ProMetal pin

4.4   Materials

4.4.1   Mouldings

The mouldings were produced in polypropylene homopolymer, Domolen 1100N (DOME Polypropylene, Holland) of MFR 12 g/10 min (230ºC/21.6 N). The data sheet of this material is included in appendix 4

4.4.2   Moulding elements

Raw materials

The moulding elements (moulding blocks and pins) were produced in various materials. Their main properties are shown in Table 4.2. Further details are presented in appendix 4.

The density of the epoxy-based composite material was determined by the impulsion method. The aluminium powder particles used for the epoxy/Al composite have an average size of 50 μm and density of 2.43 Mg.m^{-3}.

The epoxy/short steel fibre composite was developed by Sabino-Netto. The short steel carbon fibres have an average length of 453 μm and average thickness of 45 μm and density of 7.87 Mg.m^{-3} [48].

The standard moulding elements of the two hybrid moulds are in tool steel DIN WNr.1.2311.

Table 4.2 - Properties of the moulding element materials

Property	Units	Tool steel (DIN W Nr. 1.2311)	Epoxy/Al (Biresin L74 +60% Alum)	SL resin DSM Somos 11120/2	Epoxy/SSF (Biresin L74 +15% SSF)	ProMetal S4
Density	[Mg.m^{-3}]	7.80	1.65	1.12	2.10	7.50
Specific heat	[J.kg^{-1}.K^{-1}]	460	1279	286	_	418
Thermal conductivity	[W.m^{-1}. K^{-1}]	29.00	0.61	0.17	0.39	22.60
Thermal diffusivity	[m^2.s^{-1}]	8.08×10^{-6}	0.29×10^{-6}	0.52×10^{-6}		7.20×10^{-6}
Coef. of thermal expansion	[K^{-1}]	1.20×10^{-5}	6.00×10^{-5}	9.50×10^{-5}	_	_
Flexural modulus @20ºC	[GPa]	200.0	5.2-6.0	2.0-2.4	3.0-3.5	147.0

The properties of the Biresin L74 epoxy used for the composites are listed in Table 4.3.

Table 4.3 - Epoxy resin properties (Biresin L74).

Material (trade name)	Coefficient of thermal expansion* @100ºC [K^{-1}]	Hardness* [shore D]	Impact strength* [$kJ.m^{-2}$]	Heat deflection* temperature [ºC]	Density [$Mg.m^{-3}$]
BiresinL74	6.8×10^{-5}	85	29	160	1.1

* Values after post curing: 3h/60ºC + 3h/140ºC

Moulding blocks

The mouldings with HM-2 were produced using four combinations of materials in the moulding blocks:

1. Epoxy/60% aluminium powder (Biresin L74) in the core and steel in the cavity (identified as $Resin_1$/Steel or R_1S combination);

2. SL resin (DSM Somos 11120/2) in core and steel in cavity ($Resin_2$/Steel or R_2S);

3. Epoxy/15% short steel fibres (Biresin L74) in core and steel in cavity ($Resin_3$/Steel or R_3S) and

4. Steel in core and steel in cavity (Steel/Steel or SS). Figure 4.12 shows the example of the ejection side of the HM-2 fitted with the SL core moulding block.
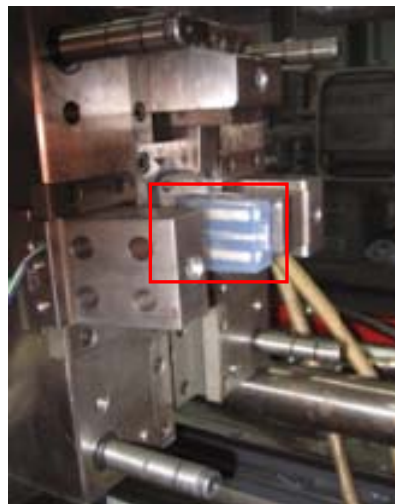
a   **b**

Figure 4.12 - Ejection side of the HM-2 (a) fitted with the SL core moulding block (b)

Moulding pins

To define the back hole of the support box a moulding pin was designed and produced with the main dimensions shown in Figure 4.13.
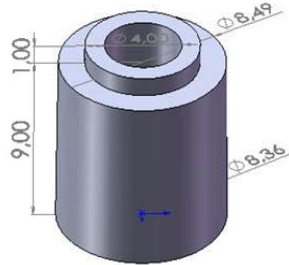
Figure 4.13 - Moulding pin main dimensions

The materials used to produce the moulding pins for tests were: (1) Tool steel (Pin$_1$); (2) Epoxy (Biresin L74) filled with 60% (in weight) aluminium powder (Pin$_2$); (3) SL resin (DSM Somos 11120/2), (Pin$_3$); (4) Epoxy (Biresin L74)/15% (in volume) short steel fibres (Pin$_4$); (5) ProMetal (Pin$_5$). The main properties of the materials used in the moulding elements are presented in Table 4.2.

4.5   Rapid tooling

4.5.1   Masters

In this study, the standard steel moulding blocks were used as *masters* (physical models for the moulding blocks in silicone moulds) for replication. The Figures 4.14 and 4.15 show the HM-1 steel moulding blocks and the HM-2 steel core block, respectively.

a   **b**

Figure 4.14 – HM-1 steel moulding blocks used as masters: a) core, b) cavity

Figure 4.15 - HM-2 steel core used as master

4.5.2 Silicone moulds

The silicone moulds were produced to replicate epoxy-composite moulding blocks for the hybrid moulds. The process to produce the silicone moulds in both cases was similar. The main steps of the process are detailed for the case of HM-2, and are as follows:

1. *Frame construction for silicone casting* using the steel core as a master (Figure 4.16);

Figure 4.16 - Structure for silicone casting and definition of the master position

2. *Definition of the parting plane* depending on the master position Figure 4.17;

| **a** | **b** |

Figure 4.17 - Structure for silicone casting: a) Parting plane definition and holed for silicone cast,

b) Structure ready for casting

3. *Preparation of the silicone* by mixing the Köraform components A50 (Technical data in appendix 4) and degassing in the MCP dynamic vacuum equipment (MCP, Spain);

4. *Casting of the silicone* into the frame and second degassing;

5. *Curing* of the cast silicone at room temperature;

6. *Demoulding of the master*. After the master is removed the silicone mould is ready to produce the mouldings by vacuum casting (Figure 4.18).

Figure 4.18 - Silicone mould and master

4.5.3 Epoxy tooling

The resin moulding blocks were produced by vacuum casting in silicone moulds as shown in Figure 4.19 for the HM-2 core. This shows the successive phases of the process from the CAD model to the core blocks.

a   b   c   d
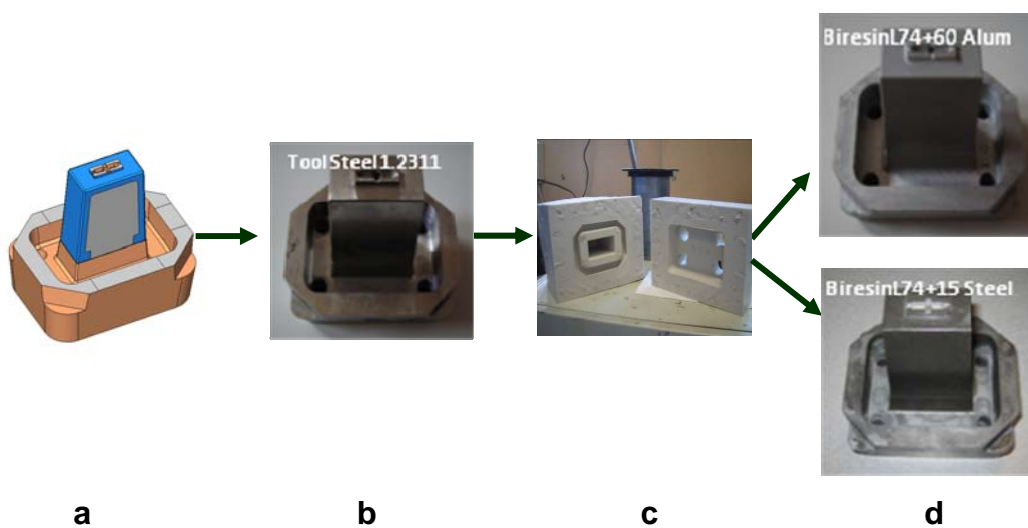
Figure 4.19 - Phases of the epoxy tooling process: a) CAD model, b) steel master, c) silicone moulds, d) Epoxy composite blocks

The manufacturing route for the epoxy resin moulding blocks included:

1. *Mixture* the resin components in indicated proportions;

2. *Degassing* of the resin in the MCP dynamic vacuum equipment during 30 minutes;

3. *Casting*;

4. *Curing* of the cast resin at room temperature (24 h);

5. *Post cure* (3 h at 60ºC and 3 h at 140ºC for the Biresin L74, according to the technical data in appendix 4. The heating and cooling were made at a rate of 10ºC/h;

6. *Finishing operations* for fitting the instrumentation and fitting the moulding blocks into the mould structure.

In the case of epoxy resin with 15% of short steel fibres core moulding block the cure up to gel time at room temperature, was done using a dynamic process to avoid steel fibre sedimentation [41]. In this process the mould is continuously rotated on the apparatus at 5 rpm. The anti-sedimentation equipment is shown in Figure 4.20.

a   **b**

Figure 4.20 - Anti-sedimentation equipment: a) overall view, b) equipment in operation

4.5.4   Stereolithography tools

The stereolithography (SL) resin core moulding blocks were produced using the so called ACES build style for epoxy resins with a 3D Systems SLA 3500 equipment (3D Systems, USA). This is the standard build style for SLA machines. The layer thickness was 0.1 mm. An extra thickness of 0.3 mm was used in the final block for adjustment into the mould structure. Figure 4.21 shows the successive phases of the SL process, from the CAD model of the core moulding block (Figure 4.21a) to the final SL resin core moulding block (Figure 4.21d). The shrinkage of the SL resins used is close to zero.
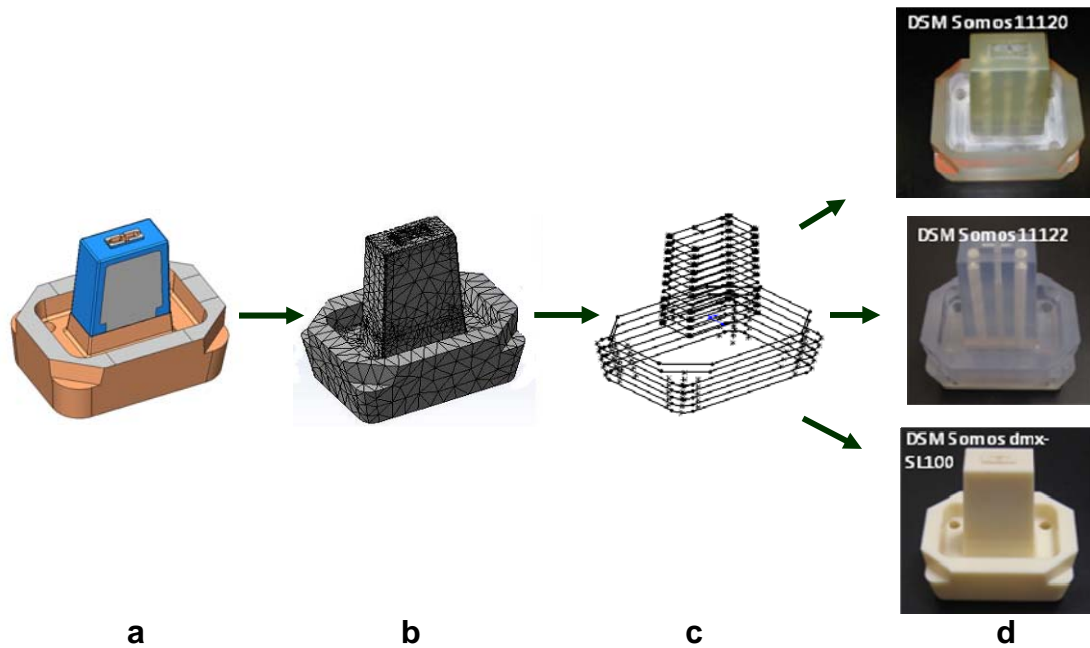
Figure 4.21 - Phases of the production of SL moulding blocks: a) CAD model, b) STL model, c) SLI model, d) SL resin blocks

The orientation of moulding blocks was on that way that the core side was on top, so that supports do not damage the surface of the part. After building the parts on the machine, they were cleaned with standard acetone and isolpropanole, and afterwards during 20 minutes post curing in a standard UV curing furnace of 3D Systems (standard procedure). The ejector holes diameters were built little smaller to pro drill these holes afterwards, avoiding leakage of the polymer and damaging of the mould core. The layer-by-layer scanning strategy was constructed with a 0.03 mm over-cure to arrange the interconnection between the layers. It is so that the type and status of the laser (power and laser beam diameter) will affect the parameters slightly, and also as can be expected the resin itself [221].

4.5.5   3D Metal Printing tools

The 3D Metal Printing core block was produced with ProMetal R10 equipment (ProMetal, Germany). After this process the block surface is rather rough (Ra ≈ 12.5 µm). Thus, 1 mm extra thickness was considered for post processing and final block adjustments to fit into the mould structure. After the adjustments and surface finishing the final roughness came down to *ca.* 0.1 µm. The roughness measurements were made using a Perthometer M2 roughness meter (Mahr, Germany) and a light microscope Zeiss MC 80 (Carl Zeiss, USA).

In 3D Metal Printing tools it is recommended the minimum of 1 mm extra thickness to guarantee the post processing operations and surface finishing, namely in regions with great accuracy (as for mould fitting, closing planes, …).

4.6 Injection moulding

4.6.1 Equipment

The mouldings were produced in a Ferromatik Milacron K85 (Ferromatik Milacron, Germany) injection moulding machine of 850 kN clamping force. The mould temperature was controlled through a thermal regulator Piovan THN 6P (Piovan, Italy), with a heating capacity of 6 kW and a 330 W pump delivering a flow rate of 35 L/min at 300 kPa.

4.6.2 Processing conditions

In the experiments with hybrid moulds the processing conditions were set according to each combination of moulding elements, *i.e.*, core and cavity or moulding pin materials.

With the HM-1 mould the mouldings were produced using combinations of moulding blocks depending on the material used. These combinations are identified in terms of the core and cavity materials, as RR (resin core/resin cavity), RS (resin core /steel cavity), SS (steel core /steel cavity).

The material used in the steel moulding blocks was the tool steel DIN WNr.1.2311. The epoxy composite was filled with 60% (in weight) of aluminium powder. The materials properties are shown in Table 1. The processing conditions with HM-1 are detailed in Table 4.4.

Table 4.4 – HM-1 Injection moulding processing conditions

Parameter	Value		
Injection temperature [ºC]	230		
Water cooling temperature [ºC]	40		
Injection flow rate [$cm^3.s^{-1}$]	37.7		
Injection pressure [MPa]	42		
Holding time [s]	5		
Core - Cavity	**SS**	**RS**	**RR**
Holding pressure [MPa]	36	36	14
Cooling time [s]	12	25	44

In the case of the HM-2 mould the processing conditions were also set according to the materials of the moulding blocks (Table 4.5) and moulding pins (Table 4.6). In the studies on the moulding pin materials the moulding blocks were both tool steel.

Table 4.5 - Processing conditions in the programme for core moulding block material

Parameter	SS	R_1S and R_3S	R_2S
Core/Cavity materials	Steel/Steel	Epoxy/Steel	SLres/Steel
Injection temp [ºC]	230	230	230
Cooling temp [ºC]	40	40	40
Injection time [s]	1.3	1.3	3
Injection pressure [MPa]	91	70	42
Holding time [s]	5	10	10
Opening, closing and ejection time [s]	12	12	12
Holding pressure [MPa]	70	56	14
Cooling time [s]	25	35	45

Table 4.6 - Processing conditions in the programme for the moulding pin material

Parameter	Pin_1 (Steel)	Pin_2 (EP-Al)	Pin_3 (SL)	Pin_4 (SSF)	Pin_5 (ProM)
Injection temp [ºC]	230	230	230	230	230
Cooling temp [ºC]	40	40	30	40	40
Injection time [s]	1.3	1.3	1.3	1.3	1.3
Injection pressure [MPa]	91	70	70	70	91
Holding time [s]	5	5	5	5	5
Opening, closing and ejection time [s]	12	12	12	12	12
Holding pressure [MPa]	70	56	35	56	70
Cooling time [s]	25	25	35	25	25

In each processing condition, at least 25 mouldings were produced after process stabilization. For each set of new processing conditions, the first 10 injected parts were always rejected.

4.7   Characterisation techniques

The characterisation techniques include the test methods for mould materials, the techniques for the morphological studies on the mouldings, and the shrinkage assessment of the mouldings. A tribological analysis was made of pairs of materials (mould/moulding) to determine the coefficient of friction upon ejection.

4.8   Mould materials

The thermal and mechanical properties of the mould materials used in the moulding elements (blocks and pins), namely thermal conductivity, thermal diffusivity, elasticity modulus, tensile and compression strength, specific heat and density, were determined.

4.8.1   Thermal properties

The equipment used to determinate the material thermal properties, as shown in Table 4.2, is an Alambeta conductivity equipment (Sensora, Czech Republic) and the samples prepared with a diameter of 60 mm and thickness of 3 mm. The tests were carried out according to the conditions established for the equipment.

4.8.2   Physical properties

The density of the epoxy-based composite material was determined by the impulsion method. The aluminium powder particles used for the epoxy-based composite have an average size of 50 μm and density of 2.43 Mg.m^{-3}. The epoxy/short steel fibre composite was proposed by Sabino-Netto [48]. The short steel carbon fibres have an average length of 453 μm and average thickness of 45 μm and density of 7.87 Mg.m^{-3}.

4.8.3   Mechanical properties

The mechanical properties of the mould materials used in the moulding elements (blocks and pins), namely: elasticity modulus, tensile and compression strength and specific heat were determined using a Dynamic Mechanical Analyser (DMA) Tritec 2000 (Triton, UK), a universal testing machine Zwick Z100 (Zwick, Germany).

The DMA tests were complemented with tensile and compression tests according to the ISO 527-1 and ISO 604:1993(E) standards, respectively. The specimen dimensions were:

25 mm gauge length, 4 mm width and 2 mm thickness for the universal tensile tests. The specimen dimensions for the compressive tests were $10\times10\times4$ mm to determine the compressive strength and $50\times10\times4$ mm for the compressive modulus.

4.9 Morphology

The morphology study was made on HM-1 mouldings. The combinations of materials of the moulding blocks originated different morphologies in the mouldings. This was observed on thin sliced sections of approximately 10 µm cut perpendicular to the flow direction (Figure 4.22) in a microtome Anglia 0325 (Anglia Scientific Instruments, UK), using steel razor blades. The microtomed sections were placed between glass slides within a liquid of matched refractive index (Canada balsam). The samples were observed under the polarized light microscope Olympus BH-2 (Olympus, Japan) coupled with an image analyzer system with a low-power magnification to allow for a complete view of the structure through the thickness being observed.

Sliced section at mid-height and through the thickness of the moulding.
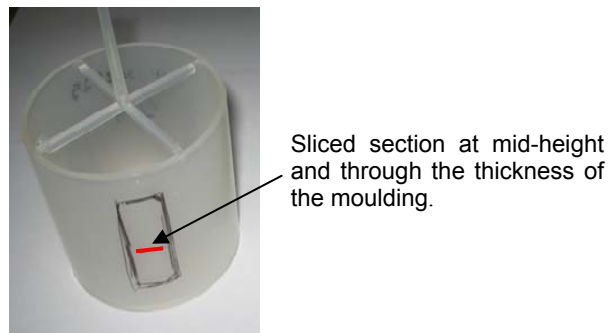
Figure 4.22 - Sample location for the morphology analysis

Dimensional changes of the tubular parts were measured at specific locations highlighted in Figure 4.23. An inside micrometer Mitutoyo SBMC-100CST (Kawazaki, Japan), using a measuring range from 50-100 mm and 1 µm resolution was used.
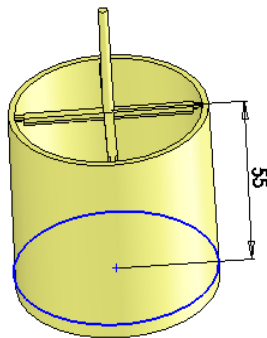
Figure 4.23 – Local part for shrinkage evaluation

The shrinkage study of the HM-2 mouldings was made considering the back detail of the support box Figure 4.24. Measurements in the testing part and moulding pins were made, in the locations of the support box shown in Figure 4.24b, with a 150 mm digital calliper.

a   **b**
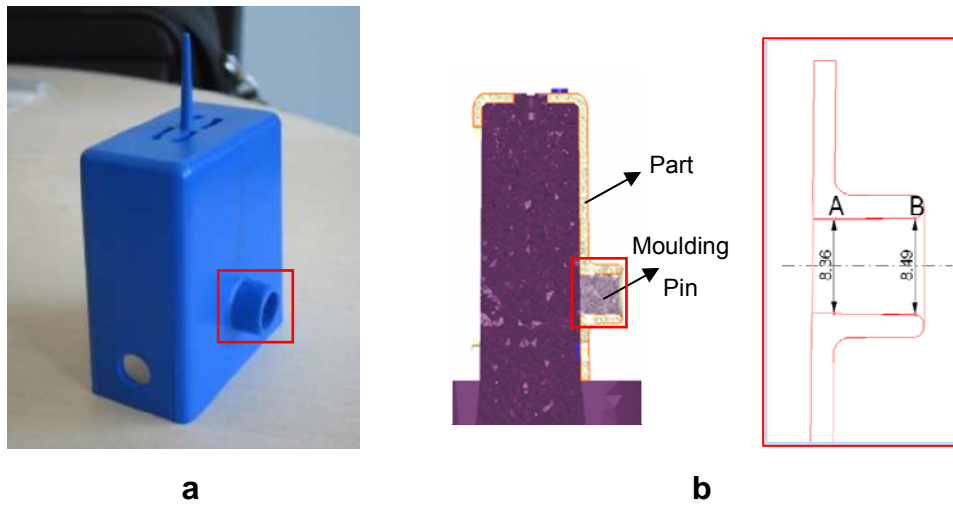
Figure 4.24 - HM-2 moulding: a) Back detail, b) Dimensions A and B for shrinkage analysis

4.10 Friction properties

The determination of the static coefficient of friction of the pairs of materials in contact was required for the studies on the ejection in the lateral castle of the support box. The coefficient of static friction was determined with the prototype apparatus that enables its determination in conditions similar to processing [126]. This friction apparatus used as an accessory of an Instron 4505 universal testing machine is shown in Figure 4.25.

The samples for the friction tests were injected in the same material of the mouldings, in a Krauss-Maffei KM60-210A injection moulding machine.

a   **b**
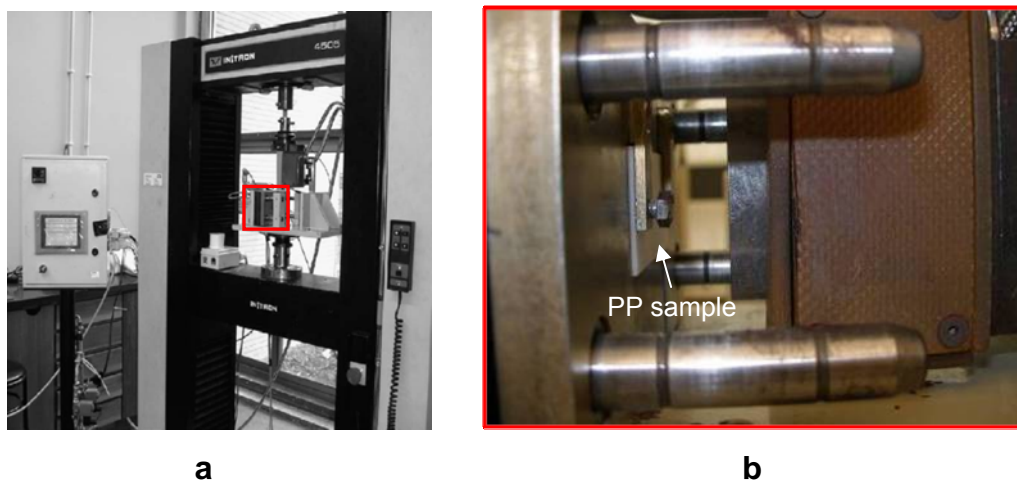
Figure 4.25 - Friction testing equipment (source: Pouzada *et al.* [126]) (a) and sample position (b)

The friction test followed the following steps:

1. Heating the moulding surface up to the replication temperature;

2. Stabilization of the temperature;

3. Application of contact pressure to get surface replication for 90 s;

4. Cooling down to the test temperature;

5. Friction test at selected cross-head speed.

The cycle time for the complete routine is typically 15–20 min.

The tests were made with the same mould materials and moulding conditions used in injection moulding. Before the friction tests the PP sample was heated up with a heat blower up to a replication temperature below the melt temperature of the material, ≈160ºC. The replication temperature was monitored with an infrared pyrometer. The friction was determined for the temperature of 65ºC (corresponding to a typical ejection temperature) and with contact pressure of 4.3 MPa. A typical curve of the evolution of the friction force obtained with the apparatus is shown in Figure 4.26.
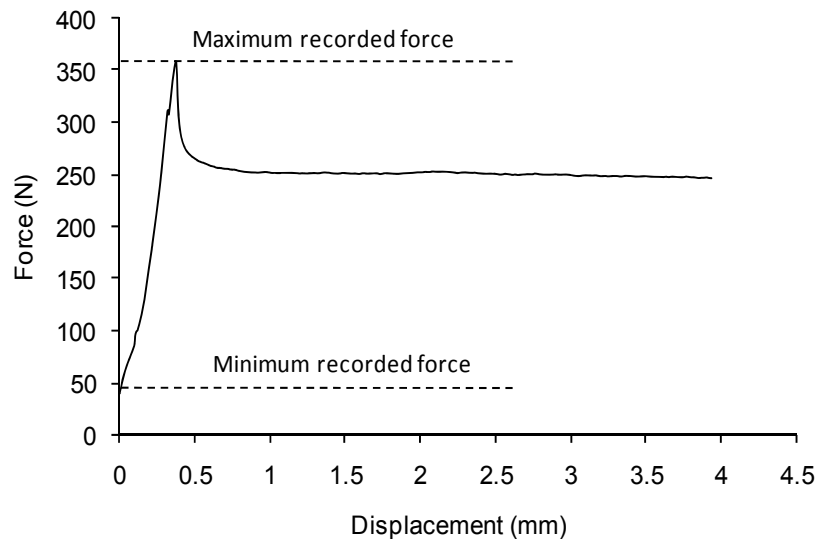
Figure 4.26 - Determination of friction force in test curve

The maximum force is used for the determination of the coefficient of friction. It was calculated as the difference between the maximum and minimum recorded forces, as in Figure 20. The static friction coefficient is the ratio:

$$\mu_s = \frac{F_a}{F_n} \tag{4.1}$$

where F_a is the friction maximum force and F_n is the normal contact force applied by the pneumatic cylinder of the apparatus.

4.10.1 Ejection forces

The ejection force required to remove the moulding pin (Figure 4.27) from the back detail of the support box (Figure 4.2) was determined analytically from the polymer shrinkage.
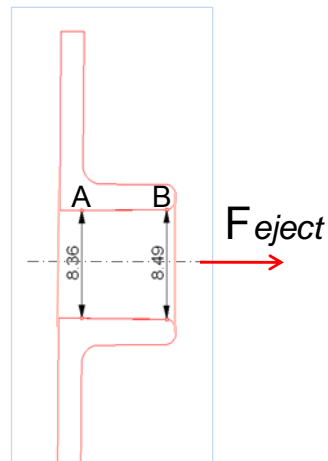
Figure 4.27 – Scheme of the ejection force required to remove the moulding pin

It was also determined experimentally using the load cell specifically designed for this study. The load cell consists in a 12×6×1 mm steel beam with a bonded strain gauge Type: KFG-2-120-C1-11 (Kyowa, Japan). The load cell was fitted into one of the slide groups and instrumented with a Wheatstone bridge system with the uniaxial steel strain gauge (see Figure 4.28).

a   **b**
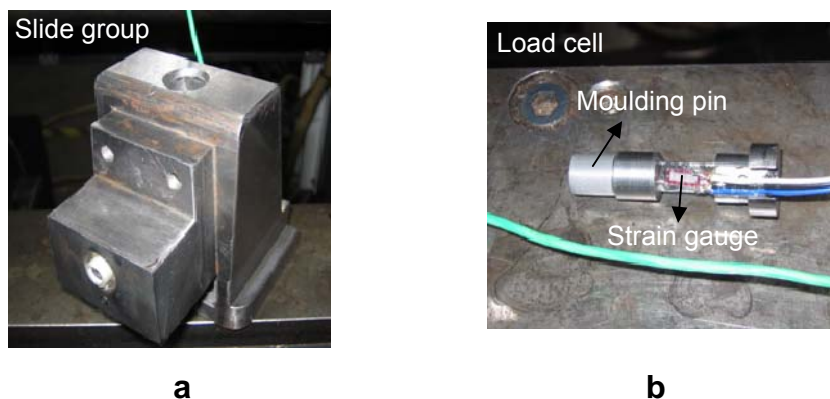
Figure 4.28- Slide group (a) and load cell instrumentation (b)

The National Instruments Compact DAQ USB data acquisition system (National Instruments, Portugal) was used to collect the deformation data, as mentioned above.

5 RESULTS AND DISCUSSION

5.1 The plastics parts

5.1.1 Tubular part

This simple plastic part is produced in specific processing conditions of this research work to study and understand important characteristics of the mouldings produced with hybrid moulds. As presented in chapter 4, section 4.3.1, the hybrid mould used to produce the 3D tubular parts (HM-1) is a simple tool (without "noise") very good for demonstrating in theoretical fundamentals. The parts are produced only with the opening and close movements of the two halves (injection and ejection sides) of the mould.

5.1.2 Support box

This testing part was defined based on the conceptual model shown in Figure 5.1. The model is defined to study the effect of lateral movements of different amplitudes (short and long) in hybrid moulds and the performance tools manufactured in alternative materials (main core and moulding elements, or moulding inserts).
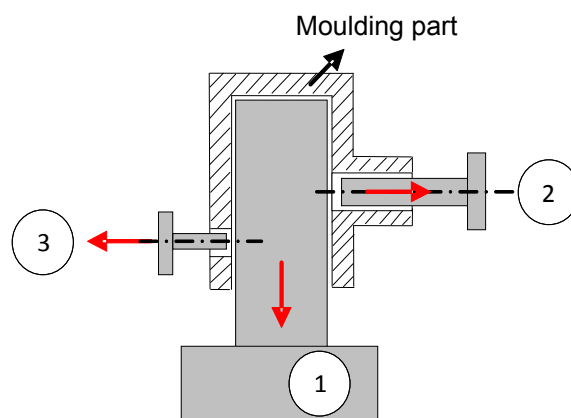
Figure 5.1 - Conceptual model. 1-deep core movement, 2-long side movement, 3-short side movement

This concept allows the study of:

- The main core (1) – it is associated to the main ejection movement and is responsible for moulding the inside shape of the part;

- The long lateral core (2) – responsible for the creation of the fitting detail on the right side of the part;

- The short lateral core (3) – responsible for the creation of the lateral opening on the left side of the part.

5.2   Hybrid mould design and manufacture

The mould HM-1 is one of the first hybrid moulds purposely designed at the University of Minho to assess the effect of the moulding blocks on the morphology and dimensional properties [185]. It was adapted to this research programme with some of the main findings already published elsewhere [195] and attached in appendix 2.

The mould HM-2 was designed for this research according to the specifications described in Chapter 4. For new designs the moulding dimensions are limited by the moulding block dimensions and only four movable elements are possible to define side details.
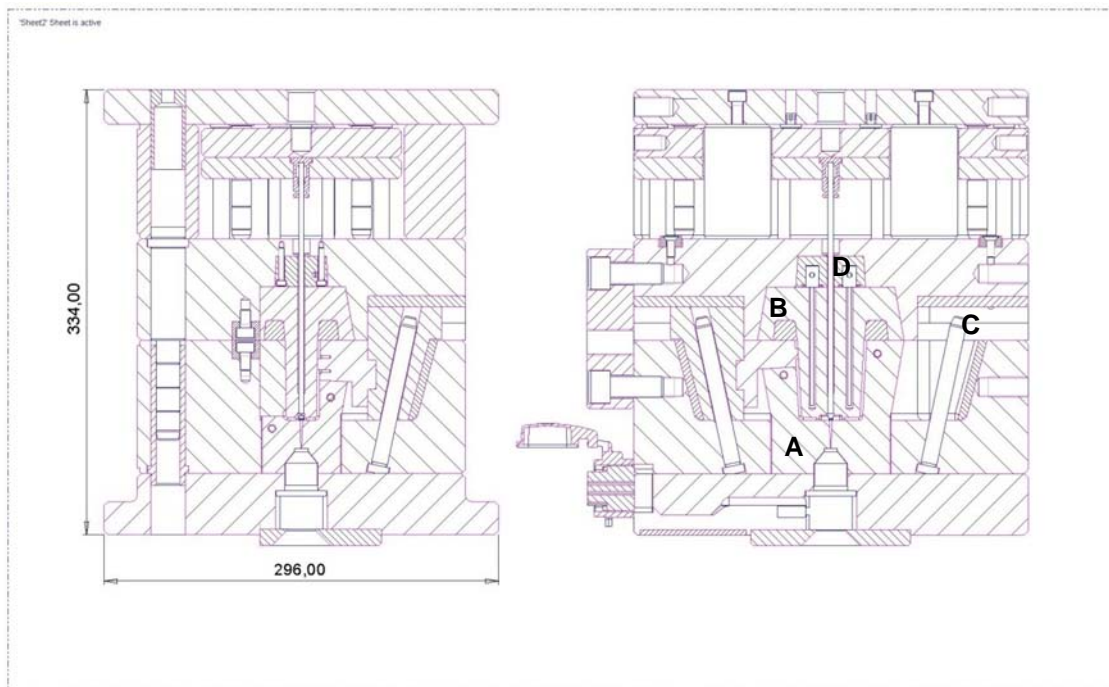
Figure 5.2 - HM-2 assembly. A-cavity moulding block, B-core moulding block, C-lateral moulding element, D-cooling cassette fitted into the core

5.2.1   Moulding blocks

The moulding blocks for the HM-2 mould were shown in Figure 4.7. These blocks can be assembled in the mould structure when the mould is open, without the need to disassemble the tool. This flexible option allows changing mould inserts without removing the mould from the injection moulding machine. The outside walls of the moulding blocks were designed with 10º draft angles, to facilitate their removal and replacement. The main dimensions of the moulding blocks are shown in appendix 3.

The moulding blocks are fixed with four bars screwed into the mould structure (Figure 5.3).
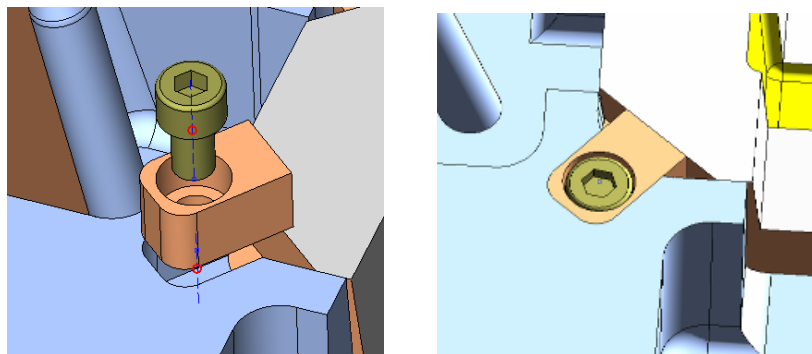
Figure 5.3 - Attaching the moulding blocks to the mould structure

5.2.2   Lateral moulding elements

The structure of the mould also enables the assembly of four side groups to define details on a generic part. Each lateral side group has a common back support that enables fitting a specific front (Figure 5.4). This design was defined to allow changing the frontal element according to the detail shape and the material for the moulding pin.
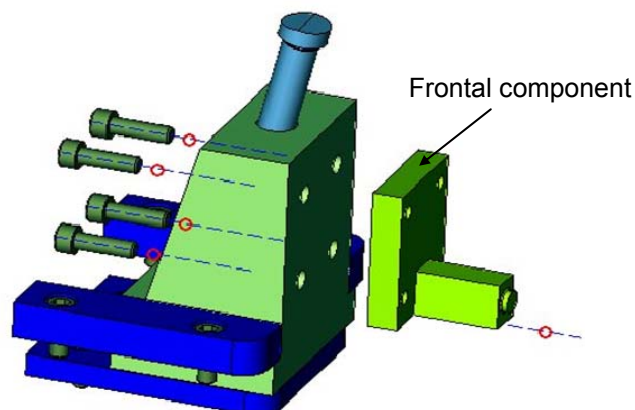
Figure 5.4 – HM-2 slide group

5.2.3   Moulding pins

The slide group is responsible for the creation of the detail on the side of the support box that requires a long side movement. The actual moulding pin was designed to allow the testing of various materials and RPT techniques (Figure 5.5).
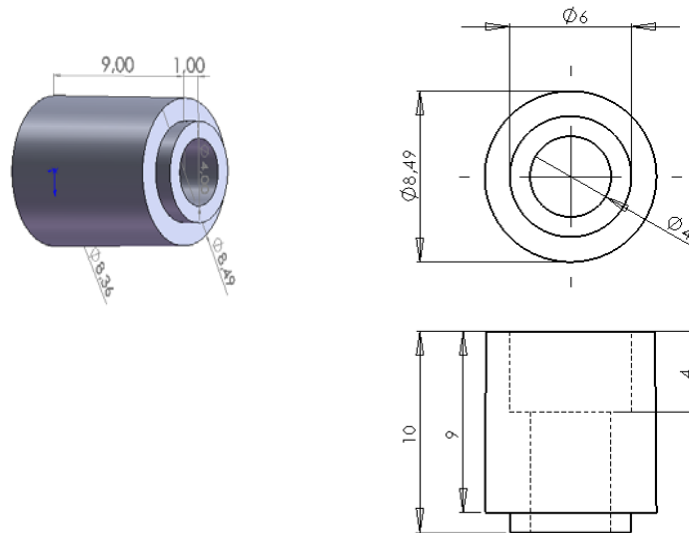
Figure 5.5 - Moulding pin design

Its performance was tested in operation during the injection cycle. It was fitted in the frontal element of the side group (Figure 5.6).
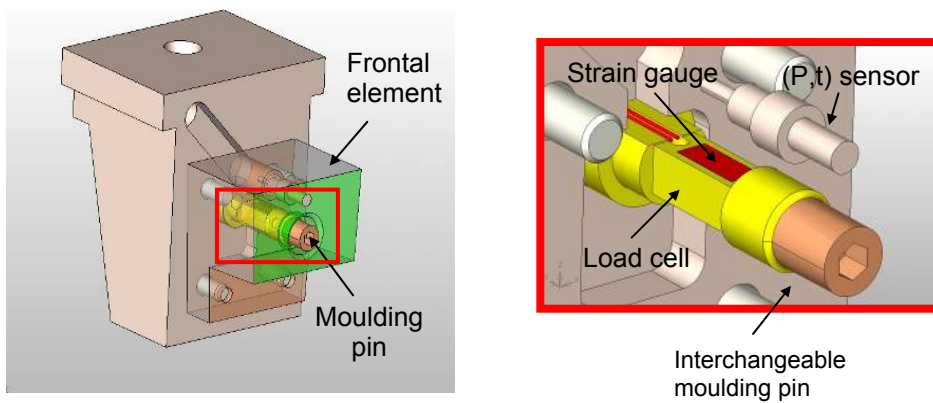
Figure 5.6 - Moulding pin fitted on the side group

5.2.4   Functional systems

The functional systems of HM-2 specifically designed for their operation as a hybrid mould are the injection, cooling and ejection systems.

Runner system

The injection system consists of a hot nozzle to add more flexibility on the sprue dimensions, as shown in Figure 5.7. The gating for this specific part, the support box, is of the spider type with four gates allowing a flow pattern as uniform as possible (Figures 5.8 and 5.9). The uniformity of the flow can be observed in the Moldex3D simulation, as exampled in Figure 5.10.
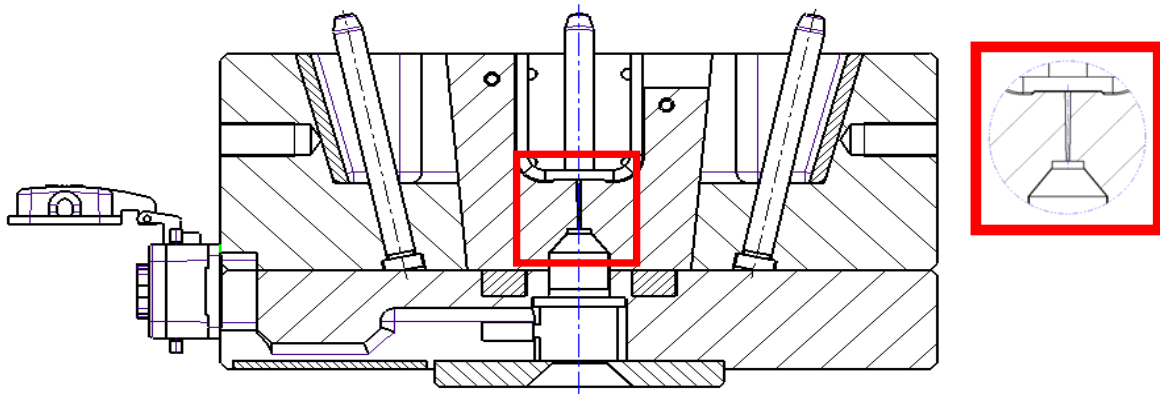
Figure 5.7 - Injection system
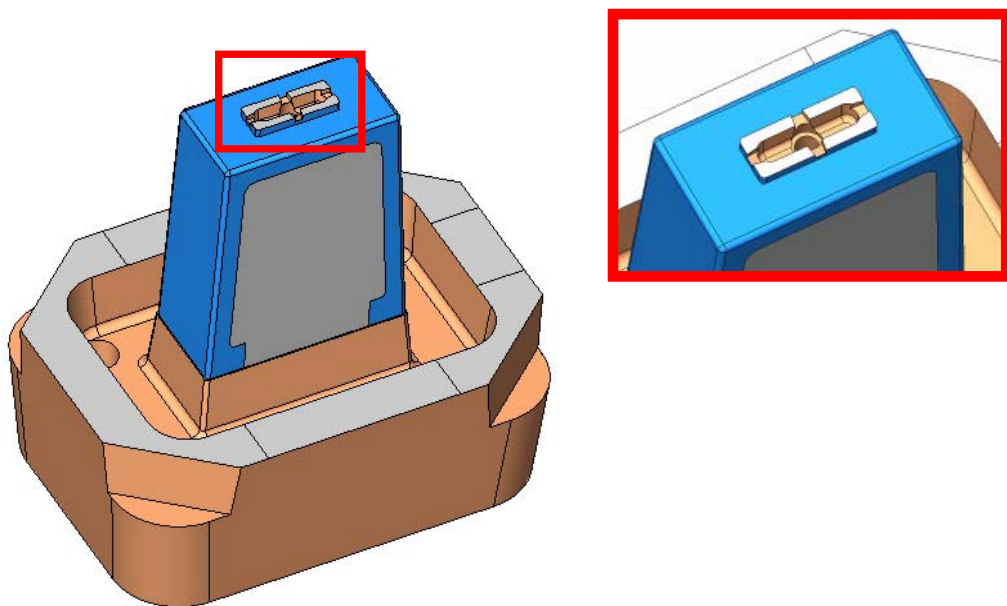
Figure 5.8 - Spider gating system with four gates

The runner system is composed by sprue, two runners and four gates. The runners have a section of 4×4 mm. The main dimensions of the feed system are shown in Figure 5.9.
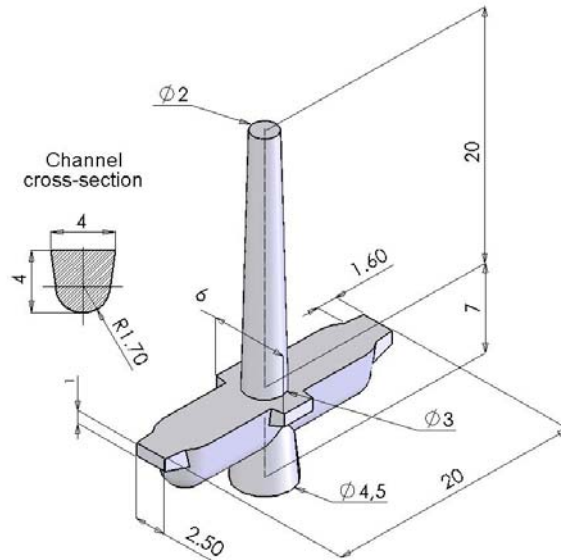
Figure 5.9 – Main dimensions of the feed system
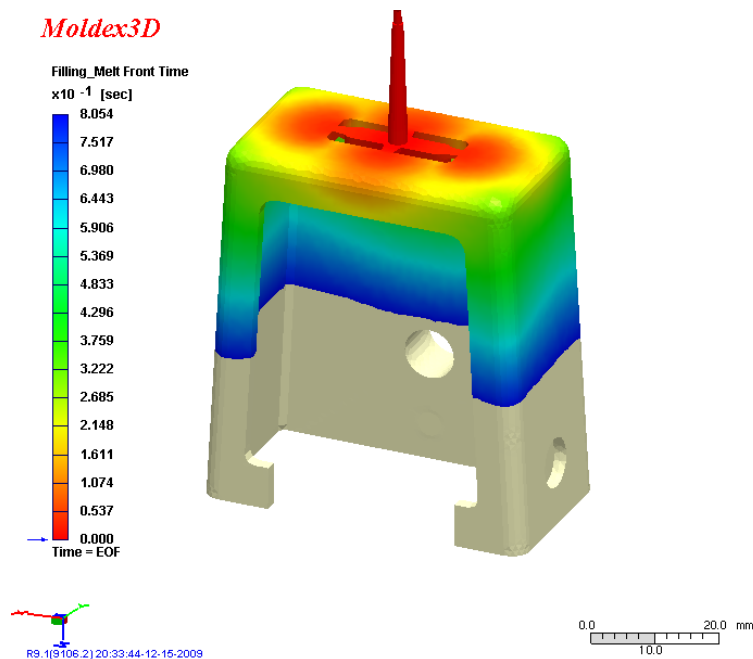
Figure 5.10 – Melt front during the filling phase, at 0.8 s

Cooling system

The cooling system was designed to make the cooling efficient and the production of the core blocks as simple as possible. In the injection side a conformal cooling architecture was implemented (Figure 5.11). The conformal cooling solution is recommendable when low thermal conductivity materials are used in the moulding elements. In the core side it is implemented as a common unit that is assemblable to any core and consists of a cooling cassette with 2 thermal pins in the ejection side of the mould (Figure 5.11).

a **b**
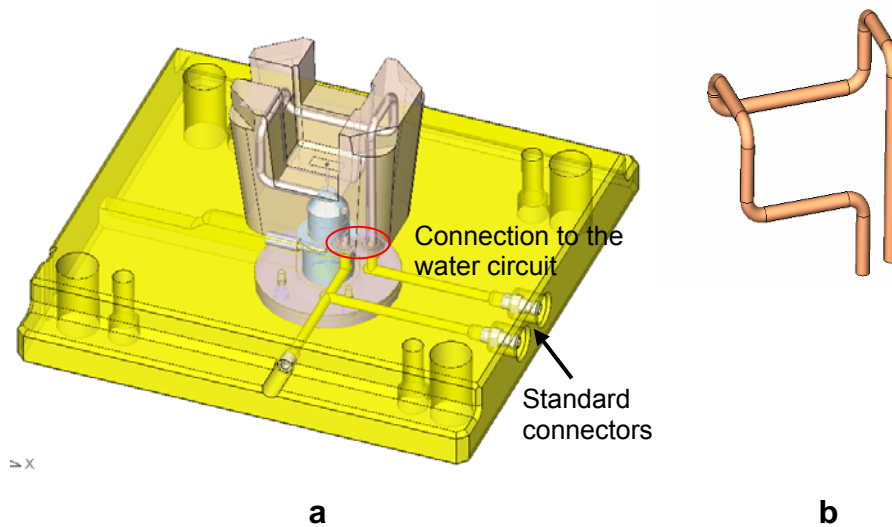
Figure 5.11 - Cooling system: a) implementation in the cavity, b) layout of the conformal cooling channel

The implemented channel layout has the flexibility for establishing various cooling paths. In this study this possibility was not explored and the cooling circuit was always the same.

The characteristics of the water control system were specified in chapter 4, section 4.6.1. The diameter of the cooling channels is 6 mm and the water flow rate, measured in the flow meter, is 6 L/min.

The cooling circuit in the interchangeable cooling cassette is shown in Figure 5.12. The cassette is fixed in the core plate and the inlet and the outlet of the cooling fluid were implemented in this plate (Figure 5.12c)). This solution allows the easy exchange of the core block without removing the cassette from the mould structure.

a **b** **c**
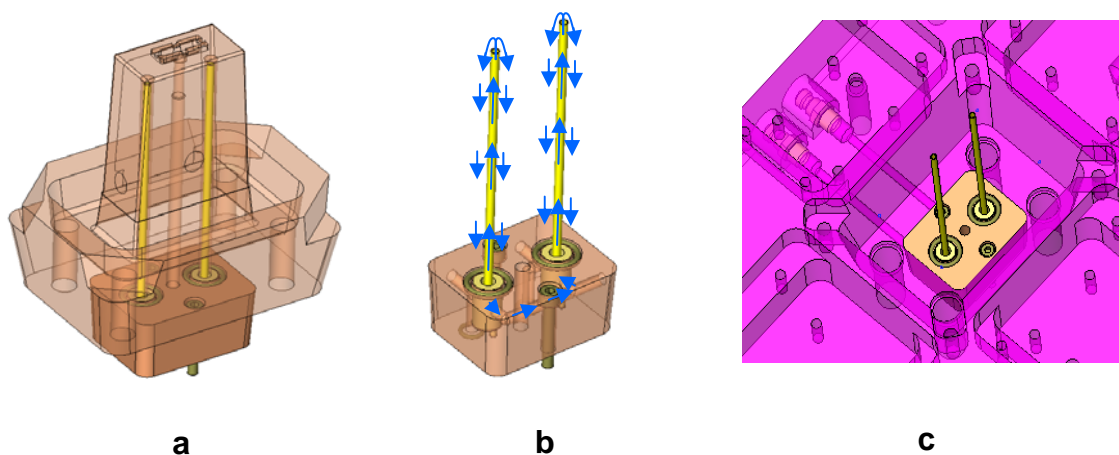
Figure 5.12 - Cooling system in the core: a) Cooling cassette fitted into the core, b) Cooling layout, c) Cooling cassette placed in the core plate

Ejection system

The ejection system consists of a stripper ring fitted in the core moulding block, to promote a smooth ejection of the part, and a 4 mm central ejector pin for the runner system (Figure 5.13).
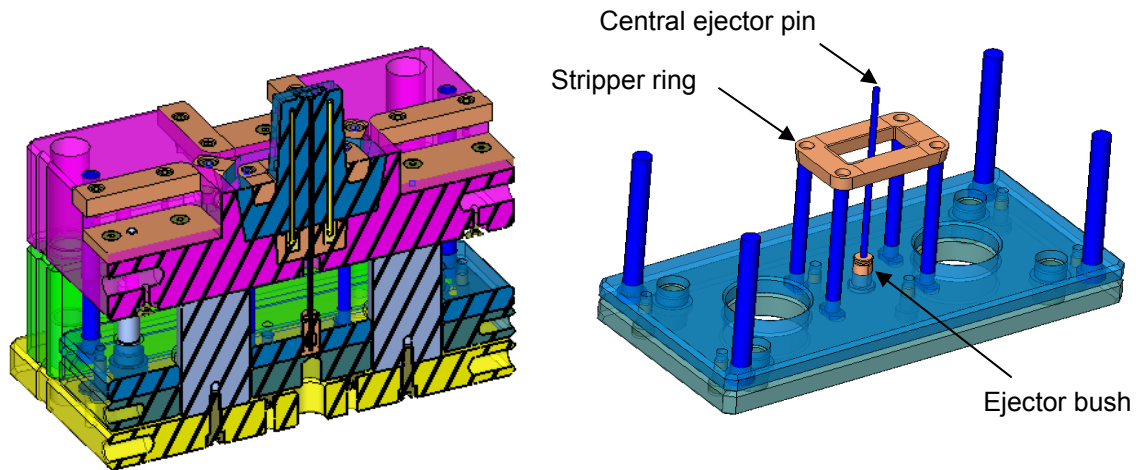

Figure 5.13 – Ejection system

The reutilisation goal was achieved by designing in the mould structure a bolster to quick exchange of the moulding blocks without removing the mould from the injection machine (Figure 5.2).

The main details of the mould design was published elsewhere [220] and attached in appendix 3.

5.2.5   Mechanical characterization

Tensile and compression tests, according to ISO 527-1 and ISO 604:1993 standards respectively, were made in the epoxy-based composites materials. The characterisation in compression complies with the fact that the moulding blocks are under this state of stress. Typical curves are shown in the Figure 5.14 and Figure 5.15 for the epoxy/Al and the epoxy/SSF composites materials, respectively.
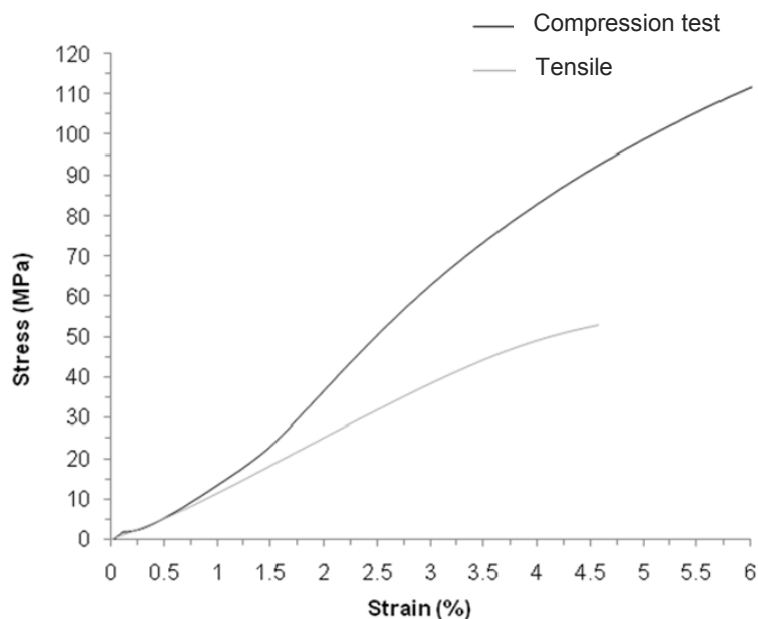
Figure 5.14 – Tensile and compression tests of the epoxy/Al composite material
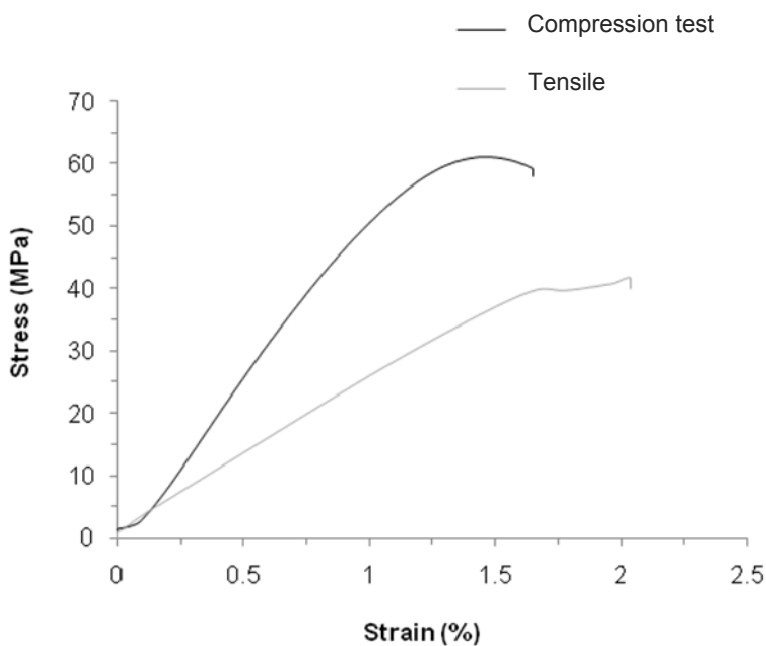

Figure 5.15 – Tensile and compression tests of the epoxy/SSF composite material

The moduli of elasticity of the epoxy/SSF composite are of 2.43 ± 0.035 GPa and 4.45 ± 0.27 for the tensile and compression tests, respectively (Table 5.1).

The properties in compression at 20ºC of the epoxy composite are listed in Table 5.1 alongside the DMA data obtained in flexure mode.

Table 5.1 – Mechanical properties of the epoxy composites at 20ºC

Material	Biresin L74+60%Al			Biresin L74+15%SSF		
Test	Tensile	Compression	DMA flexural	Tensile	Compression	DMA flexural
Maximum strength [MPa]	52.79	117.70	-	38.67	60.32	-
Modulus [GPa]	4.86	5.93	5.70	2.43	4.45	3.40

Physical properties

The variation of the moduli of elasticity in the temperature working range of the moulding blocks work, was determined from 30ºC to 100ºC. Data obtained from the DMA tests show the variation of the moduli of elasticity with temperature, in 3-point bending loading (Figure 5.16).
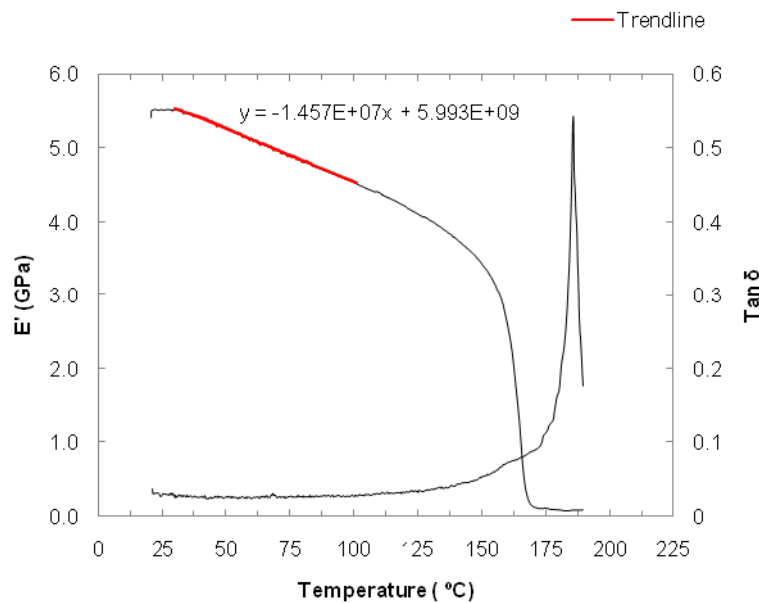
Figure 5.16 - Modulus of elasticity versus temperature of the epoxy/Al composite (DMA 3-point bending test)

The data in the two test modes show a sharp decrease of the elasticity moduli above the glass transition temperature of 120ºC. Below this transition there is a linear variation of the moduli in the range from 20ºC to 100ºC. Considering the case of the 3-point bending data it is possible to obtain a linear dependence of the modulus with temperature:

$$E(T) = -14.6 \times T + 6.0 \times 10^3 \qquad\qquad 5.1$$

where T is the temperature (ºC) and E is the modulus of elasticity (MPa).

In the range of temperatures between 20ºC and 100ºC, the epoxy/SSF composite behaves similarly as it is shown in the Figure 5.17.
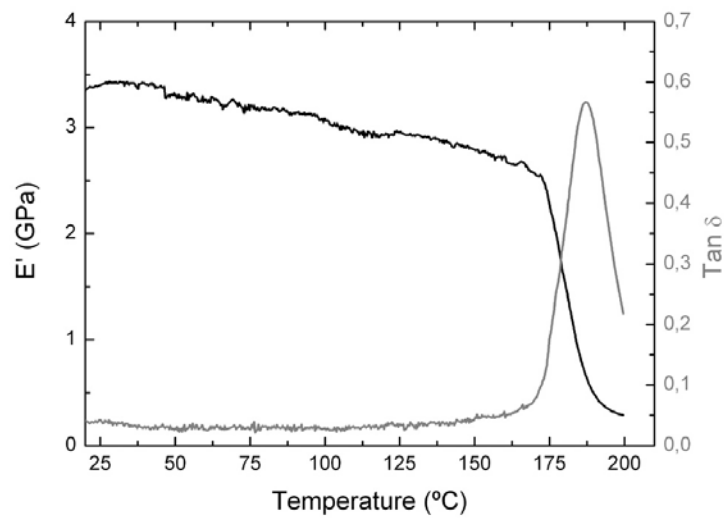

Figure 5.17 – Modulus of elasticity modulus versus temperature of the epoxy/SSF composite material (DMA 3-point bending test)

The experimental data in the temperature working range of the moulding blocks can be described by the linear equation:

$$E(T) = -5.24 \times T + 3.58 \times 10^3 \qquad\qquad 5.2$$

where T is the temperature (ºC) and E is the modulus of elasticity (MPa).

5.2.6 Thermal characterization

The thermal properties of the epoxy/Al composite are shown in Table 5.2. The thermal properties were calculated from 5 samples with 60 mm in diameter and 3 mm in thickness.

Table 5.2 – Thermal properties of the epoxy/Al composite

Thermal conductivity [W.m^{-1}. K^{-1}]	Thermal diffusivity [m^2.s^{-1}]	Thermal resistance [K.m^2.W^{-1}]	Density [Mg.m^{-3}]	Specific heat [J.kg^{-1}.K^{-1}]
0.606 ± 0.034	$0.286 \times 10^{-6} \pm 0.012 \times 10^{-6}$	$4.75 \times 10^{-3} \pm 0.25 \times 10^{-3}$	1.655 ± 0.027	1279.19

5.3   Injection moulding

5.3.1   Processing conditions

The processing conditions were set considering the installed moulding block combination and adjusted to obtain steady processing conditions. The experiments with the two hybrid moulds were identified with alphanumeric codes representing the moulding blocks combination.

In the case of HM-1 the holding pressure (MPa) and the cooling time (s) also were codified. As an example, the code RS36.25 refers to parts produced with resin core and steel cavity, 36 MPa holding pressure and cooling time of 25 s.

In case of HM-2 the code is only related to the moulding block material combination. As an example, the alphanumeric code R_1S correspond to the experiments carried out with epoxy resin filled with aluminium powder (identified as R_1) core moulding block and steel (identified as S) cavity moulding block.

In injection moulding with hybrid moulds not only the moulding properties are important but also the moulding block integrity, especially when less resistant materials are used. The setting of the process conditions was made according to each combination of core and cavity materials, namely the injection pressure, the pressure holding time and the time to fill the part.

The establishment of the holding time was made experimentally through weighing a series of shots at increasing holding time. An example is shown in Figure 5.18 for the injection material (PP Domolen 1100N), injected at a temperature of 230ºC, in the case of R_1S moulding blocks combination using a holding pressure of 56 MPa.
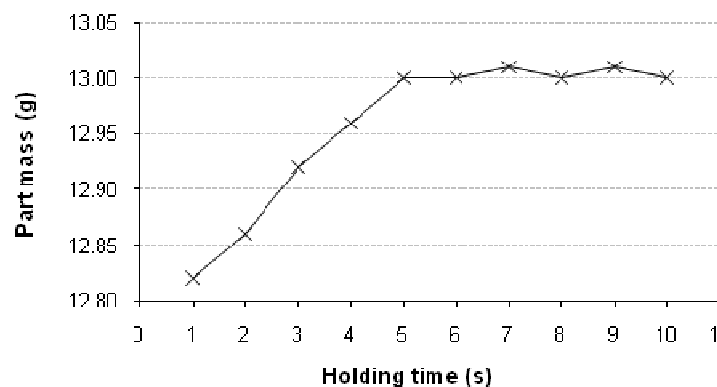

Figure 5.18 – Mass evolution with holding time for PP Domolen 1100 N, injected at 230ºC, in the case of R_1S combination

The fill time depends on the temperature and is important to set the start the beginning of the holding phase. In the Figure 5.19 the case of SS moulding block combination with a ProMetal Pin is exemplified.
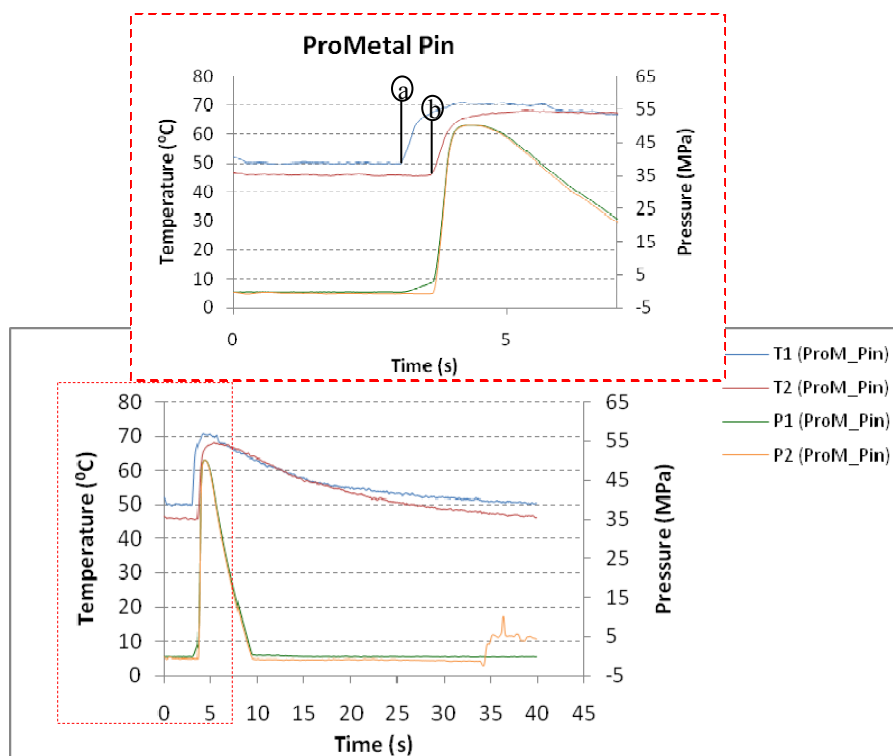

Figure 5.19 - Filling time: Injected polymer reaches the sensor 1 (spot a) and injected polymer reaches the sensor 2 (spot b). The time difference between the instants *a* and *b* is, approximately, the time required to fill the part

When using epoxy composite or SL soft cores, the processing conditions involving pressure were adjusted to cope with the poorer mechanical properties of these materials. The injection pressure and the holding pressure were reduced from that used for the steel core (by 20% for epoxy cores and up to 50% for SL). Conversely, the lower thermal conductivity of these materials leads to an increase of the cycle time up to 60 s.

5.3.2   Pressure monitoring

Typical pressure data for the SS and RS (or R_1S and R_3S) moulding block combinations are shown in Figure 5.20 where data variation over the injection cycle is recorded. These data were obtained from the HM-2 with the pressure and temperature integrated sensors placed in the cavity (P_1) and in the slide group in the core side (P_2) moulding blocks (Figures 4.7 and 4.8), in spots of the part shown in Figure 4.2.
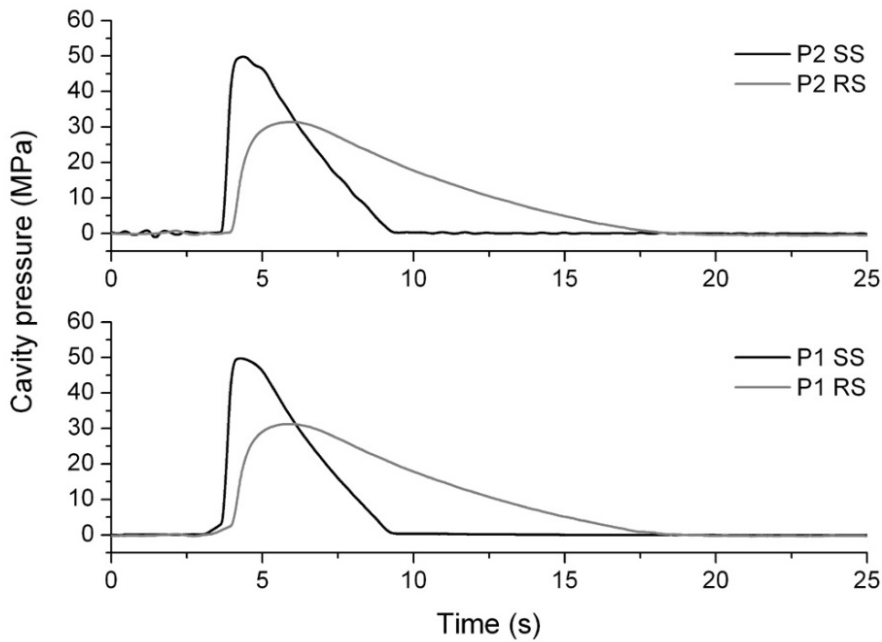
Figure 5.20 - Pressure evolution for SS and RS core/cavity combinations. P1 - cavity; P2 - core

The pressure data plot depends on the materials used in the moulding blocks. An overall view of all moulding block combinations and processing conditions for HM-2 is shown in Figure 5.21.
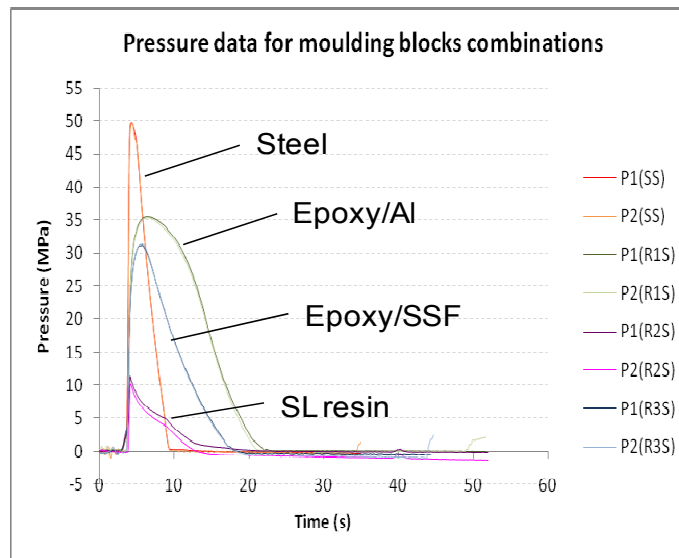

Figure 5.21 - Pressure data for the core/cavity combinations in HM-2. P1-cavity; P2-core

It may be observed that the material combinations with resin lead to a slower decrease of the cavity pressure and the maximum values are always lower than the all-steel combination. The slower drop in the combinations with soft materials reflects the slower and lengthier cooling of the melt whereas the lower maxima result from the sizeable

deformation of the resin blocks that can be estimated, *e.g.*, by structural analysis. This analysis will be more detailed in section 5.8.2.

5.3.3   Temperature monitoring

The evolution of temperature during moulding was monitored as shown in Figure 5.22 for a complete moulding cycle. The figure shows the temperature variation at the cavity moulding surface (sensor T1) and at the core (sensor T2).
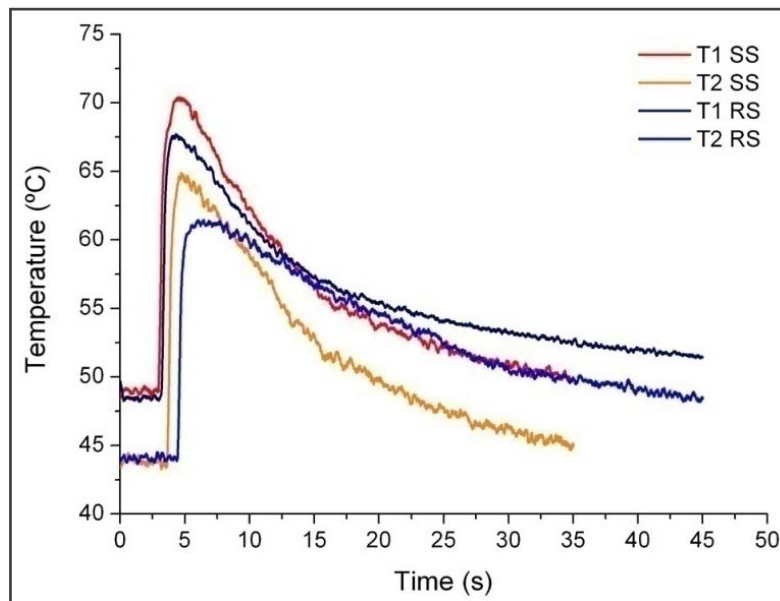

Figure 5.22 - Temperature data for the SS and RS core/cavity combinations. T1 - cavity; T2 - core

An overall view of the temperature data for all the moulding block combinations and processing conditions, when using HM-2, is shown in Figure 5.23. A characteristic feature of the curve profiles involving resin moulding blocks is the slower dropping of the temperature. The lowest temperature curve obtained for the combination R_2S is related with the number of injected parts.
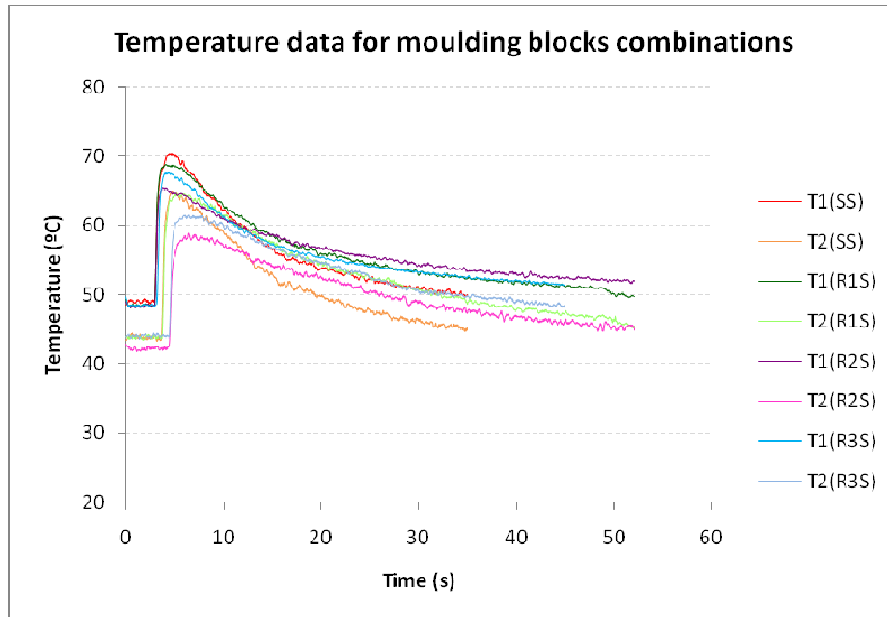
Figure 5.23 - Temperature data for the various core/cavity combinations in HM-2. T1 - cavity; T2 – core

5.3.4   Reproducibility

The reproducibility of the injection moulding process with hybrid moulds was assessed through part weighing, force data repeatability (Figure 5.24), and real time temperature (Figure 5.25) and pressure data collection, as exemplified for the case of SS combination in HM-2 with a ProMetal moulding pin material.
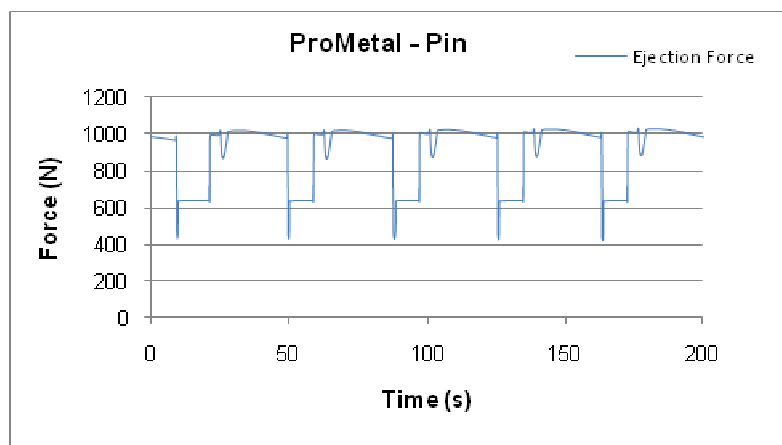

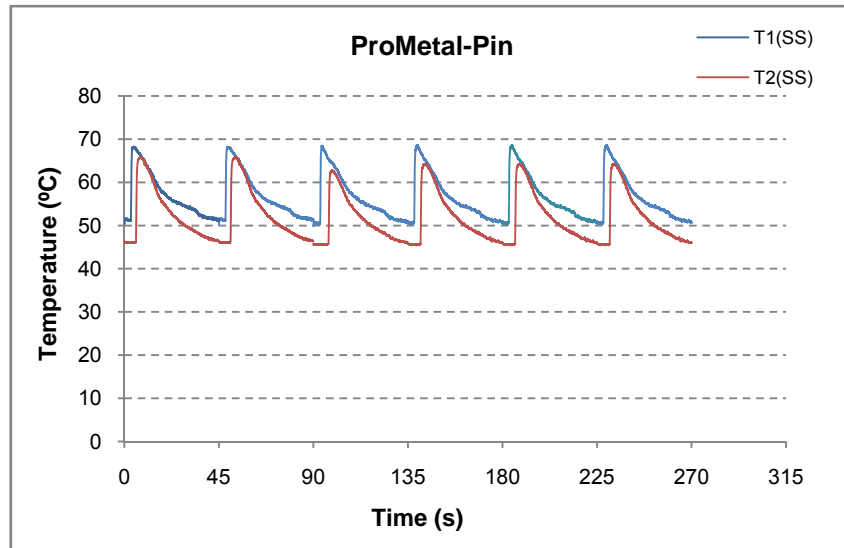Figure 5.24 – Real time ejection force data collection

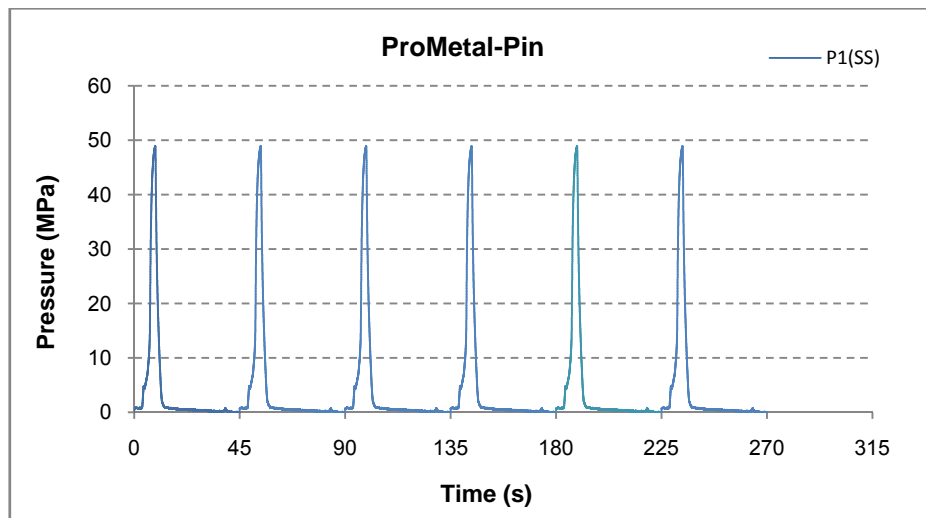Figure 5.25 – Real time temperature data collection

Figure 5.26 - Real time pressure data collection

The mouldings considered for further analyses were those whose weight was inside the range defined by the batch average weight, plus or less one standard deviation. An example for the HM-1 case study is given in Figure 5.27 and Figure 5.28, for the parts injected using identical processing conditions (identified as RS36.25 and RS14.25), *i.e.*, injection temperature of 230ºC, mould temperature of 40ºC, injection pressure of 42 MPa, holding pressure of 36 MPa and 14 MPa respectively, holding time of 5 s and cooling time of 25 s, with a total cycle time of 40 s. The statistic control limits are indicated for a batch of mouldings obtained with a RS combination (Resin-core and Steel-cavity) of moulding blocks. In general it was observed that more than 68% of the mouldings were inside the statistic control limits for all processing conditions and combination of moulding blocks.
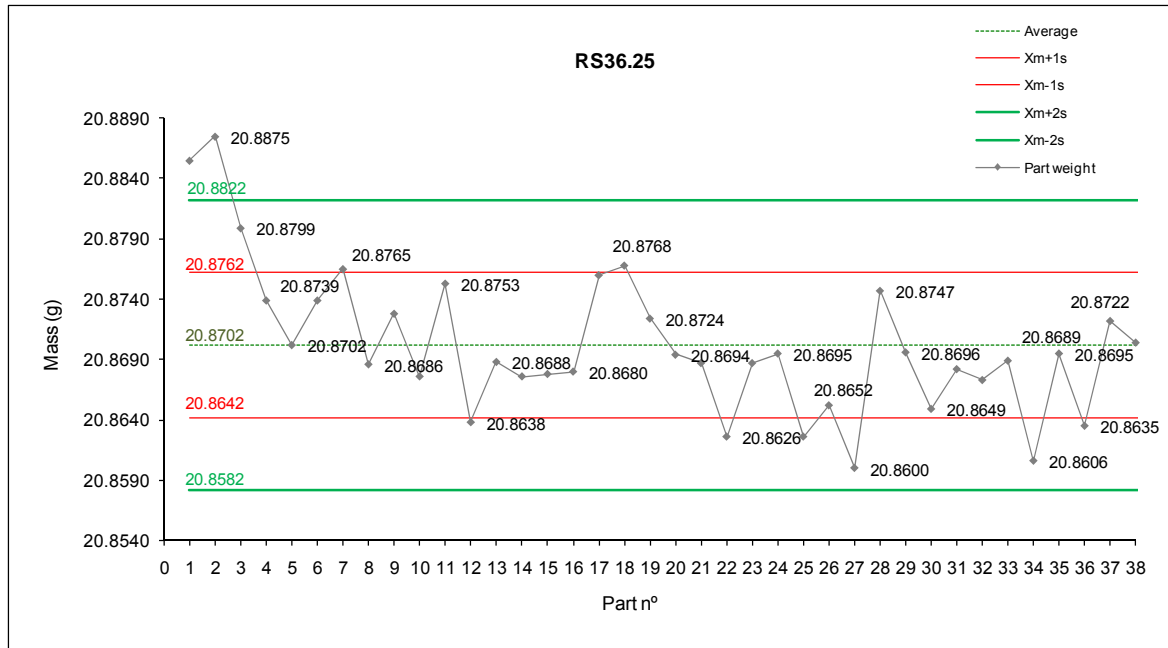
Figure 5.27 – Weight of the mouldings obtained in RS36.25 moulding conditions
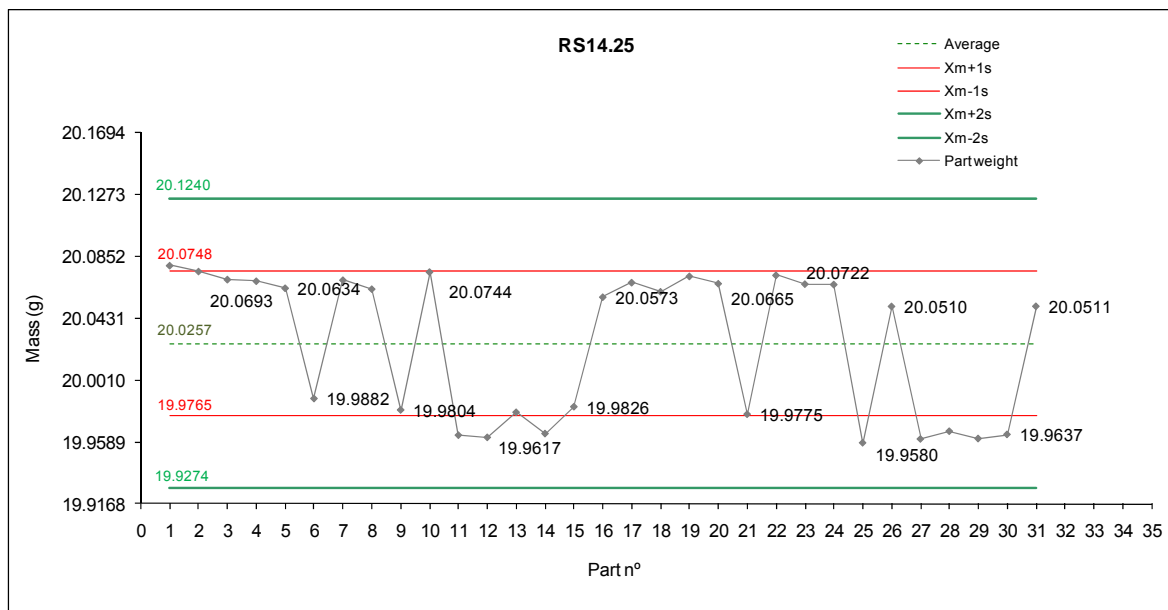

Figure 5.28 – Weight of the mouldings obtained in RS14.25 moulding conditions

A little difference on the weight of the parts obtained in identical process conditions can be observed in Figures 5.27 and 5.28. As expected, it was observed a reduction of mass in the case of lower holding pressure. Figures 5.27 and 5.28 also show that the first injected parts have a little more weight than those injected after. This effect can be associated to the epoxy composite thermal dilatation (Coefficient of thermal expansion $\approx 6.00 \times 10^{-5}$) during the first injection cycles until the mould temperature stabilizes, as it will be further discussed in section 5.8.1.

5.4 Mouldings

5.4.1 Morphology in hybrid moulds

The morphology study of parts made with hybrid moulds was made in the polypropylene 3D tubular parts. The mould HM-1 was used in the conventional all steel configuration and hybrid mould configuration with epoxy composite moulding blocks. The mouldings were produced using three moulding block combinations: Resin in core and Resin in cavity (RR combination); Resin in core and Steel in cavity (RS) and Steel in core and Steel in cavity (SS). The various combinations of core and cavity materials and injection processing conditions were used to influence the morphology of the polypropylene mouldings (Table 4.4 in chapter 4, section 4.6.2). The morphology results, presented in this section, was published elsewhere [195] and attached in appendix 2.

Table 4.4– HM-1 Injection moulding processing conditions

Parameter	Value		
Injection temperature [ºC]	230		
Water cooling temperature [ºC]	40		
Injection flow rate [$cm^3.s^{-1}$]	37.7		
Injection pressure [MPa]	42		
Holding time [s]	5		
Core - Cavity	**SS**	**RS**	**RR**
Holding pressure [MPa]	36	36	14

With semicrystalline materials, as it is the case of polypropylene, it is known that the change in processing conditions lead to important changes in the morphology of the moulded material that in turn influences the product properties [165, 170, 172]. The mouldings in this study were analysed at a mid-distance in the flow path (Figure 5.29) and the through thickness morphology was observed (Figure 5.30).
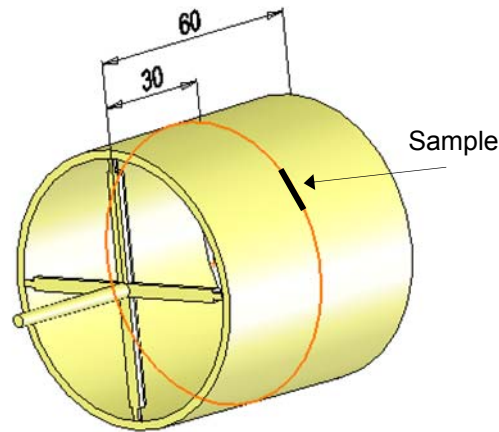
Figure 5.29 – Location of the samples for morphology analyses

The results highlight the effect of the moulding block material in the structures that develop in the mouldings. For one of the processing conditions (Table 4.4) that were used in the study, *i.e.*, injection temperature of 230ºC, mould temperature of 40ºC, injection pressure of 42 MPa, holding pressure of 14 MPa, holding time of 5 s and cooling time of 44 s, with a total cycle time of 60 s, it is evident the influence of the moulding block material thermal conductivity, *i.e.*, the cooling rate that results from it. The resulting microstructures are shown in Figure 5.30.

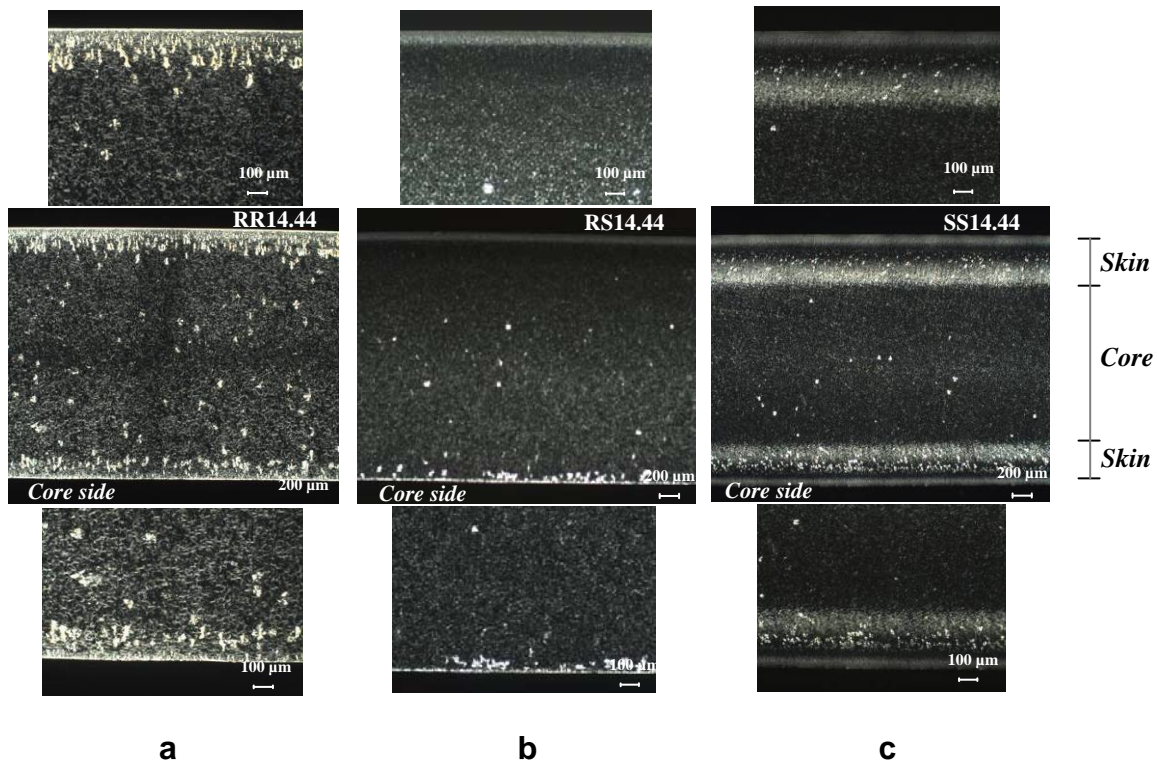**a**   **b**   **c**

Figure 5.30 – Microstructure of polypropylene mouldings in through thickness sections for the moulding blocks combinations: a) RR14.44, b) RS14.44, c) SS14.44

The cooling rates of these mouldings were calculated between the temperatures of 130ºC and 100ºC, using the HM-1 T (t) programme (Figure 3.4). Table 5.3 presents the obtained values for the processing conditions of these mouldings.

Table 5.3 – Cooling rates for processing conditions of these mouldings (T_{inj}-230ºC, T_{mould}-40ºC, t_{cool}-44)

Moulding conditions	RR14.44	RS14.44	SS14.44
Cooling rates [ºC/sec]	0.84	1.23	1.50

In Figure 5.30 different dimensions in cavity and core skins can also be observed. The skin thickness (considered as the external brighter area) and the part thickness were measured in 5 different points along the length of each sample. The average error on the measurements was 3.8% (maximum error of 5.1%). The skin ratio was then calculated by the equation of the skin-to-core thickness quotient as previously referred by Cunha *et al.* [172].

$$Skin\ ratio = \frac{Core\ skin + Cavity\ skin}{total\ thikness}$$ 5.3

Table 5.4 shows the obtained results for the RR, RS and SS moulding blocks combinations.

Table 5.4 – Skin ratio obtained for the RR, RS and SS moulding blocks combinations
(T_{inj}-230ºC, T_{mould}-40ºC, t_{cool}-44s)

	Moulding blocks combinations		
	RR14.44	RS14.44	SS14.44
Total thickness [mm]	2.01	2.01	2.00
Cavity skin [mm]	0.19	0.31	0.42
Core skin [mm]	0.17	0.13	0.33
Skin ratio	0.18	0.22	0.38

As observed in Table 5.4 the mouldings produced in hybrid moulds have smaller skin ratios than those produced in conventional moulds. These smaller ratios derive from a slower cooling process verified in the mouldings produced through hybrid moulds.

Homogeneous moulding blocks

When identical materials are used in the moulding blocks, as the RR and SS combinations, a nearly symmetrical structure develops. These structures show the characteristic laminated microstructure of injection moulded PP, featuring a layered organisation across the thickness. In the case of the SS combination, it is possible to identify the five layers referred to by Fujiyama *et al.* [175]: a spherulitic core, two intermediate crystalline and oriented layers and two highly oriented skins with a characteristic "shish kebab" type structure. However, in engineering studies it is common to consider only three layers as many authors have done [137, 165, 171, 172, 176, 222]. In this case the structure is of the type 'skin-core-skin' and it can be quantitatively described by the skin ratio. The differences found in the layer structures result from the thermo-mechanical history during the injection cycle.

When an RR is used the through-thickness morphology is more uniform and features the β-form spherulites that are associated to slow cooling. These features were observed in the "twin" HM-1 mould by Bareta *et al.* and Gomes *et al.* [148, 185]. The condition for a most favourable appearance of this kind of structure is the molecular orientation. It is required an optimal molecular orientation and cooling rates for them to grow up. As shown in Figure 5.30a, a higher density of β-form spherulites (the coarser and brighter ones) is observed close to the skins and, although the appearance of some β-form spherulites occurred, a greater amount of α-form spherulites (the darker ones) appeared in the core. In the case of the SS combination, well defined skin layers with thin spherulites were observed. It was also possible to see two different layers with thin spherulites due to a change in the molecular orientation, caused by the effect of the holding pressure. The slight difference in the skin structure between the core side and the cavity side can be related with the cooling efficiency on each side of the mould.

Heterogeneous moulding blocks

The heterogeneous RS combination, that is likely to be commonly used in hybrid moulds, gives rise to a non-symmetric distribution of the morphological features with respect to the mid-plane of the section: at the steel side a clear skin with finer spherulites and similar to the SS combination moulds is visible whereas at the resin side a coarser spherulite structure is evident. If the cycle time is shortened, *e.g.*, for 19 s, there will result a visible alteration on the morphology as it is the case of the RS14.25 moulding.

In this case (Figure 5.31) there is an increment of the heterogeneity of the morphology particularly associated to the modification in the resin side of the moulding with a region very populated with β-form spherulites.
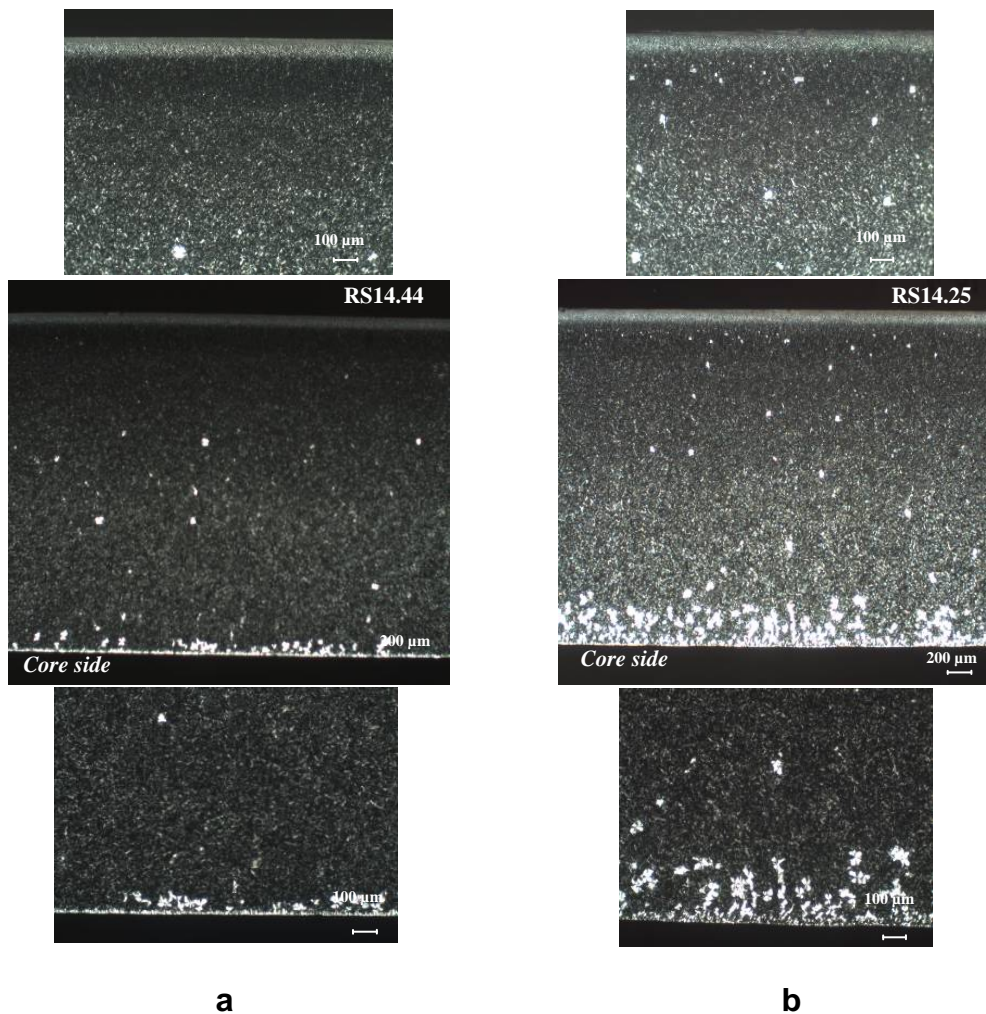

a   **b**

Figure 5.31 - Microstructure of polypropylene mouldings in through thickness sections for the moulding blocks combinations: a) RS14.44 (T_{inj}-230ºC, T_{mould}-40ºC, t_{cool}-44 s), b) RS14.25 (T_{inj}-230ºC, T_{mould}-40ºC, t_{cool}-25 s)

Differences were also obtained in the weight of the mouldings, produced under the same processing conditions but using different combinations of moulding blocks. Table 5.5 resumes the mass average (X_m) and standard deviation (STDV) for the 30 mouldings obtained in RR14.44; RS14.44 and SS14.44 moulding conditions.

Table 5.5 – Mass average and standard deviation of the 30 mouldings obtained in RR14.44, RS14.44 and SS14.44 moulding conditions (T_{inj}-230ºC, T_{mould}-40ºC, t_{cool}-44 s)

Part nº	Mass [g]		
	RR14.44	RS14.44	SS14.44
1	21.0700	20.1367	19.7488
2	21.0578	20.0550	19.7432
3	21.0510	20.0342	19.7454
4	21.0653	20.0516	19.7451
5	21.0700	20.1390	19.7475
6	21.0350	20.0441	19.7455
7	21.0705	20.0417	19.7474
8	21.0670	20.1437	19.7471
9	21.0514	20.1381	19.7463
10	21.0613	20.1310	19.7459
11	21.0517	20.0319	19.7456
12	21.0529	20.0396	19.7449
13	21.0611	20.0232	19.7483
14	21.0392	20.0271	19.7472
15	21.0446	20.0395	19.7435
16	21.0529	20.1265	19.7452
17	21.0456	20.1285	19.7446
18	21.0441	20.1113	19.7474
19	21.0503	20.0498	19.7459
20	21.0415	20.1631	19.7447
21	21.0501	20.0780	19.7451
22	21.0464	20.0694	19.7439
23	21.0434	20.1494	19.7438
24	21.0583	20.0704	19.7557
25	21.0320	20.1617	19.7456
26	21.0336	20.0555	19.7405
27	21.0472	20.0722	19.7438
28	21.0438	20.0718	19.7646
29	21.0487	20.1435	19.7678
30	21.0344	20.0803	19.7560
Xm	21.0507	20.0869	19.7475
STDV	0.0111	0.0466	0.0060

As it can be observed in Table 5.5, the average mass for the RR moulding blocks combination is higher than for the SS combination. Although the coefficient of thermal expansion of the epoxy composite is higher than the steel (Table 4.2), this fact is associated to dimensional and moulding blocks deformation issues. The first ones are related with the shrinkage chain during the production of the epoxy composite moulding blocks (since the master considered was the steel core). The latter deformation issues derive from the use of soft materials, which are submitted to the injection pressures of the moulding cycle.

The mass average and the standard deviation obtained in all moulding conditions considered in HM-1 studies, are shown in Table 5.6.

Table 5.6 - Mass average and standard deviation of the mouldings obtained in HM-1 with the considered moulding conditions (T_{inj}-230ºC, T_{mould}-40ºC, P_{inj}-42 MPa)

Moulding block combination (Core/Cavity)	Cooling time (t_{cool}) [s]	Holding pressure (P_{hold}) [MPa]	Mass average [g]	STDV
Steel/Steel (SS)	12	14	19.6843	0.0031
		36	20.0372	0.0025
	25	14	19.7256	0.0107
		36	20.0676	0.0019
	44	14	19.7488	0.0059
		36	20.0868	0.0062
Resin/Steel (RS)	12	14	19.8534	0.0536
		36	20.7633	0.0379
	25	14	20.0257	0.0491
		36	20.8702	0.0060
	44	14	20.1016	0.0461
		36	21.0044	0.0054
Resin/Resin (RR)	44	14	21.0556	0.0154

5.4.2   Performance analysis

For every processing condition using hybrid moulds it is possible to observe that the material combinations using resin lead to a slower decrease of the cavity pressure and maximum values are always lower than with the steel combinations. This is due to the smaller elasticity modulus of the composite (Table 4.2) used in the moulding blocks and the longer time of the injected polymer until solidification. Usually the most time consuming during the moulding cycle is in the cooling stage, so it is recommended to minimize this period as much as possible.

The cooling time can be estimated applying the Wuebken equation:

$$t_k = \frac{s^2}{\alpha \pi^2} \times ln\left[\frac{8}{\pi^2} \times \frac{T_{inj} - T_W}{T_{eject} - T_W}\right]$$ 5.4

where, α is the material thermal diffusivity, *s* is the part thickness, T_{inj} is the injection temperature, T_{eject} is the average ejection temperature and T_w is the medium mould temperature.

Pressure

These pressure data (Figure 5.32) suggesting a sizeable deformation of the resin blocks evidence the need for structural analysis in those cases. As an example it is possible to see in Figure 5.32 that the pressure curves obtained considering the same processing conditions but with different moulding blocks combinations (SS36.12 and RS36.12) show lower values in the epoxy resin core.
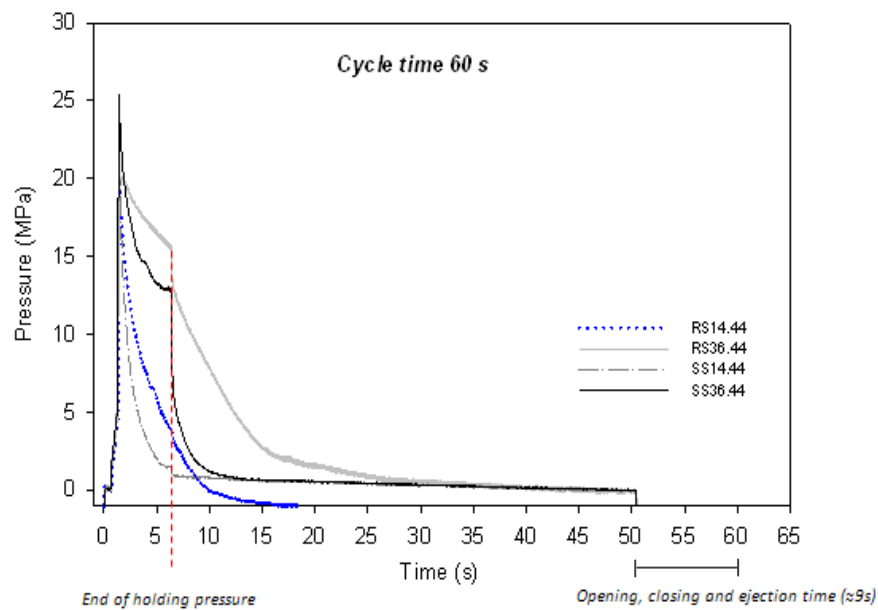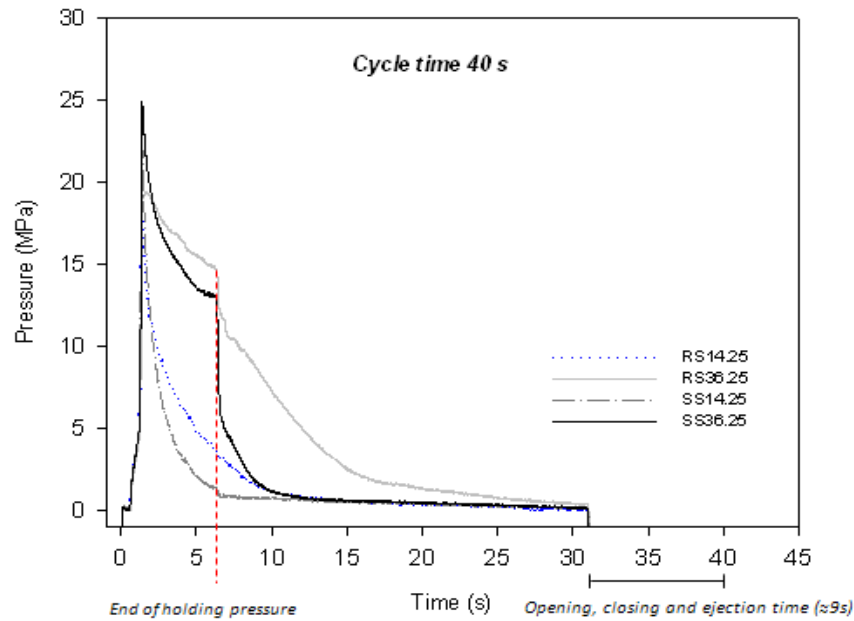

a

b

c
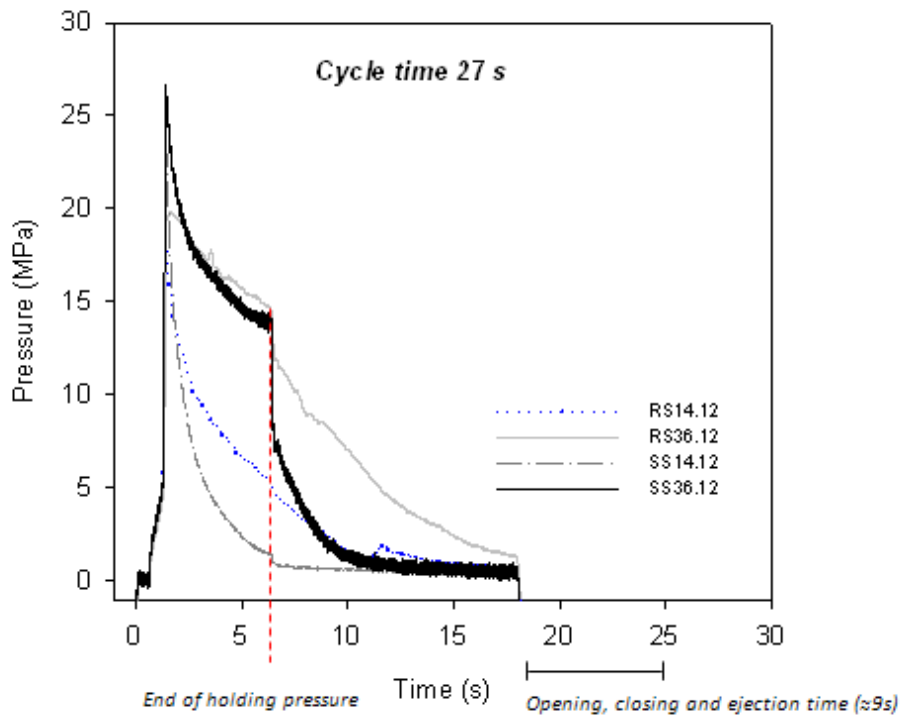
Figure 5.32 - Pressure *vs* time obtained in the indicated moulding conditions: a) 27 s cycle time, b) 40 s cycle time, c) 60 s cycle time

As mentioned before adjustments on the processing conditions, namely, reducing the injection pressures and increasing the cooling time help the hybrid mould performance. In this case, due to the poorer mechanical properties of the resin core material, although the injection pressure was the same from that used for the steel core, the holding pressure was reduced by 40%. The cycle time was increased up to 60 s.

Temperature

The combination of materials in the core and cavity also implies different temperature running levels (Figure 5.33). In Figure 5.33 it is also visible how the temperature varies during consecutive cycles, inside the core (sensor T_5) and at moulding surface of the cavity (sensor T_4). The repeatability between cycles is clear.
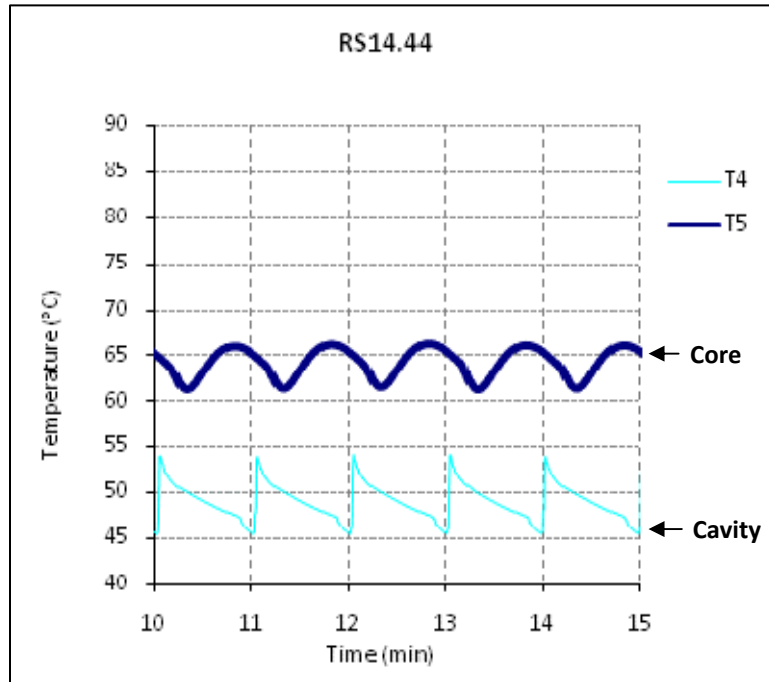

Figure 5.33 - Temperature vs time obtained with RS14.44 moulding conditions (T_{inj}-230ºC, T_{mould}-40ºC, t_{cool}-44 s)

For keeping the moulding cycle within reasonable limits, the moulding blocks of lower thermal conductivity should run at temperatures substantially higher than the coolant medium (typically at 40ºC). The regime temperature must be such that the moulding surface at the beginning of each cycle is always the same.

In the case of both blocks being in epoxy composite the temperature difference between the coolant and the moulding surface is of the order of 40ºC (Figure 5.34). The heterogeneous combination (RS) requires a running temperature in the resin block around 20ºC higher (Figure 5.33) whereas the all-steel mould (SS) runs approximately at 10ºC higher than the coolant medium (Figure 5.35).
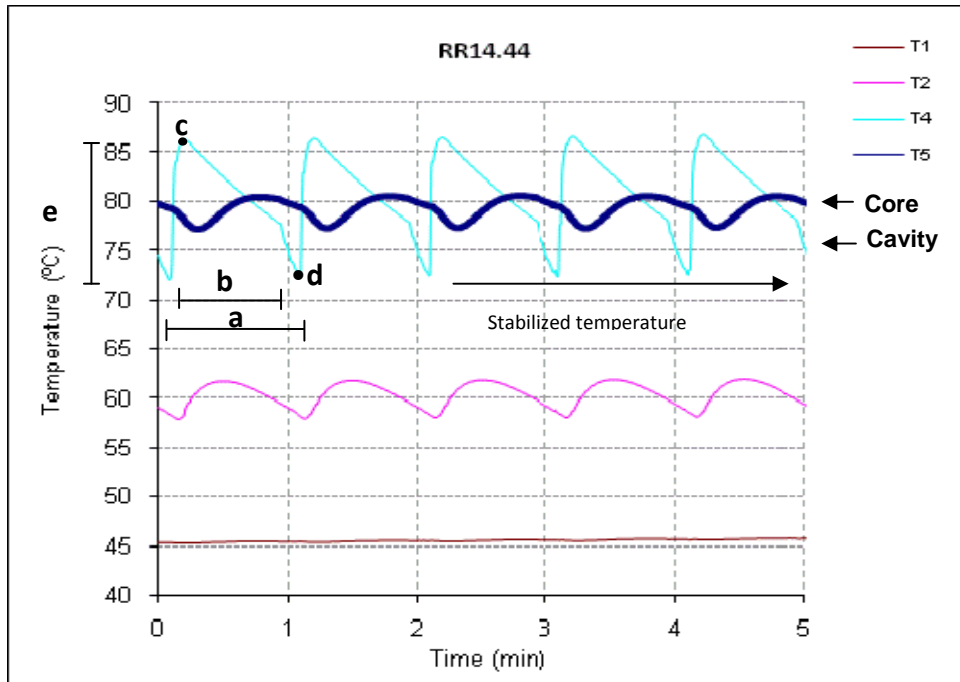
Figure 5.34 - Temperature vs time obtained with RR configuration (T_{inj}-230ºC, T_{mould}-40ºC, t_{cool}-44 s)
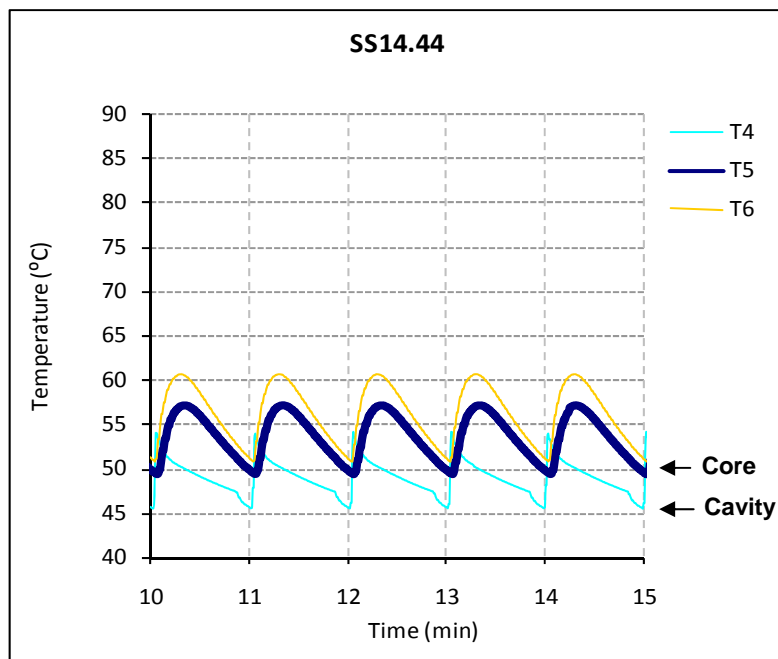

Figure 5.35 - Temperature vs time obtained with SS configuration (T_{inj}-230ºC, T_{mould}-40ºC, t_{cool}-44 s)

These variations result from the combined effect of conductivity of the materials and the expected total cycle time. The cycles depicted in the Figure 5.34 were recorded after the temperatures at the moulding blocks having stabilized, *i.e.*, the temperature at the beginning of the cycle being the same at the end. The temperature monitored by the sensor T_4, at the cavity, shows the steep rise during injection, up to the maximum, **c**, the steady

cooling during the cooling phase, **b**, and the quicker cooling after the opening of the mould down to the start temperature, **d**. It may also be observed the thermal amplitude, **e**, recorded at one of the gates of the impression, and the large gradient between the moulding surface (T_4) and the coolant (T_1), with an intermediate value being recorded by the sensor T_2. These differences are more evident if a comparison is made with the data recorded with the all steel SS configuration (Figure 5.35).

It may also be noted that if the total cycle time is shortened the running temperature of the resin block increases. This is exemplified in the Figure 5.36 that corresponds to a case where the total cycle time was decreased by 19 s compared with the case of the Figure 5.33. The result was an increase of the running temperature of about 10ºC.
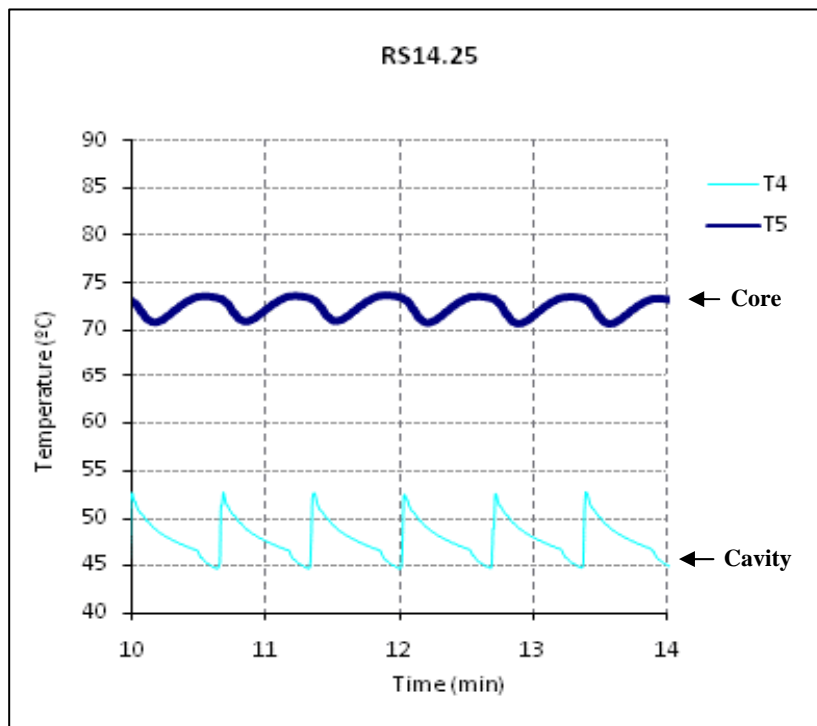

Figure 5.36 - Temperature *vs* time obtained with RS configuration (T_{inj}-230ºC, T_{mould}-40ºC, t_{cool}-25 s)

5.5   Shrinkage in hybrid moulds

Mould temperatures and holding pressure mainly affect the final dimensions of the mouldings. Generally, as observed by Pontes and co-workers, increasing the mould temperature or decreasing the holding pressure lead to higher shrinkage parts [127, 137]. In semicrystalline materials the expected shrinkage percentage can vary from 1% to 2.5%. The shrinkage observed in this study is within this range.

3D tubular parts

The shrinkage of the HM-1 moulded parts was evaluated in terms of the internal diameter of 60 mm of the 3D tubular parts (Figure 4.1). The shrinkage observed in mouldings using resin moulding blocks is much higher than in the SS counterparts (Figure 5.37). It is known that the shrinkage of injection mouldings is governed mainly by the thermal and pressure history during the moulding cycle. In these circumstances these results appear somewhat strange, as the variables involved are not that different apart. Therefore, one could expect that this situation must not be related only to the actual plastics shrinkage but also to the actual deformation of the core during the injection and holding phases of the moulding cycle. This analysis is further detailed in section 5.8.2 through structural simulation of the cores.
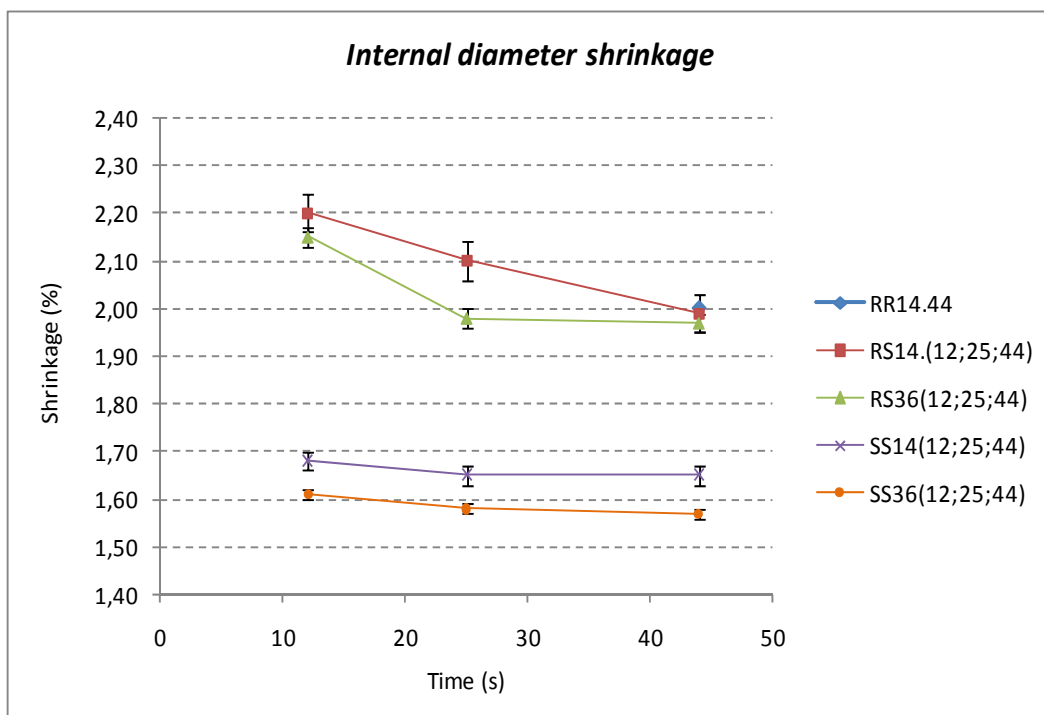

Figure 5.37 - Internal diameter shrinkage

Table 5.7 summarises the main results emerging from the shrinkage study where the holding pressure, the cooling rate and the mould temperature effects were considered.

Table 5.7 - Internal diameter shrinkage in 3D tubular parts

Moulding block combination (Core/Cavity)	Cooling time [s]	Mould temperature [ºC]	Holding pressure [MPa]	Inner diameter shrinkage [%]
Steel/Steel (SS)	12	65	14	1.68
			36	1.61
	25	57	14	1.65
			36	1.58
	44	49	14	1.65
			36	1.57
Resin/Steel (RS)	12	74	14	2.20
			36	2.15
	25	71	14	2.10
			36	1.98
	44	61	14	1.99
			36	1.97
Resin/Resin (RR)	44	78	14	2.00

As it can be observed in Table 5.7, for all cases the smaller shrinkage occurs for higher holding pressure and lower mould temperatures. The results also reveal that shorter cooling times and resin combinations increase the mould temperatures since the cooling water circuit temperature was established on 40ºC.

Support box

The shrinkage of the HM-2 moulded parts was made in selected dimensions of the support box (L1, L2 and L3), as shown in Figure 5.38, and correspondent dimensions of the core moulding blocks. Numerical simulations were carried out using Moldex3D release 9.1 to predict the shrinkage and compare it to the actual part. A further study of warpage in specific locations of this part was published elsewhere [40].
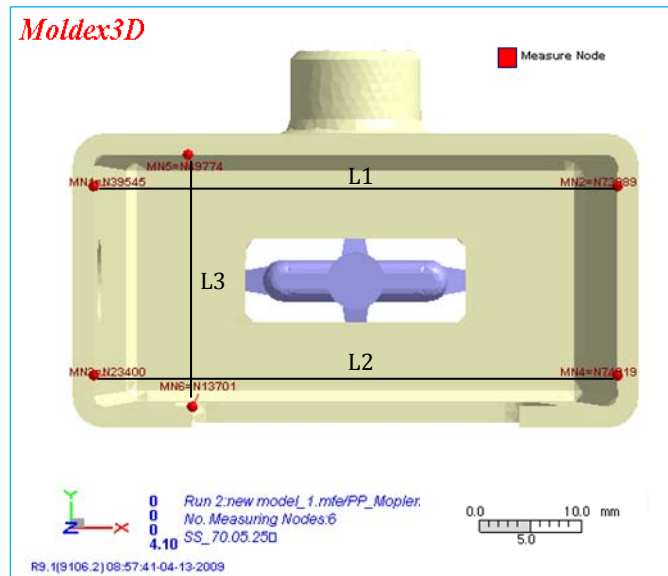
Figure 5.38 - Top view of the support box with nodes and dimensions L1, L2 and L3 for the shrinkage analysis using Moldex3D 9.1

The actual shrinkage, as shown in Table 5.8, is within the expected shrinkage percentage range for the SS combination. For the R_1S (Epoxy-Alum/steel) combination higher shrinkage values were obtained at the specified locations.

Table 5.8 - Shrinkage data at specific locations of the part

Shrinkage [%]	Experimental		Moldex3D 9.1	
	SS	R_1S	SS	R_1S
L1	0.9790	3.6522	1.0341	1.3184
L2	0.8425	12.5843	0.8602	6.5699
L3	1.2634	11.6279	1.3358	1.3358

The shrinkage observed in the moulded parts with resin moulding blocks is much higher than in the SS counterparts (Table 5.8). Similarly to the case of 3D tubular parts, this situation must not be related only to the actual plastics shrinkage but also to the deformation of the core during the injection and holding phases of the moulding cycle.

5.6   **Tribological aspects in hybrid moulds**

As mentioned in chapter 2, section 2.3.3, an important aspect of the operation of hybrid moulds is the wear produced by shrinkage and friction during ejection. During the ejection phase, friction forces are generated between the part (plastic) and the core (typically steel). The coefficient of friction between plastic/steel depends on the surface texture of the core and the ejection temperature [126]. Generally, the ejection force is considered as the result of the contribution of part geometry, mould geometry and material, moulding material and processing conditions [127]. The scheme in the Figure 5.39 gives an idea about the polymer contribution to the ejection force calculation.
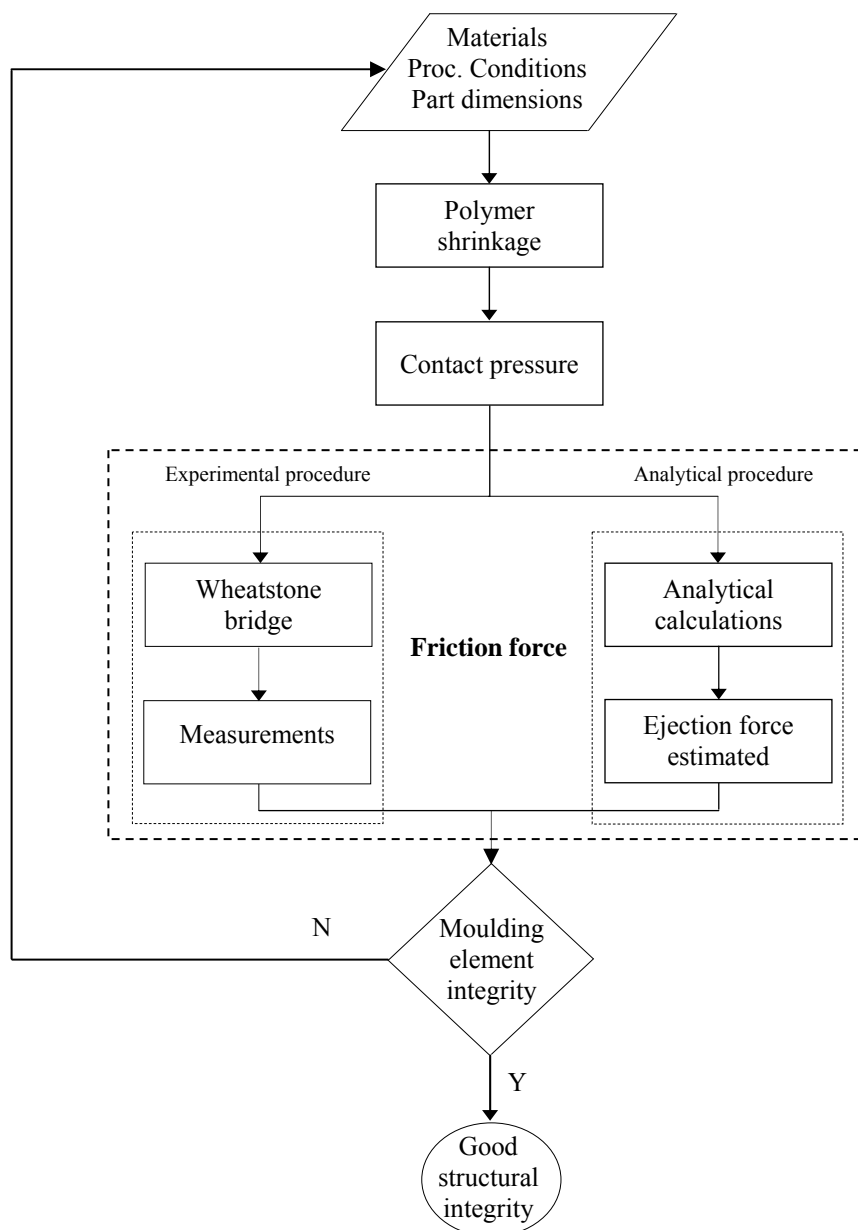

Figure 5.39 - Procedure for the ejection force determination

As shown in Figure 5.39, besides the known dependences on the ejection forces intensity, also aspects related with moulding pins, namely: deformations due to injection pressures, deformations related with the thermal polymer shrinkage, the moulding removal and the mould tension field should be considered on moulding pin structural integrity evaluation.

As mentioned in chapter 4, the tribological study in this work was focused in the HM-2 mouldings, considering the back detail of the support box (Figure 4.24) defined with a moulding pin with a long side movement.

Polymer shrinkage

For assessment and comparison of the shrinkage in the moulding pin region, measurements were made in the points A and B (Figure 5.40) of the seven mouldings after ejection. The results are shown in Table 5.9.

Figure 5.40 - Dimensions A and B for shrinkage analysis in pin region

Table 5.9 – Dimensions obtained in the points A and B of the mouldings measured

Moulding pin material	Epoxy/Al		DSM Somos 11120/2		Epoxy/SSF		ProMetal S4		Steel 1.2311	
Part Nº	A	B	A	B	A	B	A	B	A	B
1	8.20	8.25	8.27	8.17	8.21	8.27	8.15	8.23	8.15	8.35
2	8.19	8.26	8.26	8.18	8.19	8.29	8.14	8.24	8.16	8.34
3	8.18	8.26	8.24	8.18	8.20	8.27	8.12	8.24	8.17	8.30
4	8.19	8.25	8.22	8.17	8.22	8.27	8.14	8.22	8.15	8.31
5	8.20	8.24	7.95	8.19	8.23	8.28	8.13	8.25	8.17	8.33
6	8.22	8.25	7.78	8.17	8.21	8.28	8.15	8.26	8.16	8.34
7	8.21	8.26	7.77	8.18	8.20	8.29	8.15	8.21	8.16	8.31
Average dimension	8.20	8.25	8.07	8.18	8.21	8.28	8.14	8.24	8.16	8.33
STDV	0.01	0.01	0.21	0.01	0.01	0.01	0.01	0.01	0.01	0.02

The initial moulding pin dimensions (before injection) and the A and B average dimensions on parts are shown in Table 5.10. The materials used in the moulding pins are described in chapter 4, section 4.4.2.

Table 5.10 –Moulding pins dimensions and A and B parts dimensions

Molding pin material	Moulding pin dimension [mm] (before injection)		Part dimension [mm]	
	A	B	A	B
Steel DIN W Nr. 1.2311	8.36	8.49	8.16	8.33
Epoxy/Al	8.38	8.45	8.20	8.25
DSM Somos 11120/2	8.28	8.39	8.07	8.18
Epoxy/SSF	8.40	8.51	8.21	8.28
ProMetal S4	8.34	8.41	8.14	8.24

The predicted shrinkage and the measured values at the moulding pin region, for steel and soft materials, are shown in Table 5.11. This results was already published elsewhere [223] and attached in appendix 2.

Table 5.11- Measurements in the moulding pin of the support box and predictions obtained in Moldex3D 9.1

Molding pin material	Shrinkage [%] (Measured on the part)		Shrinkage [%] (Moldex3D 9.1)		Moldex3D 9.1 Relative Error [%]	
	A	B	A	B	A	B
Steel DIN W Nr. 1.2311	2.39	1.88	2.51	1.81	5.02	3.72
Epoxy/Al	2.15	2.37	2.13	2.50	0.09	5.20
DSM Somos 11120/2	2.54	2.50	1.99	2.95	21.65	18.00
Epoxy/SSF	2.26	2.70	2.18	2.63	3.54	2.59
ProMetal S4	2.40	2.02	2.48	1.87	3.23	7.4
				Average	3.85	
				STDV	2.14	

Friction force

The friction force evolution is registered during the friction test depending on the relative displacement between the stample and the moulding specimen. In the typical curve obtained it is important to identificate the maximum friction force [126]. Due to the initial force of the starting test, the friction force to be considered is the difference between the maximum and the minimum registered forces, given by the equation 5.5:

$$F_a{}^{máx} = F_{max} - F_{min} \qquad\qquad 5.5$$

Where, F_{max} is the maximum recorded force and $F_{mín}$ is the minimum recorded force.

The normal force acting on the friction specimen is directly proporcional to the force regulated in the pneumatic device of the apparatus for measuring the friction force. To reach the force aplied efectively on the friction specimen the system was calibrated. The normal force depends of the contact pressure applied by the pneumatic cylinder. The linear equation obtained in the system calibration [48] was:

$$F_n = 1.85 \times p_{ap} \times 10^3 + 14.43 \qquad\qquad 5.6$$

where: p_{ap} is the contact pressure applied by the pneumatic cylinder.

This equation was derived from a linear regression obtained with experimental data (Figure 5.41).
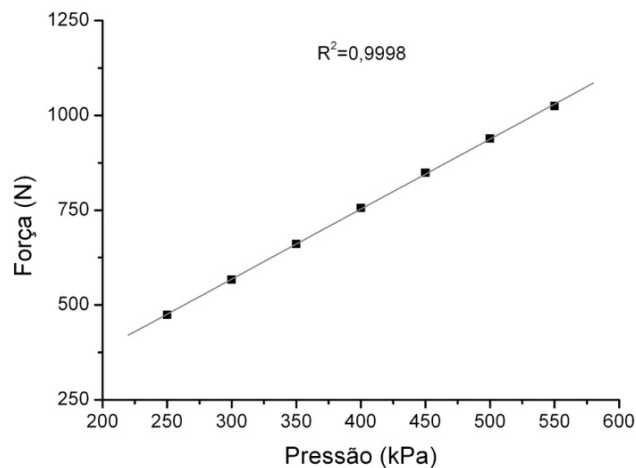
Figure 5.41 – Linear regression of the experimental data for system calibration (source: Sabino-Netto [48])

Ejection force

The ejection forces are recorded and estimated for the various pin materials used. These data are derived from recorded graphs as in Figure 5.24 after defining the baseline.

The estimated values of the ejection force were calculated as mentioned in chapter 3, section 3.1.3., using the equation:

$$F_{eject} = \mu_e \times p_c \times A_c$$

The coefficient of static friction, μ_e, was determined experimentally in as-moulding conditions and the corresponding data is detailed in the Table 5.12 for each pair of materials in contact.

Table 5.12 - Coefficient of static friction determined experimentally

Stamp material	Pressure (p_{ap}) [bar]	Temperature [ºC]	Fn [N] ($Fn=1,85 \times p_{ap} \times 10^3 + 14,43$)	Friction force [N]	Coefficient of friction
Steel (DIN W Nr. 1.2311)	6.5	65.0	1216.93	313.7	0.258
Epoxy/Al	3.5	65.0	661.9	213.9	0.323
Epoxy/SSF	3.5	65.0	661.9	205.2	0.310
ProMetal S4	5.0	65.0	939.4	241.4	0.257

The contact pressure acting on the moulding pin (p_c) was calculated taking into account, shrinkage of the polymer, the thermal expansion and the deformation of the moulding, as mentioned in chapter 3, section 3.1.3. In the Table 5.13 is shown the recorded ejection forces and the estimated ones.

Table 5.13 - Recorded ejection forces with the use of steel and soft materials

Molding pin material	Ejection force (N) measured by the load cell $F_{eject}= ((\varepsilon -0.0006)/ (8 \times 10^{-6})) \times 9.81$	Coefficient of static friction Measured	Ejection force (N) estimated $F_{eject}= \mu_e \times p_c \times A_c$	Relative Error (%)
Steel (DIN W Nr. 1.2311)	415.58	0.258	434.87	4.64
Epoxy/Al	613.12	0.323	723.66	18.03
DSM Somos 11120/2	689.70	0.475	898.75	-
Epoxy/SSF	619.50	0.310	747.93	20.73
ProMetal S4	423.79	0.257	446.50	5.36

5.7 Tool integrity

Several problems are connected to the structural integrity of moulding elements when "soft" materials are used. This section shows the results obtained in this research work, with the moulding blocks produced in SL and epoxy-based composite materials. Possible associated reasons and related work are also discussed. The results presented in this section was already published elsewhere [213] and attached in appendix 2.

5.7.1 Stereolithography blocks

In the case of the R_2S combination, soon the runner system damaged itself, as shown in Figure 5.44. The failure of the SL core started at the gating region as already observed by Ribeiro Jr, 2003. The complete filling of the parts was only possible with injection pressure of 42 MPa. However at 28 MPa vestiges of resin in the mouldings started to appear, as shown in Figure 5.45. This is associated to the thermal effects and the shrinkage and resulting stresses. These influence the ejection forces at the gating zone as it was also pointed out by other authors (*e.g.* [9, 57, 184, 192]). For instance, Figure 5.42 shows the part temperature for the case of R_2S (SL resin/Steel - core/cavity combination).
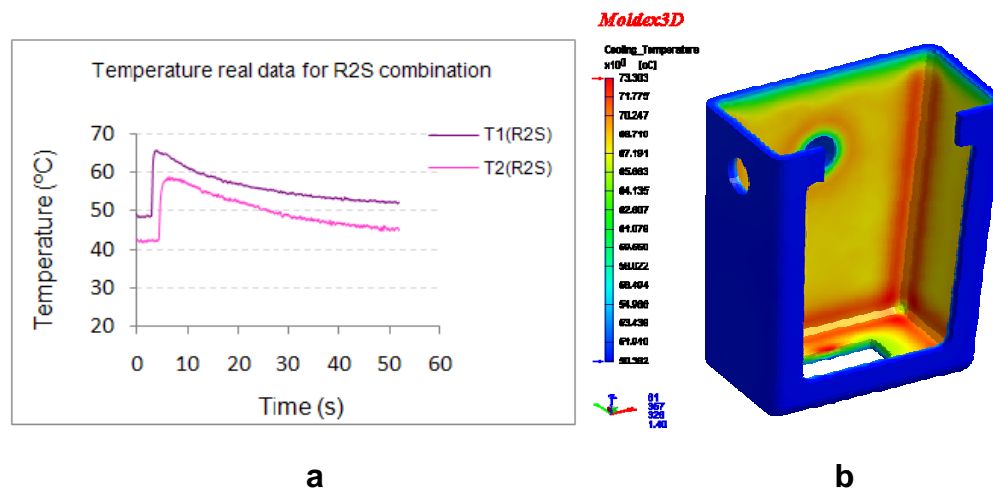
Figure 5.42 – Part temperature for the case of R_2S (SL resin/ Steel - core/cavity combination): a) measured on part sensors locations, b) predicted by Moldex3D 9.1

As it was observed in the real profiles and part field temperatures predicted by Moldex3D 9.1 (Figure 5.42) the minimum value reached, during the moulding cycle, is about 42ºC (at the starting cycle) and maximum values are never lower than 58ºC. The glass transition temperature of the SL resin used is approximately 45ºC (DSM Somos 11120 data sheet). In these thermal conditions, the SL resin loses some of its mechanical strength and stiffness,

i.e., shifts from an elastic state to a viscoelastic state. Thus, it is convenient to use resins with glass transition temperature at least 15ºC higher than the working temperature of the mould.

During the filling stage of the moulding cycle the mould temperature rises because of the heat transferred from the melt to the mould wall by heat conduction. A typical mould temperature variation cycle during the first shots, in a hybrid mould with steady coolant action, is illustrated in Figure 5.43.
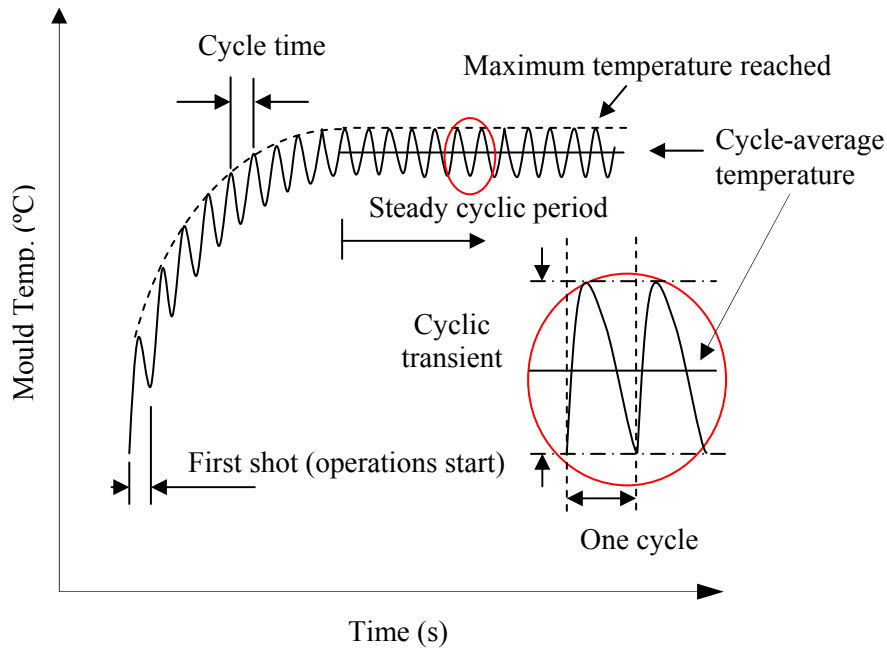
Figure 5.43 – Typical mould temperature evolution in first injection cycles

At the beginning of the moulding series, the temperature variation is significant during some shots. Then, it gets to a steady state which is maintained during the moulding production. Hence, conventionally, it is reasonable to use the cycle-average temperature as the mould temperature along the time. However, with the use of specific materials in moulding elements, such as the SL resins with low glass transition temperature and low thermal conductivity, it is most important to control the maximum temperature reached during the injection cycle.

Also the material chemical affinity is associated to mould failure. The Hildebrand parameter (ξ), reflects the material solubility and can provide information useful to design [122]. Although adhesion between the injected material (ξ =18 MPa$^{1/2}$) and the moulding block material (ξ =22 MPa$^{1/2}$) was verified in the runner system (Figure 4.44).

<center>**a**   **b**</center>
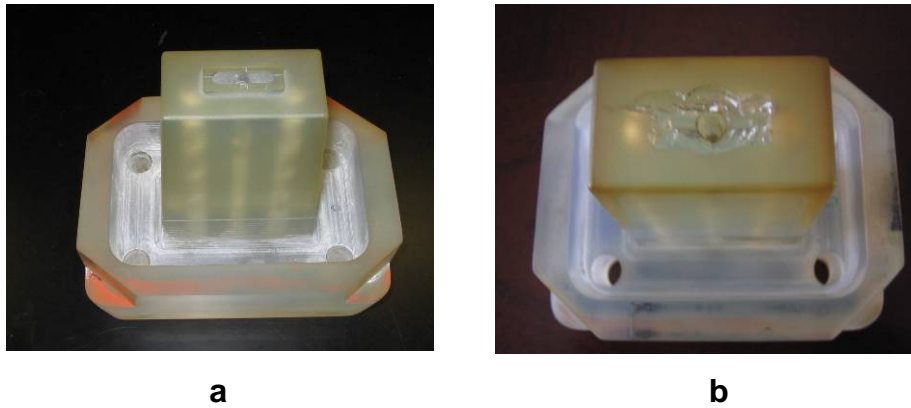
Figure 5.44 - Runner system of the Somos 11120 resin core moulding blocks: a) before injections, b) after injections

As a result of the core damage the quality of the injection was not good. Experimentally, it was possible to fill the part using low injection pressure values. Upon increasing the pressure of injection (values of 20 to 25 bar hydraulic pressure) debris of resin began to appear on the mouldings (Figure 5.45).

<center>Figure 5.45 - Residues of SL resin in the mouldings</center>

At 30 bar, it was possible to fill completely the impression and form the part. Using a holding pressure of 10 bar during 2 s it was possible to inject 17 parts before the runner

system was completely damaged (Figure 5.46). A slightly longer life was obtained using lower mould temperature of 22ºC.
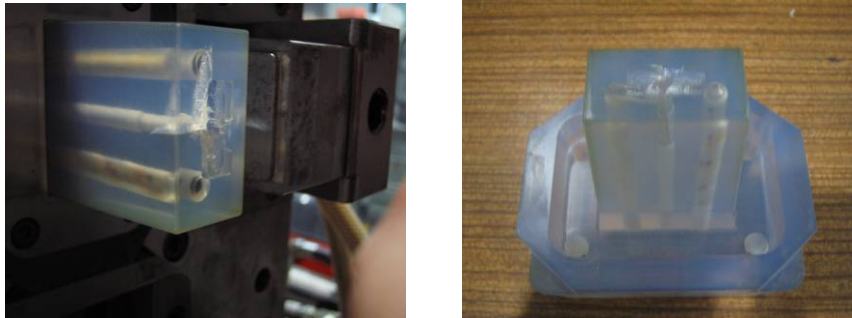
Figure 5.46 - Runner system of the Somos 11122 resin core moulding blocks after injections

This poor lifewise performance of SL tools were in line with observations by Hopkinson and co-workers [57, 192].

5.7.2 Epoxy-composite blocks

The operation of the hybrid mould using the R_1S configuration with epoxy composite in the core block was more long lasting (Figure 5.47). Failure happened eventually, starting at gate area and at the moulding surfaces.

a   **b**
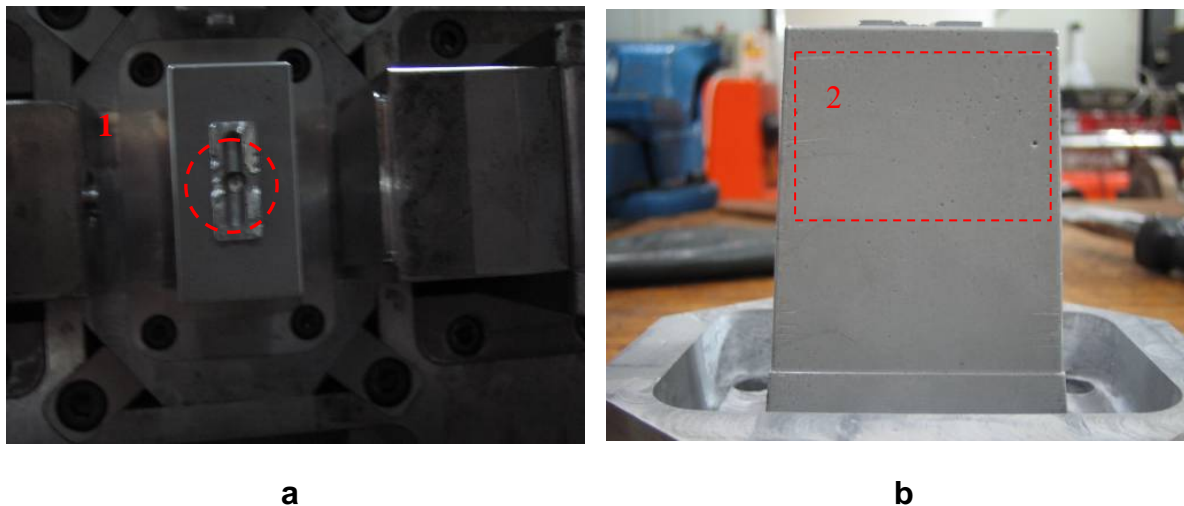
Figure 5.47 - Failure of the epoxy/Al core moulding block: a) runner system, b) moulding surface

The failure at the gate area, also verified by Bareta 2007, is most probably associated to the thermal fatigue. The pitting at the moulding surfaces could be associated two distinct effects: the erosion originated by the consequently injection pressures that leads to the loosening of particles or the adhesion between the aluminium particles and the injected polymer due Hildebrand parameters of the two materials in contact that these loosen

particles penetrate into downstream zones of the block causing surface degradation. It is also possible but less probable, that these loosen particles penetrate into downstream zones of the block causing surface degradation. The erosion effect was previously mentioned and observed by Bareta, as shown in Figure 2.14 [95], and the adhesion effect was also previously mentioned by Gonçalves and co-workers [93].

The R_1S combination is adequate for production of series of several hundred parts. After 300 mouldings no visible defects were seen in the composite core. The equivalent R_3S combination, with the epoxy/SSF composite core, starts to deteriorate close to the gate, as shown in Figure 5.48.

| a | b |
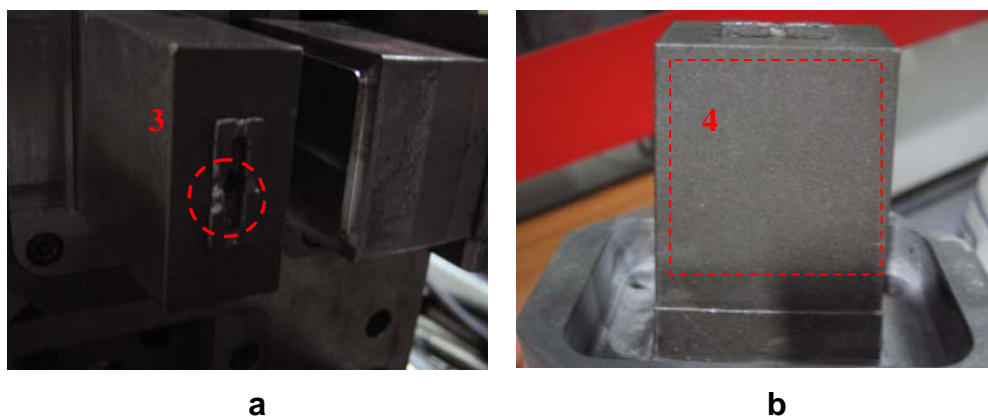
Figure 5.48 - Epoxy/SSF core moulding block failures: a) runner system, b) moulding zone

The composite with SSF is prone to additional mechanical problems, especially in the sliding zones. Some steel particles from the core cause seizing in the mould surfaces in contact, as illustrated in the Figure 5.49. The block faces did not show any defects after the production run. However this problem is easily solved if higher gap tolerances are used in the sliding zones.

a

b

c
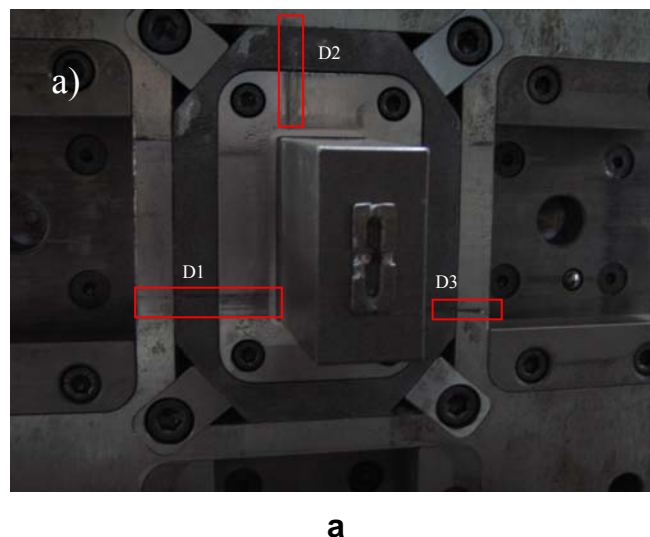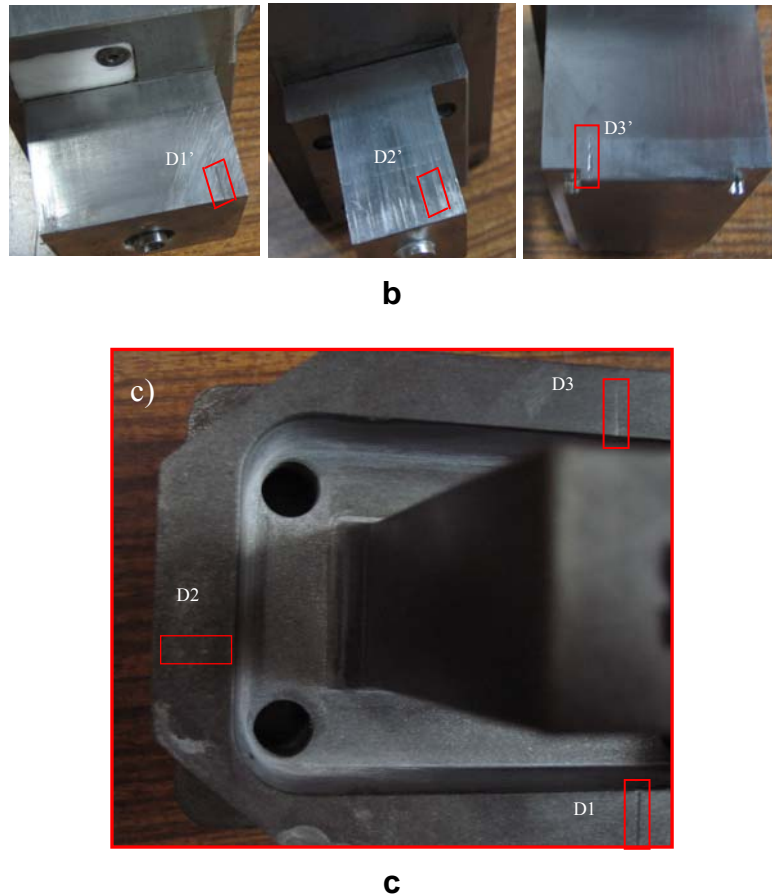
Figure 5.49 - Seizing in steel components when epoxy/SSF composites are used in the core: a) scratching zones, b) and c) seized components

5.7.3   Moulding pins

Regarding the performance and structural integrity of the different moulding pins materials used, to define the back detail of the support box, it was observed that only those made from stereolithography presented problems. After about 20 shots the failure of the SL inserts occurred as depicted in the Figure 5.50.

a   **b** (19th shot)   **c** (20th shot)
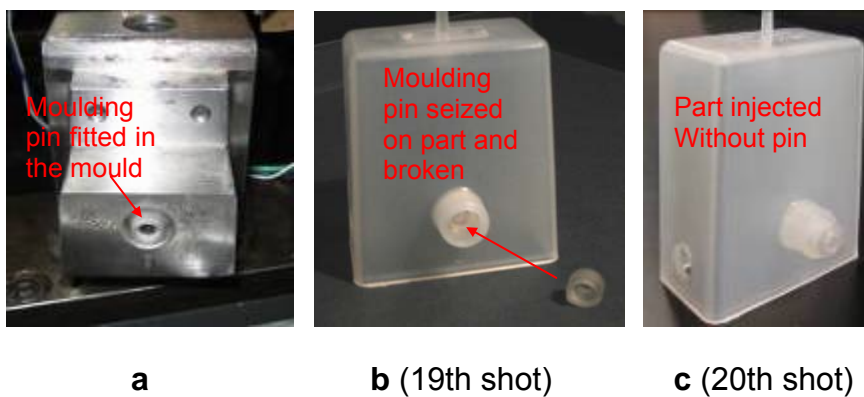
Figure 5.50 - Moulding pin part zone when using the Somos 11120 pin: a) moulding pin fitted in the mould, b) and c) aspects of the failure of the pin when moulding PP

The failure was a combined result of the shrinkage and resulting stresses in this zone. The problem was worsened by the adhesion between the moulded material and the moulding pin material. The adhesion is likely when the Hildebrand factors of the materials are close to each other [125]. PP and epoxy have Hildebrand factors rather close, 18 MPa$^{1/2}$ for the PP and 22 MPa$^{1/2}$ for the epoxy. The low glass temperature of the SL resin (≈45ºC) is an additional problem considering the running temperature of the mould (≈50ºC) and the maximum temperature reached (between 65ºC and 70ºC). These results suggest that the use of SL in core blocks is not recommended for productions runs over 10-20 parts.

5.8 Simulations

In hybrid moulds for plastics materials with low thermal conductivity as epoxy composites or stereolithography resins require a *warming up* period so that a regime mould temperature is achieved. Also, the temperature at the interface 'moulding surface–polymer moulding' has characteristics that are not commonly integrated in design tools. Furthermore the lower stiffness and strength of epoxy composites used in the moulding blocks make necessary an accurate prediction of the pressure field during the moulding cycle for guaranteeing moulding repeatability and block reliability. The complexity of these problems imposes the use of computing tools in the design process.

The main objective of the numerical simulations in hybrid mould design is to predict its performance during the moulding process. In this work the thermal and flow processes were simulated using the commercial software Moldex3D 9.1. The structural integrity and performance of moulding blocks produced in "soft materials" was estimated using the software ANSYS Workbench 11.0. These predictions were compared with experimental data gathered with the pressure and temperature sensors that were used in the instrumentation of the hybrid moulds.

5.8.1 Thermal analysis

The simulation of the injection moulding process with Moldex3D was focused on the HM-2 injection moulding studies. The simulations were made using the same processing conditions used in the experimental work.

In the modelling of the hybrid mould the architecture of the cooling system, the impression, the runner system layout and injector were included as shown in Figure 5.51.
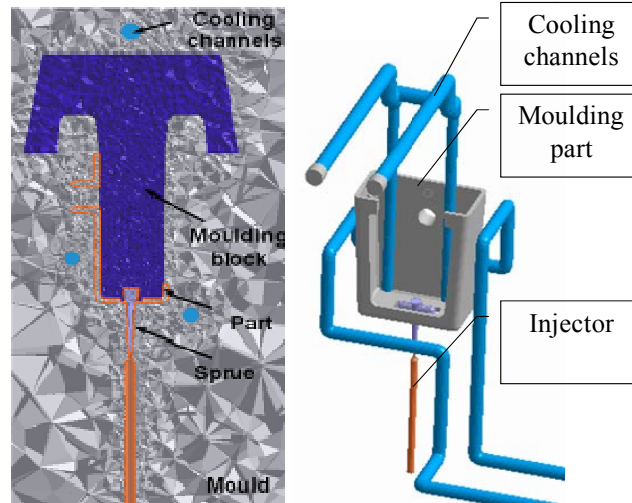
Figure 5.51 - Model and cooling architecture used in Moldex3D

The software was assessed by comparing the simulations with thermal and flow data from the mould with standard DIN WNr.1.2311 tool steel moulding blocks. For the hybrid moulds the prediction of the temperature and the pressure fields was also made for successive injection cycles.

The prediction of the shrinkage was made in the region of the moulding pin showed in Figure 4.24.

Thermal performance

The numerical simulations of the thermal performance were focused in support box produced with HM-2. The evolution of the temperature during moulding was monitored, as exemplified in Figure 5.52, for a complete moulding cycle, when using the tool steel and the epoxy-based composite aluminium, with the respective processing conditions showed in Table 4.4. The temperature at the moulding surface of the cavity was monitored with the sensor T_1, and at the core with the sensor T_2, as shown in Figure 5.53. The main findings presented in this section were previously published elsewhere [213, 214, 223] and attached in appendix 2.
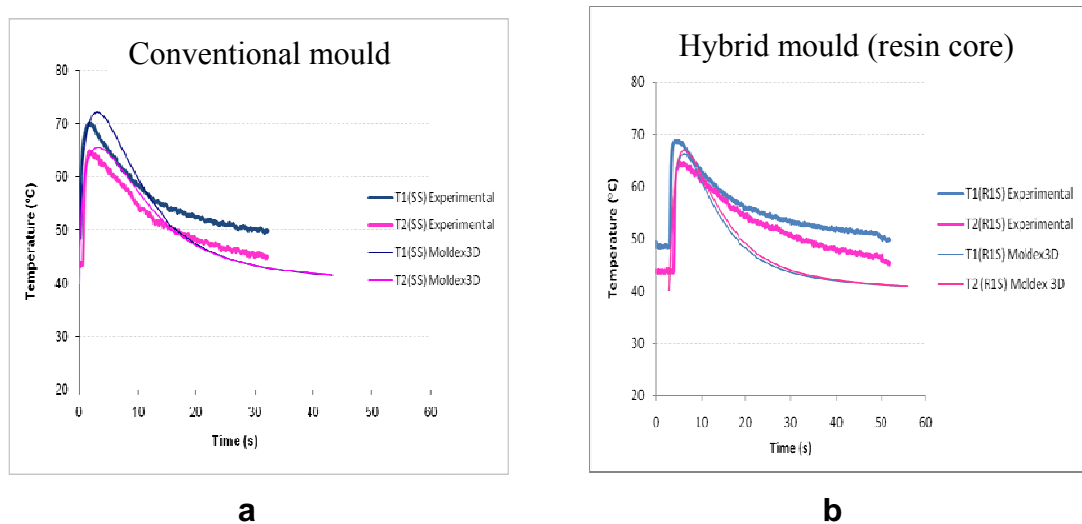
Figure 5.52 - Temperature comparison between experimental and predicted values for the: a) steel/steel and b) epoxy-Al/steel, cavity/core combinations. T_1 - cavity; T_2 – core
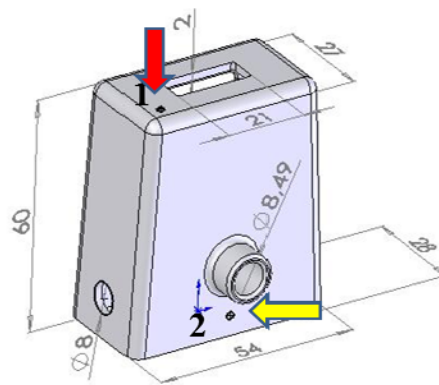
Figure 5.53 - Sensor location on the part (T_1 placed on the cavity side and T_2 on the core side)

The data obtained with T_2 in the conventional and the hybrid moulds highlight the influence of the higher thermal resistance of the moulding blocks with lower thermal conductivity (Figure 5.52). This fact also contributes for longer cycle times to produce parts in hybrid moulds and higher regime mould temperatures.

Figure 5.54 shows the temperature evolution over a complete cycle at the moulding surface of the core (T_2) in the conventional mould and in the hybrid mould with different core moulding blocks materials. These data highlight the major influence of the thermal conductivity of the materials used in the moulding blocks on the temperature evolution at the parts. The parts produced in moulding blocks made with resin reach a higher temperature, especially throughout the cooling time, when compared with the conventional mould.

The slower temperature decay observed for the combination R_2S (Figure 5.54) is caused by the lower thermal conductivity of the stereolithography resin of the core.
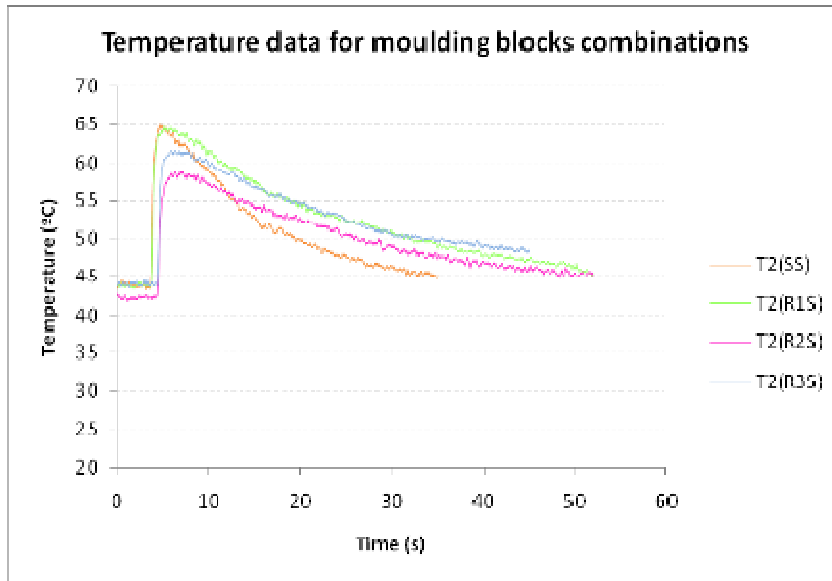
Figure 5.54 - Temperature data at the core side

In the pin region, the field of temperatures as predicted by Moldex3D 9.1 is depicted in the Table 5.14. As mentioned before, in these experiments only the moulding pin was changed, the core and the cavity moulding blocks was always in tool steel. Further simulation analyses are presented in appendix 5.

Table 5.14 - Field of temperatures predicted for different materials in moulding pin

Steel DIN W Nr. 1.2311	ProMetal S4	Epoxy/Al	Epoxy/SSF
52ºC Max Temperature	51ºC Max Temperature	77ºC Max Temperature	87ºC Max Temperature

For the steel and ProMetal moulding pins the field of temperatures are similar. Higher temperatures are reached when epoxy-based composites are used, contributing, in these cases, to the higher polymer shrinkage (Table 5.11).

Mould temperature stabilization

When low thermal conductivity materials are used the temperature evolution in the first injection cycles changes until stabilization is reached. This stabilization depends on the expected cycle time. Thus it is necessary to know which the mould temperature is when the moulding cycle is stabilized.

Figure 5.55 shows the simulation of the mould temperature evolution during the initial injection cycles. In the case of SS combination (Steel/Steel in Core/Cavity), when using the PP Domolen 1100 N, the processing conditions showed in Table 4.5 (T_{inj} 230ºC, T_{mould} 40ºC, P_{inj} 91 MPa, P_{hold} 70 MPa, t_{hold} 5 s, t_{cool} 25 s) and a cycle time of 43.3 s, the mould temperature stabilizes after 4 cycles. In the case of the RS combination (Epoxy-Al/Steel in Core/Cavity), when using the PP Domolen 1100N, the processing conditions showed in Table 4.5 (T_{inj} 230ºC, T_{mould} 40ºC, P_{inj} 70 MPa, P_{hold} 56 MPa, t_{hold} 10 s, t_{cool} 35 s) and a cycle time of 58.3 s, 10 shots are required until the process is stabilized, *i.e.*, the temperature at the beginning of the cycle is identical to the end.
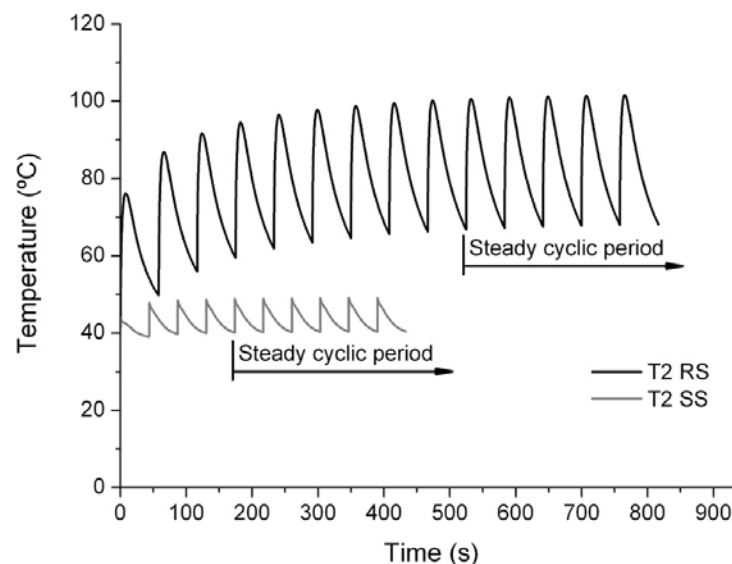
Figure 5.55 - Temperature evolution in first injection cycles predicted by Moldex3D (SS cycle time = 43,3 s; RS cycle time = 58,3 s)

Therefore, the definition of the moulding surface temperature at the beginning of the moulding cycle, in stabilized conditions, depends of the required cycle time. Rapid cycling leads to higher service temperatures, as shown in the Moldex3D 9.1 simulation conclusions in Figure 5.56 for the case of RS combination with the injected material and processing conditions mentioned above.
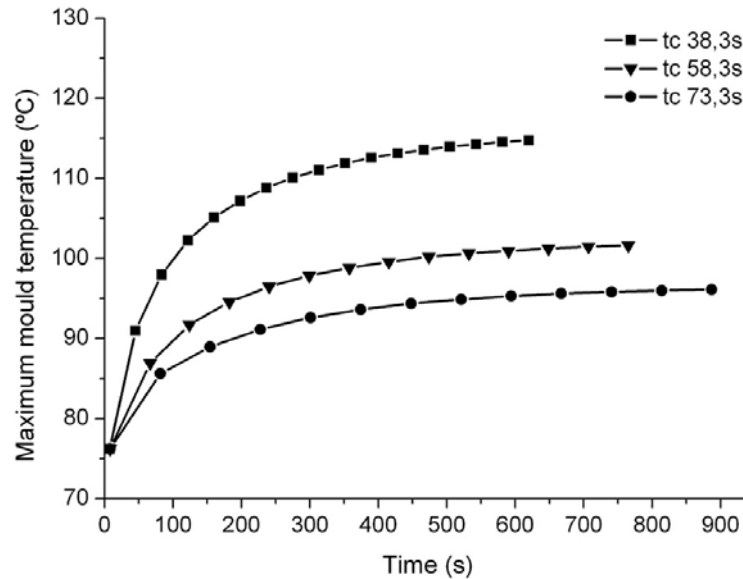

Figure 5.56 - Temperature evolution during the initial injection cycles of the RS combination, as predicted by Moldex3D 9.1 for different injection cycle times

The computer simulation tools show accordance between the experimental values and the predicted ones.

5.8.2   Structural analyses

The structural analyses in the two hybrid moulds were made with the software ANSYS Workbench 11.0. The pressure and temperature fields during the injection cycle were considered in the simulations.

Mould HM-1

In the HM-1 studies the structural simulations were made to compare the deformation of steel and resin composite cores.

As boundary conditions to use in the simulations, it was considered that the bottom face of the core was bonded to the mould plate (Figure 5.57), and the temperature of the core in the moulding region increased linearly from 40ºC up to the actually monitored temperature

in each of the studied cases . For the actual calculations the properties of the materials shown in Table 4.2 were input in the program database (Figure 5.58), as well as the pressure *p* recorded during the tests.
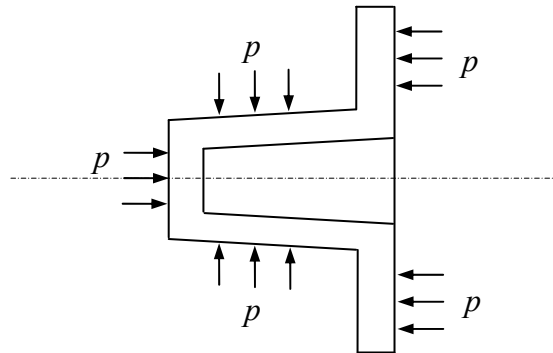
Figure 5.57 - Boundary conditions imposed in the program database

Figure 5.58 – Properties of the Epoxy/Al resin inputted in the program database

Figure 5.59 shows the simulation results of the radial elastic strain field of the steel core is and establishes a maximum strain of 0.0085% at the middle region of the core. Further details are presented in appendix 6.
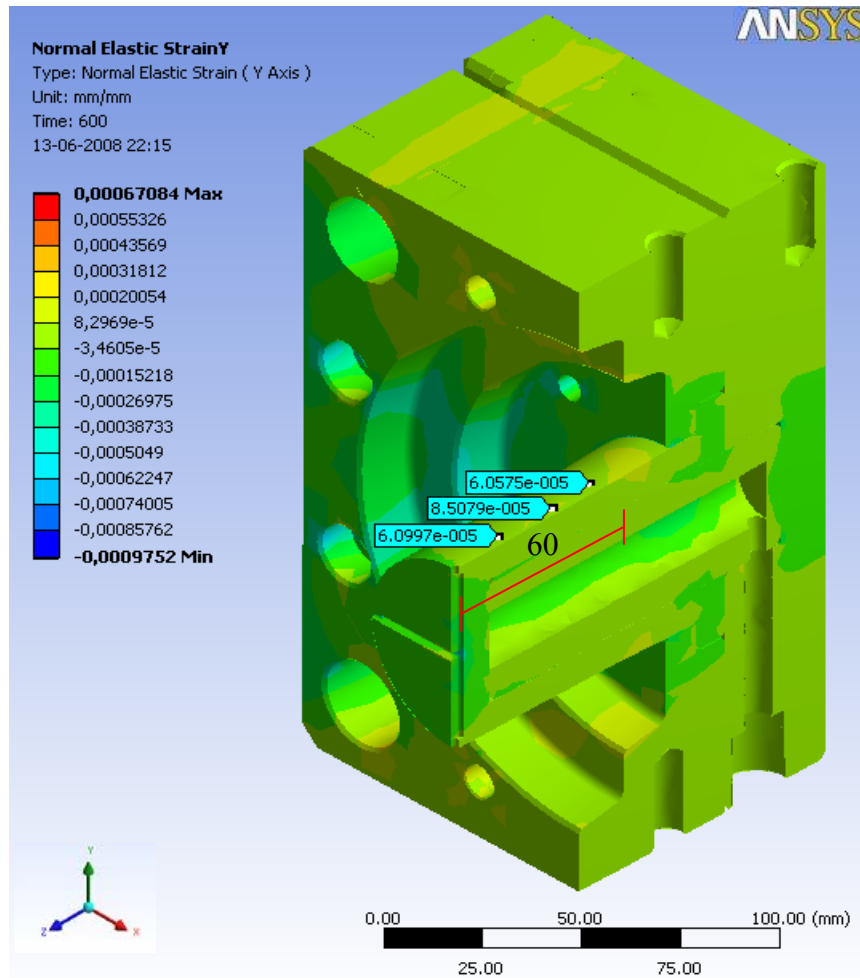
Figure 5.59 - The radial elastic strain field simulation of the steel core moulding block

The radial strain field of the resin moulding block subjected to the pressure corresponding to the RS combination with holding pressure of 36 MPa is depicted in the Figure 5.60 and shows a maximum strain of 0.036% at the point mentioned before.
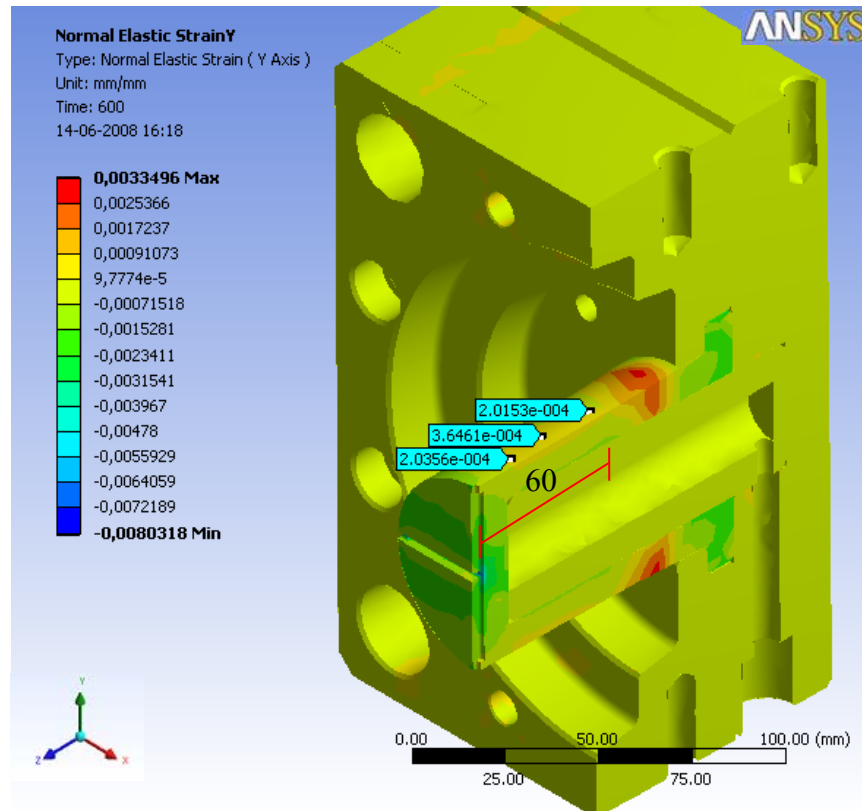
Figure 5.60 - The radial elastic strain field simulation of the epoxy resin composite moulding block

The one order of magnitude higher deformation of the moulding blocks produced in epoxy-based composites materials suggests their bigger sensitivity to the injection moulding pressures. This fact reveal the importance for the strictly control of the injection moulding process conditions and the influence on the parts produced as mentioned above.

The obtained results presented above were published elsewhere [195] and attached in appendix 2.

Mould HM-2

The structural analyses of the mould HM-2 were focused in the moulding pin element. The software ANSYS Workbench 11.0 was used to predict the pin structural integrity for each material used. In the simulations it was considered as boundary conditions that the bottom face of the moulding pin was bonded to the load cell wall and the contact pressure was that caused by the moulding at the moment of ejection. The pressure information obtained in the experimental tests, the pressure data associated to shrinkage of the moulded material and the resin composite material data were used as inputs. Some of the obtained results were published elsewhere [223] and attached in appendix 2.

The integrity of moulding pins, at the ejection phase of the injection cycle, was estimated using the pressure data associated to shrinkage of the injected material and the boundary conditions schematized in Figure 5.61.
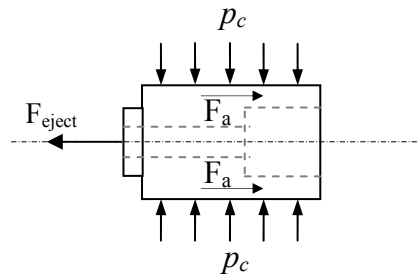

Figure 5.61 - Boundary conditions established for the structural analyses in pins inserts

F_{eject} the ejection force to remove the pin from the back detail of the part, F_a is the friction force and (p_c) is the contact pressure that can be calculated, as shown in Chapter 3, section 3.1.3, by the equation 3.23:

$$p_c = E(T_{eject})_{pol} \times Sh_i$$

Considering the value of the elasticity modulus of the injected polymer at ejection temperature (E $(T_{eject})_{pol}$), 600×10^6 Pa (Modulus curves of the PP for 1% strain at 60°C) and the value of shrinkage obtained experimentally (Sh_i) 0.0252 (Table 5.11) in the case of SL resin pin (DSM Somos 11120), the obtained contact pressure is 15.12 MPa.

Figure 5.62, shows the simulation of the equivalent elastic strain and stress for the case of epoxy based composite filled with aluminium powder used in the moulding pin.
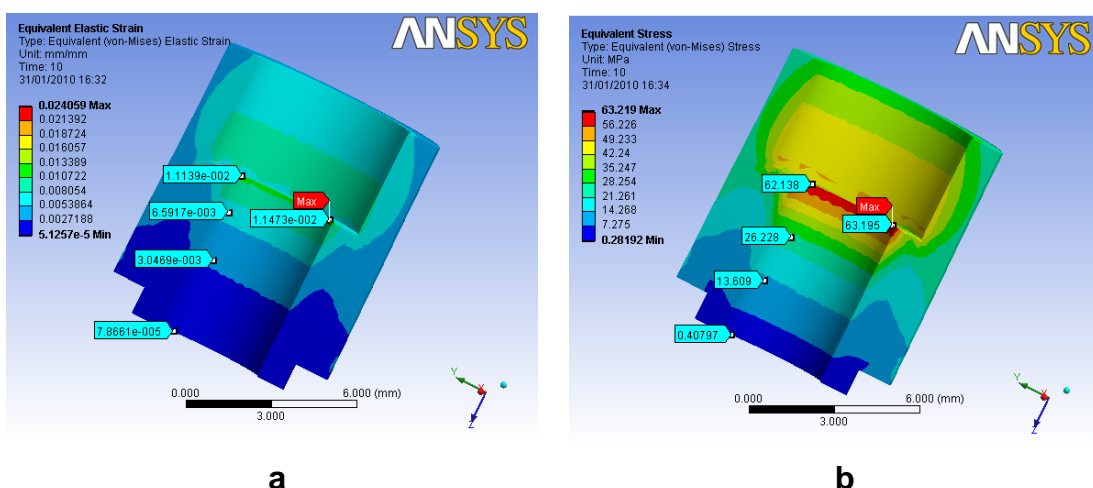

Figure 5.62 - Epoxy/Al pin: a) equivalent elastic strain, b) equivalent stress

Comparisons between the equivalent elastic strain and the equivalent stress, with the use of different materials in moulding pins, were made in the minimum (A) and maximum (or

critical B) points. Further details of simulation analyses are included in appendix 6. Table 5.15 shows the obtained results.

Table 5.15 – Equivalent elastic strain and stress in points A and B of the moulding pins in different materials

Property *vs* Material		Tool steel	ProMetal	Epoxy/SSF	Epoxy/Al	SLresin
Elastic strain [%]	A	0.0029	0.0039	0.0057	0.0051	0.0166
	B	0.0202	0.0389	1.3219	1.1473	2.3890
Stress [MPa]	A	3.55	3.38	0.45	0.28	0.45
	B	56.10	58.84	60.70	63.19	60.32

The structural analyses using the software ANSYS Workbench show that the larger deformation of the resin core and soft moulding pins materials adds to the actual shrinkage resulting from the crystallization and thermal shrinkage of the moulded material.

The pressure evolution during the injection moulding cycle, for the different core/cavity combinations, can be observed in Figure 5.63. The maximum values reached for the cores in epoxy-based composite resin are lower than steel one, as required in moulding conditions for these type of materials. Further details are presented appendix 5.
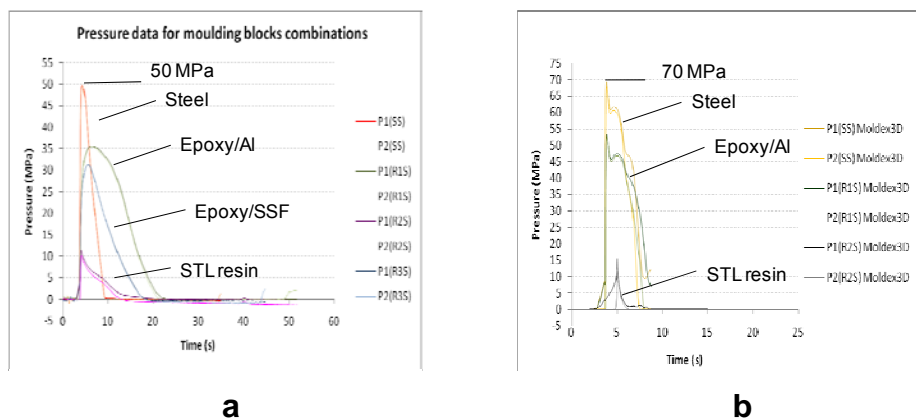

Figure 5.63 - Pressure data for the different core/cavity combinations: a) experimental, b) predicted evolution in Moldex3D 9.1. P1 - cavity, P2 - core

The lower profile for the SL resin is also related with the processing conditions established for this kind material. The pressure was simulated as a value somewhat higher than the measured (Figure 5.63b).

As mentioned above, the SL pin structural integrity failed after 20 shots, as depicted in the Figure 5.64.
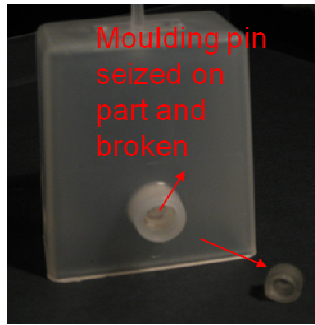
Figure 5.64 – Failure of the SL inserts

The main mechanical properties of the SL resin are shown in Table 5.16.

Table 5.16 - Main mechanical properties of the SL resin

Mechanical properties	SL resin DSM Somos 11120/2
Tensile strength [MPa]	47,1 – 53,6
Elongation at break [%]	11 - 20
Elongation at yield [%]	3,3 – 3,5
Modulus of Elasticity [GPa]	2,65 – 2,88
Izod Impact Notched [J.cm^{-1}]	0,2 – 0,3

Source: DSM Somos (New Castle, USA) data sheet

The equivalent stress (Von-Mises) was simulated and the maximum value of 64.32 MPa was obtained in the regions coloured in red for the elastic strain of 2.39% (Figure 5.65).
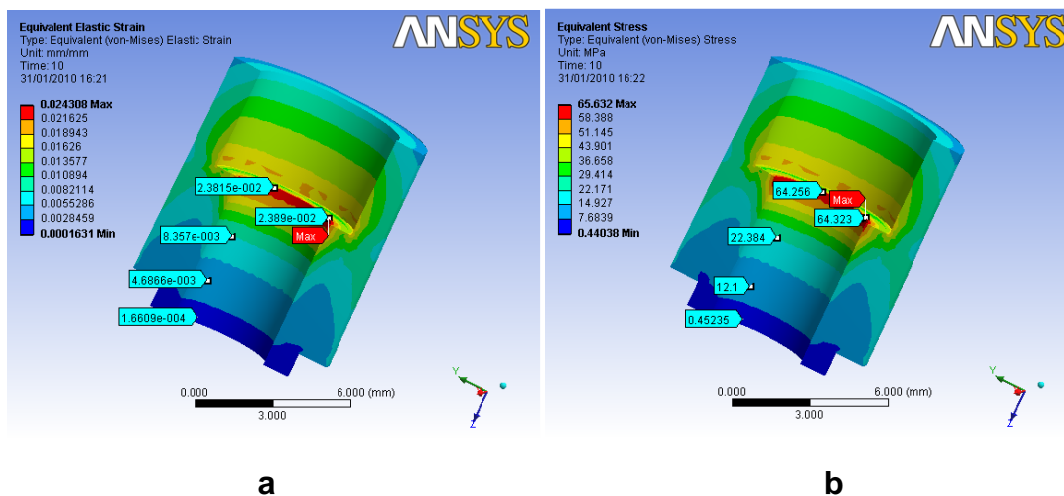

a   **b**

Figure 5.65 – SL resin pin: a) equivalent elastic strain, b) equivalent stress

Analyzing the mechanical properties of the SL resin Table 5.16 and the field of stresses obtained in the ANSYS structural analyses of the pins, in as moulding conditions during the ejection phase, *i.e.*, temperature $\approx 60^{\circ}$C, ejection force ≈ 690 N and contact pressure provoked by the polymer shrinkage ≈ 15.12 MPa, it can be observed that the failure occur, most probably, during this phase of the injection cycle.

Determining analytically the equivalent stress, for this case of study, it was also verified that the equivalent stress is higher than the interval of values admissible for the tensile strength of the SL resin. For this calculus it was considered the load state of the pins during the ejection phase and then applying one of the known strength materials criterions' (Van Mises or Tresca), *i.e.*, the ejection force measured through the load cell (689.70 N for the case of SL resin, Table 5.13) and the lower transversal section shown in Figure 5.5, (A = 28.34 $\times 10^{-6}$ m^2) the normal strength in the pin is ≈ 24.34 MPa. For the compression stress it was considered the field of stresses obtained through the ANSYS structural analysis (Figure 5.66) with a maximum value of 42.23 MPa, when the pin is only subjected to the contact pressure due the polymer shrinkage.
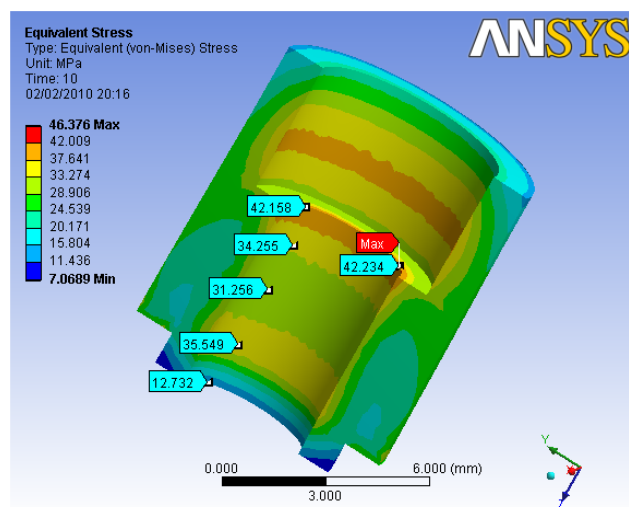

Figure 5.66 – Compression stresses on the moulding pin due the polymer shrinkage

Analysing the Mohr's circle for plane stress (Figure 5.67) and considering $\sigma_1 = 24.34$ MPa and $\sigma_2 = 42.23$ MPa, the equivalent stress, applying the Tresca's criterion ($\sigma_{yield} \geq |\sigma_1 - \sigma_2|$), is 66.57 MPa, *i.e.*, above the upper limit admissible for the tensile strength, as shown in Table 5.16.
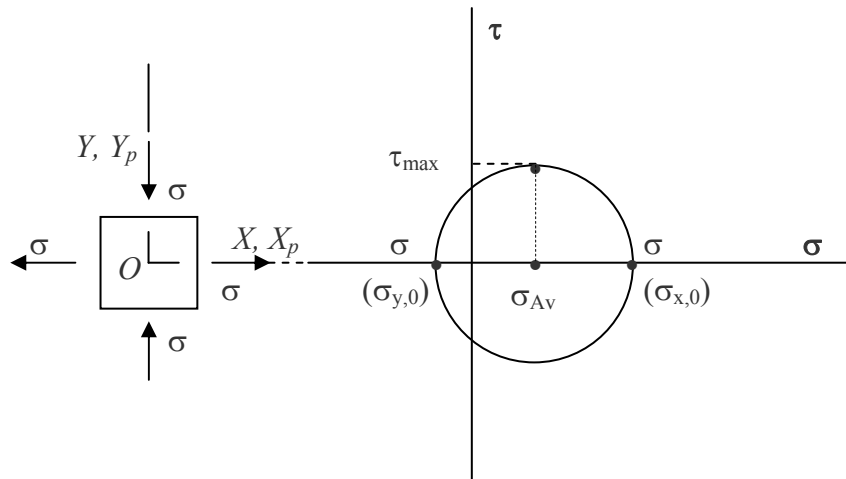
Figure 5.67 - Mohr's circle for plane stress for the case of $\tau_{xy} = 0$ and $\sigma_x > \sigma_y$

Pin deformation comparison between steel and soft materials using the *ANSYS Workbench* ®11.0 software

As expected, the deformations of the pins in Steel and ProMetal are similar (Figures 5.68 and 5.69) as well as the cases of Epoxy/Al and Epoxy/SSF composites.
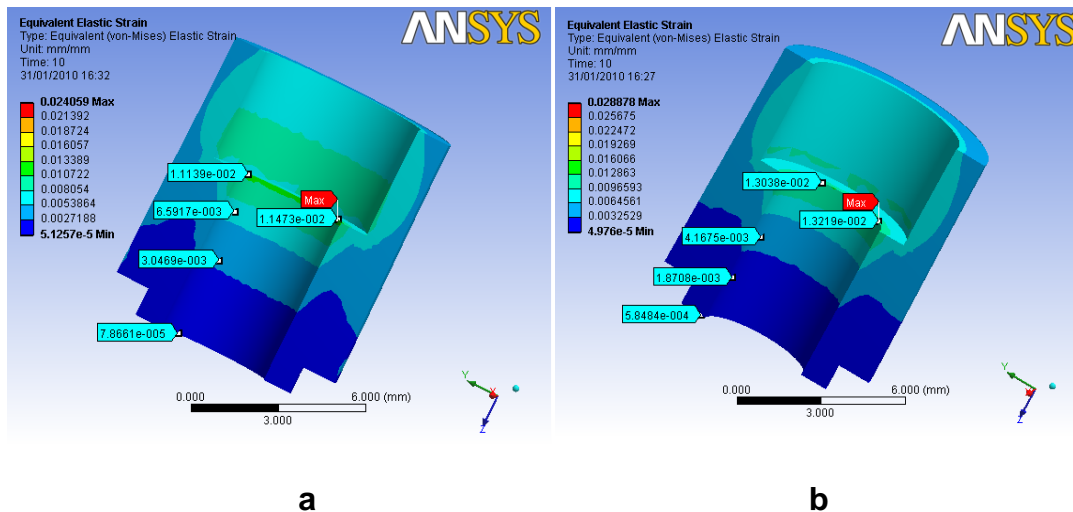

a   **b**

Figure 5.68 - Equivalent elastic strain of the moulding pins simulated in ANSYS Workbench: a) Epoxy/Al, b) Epoxy/SSF
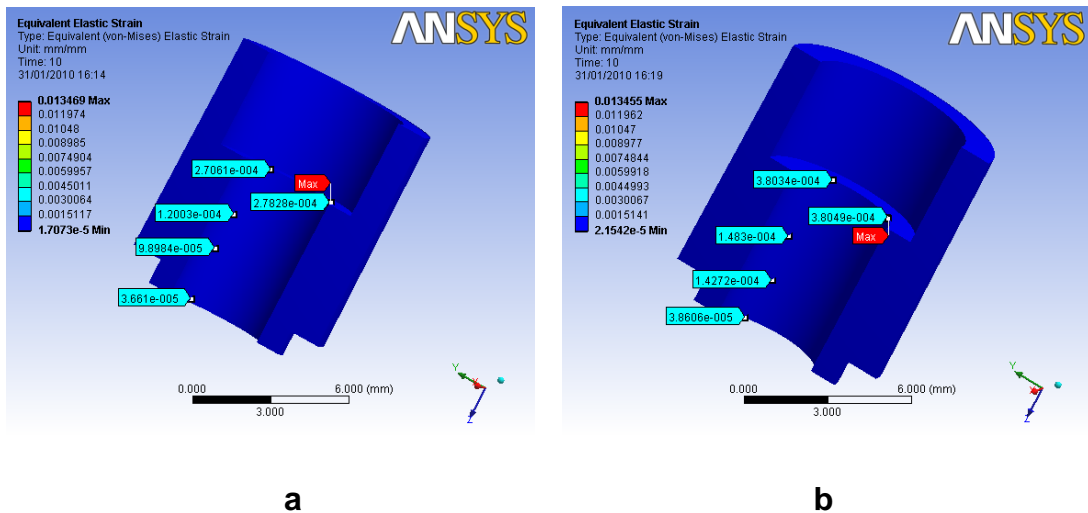
a **b**

Figure 5.69 - Equivalent elastic strain of the moulding pins simulated in ANSYS Workbench a) Steel b) ProMetal

The structural analyses observed in the moulding pins (Figure 5.69) shows that the equivalent elastic strain in the critical zones of the pins produced in softer materials are higher. Just for the cases of Epoxy/Al and Epoxy/SSF, if it were taking into account the moulding pins deformation, the achieved relative errors of the estimated ejection forces reduces *ca.* 40%.

These results suggest the importance of considering the deformation of the moulding elements, essentially when soft materials are used, due the involved pressures. This deformation influences the plastic part shrinkage and, consequently, the ejection forces.

CONCLUSIONS

This research work aimed at developing a solution for hybrid moulds with features applicable in the industrial practice and analysing aspects related with its performance. The main conclusions of the work were:

a) A mould was designed with features for analysing short and long side movements, warpage and ejection forces. The solution developed enabled the reutilisation by keeping the structure of the mould and changing the moulding blocks. It was instrumented for monitoring pressure, temperature and ejection forces in operation.

b) Rapid prototyping and tooling solutions were used for processing moulding elements, namely direct processes as Stereolithography and ProMetal three dimensional printing and indirect processes as Vacuum Casting of epoxy composites and silicone moulds.

c) A model was developed for predicting the temperature field during the injection moulding. It was concluded that in the care of hybrid moulds it is important to consider the effect of the thermal contact resistance.

d) A model was also developed for predicting the shrinkage of mouldings when soft moulding blocks are used. This demonstrable the contribution of these blocks in the overall product shrinkage.

e) The hybrid moulds with soft cores require a longer initial running period for stabilisation of the processing temperatures, namely in the mould. This is caused by the lower thermal conductivity of polymer based composites.

f) The pressure evolution in the impression of hybrid moulds with soft moulding cores is different from conventional steel cores showing a slower reduction of this variable and also a lower pressure profile.

g) The mouldings obtained with hybrid moulds are heavier and have a larger dispersion than the ones obtained with conventional moulds. The mouldings produced with resin and steel combinations in the moulding blocks are lighter than the ones produced in all-resin moulding blocks, but heavier than the mouldings produced in steel moulding blocks.

h) The morphology of the polypropylene mouldings obtained with hybrid moulds displays a smaller skin ratio and different spherulite types than with conventional moulds.

Particularly, the occurrence of β-form spherulites is a visible feature in hybrid moulds, and dependent on their cooling ratios.

i) The shrinkage in mouldings produced in hybrid moulds is of the order of 60% larger than conventional moulds, this being attributable to the deformation of the core moulding blocks caused by the injection pressure.

j) The static coefficient of friction in the ejection is similar for the steel and ProMetal materials and lower than the obtained for epoxy composites. Although the difference found in this coefficient, the main reason for the discrepancy obtained in the ejection forces needed to remove de moulding pins from the parts is associated to the deformation of the soft moulding elements.

k) It is possible to predict the temperature evolution in the mould providence the software is provided with a routine that accommodate the effect of the thermal contact resistance.

l) It is also possible to predict the number of cycles required for the stabilization of the moulding blocks using the software Moldex3D.

m) It was confirmed by simulation that the strain in moulding cores made by epoxy composites is one order of magnitude higher than steel, thus implying the need of accounting with it for the prediction of the moulding shrinkage.

n) The structural integrity of moulding elements is an issue in hybrid moulds, this being particularly critical when stereolithography elements are used.

o) The mould elements made from stereolithography tend to break prematurely and consequently are not recommendable for injection moulds. However, its application is envisageable if it is possible to guarantee the working temperature below 15ºC above the glass transition temperature of the resin.

p) The failure of the moulding elements in hybrid moulds is usually associated to the stresses that are raised during ejection and depend on the shrinkage and coefficient of friction between the mould and the moulding.

q) There is a tendency to the chipping of the moulding blocks near to the gates possibly due the thermal and stress fatigue.

r) When polymer composites are used in the moulding blocks pitting at the moulding surfaces are likely to appear as a possible joint result of the adhesion of the two materials and the removal of filler particles.

s) Hybrid moulds are a viable processing solution for injection moulding, considering the design, manufacturing, processing and economical issues. This kind of moulds represents an important tool for short and medium series. It is the most indicated solution, essentially, for quick production and for products with specific requirements, such as complex features, zones with difficult cooling and larger parts (≈ 1 m^2) in short production series.

The consideration of the shrinkage is of great importance on designing plastics parts with narrow precision tolerances. This study evidences that the final dimensions of the parts produced in hybrid moulds depend on the plastics shrinkage but also on the core deformation occurred in non-metallic core, due to the processing pressure. The performance of hybrid moulds is related with the moulding elements structural integrity. Therefore, it is important to consider a preliminary analysis on these elements through the use of adequate simulation tools.

The work reported herewith is being pursued with experiments on parts of more complex shapes that are usually subjected to mould filling simulation. Some improvements, such as the ability to accommodate the effect of deformation and the poor thermal behaviour of the non-metallic moulding blocks, are required in the actual computer simulation tools to ensure reliability.

FURTHER WORK

This work pointed out some studies possibilities on the use of hybrid moulds for injection moulding and understanding the relationships between the processing and the mould design. Based on the results, arguments presented and experience acquired along this work, it is suggested to further work:

- Study of the shrinkage and ejection forces in the context of other injection materials: amorphous, semi-crystalline and short fibre reinforced;

- Assessment the main factors that influence the mould wear, namely the hardness of the materials, the roughness of the moulding elements, the chemical affinity and the adhesion of the fillers to the polymer in the composite

- Study the possible improvements on strength, surface finish and reliability of the parts produced by RPT techniques;

- Optimization the runner system design to improve its life;

- Experimental evaluation of the soft moulding blocks deformation during the injection cycle;

- Implementation of conformal cooling layouts using the principle of fusible cores;

- Implementation of hybrid mould solutions for large plastics parts (such as 1 m2 of area), the equipment required to produce small series (around 500 parts) and the viability of an industrial production unit (unit of pilot production) for this kind of products;

- Development of design methodologies for hybrid moulds philosophy;

- Implementation of software routines in simulation packages for improving the temperature prediction accuracy and the ejection force and resulting stress prediction.

REFERENCES

1. Feygin, M., *Apparatus and method for forming an integral object from laminations.* 1988: US Patent.

2. Hull, C. W., *Apparatus for production of three-dimensional objects by stereolithography.* 1986: US Patent.

3. Brown, C. O., Breinan, E. M., Kear, B. H., *Method for fabricating articles by sequential layer deposition.* 1982: US Patent.

4. Kruth, J. P., Leu, M. C., Nakagawa, T., *Progress in Additive Manufacturing and Rapid Prototyping.* Annals CIRP, 1998. **47**(2): p. 525 - 540.

5. Chua, C. K. Leong, K. F., *Rapid Prototyping: Principles and applications in manufacturing.* 1997: John Wiley.

6. Saraiva, V. M., Lima, M., Pouzada, A. S. *Towards a new conceptual design of injection moulds.* 44th Int Scientific Colloquium. 1999. Ilmenau, Germany.

7. Muller, H. Sladojevic, J., *Rapid tooling approaches for small lot production of sheet metal parts.* Journal of Materials Processing Technology, 2001. **115**: p. 97 - 103.

8. Hernández, P., Ares, E., Pouzada, A. S. *New trends on the design and manufacture of injection moulds - Reusability and Recycling.* PMI 2005 - Int. Conf. on Polymers & Moulds Innovations. 2005. Ghent, Belgium.

9. Hopkinson, N. Dickens, P., *A comparison between stereolithography and aluminium injection moulding tooling.* Rapid Prototyping Journal, 2000. **6**(4): p. 253-258.

10. Karunakaran, K. P., Dibbi, S., Shanmuganathan, P. V., Raju, D. S., Kakaraparti, S., *Efficient stock cutting for laminated manufacturing. Computed-Aided Design.* 2002. p. 281-298.

11. Pontes, A. J., Gago, P., Bártolo, P. J., Soares, R., Pouzada, A. S., *Hibridmolde - A Project towards the new mould generation.* O Molde, 2005. **66**: p. 16-20.

12. Campbell, I., Combrinck, J., Beer, D., Barnard, L., *Stereolithography build time estimation based on volumetric calculations.* Rapid Prototyping Journal, 2008. **14**(5): p. 271-279.

13. Pouzada, A. S., *Hybrid moulds: a case of integration of alternative materials and rapid prototyping for tooling.* Virtual and Physical Prototyping, 2009. **4**(4): p. 195-202.

14. Bareta, D. R., Zeilmann, R. P., Costa, C. A., Pouzada, A. S. *Application of alternative materials in hybrid mould cores.* RPD 2006 - Building the future by innovation. 2006. Marinha Grande, Portugal.

15. Engelmann, P., Hayden, K., Guichelaar, P., Dealey, R., Monfore, M. *Understanding wear mechanisms: The key to mold life.* Proceedings ANTEC 2000 Conference. 2000. Orlando, USA.

16. Voet, A., Mingneau, J., Dehaes, J., Kruth, J. P., Van Vaerenbergh, J. *Study of the Wear Behaviour of Conventional and Rapid Tooling Mould Materials.* PMI 2005 - Int. Conf. on Polymers & Moulds Innovations. 2005. Ghent, Belgium.

17. Peças, P., Ribeiro, I., Henriques, E., Pouzada, A. S., Pontes, A. J. *The importance of applying life-cycle approaches in the design decision of injection moulded plastics parts*. PMI 2008 - Int Conf. Polymers & Moulds Innovations. 2008. Ghent, Belgium.

18. Drizo, A. Pegna, J., *Environmental impacts of rapid prototyping: an overview of research to date.* Rapid Prototyping Journal, 2006. **12** (2): p. 64-71.

19. Peças, P., Ribeiro, I., Folgado, R., Henriques, E., *A Life Cycle Engineering model for technology selection: a case study on plastic injection moulds for low production volumes.* Journal of Cleaner Production, 2009. **17**: p. 846 - 856.

20. Chua, C. K., Hong, K. H., Ho, S. L., *Rapid tooling technology. Part 1: A comparative study.* International Journal of Advanced Manufacturing Technology, 1999. **15**: p. 604-605.

21. Menges, G., Michaeli, W., Mohren, P., *How To Make Injection Molds*. 3rd ed. ed. 2001, Munich: Hanser Pulishers.

22. Williams, J. A., *Rapid tooling applications: an overview and reality check.* Rapid News (Time Compression Technologies), 1997. **5**(3): p. 48.- 54.

23. King, D. Tansey, T., *Alternative materials for rapid tooling.* Journal of Materials Processing Technology, 2002. **121**: p. 313-317.

24. Rosochowski, A. Matuszak, A., *Rapid tooling: the state of the art.* Journal of Materials Processing Technology, 2000. **106**: p. 191-199.

25. Chua, C. K., Hong, K. H., Ho, S. L., *Rapid tooling technology. Part 2: A case study using arc spray metal tooling.* International Journal of Advanced Manufacturing Technology, 1999. **15**: p. 609-614.

26. Chua, C. K., Chou, S. M., Wong, T. S., *A study of the state of the art rapid prototyping tecnologies.* International Journal of Advanced Manufacturing Technology, 1998. **14**: p. 146-152.

27. Himmer, T., Techel, A., Nowotny, S., Beyer, E. *Recent developments in Metal Laminated Tooling by Multiple Laser Processing*. 13th Solid Freeform Fabrication Symposium. 2002. Austin, TX (USA).

28. Himmer, T., Stiles, E., Techel, A., Nowotny, S., Beyer, E. *MOLDDESIGN*. Metal Laminated Tooling-Process Chain 2009 [cited 2009 29th October]; MoldMaking Technology Online:[Available from: http://www.moldmakingtechnology.com/articles/030501.html.

29. Pham, D. T. Dimov, S. S., *Rapid prototyping and rapid tooling-the key enablers for rapid manufacturing.* Proceedings of the Institution of Mechanical Engineers, Part C: Journal of Mechanical Engineering Science, 2003. **217**(1): p. 1-23.

30. Du, Z. H., Chua, C. K., Chua, Y. S., Loh-Lee, K. G., Lim, S. T., *Rapid sheet metal manufacturing. Part 1: Indirect rapid tooling.* International Journal of Advanced Manufacturer Technology, 2002. **19**: p. 411-417.

31. Beck, E. W. Smith, S. B., *Silicone mold and elastomer tool life.* 1990, Dow Corner Corporation, Midland, Mich.: US Patent.

32. Curfman, W. A., *Method of making an epoxy mold.* 1989, General Motors Corporation, Detroit, Mich.: US Patent.

33. Palma, J. M., *Metal spray tool repair system.* 1999, The Boeing compant, Seattle Wach.: US Patent.

34. Cheah, C. M., Chua, C. K., Ong, H. S., *Rapid moulding using epoxy tooling resin.* International Journal Advanced Manufacturing Technology, 2002. **20** (55): p. 368-374.

35. Pham, D. T., Dimov, S., Lacan, F., *Firm Tooling: bridging the gap between hard and soft tooling. Prototyping Technology International.* 1998, UK & Int. Press, England. p. 196-203.

36. Dunne, P., Soe, S. P., Byrne, G., Venus, A., Wheatley, A. R., *Some demands on rapid prototypes used as master patterns in rapid tooling for injection moulding.* Journal of Materials Processing Technology, 2004. **150**: p. 201-207.

37. Jacobs, P. F., *Stereolithography and other RP&M technologies: From Rapid Prototyping to Rapid Tooling.* 1995, Dearborn MI: SME. 392.

38. Venus, A. D., Crommert, S. J., Hagan, S. O. *The feasibility of silicon rubber as an injection mould tooling process using rapid prototyped pattern.* Second National Conference on Rapid Prototyping and Tooling Research. 1996.

39. Dickens, P. M. *Rapid tooling techniques.* EuroMold'99 Conference - RP's Strategic Benefits and Risks. 1999. Frankfurt/Germany.

40. Silva, M. A., Martinho, P. G., Pouzada, A. S. *Warpage of injection mouldings in hybrid moulds with epoxy-aluminium composite core.* VR@P 2009 conference 2009. Leiria, Portugal.

41. Sabino-Netto, A. C., Salmoria, G. V., Ahrens, C. H., Pouzada, A. S. *On the effect of the cure process on the mechanical properties of steel fibre reinforced epoxy composites.* PPS 24th Annual Meeting. 2008. Salerno, Italy.

42. Ramos, A. M., Relvas, C., Simões, J. A., *Vacuum casting with room temperature vulcanising rubber and aluminium moulds for rapid manufacturing of quality parts: a comparative study.* Rapid Prototyping Journal, 2003. **9**(2): p. 111-115.

43. Vasconcelos, P. V., Lino, F. J., Neto, R. J. *Importance of the vacuum in rapid tooling of polymeric-based moulds.* RPD 2004 - Rapid Product Development. 2004. Marinha Grande, Portugal.

44. Lima, P., Ramos, J., Pouzada, A. S. *Thermal performance of hybrid injection molds with epoxy inserts.* Proceedings ANTEC 2003 Conference. 2003. Nashville, USA.

45. Ma, S., Gibson, I., Balaji, G., Hu, Q. J., *Development of epoxy matrix composites for rapid tooling applications.* Journal of Materials Processing Technology, 2007. **192-193**: p. 75-82.

46. Vasconcelos, P. V., Lino, F. J., Batista, A. M., Neto, R. J. L., *Tribological behaviour of epoxy based composites for rapid tooling.* Wear, 2006. **260**: p. 30-40.

47. Sabino-Netto, A. C., Salmoria, G. V., Ahrens, C. H., Pouzada, A. S., *Mechanical Properties of Epoxy Composites Filled with Short Steel Fibres for Hybrid Injection Moulds.* Advanced Materials Forum IV, 2008. **587-588**: p. 222-226.

48. Sabino-Netto, A. C., *Desenvolvimento e avaliação de compósito de resina epóxi reforçado com fibras de aço na fabricação de blocos moldantes para moldagem por injeção.* Florianópolis: Universidade Federal de Santa Catarina, 2008. 200 p. PhD Thesis

49.   Sabino-Netto, A., Salmoria, G. V., Jesus, M. S., Ahrens, C. H. *Investigation of thermal and mechanical performance of an iron-epoxy composite for rapid tooling.* RPD 2006 - Building the future by innovation. 2006. Marinha Grande, Portugal.

50.   Pontes, A. J., Queirós, M. P., Bartolo, P. J., Pouzada, A. S. *A Study on design and performance of hybrid moulds for injection moulding.* ICIT 2005 - 5th International Conference of Industrial Tools. 2005. Bled, Slovenia.

51.   Feenstra, F., Holmer, B., Pohl, H., Tromans, G., Moos, N., Mieritz, B. *RP, RT, RM Trends and developments/research survey.* Rapid Prototyping Industrial Applications (RAPTIA). 2002.

52.   Kodama, H., *Automatic method for fabricating a three-dimensional plastic model with photo-hardening polymer.* Review of Scientific Instruments, 1981. **52**(11): p. 1770-1773.

53.   Jardini, A. L., Maciel, R. F., Scarparo, M. A., Andrade, S. R., Moura, L. F., *Infrared laser stereolithography: prototype construction using special combination of compounds and laser parameters in localised curing process.* International Journal of Materials and Product Technology, 2004. **21**(4): p. 241 - 254.

54.   Chen, H., Corbel, S., Allanic, A. L., Andre, J. C. *Solid fabrication induced by thermal IR lasers.* Proceedings of the Third International Conference on Rapid Prototyping. 1992. Ohio, USA.

55.   Bártolo, P. J. Mitchell, G., *Stereo-thermal-lithography: a new principle for rapid prototyping.* Rapid Prototyping Journal, 2003. **9**(3): p. 150 - 156.

56.   Li, Y., Gargiulo, E. P., Keefe, M., *Studies in direct tooling using stereolithography.* Journal of Manufacturing Science and Engineering, 2000. **122** (2): p. 316 - 322.

57.   Ribeiro Jr, A. R., Hopkinson, N., Ahrens, C. H., *Thermal effects on stereolithography tools during injection moulding.* Rapid Prototyping Journal, 2004. **10**(3): p. 176-180.

58.   Harris, R. A., Hague, R. J., Dickens, P. M., *Crystallinity control in parts produced from stereolithography injection mould tooling.* J. Materials: Design and Applications, 2003. **217**(part L): p. 269-276.

59.   Salmoria, G. V., Gonzalez, V. J., Ahrens, C. H., Soldi, V., Pires, A. T. N., *Stereolithography Somos 7110 photosensitive resin: study of curing kinetic and thermal degradation.* Journal of Materials Processing Technology, 2005. **168**(1): p. 164 - 171.

60.   Cheah, C. M., Nee, A. Y. C., Fuh, J. Y. H., Lu, L., Choo, Y. S., Miyazawa, T., *Characteristics of photopolymeric material used in rapid prototypes. Part I. Mechanical properties in the green state.* Journal of Materials Processing Technology, 1997. **67**: p. 41-45.

61.   Wohlers, T., *Wohlers Report 2009 - State of the industry. Annual Worldwide Progress Report.* 2009: Colorado (USA).

62.   Koster, R. Ragaert, K. *Bioplastics injection moulding and modern mould opportunities.* PMI 2007 - Int. Conf. on Polymers & Moulds Innovations. 2007. Gent, Belgium.

63.   Deckard, C. R., *Method and apparatus for producing parts by selective sintering.* 1989: US Patent.

64. Deckard, C. R., *Selective Laser Sintering*. Austin: University of Texas at Austin, 1988. PhD Thesis

65. Badrinarayan, H. Harlow, J. W. *Manufacture of Injection Moulds using SLS*. Solid Freeform Fabrication Proceeding. 1994.

66. Beaman, J. J., Marcus, H. L., Bourell, D. L., Barlow, J. W., Crawford, R. H., *Solid Freeform Fabrication: A New Direction in Manufacturing*. 1997, Kluwer Academic Publishers: Dordrecht London. p. 330.

67. Tolochko, N., Mozzharov, S., Laoui, T., Froyen, L., *Selective laser sintering of single- and two-component metal powders*. Rapid Prototyping Journal, 2003. **9**(2): p. 68-78.

68. Kruth, J. P., Levy, G., Klocke, F., Childs, T. H. C., *Consolidation phenomena in laser and powder-bed based layered manufacturing*. Annals of the CIRP, 2007. **56**(2): p. 1-30.

69. Wu, W. Z. Yan, M. G., *Development of polymer coated metallic powder for selective laser sintering (SLS) process*. Journal of Advanced Materials, 2002. **34**(2): p. 25-28.

70. Bourell, D. L., Marcus, H. L., Barlow, J. W., Beaman, J. J., *Selective laser sintering of metals and ceramics*. International journal Powder Metallurgy, 1992. **28**(4): p. 369-381.

71. Kruth, J. P., Mercelis, P., Vaerenbergh, J. V., Froyen, L., Rombouts, M. *Advances in Selective Laser Sintering*. Advanced Research in Virtual and Rapid Prototyping. 2003. Leiria/Portugal.

72. Dimov, S. S., Pham, D. T., Lacan, F., Dotchev, K. D., *Rapid tooling applications of the selective laser sintering process*. Assembly Automation, 2001. **21**(4): p. 296-302.

73. Pontes, A. J., Queirós, M. P., Soares, R., Pouzada, A. S. *Hybrid moulds with SLS inserts: Design and performance assessment*. PPS Americas Reg. Meeting. 2004. Florianópolis, Brasil.

74. Kruth, J. P., Vandenbroucke, B., Vaerenbergh, J. V., Mercelis, P. *Benchmarking of different SLS/SLM processes as rapid manufacturing techniques*. PMI 2005 - Int. Conf. on Polymers & Moulds Innovations. 2005. Ghent, Belgium.

75. Lohner, A., *Laser sintering ushers in new route to PM parts. Metal Powder Report*. 1997. p. 24 - 27.

76. Khaing, M. W., Fuh, J. Y. H., Lu, L., *Direct metal laser sintering for rapid tooling: processing and characterization of EOS parts*. Journal of Materials Processing Technology, 2001. **113**: p. 269 - 272.

77. Geiger, M., Precht, M., Niebling, F., Otto, A. *Laser assisted rapid prototyping - processes, applications and developments in the field of additive processes*. ICIT 2003 - 4th International Conference of Industrial Tools. 2003. Bled, Slovenia.

78. Wimpenny, D., *Rapid tooling options compared*, ed. W.M. Group. 2003, Coventry, UK: University of Warwick

79. Sachs, E. M., Haggerty, J. S., Cima, M. J., Williams, P. A., *Three-dimensional Printing Techniques*. 1994: US Patent.

80. Gravet, D. *3DPrinting metal: A new way of thinking*. PMI 2008 - Int. Conf. on Polymers & Moulds Innovations. 2008. Ghent, Belgium.

81. Cima, M., Haggerty, J., Sachs, E., *Three-dimensional printing techniques* 1989: US Patent.

82. Dormal, T. *3D Printing metal: the fastest solution for complex metal parts and inserts*. Rapid Product Development. 2004. Marinha Grande (Portugal).

83. Godlinski, D. *Rapid Manufacturing of dense stainless steel parts*. Euro PM. 2003. Valencia (Spain).

84. Meiners, W., Wissenbach, K., Gasser, A., *Selective laser sintering at melting temperature* 1996: US Patent.

85. Levy, G. N., Schindel, R., Kruth , J. P., *Rapid manufacturing and rapid tooling with layer manufacturing (LM) technologies, state of the art and future perspectives.* CIRP Annals - Manufacturing Technology, 2003. **52**(2): p. 589-609.

86. *MCP HEK - GmbH*. 2009   [cited 2009 October, 20th]; Available from: http://www.mcp-hek.de.

87. Shiomi, M., Yoshidome, A., Abe, F., Osakada, K., *Finite elements analysis of melting and solidifying processes in laser rapid prototyping of metallic powders.* International Journal of Machine Tools & Manufacture, 1999. **39**(2): p. 237-252.

88. Mateus, A., Gago, P., Oliveira, V., Saraiva, V. M., Lima, M., Monteiro, A. C., Pouzada, A. S. *Hybrid moulds - integration of alternative materials and manufacturing processes*. 16th Int. Conf. on Production Research 2001. Prague/Czech Republic.

89. Martinho, P. G., Bártolo, P. J., Queirós, M. P., Pontes, A. J., Pouzada, A. S., *Hybrid Moulds: The use of combined techniques for the rapid manufacturing of injection moulds*, in *Virtual Modelling and Rapid Manufacturing*, P.J. Bártolo, et al., Editor. 2005, Taylor and Francis: Leiria. p. 421.

90. Saurkar, S., Malloy, R. A., McCarthy, S. *Rapid tooling: a study of different cooling techniques for mold inserts used in the direct aim (ACES injection molding) process*. Proceedings ANTEC 2005 Conference. 2005. Boston, USA.

91. Segal, J. I. Campbell, R. I., *A review of research into the effects of rapid tooling on part properties.* Rapid Prototyping Journal, 2001. **7**(2): p. 90-98.

92. Volpato, N., Foggiatto, J. A., Amorim, J. R., Filho, O. D. *A proposed data base to aid material selection for prototype tooling*. RPD 2006 - Building the future by innovation. 2006. Marinha Grande, Portugal.

93. Gonçalves, M. W., Pouzada, A. S., Salmoria, G. V., Ahrens, C. H. *Performance and friction properties of injection hybrid moulds with stereolitography moulding zones*. Materiais 2005 - 3rd Int Materials Symposium. 2005. Aveiro.

94. Roobaert, S., Behl, P., Queiros, M. P., Cardon, L., Pontes, A. J., Pouzada, A. S. *Characterisation of polypropylene mouldings made using different core materials*. PMI 2008 - Int. Conf. on Polymers & Moulds Innovations. 2008. Ghent/Belgium.

95. Bareta, D. R., *Estudo comparativo e experimental de materiais aplicados a insertos machos de moldes de injecção dentro do conceito de molde híbrido*. Caxias do Sul: Universidade de Caxias do Sul, 2007. 123 p. Master Thesis

96. Roobaert, S., Behl, P., Queirós, M. P., Cardon, L., Pontes, A. J., Pouzada, A. S. *Characterisation of polypropylene mouldings made using different core materials.* PMI 2008 - Int. Conf. on Polymers & Moulds Innovations. 2008. Ghent, Belgium.

97. Ragaert, K., Cardon, L., Vancampenhout, J. *Hybrid injection moulds: a practical approach for implementation.* RPD 2006 - Rapid Product Development. 2006. Marinha Grande, Portugal.

98. Yang, S. Y. Chang, H. C., *Study on the performance of cooling systems in precision injection molds.* International Polymer Processing, 1995. **10**(2): p. 255-261.

99. Singh, K. J., *Mold Cooling*, in *CAE: Computer Aided Engineering for Injection Molding*, E.C. BERNHARDT, Editor. 1983, Carl Hanser Verlag: Munich.

100. Malloy, R. A., *Plastic part design for injection molding.* 1994, New York: Hanser Pulishers.

101. Zollner, O., *Optimised mould temperature control.* Application Technology Information, 1997: p. 1104 -1109.

102. Ahrens, C. H., Ribeiro Jr., A. S., Beal, V. E., *Heat Flux Canals (HFC) technique: an alternative to cool down stereolithography moulds.* Revista Brasileira de Ciências Mecânicas, 2003. **XXV**(3): p. 254-258.

103. Xu, X., Sachs, E., Allep, S., *The design of conformal cooling channels in injection molding tooling.* Polymer Engineering and Science, 2001. **41**(7): p. 1265-1279.

104. Xu, X., *Conformal Cooling and Rapid Thermal Cycling in Injection Molding by 3D Printed Tools*. Massachusets: Massachusetts Institute of Technology 1999. 122 p. PhD Thesis

105. Sachs, E., Wylonis, E., Allen, S., Cima, M., Guo, H., *Production of injection molding tooling with conformal cooling channels using the three dimensional printing process.* Polymer Engineering and Science, 2004. **40**(5): p. 1232 - 1247.

106. Ferreira, E. C. Mateus, A., *Studies of rapid soft tooling with conformal cooling channels for plastic injection moulding.* Journal of Materials Processing Technology, 2003. **142**(2): p. 508-516.

107. Voet, A., Pee, B. V., Mingneau, J., Cardon, L., Houtekier, R. *Optimization of conformal cooling by using new materials and production techniques.* PMI 2007 - Int. Conf. on Polymers & Moulds Innovations. 2007. Ghent, Belgium.

108. Peixoto, F. L., Cavalheiro, A. Z., Salmoria, G. V., Ahrens, C. H., Fascin, H. M., Hildebrand, C. P. *Thin wall plastic part design assisted by rapid tooling and cae technologies* RPD 2006 - Building the future by innovation. 2006. Marinha Grande, Portugal.

109. Pontes, A. J., Sousa, C., Gomes, C., Pouzada, A. S. *Characterization of composite systems used in the production of resin casting moulds.* PPS 24th Annual Meeting 2008. Salerno, Italy.

110. Sabino-Netto, A., Yañez, F. A., Ahrens, C. H., Salmoria, G. V. *Effects of mixing parameters on the quality of composite epoxy-aluminium tools.* PPS Americas Reg. Meeting. 2004. Florianópolis, Brazil.

111. Volpato, N. Derenievicki, O. F. *Uma Análise da Usinagem de Resinas para Ferramental Rápido.* III COBEF, ABCM. 2005. Joinville, Brasil.

112. Lanz, W. R., Melkote, S. N., Kotnis, M. A., *Machinability of rapid tooling composite board.* Journal of Materials Processing Technology, 2002(5760): p. 1-4.

113. Rosato, D. V., Rosato, D. V., Rosato, M. G., *Injection Molding Handbook.* 3rd ed. 2000, New York: Springer. 1488.

114. Cracknell, P. S. Dyson, R. W., *Handbook of thermoplastics injection mould design.* 1st Edition ed. 1993, London: Chapman & Hall. 144.

115. Strong, A. B., *Plastics, Materials and Processing.* 2nd ed. 1999, New Jersey: Prentice-Hall. 811.

116. Saraiva, V. Soares, R., eds. *Processos e Técnicas não convencionais - Manual do projectista para moldes de injeção de plástico.* Vol. 9. 2003, CENTIMFE: Marinha Grande, Portugal.

117. Dimla, D. E., Camilotto, M., Miani, F., *Design and optimisation of conformal cooling channels in injection moulding tools.* Journal of Materials Processing Technology, 2005. **164**: p. 1294-1300.

118. HibridMolde, *Moldes híbridos (Elementos de projecto em SLSm e RM).* 2005, Moliporex, S. A.; Universidade do Minho; Instituto Politécnico de Leiria; Centimfe, Lda.: Marinha Grande, Portugal. p. 108.

119. Queirós, M. P., Pontes, A. J., Pouzada, A. S. *Performance Assessment of Hybrid Moulds for Injection Moulding.* PMI 2005 - International Conference on Polymers & Moulds Innovations. 2005. Ghent, Belgium.

120. Barthés-Labrousse, M. G., *Adhesion mechanisms at amine-cured epoxy/aluminium interfaces.* Journal of Adhesion, 1996. **57**: p. 65-76.

121. Marsh, J., Minel, L., Barthés-Labrousse, M. G., Gorse, D., *Interaction of epoxy model molecules with aluminium, anodised titanium and copper surfaces: an XPS study.* Applied Surface Science, 1998. **133**: p. 270-286.

122. Brandrup, J., Immergut, E. H., Grulke, E. A., *Polymer Handbook.* 4th Edition ed. 2003, New York: Wiley-Interscience. 2336.

123. Westphal, M. G., Pouzada, A. S., Salmoria, G. V., Ahrens, C. H., *Performance and friction properties of injection hybrid moulds with stereolitography moulding zones.* Materials Science Forum, 2006. **514-516**: p. 1673-1677.

124. Palmer, A. E. Colton, J. S., *Failure Mechanisms in Stereolithography Injection Molding Tooling.* Polymer Engineering and Science, 2000. **40**(6): p. 1395-1404.

125. Gonçalves, M. W., Salmoria, G. V., Ahrens, C. H., Pouzada, A. S., *Study of tribological properties of moulds obtained by stereolithography.* Virtual and Physical Prototyping, 2007. **2**(1): p. 29-36.

126. Pouzada, A. S., Ferreira, E. C., Pontes, A. J., *Friction Properties on Moulding Thermoplastics.* Polymer Testing, 2006. **25**: p. 1017-1023.

127. Pontes, A. J. Pouzada, A. S., *Ejection force in tubular injection moldings. Part I: Effect of processing conditions.* Polymer Engineering and Science, 2004. **44** p. 891-898.

128. Lavielle, L., *Polymer - polymer friction: Relation to adhesion.* Wear, 1991. **151**: p. 63 - 75.

129. Fourche, G., *An overview of the basic aspects of polymer adhesion, Part I: Fundamentals.* Polymer Engineering and Science, 1995. **35**(12): p. 957-967.

130. Araújo, B. J. Pouzada, A. S., *Projecto de sistemas de extracção em moldes de injecção.* O Molde, 2002. **54**.

131. Voet, A., Dehaes, J., Mingneau, J., Kruth, J. P., Van Vaerenbergh, J. *Laser sintered injection moulds, case studies made in Belgium.* PMI 2005 - Int. Conf. on Polymers & Moulds Innovations. 2005. Ghent, Belgium.

132. Pontes, A. J., Ferreira, E. C., Pouzada, A. S. *Tribological aspects during ejection in injection moulds.* RPD 2004 - Agile Development for Productivity. 2004. Marinha Grande, Portugal.

133. Neto, V. F., Vaz , R., Ali, N., Oliveira, M. S. A., Grácio, J., *Performance of sub-micron diamond films coated on mould inserts for plastic injection moulding.* Journal of Materials and Science, 2008. **43**: p. 3392-3399.

134. Cardon, L., Houtekier, R., Ragaert, K., Moerman, M., *The effect of the mould material selection and production methodology on the thermal behaviour and tribology of injection moulds* in *Virtual and rapid manufacturing*, P.J. Bártolo, et al., Editor. 2008, Taylor and Francis: Leiria. p. 425 - 429.

135. Bryce, D. M., *Plastic Injection Molding: manufacturing process fundamentals* Fundamentals of injection molding series. 1996, Dearborn: Society of Manufacturing Engineers 277.

136. Pontes, A. J., Pantani, R., Titomanlio, G., Pouzada, A. S., *Solidification criterion on shrinkage predictions for semi-crystalline injection moulded samples, Vol. 15: nº 3 (2000) , p 284.* International Polymer Processing, 2000. **15**(3).

137. Pontes, A. J., Oliveira, M. J., Pouzada, A. S., *The effect of holding pressure on the shrinkage and birefringence of injection moulded polypropylene plates.* Materials Science Forum, 2004. **455-456**: p. 814-817.

138. Pontes, A. J., *Shrinkage and ejection forces in injection moulded products.* Guimarães: University of Minho, 2002. 198 p. PhD Thesis

139. Morelli, C. L., Sousa, J. A., Pouzada, A. S., *Assessment of weld line performance of pp/talc moldings produced in hot runner injection moulds.* Journal of Vinyl and Additive Technology, 2007. **13**: p. 159-165.

140. Martinez-Gamba, M., Pouzada, A. S., Frontini, P. M., *Impact properties and microhardness of double-gated glass reinforced polypropylene injection moldings.* Polym. Eng. Sci., 2009. **49**(9): p. 1688-1695.

141. Wang, Z., Lee, K. S., Fuh, J. Y. H., Li, Z., Zhang, Y. F., Nee, A. Y. C., Yang, D. C. H., *Optimum ejector system design for plastic injection mould.* International Journal of Materials & Product Technology 1996. **11**(5 and 6): p. 371-385.

142. Potsch, G. Michaeli, W., *Injection molding: An introduction.* 1995, Munich: Carl Hanser Verlag. 195.

143. Wang, T. J. Yoon, C. K. *Shrinkage and warpage analysis of injection-molded parts.* Proceedings ANTEC 2000 Conference. 2000. Orlando, USA.

144. Pontes, A. J., Pinho, A. M., Miranda, A. S., Pouzada, A. S., *Effect of processing conditions on ejection forces in injection moulds. O Molde.* 1997. p. 25 - 33.

145. Sasaki, T., Koga, N., Shirai, K., Kobayashi, Y., Toyoshima, A., *An experimental study on ejection force of injection molding.* Journal of Precision Engineering, 2000. **24**(3): p. 270 - 273.

146. Balsamo, R., Hayward, D., Malloy, R. *An experimental evaluation of ejection forces: frictional effects.* Proceedings ANTEC 1993 Conference. 1993. New Orleans, USA.

147. Pontes, A. J., Titomanlio, G., Pouzada, A. S. *The influence of processing conditions in ejection forces of injection moulded parts.* PPS 15th Annual Meeting. 1999. 'S Hertogenbosh, Netherlands.

148. Bareta, D. R., Pouzada, A. S., Costa, C. A. *The effect of rapid tooling materials on mechanical properties of tubular mouldings.* PMI 2007 - Int. Conf. on Polymers & Moulds Innovations. 2007. Ghent, Belgium.

149. Willis, S. *Rapid tooling for injection moulds: composite tooling/machine tooling comparison.* Proceedings of Rapid Prototyping and Manufacturing '97. 1997. Dearborn MI, USA.

150. Rahmati, S. Dickens, P. *Stereolithography injection moulding tooling.* Proceedings of the 6th European Conference on Rapid Prototyping and Manufacturing. 1997. Nottingham, UK.

151. Rahmati, S., Brown, S., Wykes, C. *Failure mechanisms of stereolithography tooling.* 8th European Conference on Rapid Prototyping and Manufacturing. 1999.

152. Hopkinson, N. Dickens, P., *Study of ejection forces in the AIM process.* Materials and Design, 1999. **20**(2): p. 99 - 105.

153. Ludema, K. C., ed. *Sliding and adhesive wear.* ASM Handbook - Friction, Lubrification and Wear Technology, ed. M. Park. Vol. 18. 1992: Ohio/USA.

154. Ludema, K. C., *Friction wear lubrification: a textbook in tribology.* 1 ed. 1996, Michigan: CRC-Press. 272.

155. Blau, P. J., ed. *Friction and wear of components.* ASM Handbook - Friction, Lubrification and Wear Technology. Vol. 18. 1992, American Society for Metals: Ohio. 499-692.

156. Menges, G. Bangert, H., *Measurement of coefficient of static friction as a means of determining opening and demoulding forces in injection moulds.* Kunststoffe German Plastics, 1981. **71**(9): p. 552 - 557.

157. Ferreira, E. C., Costa, M. F., Laranjeiro, C. R., Oliveira, M. J., Pouzada, A. S., *Comparative study, by optical techniques of the interface polymer/steel in replication conditions* Materials Science Forum, 2004. **455-456** p. 467-471.

158. Engelmann, P., Hayden, K., Guichelaar, P., Monfore, M. *Undercutting mold performance: Ejection wear.* Proceedings ANTEC 2002 Conference. 2002. San Francisco, USA.

159. Correia, M., Capela, C., Pouzada, A. S., Miranda, A. S. *Contributions to the modelling of ejection in injection moulding.* PMI 2007 - Int. Conf. on Polymers & Moulds Innovations. 2007. Ghent, Belgium.

160. Pontes, A. J., Pantani, R., Titomanlio, G., Pouzada, A. S. *On the prediction of ejection forces for tubular moldings.* Proceedings ANTEC 2002 Conference. 2002. San Francisco, USA.

161. Petrie, E. M., *Handbook of adhesives and sealants*. 2000, New York: McGraw-Hill.

162. Viana, J. C., Cunha, A. M., Billon, N., *The tensile behaviour of an injection moulding propylene-ethylene copolymer: effect of the local thermomechanical conditions*. International Polymer Processing, 1997(43): p. 159-166.

163. Jansen, K. M. B., *Residual stresses in quenched and injection moulded products*. International Polymer Processing, 1994. **9**(1): p. 82-89.

164. Viana, J. C., *Mechanical Characterisation of Injection Moulded Plates*. Guimarães: Universidade do Minho, 1999. PhD Thesis

165. Brito, A. M., Cunha, A. M., Pouzada, A. S., Crawford, R. J., *Predicting the skin-core boundary location in injection moldings*. International Polymer Processing, 1991. **6**(4): p. 370-377.

166. Kistler, I. A., *Plastics Processing. Injection Molding, Extrusion, Die Casting*. 1998, Kistler Instrumente AG: Winterthur.

167. Johannaber, F., *Injection molding machines*. 3rd ed. ed. 1994, New York: Hanser Publishers. 315.

168. Viana, J. C., Billon, N., Cunha, A. M., *The thermomechanical environment and the mechanical properties of injection moldings* Polymer Engineering and Science, 2004. **44**(8): p. 1522-1533.

169. Viana, J. C., Cunha, A. M., Billon, N., *The thermomechanical environment and the microstructure of an injection moulded polypropylene copolymer*. Polymer, 2002. **43**(15): p. 4185-4196.

170. Oliveira, M. J., Bernardo, C. A., Hemsley, D. A., *Morphology and mechanical behavior of polypropylene hot plate welds*. Polymer Engineering and Science, 2001. **41**(11): p. 1913-1922.

171. Viana, J. Cunha, A. M. *Impact Performance of Injection Molded PP Plates*. PPS 12th Annual Meeting. 1996. Sorrento/Italy.

172. Cunha, A. M., Pouzada, A. S., Crawford, R. J., *A study of the impact behaviour of injection moulded polypropylene using two different modes of testing*. Plastics Rubber and Composites Processing and Applications, 1992. **18** (2): p. 79-90.

173. Oliveira, M. J., *Microscopia Óptica*, in *Técnicas de Caracterização de Polímeros*, S.V. Canevarolo, Editor. 2004, Artliber: São Paulo.

174. Hemsley, D. A., *Applied Polymer Light Microscopy*. 1989, Barking: Elsevier Applied Science.

175. Fujiyama, M., Wakino, T., Kawasaki, Y., *Structure of the skin layer in injection-molded polypropylene*. Journal of Applying Polymer Science, 1988. **35**(11): p. 29-49.

176. Pouzada, A. S. *Predicting the mechanical behaviour of anisotropic moulded plates*. 3rd Japan Int SAMPE Symposium. 1993. Tokyo, Japan.

177. Tordjeman, P., Robert, C., Marin, G., Gerard, P., *The effect of α, β crystalline structure on the mechanical properties of polypropylene*. European Physical Journal E, 2001. **4**(4): p. 459-465.

178.   Tjong, S. C., Shen, J. S., Li, R. K. Y., *Morphological behaviour and instrumented dart impact properties of β-crystalline-phase polypropylene.* Polymer Engineering and Science, 1995. **37**(12): p. 2309-2316.

179.   Yuan, Y., Chen, B., Zhan, X., *Study on the formation of b-crystal during the crystallization process of polypropylene reactor granule.* Polymer Engineering and Science, 2007. **48** p. 5480-5483.

180.   Williams, R. F. Pacoast, L. H. *Effect of process variables on mold shrinkage.* Modern Plastics International. 1967.

181.   Fischer, J. M. Maier, C., *Handbook of molded part shrinkage and warpage*, ed. W. Andrew. 2003, Morris, NY: Plastics Design Library. 252.

182.   Voet, A., Pee, B. V., Mingneau, J., Cardon, L., Houtekier, R. *Optimization of conformal cooling by use of "design of experiments": industrial case study of an injection molded product.* RPD 2006 - Rapid Product Development. 2006. Marinha Grande, Portugal.

183.   Cardon, L., *A generic procedure for mould material thermal behaviour modelling using finite element simulation of hybrid injection moulds.* 2005. Ph D

184.   Guimarães, D. A., Alves, A., Pontes, A. J. *Thermal study of stereolithography moulding inserts.* RPD 2006 - Building the future by innovation. 2006. Marinha Grande, Portugal.

185.   Gomes, C., Lino, J., Cardon, L., Pouzada, A. S., Pontes, A. J. *An insight on the thermo-mechanical behaviour of deep core hybrid moulds.* PMI 2007 - Int. Conf. on Polymers & Moulds Innovations. 2007. Gent, Belgium.

186.   Candal, M. V. Morales, R. A., *Design of plastic pieces and their molds using CAD/CAE Tools.* Computer Applications in Engineering Education, 2005. **13**(4): p. 233-239.

187.   Shan, Z., Yan, Y., Zhang, R., Lu, Q., Guan, L., *Rapid manufacture of metal tooling by rapid prototyping.* International Journal of Advanced Manufacturing Technology, 2003. **21**: p. 469-475.

188.   Nagahanumaiah, Ravi, B., Mukherjee, N. P., *An integrated framework for die a mold cost estimation using design features and tooling parameters.* International Journal of Advanced Manufacturing Technology, 2005. **26**(9-10): p. 1138-1149.

189.   Peças, P., Henriques, E., Ribeiro, I., Pouzada, A. S., Pontes, A. J. *The use of RPT for low and very low production series: A case-study analysis.* RPD2008 - Designing the Industry of the Future. 2008. Oliveira de Azeméis, Portugal.

190.   Zhou, G. J., Hercovici, D., Calvin, C. C., *Parametric process optimization to improve the accuracy of rapid prototyped stereolithography parts.* International Journal of Machine Tools & Manufacture, 1996. **2**(3): p. 4-15.

191.   Peças, P., Henriques, E., Quinas, P., Gomes, C., Pouzada, A. S., Pontes, A. J. *A contribution to the life cycle management application to mould making business.* RPD 2006 - Building the future by innovation. 2006. Marinha Grande, Portugal.

192.   Hopkinson, N. Dickens, P. M., *Predicting stereolithography injection mould tool behavior using models to predict ejection force and tool strength.* International Journal of Production Research, 2000. **38**(16): p. 3747-3757.

193. Incropera, F. P., Dewitt, D. P., Bergman, T. L., S., L. A., *Fundamentals of Heat and Mass Transfer*. 6th ed. ed. 2007, New York: John Wiley & Sons, Inc. 997.

194. Holman, J. P., *Heat Transfer*. 1989, New York: MacGraw Hill, Inc.

195. Martinho, P. G., Bartolo, P. J., Pouzada, A. S., *Hybrid moulds: effect of the moulding blocks on the morphology and dimensional properties*. Rapid Prototyping Journal, 2009. **15** (1): p. 71-82.

196. White, F. M., *Fluid Mechanics*. 2006, New York: McGraw-Hill Inc. 864.

197. Hele-Shaw, H. S., *The flow of water*. Nature, 1898. **58**(34).

198. Kennedy, P., ed. *Flow Analysis of injection molds*. 1995, Moldflow Pty. Ltd.,Hanser: New York. 237.

199. Wang, V. W., Hieber, C. A., Wang, K. K., *Dynamic simulation and graphics for the injection molding of three-dimensional thin parts*. Journal of Polymer Engineering, 1986. **7**(21).

200. Yu, L., Lee, L. J., Koelling, K. W., *Flow and heat transfer simulation of injection molding with microstructures*. Polymer Engineering and Science, 2004. **44**(10): p. 10.

201. Hetu, J. F., Gao, D. M., Garcia-Rejon, A., Salloum, G., *3D finite element method for the simulation of the filling stage in injection molding*. Polymer Engineering and Science, 1998. **38**(2): p. 223-236.

202. CoreTech, *Moldex3D User's Manual*. Vol. Document No. MDXR9.1-v01-081130. 2009, Taichung: CoreTech System Co.

203. Shoemaker, J., *Moldflow Design Guide* 2006, Chicago: Hanser Gardner Publications 326.

204. Maier, C., *Moldex3D moves in. British Plastics & Rubber*. 2003, MCM, Caterham, ROYAUME-UNI. p. 39-40.

205. Cao, W., Wang, R., Shen, C. Y., *A dual domain method for 3-D flow simulation* Polymer - Plastics Technology and Engineering 2004. **43**(5): p. 1471-1486.

206. Araújo, B. J., Teixeira, J. C. F., Cunha, A. M., Groth, C. P. T., *Parallel three-dimensional simulation of the injection molding process*. International journal for numerical methods in fluids, 2009. **59**(7): p. 801–815.

207. Ilinca, F. Hétu, J.-F., *Three-dimensional filling and post-filling simulation of polymer injection molding*. International Polymer Processing 2001. **16**: p. 291-301.

208. Chung, S. T. Kwon, T. H., *Numerical-simulation of fiber orientation in injection-molding of short-fiber-reinforced thermoplastics*. Polymer Engineering and Science 1995. **35**(7): p. 604-618.

209. Cutler, B., Dorsey, J., McMillan, L. *Simplification and improvement of tetrahedral models for simulation*. Proceedings of the 2004 Eurographics/ACM SIGGRAPH Symposium on Geometry Processing. 2004. Nice, France.

210. Martinho, P. G., Bártolo, P. J., Pontes, A. J., Pouzada, A. S. *Structural and thermal aspects of the performance of hybrid moulds with SLS*. Proceedings ANTEC 2006 Conference. 2006. Charlotte, USA.

211.   Attanasio, D. C., Hopkinson, N., Kehrberger, R., Sridhar, A., Witt, G., *Application and modelling of hybrid stereolithography injection mould tooling* Virtual and Physical Prototyping 2006. **1**(3): p. 197 - 206.

212.   Aluru, R., Keefe, M., Advani, S., *Simulation of injection molding into rapid-prototyped molds.* Rapid Prototyping Journal, 2001. **7**(1): p. 42-51.

213.   Martinho, P. G., Cardon, L., Neves, T., Bartolo, P. J., Pouzada, A. S. *On the influence of the materials used on the moulding blocks of hybrid moulds*. PMI 2008 - Int. Conf. on Polymers & Moulds Innovations. 2008. Ghent, Belgium.

214.   Martinho, P. G., Neves, T., Bártolo, P. J., Pouzada, A. S., *The use of Moldex3D to predict flow, thermal and shrinkage on injection moulding with hybrid moulds.* E.U. Meeting, Editor. 2008: Chester, UK.

215.   Shojaefard, M. H. Goudarzi, K., *The numerical estimation of thermal contact resistance in contacting surfaces.* American Journal of Applied Sciences 2008.

216.   Madhusudana, C. V., *Thermal contact conductance.* 1996, Berlin: Springer.

217.   Thompson, M. K. Thompson, J. M., *Considerations for predicting Thermal Contact Resistance in ANSYS.* 2007, KAIST-Korea Advanced Institute of Science and Technology: Daejeon, South Korea.

218.   Thompson, M. K., *A multi-scale iterative approach for finite element modeling of Thermal Contact Resistance* Massachusetts: Massachusetts Institute of Technology, 2007. PhD Thesis

219.   Moldflow, P. I., ed. *Simulation Fundamentals Training Practice.* 2006, Moldflow Corporation Inc.: Chicago. 512.

220.   Martinho, P. G., Bártolo, P. J., Pouzada, A. S. *Efficient design solutions for hybrid moulds and the widening of the lifecycle of injection moulds*. PMI 2007 - Int. Conf. on Polymers & Moulds Innovations. 2007. Ghent, Belgium.

221.   Jacobs, P. F., *Rapid Prototyping & Manufacturing: Fundamentals of StereoLithography*. 1st ed. 1992, Dearborn MI: SME. 434.

222.   Tenma, M. Yamaguchi, M., *Structure and properties of injection-molded polypropylene with sorbitol-based clarifier.* Polymer Engineering and Science, 2007. **47**(9): p. 1441-1446.

223.   Martinho, P. G., Cardon, L., Neves, T., Bártolo, P. J., Pouzada, A. S. *A study of the ejection forces on moulding inserts obtained by RPT techniques*. RPD2008 - Designing the Industry of the Future. 2008. Oliveira de Azeméis, Portugal.

Appendixes

Appendix 1

Mathcad program

1. Algorithm of the HM-1 T(t) program

Determination the transient temperature along the HM-1 moulding zone thickness, Figure 70 (cooling layer, core and cavity moulding blocks and injected polymer).
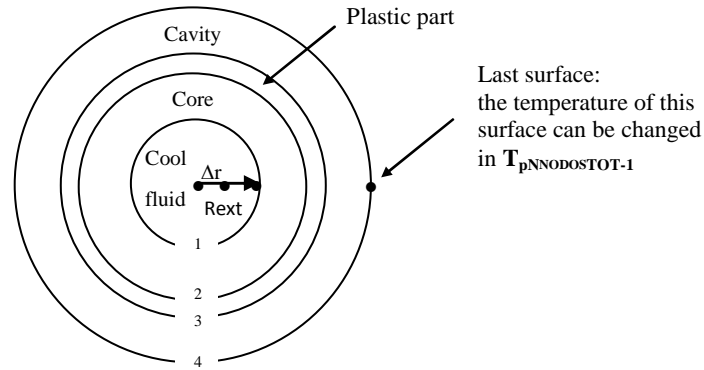
Figure 70 - Top view of the HM-1 moulding zone (moulding blocks and plastic part or impression)

In this case study was considered 4 layers. Each layer has respective external radius (Rext):

NCamadas := 4
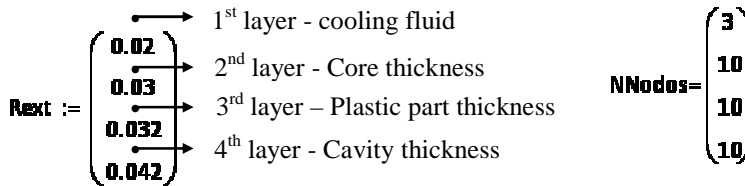
$$\text{Rext} := \begin{pmatrix} 0.02 \\ 0.03 \\ 0.032 \\ 0.042 \end{pmatrix}$$

1st layer - cooling fluid
2nd layer - Core thickness
3rd layer – Plastic part thickness
4th layer - Cavity thickness

$$\text{NNodos} = \begin{pmatrix} 3 \\ 10 \\ 10 \\ 10 \end{pmatrix}$$

The HM-1 moulding zone was discretized in 30 nodes (the first one, in the centre of the problem, is the number zero) once 3 nodes, positioned in layers interfaces, are shared by the respective adjacent layers.

1. Input data

1.1. Geometry

1.2. Mesh parameters

1.3. Materials

1.3.1. Input the cooling fluid and the mould material specific heat in respective layers (cP(Tempera))

1.3.3. Input the material density in each layer (ρ (Tempera))

1.3.4. Input material thermal conductivity in each layer (k (Tempera))

1.3.5. Input the cycle time for simulation (t_{Tot})

1.3.6. Input the border conditions

1.3.6.2. Cooling fluid temperature (T if *Camada Actual* (r) = 0)

1.3.6.2. Core moulding block temperature (T if *Camada Actual* (r) = 1)

1.3.6.3. Initial plastic temperature (T if *Camada Actual* (r) = 2)

1.3.6.4. Cavity moulding block temperature (T if *Camada Actual* (r) = 3)

Example:

$$
\text{TPerm}\,(r) := \begin{vmatrix} T \leftarrow 40\ ^\circ C & \text{if} & \text{CamadaActual}\ (r) = 0 \\ T \leftarrow 40\ ^\circ C & \text{if} & \text{CamadaActual}\ (r) = 1 \\ T \leftarrow 250\ ^\circ C & \text{if} & \text{CamadaActual}\ (r) = 2 \\ T \leftarrow 40\ ^\circ C & \text{if} & \text{CamadaActual}\ (r) = 3 \end{vmatrix}
$$

2. Program

2.1. Mesh generation

2.1.1. Number total of nodes (NNodosTot)

Example:

$$
\text{NNodosTot} := \begin{vmatrix} \text{for}\ \ i \in 1..\text{NCamadas}\ -1 \\ \quad \text{NNodosTotParcial} \leftarrow \text{NNodosTotParcial} + \left(\text{NNodos}_i - 1\right) \\ \text{NNodosTot} \leftarrow \text{NNodos}_0 + \text{NNodosTotParcial} \end{vmatrix} = 30\ \blacksquare
$$

2.1.2. Distance between nodes in each layer (Δr)

The distance between nodes (Δr) in each layer depends on the layer thickness and number of nodes considered in the respective layer.

Example: the dimension of the first layer is 0.02 m (Figure 1) and the first layer was discretized in 3 nodes (that corresponds to 2 distances). So the distance between nodes is 0.01 m.

$$
\Delta r := \text{for}\ \ i \in 0..\text{NCamadas}\ -1 \quad = \begin{pmatrix} 0.01 \\ 1.111 \times 10^{-3} \\ 2.222 \times 10^{-4} \\ 1.111 \times 10^{-3} \end{pmatrix} m\ \blacksquare
$$

$$
\begin{vmatrix} \Delta r_i \leftarrow \dfrac{\text{Rext}_i}{\text{NNodos}_i - 1} & \text{if}\ \ i = 0 \\[2mm] \Delta r_i \leftarrow \dfrac{\text{Rext}_i - \text{Rext}_{i-1}}{\text{NNodos}_i - 1} & \text{if}\ \ i > 0 \\[2mm] \Delta r \end{vmatrix}
$$

2.1.3. Distance from centre to each node (r)

Example:

	0
14	0.0307
15	0.0309
16	0.0311
17	0.0313
18	0.0316
19	0.0318
20	0.032
21	0.0331
22	0.0342
23	0.0353
24	0.0364
25	0.0376
26	0.0387
27	0.0398
28	0.0409
29	...

$$rm := \begin{array}{|l} k \leftarrow 0 \\ rmacumulado \leftarrow 0 \\ \quad \text{for} \quad i \in 0\,..\, NCamadas \, -1 \\ \qquad \begin{array}{|l} \text{for} \quad j \in 0\,..\, NNodos_i - 1 \\ \qquad \begin{array}{|l} rm_k \leftarrow \Delta r_i \cdot j \\ rm_k \leftarrow rmacumulado \, + rm_k \\ lastrm \, \leftarrow rm_k \quad \text{if} \quad j = NNodos_i - 1 \\ k \leftarrow k + 1 \end{array} \\ rmacumulado \, \leftarrow lastrm \\ k \leftarrow k - 1 \end{array} \\ rm \end{array} = \begin{array}{} \end{array} \, m \, \blacksquare$$

2.2. Determination the materials properties necessary to the numerical calculus

2.2.1. Determination the plastic material specific heat variation with temperature (cP(Tempera))= f (T))

The expressions cPL, cPT and cPS were used to calculate the cPPlastic, depending on the temperature of the graph of the Figure 71 (in this case for the PP material).

$$cPL(Tempera) := 0.837 \cdot Tempera \cdot \frac{m^2}{K^2 \cdot s^2} + 2.221 \times 10^3 \cdot \frac{m^2}{K \cdot s^2}$$

$$cPT(Tempera) := \frac{686.72137 \cdot Tempera}{480.97208 \ K - Tempera} \cdot \frac{m^2}{K \cdot s^2}$$

$$cPS(Tempera) := 8.039 \cdot Tempera \cdot \frac{m^2}{K^2 \cdot s^2} - 705.258 \cdot \frac{m^2}{K \cdot s^2}$$

$$cPPlástico \, (Tempera) := \begin{array}{|ll} cPL(Tempera) & \text{if} \quad Tempera \geq 448.15 \ K \\ cPT(Tempera) & \text{if} \quad 370 \ K < Tempera \leq 448.15 \ K \\ cPS(Tempera) & \text{otherwise} \end{array}$$

Tempera := 0K, 1K .. 500K

Figure 71 – Specific heat variation with the temperature for the injected plastic used (PP)

2.2.2. Determination the materials thermal diffusivity in respective layers (α(Tempera))= f (T))

The expression α (Tempera) was used to calculate the materials diffusivity in respective layers

$$\alpha(\text{Tempera}) := \text{for } i \in 0 .. \text{NCamadas } -1$$
$$\alpha_i \leftarrow \frac{\text{CondT (Tempera)}_i}{\rho(\text{Tempera })_i \text{ cP(Tempera)}_i} \qquad \alpha(100\,°C) = \begin{pmatrix} 1 \times 10^{-7} \\ 8.082 \times 10^{-6} \\ 6.949 \times 10^{-8} \\ 8.082 \times 10^{-6} \end{pmatrix} \frac{m^2}{s} \blacksquare$$
$$\alpha$$

2.2.3. Determination the $\Delta t_{\text{máximo}}$ per iteration

The calculation of the maximum possible time break ($\Delta t_{\text{máximo}}$) per iteration, for convergence solution, was based on stability criteria:

1-4 $F_0 \geq 0$ (more unfavourable way, node 0)

where F_0 is the Fourier number.

$$\text{Fo (Tempera)} := \text{for } i \in 0 .. \text{NCamadas } -1$$
$$\text{Fo}_i \leftarrow \frac{\alpha(\text{Tempera })_i \cdot \Delta \text{tmaxass}}{(\Delta r_i)^2}$$
$$\text{Fo}$$

where,

$$\Delta tmax := \text{for} \quad i \in 0..\text{NCamadas} - 1$$

$$\left| \begin{array}{l} \Delta tmax_i \leftarrow \dfrac{1}{4} \cdot \dfrac{(\Delta r_i)^2}{\alpha(\text{TemperaMin})_i} \\[2mm] \Delta tmax \end{array} \right.$$

$$\Delta tmax := \min(\Delta tmax)$$

$$\Delta tmax = 0.038 \text{ s } \blacksquare$$

Supposing a Δt value 5 % inferior to the maximum of the stability criteria (convergence), *i. e.*,

$$\Delta tmaxass := 0.95 \cdot \min(\Delta tmax)$$

$$\Delta tmaxass = 0.036 \text{ s } \blacksquare$$

2.3. Determination the equivalent properties in the nodes of the layers transition (ρ_{eq}, cp_{eq}, α_{eq}, F_{0eq})

For the layers transitions, i.e. for the border nodes (the nodes in the interfaces) it was defined equivalent properties, because there are different materials to be considered in the volume of control around these nodes.

2.3.1. Density equivalent

$$\rho eq(\text{Tempera}) := \text{for} \quad i \in 0..\text{NCamadas} - 2$$

$$\left| \begin{array}{l} \rho eq_i \leftarrow \dfrac{\rho(\text{Tempera})_i \cdot \left(\text{Rext}_i - \dfrac{\Delta r_i}{4}\right) \cdot \dfrac{\Delta r_i}{2} + \rho(\text{Tempera})_{i+1} \cdot \left(\text{Rext}_i + \dfrac{\Delta r_1}{4}\right) \cdot \dfrac{\Delta r_{i+1}}{2}}{\left(\text{Rext}_i - \dfrac{\Delta r_i}{4}\right) \cdot \dfrac{\Delta r_i}{2} + \left(\text{Rext}_i + \dfrac{\Delta r_{i+1}}{4}\right) \cdot \dfrac{\Delta r_{i+1}}{2}} \\[4mm] \rho eq \end{array} \right.$$

2.3.2. Specific heat equivalent

$$cPeq(\text{Tempera}) := \text{for} \quad i \in 0..\text{NCamadas} - 2$$

$$\left| \begin{array}{l} cPeq_i \leftarrow \dfrac{\rho(\text{Tempera})_i \cdot cP(\text{Tempera})_i \cdot \left(\text{Rext}_i - \dfrac{\Delta r_i}{4}\right) \cdot \dfrac{\Delta r_i}{2} + \rho(\text{Tempera})_{i+1} \cdot cP(\text{Tempera})_{i+1} \cdot \left(\text{Rext}_i + \dfrac{\Delta r_1}{4}\right) \cdot \dfrac{\Delta r_{i+1}}{2}}{\rho eq(\text{Tempera})_i \cdot \left[\left(\text{Rext}_i - \dfrac{\Delta r_i}{4}\right) \cdot \dfrac{\Delta r_i}{2} + \left(\text{Rext}_i + \dfrac{\Delta r_{i+1}}{4}\right) \cdot \dfrac{\Delta r_{i+1}}{2}\right]} \\[4mm] cPeq \end{array} \right.$$

2.3.3. Thermal diffusivity equivalent

The thermal diffusivity equivalent on the left and on the right of the node was determined by the equations respectively:

$\alpha eqe\ (Tempera\ ) := for\quad i \in 0..\ NCamadas\ -2$

$$\alpha eqe_i \leftarrow \frac{CondT\ (Tempera\ )_i}{\rho eq\ (Tempera\ )_i \cdot cPeq\ (Tempera\ )_i}$$

$$\alpha eqe$$

$\alpha eqd\ (Tempera\ ) := for\quad i \in 0..\ NCamadas\ -2$

$$\alpha eqd_i \leftarrow \frac{CondT\ (Tempera\ )_{i+1}}{\rho eq\ (Tempera\ )_i \cdot cPeq\ (Tempera\ )_i}$$

$$\alpha eqd$$

2.3.4. Fourier number equivalent

The Fourier number equivalent, on the left and on the right of the node, was determined by the equations, respectively:

$Foeqe\ (Tempera\ ) := for\quad i \in 0..\ NCamadas\ -2$

$$Foeqe_i \leftarrow \frac{\Delta tmaxass\ \cdot \alpha eqe\ (Tempera\ )_i}{(\Delta r_i)^2}$$

$$Foeqe$$

$Foeqd\ (Tempera\ ) := for\quad i \in 0..\ NCamadas\ -2$

$$Foeqd_i \leftarrow \frac{\Delta tmaxass\ \cdot \alpha eqd\ (Tempera\ )_i}{(\Delta r_{i+1})^2}$$

$$Foeqd$$

Note: By the Fourier number definition, it is verified that Foeq will be stayed between Fo on the left and Fo on the right, therefore it is not necessary to consider the intermediary nodes to fulfill the convergence criteria.

2.4. Determination of the total iterations number (NIT)

$$NIT := floor\left(\frac{tTot}{\Delta tmaxass}\right) + 1 = 1.654 \times 10^3 \blacksquare$$

2.5. Calculation the transient temperatures in the materials

List of the developed program (appendix…)

3. Results

3.1. Print the temperature results

3.2. End program

Notes about temperature results

Table 17 shows the temperature results in the different nodes of the problem at the instant times represented by the lines of the iteration number.

Table 17 – Temperature results

	0	1	2		27	28	29
0	40	40	40		40	40	40
1	40	40	40		40	40	40
2	40	40	40		40	40	40
3	40	40	40		40	40	40
4	40	40	40		40	40	40
5	40	40	40		40	40	40
6	40	40	40		40	40	40
7	40	40	40		40.008	40	40
8	40	40	40		40.034	40.002	40
9	40	40	40		40.086	40.009	40
10	40	40	40		40.167	40.025	40
11	40	40	40		40.277	40.052	40
12	40	40	40		40.415	40.092	40
13	40	40	40		40.576	40.146	40
14	40	40	40		40.757	40.211	40
15	40	40	40		40.952	40.288	...

$\text{TTransiente} =$ (table above) $\cdot °C$

The columns numbers represents the nodes of the problem (from 0-centre to 29-last surface). The line numbers represents the iteration number that multiplied by the time between 2 consecutive iterations gives us the correspondent instant of time:

e.g., 0.03628 x 3 = 0.1s (the third line corresponds to the instant of 0.1 s)

0.03628 x 275 = 9.977s (the 275 line corresponds to the instant of ≈ 10s)

To know at what line of the table corresponds the instant t, it is only necessary make the relation between t and Δtmaxass (t/Δtmaxass):

e.g., the line that corresponds to the instant of 40s is 40/0.03628 = <u>1102</u>

The total number of iterations needed for 60s cycle time is given by NIT

$\text{NIT} = 1.654 \times 10^3 \blacksquare$

The minimum time between iterations is 0.03628 s

$\Delta\text{tmaxass} = 0.03628 \text{ s} \blacksquare$

Δr is the distance between nodes in each layer.

$$\Delta r = \begin{pmatrix} 0.01 \\ 1.111 \times 10^{-3} \\ 2.222 \times 10^{-4} \\ 1.111 \times 10^{-3} \end{pmatrix} \text{ m} \blacksquare$$

e. g. the first layer has a radium value of 0.02 m and it is discretized in 3 nodes. Dividing by 2 spaces the distance between nodes in this layer is 0.01 m.

Selection the breaks of time for representation

$\text{NIntervalos} := 10$

$$Tt := \begin{array}{|l} Tt_0 \leftarrow \text{submatrix}\,(\text{TTransiente}\,,0\,,0\,,0\,,\text{NNodosTot}\ -1) \\[4pt] \text{for}\quad i \in 1\,..\,\text{NIntervalos} \\[4pt] \qquad \begin{array}{|l} ac \leftarrow i \cdot \dfrac{\text{NIT}}{\text{NIntervalos}} + ac \\[6pt] \qquad \displaystyle\sum_{n\,=\,1} n \\[6pt] Tt_i \leftarrow \text{submatrix}\,(\text{TTransiente}\,,\text{floor}\,(ac)\,,\text{floor}\,(ac)\,,0\,,\text{NNodosTot}\ -1) \end{array} \\[4pt] Tt \end{array}$$

$$Tt = \begin{array}{|c|c|} \hline & 0 \\ \hline 0 & [1,\,30] \\ \hline 1 & [1,\,30] \\ \hline 2 & [1,\,30] \\ \hline 3 & [1,\,30] \\ \hline 4 & [1,\,30] \\ \hline 5 & [1,\,30] \\ \hline 6 & [1,\,30] \\ \hline 7 & [1,\,30] \\ \hline 8 & [1,\,30] \\ \hline 9 & [1,\,30] \\ \hline 10 & [1,\,30] \\ \hline \end{array} \cdot °C$$

$$Tt_0^{\ T} = \begin{array}{|c|c|} \hline & 0 \\ \hline 0 & 40 \\ \hline 1 & 40 \\ \hline 2 & 40 \\ \hline 3 & 40 \\ \hline 4 & 40 \\ \hline 5 & 40 \\ \hline 6 & 40 \\ \hline 7 & 40 \\ \hline 8 & 40 \\ \hline 9 & 40 \\ \hline 10 & 40 \\ \hline 11 & 250 \\ \hline 12 & 250 \\ \hline 13 & 250 \\ \hline 14 & 250 \\ \hline 15 & \dots \\ \hline \end{array} \cdot °C \quad rm = \begin{array}{|c|c|} \hline & 0 \\ \hline 0 & 0 \\ \hline 1 & 0.01 \\ \hline 2 & 0.02 \\ \hline 3 & 0.021 \\ \hline 4 & 0.022 \\ \hline 5 & 0.023 \\ \hline 6 & 0.024 \\ \hline 7 & 0.026 \\ \hline 8 & 0.027 \\ \hline 9 & 0.028 \\ \hline 10 & 0.029 \\ \hline 11 & 0.03 \\ \hline 12 & 0.03 \\ \hline 13 & 0.03 \\ \hline 14 & 0.031 \\ \hline 15 & \dots \\ \hline \end{array} \cdot m \blacksquare$$

Temperature results representation in the instants of time pre-defined

Figure 72 shows the representation curves of the temperature variation along the different layers defined in the problem (defined in *x* axis by the Rext (m)) and in the 11 different instants of time (defined by the curves) including the initial one (grey curve) as the correspondence showed in the table "Tempo".

$$\text{acumulador} := \left[\sum_{n\,=\,1}^{\text{NIntervalos}} (\text{const} \cdot n) \right]$$

$$\sum_{n\,=\,1}^{NIntervalos} (const \cdot n) \le NIT$$

$$const \le \frac{NIT}{\displaystyle\sum_{n\,=\,1}^{NIntervalos} (n)}$$

	0
0	0
1	1.091
2	3.273
3	6.546
4	10.91
5	16.364
6	22.91
7	30.547
8	39.274
9	49.093
10	60.002

$Tempo =$ ... $\cdot s$ ∎

Figure 72 – Temperature representation curves in different instants of time

Auxiliary data

The data exemplified below possibility the calculus of cooling rates in different instants of time during the injection cycle in each node characterized in the problem.

$T1 := submatrix \; (TTransiente \;, 28\,, 28\,, 0\,, NNodosTot \; - 1)$

$T1 =$

	0	1	2	3	4	5	6
0	40	40	40	42.208	44.811	48.19	...

$\cdot\; °C$

$T10 := submatrix \; (TTransiente \;, 275\,, 275\,, 0\,, NNodosTot \; - 1)$

$T10 =$

	0	1	2	3	4	5	6
0	40	40	40	42.526	44.892	47.083	...

$\cdot\; °C$

2. List of the program

List of a program (*Mathcad*) developed to numerically solve the heat diffusion equation applied to the HM-1 mould (cylindrical coordinates). From this program the temperature fields, both in the injected plastic part and in the moulding blocks, can be numerically predicted for the similar conditions of the experimented ones.

Input data

- Geometry and mesh parameter:

i) Number of cylindrical layers (materials) and respective thickness;

ii) Number of intended nodes in each layer for mesh generation

In the Figure **73** (*Example:* For the studied case) was considered 4 layers. Each layer has the respective external radius showed below:

External radius   and nº of nodes in each layer are shown below

NCamadas := 4
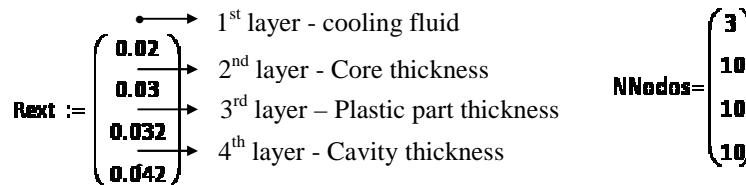
The HM-1 moulding zone was discretized in 30 nodes (the first one, in the centre of the problem, is the number zero) once 3 nodes, positioned in layers interfaces, are shared by the respective adjacent layers.
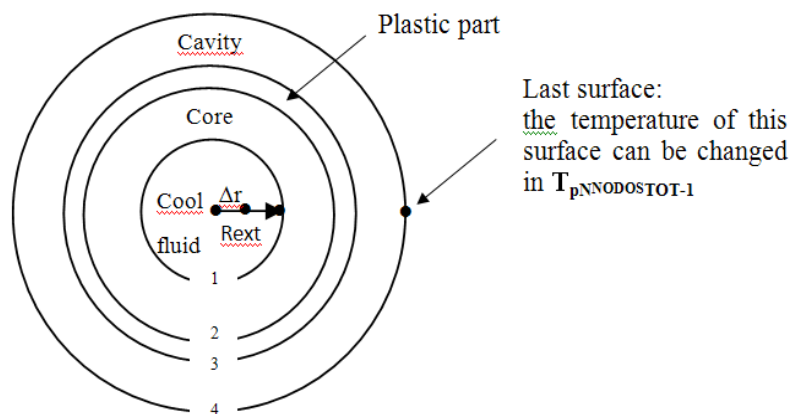
Figure 73 - Top view of the HM-1 moulding zone (moulding blocks and plastic part (or impression)

$$
\text{NNodosTot} := \left| \begin{array}{l} \text{for} \quad i \in 1..\text{NCamadas} \; - 1 \\ \quad \text{NNodosTotParcial} \; \leftarrow \text{NNodosTotParcial} \; + \left(\text{NNodos}_i - 1\right) \\ \text{NNodosTot} \; \leftarrow \text{NNodos}_0 + \text{NNodosTotParcial} \end{array} \right. = 30 \; \blacksquare
$$

The dimension between nodes (Δr) depends on the layer thickness and number of nodes considered in the respective layer, e.g., the dimension of the first layer is 0.02 m (Figure **70**) and the first layer was discretized in 3 nodes (that corresponds to 2 distances). So the distance between nodes is 0.01 m.

$$
\Delta r := \left| \begin{array}{l} \text{for} \quad i \in 0..\text{NCamadas} \; - 1 \\ \quad \left| \begin{array}{l} \Delta r_i \leftarrow \dfrac{\text{Rext}_i}{\text{NNodos}_i - 1} \quad \text{if} \quad i = 0 \\ \Delta r_i \leftarrow \dfrac{\text{Rext}_i - \text{Rext}_{i-1}}{\text{NNodos}_i - 1} \quad \text{if} \quad i > 0 \\ \end{array} \right. \\ \Delta r \end{array} \right. = \begin{pmatrix} 0.01 \\ 1.111 \times 10^{-3} \\ 2.222 \times 10^{-4} \\ 1.111 \times 10^{-3} \end{pmatrix} \text{m} \; \blacksquare
$$

$$
\text{rm} := \left| \begin{array}{l} k \leftarrow 0 \\ \text{rmacumulado} \; \leftarrow 0 \\ \text{for} \quad i \in 0..\text{NCamadas} \; - 1 \\ \quad \left| \begin{array}{l} \text{for} \quad j \in 0..\text{NNodos}_i - 1 \\ \quad \left| \begin{array}{l} \text{rm}_k \leftarrow \Delta r_i \cdot j \\ \text{rm}_k \leftarrow \text{rmacumulado} \; + \text{rm}_k \\ \text{lastrm} \; \leftarrow \text{rm}_k \quad \text{if} \quad j = \text{NNodos}_i - 1 \\ k \leftarrow k + 1 \end{array} \right. \\ \text{rmacumulado} \; \leftarrow \text{lastrm} \\ k \leftarrow k - 1 \end{array} \right. \\ \text{rm} \end{array} \right. =
$$

	0
14	0.0307
15	0.0309
16	0.0311
17	0.0313
18	0.0316
19	0.0318
20	0.032
21	0.0331
22	0.0342
23	0.0353
24	0.0364
25	0.0376
26	0.0387
27	0.0398
28	0.0409
29	...

m $\blacksquare$

- Material

Plastic specific heat (c_p) variation with temperature: the expressions cPL, cPT and cPS were used to calculate the cPPlastic, depending on the temperature of the graph of the Figure 71 (in this case for the PP material).

$$cPL(Tempera) := 0.837 \cdot Tempera \cdot \frac{m^2}{K^2 \cdot s^2} + 2.221 \times 10^3 \cdot \frac{m^2}{K \cdot s^2}$$

$$cPT(Tempera) := \frac{686.72137 \cdot Tempera}{480.97208 \; K - Tempera} \cdot \frac{m^2}{K \cdot s^2}$$

$$cPS(Tempera) := 8.039 \cdot Tempera \cdot \frac{m^2}{K^2 \cdot s^2} - 705.258 \cdot \frac{m^2}{K \cdot s^2}$$

$$cPPlástico \; (Tempera) := \begin{cases} cPL(Tempera) & \text{if} \quad Tempera \geq 448.15 \; K \\ cPT(Tempera) & \text{if} \quad 370 \; K < Tempera \leq 448.15 \; K \\ cPS(Tempera) & \text{otherwise} \end{cases}$$

$Tempera := 0K, 1K .. 500K$
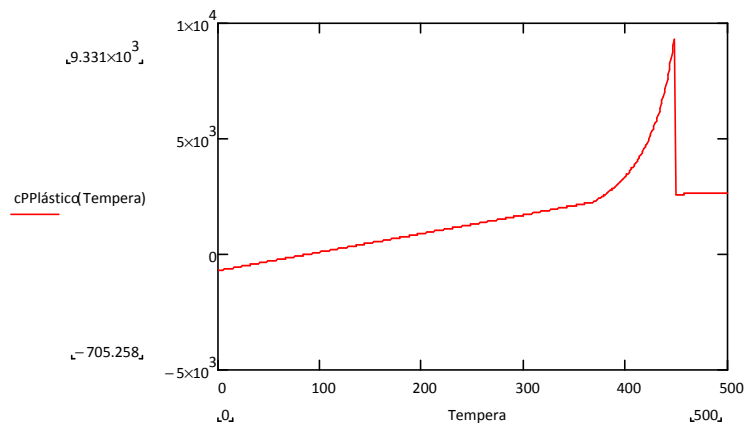
Figure 74 – Specific heat variation with the temperature for the injected plastic used (PP)

Other material properties:

$$\rho(\text{Tempera}) := \begin{pmatrix} 1000 \\ 7800 \\ 912.5 \\ 7800 \\ 1000 \end{pmatrix} \cdot \frac{kg}{m^3}$$

$$\text{CondT}(\text{Tempera}) := \begin{pmatrix} 0.5 \\ 29 \\ 0.1507 \\ 29 \\ 0.5 \end{pmatrix} \frac{W}{m \cdot K}$$

$$\text{cP}(\text{Tempera}) := \begin{pmatrix} 5000 \cdot \dfrac{J}{kg \cdot K} \\[4pt] 460 \cdot \dfrac{J}{kg \cdot K} \\[4pt] \begin{vmatrix} \text{cPL}(\text{Tempera}) & \text{if} \quad \text{Tempera} \geq 448.15 \ K \\ \text{cPT}(\text{Tempera}) & \text{if} \quad 370 \ K < \text{Tempera} \leq 448.15 \ K \\ \text{cPS}(\text{Tempera}) & \text{otherwise} \end{vmatrix} \\[4pt] 460 \cdot \dfrac{J}{kg \cdot K} \\[4pt] 5000 \cdot \dfrac{J}{kg \cdot K} \end{pmatrix}$$

Thermal diffusivity calculation:

$$\alpha(\text{Tempera}) := \begin{array}{|l} \text{for} \quad i \in 0 .. \text{NCamadas} \ - 1 \\ \quad \begin{array}{|l} \alpha_i \leftarrow \dfrac{\text{CondT}(\text{Tempera})_i}{\rho(\text{Tempera})_i \ \text{cP}(\text{Tempera})_i} \\ \alpha \end{array} \end{array}$$

$$\alpha(100 \ ^\circ C) = \begin{pmatrix} 1 \times 10^{-7} \\ 8.082 \times 10^{-6} \\ 6.949 \times 10^{-8} \\ 8.082 \times 10^{-6} \end{pmatrix} \frac{m^2}{s} \ \blacksquare$$

Time required for simulation (i.e. cycle time), should be placed in seconds.

$$\text{tTot} := 60 \ s$$

Stability criteria and the Fourier number

$$\text{Fo} := \frac{\alpha \cdot \Delta t}{\Delta r^2}$$

The stability criteria in the node 0 (Centre of the cylinder):

$$\text{TemperaMin} := 40 \ ^\circ C$$

$$1 - 4 \cdot \text{Fo} \geq 0,$$

Verify if it is minimum or maximum. Analysing the expressions it seems that is minimum, it corresponds to the minimum value of cp, so the maximum value of α and the minor of Δt.

$$\Delta \text{tmax} := \begin{array}{|l} \text{for} \quad i \in 0 .. \text{NCamadas} \ - 1 \\ \quad \begin{array}{|l} \Delta \text{tmax}_i \leftarrow \dfrac{1}{4} \cdot \dfrac{(\Delta r_i)^2}{\alpha(\text{TemperaMin})_i} \\ \Delta \text{tmax} \end{array} \end{array}$$

Δtmax $:=$ min (Δtmax)

Δtmax $= 0.038$ s ∎

Supposing a Δt value 5 % inferior to the maximum of the stability criteria (convergence), *i. e.,*

Δtmaxass $:= 0.95 \cdot$ min (Δtmax)

Δtmaxass $= 0.036$ s ∎

Note: In the intermediate nodes the convergence criteria will be $1\text{-}2.F_0 \geq 0$, therefore less exigent. So, the Fourier for each layer is

Fo (Tempera) $:=$ for   i $\in 0 ..$ NCamadas $- 1$

$$\text{Fo}_i \leftarrow \frac{\alpha(\text{Tempera })_i \cdot \Delta\text{tmaxass}}{\left(\Delta r_i\right)^2}$$

Fo

For the layers transitions, i.e. for the border nodes (the nodes in the interfaces)

It was defined equivalent properties, because there are different materials to be considered in the volume of control around these nodes.

i) Density equivalent

ρeq (Tempera) $:=$ for   i $\in 0 ..$ NCamadas $- 2$

$$\rho\text{eq}_i \leftarrow \frac{\rho(\text{Tempera })_i \cdot \left(\text{Rext}_i - \dfrac{\Delta r_i}{4}\right) \cdot \dfrac{\Delta r_i}{2} + \rho(\text{Tempera })_{i+1} \cdot \left(\text{Rext}_i + \dfrac{\Delta r_1}{4}\right) \cdot \dfrac{\Delta r_{i+1}}{2}}{\left(\text{Rext}_i - \dfrac{\Delta r_i}{4}\right) \cdot \dfrac{\Delta r_i}{2} + \left(\text{Rext}_i + \dfrac{\Delta r_{i+1}}{4}\right) \cdot \dfrac{\Delta r_{i+1}}{2}}$$

ρeq

ii) Thermal capacity equivalent

cPeq (Tempera) $:=$ for   i $\in 0 ..$ NCamadas $- 2$

$$\text{cPeq}_i \leftarrow \frac{\rho(\text{Tempera })_i \cdot \text{cP}(\text{Tempera })_i \cdot \left(\text{Rext}_i - \dfrac{\Delta r_i}{4}\right) \cdot \dfrac{\Delta r_i}{2} + \rho(\text{Tempera })_{i+1} \cdot \text{cP}(\text{Tempera })_{i+1} \cdot \left(\text{Rext}_i + \dfrac{\Delta r_1}{4}\right) \cdot \dfrac{\Delta r_{i+1}}{2}}{\rho\text{eq}(\text{Tempera })_i \cdot \left[\left(\text{Rext}_i - \dfrac{\Delta r_i}{4}\right) \cdot \dfrac{\Delta r_i}{2} + \left(\text{Rext}_i + \dfrac{\Delta r_{i+1}}{4}\right) \cdot \dfrac{\Delta r_{i+1}}{2}\right]}$$

cPeq

iii) Thermal diffusivity equivalent (in this case, on the left and on the right of the node as shown through the definition

αeqe (Tempera) $:=$ for   i $\in 0 ..$ NCamadas $- 2$

$$\alpha\text{eqe}_i \leftarrow \frac{\text{CondT}(\text{Tempera })_i}{\rho\text{eq}(\text{Tempera })_i \cdot \text{cPeq}(\text{Tempera })_i}$$

αeqe

αeqd (Tempera) $:=$ for   i $\in 0 ..$ NCamadas $- 2$

$$\alpha\text{eqd}_i \leftarrow \frac{\text{CondT}(\text{Tempera })_{i+1}}{\rho\text{eq}(\text{Tempera })_i \cdot \text{cPeq}(\text{Tempera })_i}$$

αeqd

iv) Fourier number equivalent (in this case, on the left and on the right of the node as shown through the definition

$$\text{Foeqe (Tempera)} := \text{for } i \in 0 .. \text{NCamadas } - 2$$
$$\text{Foeqe }_i \leftarrow \frac{\Delta tmaxass \cdot \alpha eqe \text{ (Tempera)}_i}{(\Delta r_i)^2}$$
$$\text{Foeqe}$$

$$\text{Foeqd (Tempera)} := \text{for } i \in 0 .. \text{NCamadas } - 2$$
$$\text{Foeqd }_i \leftarrow \frac{\Delta tmaxass \cdot \alpha eqd \text{ (Tempera)}_i}{(\Delta r_{i+1})^2}$$
$$\text{Foeqd}$$

Note: By the Fourier number definition, it is verified that Foeq will be stayed between Fo on the left and Fo on the right, therefore it is not necessary to consider the intermediary nodes to fulfill the convergence criteria.

Determination of the iterations number

$$\text{NIT} := \text{floor}\left(\frac{tTot}{\Delta tmaxass}\right) + 1 = 1.654 \times 10^3 \blacksquare$$

Establishment of the initial conditions

Cycle for determination the **layer** position in function of *r* (*e.g.* CamadaActual (0.025 m) = 2)

$$\text{CamadaActual (r)} := \begin{array}{|l}
\text{CamadaActual } \leftarrow 0 \quad \text{if } r < \text{Rext}_0 \\
\text{CamadaActual } \leftarrow 1 \quad \text{if } \text{Rext}_0 \leq r < \text{Rext}_1 \\
\text{CamadaActual } \leftarrow 2 \quad \text{if } \text{Rext}_1 \leq r \leq \text{Rext}_2 \\
\text{CamadaActual } \leftarrow 3 \quad \text{otherwise}
\end{array}$$

CamadaActual (0.033 m) = 3 $\blacksquare$

Note: 4 layers (0, 1, 2, 3) delimited by 4 (1, 2, 3, 4) surfaces

Initial temperature in function of r

<u>*Input data*</u>

$$\text{TPerm (r)} := \begin{array}{|l}
T \leftarrow 40 \text{ °C} \quad \text{if } \text{CamadaActual (r)} = 0 \\
T \leftarrow 40 \text{ °C} \quad \text{if } \text{CamadaActual (r)} = 1 \\
T \leftarrow 250 \text{ °C} \quad \text{if } \text{CamadaActual (r)} = 2 \\
T \leftarrow 40 \text{ °C} \quad \text{if } \text{CamadaActual (r)} = 3
\end{array}$$

$$r := 0, 0.00005 \text{ m} .. \text{Rext}_{\text{NCamadas}-1}$$

These initial temperature conditions mean that the cooling fluid in the core is at 40ºC, the core moulding block temperature is 40ºC, the plastic is injected at 250ºC and the cavity moulding block temperature is 40ºC. Figure 75 shows the initial temperature conditions established in the input data.
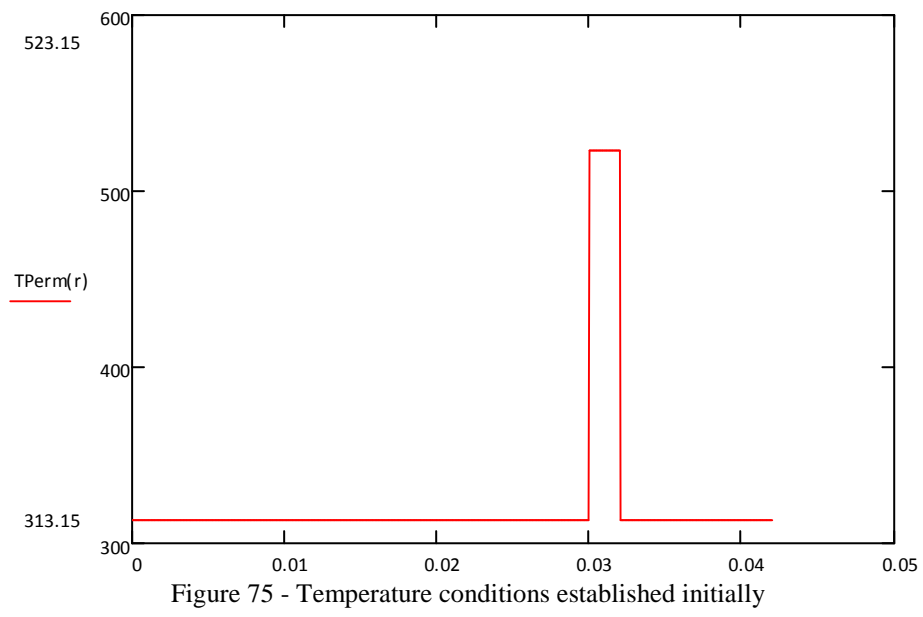
Figure 75 - Temperature conditions established initially

Initial nodes conditions

$$\text{Tpini} := \begin{vmatrix} \text{for} & i \in 0 .. \text{NNodosTot} - 1 \\ & \text{Tpini}_i \leftarrow \text{TPerm}(\text{rm}_i) \\ \text{Tpini} & \end{vmatrix} = $$

	0
0	40
1	40
2	40
3	40
4	40
5	40
6	40
7	40
8	40
9	40
10	40
11	250
12	250
13	250
14	250
15	...

·°C

rm =

	0
0	0
1	0.01
2	0.02
3	0.021
4	0.022
5	0.023
6	0.024
7	0.026
8	0.027
9	0.028
10	0.029
11	0.03
12	0.03
13	0.03
14	0.031
15	...

m ■
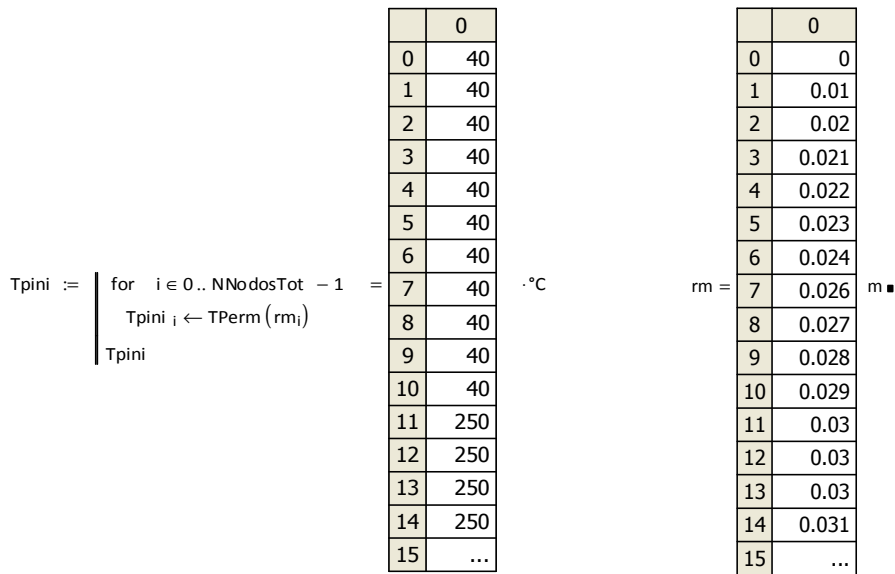
Figure 76 shows the graph with temperature conditions established initially (mentioned above) before the simulation. The nodes on the interfaces are connected for the temperatures of the injected plastic (250ºC) and moulding blocks (40ºC). So the vertical line of the Figure 75 appears as a slope line in Figure 76.
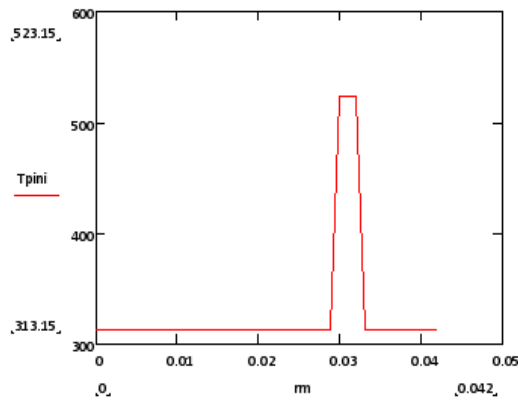
Figure 76 – Initial instant before simulation

PROGRAM (resolution)

Calculation of the transient temperatures after the initial established conditions

$$
\begin{aligned}
TTransiente := \quad & \text{for } l \in NNodosTot - 1..0 \\
& \quad T_{0,l} \leftarrow Tpini_l \\
& \quad Tpp_l \leftarrow T_{0,l} \\
& \text{for } i \in 1..NIT \\
& \quad acumulador \leftarrow 0 \\
& \quad Tp_{NNodosTot-1} \leftarrow 40\,^\circ C \\
& \quad \text{for } n \in 0..NNodos_0 - 1 \\
& \quad\quad Tp_n \leftarrow 40\,^\circ C \\
& \quad \text{for } l \in NNodosTot - 2..0 \\
& \quad\quad Tp_l \leftarrow Tpp_l \\
& \quad\quad Tp_{NNodos_0 - 1} \leftarrow 40\,^\circ C \\
& \quad \text{for } j \in NCamadas - 1..0 \\
& \quad\quad \text{for } k \in NNodos_j - 2..0 \\
& \quad\quad\quad NodoActual \leftarrow NNodosTot - 2 - acumulador
\end{aligned}
$$

$$
Tpp_{NodoActual} \leftarrow Fo\left(Tp_{NodoActual}\right)_j \cdot \left[\left(1 - \frac{\Delta r_j}{2 \cdot rm_{NodoActual}}\right) \cdot Tp_{NodoActual-1} + \left(1 + \frac{\Delta r_j}{2 \cdot rm_{NodoActual}}\right) \cdot Tp_{NodoActual+1}\right] + \left(1 - 2 \cdot Fo\left(Tp_{NodoActual}\right)_j\right) \cdot Tp_{NodoActual} \quad \text{if } NodoActual > 0 \wedge k \neq 0
$$

$$
Tpp_{NodoActual} \leftarrow 4 \cdot Foeqe\left(Tp_{NodoActual}\right)_{j-1} \cdot \frac{\left(2 \cdot rm_{NodoActual} - \Delta r_{j-1}\right) \cdot \Delta r_{j-1}}{\left(\Delta r_{j-1} + \Delta r_j\right) \cdot \left(4 \cdot rm_{NodoActual} - \Delta r_{j-1} + \Delta r_j\right)} \cdot Tp_{NodoActual-1} + 4 \cdot Foeqd\left(Tp_{NodoActual}\right)_{j-1} \cdot \frac{\left(2 \cdot rm_{NodoActual} + \Delta r_j\right) \cdot \Delta r_j}{\left(\Delta r_{j-1} + \Delta r_j\right) \cdot \left(4 \cdot rm_{NodoActual} - \Delta r_{j-1} + \Delta r_j\right)} \cdot Tp_{NodoActual+1} + \left[1 - Foeqe\left(Tp_{NodoActual}\right)_{j-1} \cdot \frac{4 \cdot \left(2 \cdot rm_{NodoActual} - \Delta r_{j-1}\right) \cdot \Delta r_{j-1}}{\left(\Delta r_{j-1} + \Delta r_j\right) \cdot \left(4 \cdot rm_{NodoActual} - \Delta r_{j-1} + \Delta r_j\right)} - Foeqd\left(Tp_{NodoActual}\right)_{j-1} \cdot \frac{4 \cdot \left(2 \cdot rm_{NodoActual} + \Delta r_j\right) \cdot \Delta r_j}{\left(\Delta r_{j-1} + \Delta r_j\right) \cdot \left(4 \cdot rm_{NodoActual} - \Delta r_{j-1} + \Delta r_j\right)}\right] \cdot Tp_{NodoActual} \quad \text{if } NodoActual > 0 \wedge k = 0
$$

$$
\begin{aligned}
& Tpp_{\left(NNodos_0 - 1\right)} \leftarrow 40\,^\circ C \\
& acumulador \leftarrow acumulador + 1 \\
& T_{i,NodoActual} \leftarrow Tpp_{NodoActual} \\
& T_{i,NNodosTot-1} \leftarrow Tp_{NNodosTot-1} \\
& T
\end{aligned}
$$

Notes:

1) As mentioned in Figure the temperature of the last surface can be changed in **T$_{pNNODOSTOT-1}$**. In the establishment of this temperature it should exists a co-relation between the values attributed to the **T$_{pNNODOSTOT-1}$** and the values attributed to the layers, in the initial temperature in function of *r*.

2) The temperature of the cooling fluid on the cavity side only can be changed in **T$_{pNNODOSTOT-1}$**. This is a simplification o the developed numerical method to solve the problem. By the way, the problem resolution is approached to a heat transfer by conduction. To solve the real problem it will be necessary to consider another layer from the **T$_{pNNODOSTOT-1}$** (see Figure 77) delimited by a new surface. In this layer it will be necessary to consider the cooling channels, or the used cooling system, and solve the problem in this layer as a heat transfer by convection.
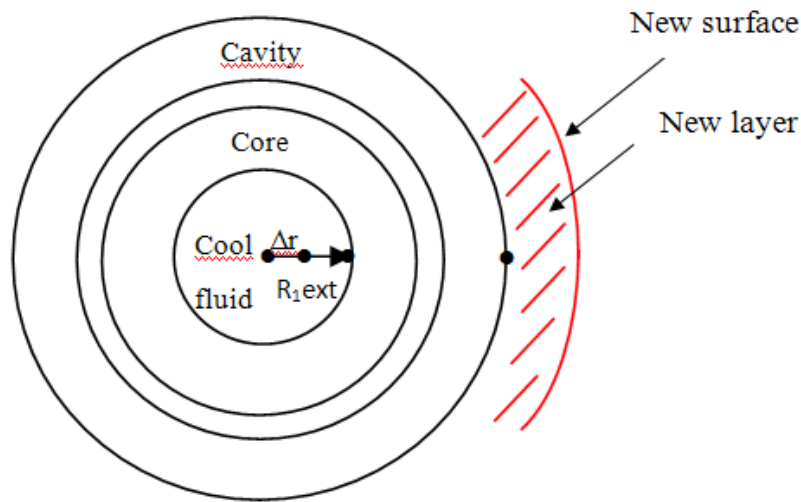
Figure 77 – New delimited layer needed to define heat transfer by convection (as the real problem)

Temperature results

Table 18 shows the temperature results in the different nodes of the problem at the instant times represented by the lines of the iteration number.

Table 18 – Temperature results

		0	1	2		27	28	29	
	0	40	40	40		40	40	40	
	1	40	40	40		40	40	40	
	2	40	40	40		40	40	40	
	3	40	40	40		40	40	40	
	4	40	40	40		40	40	40	
	5	40	40	40		40	40	40	
	6	40	40	40		40	40	40	
TTransiente =	7	40	40	40		40.008	40	40	·°C
	8	40	40	40		40.034	40.002	40	
	9	40	40	40		40.086	40.009	40	
	10	40	40	40		40.167	40.025	40	
	11	40	40	40		40.277	40.052	40	
	12	40	40	40		40.415	40.092	40	
	13	40	40	40		40.576	40.146	40	
	14	40	40	40		40.757	40.211	40	
	15	40	40	40		40.952	40.288	...	

The columns numbers represents the nodes of the problem (from 0-centre to 29-last surface)

The line numbers represents the iteration number that multiplied by the time between 2 consecutive iterations gives us the correspondent instant of time:

e.g., 0.03628 x 3 = 0.1s (the third line corresponds to the instant of 0.1 s)

0.03628 x 275 = 9.977s (the 275 line corresponds to the instant of ≈ 10s)

To know at what line of the table corresponds the instant t, it is only necessary make the relation between t and Δtmaxass (t/Δtmaxass):

e.g., the line that corresponds to the instant of 40s is 40/0.03628 = <u>1102</u>

The total number of iterations needed for 60s cycle time is given by NIT

$NIT = 1.654 \times 10^3$ ∎

The minimum time between iterations is 0.03628 s

$\Delta tmaxass = 0.03628$ s ∎

Δr is the distance between nodes in each layer.

$$\Delta r = \begin{pmatrix} 0.01 \\ 1.111 \times 10^{-3} \\ 2.222 \times 10^{-4} \\ 1.111 \times 10^{-3} \end{pmatrix} m \blacksquare$$

e. g. the first layer has a radium value of 0.02 m and it is discretized in 3 nodes. Dividing by 2 spaces the distance between nodes in this layer is 0.01 m.

Selection the breaks of time for representation

$NIntervalos := 10$

$$Tt := \begin{Vmatrix} Tt_0 \leftarrow submatrix\ (TTransiente\ , 0, 0, 0, NNodosTot\ -1) \\ for\ \ i \in 1 .. NIntervalos \\ \quad \begin{Vmatrix} ac \leftarrow i \cdot \dfrac{NIT}{NIntervalos} + ac \\ \displaystyle\sum_{n=1} n \\ Tt_i \leftarrow submatrix\ (TTransiente\ , floor\ (ac)\ , floor\ (ac)\ , 0, NNodosTot\ -1) \end{Vmatrix} \\ Tt \end{Vmatrix}$$

Tt =

	0
0	[1, 30]
1	[1, 30]
2	[1, 30]
3	[1, 30]
4	[1, 30]
5	[1, 30]
6	[1, 30]
7	[1, 30]
8	[1, 30]
9	[1, 30]
10	[1, 30]

·°C

$Tt_0^T =$

	0
0	40
1	40
2	40
3	40
4	40
5	40
6	40
7	40
8	40
9	40
10	40
11	250
12	250
13	250
14	250
15	...

·°C rm =

	0
0	0
1	0.01
2	0.02
3	0.021
4	0.022
5	0.023
6	0.024
7	0.026
8	0.027
9	0.028
10	0.029
11	0.03
12	0.03
13	0.03
14	0.031
15	...

m ∎

Temperature results representation in the instants of time pre-defined

Figure 72 shows the representation curves of the temperature variation along the different layers defined in the problem (defined in *x* axis by the Rext (m)) and in the 11 different instants of time (defined by the curves) including the initial one (grey curve) as the correspondence showed in the table "Tempo".

$$\text{acumulador} := \left[\sum_{n=1}^{\text{NIntervalos}} (\text{const} \cdot n) \right]$$

$$\sum_{n=1}^{\text{NIntervalos}} (\text{const} \cdot n) \leq \text{NIT}$$

$$\text{const} \leq \frac{\text{NIT}}{\displaystyle\sum_{n=1}^{\text{NIntervalos}} (n)}$$

Figure 78 – Temperature representation curves in different instants of time

Auxiliary data

The data exemplified below possibility the calculus of cooling rates in different instants of time during the injection cycle in each node characterized in the problem.

T1 := submatrix (TTransiente , 28 , 28 , 0 , NNodosTot − 1)

T1 =	0	1	2	3	4	5	6	· °C
0	40	40	40	42.208	44.811	48.19	...	

T10 := submatrix (TTransiente , 275 , 275 , 0 , NNodosTot − 1)

T10 =	0	1	2	3	4	5	6	· °C
0	40	40	40	42.526	44.892	47.083	...	

Appendix 2

Publications

Rapid Prototyping Journal

Hybrid moulds: effect of the moulding blocks on the morphology and dimensional properties

Pedro Gonçalves Martinho
Polytechnic Institute of Leiria, School of Technology and Management, Leiria, Portugal
Paulo Jorge Bártolo
CDRSP, Polytechnic Institute of Leiria, Leiria, Portugal
António Sérgio Pouzada
Institute for Polymers and Composites, University of Minho, Guimarães, Portugal

Editor Dr Ian Campbell
*Department of Design and Technology, Loughborough
University, Loughborough, Leicestershire LE11 3TU, UK*
Regional Editor – Asia and Australasia Dr Ian Gibson
*Department of Mechanical Engineering,
National University of Singapore, Singapore*
Regional Editor – North and South America
Dr Brent Stucker
*Department of Mechanical & Aerospace Engineering
Utah State University, USA*
Publisher Harry Colson

Typeset in Europe by the Alden Group, Oxfordshire

Mission Statement
Rapid Prototyping Journal provides industrialists and academics
with essential information regarding research into the
development and application of rapid prototyping and related
technologies. The journal concentrates on rapid product
development in a manufacturing environment but applications
within other areas, such as medicine and construction, are also
covered. A double-blind review process ensures the content's
validity and relevance.

Hybrid moulds: effect of the moulding blocks on the morphology and dimensional properties

Pedro Gonçalves Martinho
Polytechnic Institute of Leiria, School of Technology and Management, Leiria, Portugal

Paulo Jorge Bártolo
CDRSP, Polytechnic Institute of Leiria, Leiria, Portugal, and

António Sérgio Pouzada
Institute for Polymers and Composites, University of Minho, Guimarães, Portugal

Abstract

Purpose – This paper aims to explore the influence of the materials used in moulding blocks of hybrid moulds on the injection moulding setup and the properties of the mouldings.

Design/methodology/approach – An instrumented (pressure and temperature) hybrid mould with exchangeable moulding blocks, produced by rapid prototyping and tooling techniques (RPT), was used to produce polypropylene tubular mouldings. The configuration of the mould was varied with combinations of moulding block materials, namely, an epoxy resin composite processed by vacuum casting and steel. The processing conditions were adjusted to obtained steady processing conditions. The mouldings were assessed in terms of the microstructure and the shrinkage.

Findings – Due to the properties of the moulding block obtained by RPT being different from tool steel, the injection moulding processing conditions and the plastics parts properties are different when hybrid moulds are used. The cycle time depends on the moulding block properties and must be adjusted to the desired running temperature. The morphology of the mouldings is strongly affected by the thermal properties of the moulding block materials. When different materials are used in the core and the cavity asymmetric structures develop in the part. The shrinkage of the mouldings, when resin cores are used is also affected by the deformation of the core caused by the injection pressure.

Originality/value – This paper makes a contribution to understanding the morphology of semi-crystalline mouldings obtained using hybrid moulds and enhances the importance of the core deformation on the shrinkage of the mouldings.

Keywords Rapid prototypes, Thermoplastic polymers, Resins

Paper type Research paper

Introduction

In the last two decades, the concept of hybrid mould (Figure 1) for injection moulding has been developed to fulfil new trends of the plastics industry. Advantages of this kind of moulds are: *efficiency*, by reducing waste and energy consumption; *agility* for enabling customisation and *flexibility* for the modification and implementation of design concepts (Beal *et al.*, 2003; Ribeiro *et al.*, 2004; Martinho *et al.*, 2005; Bareta *et al.*, 2007).

Hybrid moulds were described as tools that make use of different technologies and materials to obtain the moulding blocks (Saraiva *et al.*, 1999). These can be produced by rapid prototyping and tooling (RPT) techniques: direct rapid tooling such as Direct AIM, Selective Laser Sintering or Metallic LOM, or indirect rapid tooling as Epoxy tooling or 3D KelTool (Chua *et al.*, 2003; Drizo and Pegna, 2006). Potsch and Michaeli (1995) acknowledged that using RPT technologies for moulding blocks influences the overall performance of the mould. Segal and Campbell (2001) refer that it is necessary to understand how the moulded part is affected by the RPT technique used for the moulding blocks. Some difficulties still exist in the production of technical plastics parts using hybrid moulds, which are associated to the thermal and mechanical data and behaviour of the materials being unavailable or little understood (Lima *et al.*, 2003; Ribeiro *et al.*, 2004).

Segal and Campbell (2001) recognized that the performance of parts obtained with hybrid moulds is an important issue. The injection moulded thermoplastics keep a residual molecular orientation as a combined result of the chain alignment during the mould filling followed by a high cooling rate leading (Viana and Cunha, 1996). This frozen-in orientation causes an anisotropic morphology whose pattern affects the in-service properties of the parts (Brito *et al.*, 1991; Cunha *et al.*, 1992). These authors also refer that the behaviour of the mouldings depends on the morphology built up during processing. The characterization of the microstructure of the injected parts can

Figure 1 The concept of hybrid mould

Conventional machining
for standard mould plates

The hybrid mould concept
combines old and new
fabrication techniques

Prototyping techniques
for moulding blocks

be made by polarized light microscopy (Hemsley, 1989). It may be correlated with the mechanical performance.

Vacuum casting of epoxy/aluminium composites is a common route for obtaining moulding blocks. Nevertheless, problems may arise caused by the non-uniform mixing of the components, the curing agent and the presence of trapped gases (Cheah *et al.*, 2002; Sabino-Netto *et al.*, 2004).

This work reports on a research involving the production of 3D parts using a hybrid mould. The epoxy-based composite moulding blocks were produced by vacuum casting. Various combinations of core and cavity materials and injection processing conditions were used to influence the morphology and the shrinkage of the mouldings.

Experimental

Tooling

The hybrid mould and the tubular mouldings are shown in Figures 2 and 3. The injection is made through four gates at the extremities of a spider gating system. A stripper plate is used for ejection.

The moulding blocks that are easily assembled in the mould structure are shown in Figure 4.

The mouldings were produced using three combinations of materials of the moulding blocks:
1   resin in core and resin in cavity (identified by resin/resin or RR combination);
2   resin in core and steel in cavity (resin/steel or RS); and
3   steel in core and steel in cavity (steel/steel or SS).

The resin moulding blocks were produced by vacuum casting the epoxy composites in silicone moulds. Figure 5 shows the successive phases of the process, from the CAD model (a) to the actual moulding blocks (d).

The manufacturing route for the epoxy resin moulding blocks included the degassing of the resin (35 min), the cure at room temperature (24 h) and the post cure (3 h at 60°C and 4 h at 140°C). The heating and cooling were made at a rate of 10°C/h. The machining operations for fitting the instrumentation and

getting the dimensions and adjustments for fitting the moulding blocks into the mould structure were made after the post cure.

The hybrid mould used in this work was instrumented with six sensors, as shown in Figure 4: four Type-K thermocouples (T_1, T_2, T_5 and T_6), one Hotset TEF 15 Type-K temperature sensor (Hotset, Lüdenscheid, Germany) (T_4) and one Kistler 6157 BA pressure sensor (Kistler Instruments, Winterthur, Switzerland) (P). The locations of these sensors were chosen for ascertaining these process variables at the starting point of filling and at *ca.* one third of the flow path length, this being a common practice in injection mould instrumentation. The steel moulding blocks were fitted with the T_4 and P sensors in the cavity and the T_5 and T_6 sensors in the core. The resin moulding blocks were fitted with the T_1, T_2 and T_4 sensors in the cavity and the T_5 sensor in the core. A Priamus system was used to get pressure data (Priamus System Technologies GmbH, Salach, Germany) and the temperature values were collected with a USB TC-08 Thermocouple Data Logger system (Picotech, St Neots, UK).
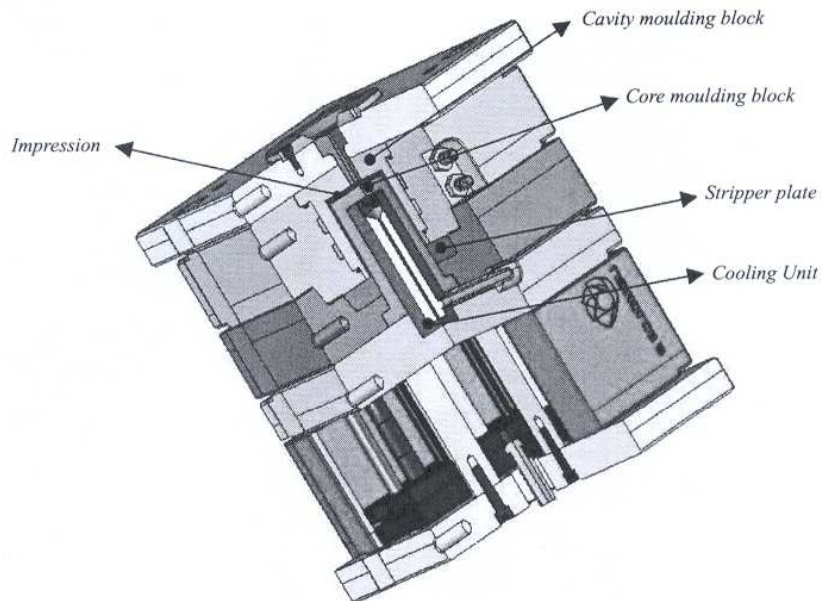
Materials

The core and cavity standard moulding blocks are in DIN W Nr. 1.2311 tool steel, with the properties shown in Table I. The alternative material used in the resin moulding blocks and selected for the studies is a composite of epoxy resin Biresin L74 (Sika, Stuttgart, Germany) with 60 per cent aluminium powder.

The Biresin L74 epoxide has the properties shown in Table II. The aluminium powder particles have an average size of 50 μm and specific gravity of 2.43 Mg m^{-3}.

Injection moulding

The mouldings were produced in polypropylene homopolymer, PP Homo Domolen 1100N (DOME Polypropylene, Rozenburg, The Netherlands) of MFR 12 g/10 min (230°C/2.16 kg) using a Ferromatik Milacron K85 injection moulding machine of 850 kN clamping force.

Figure 2 Hybrid mould design

The processing conditions were set according to each combination of core and cavity materials, as shown in Table III.

In the following the processing conditions will be referred to using an alphanumeric code representing the moulding block material combination, the holding pressure (MPa) and the cooling time (s). As an example, the code RS36.25 refers to parts produced with resin core and steel cavity, 36 MPa holding pressure and cooling time of 25 s. In each injection run, at least 25 mouldings were produced after process stabilization. For each set of new stabilized processing conditions, the first six injected parts were rejected.

Characterization tests

Thermal and mechanical properties of the materials used in the moulding blocks, namely: thermal conductivity, thermal

Figure 3 Part design

diffusivity, elasticity modulus variation, specific heat and density were determined in this study. The tests were made with an Alambeta conductivity equipment (Sensora, Liberec, Czech Republic), a dynamic mechanical analyser Tritec 2000 (Triton, Nottingham, UK) and a universal testing machine Zwick Z100 (Ulm, Germany). The density of the composite was determined by the impulsion method. The morphology of the mouldings was observed on thin sliced sections of $10\,\mu m$ obtained with a microtome model 0325 from Anglia Scientific Instruments (Cambridge, UK), using a polarized light microscope Olympus BH-2 (Tokyo, Japan). Dimensional changes of the mouldings were measured with an inside micrometer Mitutoyo SBMC-100CST (Kawazaki, Japan), using a measuring range from 50-100 mm and $1\,\mu m$ resolution and a 150 mm digital calliper.

Results and discussion

Moulding block materials

The mechanical behaviour of the epoxy/aluminium composite used in the moulding blocks was analysed in terms of the variation of the modulus of elasticity with the temperature. This analysis is necessary as the moulding blocks are expected to work over a range of temperatures, typically from 30 to 100°C. The flexural modulus variation was determined in the DMA equipment. A typical test curve is shown in Figure 6.

The sharp decrease of the modulus above 120°C is related to the approximation of the melt temperature of the material. Within the expected operating range from 20 to 100°C the experimental data can be described by the linear equation:

$$E(T) = -14.6T + 6.0 \times 10^3, \qquad (1)$$

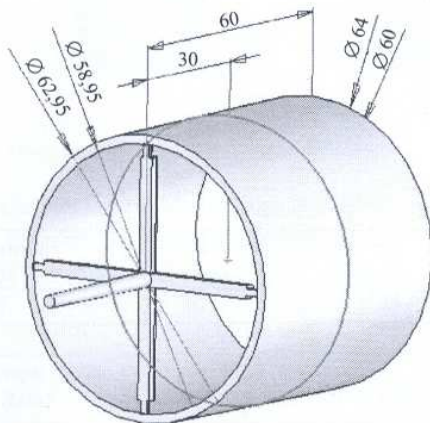where T is the temperature in °C and E is the modulus in MPa.

Figure 4 Interchangeable moulding blocks and sensors location: (a) cavity and (b) core

(a)

(b)

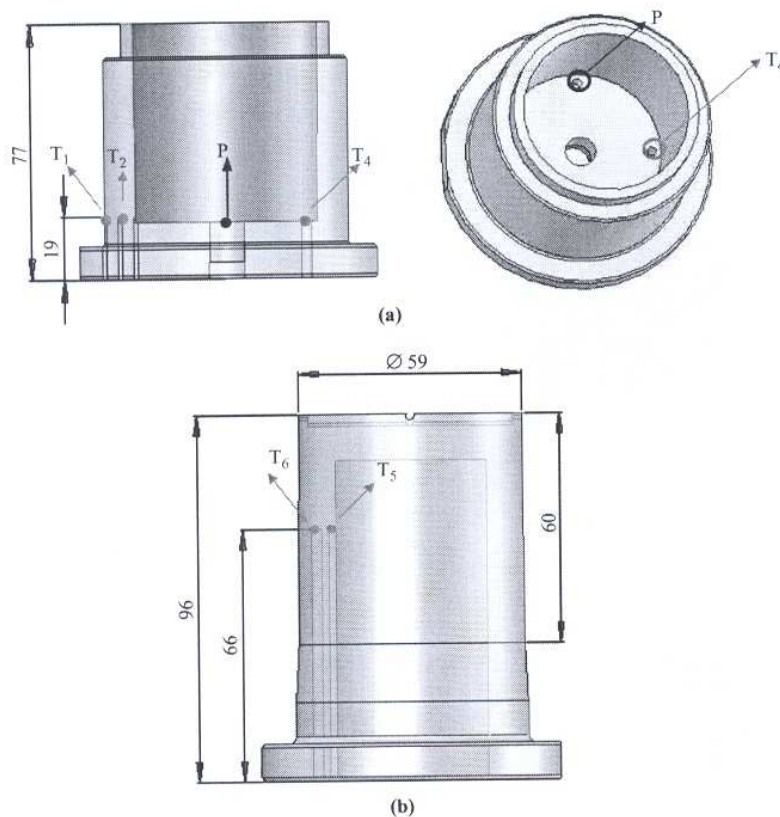**Figure 5** Silicon moulds to produce moulding blocks: (a) CAD models; (b) steel masters; (c) silicone moulds and (d) epoxy resin blocks
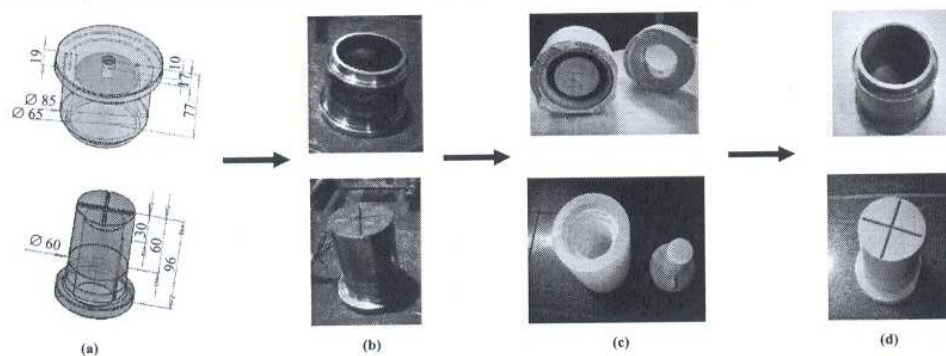

(a)   (b)   (c)   (d)

Table I Properties of the tool steel material (W Nr. 1.2311) and the epoxy resin filled with aluminium (Biresin L74 +60 per cent aluminium) material

Moulding block material	Specific gravity (Mg m^{-3})	Specific heat (J kg^{-1} K^{-1})	Thermal conductivity (W m^{-1} K^{-1})	Thermal diffusivity (m^2 s^{-1})	Thermal expansion coefficient (K^{-1})	Flexural modulus at 20°C (GPa)
Tool steel (DIN W Nr. 1.2311)	7.8	460	29	–	1.2×10^{-5}	200
Epoxy composite (Biresin L74 + 60 per cent alum.)	1.65	1279.19	0.606	0.286×10^{-6}	6×10^{-5}	5-6

Table II Epoxy resin properties (Biresin L74)

Material	Hardness[a] (shore *D*)	Impact resistance[a] (kJ m^{-2})	Heat deflection[a] temperature (°C)	Specific gravity (Mg m^{-3})
Biresin L74	85	29	160	1.1

Note: [a]Values after post curing: 3 h/60°C + 3 h/140°C

Table III Injection moulding processing conditions

Parameter		Value	
Injection temperature (°C)		230	
Water cooling temperature (°C)		40	
Injection flow rate (cm^3 s^{-1})		37.7	
Injection pressure (MPa)		42	
Holding time (s)		5	
Core-cavity:	SS	RS	RR
Holding pressure (MPa)	36	36	14
Cooling time (s)	12	25	44

Figure 6 Elasticity modulus versus temperature of the epoxy resin composite material

3-Point bending DMA analysis

$$y = -14.573.682,25x + 5.993.177.061,73$$
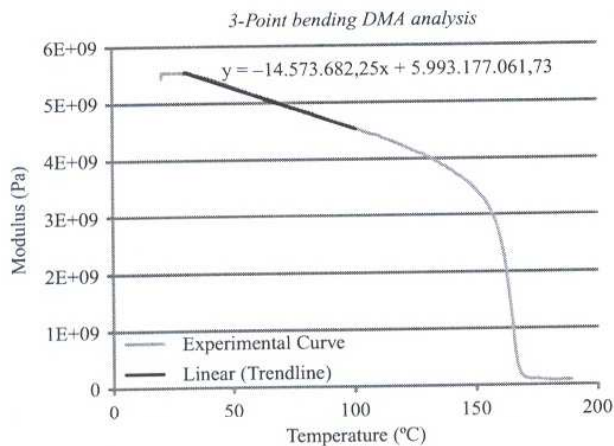
When these materials are used in moulding blocks they are essentially subjected to a compression state of stress. Therefore, the DMA tests were complemented with compression tests according to the ISO 604:1993 standard. The properties of the epoxy composite in compression at 20°C are listed in Table IV alongside the data obtained in flexure.

Table IV Properties of the epoxy composite obtained through a compression test at 20°C

Property	Test method	
	Compression test	DMA flexural test
Yield strength (MPa)	137.7	–
Modulus (MPa)	8,580	5,700

Injection moulding

Moulding reproducibility

The injection moulding process reproducibility was evaluated through moulding weighing and real time pressure and temperature data collection. The mouldings considered for further analyses were those whose weight was inside the range defined by the batch average weight, plus or less one standard deviation. An example is given in Figure 7 where statistic control limits are indicated for a batch of mouldings obtained with a RS combination of moulding blocks. In general, it was observed that more than 68 per cent of the mouldings were inside the statistic control limits for all processing conditions and combination of moulding blocks.

Pressure monitoring

Typical pressure data for some moulding block combinations and processing conditions are shown in Figure 8 where data variation is recorded over the injection cycle. It is possible to observe that the material combinations using resin lead to a slower decrease of the cavity pressure and maximum values are always lower than the steel combinations. This is due to the smaller modulus of the composite used in the moulding blocks.

These data suggesting a sizeable deformation of the resin blocks evidence the need for structural analysis in those cases. As an example it is possible to see in Figure 8 that the pressure curves obtained considering the same processing conditions but with different moulding blocks combinations (SS36.12 and RS36.12) show lower values in the epoxy resin core.

The epoxy resin core, the pressure and cycle time conditions have been adjusted due to the poorer mechanical properties of this material. Although the injection pressure was the same from that used for the steel core, the holding pressure was reduced by 40 per cent. The cycle time was increased up to 60 s.

Temperature monitoring

Information on typical recordings of the thermocouples during the moulding cycles for various moulding block combinations and cycle times is given in Figure 9. In this figure it is also visible how the temperature varies during consecutive cycles, inside the core (sensor T_5) and at moulding surface of the cavity (sensor T_4). The repeatability between cycles is clear.

Moulding cycle

The use of materials with very different mechanical and thermal properties (epoxy resin filled with aluminium powder and tool steel 1.2311) implies changes in the set up of the more appropriate processing conditions.

The combination of materials in the core and cavity determined different temperature running levels (Figure 9). In this respect the block mouldings in lower thermal conductivity materials run at temperatures substantially higher than the coolant medium (40°C). In the case of both blocks being in resin composite the difference is of the order of 40°C (Figure 9(b)). The heterogeneous combination (RR) lends to a running temperature in the resin block around 20°C higher (Figure 9(a)). The conventional all-steel mould (SS) runs approximately at 10°C higher than the coolant medium. These variations result from the conductivity of the materials in combination with the total cycle time set for the processing. In Figure 9(b) the various phases of the injection cycle are identified in the graph. The cycles depicted in the figure were recorded after the temperatures at the moulding blocks having

Figure 7 Parts weight in the indicated moulding conditions

RS36.25
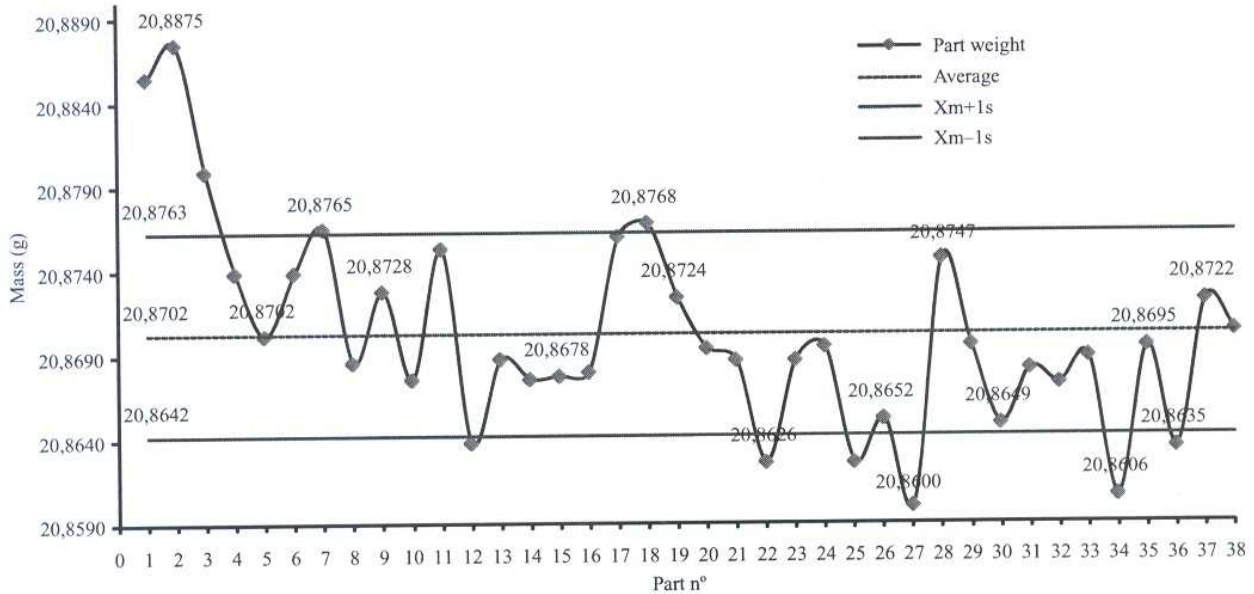
stabilized, i.e. the temperature at the beginning of the cycle being the same at the end of it. The temperature monitoring with the sensor T_4, at the cavity, clearly shows the steep rise during injection, up to the maximum point c, the steady cooling during the cooling phase (b) and the quicker cooling after the opening of the mould down to the start temperature, d. It may also be observed the thermal amplitude (e) recorded at one of the gates of the impression, and the large gradient between the moulding surface (T_4) and the coolant (T_1), with an intermediate value being recorded by the sensor T_2. These differences are more evident if a comparison is made with the data recorded with the all steel SS temperature recording (Figure 9(b)).

It may also be noted that if the total cycle time is shortened the running temperature of the resin block increases. This is exemplified in Figure 9(d)) that corresponds to a case where the total cycle time was decreased of 19 s compared with the case of Figure 9(a). The result was an increase of the running temperature of about 10°C.

Morphology

Especially, with semi-crystalline materials, as it is the case of polypropylene, it is known that the change in processing conditions lead to important changes in the morphology of the moulded material that in turn influences the product properties (Brito *et al.*, 1991; Oliveira *et al.*, 2001). The mouldings in this study were analysed at a mid-distance in the flow path and the through thickness morphology was observed. The results highlight the fundamental effect of the moulding block material in the structures that develop in the mouldings. For one of the processing conditions that were used in the study, it is evident the influence of the moulding block material thermal conductivity, i.e. the cooling rate that results from it. The resulting microstructures are shown in

Figure 10, corresponding to mouldings obtained using the same processing conditions, namely a total cycle time of 60 s and a holding pressure of 14 MPa.

Homogeneous moulding blocks

When identical materials are used in the two moulding halves, as are the cases of the RR and SS combinations, a nearly symmetrical structure develops. These structures show the characteristic laminated microstructure of injection moulded PP, featuring a layered structure across the thickness. In the case of the SS combination, the identification of five layers (Fujiyama *et al.*, 1988): a spherulitic core, two intermediate crystalline and oriented layers and two highly oriented skins with a characteristic "shish kebab" type structure or only three layers as it is preferred for engineering studies by many authors (Brito *et al.*, 1991; Cunha *et al.*, 1992; Pouzada, 1993; Viana and Cunha, 1996; Pontes *et al.*, 2004; Tenma and Yamaguchi, 2007): skin-core-skin, is straightforward. The differences found in the crystalline structures result from the thermo-mechanical conditions during the injection cycle. The inter-relationship between the morphological parameters and mechanical properties has been addressed to by several authors (Cunha *et al.*, 1992; Tjong *et al.*, 1995; Tordjeman *et al.*, 2001; Oliveira *et al.*, 2001; Yuan *et al.*, 2007). When a RR combination is used the through-thickness morphology is more uniform and features the bright β-form spherulites that are associated to slow cooling. Identical features were observed, for example, by Bareta *et al.* (2007).

Heterogeneous moulding blocks

The heterogeneous RS combination gives rise to a non-symmetric distribution of the morphological features with respect to the mid-plane of the section: at the steel side a clear skin with finer spherulites and similar to the SS combination moulds is visible whereas at the resin side a coarser spherulite

Figure 8 Pressure vs time obtained in the indicated moulding conditions: (a) 27 s cycle time; (b) 40 s cycle time and (c) 60 s cycle time
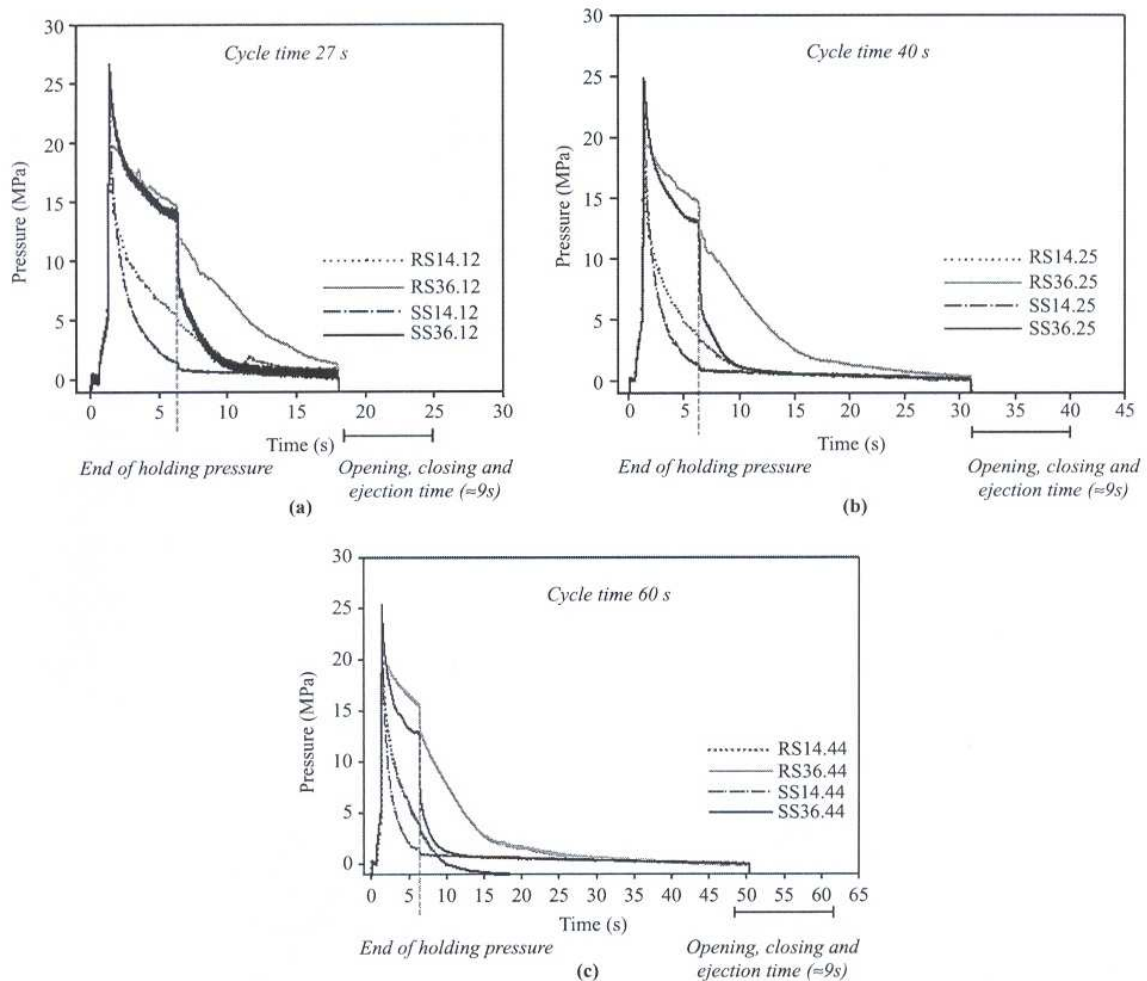
structure is evident. If the cycle time is shortened, e.g. for 19 s, there will result a visible alteration on the morphology as it is the case of the RS14.25 moulding. In this case (Figure 11) there is an increment of the heterogeneity of the morphology particularly associated to the modification in the resin side of the moulding with a region very populated with β-form spherulites.

Shrinkage

Mould temperatures and holding pressure mainly affect the final dimensions of the mouldings. Generally, as observed by Pontes *et al.* (2004) and Pontes and Pouzada (2004), increasing the mould temperature or decreasing the holding pressure lead to higher shrinkage parts. In semi-crystalline materials the expected shrinkage percentage can vary from 1 to 2.5 per cent. The shrinkage measured in this study, as shown in Figure 12, is within this range.

The shrinkage observed in the moulded parts with resin moulding blocks is much higher than in the SS counterparts (Figure 12). It is known that the shrinkage of injection mouldings is governed mainly by the thermal and pressure history during the moulding cycle. In these circumstances these results appear somewhat strange, as the variables involved are not that different apart. Therefore, one could expect that this situation must not be

related only to the actual plastics shrinkage but also to the actual deformation of the core during the injection and holding phases of the moulding cycle. This analysis is detailed below through structural simulation of the cores.

Deformation of the core

Structural simulations were made using the software *ANSYS Workbench* to compare the deformation of steel and resin composite cores. The simulations were made using the pressure information obtained during the experimental tests and the resin composite material data already referred before. Within the boundary conditions used in the simulations, it was considered that the bottom face of the core was bonded to the mould plate and the temperature of the core in the moulding region increased linearly from 40°C up to the actually monitored temperature in each of the studied cases. For the actual calculations the relevant properties of the materials (P20 steel and epoxy/aluminium composite) were input in the program database, as well as the pressure recorded during the tests.

The radial elastic strain field of the steel core is shown in Figure 13 and gives a maximum value of 0.0085 per cent at the middle region of the core.

Figure 9 Temperature vs time obtained in the indicated moulding conditions: (a) RS14.44; (b) RR14.44; (c) SS14.44 and (d) SS14.25
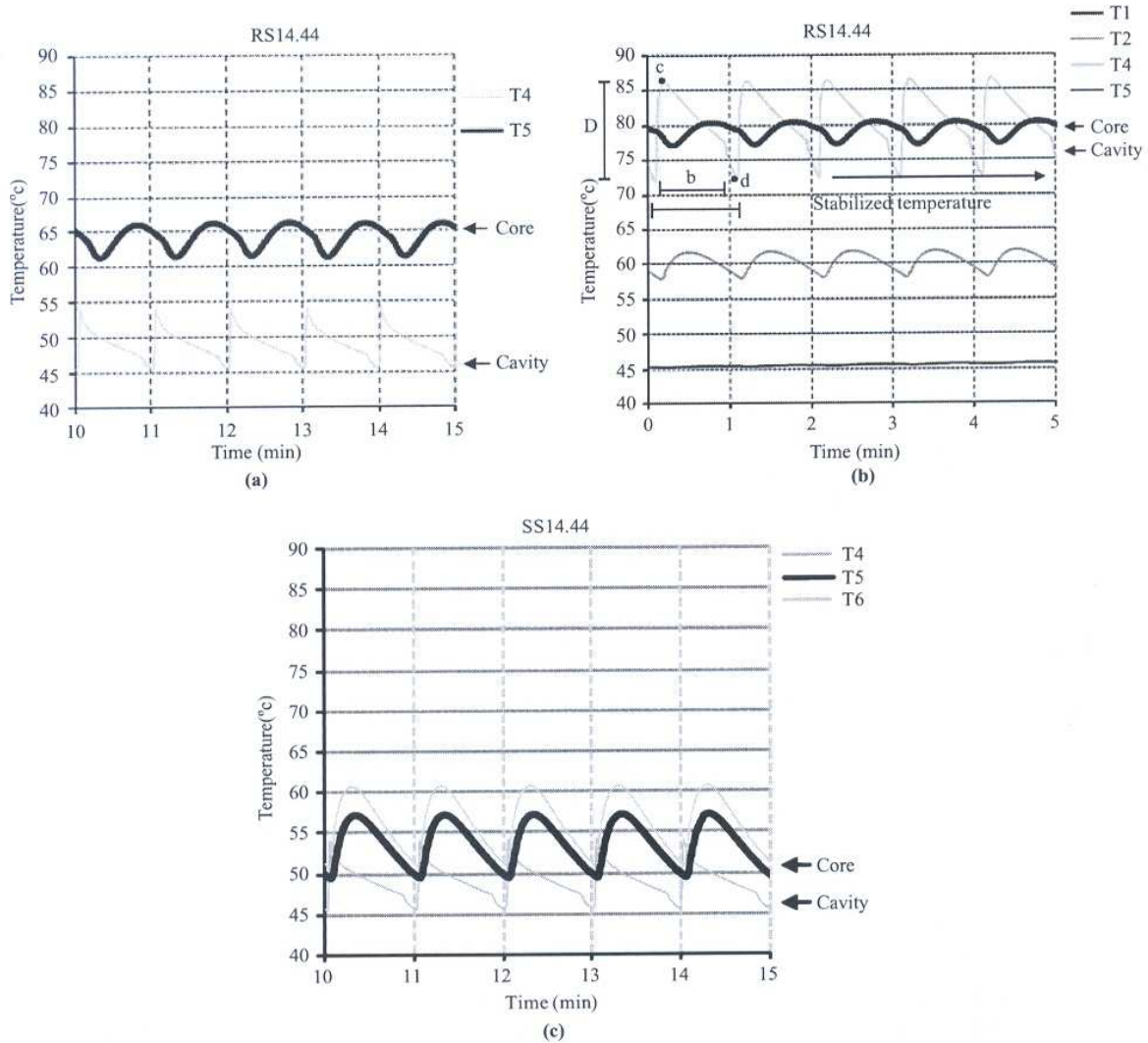
The radial strain field of the resin moulding block subjected to the pressure corresponding to the RS combination with holding pressure of 36 MPa is depicted in Figure 14 and shows a maximum value of 0.036 per cent at the point mentioned before.

The larger deformation of the resin core adds to the actual shrinkage resulting from the crystallization and thermal shrinkage of the moulded material.

It is important to evidence that when resin moulding blocks are used in injection moulds the final shrinkage of the mouldings is a consequence of the specific polymer shrinkage and the deformation of the non-metallic core deformed by the processing pressure. In this case the shrinkage of the part depends not only on the changes in the specific volume caused by the crystallization and the temperature variation but also on the core deformation caused by the injection pressure. The shrinkage in a moulded product is normally calculated in percentage as:

$$Sh_i = \frac{D_{imp} - D_{part}}{D_{imp}}, \qquad (2)$$

where D_{imp} is the dimension in the impression in the i direction at a reference temperature and D_{part} is the corresponding part dimension.

In the case of a moulding block with deformability in the range of the moulding shrinkage, the final dimension in the part is the result from the dimension variation associated to the cooling of the polymer (resulting from thermal and crystallinity/solidifying effects) and to the deformation caused by the injection pressure on the moulding block, i.e.:

$$D_{part} = D_{imp} - \delta_{plast} - \delta_{pressure}. \qquad (3)$$

Thus, the shrinkage of the part in this type of moulds, as a first approximation, will be the result of the two deformations, δ_{plast} and $\delta_{pressure}$:

$$Sh_i = \frac{\delta_{plast} + \delta_{pressure}}{D_{imp}} \qquad (4)$$

Figure 10 Microscopic part thickness analysis (material flow direction) in the indicated moulding conditions
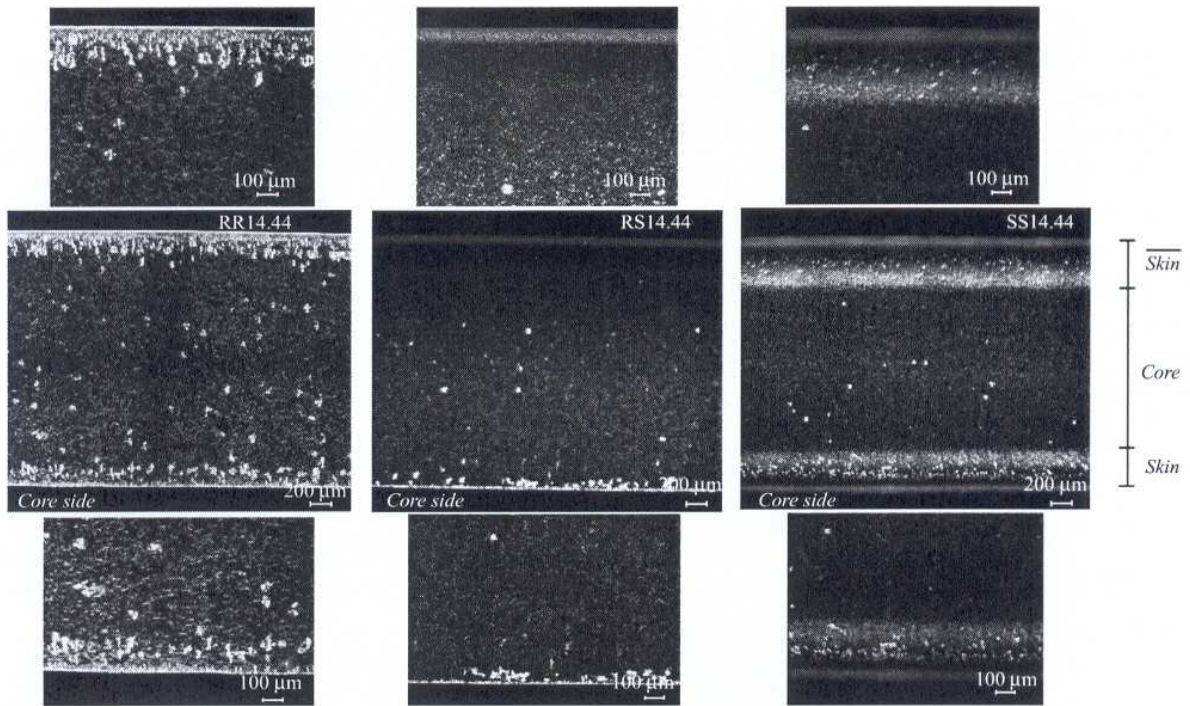

Figure 11 Microscopic part thickness analysis (material flow direction) in the parts obtained in the indicated moulding conditions and different cooling time
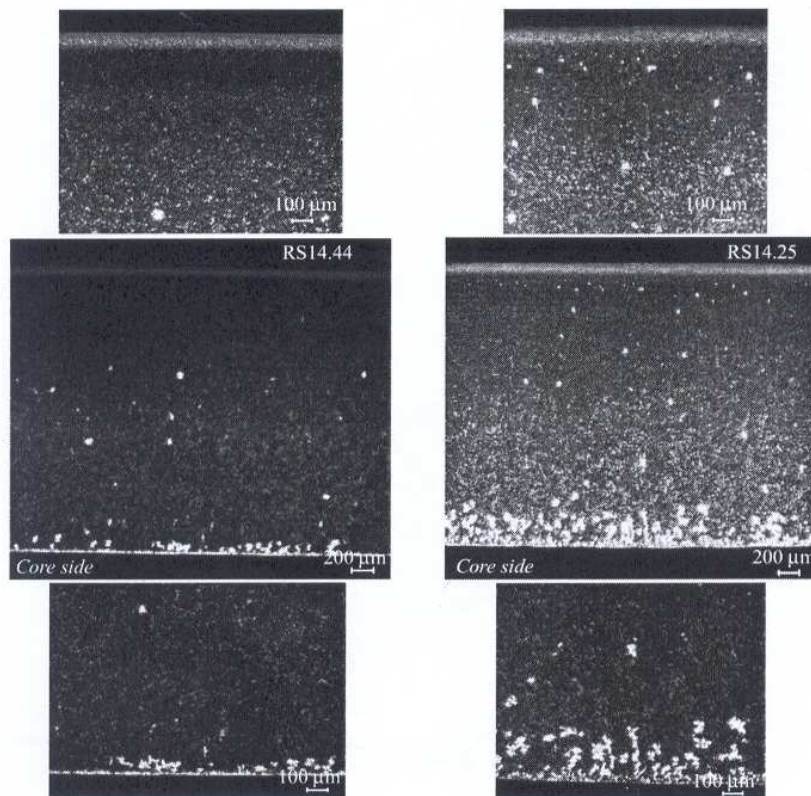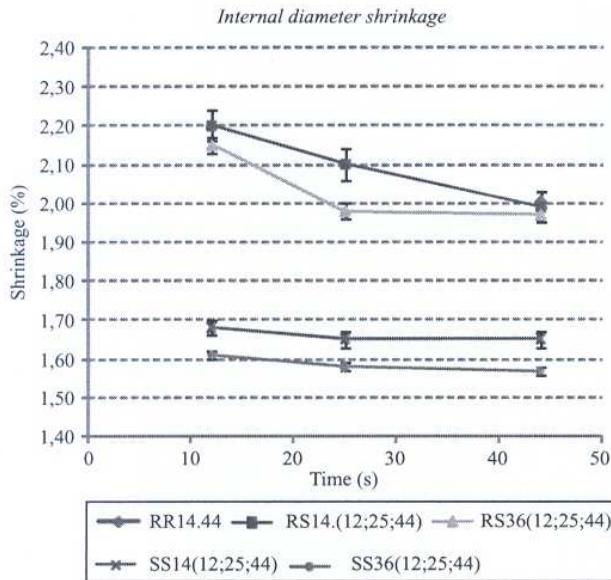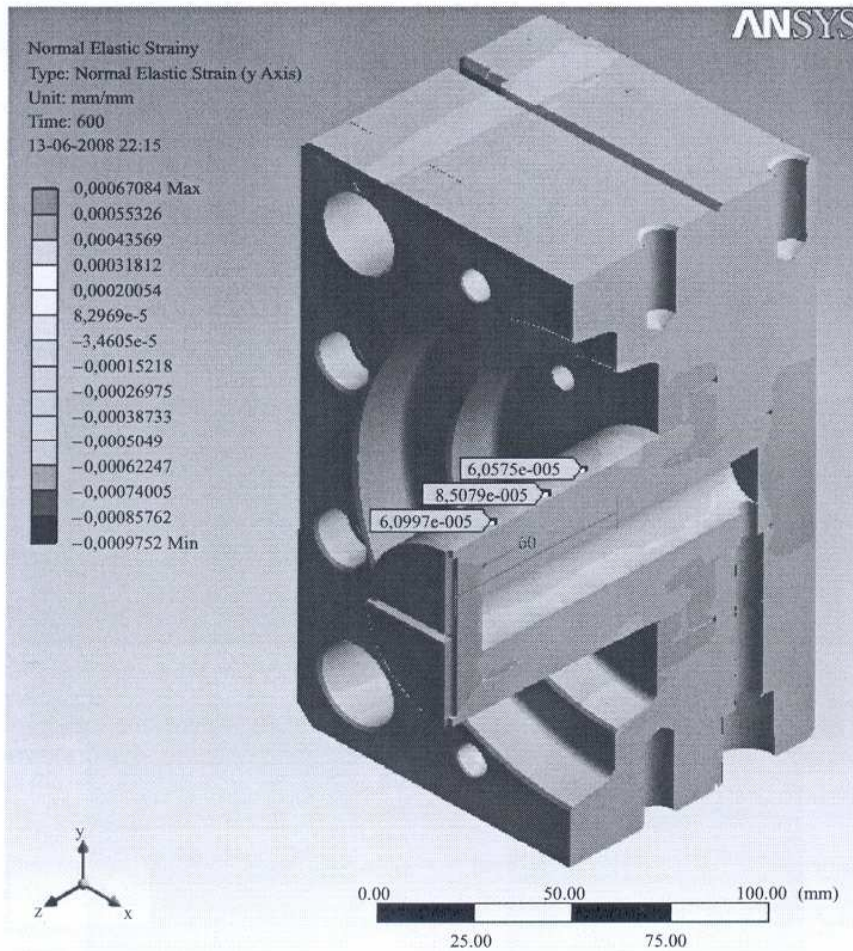
Figure 12 Parts' internal diameter shrinkage

or:

$$Sh_i = \frac{D_{imp} - D_{part}}{D_{imp}} + \varepsilon_{pressure}, \qquad (5)$$

where $\varepsilon_{pressure} = (\delta_{pressure}/D_{imp})$ introduces the effect of the deformation of the moulding block in the shrinkage.

Table V summarises the main results emerging from the shrinkage study where the holding pressure, the cooling rate and the mould temperature effects were considered.

As observed in Table V for all studied cases, the smaller shrinkage occurs for higher holding pressure and lower mould temperatures. The results also reveal that shorter cooling times and resin combinations increase the mould temperatures since the cooling water circuit temperature was established on 40°C.

Conclusions

Moulding blocks for injection moulds can be made in materials alternative to steel, using rapid tooling techniques. Vacuum casting is a economically viable option for short runs of production.

The materials used in vacuum casting have thermal and mechanical properties that imply the need of adjusting the

Figure 13 Radial elastic strain field simulation of the steel core moulding block

Figure 14 Radial elastic strain field simulation of the epoxy resin composite moulding block
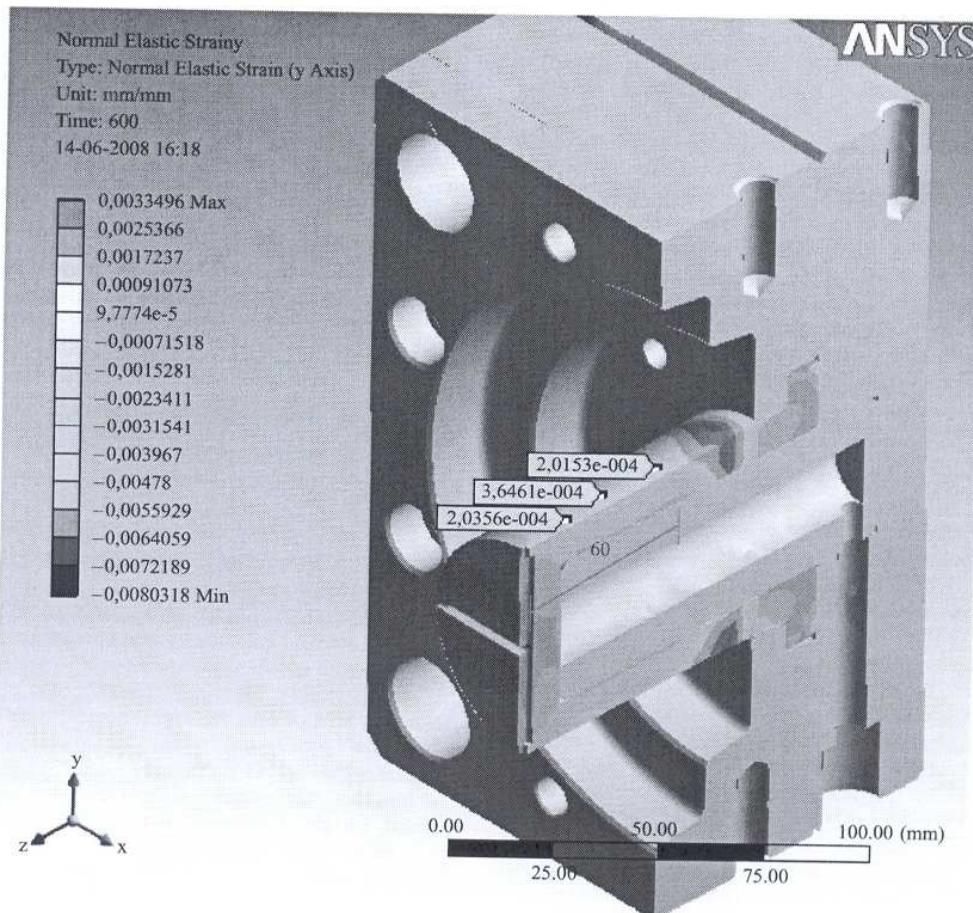

Table V Relations between the holding pressure, cooling time/mould temperature and the internal diameter shrinkage obtained on parts

Moulding block combination (core/cavity)	Cooling time (s)	Mould temperature (°C)	Holding pressure (MPa)	Inner diameter shrinkage (per cent)
Steel/steel (SS)	12	65	14	1.68
			36	1.61
	25	57	14	1.65
			36	1.58
	44	49	14	1.65
			36	1.57
Resin/steel (RS)	12	74	14	2.20
			36	2.15
	25	71	14	2.10
			36	1.98
	44	61	14	1.99
			36	1.97
Resin/resin (RR)	44	78	14	2.00

injection moulding setup. When resin moulding blocks are used, the holding pressure must be lower. Additionally, the cycle time with resin moulding blocks may become larger compared to steel unless higher running mould temperatures are used.

The plastic mouldings produced with hybrid moulds show morphological characteristics dependent on the moulding block combinations used. When different materials are used in the core and the cavity, asymmetric morphology and different crystallinity result.

These results are of practical interest on moulding thermoplastics precision parts with hybrid moulds with *soft* cores, because the actual shrinkage of the mouldings will depend on the deformation of the deformable moulding block. The consideration of the shrinkage is of great importance on designing plastics parts with narrow precision tolerances. This study evidences that the final dimensions of the parts produced in hybrid moulds depend on the plastics shrinkage but also on the core deformation of the non-metallic core deformed by the processing pressure.

The work reported herewith is being pursued with experiments on parts of more complex shapes that are usually subjected to mould filling simulation. It is desirable that the current software packages will be able to accommodate the effect of deformation and poor thermal behaviour of the non-metallic moulding blocks.

References

Bareta, D.R., Pouzada, A.S. and Costa, C.A. (2007), "The effect of rapid tooling materials on mechanical properties of tubular mouldings", paper presented at PMI 2007 International Conference on Polymers and Moulds Innovations, Gent/Belgium, April.

Beal, V.E., Ahrens, C.H. and Sabino-Netto, A.C. (2003), "Evaluating the use of aluminum inserts on stereolithography puzzle molds for injection molding of complex parts: a case study", *Proceedings ANTEC 2003 Conference, Nashville/USA, May*.

Brito, A.M., Cunha, A.M., Pouzada, A.S. and Crawford, R.J. (1991), "Predicting the skin-core boundary location in injection moldings", *International Polymer Processing*, Vol. 6 No. 4, pp. 370-7.

Cheah, C.M., Chua, C.K. and Ong, H.S. (2002), "Rapid moulding using epoxy tooling resin", *International Journal Advanced Manufacturing Technology*, Vol. 20 No. 55, pp. 368-74.

Chua, C.K., Leong, K.F. and Lim, C.S. (2003), *Rapid Prototyping – Principles and Application*, World Scientific Publishing, Singapore.

Cunha, A.M., Pouzada, A.S. and Crawford, R.J. (1992), "A study of the impact behaviour of injection moulded polypropylene using two different modes of testing", *Plastics Rubber and Composites Processing and Applications*, Vol. 18 No. 2, pp. 79-90.

Drizo, A. and Pegna, J. (2006), "Environmental impacts of rapid prototyping: an overview of research to date", *Rapid Prototyping Journal*, Vol. 12 No. 2, pp. 64-71.

Fujiyama, M., Wakino, T. and Kawasaki, Y. (1988), "Structure of the skin layer in injection-molded polypropylene", *Journal of Applied Polymer Science*, Vol. 35 No. 11, pp. 29-49.

Hemsley, D.A. (1989), *Applied Polymer Light Microscopy*, Elsevier Applied Science, Barking.

Lima, P., Ramos, J. and Pouzada, A.S. (2003), "Thermal performance of hybrid injection molds with epoxy inserts", *Proceedings ANTEC 2003 Conference, Nashville/USA, May*.

Martinho, P., Bártolo, P.J., Queirós, M.P., Pontes, A.J. and Pouzada, A.S. (2005), "Hybrid moulds: the use of combined techniques for the rapid manufacturing of injection moulds", in Bártolo, P.J. *et al.* (Eds), *Virtual Modelling and Rapid Manufacturing*, Taylor and Francis, London, pp. 421-7.

Oliveira, M.J., Bernardo, C.A. and Hemsley, D.A. (2001), "Morphology and mechanical behavior of polypropylene hot plate welds", *Polymer Engineering and Science*, Vol. 41 No. 11, pp. 1913-22.

Pontes, A.J. and Pouzada, A.S. (2004), "Ejection force in tubular injection moldings. Part I: effect of processing conditions", *Polymer Engineering and Science*, Vol. 44 No. 5, pp. 891-8.

Pontes, A.J., Oliveira, M.J. and Pouzada, A.S. (2004), "The effect of holding pressure on the shrinkage and birefringence of injection moulded polypropylene plates", *Materials Science Forum*, Vol. 455-456, pp. 814-7.

Potsch, G. and Michaeli, W. (1995), *Injection Molding: An Introduction*, Carl Hanser Verlag, Munich.

Pouzada, A.S. (1993), "Predicting the mechanical behaviour of anisotropic moulded plates", paper presented at 3rd Japan International SAMPE Symposium, Tokyo.

Ribeiro, A.R. Jr, Hopkinson, N. and Ahrens, C.H. (2004), "Thermal effects on stereolithography tools during injection moulding", *Rapid Prototyping Journal*, Vol. 10 No. 3, pp. 176-80.

Sabino-Netto, A., Yañez, F.A., Ahrens, C.H. and Salmoria, G.V. (2004), "Effects of mixing parameters on the quality of composite epoxy-aluminium tools", paper presented at PPS Americas Reg. Meeting, Florianópolis, November.

Saraiva, V.M., Lima, M. and Pouzada, A.S. (1999), "Towards a new conceptual design of injection moulds", paper presented at 44th International Scientific Colloquium, Ilmenau, September.

Segal, J.I. and Campbell, R.I. (2001), "A review of research into the effects of rapid tooling on part properties", *Rapid Prototyping Journal*, Vol. 7 No. 2, pp. 90-8.

Tenma, M. and Yamaguchi, M. (2007), "Structure and properties of injection-molded polypropylene with sorbitol-based clarifier", *Polymer Engineering and Science*, Vol. 47 No. 9, pp. 1441-6.

Tjong, S.C., Shen, J.S. and Li, R.K.Y. (1995), "Morphological behaviour and instrumented dart impact properties of β-crystalline-phase polypropylene", *Polymer*, Vol. 37 No. 12, pp. 2309-16.

Tordjeman, Ph., Robert, C., Marin, G. and Gerard, P. (2001), "The effect of α, β crystalline structure on the mechanical properties of polypropylene", *The European Physical Journal E*, Vol. 4 No. 4, pp. 459-65.

Viana, J. and Cunha, A.M. (1996), "Impact performance of injection molded PP plates", paper presented at PPS 12th Annual Meeting, Sorrento, May.

Yuan, Y., Chen, B. and Zhang, X. (2007), "Study on the formation of β-crystal during the crystallization process of polypropylene reactor granule", *Polymer*, Vol. 48 No. 19, pp. 5480-3.

Corresponding author

António Sérgio Pouzada can be contacted at: asp@dep.uminho.pt

Author guidelines

Rapid Prototyping Journal

Copyright

UK, Europe and Africa

Dr Ian Campbell, Loughborough University, Department of Design and Technology, Loughborough, Leicestershire, LE11 3TU, UK.
Tel: 01509 228312; Fax: 01509 223999
E-mail: R.I. Campbell@lboro.ac.uk

The Americas

Dr Brent Stucker, Utah State University, Department of Mechanical and Aerospace Engineering, Logan, UT 84322-4130, USA
E-mail: brent.stucker@usu.ed

Asia and Australasia

Dr Ian Gibson, Department of Mechanical Engineering, National University of Singapore, 9 Engineering Drive 1, Singapore 117576
E-mail: mpegi@nus.edu.sg

Editorial objectives

Rapid Prototyping Journal provides academics and industry decision makers with coverage of cutting-edge research in rapid prototyping and direct manufacturing techniques. The journal concentrates on rapid product development in a manufacturing environment but applications within other areas, such as medicine and construction, are also covered.

Editorial scope

The journal covers the full range of research activities related to rapid prototyping, including both technical and implementation aspects. Appropriate topic areas are:

- benchmarking
- reviews of processes/applications
- CAD and other software aspects
- case studies
- enhancement of existing processes
- integration with design process
- management implications
- materials aspects
- new rapid prototyping processes
- novel applications of rapid prototype parts
- rapid prototyping for tooling
- medical applications
- rapid/direct digital/additive manufacturing
- reverse engineering in relation to RP

For submissions involving animal or human experiments

Submissions describing animal experiments must contain a clear statement that all experiments were:

- kept to a minimum;
- only conducted where absolutely necessary;
- conducted to internationally recognised ethical and humane standards at appropriately licensed premises and conducted by appropriately licensed staff.

Articles reporting the results of experimentation involving human subjects must include a full ethical statement declaring that:

- the nature of the procedures and purpose of the research had been fully explained to all participants including their right to anonymity, privacy and to withdraw from the study at any time;
- written informed consent was obtained from all subjects;
- the research design was approved by the relevant research ethics committee of the institution at which the work was performed, including the name of the ethical committee and the date permission was granted.

The reviewing process

Each paper is reviewed by the Editors and, if it is judged suitable for this publication, it is then sent to two referees for double blind peer review. Based on their recommendations, the Editor then decides whether the paper should be accepted as is, revised or rejected. The Editor may make use of iThenticate software for checking the originality of submissions received.

Emerald Literati Editing Service

The Literati Network can recommend the services of a number of freelance copy editors, all themselves experienced authors, to contributors who wish to improve the standard of English in their paper before submission. This is particularly useful for those whose first language is not English. Please see www.emeraldinsight.com/editingservice for further details.

Submission process

Submissions to *Rapid Prototyping Journal* are made using Manuscript Central, Emerald's online submission and peer review system. Registration and access is available at http://mc.manuscriptcentral.com/rpj Full information and guidance on using Manuscript Central is available at the Emerald Manuscript Central Support Centre: http://msc.emeraldinsight.com

Registering on Manuscript Central

If you have not yet registered on Manuscript Central, please follow the instructions below:

- Please log on to http://mc.manuscriptcentral.com/rpj

- Click on "Create Account"
- Follow the on-screen instructions, filling in the requested details before proceeding
- Your username will be your e-mail address and you have to input a password of at least eight characters in length and containing two or more numbers
- Click "Finish" and your account has been created.

Submitting an article to *Rapid Prototyping Journal* on Manuscript Central

- Please log on to *Rapid Prototyping Journal* at http://mc.manuscriptcentral.com/rpj with your username and password. This will take you through to the Welcome page
- (To consult the Author Guidelines for this journal, click on the **Home Page** link in the **Resources** column)
- Click on the **Author Centre** button
- Click on the **submit a manuscript** link which will take you through to the Manuscript Submission page
- Complete all fields and browse to upload your article
- When all required sections are completed, preview your .pdf proof
- Submit your manuscript.

Manuscript requirements

The manuscript will be considered to be the definitive version of the article and should be in **MS WORD** format. Please use **single line** spacing to conserve paper during the review and production processes. Good electronic copies of all figures and tables should also be provided. All manuscripts should be run through a UK English spell check prior to submission.

As a guide, articles should be approximately 2,000 and 4,000 words in **length**. A **title** of not more than eight words should be provided. A brief **autobiographical note** should be supplied including full name, affiliation, e-mail address and full international contact details. Authors must supply a **structured abstract** set out under 4-6 sub-headings: Purpose; Design/methodology/approach; Findings; Research limitations/implications (if applicable); Practical implications (if applicable); and Originality/value of the paper. Maximum is 250 words in total. In addition provide up to six **keywords** which encapsulate the principal topics of the paper and categorize your paper under one of these **classifications**: Research paper, Viewpoint, Technical paper, Conceptual paper, Case study, Literature review or General review. For more information and guidance on structured abstracts visit: www.emeraldinsight.com/structuredabstracts

Notes or **Endnotes** should be used only if absolutely necessary and must be identified in the text by consecutive numbers, enclosed in square brackets and listed at the end of the article.

Figures should be supplied within the article itself.

All **Figures** (charts, diagrams, line drawings and photographic images) should be submitted in electronic form. Figures should be of clear quality and numbered consecutively with arabic numerals. Graphics may be supplied in colour to facilitate their appearance in colour on the online database.

Figures created in MS Word, MS PowerPoint, MS Excel, Illustrator and Freehand should be saved in their native formats.

Electronic figures created in other applications should be copied from the origination software and pasted into a blank MS Word document or saved and imported into an MS Word document by choosing "Insert" from the menu bar, "Picture" from the drop-down menu and selecting "From File ..." to select the graphic to be imported.

For figures which cannot be supplied in MS Word, acceptable standard image formats are: .pdf, .ai, .wmf and .eps. If you are unable to supply graphics in these formats then please ensure they are .tif, .jpeg, or .bmp at a resolution of at least 300dpi and at least 10cm wide.

To prepare screenshots, simultaneously press the "Alt" and "Print screen" keys on the keyboard, open a blank Microsoft Word document and simultaneously press "Ctrl" and "V" to paste the image. (Capture all the contents/windows on the computer screen to paste into MS Word, by simultaneously pressing "Ctrl" and "Print screen".)

For photographic images good quality original photographs should be submitted. If supplied electronically they should be saved as .tif or .jpeg files at a resolution of at least 300dpi and at least 10cm wide. Digital camera settings should be set at the highest resolution/quality possible.

In the text of the paper the preferred position of all tables and figures should be indicated by typing on a separate line the words "Take in Figure (No.)". Tables should be typed and included as part of the manuscript. They should not be submitted as graphic elements. Supply succinct and clear captions for all tables and figures. Ensure that tables and figures are complete with necessary superscripts shown, both next to the relevant items and with the corresponding explanations or levels of significance shown as footnotes in the tables and figures.

References to other publications must be in Harvard style and carefully checked for completeness, accuracy and consistency. This is very important in an electronic environment because it enables your readers to exploit the Reference Linking facility on the database and link back to the works you have cited through CrossRef. You should include all author names and initials and give any journal title in full.

You should cite publications in the text: (Adams, 2006) using the first named author's name or (Adams and Brown, 2006) citing both names of two, or (Adams *et al.*, 2006), when there are three or more authors. At the end of the paper a reference list in alphabetical order should be supplied:

For books: surname, initials, (year), *title of book*, publisher, place of publication, e.g. Harrow, R. (2005), *No Place to Hide*, Simon & Schuster, New York, NY.

For book chapters: surname, initials, (year), "chapter title", editor's surname, initials, *title of book*, publisher, place of publication, pages, e.g. Calabrese, F.A. (2005), "The early pathways: theory to practice – a continuum", in Stankosky, M. (Ed.), *Creating the Discipline of Knowledge Management*, Elsevier, New York, NY, pp. 15-20.

For journals: surname, initials, (year), "title of article", *journal name*, volume, number, pages, e.g. Capizzi, M.T. and Ferguson, R. (2005), "Loyalty trends for the twenty-first century", *Journal of Consumer Marketing*, Vol. 22 No. 2, pp. 72-80.

For electronic sources: if available online the full URL should be supplied at the end of the reference.

Authors' Charter

This highlights some of the main points of our Authors' Charter. For the full version visit:

www.emeraldinsight.com/charter

Your rights as an author

Emerald believes that as an author you have the right to expect your publisher to deliver:

- An efficient and courteous publishing service at all times
- Prompt acknowledgement of correspondence and manuscripts received at Emerald
- Prompt notification of publication details
- A high professional standard of accuracy and clarity of presentation
- A complimentary journal issue in which your article appeared
- Article reprints
- A premium service for permission and reprint requests
- Your moral rights as an author.

Emerald represents and protects moral rights as follows:

- To be acknowledged as the author of your work and receive due respect and credit for it
- To be able to object to derogatory treatment of your work
- Not to have your work plagiarized by others.

The Emerald Literati Network

The Emerald Literati Network is a unique service for authors which provides an international network of scholars and practitioners who write for our publications. Membership is a free and unique service for authors. It provides:

- A dedicated area of the Emerald web site for authors
- Resources and support in publishing your research
- Free registration of yourself and your work, and access to the details of potential research partners in Emerald Research Connections
- The opportunity to post and receive relevant Calls for Papers
- Information on publishing developments
- Awards for outstanding scholarship
- Usage information on authors, themes, titles and regions
- Access to tips and tools on how to further promote your work
- Awards for Excellence.

To discuss any aspect of this Charter please contact:

Emerald Literati Network, Emerald Group Publishing Limited, Howard House, Wagon Lane, Bingley BD16 1WA, United Kingdom
Telephone +44 (0)1274 777700
E-mail: **literatinetwork@emeraldinsight.com**

Emerald

The world's leading publisher of management journals and databases

A STUDY OF THE EJECTION FORCES ON MOULDING INSERTS OBTAINED BY RPT TECHNIQUES

Martinho, P.G.[1]; Cardon, L[2].; Neves, T.[3]; Bártolo, P.J.[4]; Pouzada A. S.[5]

[1] Polytechnic Institute of Leiria, Leiria, Portugal

[2] University College Ghent and Ghent University, Ghent, Belgium

[3] Simulflow-Moldex 3D, Leiria, Portugal

[4] CDRSP, Polytechnic Institute of Leiria, Leiria, Portugal

[5]Institute for Polymers and Composites, Dep. Polymer Engineering, University of Minho, Guimarães, Portugal

asp@dep.uminho.pt

Abstract

Hybrid moulds are an alternative for prototype series or short production runs of plastics products. This type of tools resorts on the use of Rapid Prototyping and Tooling (RPT). These moulds were initially sought for relatively simple geometries. However it is possible to introduce more complex details in the moulded parts if inserts with controlled tribological behaviour are used. In this study, an instrumented hybrid mould is used to test possibilities of mould construction for complex geometry products. The study includes strength and frictional behaviour of a moulding insert designed for a long side movement. The inserts were obtained by RPT techniques, namely, vacuum casting of epoxy based composites, stereolithography, 3D-printing, ProMetal and SLSm. The data obtained from polypropylene parts and their moulding inserts will be compared with simulations using the Moldex3D® software.

Introduction

Today, new plastics products should not only satisfy consumer requirements but also meet increasing product complexity and reduced lifetime. As a consequence of this new social environment, new rapid product development strategies must be adopted by the companies, which lead to tremendous challenges to their internal flexibility. Therefore, the current industrial trend is moving from mass production, *i.e.* high-volume and small-range of products for manufacturing, to small-volume and a wide range of products [1].

The search for alternative methodologies for the design and manufacturing of moulds for short runs of plastic components is a great industrial goal. This is possible through the use of rapid tooling technologies and the use of new and different materials for the moulding inserts. The idea of building moulds with moulding inserts manufactured in alternative metallic materials or in synthetic materials is the basis of the hybrid mould concept [2]. Hybrid moulds are used for short and medium run injection series. An important issue to increase the lifetime of hybrid moulds and the accuracy of their mouldings is the design for wear minimisation.

Associated to the hybrid moulds wear, three distinct mechanisms were identified [3]: abrasive, erosive, and adhesive wear. *Abrasive wear* occurs when the material is removed by contact with hard particles. The particles either may be present at the surface of a second material or may exist as loose particles between two surfaces. *Erosive wear* is caused by particles that collide on a component surface or edge and remove material from that surface due to momentum effects. According to Hayden [4], the hardness of the mould surface will influence the type of the erosion mechanism. Erosion wear produces deep, narrow furrows and pits in hard materials, and wider and shallower erosion planes in soft materials. In injection moulds this type of wear mechanism is particularly evident in areas of high shearing such as gates [5]. *Adhesive wear* occurs when two solid surfaces slide past each other under pressure. Surface projections are plastically deformed and eventually weld together by the high local pressure. As sliding continues, these bonds are broken, producing pits on the surface, projections on the second surface, and frequently tiny, abrasive particles, all of which contribute to future wear of surfaces. Polymers having the same solubility parameters and cohesive energy parameters present important adhesive characteristics [6, 7].

Various strategies were proposed to minimise the wear in injection moulds. Engelmann [8] pointed out that the strategy for wear reduction involves polishing smooth surfaces to decrease the amount of mechanical interlock between the moulding part and the moulding surface and increasing the hardness of the mould surface.

An important aspect of the operation of hybrid moulds is the wear caused by friction during ejection. During the ejection phase, friction forces are generated between the plastic part and the

core (typically steel). The coefficient of friction between plastic/steel depends on the surface texture of the core and the ejection temperature [9]. Generally, the ejection force is considered as the result of the interaction between part geometry, mould geometry and material, moulding material and processing conditions [10]. In conventional moulds where metals are used in the whole mould, the origin of the ejection forces results from the shrinkage of the thermoplastic material [7, 11]. However in hybrid moulds with resin moulding zones, the polymer-polymer contact and the chemistry adhesion are relevant especially at high temperatures. Gonçalves *et al.* [7] showed that minimising the adhesive wear is important when moulding polymers. The more favourable situation is when the Hildebrand solubility parameters are very different. It was also observed a significant elastic deformation of the cores, when resins with reduced Young modulus were used to produce the moulding blocks. In these cases the effective ejection force is lower than expected. Similarly, Salmoria *et al.* [12], who studied the use of stereolithography resins to produce moulding blocks, also showed that it is not possible to mould polymers of both higher tensile modulus and strength than the resin, due to the generalised failure of the moulds when parts were pulled out from the core. These problems can be increased if the ejection system is incorrectly designed [13].

Several researchers have investigated the effect of processing parameters on the ejection force [11, 14-16]. These studies demonstrated that the ejection force increases with the cooling time and the roughness of the mould wall.

In this paper ejection aspects associated to hybrid injection moulds are assessed. A specific part with geometrical details such as short and long lateral movable elements and a core moulding block was used. A flexible hybrid mould considering reutilisation is used to produce the injection parts.

Experimental

Tooling

The hybrid mould was designed considering reutilisation and the maximum flexibility in operation (Figure 1). Specific aspects were described elsewhere [17].

The parts are injected through a spider gating system. The main part dimensions are shown in Figure 2.

The ejection is made with a stripper ring and a central ejector pin.
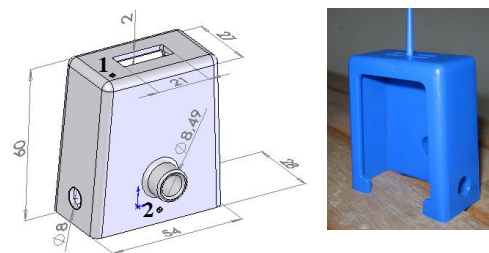

a) ejection side
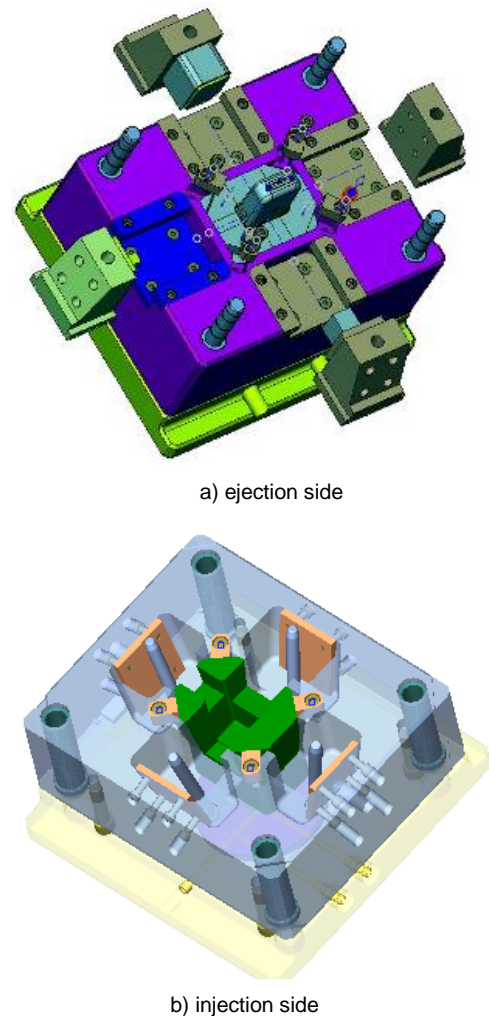
b) injection side

Fig. 1. Hybrid mould: a) ejection side; b) injection side

Fig. 2. The moulding with runner system

The hybrid mould is shown in Figure 3.

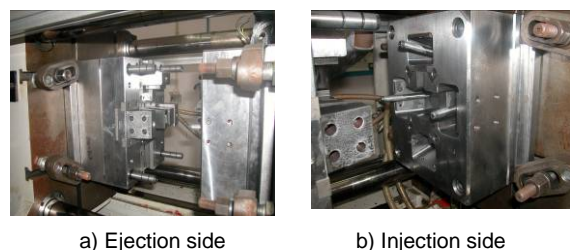
a) Ejection side   b) Injection side

Fig. 3. Hybrid mould: a) Ejection side b) Injection side

To define the back hole geometry, five moulding pins (Figure 4) were produced in: (1) Tool steel (Pin$_1$); (2) Epoxy (Biresin® L74) filled with 60% aluminium powder (Pin$_2$); (3) SL resin (DSM Somos® 11120/2), (Pin$_3$); (4) Epoxy (Biresin® L74)/15% short steel fibres (Pin$_4$); (5) ProMetal (Pin$_5$).

a) Moulding pin design

b) Produced pins

Fig. 4.   Moulding pins: a) CAD model b) as used on experimental tests

The main properties of the moulding pin materials are shown in Table 1.

Table 1: Properties of the moulding pins materials

Moulding pin material	Tool steel	Epoxy/Alum	SL resin	Epoxy/SSF	ProMetal
Properties Units	(DIN W Nr. 1.2311)	(Biresin L74 +60% Alum)	DSM Somos 11120/2	(Biresin L74 +15% SSF)	S4
Specific gravity [Mg.m^{-3}]	7.80	1.65	1.12	2.10	7.50
Specific heat [J.kg^{-1} K^{-1}]	460	1279.19	286.26	–	418
Thermal conductivity [W.m^{-1}. K^{-1}]	29	0.606	0.166	0.392	22.6
Thermal diffusivity [m^2.s^{-1}]	–	0.286 x 10^{-6}	0.519 x 10^{-6}	–	7.2 x 10^{-6}
Thermal expansion coefficient [K^{-1}]	1.20 x10^{-5}	6.00 x10^{-5}	9.50 x10^{-5}	–	–
Flexural Modulus @20ºC [GPa]	200	5-6	2-2.4	4.3-4.9	147

Instrumentation

The hybrid mould was instrumented with integrated pressure and temperature sensors (Kistler Type 6190BA) located close to the gate (1) and to the weld line (2) (see Figure 2).

The pins were screwed onto a load cell, designed for this study (Figure 5).

a) HM lateral   b) Load cell fitted in lateral component
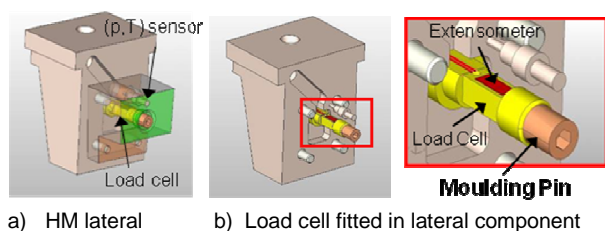
Fig. 5.   Load cell design a) hybrid mould lateral component b) load cell fitted in the lateral component

Ejection force

Typical strain data of the load cell during the injection cycles, with the use of the ProMetal moulding pin are shown in Figure 6. The strain is related to the force measured by the load cell.
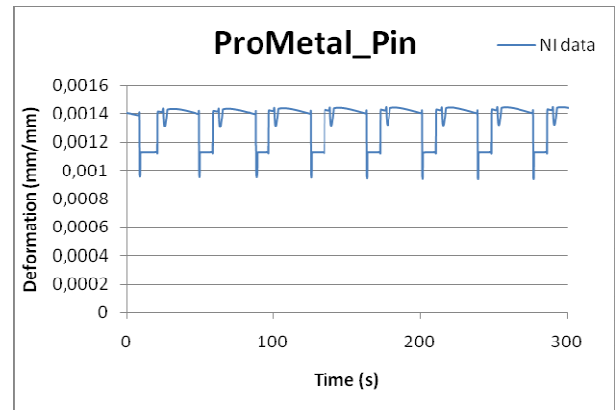
Fig. 6.   Deformation measured through the load cell during the injection cycle

The corresponding Force variation during each injection cycle is shown in Figure 7.
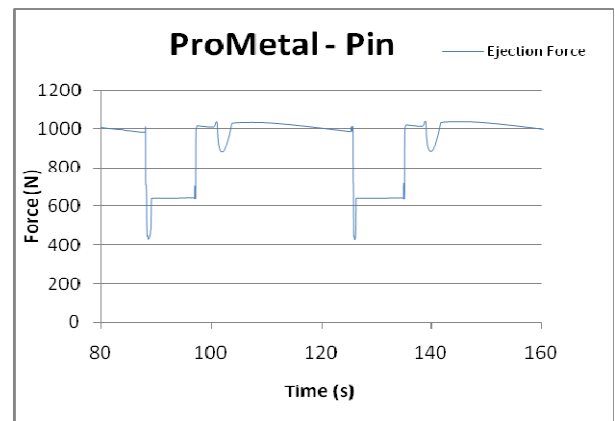
Fig. 7.   Force variation during the injection cycle

At the same time pressure and temperature data were collected during moulding (Figure 8), on the part locations shown in Figure 2.
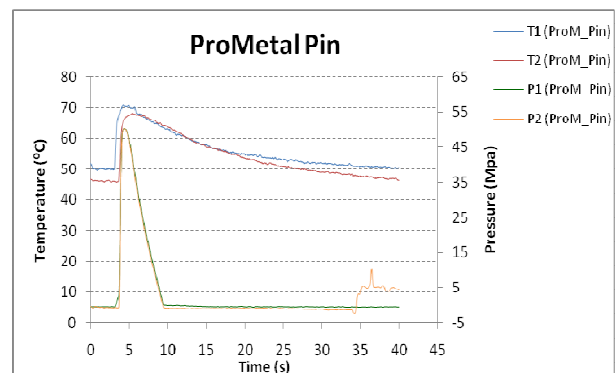

Fig. 8.   Pressure and temperature data into hybrid mould in the locations 1 and 2

Injection moulding

The mouldings were produced in polypropylene homopolymer, PP Homo Domolen 1100N (DOME Polypropylene, Rozenburg) of MFR 12 g/10min (230ºC/ 21,6 N) using a Ferromatik Milacron K85 injection moulding machine of 850 kN clamping force. The processing conditions were set according to the pin material used, as shown in Table 2.

When epoxy composite or SL pins were used, the processing conditions were adjusted to cope with the poorer mechanical properties of these materials. The injection pressure and the holding pressure were reduced by 20% from that used for the steel core. The cycle time was increased up to 50 s upon using the SL resin pin.

Table 2: Processing conditions

Parameter	Pin_1 (Steel)	Pin_2 (EP-Al)	Pin_3 (SL)	Pin_4 (SSF)	Pin_5 (ProM)
Injection temp [ºC]	230	230	230	230	230
Cooling temp [ºC]	40	40	30	40	40
Injection flow rate [$cm^3.s^{-1}$]	37.7	37.7	37,7	37.7	37.7
Injection time [s]	1.3	1.3	1.3	1.3	1.3
Injection pressure [MPa]	91	70	70	70	91
Holding time [s]	5	5	5	5	5
Opening, closing and ejection time [s]	12	12	12	12	12
Holding pressure [MPa]	70	56	35	56	70
Cooling time [s]	25	25	35	25	25

Simulation

The software Moldex3D® release 9.0 was used for the simulation of the hybrid moulds. The total number of elements used in the simulation was of 1 144 902 tetrahedrical elements. 177 792 elements were used in the part. The architecture of the cooling system (Figure 9) was considered in the simulation.
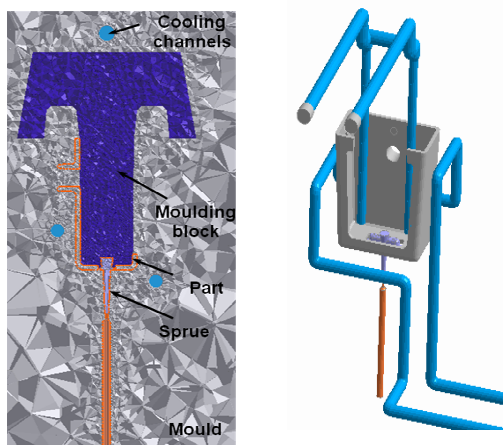
Fig. 9. Model and cooling architecture used in the Moldex3D® 9.0 simulation.

The evolution of the temperature during moulding was monitored as shown in Figure 10 for a complete moulding cycle. The figure shows how the temperature varies at the moulding surface of the cavity (sensor T_1) and in the core (sensor T_2).
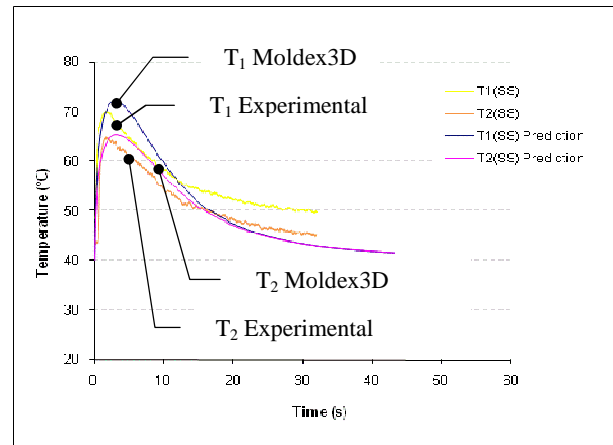
Fig. 10. Temperature data for the steel/steel (SS) cavity/core combination, T_1 - cavity; T_2 – core, and Moldex3D® 9.0 prediction values

The shrinkage prediction of the variation was made in each moulding pin, based on the dimensions shown in Figure 11.
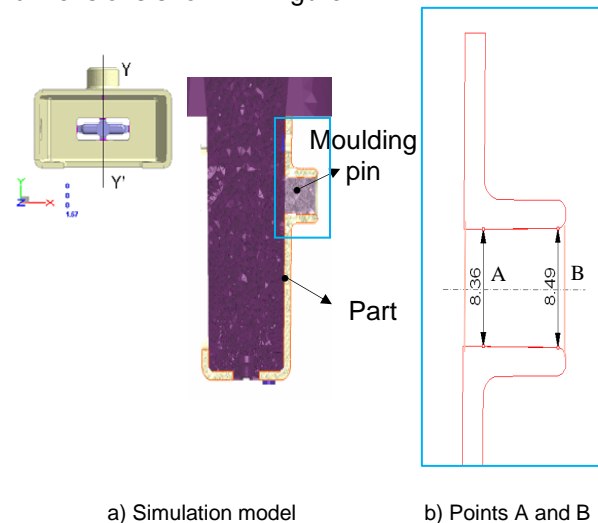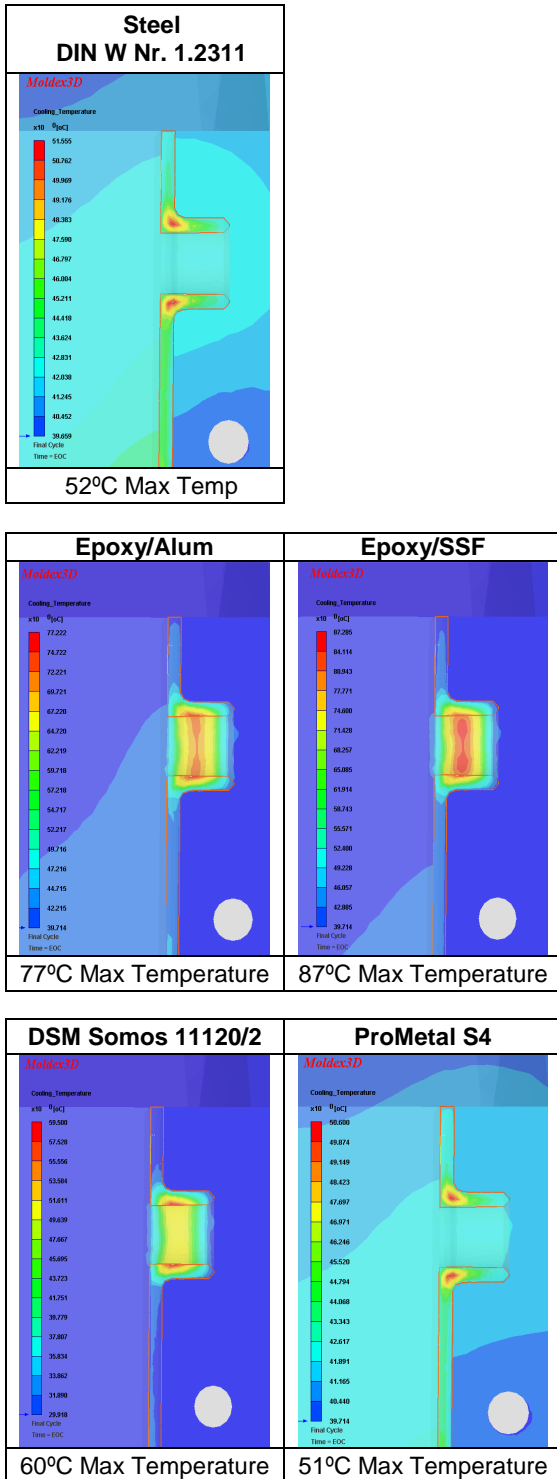

a) Simulation model   b) Points A and B

Fig. 11. Shrinkage predictions using Moldex3D® 9.0 a) Model b) Points A and B for the shrinkage analysis

The field of temperatures in the pin region as predicted by the Moldex3D® 9.0 is depicted in the Table 3.

Table 3: Field of temperatures predicted for different moulding pin materials

Steel DIN W Nr. 1.2311	
52ºC Max Temp	

Epoxy/Alum	**Epoxy/SSF**
77ºC Max Temperature	87ºC Max Temperature

DSM Somos 11120/2	**ProMetal S4**
60ºC Max Temperature	51ºC Max Temperature

Results

In injection moulding with hybrid moulds, design and processing aspects must be considered. The moulding properties and the moulding inserts integrity obtained by RPT techniques are very important, especially when less resistant materials are used. Also, the use of SL resins (DSM Somos 11120/2 – Pin$_3$) requires a strict control of the processing conditions for the durability of the inserts.

In this study, after about 20 shots the failure of the SL inserts occurs as depicted in Figure 12. This is associated to the shrinkage and resulting stresses in this zone.

a) moulding pin   b) 19th shot   c) 20th shot
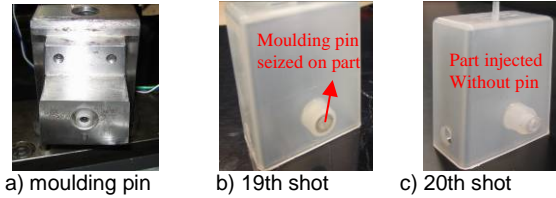
Fig. 12. Moulding pin part zone when using Somos 11120 pin. a) moulding pin fitted in the mould; b) and c) aspect of failure

The problem is worsened by the adhesion between the moulded material and the moulding pin material. PP and epoxy have Hildebrand factors rather close, 18 MPa$^{1/2}$ for the PP and 22 MPa$^{1/2}$ for the epoxy. The low glass temperature of the SL resin (~45ºC) is an additional problem considering the running temperature of the mould. The results show that the use of SL core blocks is not recommended for productions runs over 10-20 parts.

For assessment and comparing the part shrinkage in the moulding pin region, measurements were made in the mouldings (between points A and B, Figure 11b).

The predicted shrinkage and the measured values in part moulding pin zone are shown in Table 4.

Table 4: Part measurements in the moulding pin region and predicted by Moldex3D® 9.0.

Molding pin material	Ejection Force (N) Measured trough the load cell	Shrinkage (%) (Measured on the part)		Shrinkage (%) (Moldex3D® 9.0)	
	Between A and B	**A**	**B**	**A**	**B**
Steel DIN W Nr. 1.2311	415,58	2,39	1,88	2.51	1.81
Epoxy/Alum	613,12	2,15	2,37	2.13	2.50
DSM Somos 11120/2	609,70	2,54	2,50	1.99	2.95
Epoxy/SSF	619,50	2,26	2,70	2.18	2.63
ProMetal S4	423,79	2,40	2,02	2.48	1.87

The recorded ejection forces with the various pin materials are also presented in Table 4. These data are derived from recorded graphs as in Figure 7 after defining the correct baseline. In the near future the coefficient of friction, μ of pairs of materials will be determined to enable the calculation of ejection forces.

Conclusions

Moulding inserts produced by different RPT techniques imply different localized shrinkage on parts produced and consequently different ejection forces.

The number of parts that can be produced with SL moulding pin is very limited.

A good correlation is achievable between the experimental results and the predicted ones when using the software Moldex3D® 9.0.

Acknowledgements

Bibliography

[1] Martinho, P.; Bártolo, P. J.; Queirós, M. P.; Pontes, A.; Pouzada, A. - Hybrid Moulds: the Use of Combined Techniques for the Rapid Manufacturing of Injection Moulds. Virtual Modelling and Rapid Manufacturing. Edited by P.J. Bártolo *et al*, pp. 421-427, Taylor&Francis, London, 2005.

[2] Saraiva, V.M.; Lima, M.; Pouzada, A.S. - Towards a new conceptual design of injection moulds", 44th Int. Scientific Coll., Ilmenau/Germany, September 1999.

[3] Engelmann, P.; Hayden, K.; Guichelaar, P.; Dealey, R.; Monfore, M. - Understanding wear mechanisms: the key to mold life, ANTEC 2000, Brookfield, 2000.

[4] Hayden, K.; Engelmann, P.; Dealey, R.; Monfore, M. - Mold Wear vs Wall Thickness - Critical Information for Thin Wall Molding. ANTEC 1999, Brookfield, 1999.

[5] Lima, P.; Ramos, J.; Pouzada, A.S. - Thermal performance of hybrid injection molds with epoxy inserts. ANTEC 2003, Nashville: May 2003.

[6] Petrie, E.M. Handbook of adhesives and sealants. McGraw-Hill, New York, 2000.

[7] Gonçalves, M.W.; Salmoria, G.V.; Pouzada, A.S. - Study of tribological properties of moulds obtained by stereolithography, Virtual and Physical Prototyping, 2007.

[8] Engelmann, P.; Hayden, K.; Guichelaar, P.; Monfore, M. - Undercutting mold performance: Ejection wear. ANTEC 2002, Brookfield, 2002.

[9] Pouzada, A.S.; Ferreira, E.C.; Pontes, A.J. – Friction Properties on Moulding Thermoplastics. Polymer Testing, vol. 25 (2006). pp. 1017–1023.

[10] Pontes, A.J.; Ferreira, E.C.; Pouzada A.S. - Tribological aspects during ejection in injection moulds, RPD 2004 – Agile Development for Productivity, Marinha Grande, 2004.

[11] Pontes, A.J.; Pouzada, A.S. - Ejection force in tubular injection moldings. Part I: Effect of processing conditions. Polym. Eng. Sci., Vol. 44 (2004), pp. 891-898.

[12] Salmoria, G.V.; Ahrens, C.H.; Fredel, M.; Soldi, V.; Pires, A.T.N. - Stereolithography Somos 7110 resin: Mechanical behaviour and fractography of parts post-cured by different methods. Polymer Testing, 24(2), pp. 157-162, 2005.

[13] Araújo, B.J.; Pouzada, A. S. - Projecto de sistemas de extracção em moldes de injecção, O Molde, 54, pp.36-38, 2002.

[14] Burke, C.; Malloy, R. - An experimental study of the ejection forces encountered during injection molding. ANTEC 1991. Montreal, pp. 1781-1787, 1991.

[15] Balsamo, R.; Hayward, D.; Malloy, R. - An experimental evaluation of ejection forces: frictional effects. ANTEC 1993. New Orleans, 1993.

[16] Sasaki, T.; Koga, N.; Shirai, K.; Kobayashi, Y.; Toyoshima, A. - An experimental study on ejection force of injection molding, Journal of Precision Engineering, 24(3), pp.270-273, 2000.

[17] Martinho, P.G.; Bártolo, P. J.; Pouzada, A. S. - Efficient design solutions for hybrid moulds and the widening of the lifecycle of injection moulds, PMI 2007 – Int. Conf. on Polymers & Moulds Innovations. Ghent – Belgium: April 2007.

ON THE INFLUENCE OF THE MATERIALS USED ON THE MOULDING BLOCKS OF HYBRID MOULDS

Martinho, P.G.[1]; Cardon, L.[2] Neves, T.[3]; Bártolo, P.J.[4]; Pouzada A. S.[5]

[1] *Polytechnic Institute of Leiria, Leiria, Portugal;* [2] *University College Ghent and Ghent University, Ghent, Belgium;* [3] *Simulflow-Moldex 3D, Leiria, Portugal;* [4] *CDRSP, Polytechnic Institute of Leiria, Leiria, Portugal;* [5] *Institute for Polymers and Composites, Dep. Polymer Engineering, University of Minho, Guimarães, Portugal*

asp@dep.uminho.pt

Abstract

In the last few decades advances in manufacturing technologies made possible the utilisation of materials in alternative to steel in the moulding blocks of injection moulds. Hybrid moulds are an increasingly considered alternative for prototype series or short production runs. Various Rapid Prototyping and Tooling (RPT) options are available for the production of alternative moulding cores.

A development hybrid mould was developed for testing the various possibilities of mould construction for complex geometry products. This paper will present results obtained with moulding cores produced by epoxy tooling with various fillers and stereolithography. The data obtained in the instrumented mould was compared with injection moulding simulations using the MOLDEX 3D simulation software.

Introduction

Advances in manufacturing technologies observed since the 1980's have been thriving for the use of materials in alternative to steel in the moulding blocks of injection moulds. Nowadays, hybrid moulds are an increasingly considered alternative for prototype series or short production runs [1]. Various RPT options are available for the production of alternative moulding cores. The possibility of getting quickly moulding blocks in alternative materials is also the main interest for this solution. Nevertheless, several problems have been identified by researchers working with hybrid moulds. Some problems are associated to the material selection for the moulding blocks [1-4], the plastic material to be injected and the complex part geometry typical of injection mouldings [5, 6].

The moulding blocks can be produced by various RPT techniques: direct rapid tooling such as Direct AIM, Selective Laser Sintering or Metallic LOM, or indirect processes such as Epoxy tooling, Spray tooling, 3D KelTool [7, 8]. The vacuum casting of epoxy composites is commonly used for moulding blocks. However, problems were reported in respect to the non-uniform mixing of the composite components, the curing agent and also the presence of trapped gases in the mixture

[9, 10]. The stereolithography (SL) process has also been used to produce hybrid mould blocks for very short production series. Ribeiro Jr. *et al.* [2] and Guimarães *et al.* [11], studied the use of SL to directly produce these inserts. Several authors [11-13] reported that the major problem of SL moulding blocks is the thermal performance associated to the lower thermal conductivity of the SL resins in comparison with aluminium or steel. As mentioned by Guimarães *et al.* [10], this fact implies longer moulding cycles and the need of considering different cooling strategies.

Gonçalves *et al.* [12] studied the behaviour of hybrid moulds using moulding blocks made from SL resin Vantico 5260. They concluded in their studies that when a material of reduced stiffness (like the aforementioned resin) is used, a substantial elastic deformation of the core occurs. They also observed that polymers with Hildebrand solubility parameter (δ) close to the resins showed adhesion characteristics that were not observed in other polymers where these values were further apart. Salmoria *et al.* [13] studied a SL resin and concluded that it was not possible to mould polymers of tensile modulus and strength higher than the resin. Impact strength is also very important due to impact forces at injection point, with higher injection pressures. According to Gonçalves *et al.* [14], the choice of the best SL resin for the moulding blocks of a hybrid mould, leads preferentially to a resin with high tensile strength and glass temperature (T_g), but with an intermediate elastic modulus, in order to enable the absorption of more energy. It is also important, considering the Hildebrand parameters, to check the chemical affinity between the injected polymer and the moulding block material.

This paper addresses the performance of a hybrid mould with a steel cavity and several core moulding blocks produced using alternative materials: Epoxy/aluminium composite; Epoxy/short steel fibres composite (SSF), and SL resin. Pressure and temperature data were collected from the various core/cavity combinations. These data were compared with data from the mould with standard DIN WNr.1.2311 tool steel moulding blocks in terms of the thermal, mechanical and flow performance. Comparisons were also made with predictions simulated with the MOLDEX 3D software.

PMI 2008

Influence of the materials used on the moulding blocks of hybrid moulds — Martinho, P.G. *et al.*.

Experimental

Tooling

The hybrid mould that enables the quick interchangeability of the moulding blocks was described elsewhere [15]. The moulding blocks are shown in Figure 1.
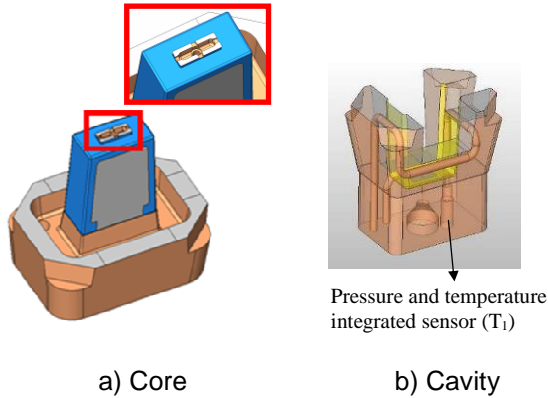

a) Core   b) Cavity

Fig. 1. Moulding blocks. a) core; b) cavity

The parts are injected through 4 gates of a spider gating system (Figure 2). The ejection is made with a stripper ring and a central ejector pin.
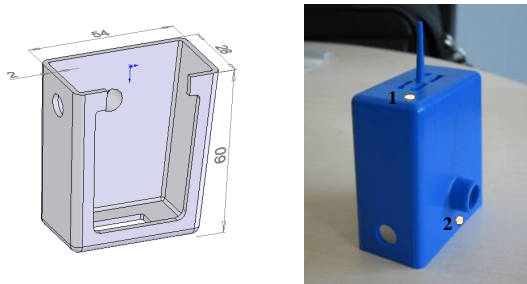
Fig. 2. The moulding with runner system

The mouldings were produced using four combinations of materials in the moulding blocks: (1) Epoxy/60% aluminium powder (Biresin® L74) in the core and steel in the cavity (identified as Resin$_1$/Steel or R$_1$S combination); (2) SL resin (DSM Somos® 11120/2) in core and steel in cavity (Resin$_2$/Steel or R$_2$S); (3) Epoxy/15% short steel fibres (Biresin® L74) in core and steel in cavity (Resin$_3$/Steel or R$_3$S) and (4) Steel in core and steel in cavity (Steel/Steel or SS).

The integrated pressure and temperature sensor (Kistler Type 6190BA) collected the data close to the gate location (1) and at the welding line location (2) of the part.

The thermal and mechanical properties of the materials used in the moulding blocks are shown in Table 1. They were determined with an Alambeta conductivity equipment (Sensora, Liberec) for the thermal properties, a dynamic mechanical analyser Tritec 2000 (Triton, Nottingham) and a universal testing machine Zwick Z100 (Ulm) for the mechanical properties.

The density of the epoxy/aluminium composite was determined by the impulsion method. The epoxy/short steel fibre composite was proposed by Sabino Netto *et al.* [16] and its density estimated with the law of the mixtures.

Table 1: Properties of the moulding blocks materials

Moulding block material		Tool steel	Epoxy/Alum	SL resin	Epoxy/SSF
Properties	Units	(DIN W Nr. 1.2311)	(Biresin L74 +60% Alum)	DSM Somos 11120/2	(Biresin L74 +15% SSF)
Specific gravity	[Mg.m^{-3}]	7.80	1.65	1.12	2.10
Specific heat	[J.kg^{-1} K^{-1}]	460	1279.19	286.26	–
Thermal conductivity	[W.m^{-1}. K^{-1}]	29	0.606	0.166	0.392
Thermal diffusivity	[m^2.s^{-1}]	–	0.286 x 10^{-6}	0.519 x 10^{-6}	–
Thermal expansion coefficient	[K^{-1}]	1.20 x10^{-5}	6.00 x10^{-5}	9.50 x10^{-5}	–
Flexural Modulus @20ºC	[GPa]	200	5-6	2-2.4	4.3-4.9

The aluminium powder particles used for the Epoxy/60% aluminium composite have an average size of 50 µm and specific gravity of 2.43 Mg.m^{-3}. The low steel carbon fibres have an average length of 453 µm and average thickness of 45 µm [16] and specific gravity of 7.87 Mg.m^{-3}. The epoxyde Biresin L74 used for preparing the composites has a Heat Deflection Temperature of 160ºC.

The standard steel moulding blocks and the mould structure are shown in the Figure 3.
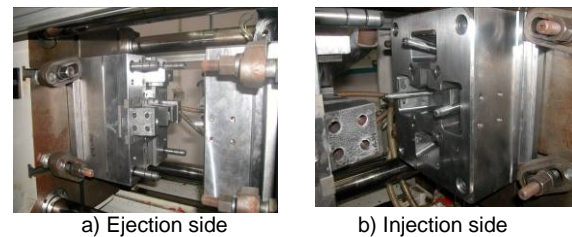

a) Ejection side   b) Injection side

Fig. 3. Standard moulding blocks fitted in the mould structure. a) Ejection side b) Injection side

The epoxy composite resin cores were produced by vacuum casting in silicone moulds. These cores were made using the actual steel core as a master.

The vacuum casting route included a preliminary degassing of the resin composite during 15 min, the degassing of the cast resin during 20 min, the cure of the cast resin at room temperature during 24 h and the post cure at 60ºC during 3 h and 140ºC during 3 h. The heating and cooling rates were set at 10ºC/h.

The SL resin core block was produced with 3-D Systems SLA 3500 equipment.

PMI 2008

Influence of the materials used on the moulding blocks of hybrid moulds | Martinho, P.G. *et al.*.

Injection moulding

The mouldings were produced in polypropylene homopolymer, PP Homo Domolen 1100N (DOME Polypropylene, Rozenburg) of MFR 12 g/10min (230ºC/ 2,16 kg) using a Ferromatik Milacron K85 injection moulding machine of 850 kN clamping force. The processing conditions were set according to each combination of core and cavity materials, as shown in Table 2.

When using the epoxy composite cores or the SL core, the processing conditions (pressure and cycle phases) were adjusted to cope with the poorer mechanical properties of these materials. The injection pressure and the holding pressure were reduced from that used for the steel core (by 20% for epoxy cores and up to 50% for SL core). The cycle time was increased up to 60s in all resin core combinations.

Table 2: Processing conditions

Parameter	SS	R_1S and R_3S	R_2S
Core/Cavity materials	Steel/Steel	EPres/Steel	SLres/Steel
Injection temp [ºC]	230	230	230
Cooling temp [ºC]	40	40	40
Injection flow rate [cm^3.s^{-1}]	37.7	37.7	37,7
Injection time [s]	1.3	1.3	3
Injection pressure [MPa]	91	70	42
Holding time [s]	5	10	10
Opening, closing and ejection time [s]	12	12	12
Holding pressure [MPa]	70	56	14
Cooling time [s]	25	35	45

Pressure monitoring

Typical pressure data for the moulding blocks combinations and processing conditions are shown in Figure 4 where data variation over the injection cycle is recorded.
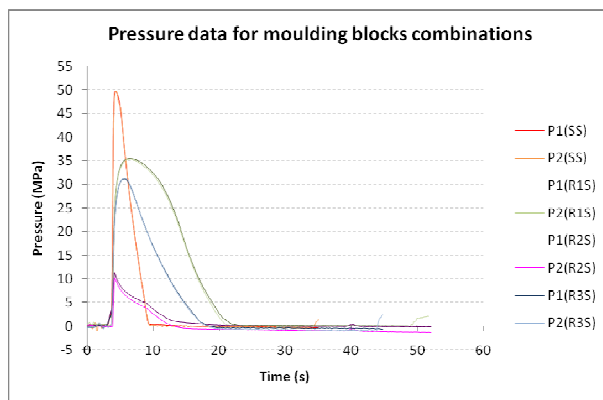
Fig. 4. Pressure data for the various cavity/core combinations. P1 - cavity; P2 - core

It may be observed that the material combinations with resin lead to a slower decrease of the cavity pressure and the maximum values

are always lower than the all-steel combination. These data can only be derived from a sizeable deformation of the resin blocks that needs to be estimated, *e.g.,* by structural analysis.

Temperature monitoring

The evolution of temperature during moulding was monitored as shown in Figure 5 for a complete moulding cycle. The figure shows how the temperature varies during each cycle at moulding surface of the cavity (sensor T_1) and in the core (sensor T_2).
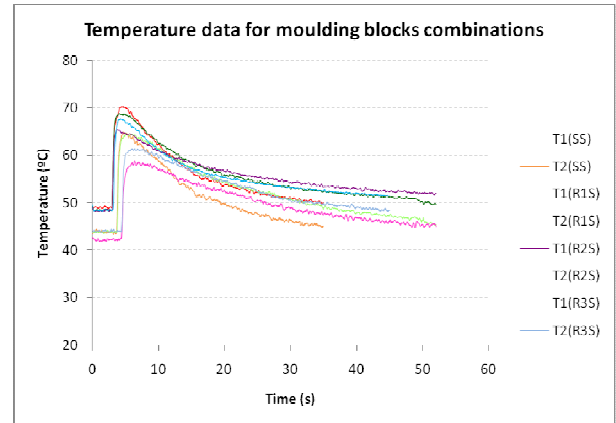
Fig. 5. Temperature data for the various cavity/core combinations. T_1 - cavity; T_2 - core

The data obtained with sensor T_2, repeated for clarity in Figure 6, highlights the influence of the higher thermal resistance of the moulding blocks with lower thermal conductivity.
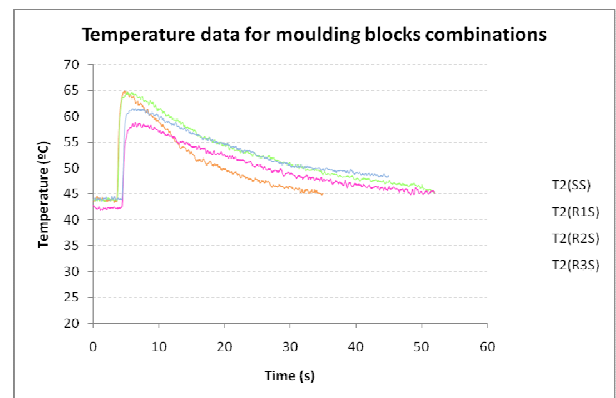
Fig. 6. Temperature data at the core side

The temperature evolution in the first injection cycles is important when low thermal conductivity materials are used and it is necessary to know the stabilized mould temperature. The definition of this regime temperature depends of the imposed cycle time. Rapid cycling leads to higher service temperatures. The Figures 7 and 8 show the temperature evolution in the first injection cycles of the SS and R_1S combinations. In the case of SS combination the mould temperature stabilizes after 7 injections whereas for the R_1S combination 12

PMI 2008

Influence of the materials used on the moulding blocks of hybrid moulds   Martinho, P.G. *et al.*.

shots are required. The evolution repeatability after this stabilization is also evident for each case.
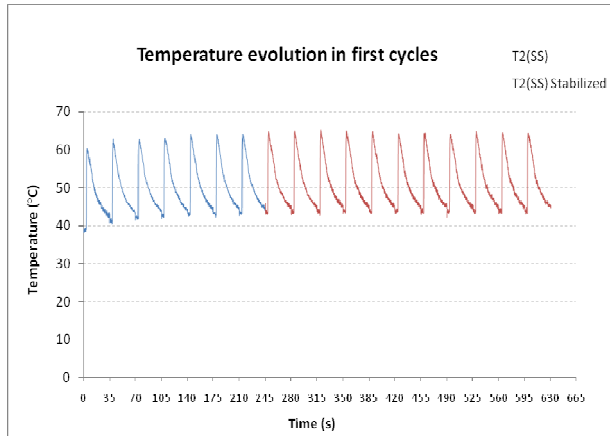

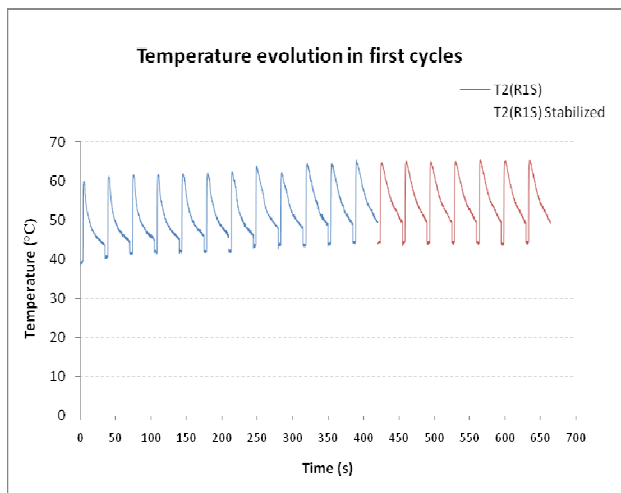**Fig. 7.**   Temperature evolution in first injection cycles of the SS combination

Fig. 8.   Temperature evolution in first injection cycles of the R_1S combination

Simulation analysis

The combination of various materials in the core and cavity blocks determined different temperature running levels (Figure 5). It was also observed that materials of low conductivity as epoxy composites or SL resins require a *warming up* period, so that a regime mould temperature is achieved. These facts imply the need of simulating the running of the moulding cycle for moulding repeatability and moulding block reliability.

The software Moldex3D release 9.0 was used for the process simulation of the hybrid moulds. The prediction of the temperature and the pressure variation were made in each injection cycle, as shown in Figures 9 and 10.
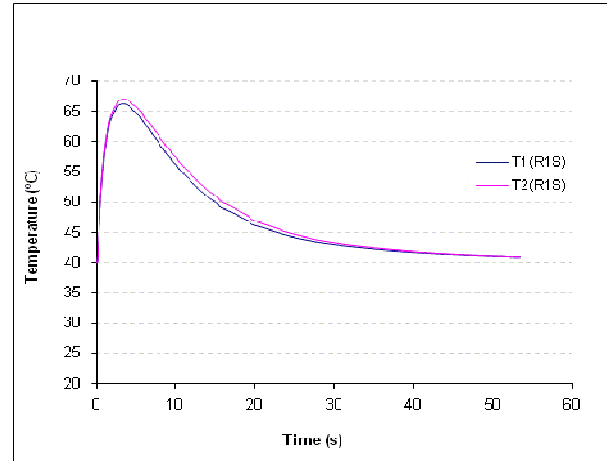
Fig. 9.   Prediction of the temperature evolution in the hybrid mould with epoxy/60% aluminium composite core using Moldex3D® 9.0
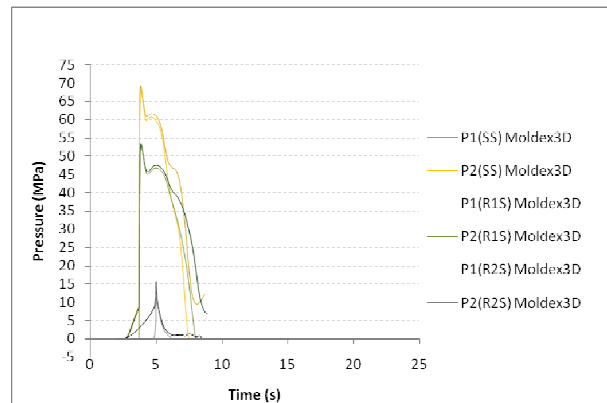
Fig. 10.   Pressure simulation of the various moulding block combinations using Moldex3D® 9.0

The total number of elements used in the Moldex simulation was of 1 144 902 tetrahedrical elements, the part using 177 792 of them. The architecture of the cooling system was included in the simulation as shown in Figure 11.
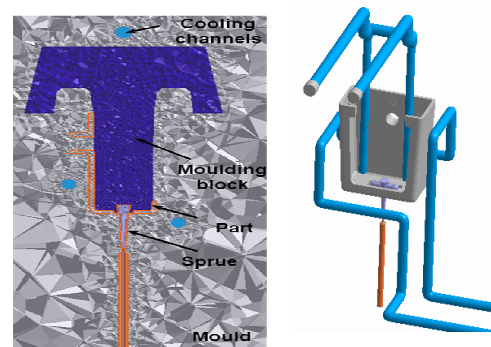
Fig. 11.   Model and cooling architecture used in the simulation with Moldex3D® 9.0

Results and discussion

Tooling
The use of epoxy composites with high density fillers as the short steel fibres require curing

PMI 2008

Influence of the materials used on the moulding blocks of hybrid moulds   Martinho, P.G. *et al.*.

methods that prevent sedimentation until the gel time is achieved. The dynamic process using the apparatus recommended by Sabino Netto *et al.* [16] at 5 rpm was adequate for this purpose. The SL core was produced with an extra thickness of 0.3 mm for the final adjustment of the block to fit into the mould frame.

Injection moulding

In injection moulding with hybrid moulds not only the moulding properties are important but also the moulding block integrity, especially when less resistant materials are used. Therefore, when SL resins (R_2S combination) are used, the control of the processing conditions is very important for the durability of the moulds. It is recommendable that the process starts with incomplete mouldings produced at lower pressure and increase the pressure until the complete filling of the mould is obtained.

The failure of the SL core started at the gating region as depicted in Figure 12. The complete filling of the parts was only possible at the injection pressure of 42 MPa. However at 28 MPa vestiges of resin in the mouldings start to appear, as shown in Figure 13. This is associated to the shrinkage and resulting stresses at the gating zone.

a) before moulding   b) after failure
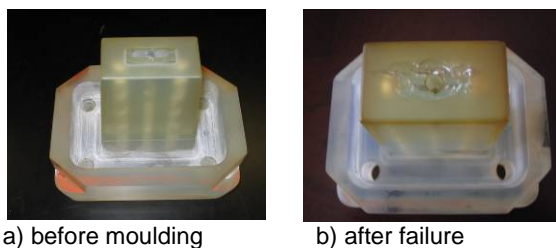
Fig. 12. Feeding system of the Somos 11120 resin core moulding blocks a) before injection b) after injection

Fig. 13. Vestiges of SL resin in the mouldings

The problem is worsened by the adhesion between the moulded material and the block material. They have Hildebrand factors rather close, 18 $MPa^{1/2}$ for the PP and 22 $MPa^{1/2}$ for the epoxy resin. The low glass temperature of the SL resin (~45ºC) is also an additional problem considering the running temperature of the mould over 60 ºC. Thus, the results show that the use of SL core blocks is not recommended for productions runs over 20 parts.

The lowest temperature curve obtained for the combination R_2S (Figure 5) is also related with the number of parts injected.

The use of epoxy composites, as the one in the R_1S combination is more adequate for production. After 300 mouldings no visible defects were seen in the composite core. The R_3S combination with the epoxy/SSF composite in the core leads to a thermal and mechanical performance similar to the R_1S. However it was noticed that especially in sliding zones, small steel particles start to detach from the core causing some seizing in the steel mould surfaces in contact, as shown in Figure 14. To avoid this problem it is recommended to use higher gap tolerances in the sliding zones.
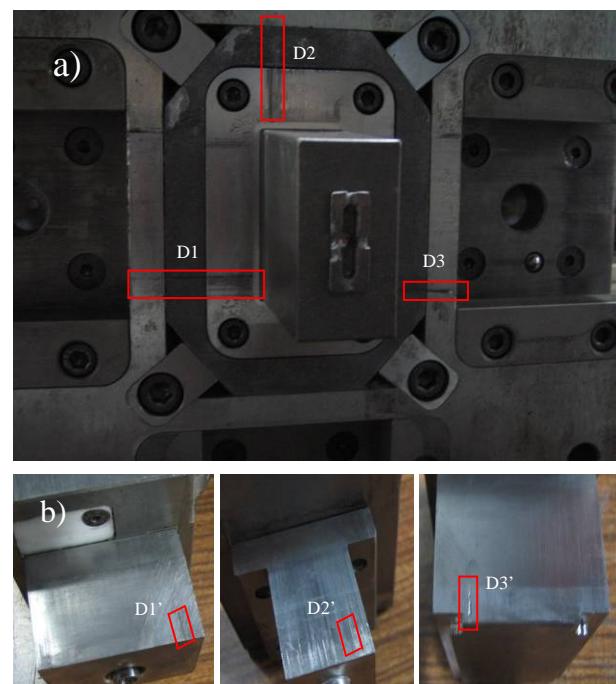

Fig. 14. Seizing in steel components when epoxy/SSF composites are used in the core. a) Scratching zones; b) Seized components

Simulation analyses

The simulation of the mould temperature taking into account the actual structure of the mould yield results quite close to the measured values, as exemplified in Figures 15 and 16 for the cases of the R_1S and SS combinations. It is noticeable that the simulation, where the cooling medium temperature was input, considered the starting temperature at 40ºC and not to the actual running temperature of the mould. The profiles of temperature at the mould/part interface show a good correlation between experimental and predicted values as shown in Figures 15 and 16.
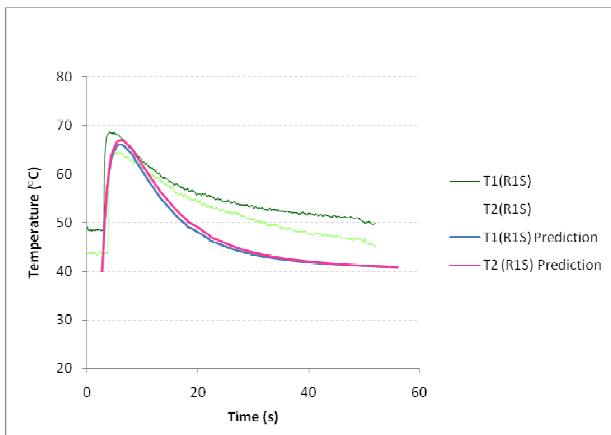
PMI 2008

Influence of the materials used on the moulding blocks of hybrid moulds   Martinho, P.G. *et al.*.

Fig. 15. Prediction of the mould temperature for the R_1S combination using Moldex3D® 9.0.
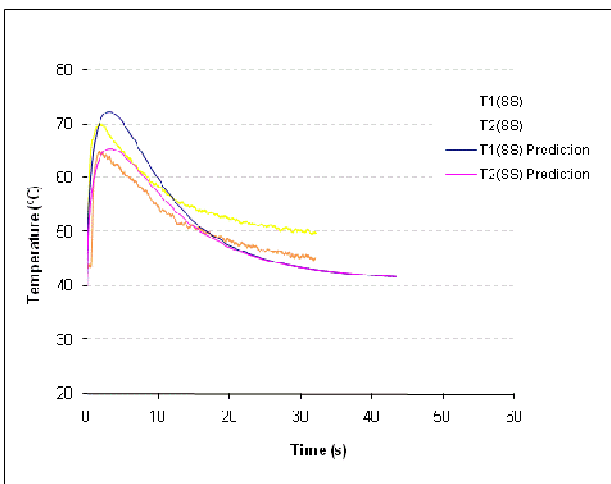

Fig. 16. Prediction of the mould temperature for the SS combination using Moldex3D® 9.0.

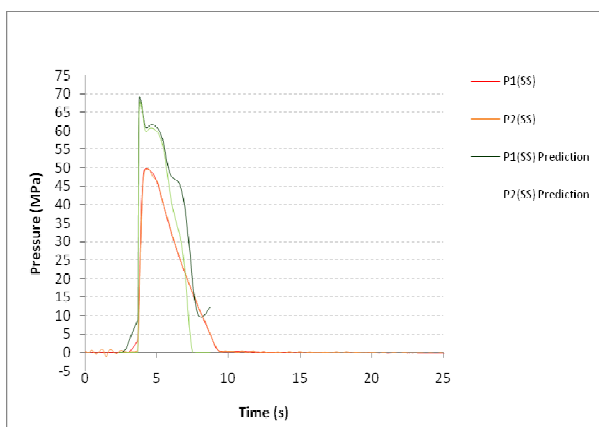The simulation of the pressure was not so precise predicting a somewhat higher value of the maximum pressure, as shown in Figure 17 for the case of the SS combination.

Fig. 17. Prediction of the pressure for the SS combination using Moldex3D® 9.0

Conclusions

Hybrid moulds are a suitable solution for producing mouldings of relatively complex shapes. When less stiff materials are used as an alternative to steel, it is important for the integrity of the moulding blocks to establish appropriate processing conditions.

The number of parts that can be produced with SL cores is very limited due to the poor resistance and low glass transition temperature compared with the mould running temperatures.

The results suggest the importance of predicting the regime mould temperature when low thermal conductivity materials are used in moulding blocks. This temperature depends on the desired cycle time.

Computer simulation can be used to predict the thermal behaviour of the mould but it appears to be recommendable that the actual structure of the mould is considered in the simulation, namely the air gaps that may condition the heat transfer process.

Acknowledgements

Bibliography

[1] Lima, P., Ramos, J., Pouzada, A.S. - Thermal performance of hybrid injection molds with epoxy inserts. Proceedings ANTEC 2003 Conf, Nashville: May 2003.

[2] Ribeiro Jr., A.R., Hopkinson, N. and Ahrens, C.H. (2004), - Thermal effects on stereolithography tools during injection moulding, Rapid Prototyping Journal. 10 No. 3, pp. 176.

[3] Pontes, A.J., Queirós, M., Bártolo, P., Pouzada, A.S. - A Study on Design and Performance of Hybrid moulds for Injection Moulding. ICIT 2005 – 5th Int. Conf. of Industrial Tools. Bled: April 2005.

[4] Martinho, P., Bártolo, P. J., Queirós, M. P., Pontes, A., Pouzada, A. - Hybrid Moulds: the Use of Combined Techniques for the Rapid Manufacturing of Injection Moulds. Virtual Modelling and Rapid Manufacturing. Edited by P.J. Bártolo et al, pp. 421, Taylor&Francis, London, 2005.

[5] Saurkar, S., Malloy, R., McCarthy, S. - Rapid tooling: a study of different cooling techniques for mold inserts used in the direct aim (ACES injection molding) process. ANTEC 2005 Conf, Boston: May 2005.

[6] Volpato, N., Foggiatto, J.A., Amorim, J.R. de, Filho, O.D. - A proposed data base to aid material selection for prototype tooling. RPD 2006, Marinha: November 2006.

[7] Chua, C.K., Leong, K.F. and Lim, C.S. - Rapid Prototyping – Principles and Application. World Scientific Publishing, Singapore: 2003.

[8] Drizo, A. and Pegna, J. (2006) - Environmental impacts of rapid prototyping: an overview of research to date. Rapid Prototyping Journal, Vol. 12 No. 2, pp. 64.

[9] Cheah, C. M., Chua, C. K. and Ong, H. S. (2002) - Rapid Moulding Using Epoxy Tooling Resin. International Journal Advanced Manufacturing Technology, Vol. 20, pp. 368.

[10] Sabino-Netto, A., Yañez, F. A., Ahrens, C. H. and Salmoria, G. V. (2004) - Effects of mixing parameters on the quality of composite epoxy-aluminium tools. PPS Americas Reg. Meeting, Florianópolis: November 2004.

[11] Guimarães, D. A., Alves, A., Pontes, A.J. - Thermal study of stereolithography moulding inserts. RPD 2006 – Building the future by innovation, Marinha Grande: November 2006.

[12] Gonçalves, M. W., Pouzada, A.S., Salmoria, G.V., Ahrens, C.H. – Performance and friction properties of injection hybrid moulds with stereolitography moulding zones. Materiais 2005 - 3rd Int Materials Symp. Aveiro: April, 2005.

[13] Salmoria, G.V., Ahrens, C.H., Fredel, M., Soldi, V., Pires, A.T.N. - Stereolithography Somos 7110 resin: Mechanical behaviour and fractography of parts post-cured by different methods. Polymer Testing, 24, pp. 157, 2005.

[14] Gonçalves, M.W.; Salmoria, G.V.; Pouzada, A.S. - Study of tribological properties of moulds obtained by stereolithography, Virtual and Physical Prototyping, 2, pp. 29, 2007.

[15] Martinho, P.G., Bártolo, P.J., Pouzada, A.S. - Efficient design solutions for hybrid moulds and the widening of the lifecycle of injection moulds, PMI 2007 – Int Conf. Polymers & Moulds Innovations, Ghent: April 2007.

[16] Sabino-Netto, A.C., Salmoria, G.V, Ahrens, C.H., Pouzada, A.S. - On the effect of the cure process on the mechanical Properties of steel fibre reinforced epoxy composites, PPS-24 - Polymer Processing Society 24th Annual Meeting, Salerno: June 2008.

EFFICIENT DESIGN SOLUTIONS FOR HYBRID MOULDS AND THE WIDENING OF THE LIFECYCLE OF INJECTION MOULDS

P. G. Martinho[1], P. J. Bártolo[1] and A. S. Pouzada[2]

[1]Polytechnic Institute of Leiria, School of Technology and Management, 2401-951 Leiria, Portugal
[2] Institute for Polymers and Composites, University of Minho, Guimarães, Portugal

Abstract

The development and manufacture of the mould is one of the most time-consuming phases in the development of new plastic products. In the last two decades advances in manufacturing technologies made possible the utilisation of material alternative to steel in the moulding blocks. The associated design solutions gave rise to the concept of hybrid moulds that may contribute for speeding the time to market or to lowering product costs. The reutilization of the injection moulds is an issue currently used by the mouldmakers to be included in the mould lifecycle. One possible reutilization strategy implies the use of the existing mould structures or parts thereof. Hybrid moulds are a design solution that includes the moulding blocks as the mould components to be directly connected to the envisaged part. This study analyses some reutilisation possibilities in the design process of hybrid moulds. Design aspects in the study include some critical aspects, namely lateral movements, cooling and ejection systems. The study is part of a research programme with the goals of optimizing functional solutions for hybrid mould structures and ascertaining the reliability of moulding blocks obtained by RP techniques.

Introduction

Today, in the highly competitive marketplace with short life-cycles of products, developing a new product to meet the consumer needs in a shorter lead-time is crucial for a successful company. New products should not only satisfy consumers' physical requirements but also should satisfy their needs, increasing product complexity and reducing its lifetime. Companies must also meet increasing customer expectations in terms of both quality and cost of products. As a consequence of this new social environment, new rapid product development strategies must be adopted by modern companies, which lead to tremendous challenges to their internal flexibility. As a consequence, the current industrial trend is moving from mass production, *i.e.* high-volume and small-range of products for manufacturing, to small-volume and a wide range of products [1].

Nowadays, the search for alternative methodologies for the design and manufacturing of moulds for short runs of plastic components is a great industrial goal, being possible through the use of rapid tooling technologies and the use of new and different materials for the moulding inserts. The idea of building moulds with moulding inserts manufactured in alternative metallic materials or in synthetic materials is the basis of the hybrid mould concept, which can have a significant impact in the mouldmaking industry as it is:

- Efficient: reduces waste and energy consumption;

- Agile: enables adaptability for customisation;

- Flexible: enables the rapid modification and fabrication of design concepts;

- Value chain enhancement.

However, the concept of hybrid moulds poses several challenges that need to be addressed:

- There is a demand for new materials;

- Improvements are needed on strength, surface finish, accuracy, repeatability and reliability;

- Designers and manufacturing engineers need to change their ways of thinking, as they generally think conventionally in terms of injection moulding;

- Hybrid moulds must perform "first time right", which means that better computer simulation tools are required to ensure reliability.

Currently, hybrid moulds are used for short and medium run injection series. Therefore, some of the current design strategies include the redesigning of conventional injection moulds in order to increase their lifecycle, the reuse of existing mould structures and the employment of recycling materials to produce moulding blocks. To increase the lifetime of hybrid moulds and the accuracy of their mouldings, it is also important to design for wear minimisation.

In this paper a conceptual moulding model is envisaged to study the wear mechanisms associated to hybrid injection moulds. This conceptual moulding model has specific geometrical details such as short and long lateral movable elements and a core moulding block, allowing studying wear due to mechanical interaction between the movable elements and the moulding part. A flexible hybrid mould design considering reutilisation [2] is also proposed, enabling users not only changing the moulding block materials but also to produce different parts by changing the moulding blocks themselves.

PMI 2007

Efficient design solutions for hybrid moulds   Martinho, P.G. *et al.*.

An approach to mechanical design of reusable/usable elements in hybrid moulds

Wear mechanisms

Three distinct wear mechanisms have been identified [3]: abrasive, erosive, and adhesive wear.

Abrasive wear occurs when material is removed by contact with hard particles. The particles either may be present at the surface of a second material or may exist as loose particles between two surfaces.

Erosive wear is caused by particles that collide on a component surface or edge and remove material from that surface due to momentum effects. This type of wear is especially important in components with high velocity flows. According to Hayden [4], the hardness of the mould surface will affect the shape of the erosion mechanism. Erosion wear produces deep, narrow furrows and pits in hard materials, and wider and shallower erosion planes in soft materials. In injection moulds this type of wear mechanism is particularly evident in areas of high shearing such as gates [5].

Adhesive wear occurs when two solid surfaces slide over one another under pressure. Surface projections are plastically deformed and eventually weld together by the high local pressure. As sliding continues, these bonds are broken, producing pits on the surface, projections on the second surface, and frequently tiny, abrasive particles, all of which contribute to future wear of surfaces. Polymers having the same solubility parameters and cohesive energy parameters present important adhesive characteristics [6, 7].

Several strategies have been proposed to minimise the wear mechanisms for injection moulds. Engelmann [8] pointed out that the strategy for wear reduction involves polishing smooth surfaces to decrease the amount of mechanical interlock between the moulding part and the moulding surface and increasing the hardness of the mould surface.

An important aspect of the operation of hybrid moulds is the wear produced by shrinkage and friction during ejection. During the ejection phase, friction forces are generated between the part (plastic) and the core (typically steel). The coefficient of friction between plastic/steel depends on the surface texture of the core and the ejection temperature [9]. Generally, the ejection force is considered as the result of the interaction between part geometry, mould geometry and material, moulding material and processing conditions [10]. In conventional injection moulds where metals are used to build the whole mould, the origin of the friction force during ejection mainly results from the roughness of the surfaces and the shrinkage of the thermoplastic material [7, 11]. However in hybrid moulds with resin moulding blocks, the contact between polymer-polymer and the chemistry adhesion are relevant especially at high temperatures. Gonçalves *et al.* [7] showed that to minimise adhesive wear it is important to inject polymers with Hildebrand solubility parameters different to the resin. It was also observed a significant elastic deformation of the cores, when resins with low Young modulus were used to produce the moulding blocks. In these cases the effective ejection force is lower than expected. Similarly, Salmoria *et al.* [12] who studied the use of stereolithography resins to produce moulding blocks, also shown that it is not possible to inject polymers of both higher tensile modulus and strength than the resin, due to the generalised failure of the moulds when parts were pulled out from the core. These problems can be increased if the ejection system is incorrectly designed [13].

Several researchers have investigated the effect of processing parameters on the ejection force [11, 14-16]. These research studies demonstrated that the ejection force increases with the cooling time and roughness of the mould wall.

The position and shape of the cavity strongly influences the wear. Voet *et al.* [17] observed significant wear mechanisms in the neighbourhood of the gate but almost no wear at the inserts, concluding that wear is mainly caused by friction between the mould and solidified product material and not by the flow of the melt in the cavity.

Lifecycle of mould and the concept of reutilization

The lifecycle of an injection mould comprises [2] five distinct stages: design, manufacturing, service, recycling and decommissioning. Usually, when injection moulds end their production life, they are kept warehoused and destroyed. The reutilisation of these moulds represents an important strategy to be followed by producers of plastic parts that is usually neglected. Some alternatives to enhance their reutilisation include: redesigning moulds in order to increase their lifecycle, reuse of existing mould structures and the employment of recycling materials to reproduce moulding blocks.

The injection parameters (moulding temperature, pressure, speed, etc.) play a relevant role in the mould life. The more severe the parameters the more damage they are expected to cause in the cavity inserts reducing their life. The adjustment of the injection moulding parameters is particularly important for hybrid moulds [18]. In this case, product shape, mould structure and mechanical design should be carefully considered to ensure that it is feasible to keep the wear within

PMI 2007

Efficient design solutions for hybrid moulds   Martinho, P.G. *et al.*.

acceptable values during the mould life [17, 19]. Additionally, hybrid tools must guarantee an injection moulding cycle time as short as possible.

To add flexibility to the hybrid mould, some special design requirements should be considered [16 (erro devia ter colocado 18)]:

- The possibility to fit as many part sizes as possible;

- Freedom in positioning the ejector pins according to the part geometry;

- An easy way to exchange the moulding blocks without the need to remove the entire mould from the injection machine.

Additionally, the concept of hybrid moulds open new design opportunities such as:

- The possibility of having conformal cooling channels, *i.e.* channels that follow the geometric shape of the part;

- Different ways to adapt injection systems, which enable to position the injection point according to the requirements without needing to redesign the plates that accommodate the respective inserts (core and cavity).

The conceptual model

The conceptual moulding model used in this research to evaluate the wear mechanism is shown in Figure 1. This model consists of a moulding part, a core moulding block and two movable elements at the side walls.
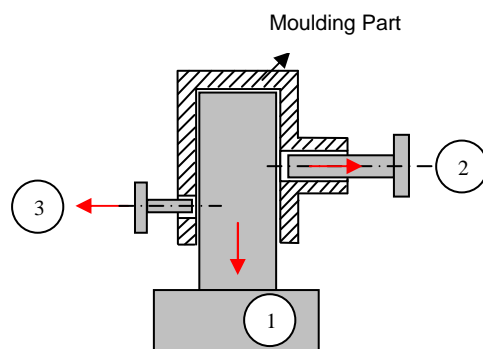
1 – Deep core movement

2 – Long side movement

3 – Short side movement

Fig. 1.   Conceptual model

This concept allows the study of:

- The main core (1) – it is associated to the main ejection movement and is responsible for moulding the inside shape of the part;

- The long lateral core (2) – responsible for the creation of the fitting detail on the right side of the part;

- The short lateral core (3) – responsible for the creation of the lateral opening on the left side of the part.

This model was defined to study the effect of lateral movements of different amplitudes (short and long) in hybrid moulds and the wear behaviour in tools manufactured in alternative materials (main core). Upon considering alternative materials for the core moulding block, and metallic materials (aluminium) for the moving lateral elements, the conceptual moulding model allows the study of tool wear as follows:

- Due to mechanical interactions between the moulded part and the lateral short and long side elements (2 and 3), the most relevant wear mechanism occurring in these moulding zones will be abrasive wear. Important factors that will influence this wear include: the hardness of used materials and the frictional forces involved. The frictional forces are also related with the temperature at which the part is removed from the hybrid mould and the roughness of the lateral movable elements (e.g. [9, 14, 16]);

- Adhesion wear will be the most relevant mechanism verified in the deep core moulding zone when non-metallic materials are used. The main factors contributing to this type of wear are the polymer-polymer contact time and temperature in the moulding zone [6, 7].

The testing part

The part considered to study and validate the conceptual model is illustrated in Figure 2.
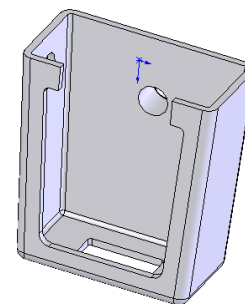
Fig. 2.   Testing part

The part (Figure 3) has a lateral circular opening on the left side, a fitting detail on the back and a main cavity (to be defined by a core moulding block). The draft angle considered for the side walls is 3º and the corners are rounded to allow manufacturing the whole insert also by machining.
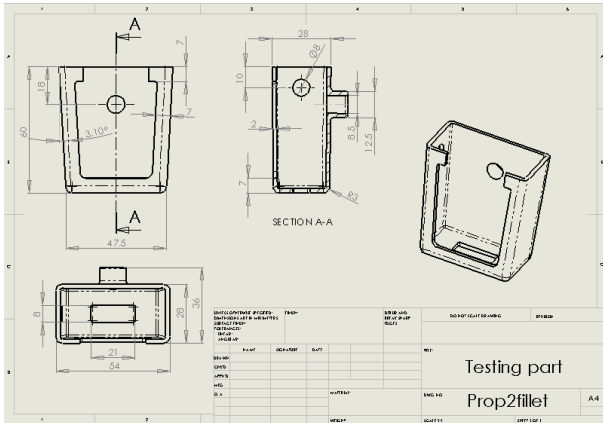
PMI 2007

Efficient design solutions for hybrid moulds
Martinho, P.G. *et al.*.

Fig. 3. Testing part dimensions

The design of the Hybrid Mould

A concept for flexibility

The mould to produce the testing part (Figure 4) was designed considering reutilisation and the maximum flexibility in operation. In particular it was considered the interchangeability of the moulding blocks (core and cavity) in the injection machine.
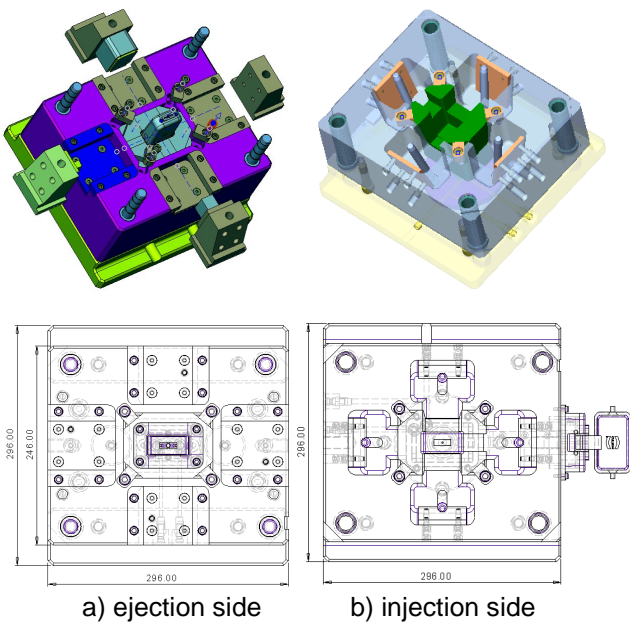

a) ejection side   b) injection side

Fig. 4. Standard Hybrid mould design a) ejection side b) injection side

Moulding blocks

The moulding blocks shown in Figure 5, are assembled in the mould structure when the mould is fully open. This option allows exchanging mould inserts from the mould structure without removing it from the injection moulding machine. The outside walls of the moulding blocks were designed with 10⁰ draft angles, to facilitate their removal and replacement.
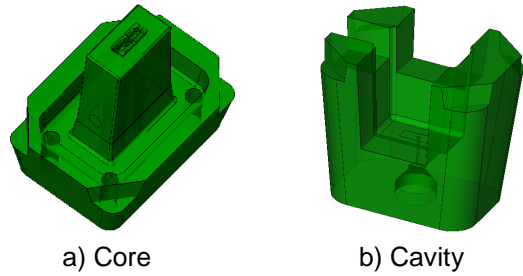
a) Core   b) Cavity

Fig. 5. Moulding blocks a) core b) cavity

Side cores

The cavity and core plates support the cavity and core blocks and allow the adjustment of lateral movements. The structure of the mould enables a maximum of four lateral movements to define details on a generic part (for the testing part it is only necessary three lateral movements). Each lateral slide group allows fitting a specific frontal element as shown in Figure 6.
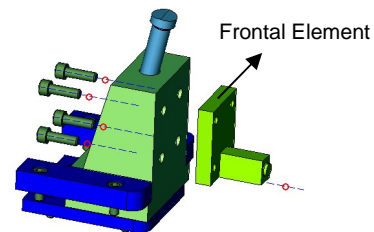
Fig. 6. HM lateral component

Cooling system

The cooling system consists of a cooling cassette in the ejection side of the hybrid mould (Figure 7a)) and of conformal cooling channels in the injection side (Figure 7b)). Other configurations for cooling channels geometry are also possible. The inlet and the outlet of the cooling fluid were designed in the core plate and in the injection fixing plate. The cooling channels must be connected to the main cooling circuit as shown in Figure 7. It is important to note that with this design solution, there is flexibility for establishing different cooling channel layouts.

a) Cooling cassette   b) Conformal cooling
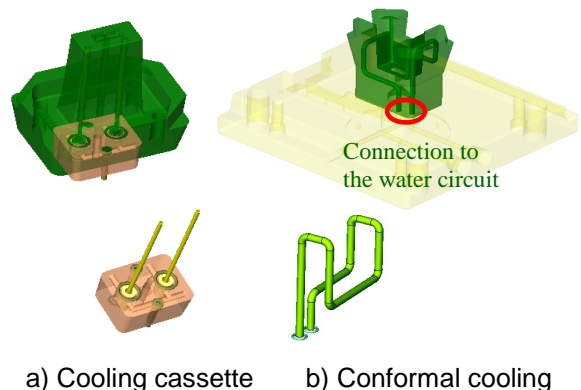
Fig. 7. Cooling system a) in the core; and b) in the cavity

PMI 2007

Efficient design solutions for hybrid moulds   Martinho, P.G. *et al.*.

The ejection system consists of an ejector plate fitted in the core moulding block and in a central extractor pin to remove the feeding system (Figure 8).
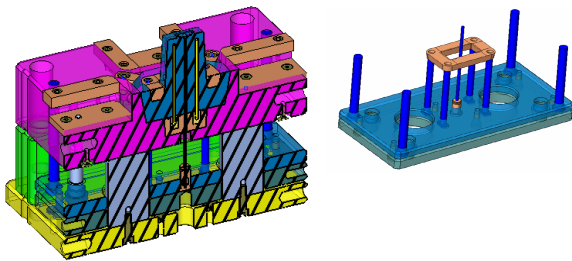
Fig. 8.   Ejection system

Conclusions

A conceptual model for the analysis of wear mechanisms in hybrid moulds is proposed. The main features of this model include the integration of lateral moving elements and deep core movements, in order to evaluate hybrid moulding zones, which are subjected to distinct wear mechanisms. The design of a testing part, corresponding to a real implementation of the proposed conceptual model, is also presented. Finally, a flexible design strategy for hybrid moulds is pointed out. This design strategy allows reutilisation, by keeping the structure of the mould and changing the moulding blocks.

Acknowledgements

Bibliography

[1] Martinho, P.; Bártolo, P. J.; Queirós, M. P.; Pontes, A.; Pouzada, A. - Hybrid Moulds: the Use of Combined Techniques for the Rapid Manufacturing of Injection Moulds. Virtual Modelling and Rapid Manufacturing. Edited by P.J. Bártolo *et al*, pp. 421-427, Taylor&Francis, London, 2005.

[2] Hernández, P.; Ares, E.; Pouzada, A. S. - New Trends on the Design and Manufacture of Injection Moulds – Reusability and Recycling, PMI 2005 – Int. Conf. on Polymers & Moulds Innovations. Gent: April, 2005.

[3] Engelmann, P.; Hayden, K.; Guichelaar, P.; Dealey, R.; Monfore, M. - Understanding wear mechanisms: the key to mold life, Proceedings ANTEC 2000 Conference, 46, pp. 952-956, Brookfield, 2000.

[4] Hayden, K.; Engelmann, P.; Dealey, R.; Monfore, M. - Mold Wear vs Wall Thickness - Critical Information for Thin Wall Molding. Proceedings ANTEC 1999 Conference, 45, pp. 1063-1067, Brookfield, 1999.

[5] Lima, P.; Ramos, J.; Pouzada, A.S. - Thermal performance of hybrid injection molds with epoxy inserts. Proceedings ANTEC 2003 Conference, Nashville: May 2003.

[6] Petrie, E.M. Handbook of adhesives and sealants. McGraw-Hill, New York, 2000.

[7] Gonçalves, M.W.; Salmoria, G.V.; Pouzada, A.S. - Study of tribological properties of moulds obtained by stereolithography, Virtual and Physical Prototyping, in print (2007).

[8] Engelmann, P.; Hayden, K.; Guichelaar, P.; Monfore, M. - Undercutting mold performance: Ejection wear. Proceedings ANTEC 2002 Conference, 48, pp. 850-854, Brookfield, 2002.

[9] Pouzada, A.S.; Ferreira, E.C.; Pontes, A.J. – Friction Properties on Moulding Thermoplastics. Polymer Testing, vol. 25 (2006). pp. 1017–1023.

[10] Pontes, A.J.; Ferreira, E.C.; Pouzada A.S. - Tribological aspects during ejection in injection moulds, RPD 2004 – Agile Development for Productivity, Marinha Grande, 10 – 15 October 2004.

[11] Pontes, A.J.; Pouzada, A.S. - Ejection force in tubular injection moldings. Part I: Effect of processing conditions. Polym. Eng. Sci., Vol. 44 (2004), pp. 891-898.

[12] Salmoria, G.V.; Ahrens, C.H.; Fredel, M.; Soldi, V.; Pires, A.T.N. - Stereolithography Somos 7110 resin: Mechanical behaviour and fractography of parts post-cured by different methods. Polymer Testing, 24(2), pp. 157-162, 2005.

[13] Araújo, B.J.; Pouzada, A. S. - Projecto de sistemas de extracção em moldes de injecção, O Molde, 54, pp.36-38, 2002.

[14] Burke, C.; Malloy, R. - An experimental study of the ejection forces encountered during injection molding. Proceedings ANTEC Conference. Montreal, pp. 1781-1787, 1991.

[15] Balsamo, R.; Hayward, D.; Malloy, R. - An experimental evaluation of ejection forces: frictional effects. Proceedings ANTEC Conference. New Orleans, 1993.

[16] Sasaki, T.; Koga, N.; Shirai, K.; Kobayashi, Y.; Toyoshima, A. - An experimental study on ejection force of injection molding, Journal of Precision Engineering, 24(3), pp.270-273, 2000.

[17] Voet A.; Mingneau J.; Dehaes J.; Kruth J.P.; Van Vaerenbergh J. - Study of the Wear Behaviour of Conventional and Rapid Tooling Mould Materials. International Conference Polymers & Moulds Innovations PMI, Gent, Belgium, April 20-23, 2005.

[18] Volpato, N.; Foggiatto, J.A.; Amorim, J.R.; Filho, O.D. - A proposed data base to aid material selection for prototype tooling, RPD 2006, Marinha Grande – Portugal, November 2006.

[19] Gonçalves, M. W.; Pouzada, A.S.; Salmoria, G.V.; Ahrens, C.H. – Performance and friction properties of injection hybrid moulds with stereolitography moulding zones. MATERIAIS 2005 - 3rd Int Materials Symp - 12º Enc. Soc. Port. Mat. Aveiro: April, 2005.

Presentation Abstract

Presentation Topic: The use of Moldex3D to predict flow and thermal performance on injection moulding with hybrid moulds

Abstract

Moulds with moulding inserts manufactured in alternative metallic materials or in synthetic materials are the basis of the hybrid mould concept. Nowadays, this kind of moulds is an increasingly considered alternative for plastic prototype series or short production runs obtained by injection moulding. The combination of various materials in moulding zones determines different temperature running levels. Materials of low conductivity as epoxy composites or stereolithography resins mean different regime mould temperatures. These facts imply the need of simulating the moulding cycle for moulding repeatability and block reliability. The processing conditions need to be adjusted to cope with the poorer mechanical properties of these materials. For the injection pressures involved, a sizeable deformation on the resin moulding zones (blocks, pins, inserts…) can occur and also need to be estimated, e.g., by structural analysis.

The information to be presented in the European Users Meeting 2008 reports on the comparisons between the thermal and flow experimental results and the predicted ones by the Moldex3D® in a hybrid mould with moulding inserts obtained by various RPT techniques. A specific part with geometrical details, designed for the studies, was produced in polypropylene homopolymer. A flexible hybrid mould was used to produce the injection parts. The mould was instrumented with integrated pressure and temperature sensors (Kistler Type 6190BA) located close to the gate and to the weld line. The simulation of the mould temperature yields results quite close to the measured values, taking into account the actual structure of the mould. The processing conditions were set according to the materials used. A good correlation is achievable between the experimental results and the predicted ones when using Moldex3D®.

The use of Moldex3D to predict flow, thermal and shrinkage on injection moulding with hybrid moulds

Universidade do Minho

IPL
escola superior
de tecnologia e gestão
instituto politécnico
de leiria
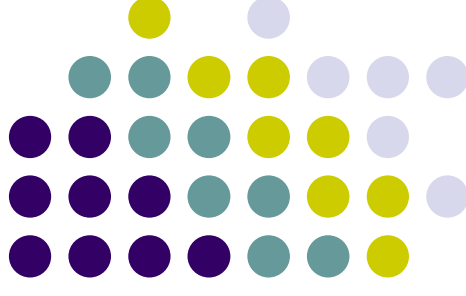
António Pouzada

Moldex3D®

- **University of Minho**

- Started in 1974
- Located in Braga and Guimarães
- 17 500 students (including post-graduates)

Universidade do Minho

Moldexs3D®

BRAGA
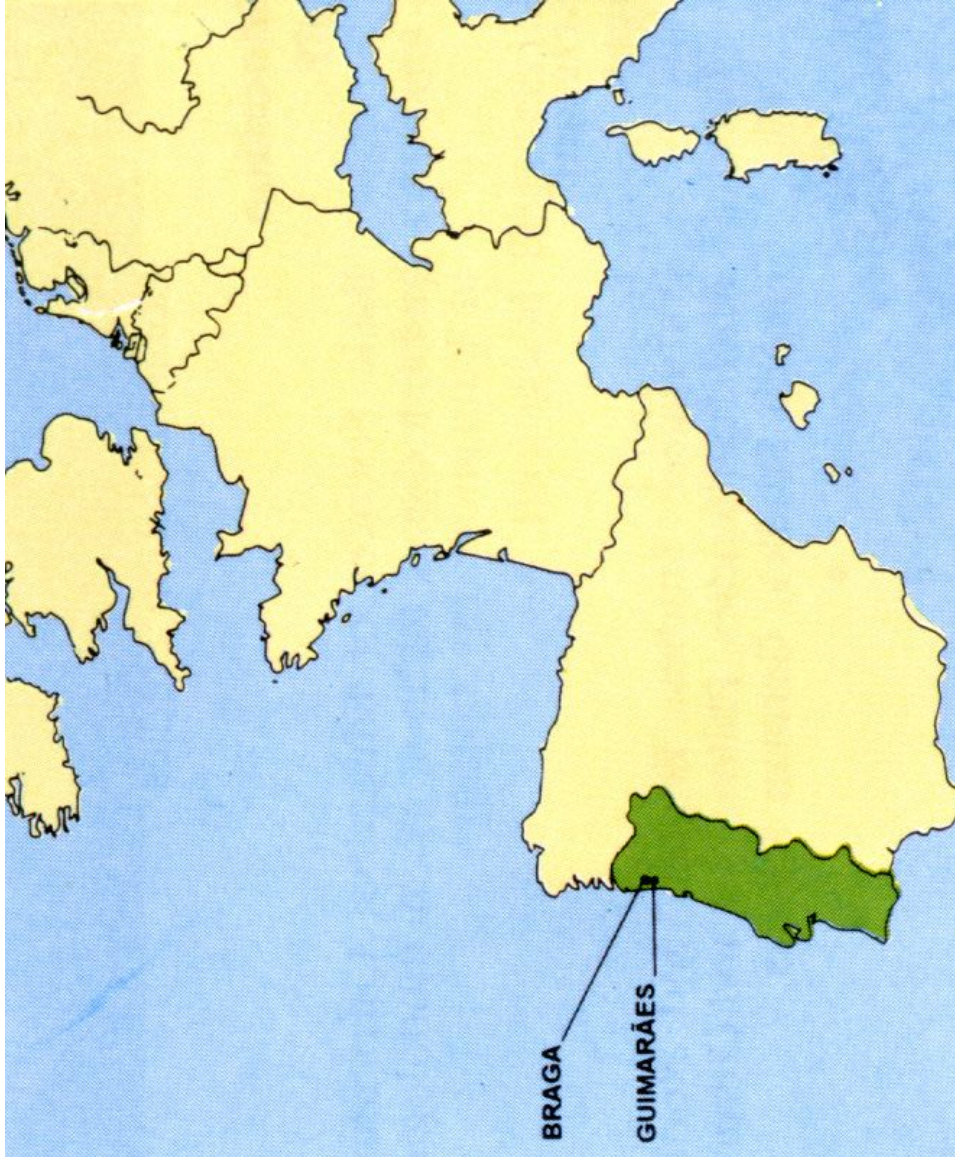
GUIMARÃES

Location of the industry
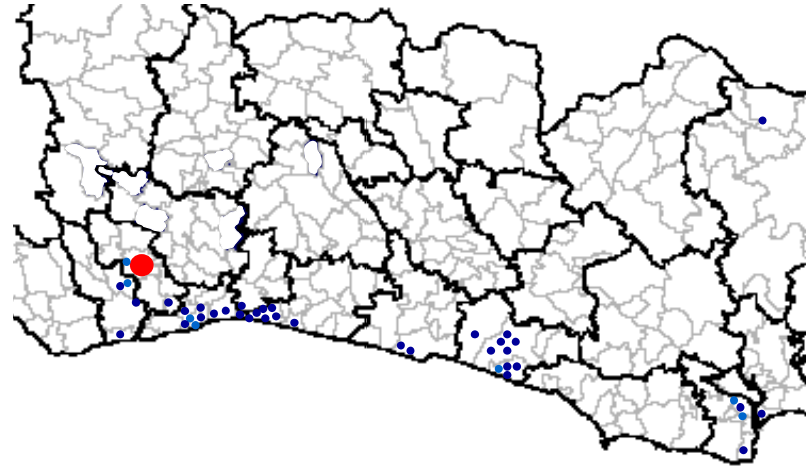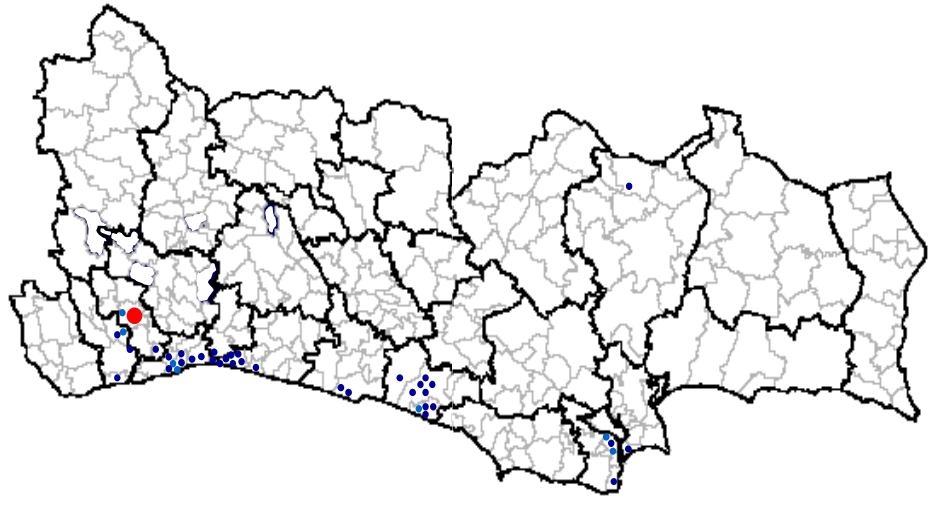
Moldex3D®

University of Minho

Campus of Azurém (Guimarães)

Moldex3D

5

Departmf Polymer Engineering

Moldex3D®

friction in ejection

- $F_{ejection} =$ *function of*

  - $p_{shrinkage}$,
  - Coefficient of friction,
  - Temperature,
  - Roughness,
  - Materials,
  - ...

Gate

Shrinkage

Ejection force

Moldex3D®
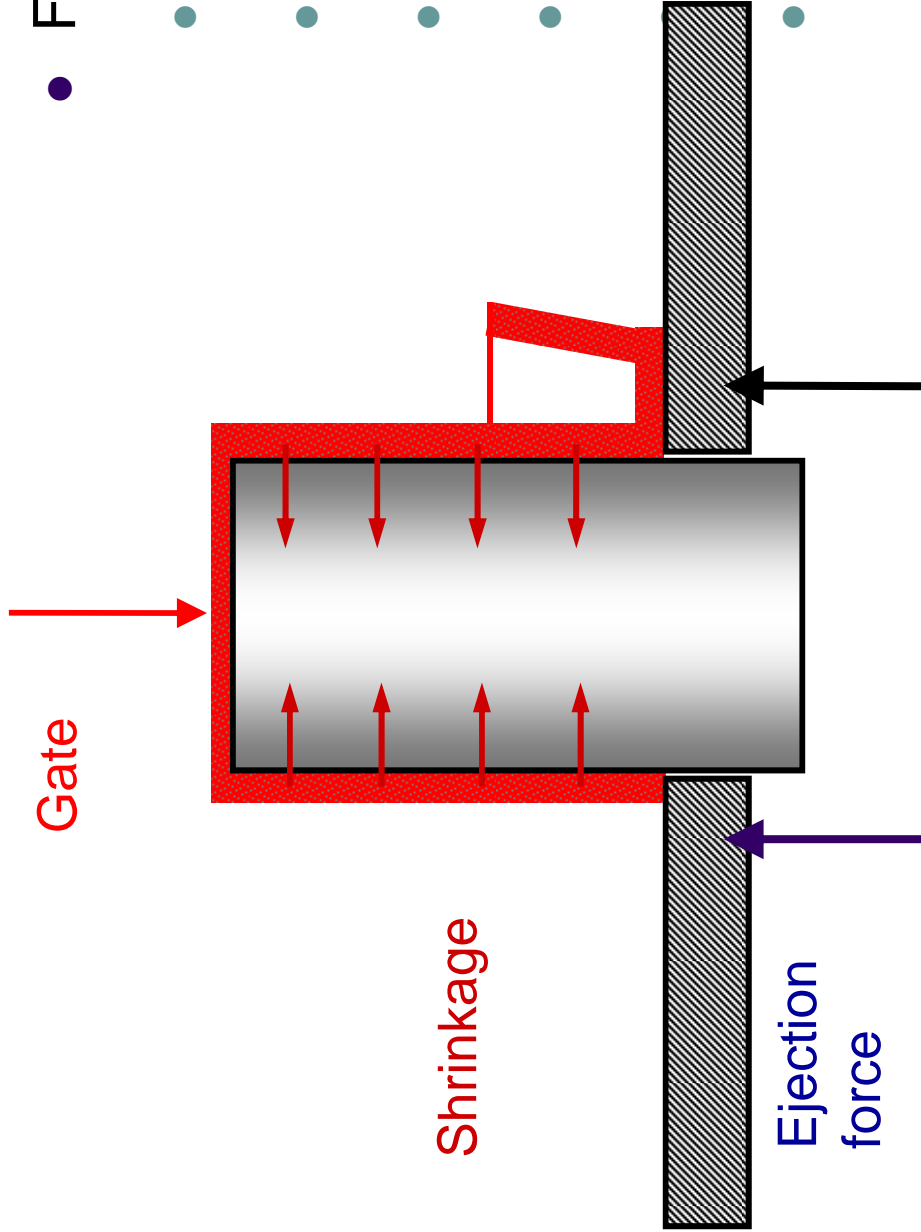
test moulding

- Moulding filled with uniaxial flow

- Hot runner mould instrumented for
  - Force
  - Temperature
  - Pressure

- Mouldable in a 600 kN injection moulding machine
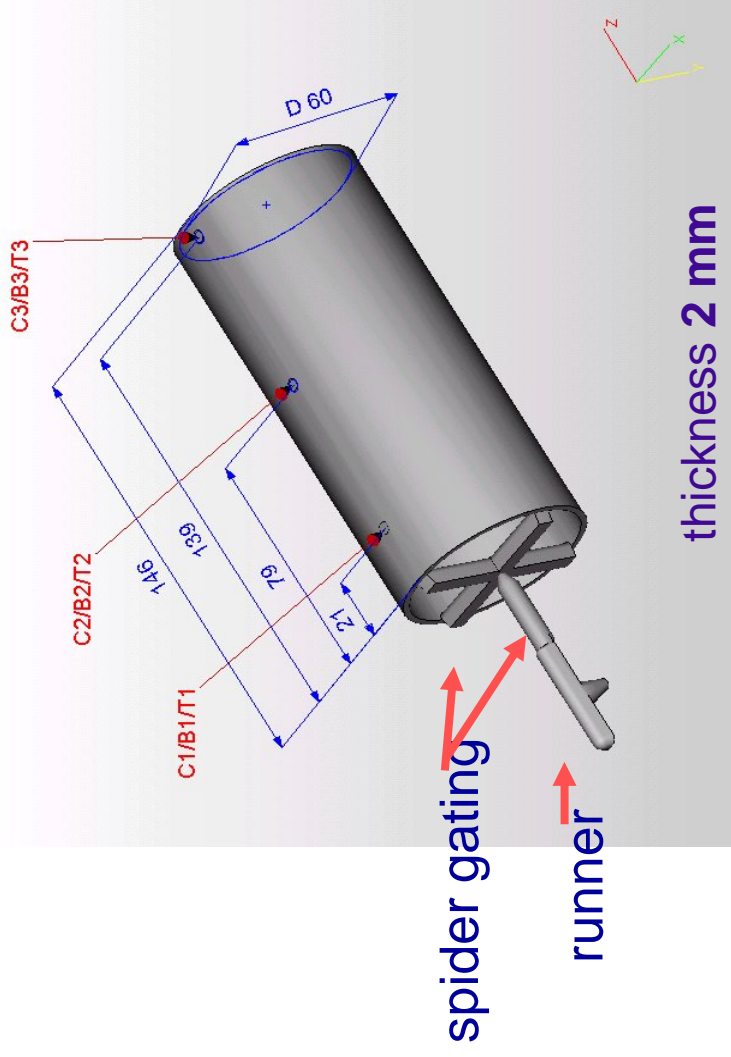
Pontes, A. J. Brito, A. M., Pouzada, A. S. J. Injection Molding Technology, Vol. 6: nº 4 (2002).

Friction testing

Heated / cooled block

Guide bearing

Steel molding surface

Pneumatic cylinder

Plastic specimen
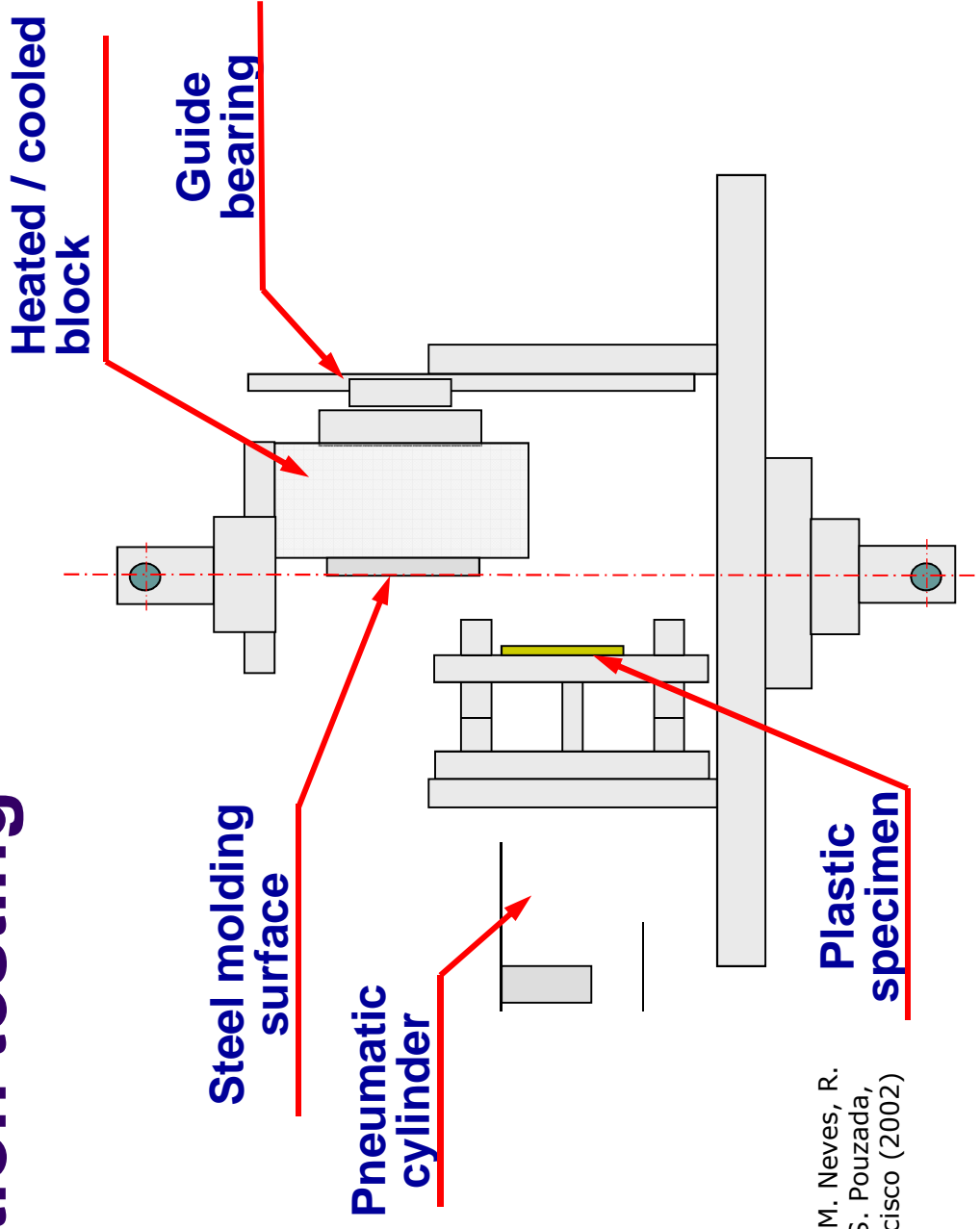
E. C. Ferreira, N. M. Neves, R. Muschalle and A.S. Pouzada, Antec'02, S. Francisco (2002)
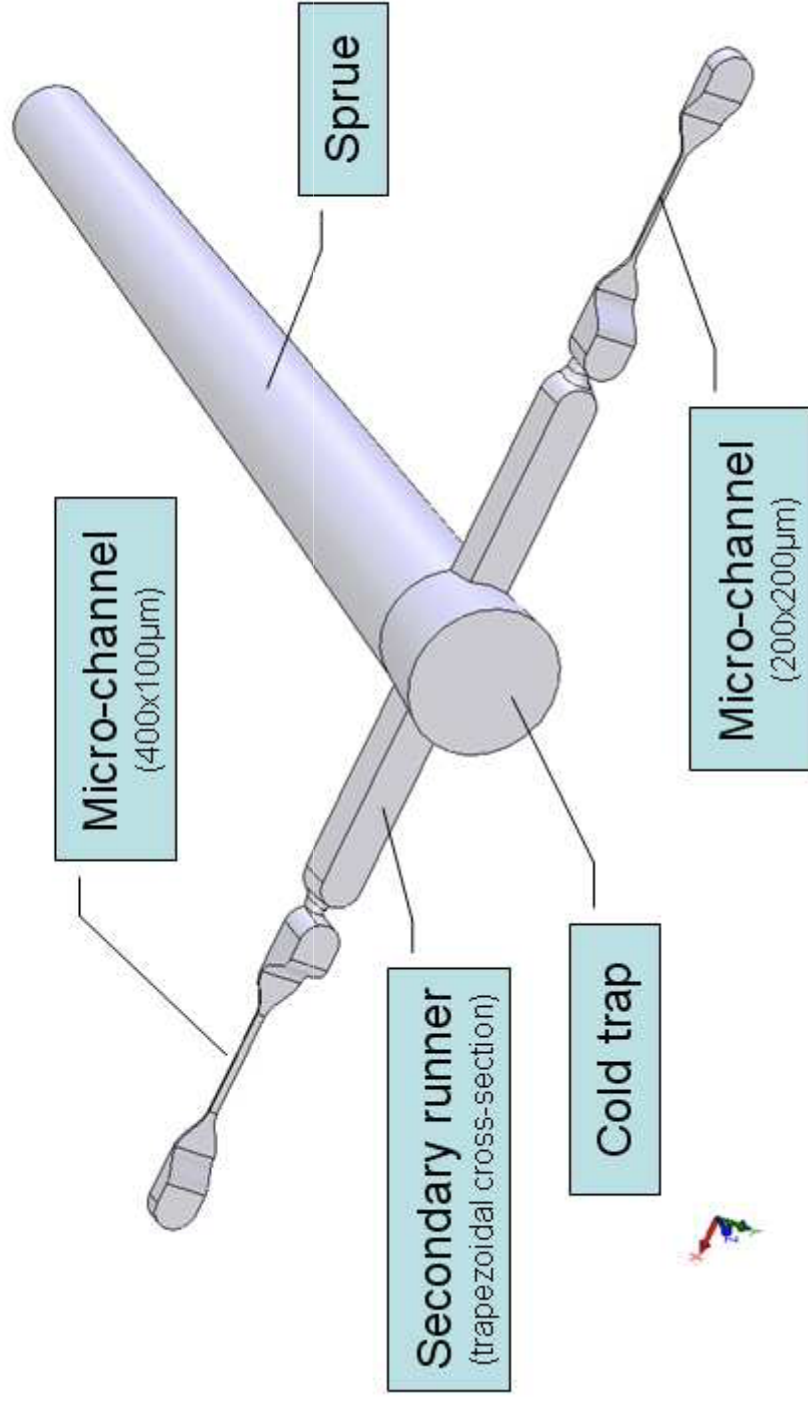
Moldex3D®

Micro-innjection moulding

Sprue

Micro-channel
(400x100µm)

Micro-channel
(200x200µm)

Secondary runner
(trapezoidal cross-section)

Cold trap

This work was developed with the support of **CoreTech** and the technical advise of **Simulflow** on the use of *Moldex 3D*.

Pedro Gonçalves Martinho[1]

Teresa Neves[2]

Paulo Jorge Bártolo[3]

António Sérgio Pouzada[4]

[1] Polytechnic Institute of Leiria, Leiria, Portugal
[2] Simulflow, Leiria, Portugal
[3] CDRSP, Polytechnic Institute of Leiria, Leiria, Portugal
[4] Institute for Polymers and Composites, University of Minho, Guimarães, Portugal

Moldex3D®

Outline

- Introduction
- Objective of the work
- Experimental
  - Test part
  - Mould and Instrumentation
  - Moulding
- Moldex 3D simulation
 - Pressure
  - Temperature
  - Shrinkage
- Conclusion

Moldex3D®

Introduction

HHybrid mould : a mould with moulding blocks fabricated in alternative metallic or synthetic materials.

There is a combination of old and new manufacturing techniques
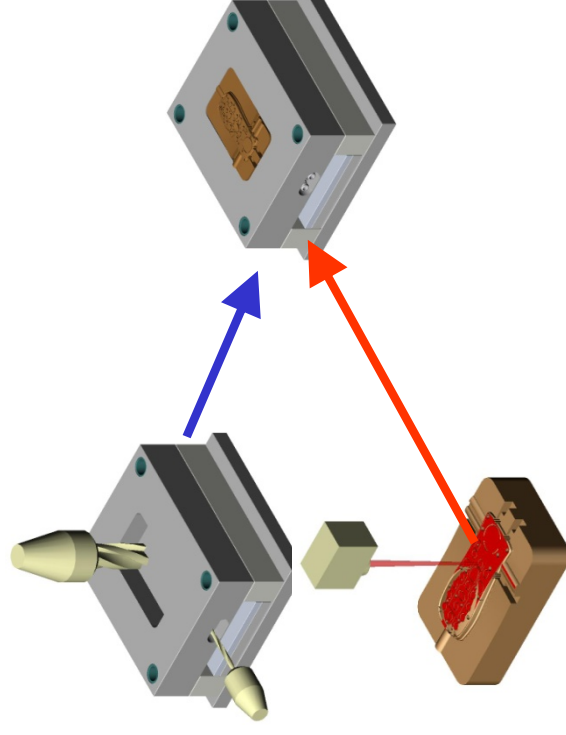
Conventional techniques for standard mould plates

Rapid prototyping techniques for moulding blocks

Universidade do Minho

IPL

Moldex3D®

Introduction

- Hybrid mould main **advantages**

  - Efficiency: waste and energy consumption reduced

  - Agility: enables adaptability for customization

  - Flexibility: rapid modification and fabrication of design concepts possible

    - Leading to chain value enhancement

Moldex3D®

Introduction

- Hybrid mould main **challenges**...

  - Search for new materials

    - Improvements are needed on strength, surface finish, and reliability

  - Exploitation of RPT possibilities

    - Limits of accuracy, repeatability, detailing

  - New design methodologies

    - Designers and manufacturing engineers need to change their ways of thinking

  - Hybrid moulds must perform "first time right"

Universidade do Minho

IPL

Moldex3D®

Universidade do Minho

IPL

- Introduction
- **Objective of the work**
- Experimental
  - Test part
  - Mould and Instrumentation
  - Moulding
- Moldex 3D simulation
  - Pressure
  - Temperature
  - Shrinkage
- Conclusions

Moldex3D®

Objective

- Predict the performance of hybrid moulds
  - Can we predict the mould temperature and pressure?
- Optimize the set up of injection moulding
  - Which are the more adequate processing conditions?
- Establish the pre-run moulding phase
  - How many cycles are required before the mould runs on cruise conditions?
- Assess shrinkage issues

Moldex3D®

- Introduction
- Objective of the work
- **Experimental**
  - **Test part**
  - **Mould and Instrumentation**
  - **Moulding**
- Moldex 3D simulation
  - Pressure
  - Temperature
  - Shrinkage
- Conclusions

**European Users' Meeting ,Chester, UK
September 24-25, 2008**

Moldex3D®

Experimental – test part

Main features

- Non-circular cross section
- lateral circular opening on the left side.
- fitting detail on the back.
- draft angle of 3⁰.
- Round corners throughout.
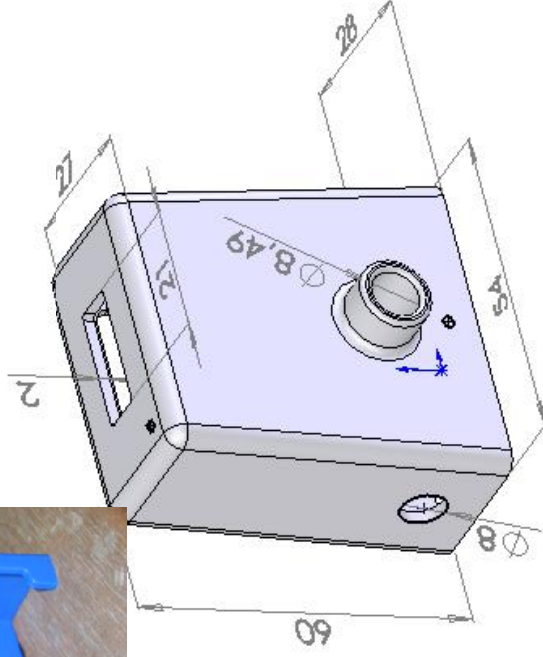
Moldex3D®

Experimental – Mould and Instrumentation

Moulding blocks are easily interchangeable with the mould in the injection machine.

Injection side

-Cavity Moulding block
-Injection system
-Cooling system

Ejection side

-Core Moulding block
-Ejection system
-Cooling system
-Movable elements

Moldex3D

Experimental - Mould and Instrumentation

Two Kistler pressure and temperature integrated sensors

1 - Close to the gate location

2 - At the weld line location (end of fill

Moldex3D®
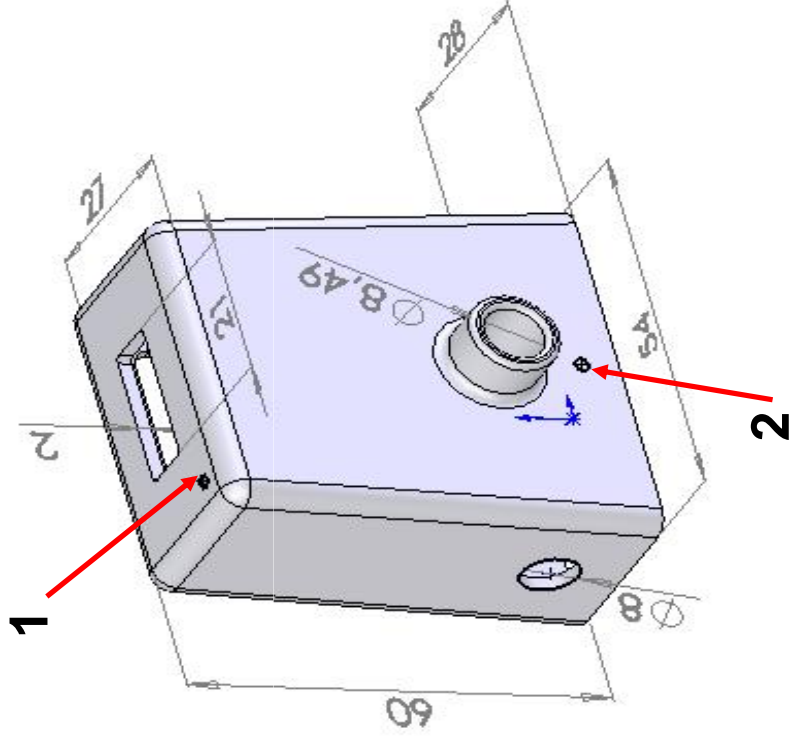
Experimental - Moulding

- Use of 3 materials in the moulding blocks

  - Epoxy/aluminium composite
  - STL resin
  - Tool steel

- Mouldings in PP

- Adjustment of processing conditions to the moulding block materials

  - Injection and holding pressure
  - Cooling time
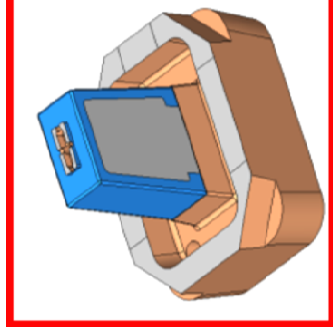
Moldex3D®

Experimental – Moulding blocks

Conventional tooling

Tool Steel 1.2311

RPT Stereolithografy

DSM Somos 11122

RPT Vacuum Casting

BiresinL74+60% Al

Core side

Cavity side

The cavity was always in tool steel

Experimental – Core materials

Moulding pin material Properties	Units	Tool steel (DIN W Nr. 1.2311)	Epoxy/Alum (Biresin L74 +60% Alum)	SL resin (DSM Somos 11120/2)	Epoxy/SSF (Biresin L74 +15% SSF)	ProMetal S4
Specific gravity	$[Mg.m^{-3}]$	7.80	1.65	1.12	2.10	7.50
Specific heat	$[J.kg^{-1} K^{-1}]$	460	1279.19	286.26	–	418
Thermal conductivity	$[W.m^{-1}.K^{-1}]$	29	0.606	0.166	0.392	22.6
Thermal diffusivity	$[m^2.s^{-1}]$	–	0.286×10^{-6}	0.519×10^{-6}	–	7.2×10^{-6}
Thermal expansion coefficient	$[K^{-1}]$	1.20×10^{-5}	6.00×10^{-5}	9.50×10^{-5}	–	–
Flexural Modulus @20°C	$[GPa]$	200	5-6	2-2.4	4.3-4.9	147

Moldex3D

Experimental – injection moulding

- Polypropylene homopolymer, PP Homo Domolen 1100N,

- Ferromatik Milacron K85 injection moulding machine of 850 kN clamping force.

- The processing conditions were set according to the material used

Parameter	SS	R$_1$S and R$_3$S	R$_2$S
Core/Cavity materials	Steel/Steel	EPres/Steel	SLres/Steel
Injection temp [ºC]	230	230	230
Cooling temp [ºC]	40	40	40
Injection flow rate [cm^3.s^{-1}]	37.7	37.7	37.7
Injection time [s]	1.3	1.3	3
Injection pressure [MPa]	91	70	42
Holding time [s]	5	10	10
Opening, closing and ejection time [s]	12	12	12
Holding pressure [MPa]	70	56	14
Cooling time [s]	25	35	45

Moldex3D®

The use of Moldex3D to predict flow, thermal and shrinkage on injection moulding with hybrid moulds

Teresa Neves

Universidade do Minho

IPL
escola superior
de tecnologia e gestão
instituto politécnico
de leiria

**European Users' Meeting ,Chester, UK
September 24-25, 2008**

Moldex3D®

- Introduction
- Objective of the work
- Experimental
  - Test part
  - Mould and Instrumentation
  - Moulding
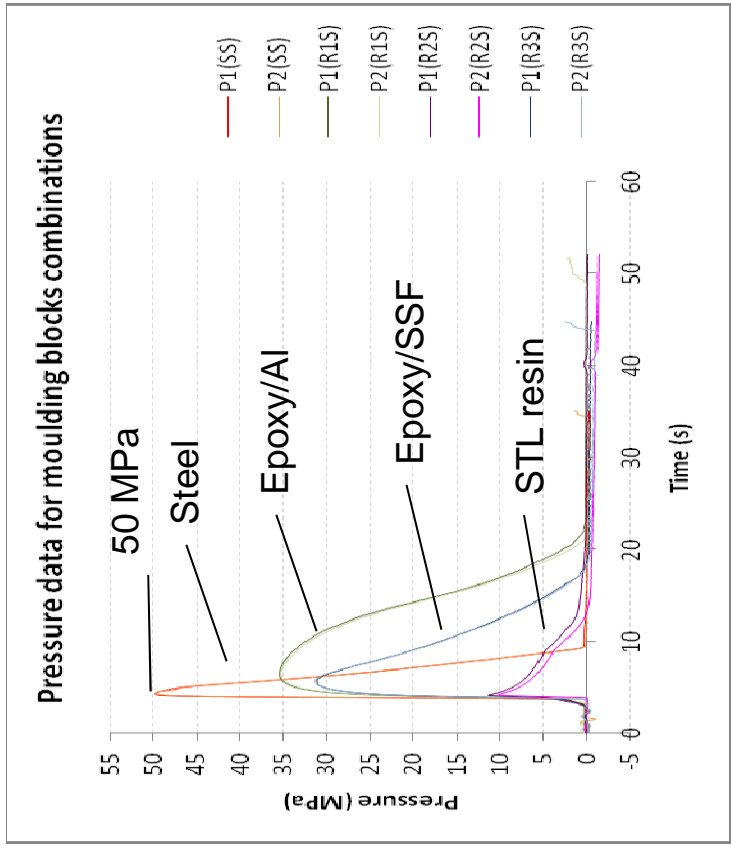- **Moldex 3D simulation**
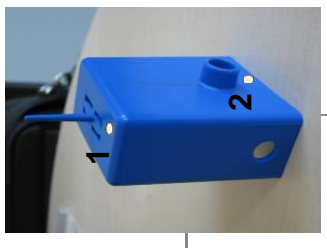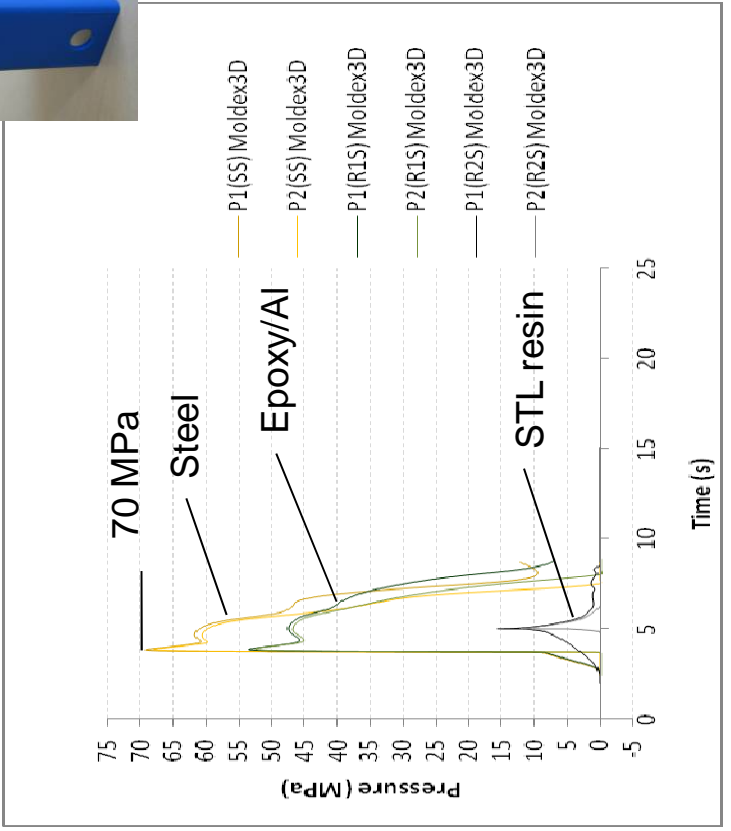 - Pressure
  - Temperature
  - Shrinkage
- Conclusions

**European Users' Meeting ,Chester, UK
September 24-25, 2008**

Moldex3D®

Moldex 3D simulation
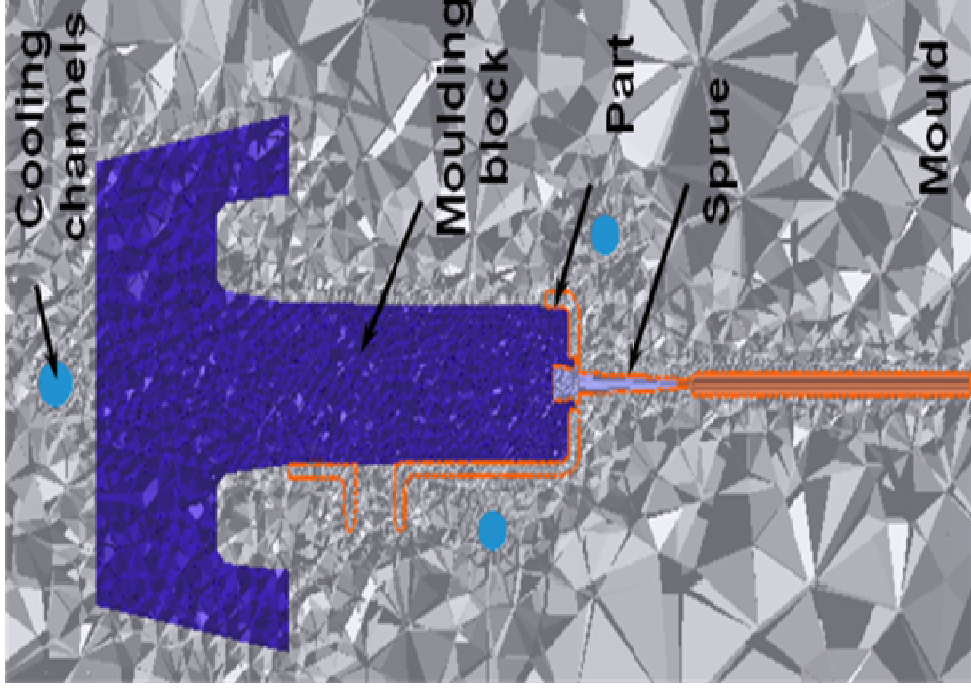
- Total number of elements – 1 144 902 tetrahedrical elements.

- 77 792 elements were used in the part.

Cooling channels

Moulding block

Part

Sprue

Mould

Moldex3D®

Moldex 3D simulation
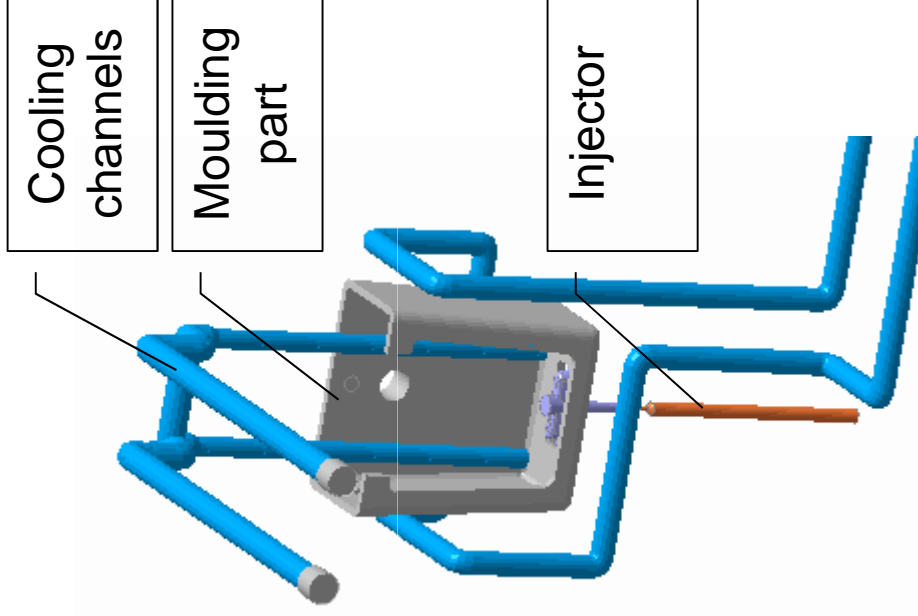
- Model and cooling architecture considered in the Moldex3D® 9.0 simulation.

Cooling channels

Moulding part

Injector

Universidade do Minho

IPL

Moldex3D®

- Introduction
- Objective of the work
- Experimental
  - Test part
  - Mould and Instrumentation
  - Moulding
- **Moldex 3D simulation**
  - **Pressure**
  - **Temperature**
  - Shrinkage
- Conclusions

Universidade do Minho

IPL

Moldex3D®

Moldex 3D simulation – pressure results

The **pressure** was simulated as a value somewhat higher than the measured.

Experimental

Pressure data for moulding blocks combinations

50 MPa · Steel · Epoxy/Al · Epoxy/SSF · STL resin

P1(SS) · P2(SS) · P1(R1S) · P2(R1S) · P1(R2S) · P2(R2S) · P1(R3S) · P2(R3S)

Simulation

70 MPa · Steel · Epoxy/Al · STL resin

P1(SS)Moldex3D · P2(SS)Moldex3D · P1(R1S)Moldex3D · P2(R1S)Moldex3D · P1(R2S)Moldex3D · P2(R2S)Moldex3D

Moldex 3D simulation – temperature results

The profiles of **temperature** at the mould/part interface show a good correlation between experimental and predicted values.

Hybrid mould (resin core)

- T1(R1S) Experimental
- T2(R1S) Experimental
- T1(R1S) Moldex3D
- T2 (R1S) Moldex 3D

Conventional mould

- T1(SS) Experimental
- T2(SS) Experimental
- T1(SS) Moldex3D
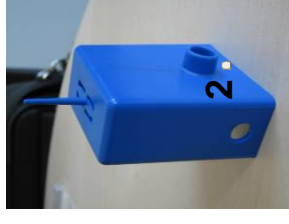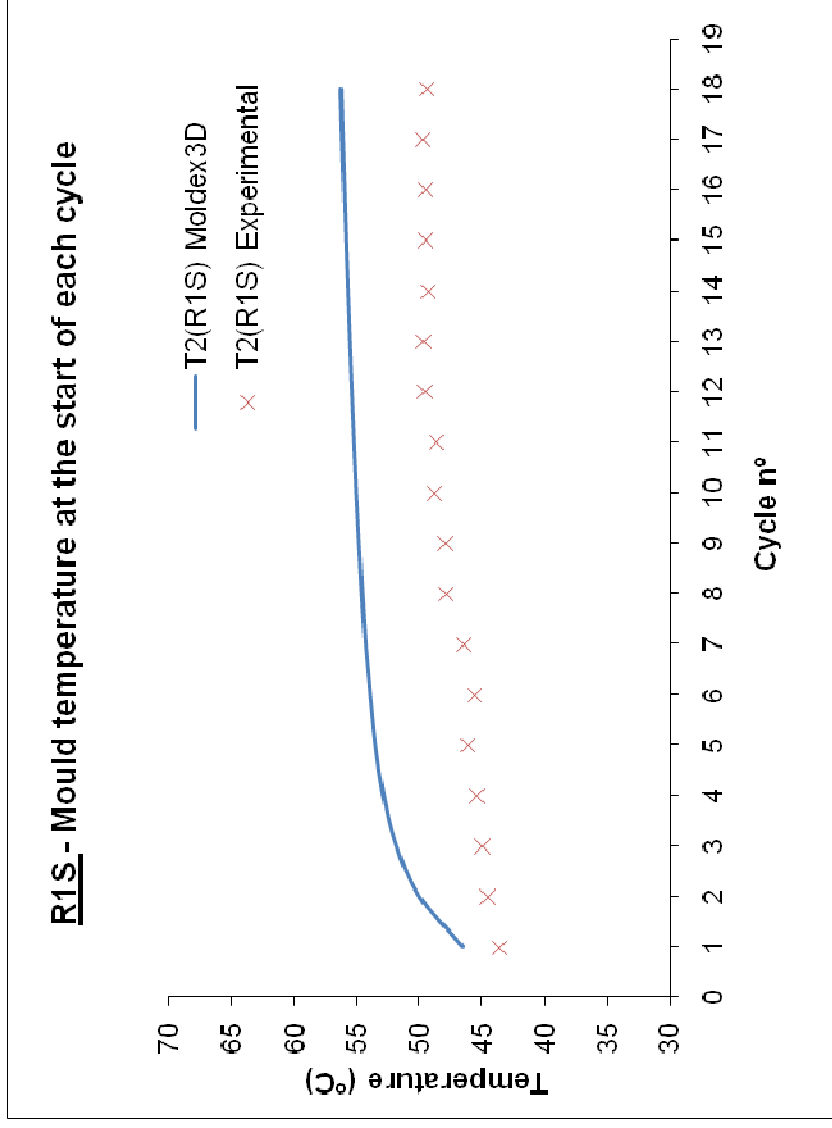- T2(SS) Moldex3D
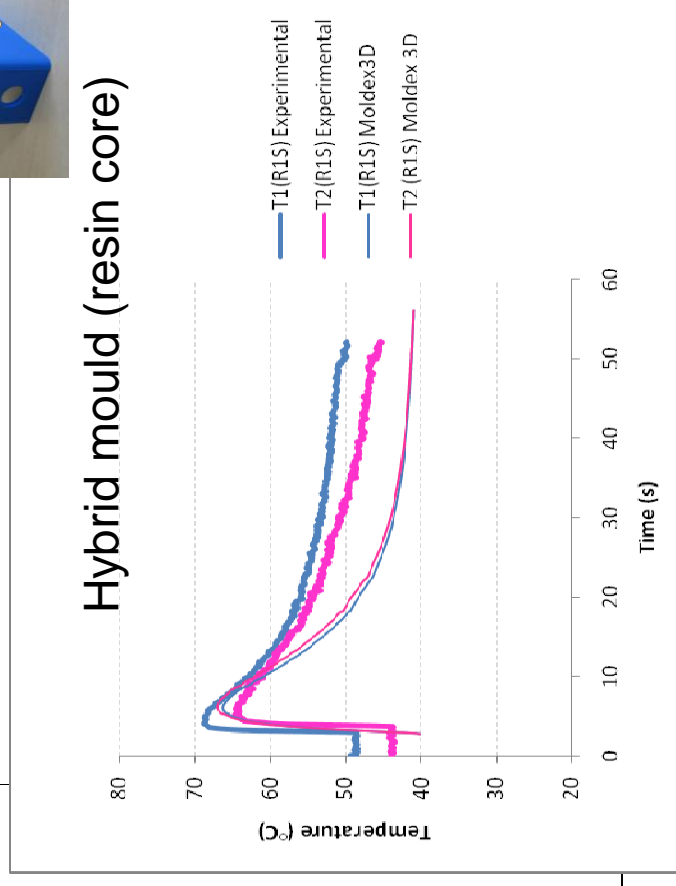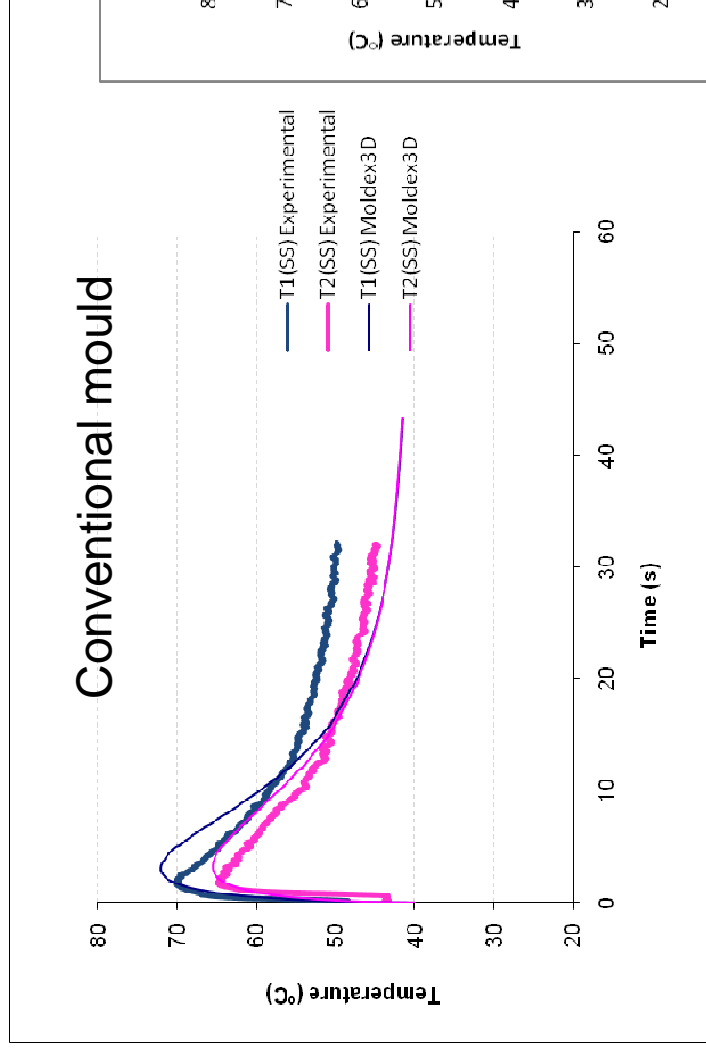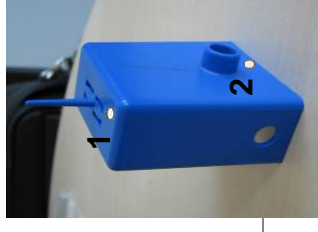
Moldex3D®

Moldex 3D simulation – stabilization results

- Experimentally, there is a slight increase of the temperature at the start of each cycle
- Case of hybrid epoxy/aluminium mould

R1S - Temperature evolution in first cycles
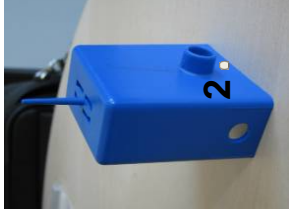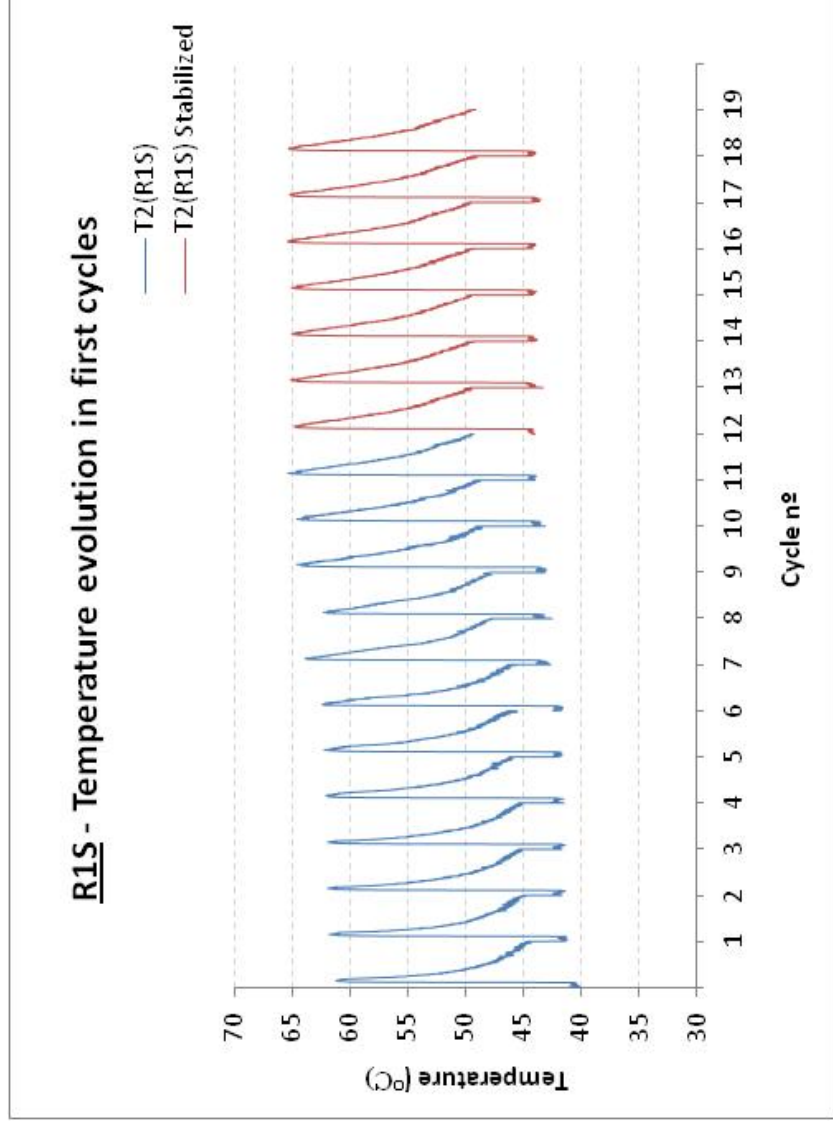
Moldex 3D simulation – stabilization results

- The simulation predicts that behaviour

- Case of hybrid epoxy/aluminium mould

R1S - Mould temperature at the start of each cycle

Temperature (°C)

— T2(R1S) Moldex 3D
× T2(R1S) Experimental

Cycle n°

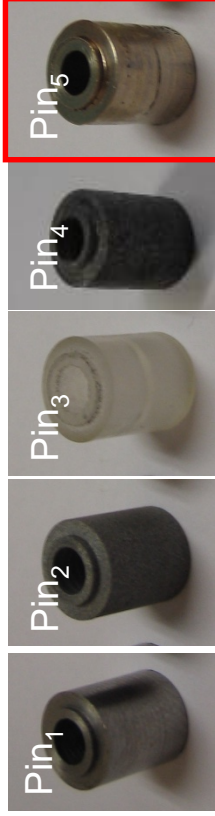Universidade do Minho

IPL

Moldex3D®

2

- Introduction
- Objective of the work
- Experimental
  - Test part
  - Mould and Instrumentation
  - Moulding
- **Moldex 3D simulation**
  - Pressure
  - Temperature
  - **Shrinkage**
- Conclusions

European Users' Meeting ,Chester, UK
September 24-25, 2008

Moldex3D®

Moldex 3D simulation – shrinkage

Conventional mould (Tool steel)
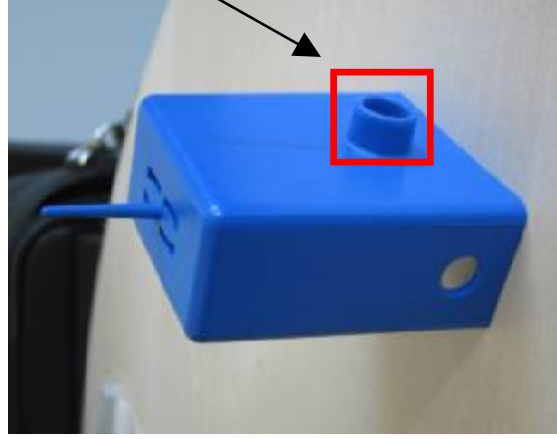
Moulding pins:

Pin$_1$: Tool steel

Pin$_2$: Epoxy (Biresin® L74) filled with

60% Al powder

Pin$_3$: STL resin (DSM Somos®

11120/2)

Pin$_4$: Epoxy (Biresin® L74)/15%

short steel fibres

Pin$_5$: ProMetal

Polypropylene mouldings

Moldex 3D simulation – shrinkage

The shrinkage was predicted at each moulding pin, based on the dimensions A and B
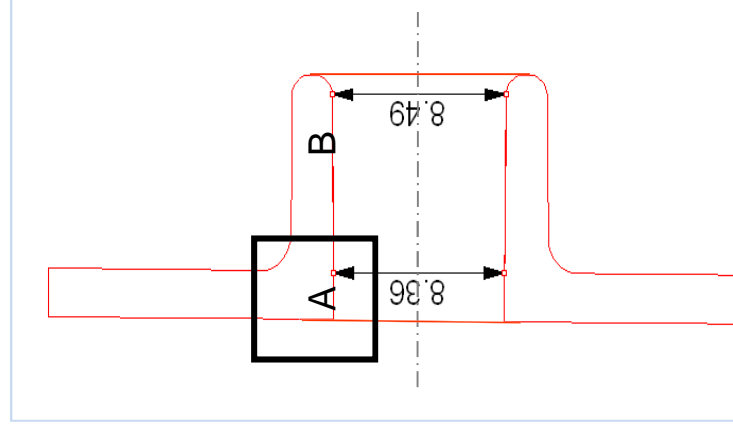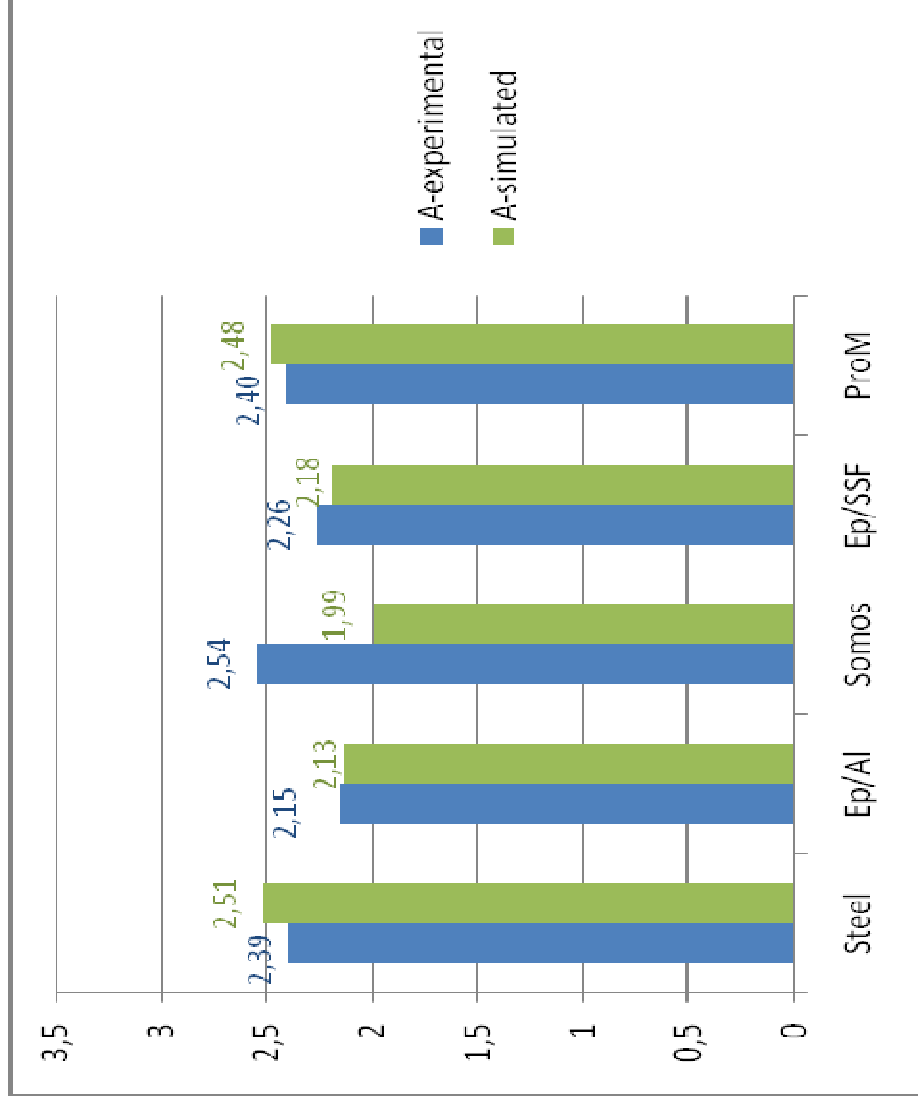
Points A and B for the shrinkage analysis
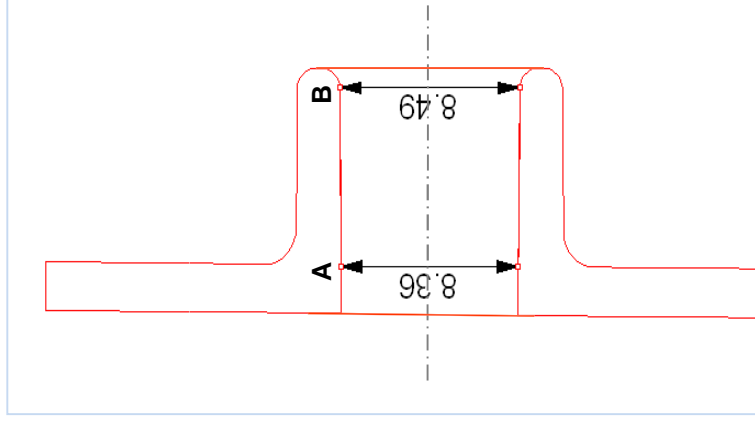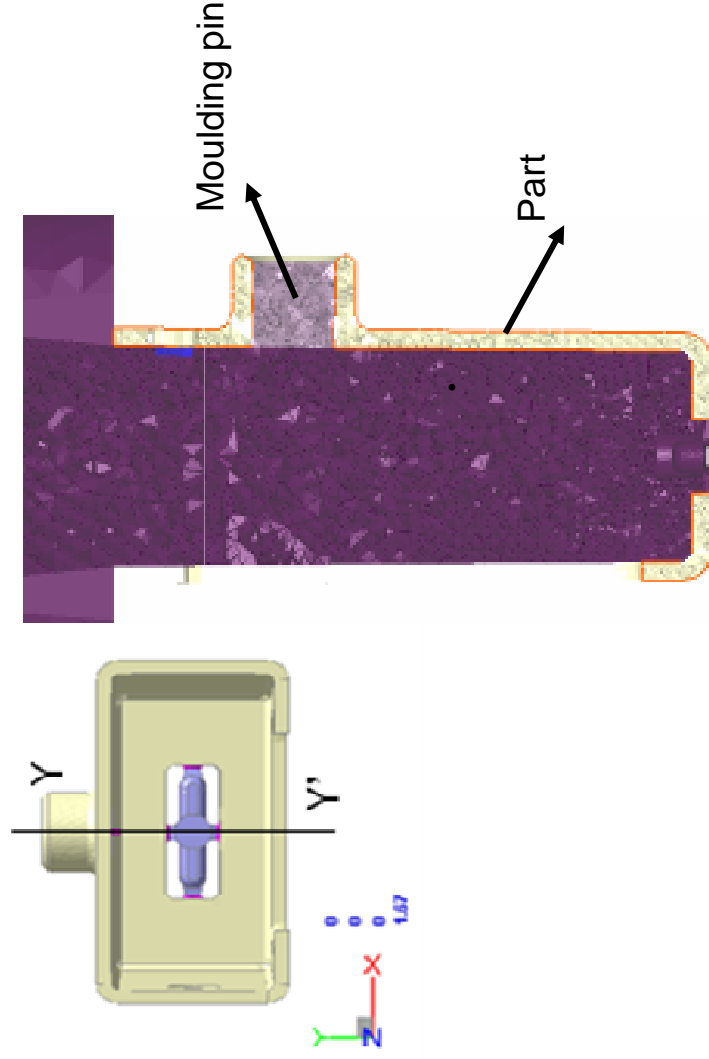
Moulding pin

Part

Moldex3D®

Moldex 3D simulation – shrinkage
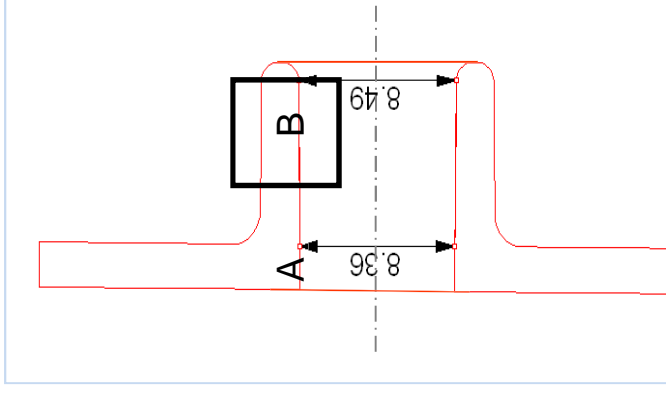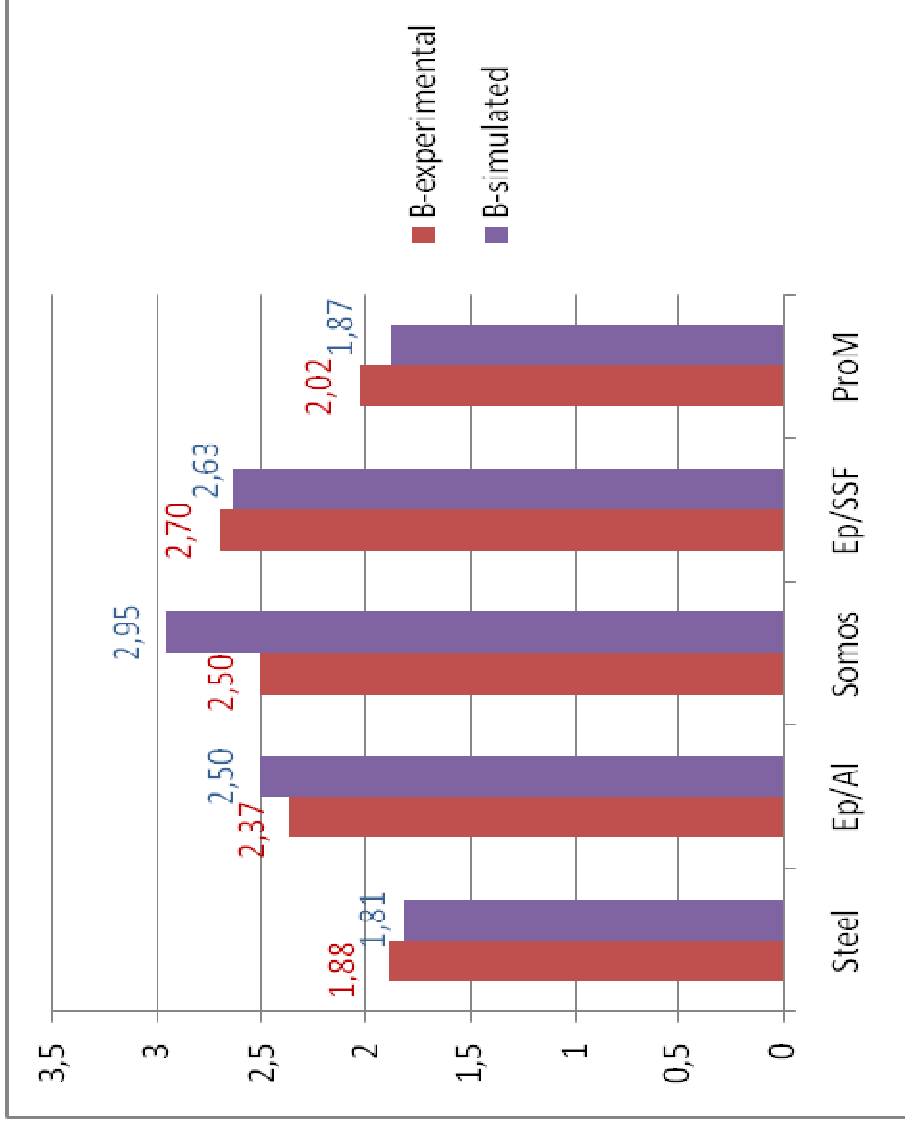
Moldex 3D simulation – shrinkage

Conclusions

- It is important to predict the mould regime temperature when low thermal conductivity materials are used in moulding blocks.

  - This temperature depends on the desired cycle time.
  - A repeatable temperature field is fundamental for the quality of the mouldings.

- Moldex 3D rel9.0 is quite precise at predicting the temperature at the mould/part interface.

- The simulation of the pressure is not as precise as a somewhat higher value for the maximum pressure is estimated.

- Moldex 3D rel9.0 is very good at predicting the shrinkage at ejection critical points.

  - The prediction of the shrinkage at these points is essential to estimate ejection forces and guaranteeing the moulding pin integrity

- Moldex 3D is an adequate tool to help the design of hybrid moulds where thermal and strength issues are critical.

Universidade do Minho

IPL

Moldex3D®

Acknowledgments

- **Coretech** and **Simulflow** for making available the use of Moldex3D® rel 9.0 and providing the expert technical support.

- **WTCM-CRIF** (Sirris) for the production of the SLA core blocks

- The Portuguese Foundation for Science and Technology, **FCT**, for the research grant to P.G. Martinho (SFRH/BD/28113/2006).

Moldex3D®

\#

Appendix 3

Hybrid mould design

The hybrid mould design is available in a CD attached to this thesis (see appendix 3).

\#

Appendix 4

Materials

Domolen
1100 N

Domolen 1100N is a good flow homopolymer with a conventional molecular weight distribution and is formulated with a general-purpose additive package. Domolen 1100 N is used for general injection moulding applications

Food Contact Applications: This grade is in compliance with most regulations regarding food contact applications (EU, FDA). Specific information is available upon request.

Properties Typical value

Properties		Unit	Test method	Value
Melt flow rate				
MFR 230 / 2. 16		g/10 min	ISO 1133	12
Technical properties				
Tensile modulus of elasticity (v = 1mm / min)		MPa	ISO 527-2	1550
Tensile yield stress (v = 50mm / min)		MPa	ISO 527-2	35
Tensile yield strain (v = 50mm / min)		%	ISO 527-2	8
Tensile strain at break (v = 50mm / min)		%	ISO 527-2	>50
Tensile creep modulus (1000h, elongation $\leq$ 0.5%)		MPa	ISO 899-1	380
Shear modulus		MPa	ISO 6721-2	800
Charpy impact strength notched	+ 23^0 C	kJ/m^2	ISO 179 / 1eA	3
	- 30^0 C	kJ/m^2	ISO 179 / 1eA	1.5
Charpy impact strength unnotched	+ 23^0 C	kJ/m^2	ISO 179 / 1eU	110
	- 30^0 C	kJ/m^2	ISO 179 / 1eU	14
Izod impact strength notched	+ 23^0 C	kJ/m^2	ISO 180 / 1A	3
	- 30^0 C	kJ/m^2	ISO 180 / 1A	1.3
Ball indentation hardness (H 132/30 - *H 358-/30)		MPa	ISO 2039-1	78*
Thermal properties				
Melting point, DSC		^{0}C	ISO 3146	163
Heat deflection temperature:				
- HDT / A (1.8 MPa)		^{0}C	ISO 75-2	55
- HDT / B (0.45 MPa)		^{0}C	ISO 75-2	85
Vicat softening temperature:				
- VST / A (10N)		^{0}C	ISO 306	154
- VST / B (50N)		^{0}C	ISO 306	90
Other properties				
Haze *1		%	ASTM D	60
Density		g/cm^3	ISO 1183	0.91
Applications				
Closures, furniture, housewares, general injection				

*1 = Injection-moulded disk, thickness = 1mm   *Issued 01/02/2004*

PRODUCT INFORMATION

Köraform A 50

KÖMMERLING
CHEMISCHE FABRIK GMBH

Addition-curing silicone mouldmaking compound with high hardness Shore A

- **low viscosity for easy pouring**

- **high mechanical strength**

- **curing practically without shrinkage at room temperature**

- **curing may be heat accelerated**

- **excellent cast resin stability**

- **Reproduction of master patterns (stereo lithography parts)**

- **Pouring of industrial parts such as damping elements, rubber elements, etc.**

TECHNICAL DATA

	Köraform A 50 A Component A	Köraform A 50 B Component B	
Colour	beige	blue	
Viscosity	60 000	1 200	mPa·s [1]
Density	1,35	0,97	DIN 53 479 [1]
	Mixture		
Mixing ratio	10 : 1		by weight
Viscosity	28 000		mPa·s	[1]
Pot Life	60		min	[1]
Earliest Demould after	12		h	[1]
	Vulcanized material		
Hardness Shore A	50		DIN 53 505 [1]
Tensile Strength	4,3		N/mm²	DIN 53 504 S 3 A [2]
Elongation at Break	370		%	DIN 53 504 S 3 A [2]
Tear Resistance	13		N/mm	ASTM D 624 Form B [2]
Linear Shrinkage	0,1		%	after 7 days [1]
1) = Measured at Standard Climate according to DIN 50 014-23/50-2			
2) = Vulcanized Material, measured after 14 days of storage at Standard Climate, DIN 50 014-23/50-2			

PROCESSING

Preparation

Köraform A 50 A- and B-component should be well stirred up prior processing in order to homogenize possibly settled fillers. The components A and B are mixed at a ratio of 10 : 1 by weight. Stirr thoroughly using a spatula or an agitator until the material has become homogeneous. The 60 minutes pot-life during which Köraform A 50 must be processed (casted or applied with a brush) starts with the mixing procedure. Demoulding can be carried out after 12 hours at the earliest.

Prior to casting, the mixed silicone has to be degassed under vacuum pressure in order to achieve a completely bubble-free vulcanized material (approx. 5 to 10 minutes at 10 to 20 mbar).

Curing Problems

(Inhibiting)

Certain substances can inhibit or even prevent curing of addition cross-linking silicones. Typical symtoms are tacky surfaces of the silicones towards the contact surfaces.

The following substances have to be particularly inspected with utmost care:

- nitrogen-containing substances (amines, polyurethanes, epoxy resins...)
- sulphurous substances (polysulfides, polysulfones, natural and synthetic rubber (EPDM))
- organometallic compounds (organotin compounds, vulcanized material and hardeners of condensation cross-linking silicones)

When casting to unknown substrates, a compatibility test must always be carried out.

CLEANING

Use Körasolv GL in order to remove fresh material. It is advisable to let residues in the mixing or casting container cure completely and then to peel them off.

SPECIAL NOTES

Storage

Köraform A 50 A and B components will retain their optimum processing characteristics for at least 6 months when stored at 5°C to 30°C in the tightly closed original container.

SAFETY

Please notice the indications on our EC-safety-data-sheets and the safety-indications on the labels of each product for the treatment of our products.

Especially the directions of the Dangerous Substance Regulation and the Accident Prevention Regulation of the Employers Liability Insurance have to be respected.

Keep the EC-safety-data-sheet of the product you treat ready to hand. It gives you valuable indications for the safe usage, disposal and in case of accidents.

PACKAGING UNITS

Köraform A 50 A: 22 kg containers
Köraform A 50 B: 2,2 kg containers

PRODUCT NUMBER

C 30187/A
C 34163/B

For safety related data please refer to the safety data sheet!

Biresin® L74

Laminating and Multi-purpose resin

Tooling & Composites

Application

- Manufacture of laminates for injection moulds and other temperature resistant moulds
- Manufacture of adhesive appliances
- For laminates with glass or carbon fibres

Properties

- Good soaking and wetting properties
- Good thermomechanical properties and high heat resistance after post curing (24 h / RT) + 3 h / 60°C + 3 h / 140°C
- Application especially in combination with surface resin **Biresin® S19**

Description

- Basis   Two-component-epoxy-system
- Resin   **Biresin® L74**, epoxy resin, yellowish-transparent, unfilled, low viscous
- Hardener   **Biresin® L74**, amine, colourless-transparent, unfilled, low viscous

Processing Data

Processing Data		
Mixing ratio resin to hardener	in parts by weight	100 : 17
Mixing viscosity, 25°C	mPas	780
Polife, 500 g / RT	min	120 - 150
Demoulding time, RT	h	24 + post curing

Physical Data (approx.-values)

Biresin® L74 resin	with hardener		Biresin® L74
Density	ISO 1183	g/cm³	1.1
Shore hardness	ISO 868	-	D 85*
E-Modulus	ISO 178	MPa	23,000* (glass fibre reinforced)
Flexural strength	ISO 178	MPa	120*
Impact resistance	ISO 179	kJ/m²	17*
Heat distortion temperature	ISO 75B	°C	160*

* values after post curing: 3h / 60°C + 3h / 140°C

Delivery

Individual components	**Biresin® L74** resin	25 kg net
	Biresin® L74 hardener	4.25 kg; 0.3 kg neto

Processing

- The material temperature must be 18 - 25°C.
- After mixing of resin and hardener component it is easily possible to incorporate additives if necessary.
- Biresin® L74 is applied quickly and easily due to its low viscosity. It will easily wet out fibres and incorporate high levels of fillers and powders with high binding force.
- The ratio between resin and selected fibre must be determined and reliably controlled.
- For laminates glass fibres with binding twill are better than binding cloth because of its better suppleness.
- It is adviced to lay up a balanced laminate to avoid distortion when de-moulding.
- Void-free glass and carbon fibre laminates are possible by processing under vacuum bag conditions to remove excess air and resin.
- To clean brushes or tools immediately Sika® Reinigungsmittel 5 is recommended.

Storage

- Minimum shelf life is 12 month under room condition (18 - 25°C), when stored in original un-opened containers.
- After prolonged storage at low temperature, crystallisation of components may occur. This is easily removed by warming sufficient time to a maximum of 80°C. Allow to cool to room temperature before use.
- Containers must be closed water tight immediately after use and prevented from moisture. The residual material has to be used up as soon as possible.

Precautions

For information and advice on the safe handling and storage of products, users should refer to the current Safety Data Sheet containing physical, ecological, toxicological and other safety related data.

Disposal considerations

Product
Recommendations: Must be disposed of in a special waste disposal unit in accordance with the corresponding regulations.
Packaging
Recommendations: Completely emptied packagings can be given for recycling. Packaging that cannot be cleaned should be disposed of as product waste.

Safety Data Sheet

according to 91/155/EEC and ISO 11014-1

1. Identification of the substance/preparation and company

Product

    Product name

    Biresin® L74 Hardener (B)

Manufacturer/supplier information

Manufacturer/supplier:	Sika Deutschland GmbH
Street/postbox:	Kornwestheimer Str. 103-107
Town/City and Post Code:	Stuttgart
Country:	Germany
Phone:	+4971180090
Telefax:	+497118009321
General information:	Product safety
Emergency information phone:	

        +49-(0)173-6774799

        Only out of office hours

2. Composition/information on ingredients

Chemical characterization

    Modified polyamine

Hazardous ingredients

    Designation according to 67/548/EEC

CAS No. EC No.	Concentration	Danger symbols	R phrases
· Cyclohex-1,2-ylendiamine			
694-83-7	50 - 100 %	Xi	38,41,43
211-776-7			

3. Hazards identification

Hazards identification

    Xi   Irritant

Information on hazards to man and to the environment

38	Irritating to skin.
41	Risk of serious damage to eyes.
43	May cause sensitization by skin contact.

4. First-aid measures

General instructions

    In any case show the physician the Safety Data Sheet

After inhalation

    In the event of symptoms take medical treatment.

4. First-aid measures (continued)

    After skin contact
        In case of contact with skin wash off immediately with soap and
        water
        Consult a doctor if skin irritation persists.

    After eye contact
        In case of contact with the eyes, rinse immediately for at least
        15 minutes with plenty of water.
        Summon a doctor immediately.

    After ingestion
        Turn a vomiting person lying on his back onto his side.
        Summon a doctor immediately.

5. Fire-fighting measures
    Suitable extinguishing media
        compatible with all usual extinguishing media

    Exposure hazard arising from the product, its combustion products or
    resulting gases
        In the event of fire the following can be released:
        Carbon monoxide (CO)
        Carbondioxide (CO2)
        Nitrogen oxides (NOx)

    Additional information
        Fire residues and contaminated firefighting medium must be disposed
        of in accordance with the local regulations.
        Collect contaminated firefighting water separately, must not
        be discharged into the drains.

6. Accidental release measures
    Personal precautions
        Ensure adequate ventilation.
        Use personal protective clothing.
        Use breathing apparatus if exposed to vapours/dust/aerosol.

    Environmental precautions
        Do not allow to enter drains or waterways
        In case of entry into waterways, soil or drains,
        inform the responsible authorities.

    Procedures for cleaning up
        Pick up with absorbent material (e.g. sand, sawdust, general-purpose
        binder).
        When picked up, treat material as prescribed under heading "Disposal".

7. Handling and storage

Handling

Instructions for safe handling
See chapter 8 / Personal protective equipment.

Instructions for fire and explosion protection
Not applicable.

Storage

Requirements for storage rooms and containers
Keep container tightly closed and dry in a cool, well-ventilated place

Combined storage instructions
Keep away from food, beverages and animal feedstocks.

Additional information regarding storage
Protect from frost.
Protect from heat and direct sunlight
Protect from atmospheric moisture and water

8. Exposure controls/personal protection

Personal protective equipment
General protective and hygiene measures
Take care for sufficient ventilation or exhaust on the workshop place.
Avoid contact with eyes and skin
Use barrier skin cream.
Remove soiled or soaked clothing immediately.
Do not eat, drink or smoke during work time.
Wash hands before breaks and after work.

Respiratory protection
Not applicable.

Hand protection
Butyl rubber/nitrile rubber gloves

Eye protection
Tightly fitting safety glasses

Body protection
Working clothes

9. Physical and chemical properties

9. Physical and chemical properties (continued)
   Appearance
          Physical state: liquid
          Colour: colourless
          Odour: amine-like

   Data relevant to safety   Method
          Flash point   > 75 °C

          Density at 20°C   approx. 0.95 g/cm3

          Solubility in water   soluble
          at 20°C

          Viscosity at 20°C   < 90 s

10. Stability and reactivity

   Materials to avoid/dangerous reactions
          No hazardous reactions when stored and handled according to
          prescribed instructions.

   Thermal decomposition and hazardous decomposition products
          No decomposition if used as prescribed.

11. Toxicological information

          Sensitization
          Sensitization/allergic reaction possible.
          Allergic reaction may be observed in sensitive persons, even
          on very low concentrations.

   Experience on humans
          When skin contact:
          Irritation.
          When eyes contact:
          Risk of serious damage to eyes.
          When inhalation:
          Irritation.
          When swallowed:
          Small amount may cause considerable health disorders.

12. Ecological information

          Additional information
          Do not allow to enter waste water drain, waterways or soil.

13. Disposal considerations

    Product

        Recommendations
        Must be disposed of in a special waste disposal unit in accordance
        with the corresponding regulations.
        See chapter 15, national regulations.

    Packaging

        Recommendations
        Completely emptied packagings can be given for recycling.
        Packaging containing remains of dangerous substances, as well as
        packagings disposed of remains can be unharmed eliminated in
        accordance with the regulations.

* 14. Transport information

    ADR/RID
        Further information
        No dangerous goods.

    IMO/IMDG
        Further information
        No dangerous goods.
        Marine pollutant: no

    IATA/ICAO
        Further information
        No dangerous goods.

15. Regulatory information

    Labelling according to EEC Directive
        The product is classified and labelled in accordance with
        EC directives/the relevant national laws.
        Relevant hazardous ingredients for labelling
        Contains: Cyclohex-1,2-ylendiamine

        Danger symbols
        Xi   Irritant

        R phrases
        38   Irritating to skin.
        41   Risk of serious damage to eyes.
        43   May cause sensitization by skin contact.

        S phrases
        24   Avoid contact with skin.
        26   In case of contact with eyes, rinse immediately with
                       plenty of water and seek medical advice.
        37/39   Wear suitable gloves and eye/face protection.

* 16. Other information
       asterisk (*) on left margin marks modification of previous version

       Recommended use: Chemical product for construction and industry

       R-phrases of the ingredients listed in chapter 2
       38   Irritating to skin.
       41   Risk of serious damage to eyes.
       43   May cause sensitization by skin contact.

The information contained in this Safety Data Sheet corresponds to our
level of knowledge at the time of publication. All warranties are ex-
cluded. Our most current General Sales Conditions shall apply. Please
consult the Technical Data Sheet prior to any use and processing.

========================

PÓ DE ALUMÍNIO

========================

DESCRIÇÃO   Pó de alumíno atomizado sem revestimento.

Pureza mínima : 99,5 %

Forma da partícula : granular

GRAU DE PUREZA   99,5 %

GRANULOMETRIA   > 150 µ : 1 % máx. *

< 150 µ : 99 % min. *

<   80 µ : 80 % *

<   45 µ : 40 % *

DENSIDADE APARENTE   1.2 g/cm^3
DENSIDADE REAL   2.43 g/cm^3

TAMANHO MÉDIO DAS PARTÍCULAS   50 µ

APLICAÇÃO   Uso Industrial.

* **Valores Médios**

   Os valores mencionados nesta Ficha Técnica devem ser considerados como valores médios e estão baseados no nosso nível actual de conhecimentos sobre este produto.

REBELCO,Lda   **Tel : 214566335**
Rua Gil Vicente, 69   **Fax :214566338**
2775-198 PAREDE   **geral@rebelco.pt**

Resistência mecânica

Cura estática

Tabela 1: Propriedades mecânicas obtidas no ensaio de tração sem controle na cura.

Condições	Resistência máxima à tração (MPa)	Módulo elástico (MPa)
0% SSF	$71,8 \pm 7,4$	1189 ± 30
10% SSF	$44,8 \pm 4,7$	1352 ± 127
15% SSF	$46,1 \pm 2,8$	1205 ± 176
20% SSF	$47,4 \pm 4,8$	1366 ± 134
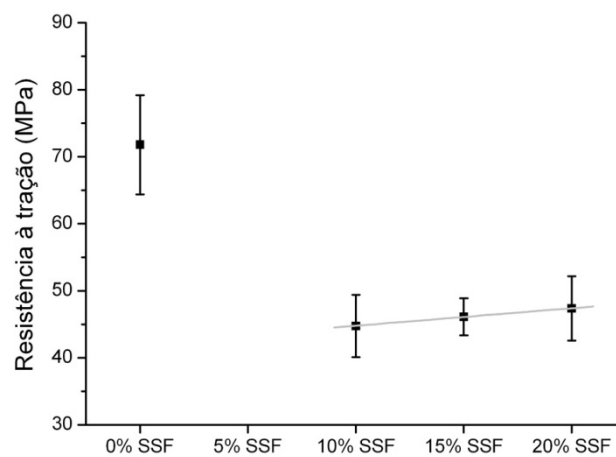
Figura 1: Resistência à tração sem controle na cura.
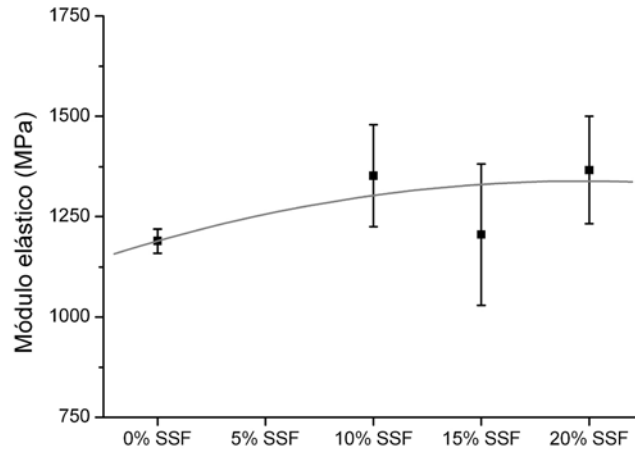
Figura 2: Módulo elástico sem controle na cura.

Cura dinâmica

Tabela 2: Propriedades mecânicas obtidas no ensaio de tração com cura dinâmica.

Condições	Resistência à tração (MPa)	Módulo elástico (MPa)
0% SSF	71,8 ± 7,4	1189 ± 30
10% SSF	64,9 ± 3,6	1731 ± 38
15% SSF	71,4 ± 3,4	1926 ± 63
20% SSF	61,0 ± 5,0	1901 ± 96
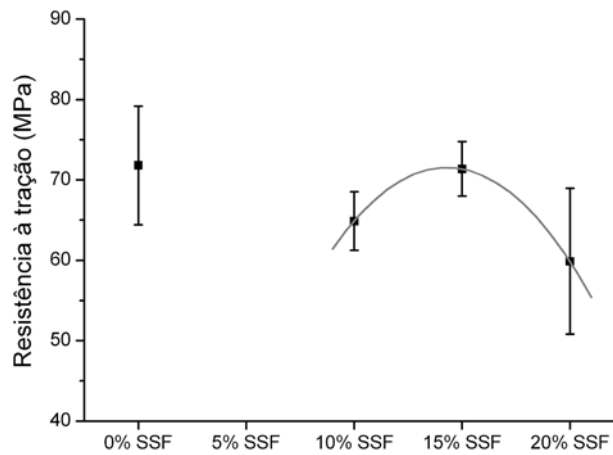
Figura 3: Resistência máxima à tração com cura dinâmica.
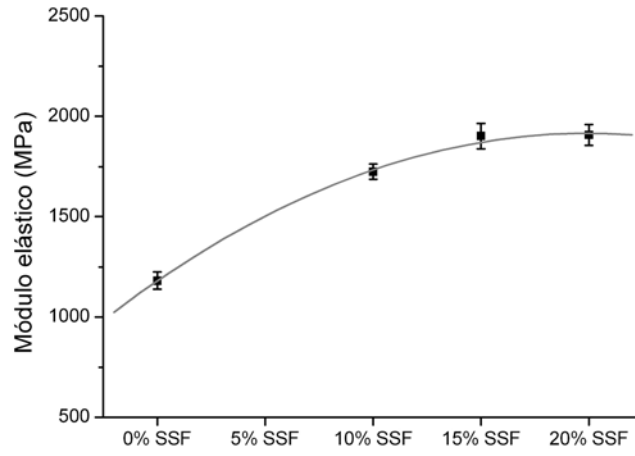
Figura 4: Módulo elástico com cura dinâmica.

Comparativo com comerciais
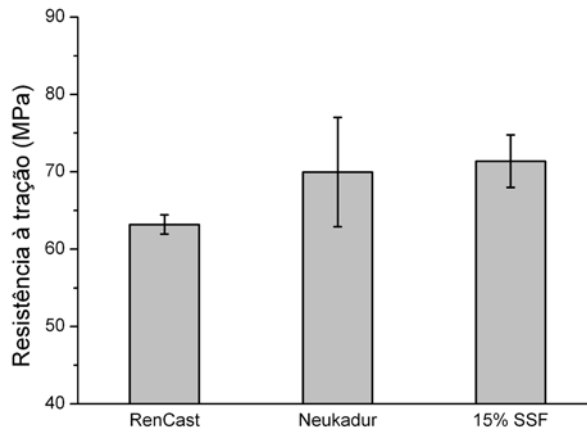
Figura 5: Comparação da resistência máxima com materiais comerciais.
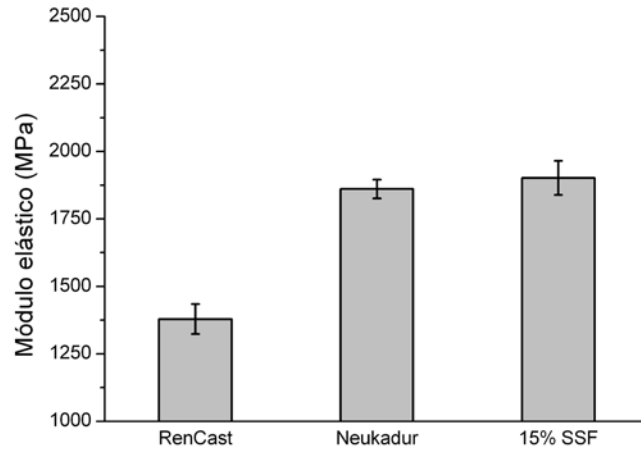
Figura 6: Comparação do módulo elástico com materiais comerciais.

Resistência ao impacto

Tabela 3: Resistência ao impacto com a adição de fibras curtas de aço.

Condições	Raio do entalhe (mm)	Resistência ao impacto Charpy $(kJ.m^{-2})$
0% SSF	0,25	$1,18 \pm 0,54$
	1	$2,15 \pm 0,32$
10% SSF	0,25	$1,64 \pm 0,16$
	1	$2,10 \pm 0,24$
15% SSF	0,25	$2,73 \pm 0,49$
	1	$2,95 \pm 0,46$
20% SSF	0,25	$3,53 \pm 0,54$
	1	$4,29 \pm 0,60$
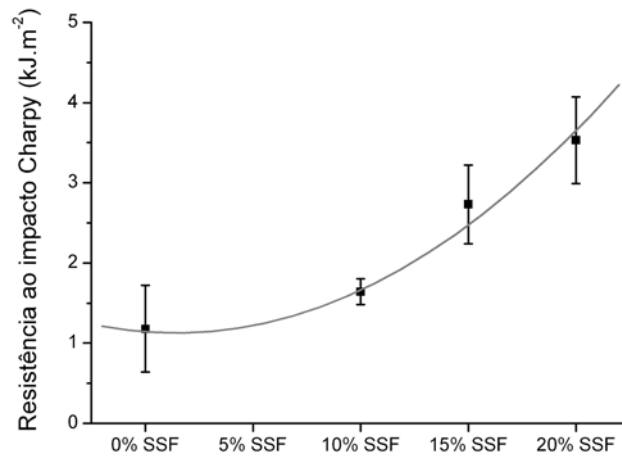
Figura 7: Resistência ao impacto Charpy de compósitos RenLam com raio de entalhe de 0,25 mm.
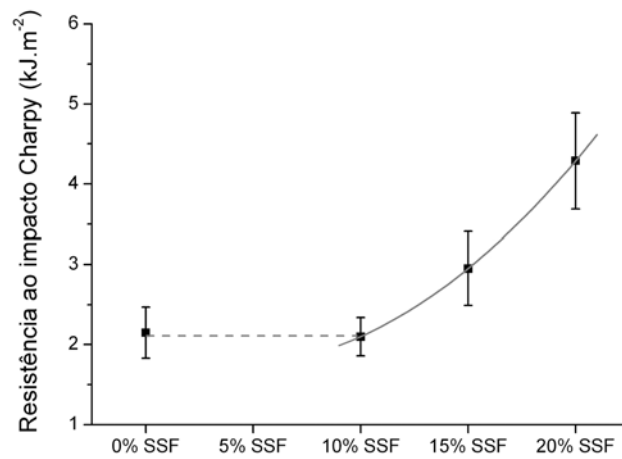
Figura 8: Resistência ao impacto Charpy com entalhe de 1 mm.

Tabela 4: Resistência ao impacto dos compósitos comerciais.

Condições	Entalhe	Resistência ao impacto Charpy $(kJ.m^{-2})$
RenCast	0,25 mm	$1,37 \pm 0,07$
	1 mm	$2,89 \pm 0,31$
Neukadur	0,25 mm	$2,06 \pm 0,38$
	1 mm	$2,69 \pm 0,33$
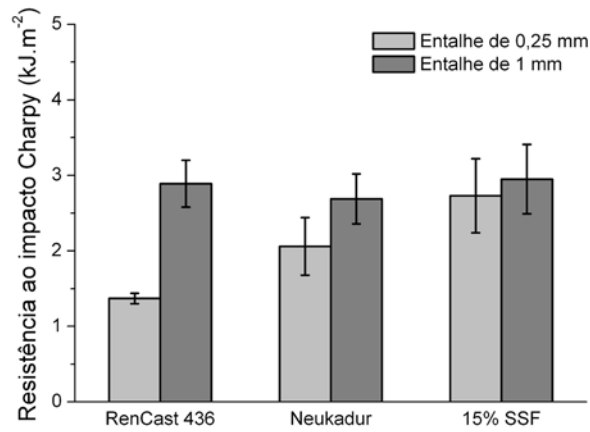
Figura 9: Comparação de resistência ao impacto Charpy.

Resistência a flexão

Tabela 5: Valores de resistência à flexão e módulo à flexão para os compósitos SSF.

Condições	Resistência à flexão (MPa)	Módulo à flexão (MPa)
0% SSF	n.p.	2147 ± 304
10% SSF	$77,4 \pm 1,8$	3828 ± 218
15% SSF	$84,2 \pm 3,0$	4658 ± 307
20% SSF	$64,7 \pm 3,3$	4249 ± 260

n.p. - Ruptura não verificada até o limite de carga da máquina.
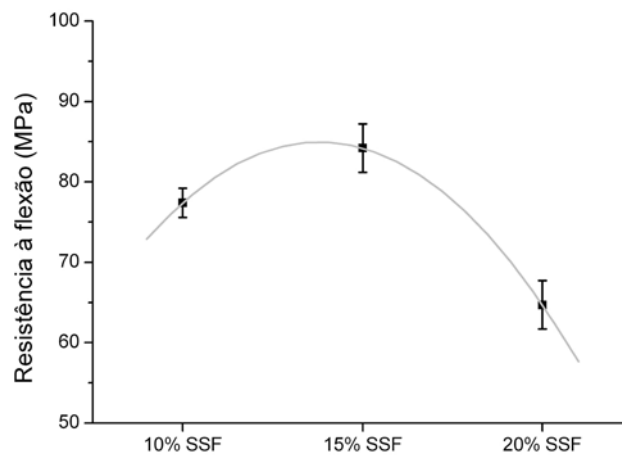
Figura 10: Variação da resistência à flexão para os compósitos SSF.
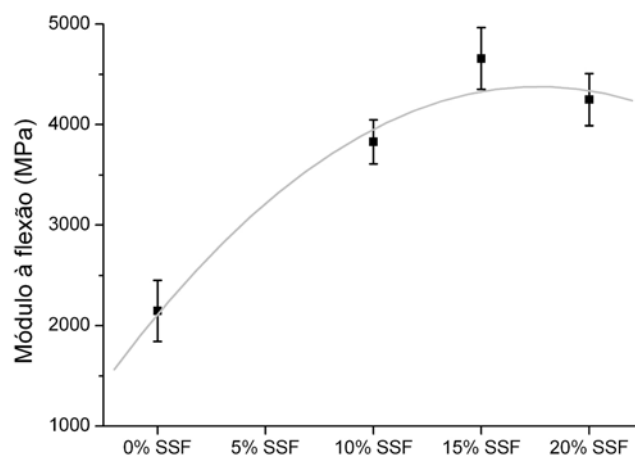
Figura 11: Variação do módulo à flexão para os compósitos SSF.

Tabela 6: Valores de resistência à flexão e módulo à flexão para os compósitos comerciais.

Condições	Resistência à flexão (MPa)	Módulo à flexão (MPa)
RenCast	$69,1 \pm 3,3$	4474 ± 159
15% SSF	$84,2 \pm 3,0$	4658 ± 307
Neukadur	$87,3 \pm 4,7$	6148 ± 240
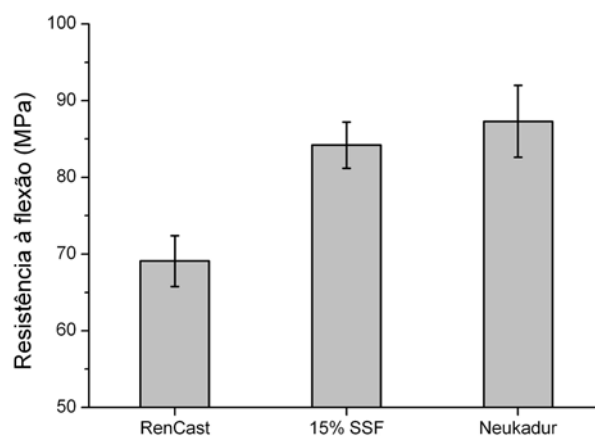
Figura 12: Comparação da resistência à flexão dos compósitos comerciais com o compósito 15% SSF.
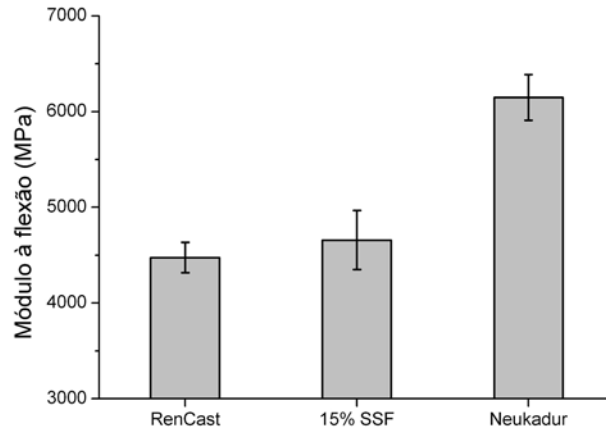
Figura 13: Comparação do módulo à flexão dos compósitos comerciais com o compósito 15% SSF.
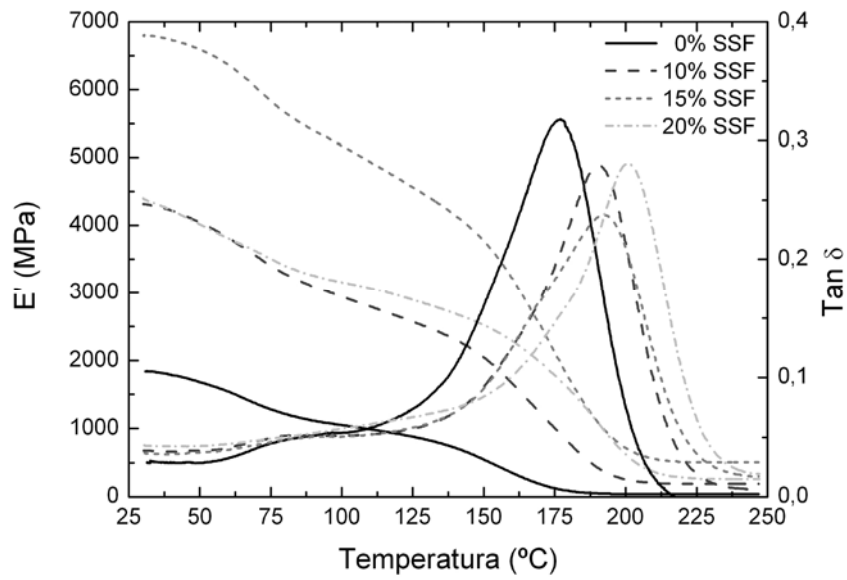
Figura 14: Variação do comportamento viscoelástico à flexão com aumento da temperatura nos compósitos SSF.
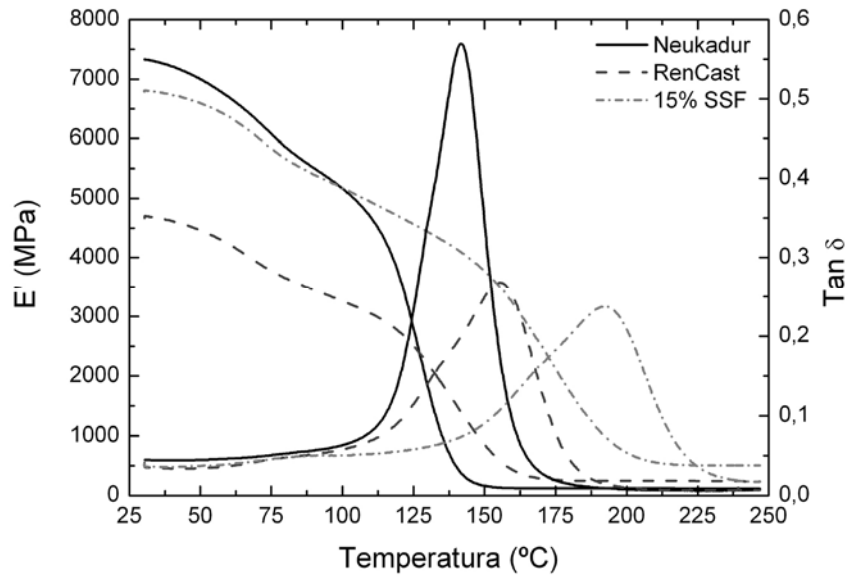
Figura 15: Comparação do comportamento viscoelástico à flexão dos compósitos comerciais com o compósito 15% SSF.

Condutividade térmica

Tabela 7: Valores de condutividade térmica para os compósitos SSF.

Condições	Condutividade térmica $(W.m^{-1}.K^{-1})$
0% SSF	0,198
10% SSF	0,353
15% SSF	0,392
20% SSF	0,453
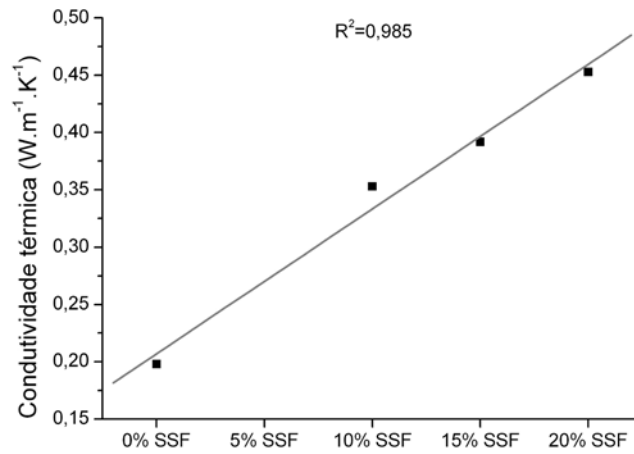
Figura 16: Variação na condutividade térmica com aumento da fração em volume de SSF.

Tabela 8: Valores de condutividade térmica para os compósitos comerciais.

Condições	Condutividade térmica (W.m^{-1}.K^{-1})
RenCast	0,361
15% SSF	0,392
Neukadur	0,494
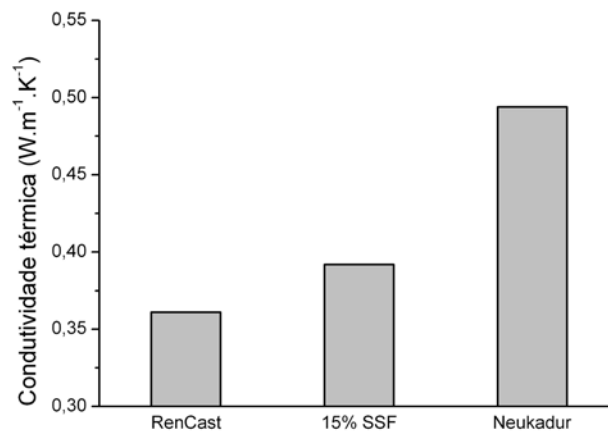
Figura 17: Comparação da condutividade térmica dos compósitos comerciais com o compósito 15% SSF.

WaterShed® XC 11122

**Clear, near colorless, durable, water-resistant resin for Stereolithography
For Solid State (355 nm) Laser Systems**

DSM Somos®
1122 St. Charles Street
Elgin, IL 60120 USA
Tel: 800.223.7191 (in USA)
Tel: 847.697.0400 (outside USA)
Fax: 847.468.7785

DSM Desotech bv
3150 AB Hoek van Holland
The Netherlands
Tel: +31 1743.15391
Fax: +31 1743.15530

www.dsmsomos.com

Email:
Americas@dsmsomos.info
Europe@dsmsomos.info
Asia@dsmsomos.info

Description

WaterShed XC is a low viscosity liquid photopolymer that produces strong, tough, water-resistant, ABS-like parts. Most importantly parts created with WaterShed 11122 are nearly colorless, and look more like true, clear engineered plastic.

In addition, WaterShed XC has been formulated with the DSM Somos Oxetane Advantage™— an advanced chemistry platform that produces parts with outstanding water resistance and high dimensional stability.

Application

WaterShed XC 11122 offers many properties that mimic traditional engineering plastics including ABS and PBT. This makes the material ideal for many applications in the automotive, medical and consumer electronics markets and include:

- Lenses
- Packaging
- Water flow analysis
- RTV patterns
- Durable concept models
- Wind tunnel testing
- Quickcast patterns

WaterShed 11120   WaterShed XC 1122

Photo courtesy of Dynacept

Physical Properties – Liquid

Appearance	Optically clear, near Colorless
Viscosity	~260 cps at 30°C
Density	~1.12 g/cm³ at 25°C

Optical Properties at 355 nm

E_c ~11.5 mJ/cm²
[critical exposure]

D_p 0.16 mm (~.0065 inch)
[slope of cure-depth vs. ln(E) curve]

E_{10} 54 mJ/cm²
[exposure that gives 0.254 mm (.010 inch) thickness]

Mechanical Properties (Metric)

ASTM Method	Description	WaterShed® XC 11122	ABS* (transparent)	Polybutylene Terephthalate*
D638M	Tensile Strength	47.1 - 53.6 MPa	45.7 MPa	55 MPa
	Elongation at Break	11 - 20 %	41.6 %	20 %
	Elongation at Yield	3.3 - 3.5 %	N/A	3.5 - 9 %
	Modulus of Elasticity	2,650 - 2,880	2,000 MPa	2,700 MPa
D790M	Flexural Strength	63.1 - 74.2 MPa	73.5 MPa	80 MPa
	Flexural Modulus	2,040 - 2,370 MPa	2,300 MPa	2,500 MPa
D256A	Izod Impact-Notched	0.2 - 0.3 J/cm	1.6 J/cm	1.2 J/cm
D542	Index of Refraction	1.512 - 1.515	1.52	N/A
D2240	Hardness (Shore D)	N/A	N/A	98 - 120 (Rockwell R)
D1004	Graves Tear	150,288 N/m	N/A	N/A
D570-98	Water Absorption	0.35 %	0.20 – 0.45 %	0.16 %

* http://www.matweb.com   N/A: Not Available

Thermal & Electrical Properties (Metric)

ASTM Method	Description	WaterShed® XC 11122	ABS* (transparent)	Polybutylene Terephthalate*
E831-00	C.T. E. -40°C – 0°C	66 - 67 μm/m-°C		
	C.T. E. 0°C – 50°C	90 - 96 μm/m-°C	60 – 130 μm/m-°C (no temp range given)	50 - 145 μm/m-°C (no temp range given)
	C.T. E. 50°C – 100°C	170 - 189 μm/m-°C		
	C.T. E. 100°C – 150°C	185 - 189 μm/m-°C		
D150-98	Dielectric Constant 60Hz	3.9 - 4.1	3.7	
	Dielectric Constant 1KHz	3.7 - 3.9		2.9 - 4.0 (no frequency specified)
	Dielectric Constant 1MHz	3.4 - 3.5	3.7	
D149-97a	Dielectric Strength	15.4 - 16.3 kV/mm	13.8 – 19.7 kV/mm	14.7 - 30 kV/mm
E1545-00	Tg	39 - 46 °C		41 °C
D648-98c	HDT @ 0.46 MPa	45.9 - 54.5 °C	94 – 207 °C	150 °C
	HDT @ 1.81 MPa	49.0 -49.7 °C	86.4 – 194 °C	61.3 °C

* http://www.matweb.com   N/A: Not Available

Mechanical Properties (Imperial)

ASTM Method	Description	WaterShed® XC 11122	ABS* (transparent)	Polybutylene Terephthalate*
D638M	Tensile Strength	6831 - 7774 psi	6,628 psi	7977 psi
	Elongation at Break	11 - 20 %	41.6 %	20 %
	Elongation at Yield	3.3 - 3.5 %	N/A	3.5 - 9 %
	Modulus of Elasticity	384 - 418 kpsi	290,000 psi	391,602 psi
D790M	Flexural Strength	9,152 - 10,756 psi	10,660 psi	11,603 psi
	Flexural Modulus	296 - 344 kpsi	344,000 psi	362,594 psi
D256A	Izod Impact-Notched	0.4 - 0.6 ft lb/in	1.5 - 2.0 ft lb/in	0.56 ft lb/in
D542	Index of Refraction	1.513 - 1.515	1.52	N/A
D2240	Hardness (Shore D)	N/A	N/A	98 - 120 (Rockwell R)
D1004	Graves Tear	833 - 858 lbf/in	N/A	N/A
D570-98	Water Absorption	0.35 %	0.2 - 0.45 %	0.16 %

N/A: Not Available

Thermal & Electrical Properties (Imperial)

ASTM Method	Description	WaterShed® XC 11122	ABS* (transparent)	Polybutylene Terephthalate*
E831-00	C.T.E. 10°F – 32°F	37 μin/in-°F		
	C.T.E. 32°F – 60°F	50 - 53 μin/in-°F	33 – 72 μin/in-°F (no temp range given)	28 - 81 μin/in-°F (no temp range given)
	C.T.E. 60°F – 88°F	94 - 105 μin/in-°F		
	C.T.E. 88°F – 115°F	103 - 105 μin/in-°F		
D150-98	Dielectric Constant 60Hz	3.9 - 4.1	3.7	
	Dielectric Constant 1KHz	3.7 - 3.9		2.9 - 4.0 (no frequency specified)
	Dielectric Constant 1MHz	3.4 - 3.5	3.7	
D149-97a	Dielectric Strength	390 - 413 V/mil	350 - 500 V/mil	373 -762 V/mil
E1545-00	Tg	102 - 109 °F		106 °F
D648-98c	HDT @ 0.46 MPa	115 - 130 °F	201 - 405 °F	302 °F
	HDT @ 1.81 MPa	120 °F	187 - 381 °F	142.3 °F

N/A: Not Available

WaterShed™ 11120

Durable, strong, semi-transparent, water-resistant resin for stereolithography
For Solid State (355 nm) Laser Systems

Description

DSM Somos® 11120 is a low viscosity liquid photopolymer that produces strong, tough, water-resistant parts. Parts created with Somos® 11120 have a light green tinge, similar in color to plate glass.

Application

Somos® 11120 offers many properties that mimic traditional engineering plastics including ABS and PBT. This makes the material ideal for many applications in the automotive, medical and consumer electronics markets and include:

- Water flow analysis
- RTV patterns
- Durable concept models
- Wind tunnel testing
- Quickcast patterns
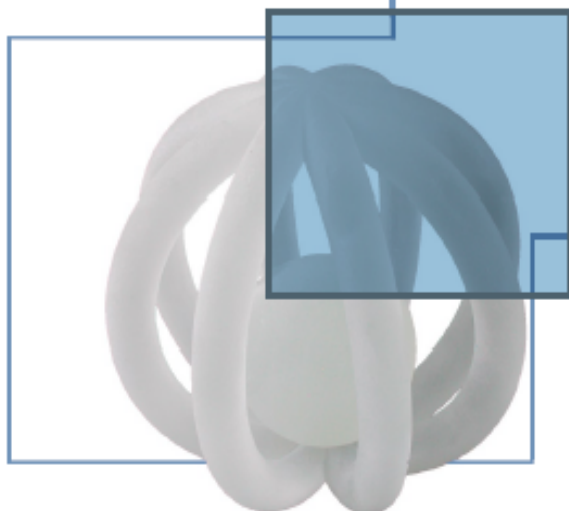
Physical Properties – Liquid

Appearance	Optically clear
Viscosity	~260 cps at 30°C
Density	~1.12 g/cm³ at 25°C

Optical Properties at 355 nm

E_c ~11.5 mJ/cm² (critical exposure)

D_p 0.16 mm (~.0065 inch) (slope of cure-depth vs. ln(E) curve)

E_{10} 54 mJ/cm² (exposure that gives 0.254 mm (.010 inch) thickness)

DSM Somos®
2 Penn's Way, Suite 401
New Castle, DE 19720, USA
Tel: +1 302.326.8100
Fax: +1 302.326.8121

DSM Desotech bv
3150 AB Hoek van Holland
The Netherlands
Tel: +31 1743.15391
Fax: +31 1743.15530

www.dsmsomos.com

Email:
Americas@dsmsomos.info
Europe@dsmsomos.info
Asia@dsmsomos.info

Mechanical Properties (Metric)

ASTM Method	Description	WaterShed™ 11120	ABS* (transparent)	Polybutylene Terephthalate*
D638M	Tensile Strength	47.1 - 53.6 MPa	45.7 MPa	55 MPa
	Elongation at Break	11 - 20 %	41.6 %	20 %
	Elongation at Yield	3.3 - 3.5 %	N/A	3.5 - 9 %
	Modulus of Elasticity	2,650 - 2880 MPa	2,000 MPa	2,700 MPa
D790M	Flexural Strength	63.1 - 74.16 MPa	73.5 MPa	80 MPa
	Flexural Modulus	2,040 - 2370 MPa	2,300 MPa	2,500 MPa
D256A	Izod Impact-Notched	0.2 - 0.3 J/cm	1.6 J/cm	1.2 J/cm
D542	Index of Refraction	1.512 - 1.515	1.52	N/A
D2240	Hardness (Shore D)	N/A	N/A	98 - 120 (Rockwell R)
D1004	Graves Tear	150,288 N/m	N/A	N/A
D570-98	Water Absorption	0.35 %	0.20 – 0.45 %	0.16 %

* http://www.matweb.com   N/A: Not Available

Thermal & Electrical Properties (Metric)

ASTM Method	Description	WaterShed™ 11120	ABS* (transparent)	Polybutylene Terephthalate*
E831-00	C.T.E. -40°C – 0°C	66 - 67 µm/m-°C		
	C.T.E. 0°C – 50°C	90 - 96 µm/m-°C	60 – 130 µm/m-°C (no temp range given)	50 - 145 µm/m-°C (no temp range given)
	C.T.E. 50°C – 100°C	170 - 189 µm/m-°C		
	C.T.E. 100°C – 150°C	185 - 189 µm/m-°C		
D150-98	Dielectric Constant 60Hz	3.9 - 4.1	3.7	
	Dielectric Constant 1KHz	3.7 - 3.9		2.9 - 4.0 (no frequency specified)
	Dielectric Constant 1MHz	3.4 - 3.5	3.7	
D149-97a	Dielectric Strength	15.4 - 16.3 kV/mm	13.8 – 19.7 kV/mm	14.7 - 30 kV/mm
E1545-00	Tg	39 - 46 °C		41 °C
D648-98c	HDT @ 0.46 MPa	45.9 - 54.5 °C	94 – 207 °C	150 °C
	HDT @ 1.81 MPa	49.0 -49.7 °C	86.4 – 194 °C	61.3 °C

* http://www.matweb.com   N/A: Not Available

Mechanical Properties (Imperial)

ASTM Method	Description	WaterShed™ 11120	ABS* (transparent)	Polybutylene Terephthalate*
D638M	Tensile Strength	6831 - 7774 psi	6,628 psi	7977 psi
	Elongation at Break	11 - 20 %	41.6 %	20 %
	Elongation at Yield	3.3 - 3.5 %	N/A	3.5 - 9 %
	Modulus of Elasticity	384 - 418 kpsi	290,000 psi	391,602 psi
D790M	Flexural Strength	9,152 - 10,756 psi	10,660 psi	11,603 psi
	Flexural Modulus	296 - 344 kpsi	344,000 psi	362,594 psi
D256A	Izod Impact-Notched	0.4 - 0.6 ft lb/in	1.5 - 2.0 ft lb/in	0.56 ft lb/in
D542	Index of Refraction	1.513 - 1.515	1.52	N/A
D2240	Hardness (Shore D)	N/A	N/A	98 - 120 (Rockwell R)
D1004	Graves Tear	833 - 858 lbf/in	N/A	N/A
D570-98	Water Absorption	0.35 %	0.2 - 0.45 %	0.16 %

* http://www.matweb.com   N/A: Not Available

Thermal & Electrical Properties (Imperial)

ASTM Method	Description	WaterShed™ 11120	ABS* (transparent)	Polybutylene Terephthalate*
E831-00	C.T.E. -40°F – 32°F	37 μin/in-°F		
	C.T.E. 32°F – 122°F	50 - 53 μin/in-°F	33 – 72 μin/in-°F (no temp range given)	28 - 81 μin/in-°F (no temp range given)
	C.T.E. 122°F – 212°F	94 - 105 μin/in-°F		
	C.T.E. 212°F – 302°F	103 - 105 μin/in-°F		
D150-98	Dielectric Constant 60Hz	3.9 - 4.1	3.7	
	Dielectric Constant 1KHz	3.7 - 3.9		2.9 - 4.0 (no frequency specified)
	Dielectric Constant 1MHz	3.4 - 3.5	3.7	
D149-97a	Dielectric Strength	390 - 413 V/mil	350 - 500 V/mil	373 -762 V/mil
E1545-00	Tg	102 - 109 °F		106 °F
D648-98c	HDT @ 0.46 MPa	115 - 130 °F	201 - 405 °F	302 °F
	HDT @ 1.81 MPa	120 °F	187 - 381 °F	142.3 °F

* http://www.matweb.com   N/A: Not Available

ProMetal Direct Metal Properties

	MATERIAL			For Comparison	
	S3	**S4**	**S4H**	**Carbon Steel** 1040 Normalized	**Aluminum** 6061-T6
Alloy Family	316 SS+Bronze	420 SS+Bronze	420 SS+Bronze		
UTS	59 KSI (406 MPa)	99 KSI (682 MPa)	111 KSI (765 MPa)	86 KSI (595 MPa)	45 KSI (310 MPa)
Yield	34 KSI (234 MPa)	66 KSI (455 MPa)	83 KSI (572 MPa)	54 KSI (370 MPa)	40 KSI (275 MPa)
Modulus	21.5 MPSI (148 GPa)	21.4 MPSI (147 GPa)	22 MPSI (151 GPa)	29 MPSI (200 GPa)	10 MPSI (69 GPa)
Elongation	3.00%	2.30%	3.80%		
Hardness	60 HRb	25-30 HRc	30-35 HRc	170 HB	
Parts functional prototypes replacement parts, etc.	x	x	x		
Tools injection molds casting molds, etc.		x	x		

PROMETAL®

\#

Appendix 5

Moldex3D simulations

\#

SOLID MESH
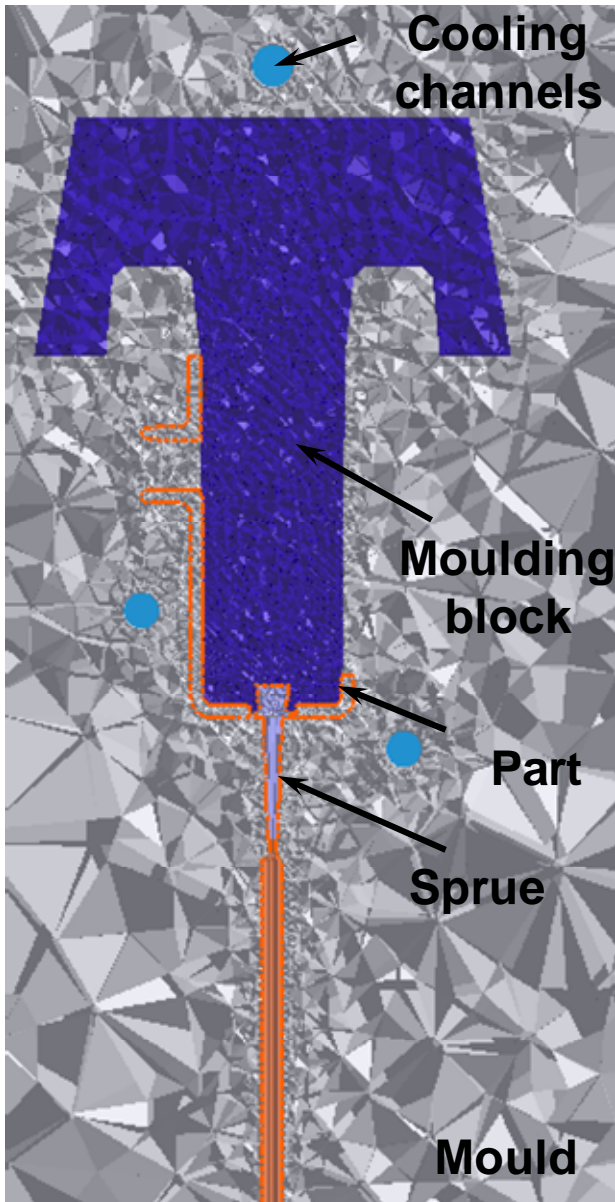
"Moldex3D Release 9.1"

Elements of the solid mesh:

- Part: **177 792**

- Runner channels: **32 909**

- Cooling channels: **33 769**

- Mould: **425016**

- Moulding block: **475 416**

- Total elments of the model: **1 144 902.**
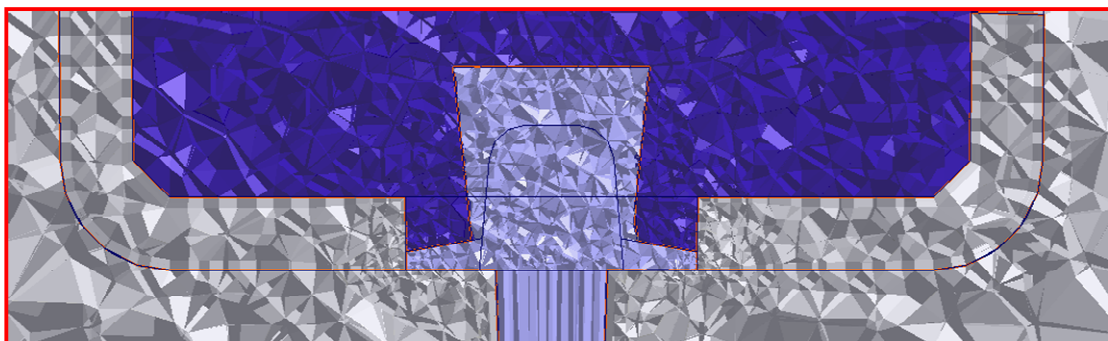
COOLING SYSTEM LAYOUT
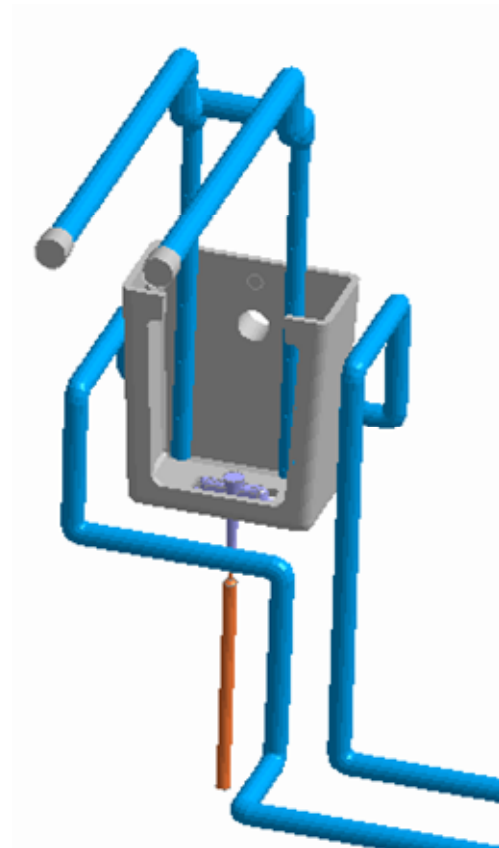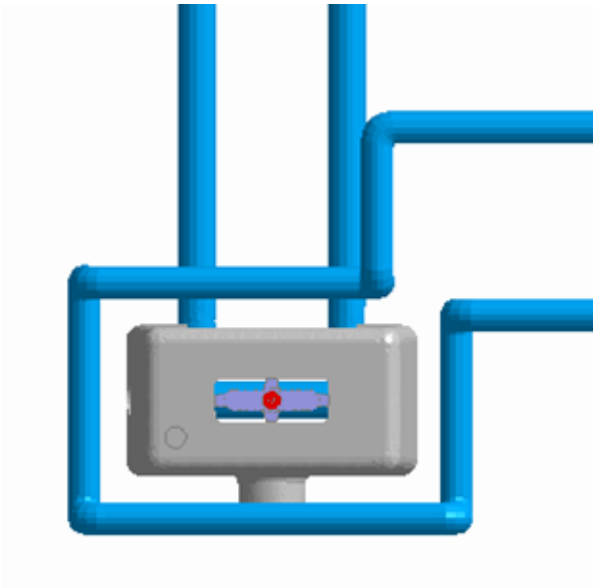
MODEL
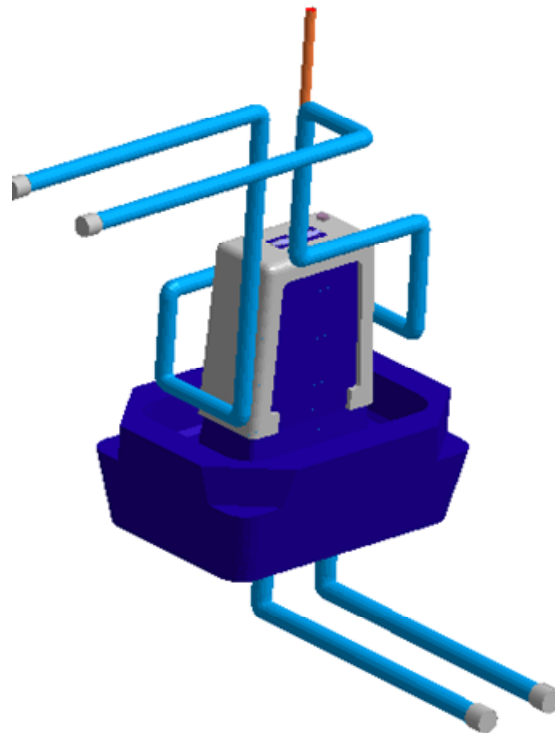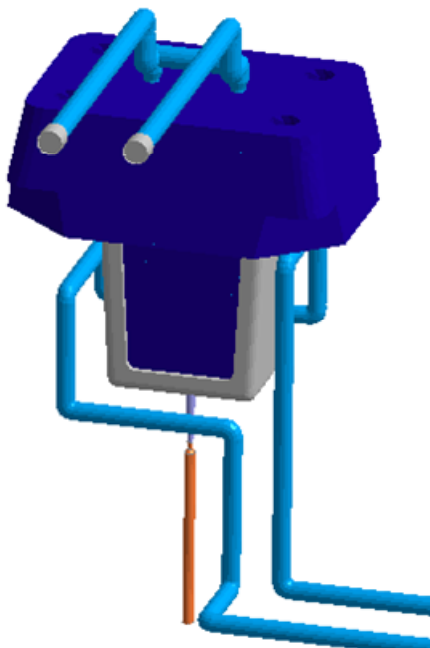
HM-2 SS (all-steel)

Pressure - Final of filling
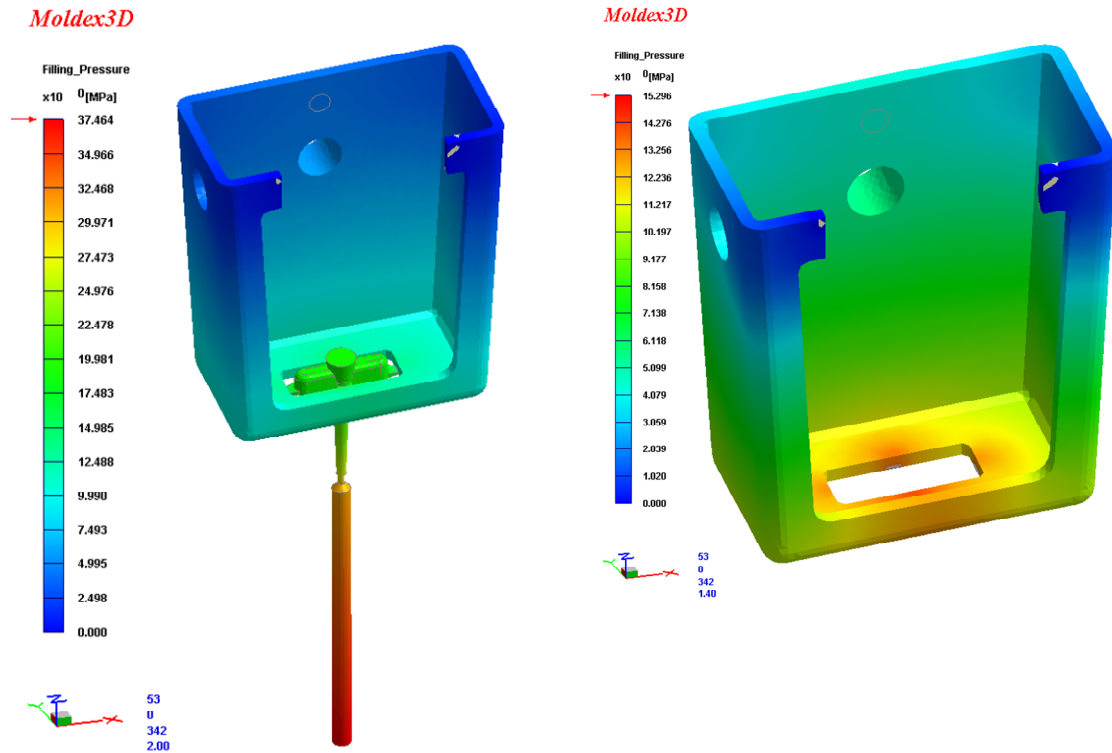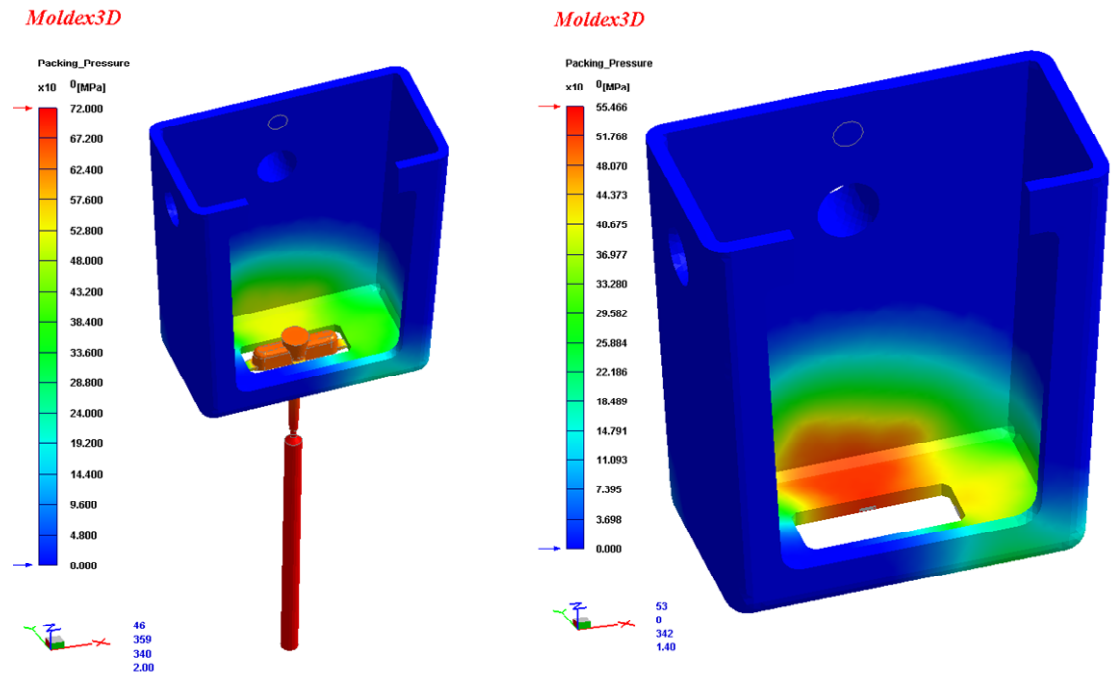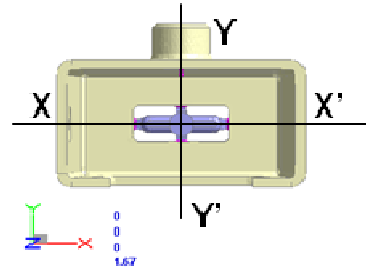
Pressure - Final of packing

Temperature - Final of filling
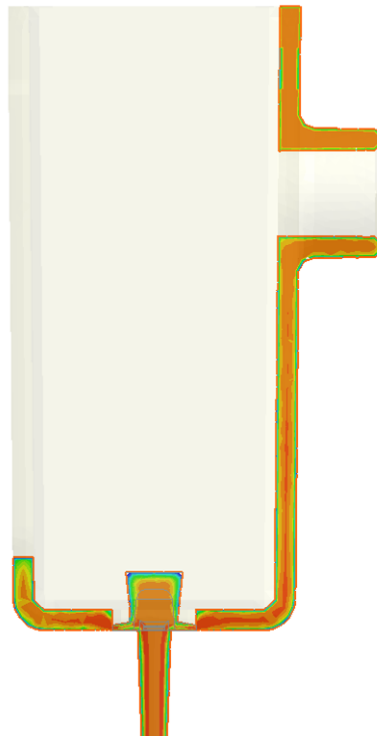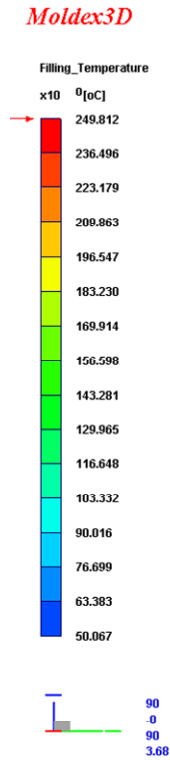
Section YY'
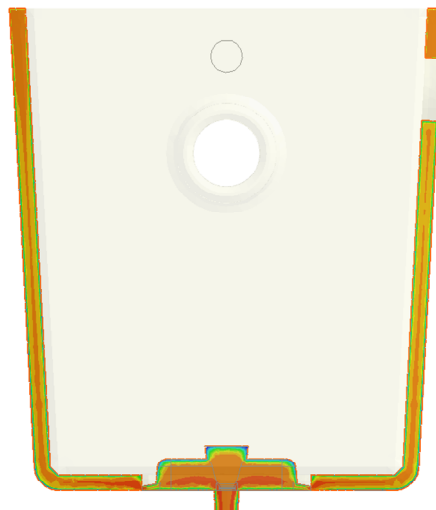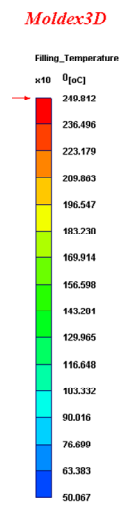
Section XX'

Temperature - Final of cooling
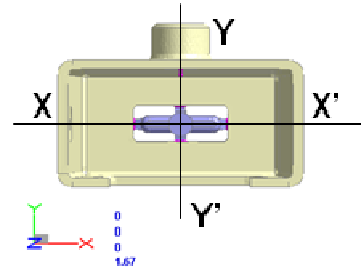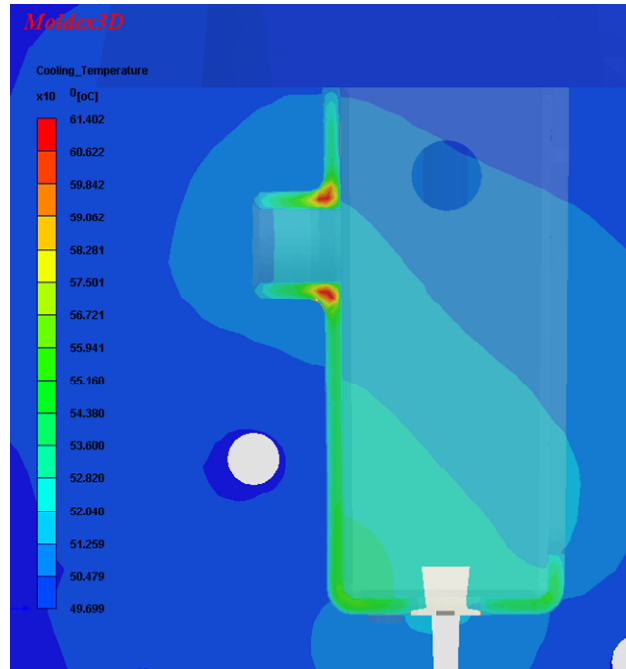
Section YY'

Section XX'
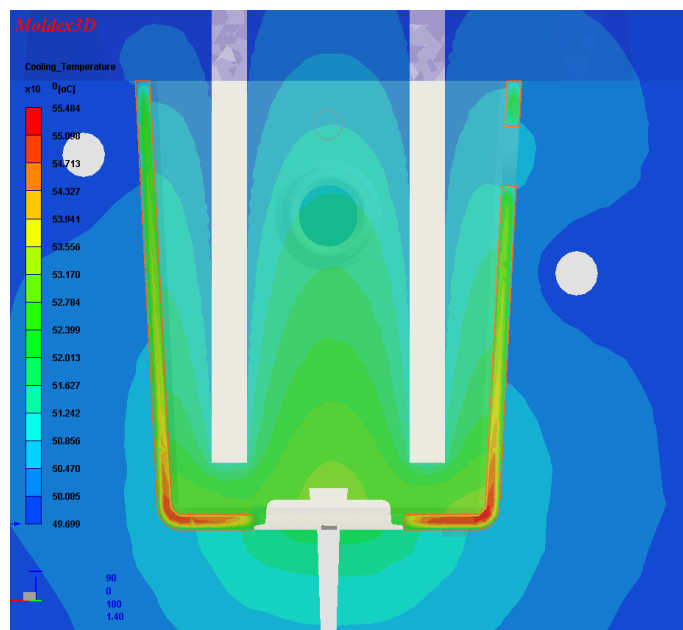
Surface Temperature - Final of cooling

Core side
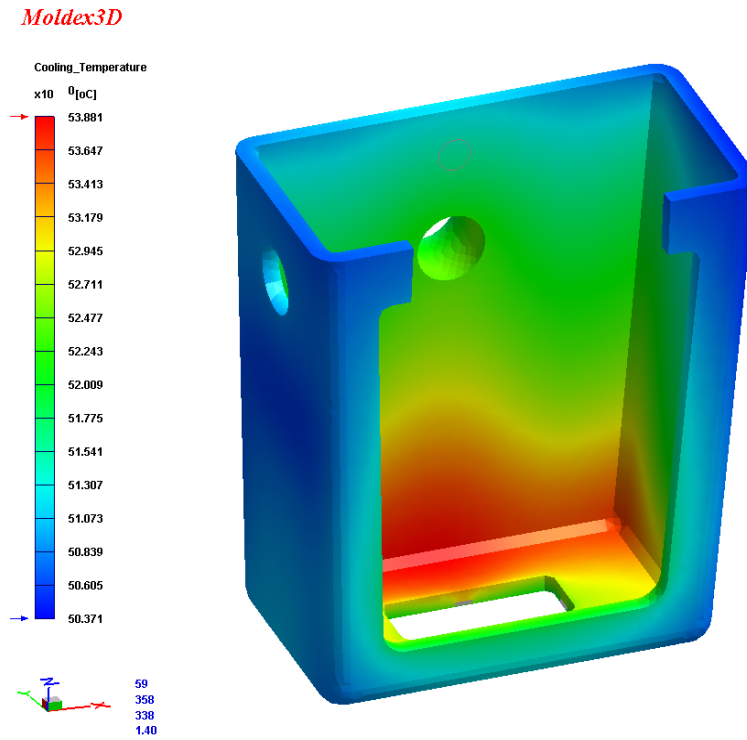
Cavity side
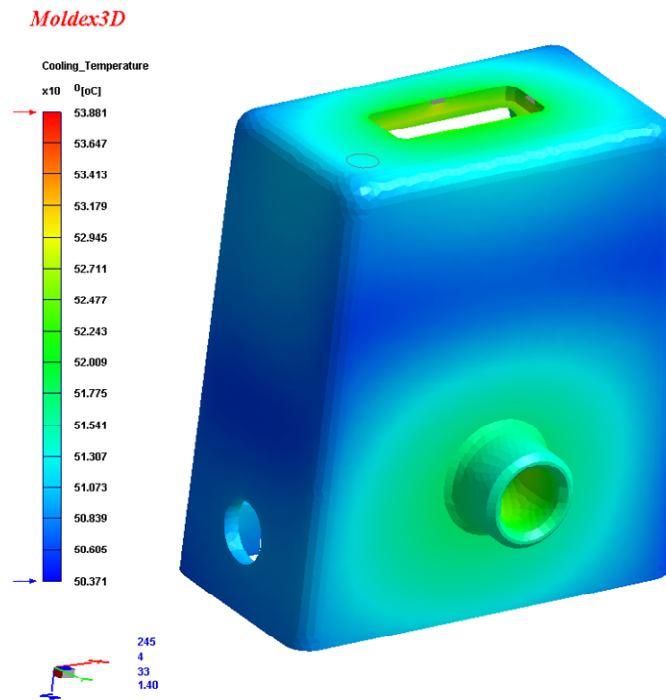
Temperature stabilization
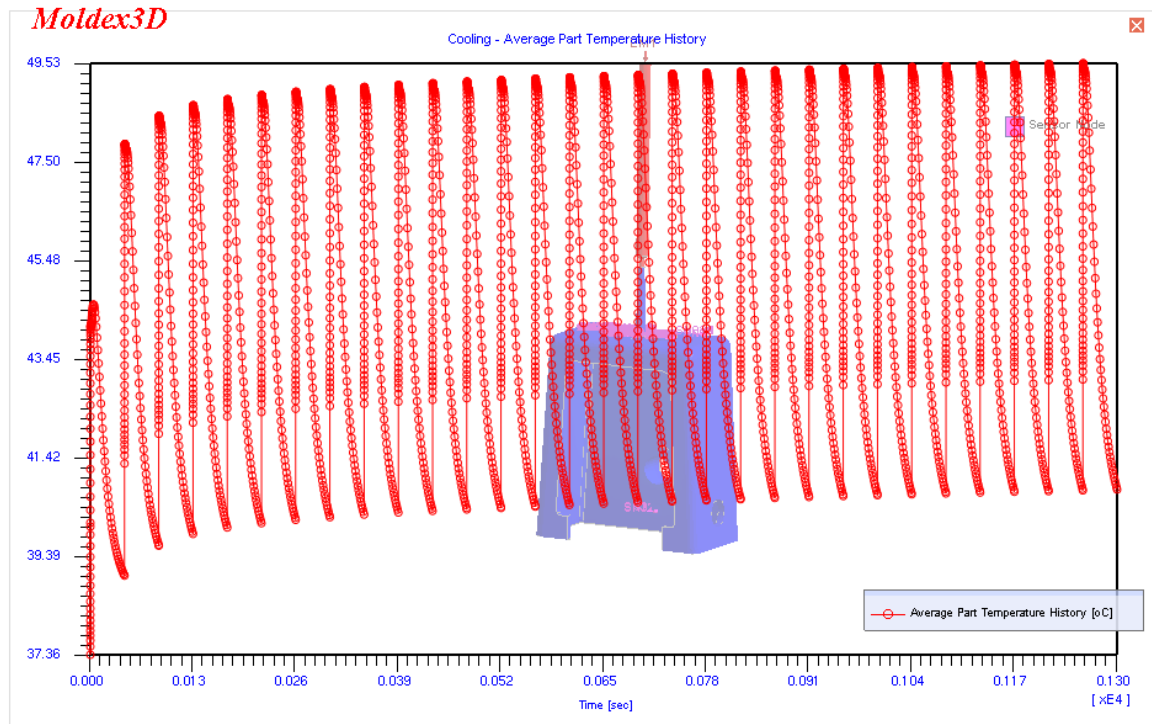
HM2 R$_1$S (BiResin L74 + 60% Al) -

Pressure - Final of filling
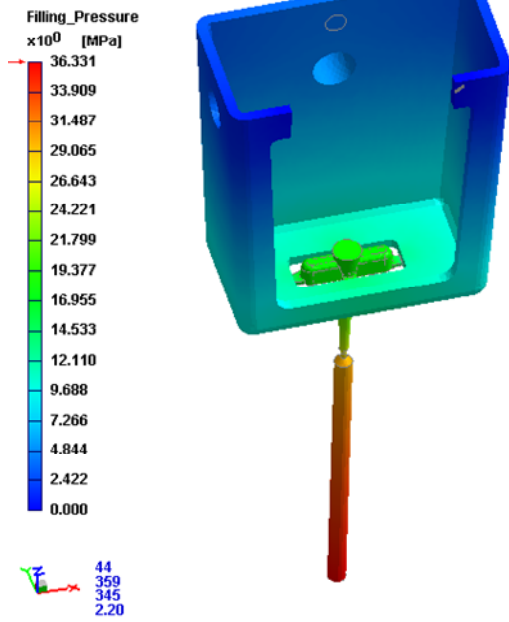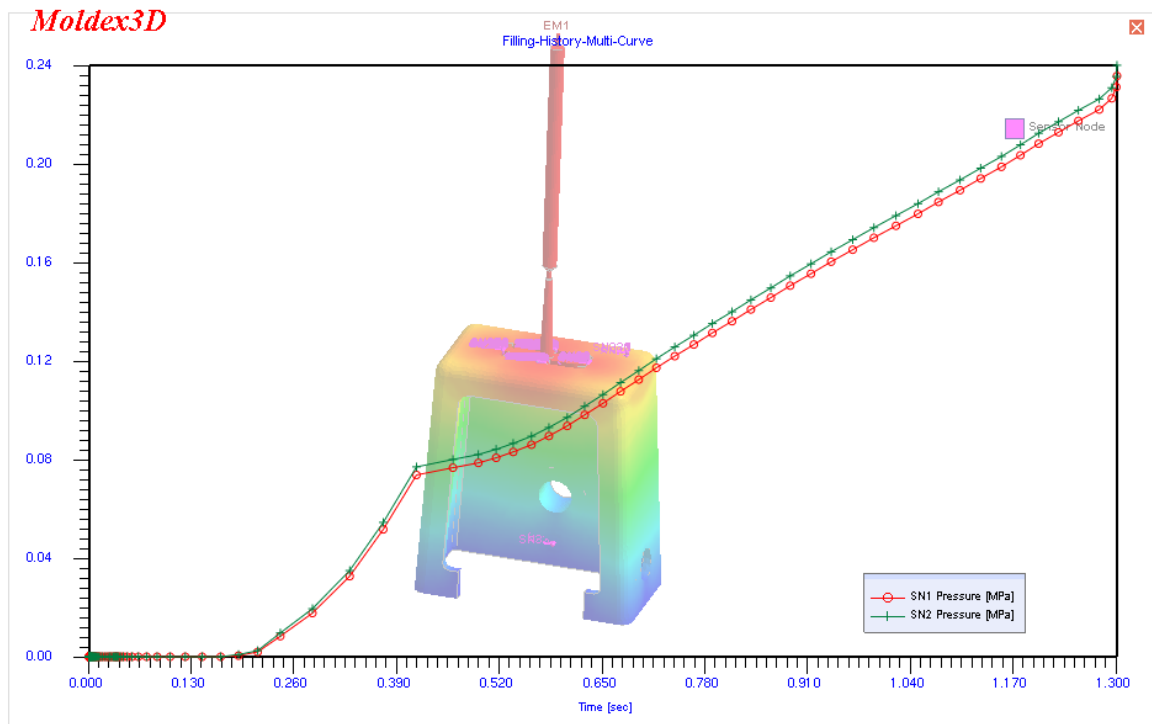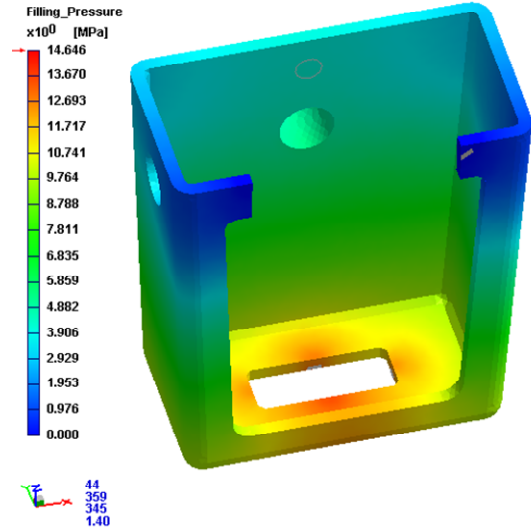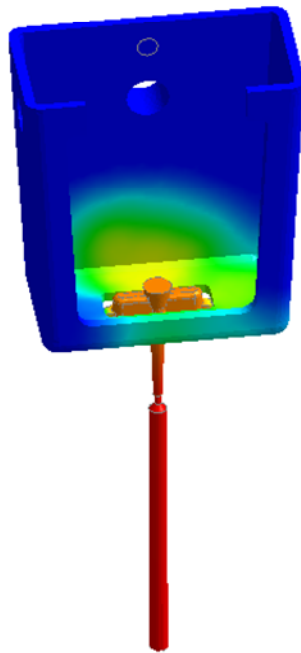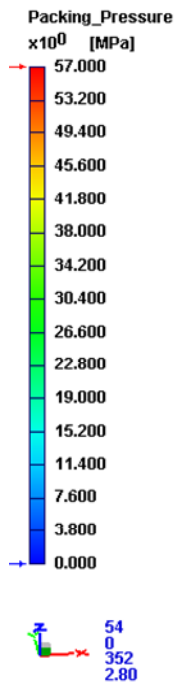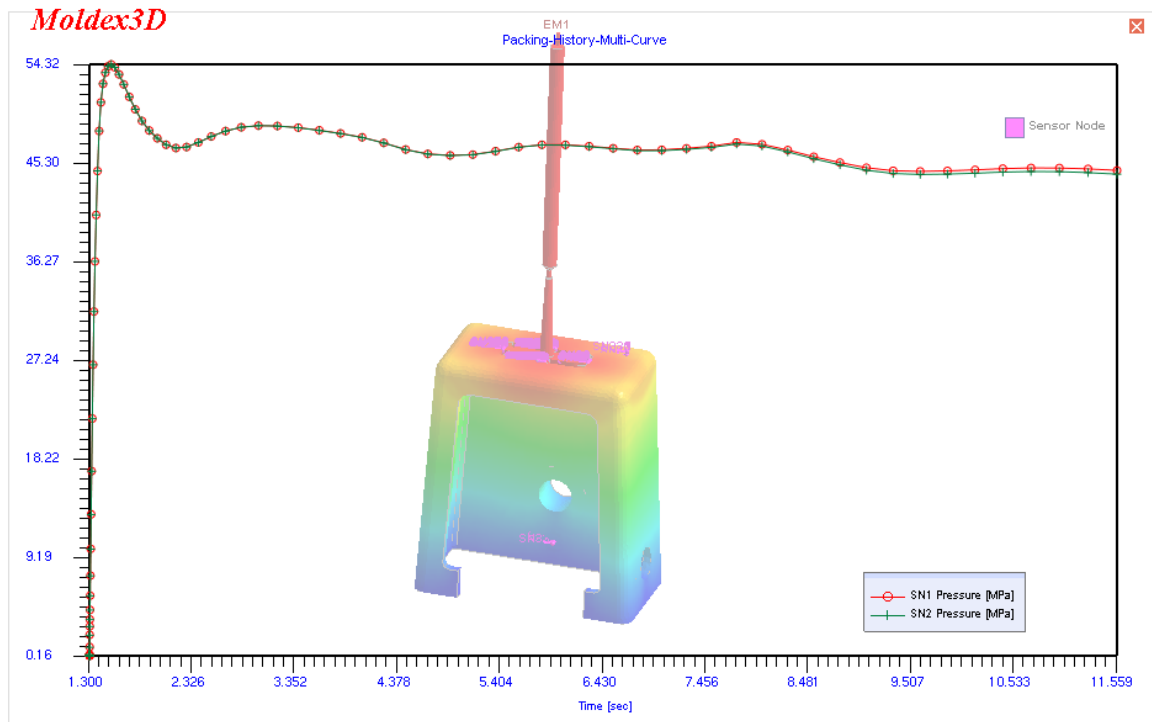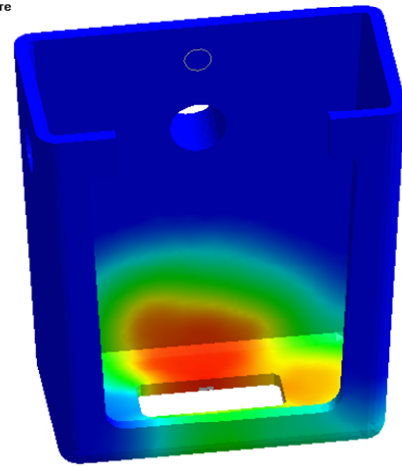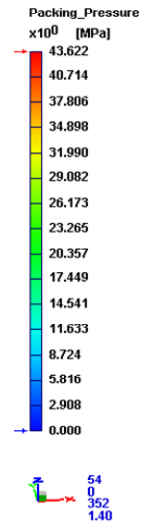
Pressure - Final of packing
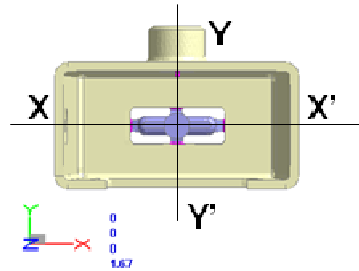
Temperature - Final of filling
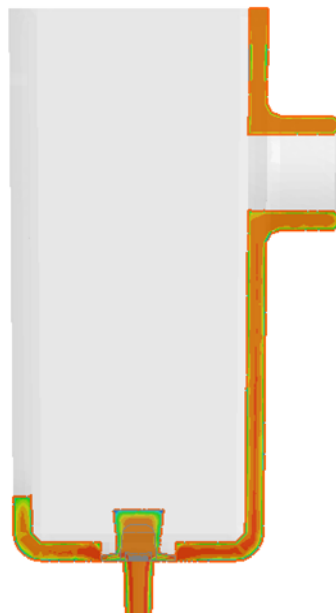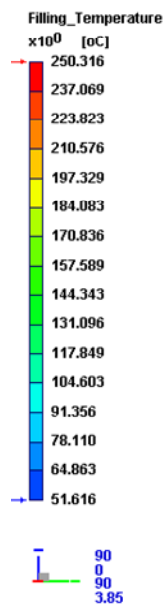
Section YY'
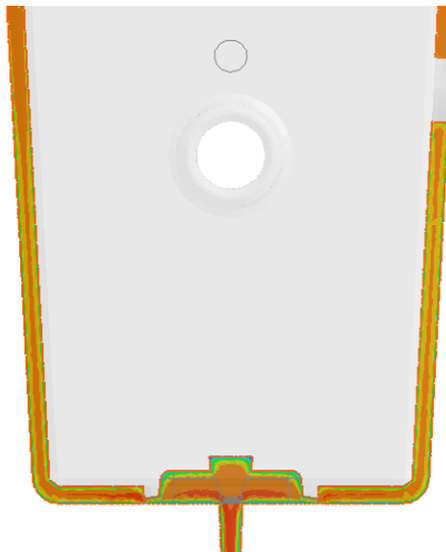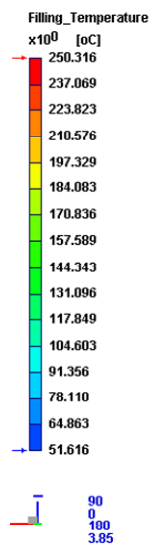
Section XX'

Temperature - Final of cooling
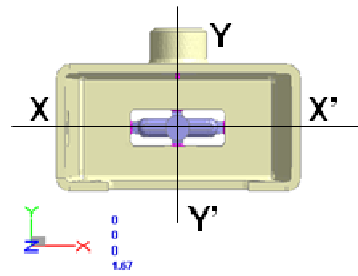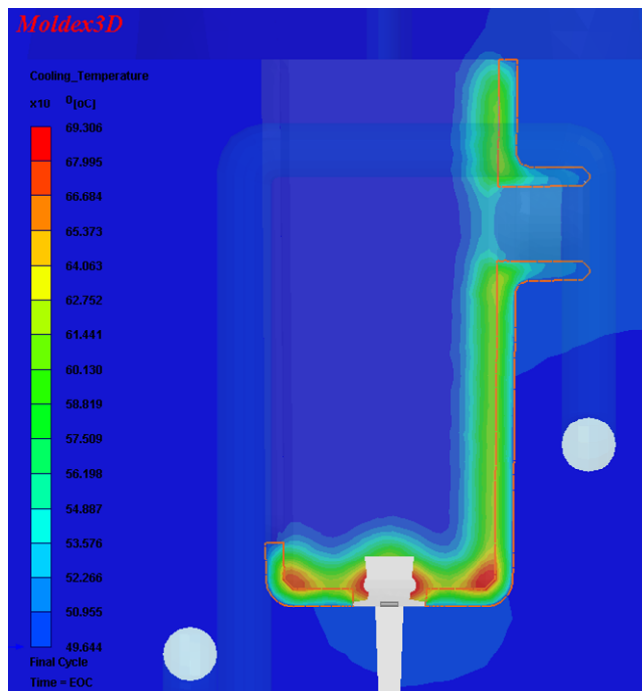
Section YY'
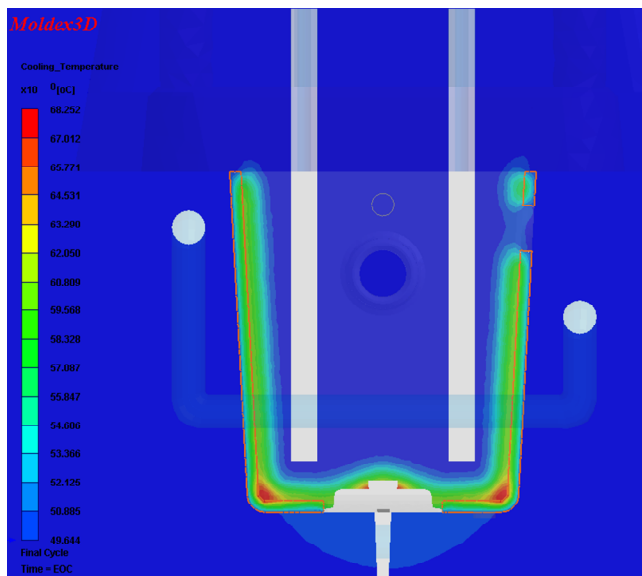
Section XX'

Surface Temperature - Final of cooling

Core side
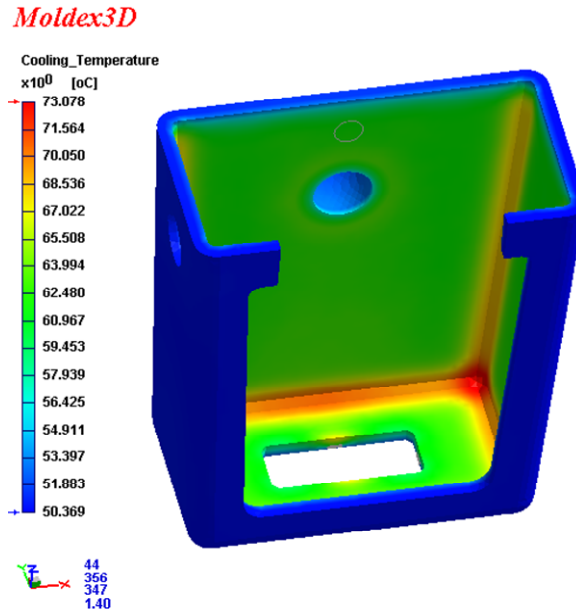
Cavity side
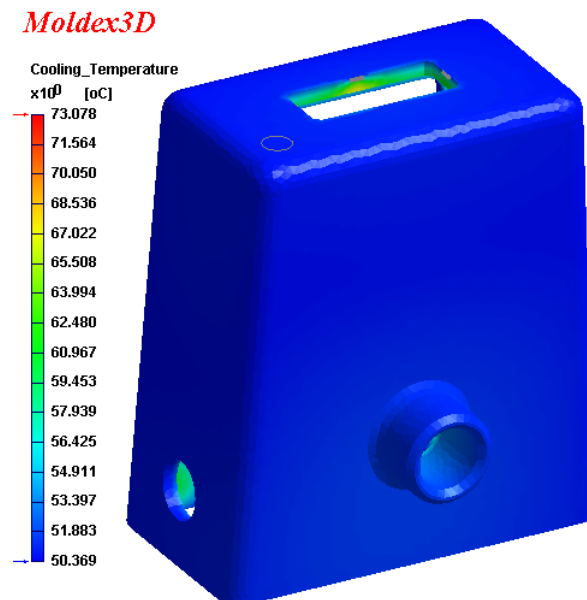
Temperature stabilization
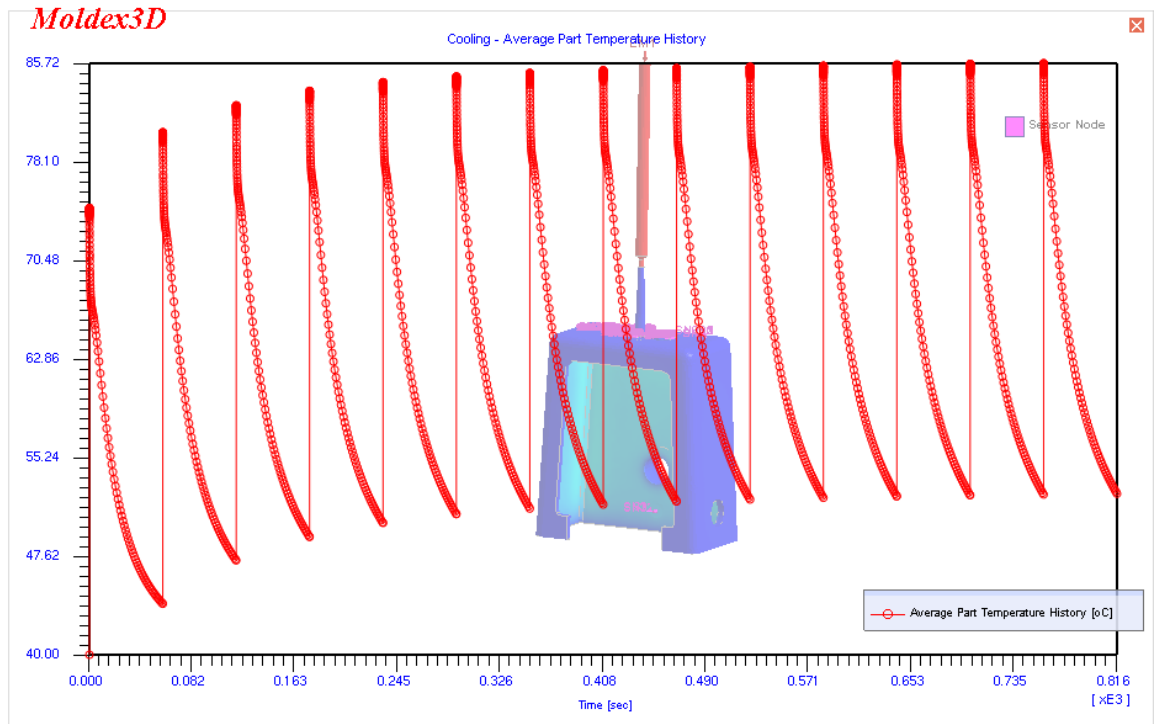
Pressure - Final of filling
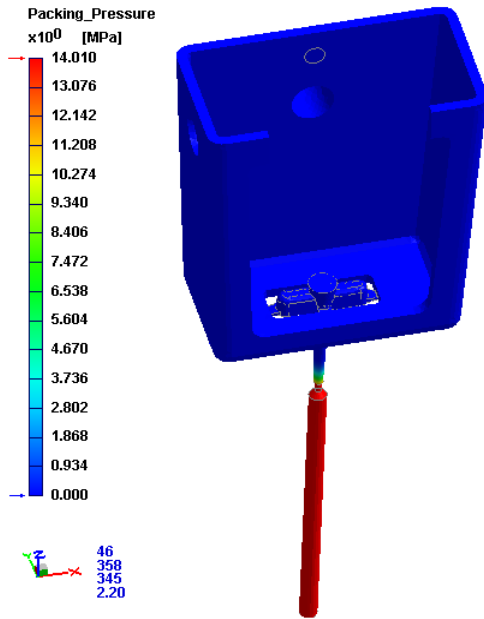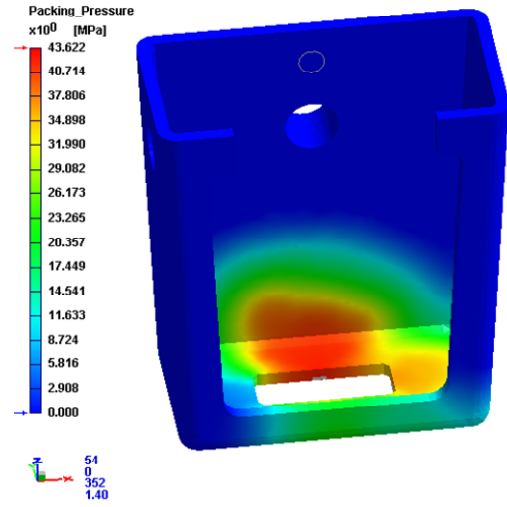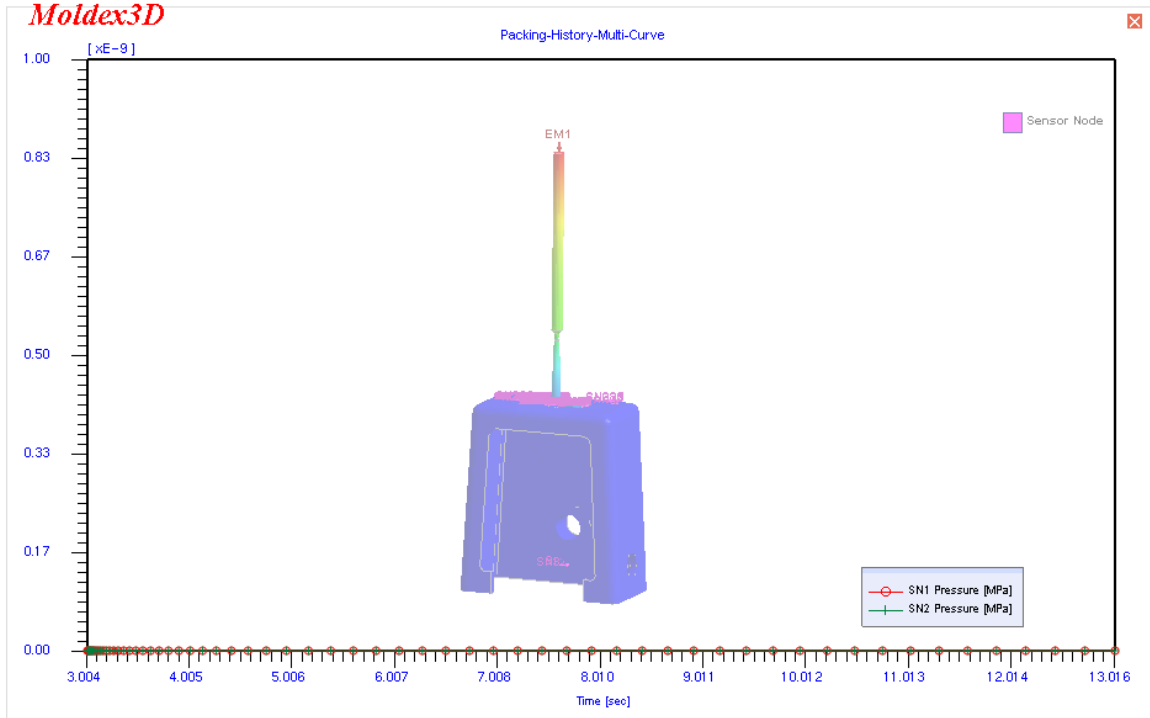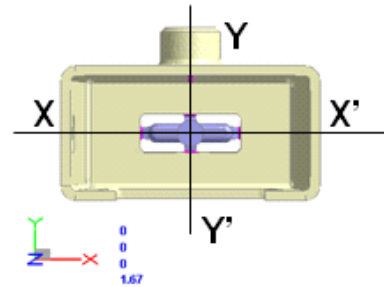
Pressure - Final of packing

Temperature - Final of filling
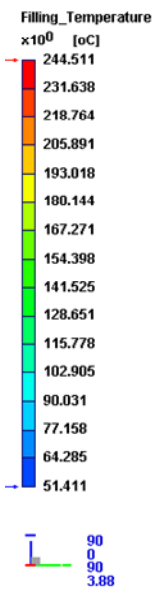
Section YY'
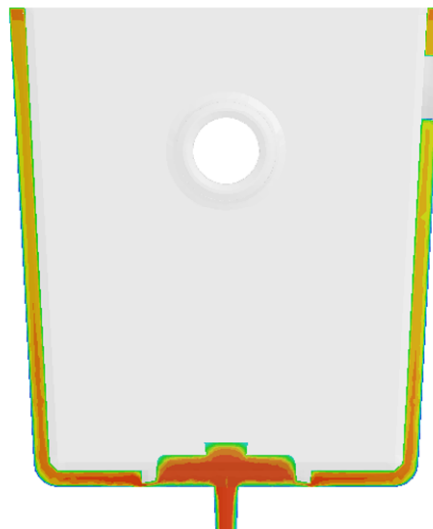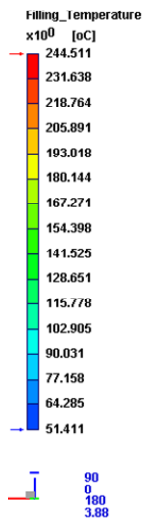
Section XX'

Temperature - Final of cooling
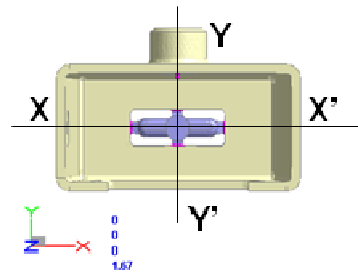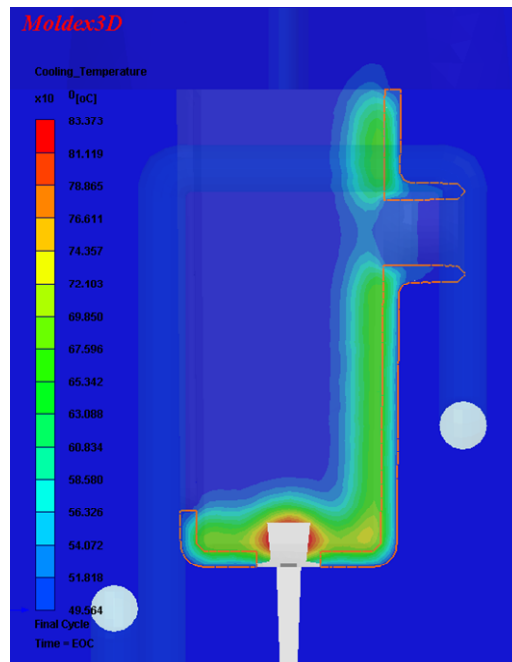
Section YY'
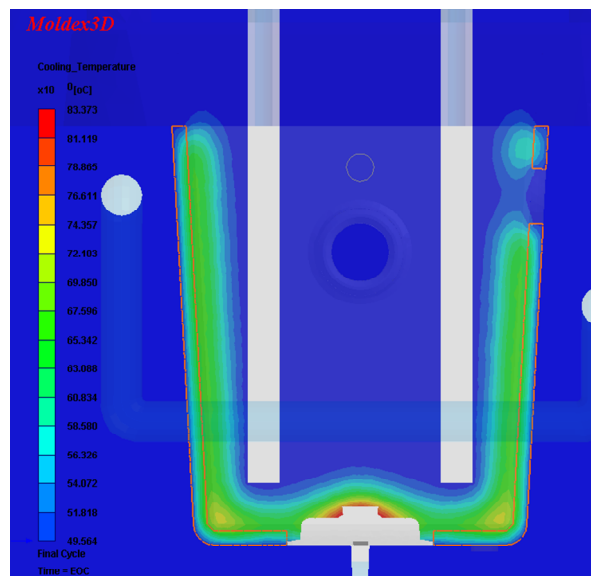
Section XX'

Surface Temperature - Final of cooling

Core side
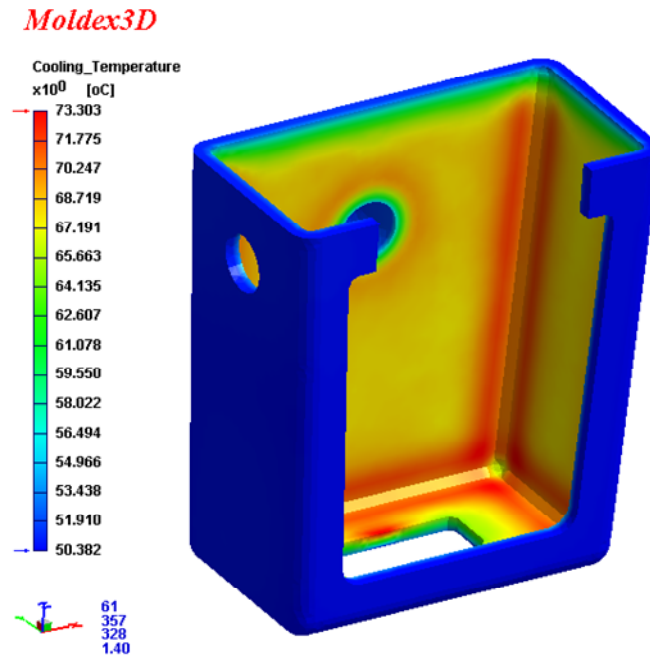
Cavity side
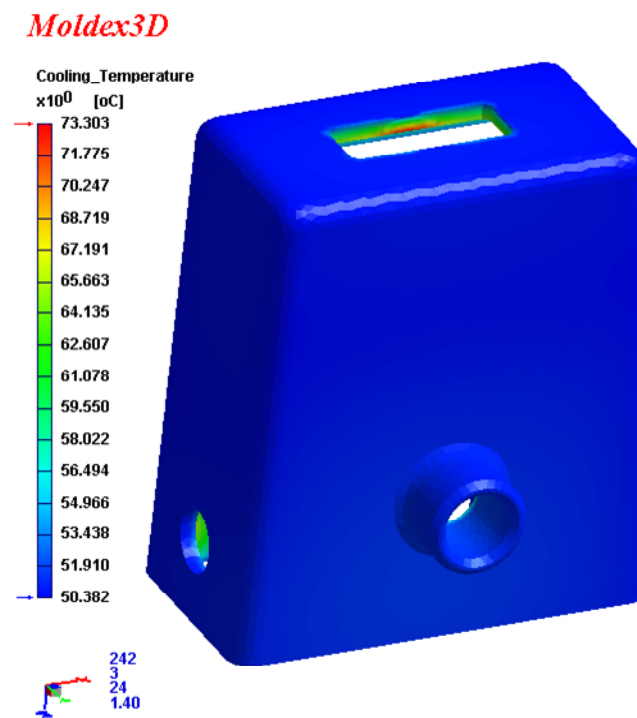
MOULDING PINS

Section YY'

A1   B1

8.36   8.49

A2   B2

Molding pin

Part
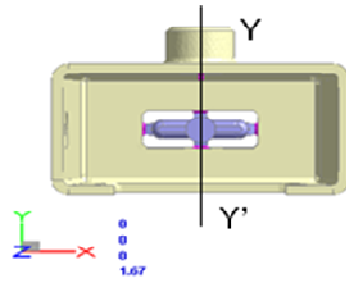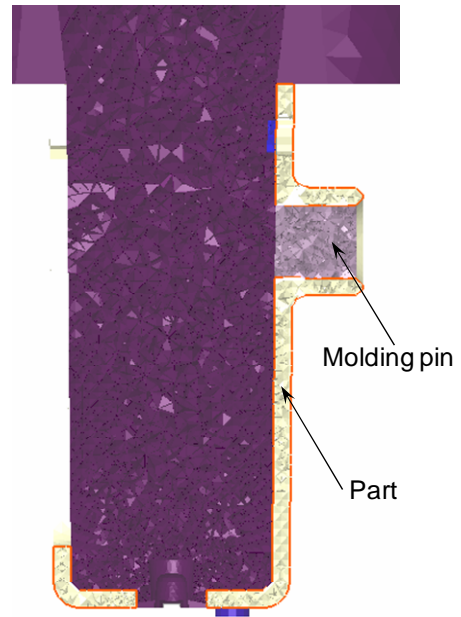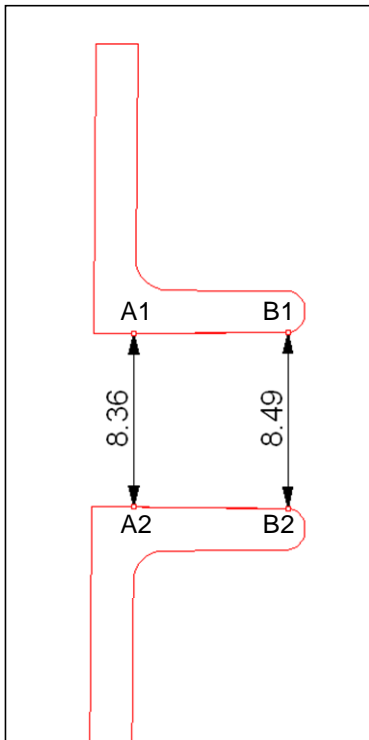
Temperature

STEEL
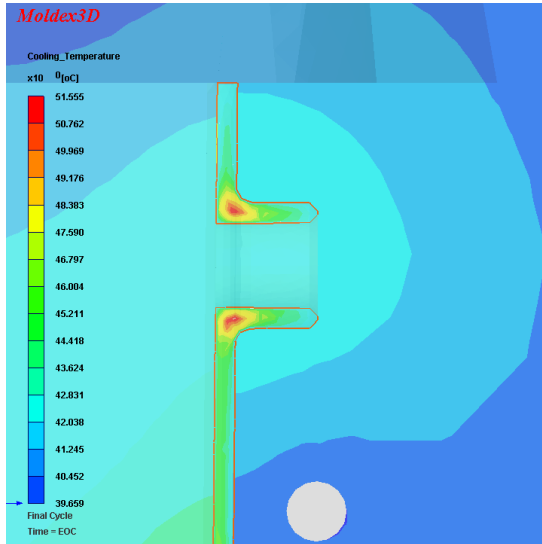
ProMetal
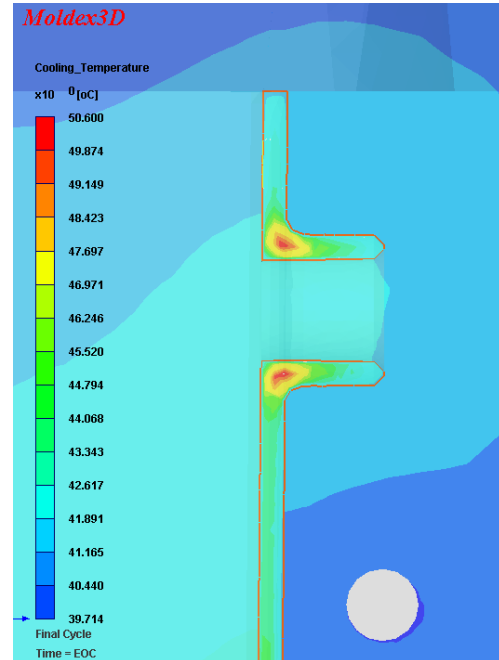
BIRESIN L74 + AL
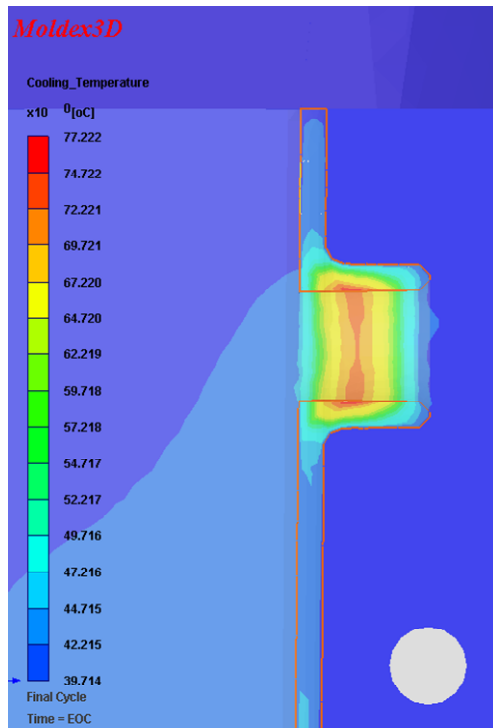
BIRESIN L74 + SSF
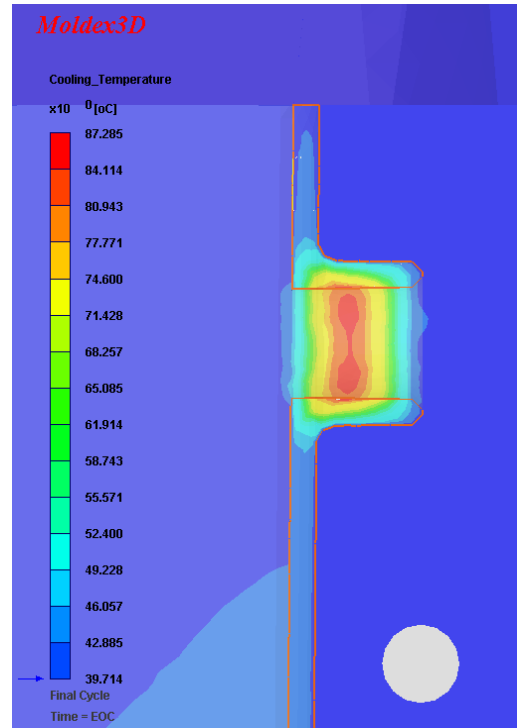
Moldex3D Report for Project

Run20
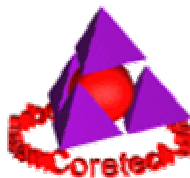
Company : *Moldex3D User*

Project Name : *HM2_exp*

Software : *Moldex3D R9.1 (9106.2)*

Author : *Administrator*

Date : Tuesday, February 09, 2010

1. Summary

Summary of the project

1.1. Summary

Mesh	Material(Part)	Process	Computation parameters
new model_1.mfe	PP_MoplenHP500N_1_2.mtr	HM2_exp_R1S.pro	HM2_exp20.cmx

1.2. Mesh Summary

Mesh Type	Mixed/BLM
No. cooling channel	2
Part dimension	54.54 x 36.31 x 60.63 (mm)
Mold dimension	290.04 x 240.00 x 222.00 (mm)
Cavity(Part) volume	15.9031 (cc)
Cold runner volume	0.397341 (cc)
Hot runner volume	0.551802 (cc)
Mold base volume	15383 (cc)
Cooling channel volume	34.5873 (cc)
Element number	1194203
Part elements	212517
Node number	239615

1.3. Material Summary
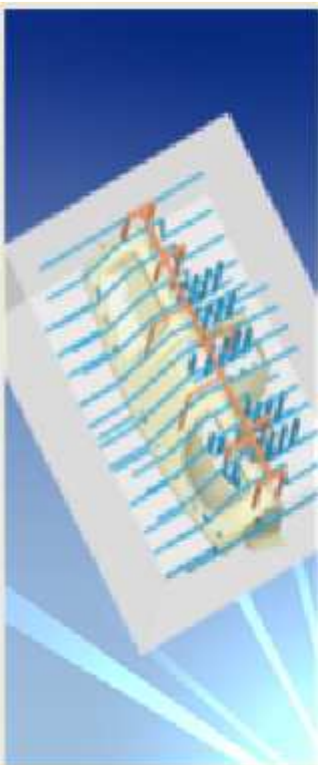
Material type	Thermoplastic
Generic name	PP
Supplier	Basell
Trade name	Moplen HP500N_1
MFI	Unavailable
Fiber percent	0.00 (%)
Linear shrinkage	2.40 (%)
Melt temperature range	220 - 250 (oC)
Mold temperature range	20 - 50 (oC)
Ejection temperature	103 (oC)
Freeze temperature	150 (oC)

1.4. Process Summary

Filling Time	1.3000 (sec)
Melt Temperature	230.0 (oC)
Mold Temperature	40.0 (oC)

Injection Pressure	500.00 (MPa)
PreFillPercentage	100.00 (%)
Injection Volume	16.3004 (cc)
Packing Time	10.0000 (sec)
Packing Pressure	56.00 (MPa)
VP Switch by volume(%) filled	98.00 (%)
Mold Opening Time	12.0000 (-)
Ejection Temperature	103.0 (oC)
Air Temperature	25.0 (oC)

Process - Project Settings

Setting method : CAE mode

In this mode, process parameters are not derived from the molding machine informations. You may freely specify process conditions for simulation.

Process File : HM2_exp_R1S.pro

Mesh File : new model_1.mfe

Material File : PP_MoplenHP500N_1_2.mtr
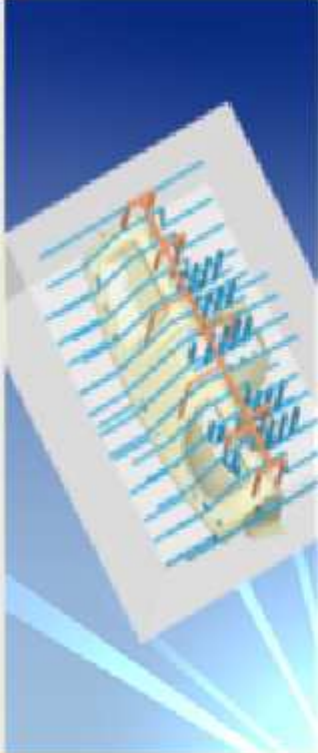
Maximum injection pressure	500	MPa
Maximum packing pressure	56	MPa

Process - Filling/Packing Settings
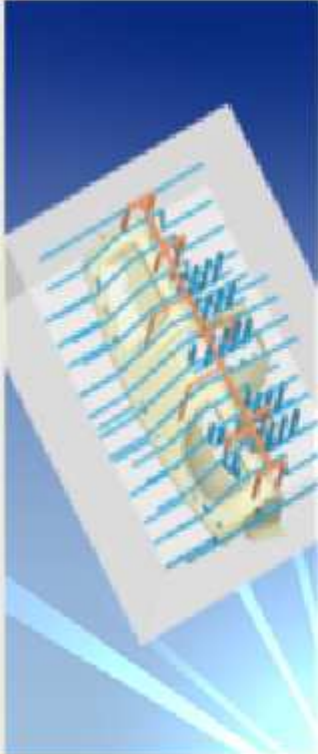
Filling setting

Filling time : 1.3 sec

Flow rate profile (1)...

Injection pressure profile (1)...

VP switch-over

By volume(%) filled   as   98   %

Packing setting

Packing time : 10 sec

Packing pressure refer to machine pressure

Packing pressure profile (1)...
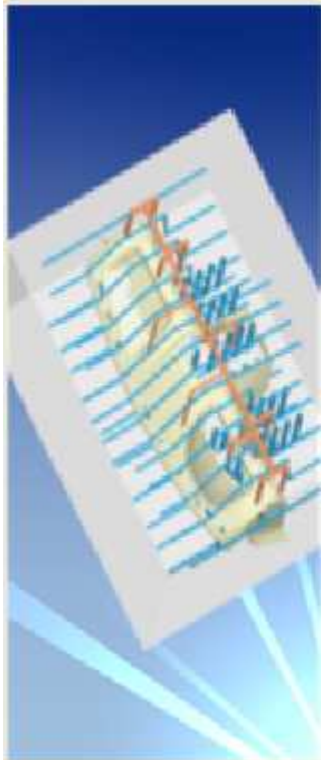
| Melt Temperature | 230 | oC |
| Mold Temperature | 40 | oC |

Advanced Setting...

Process - Cooling Settings

Item	Value	Unit
Air Temperature	25	oC
Eject Temperature	103	oC
Cooling Time	35	sec
Mold-Open Time	12	sec

Cooling Channel/Heating Rod...   Mold Metal Material...

Eject Criteria...   Part Insert Initial Temperature...

Estimate Cooling Time...

Process - Summary

[Filling]	
Filling time (sec)	1.3
Melt Temperature (oC)	230
Mold Temperature (oC)	40
Maximum injection pressure (MPa)	500
Injection volume (cm^3)	16.3004
[Packing]	
Packing Time (sec)	10
Maximum packing pressure (MPa)	56
[Cooling]	
Cooling Time (sec)	35
Mold-Open Time (sec)	12
Eject Temperature (oC)	103
Air Temperature (oC)	25
[Miscellaneous]	
Cycle time (sec)	58.3
Mesh file	new model_1.mfe
Material file	PP_MoplenHP500N_1_2.mtr

Moldex3D Report for Project

Run20 - Cooling

1. Table of content

2. Temperature

Result remark	Statistics plot
Temperature distribution of current state.	
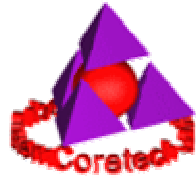
Temperature

Back

3. Cooling Time

Result remark	Statistics plot
This is the estimated cooling time required to be cooled enough to be ejected under the given design and process conditions. In other words, it means the time required to cool down below eject temperature. Use [Slicing] or [Clipping] function to view interior distribution.	

Cooling Time

4. Density

Result remark	Statistics plot
This shows the density distribution. In general, frozen region will show a greater value of density and molten region will have a lower density value. Non-uniformity in density is a source of part warpage.	

Density

Back

5. Heat Flux

Result remark	Statistics plot
This is the heat flux of the part/mold surface. This value means the heat-dissipation rate per unit area (flux) of part-mold interface. In Cycle average Analysis, it shows the average heat flux during the cycle time. In Transient Analysis, it shows the heat flux in this instant, A higher heat flux value indicates better cooling efficiency.	

Heat Flux

Back

6. Heat Load

Result remark	Statistics plot
This is the heat load of the interface of the part/moldbase/cooling channel. This value means the heat-released accumulation of the part via the part-mold interface.	

Heat Load
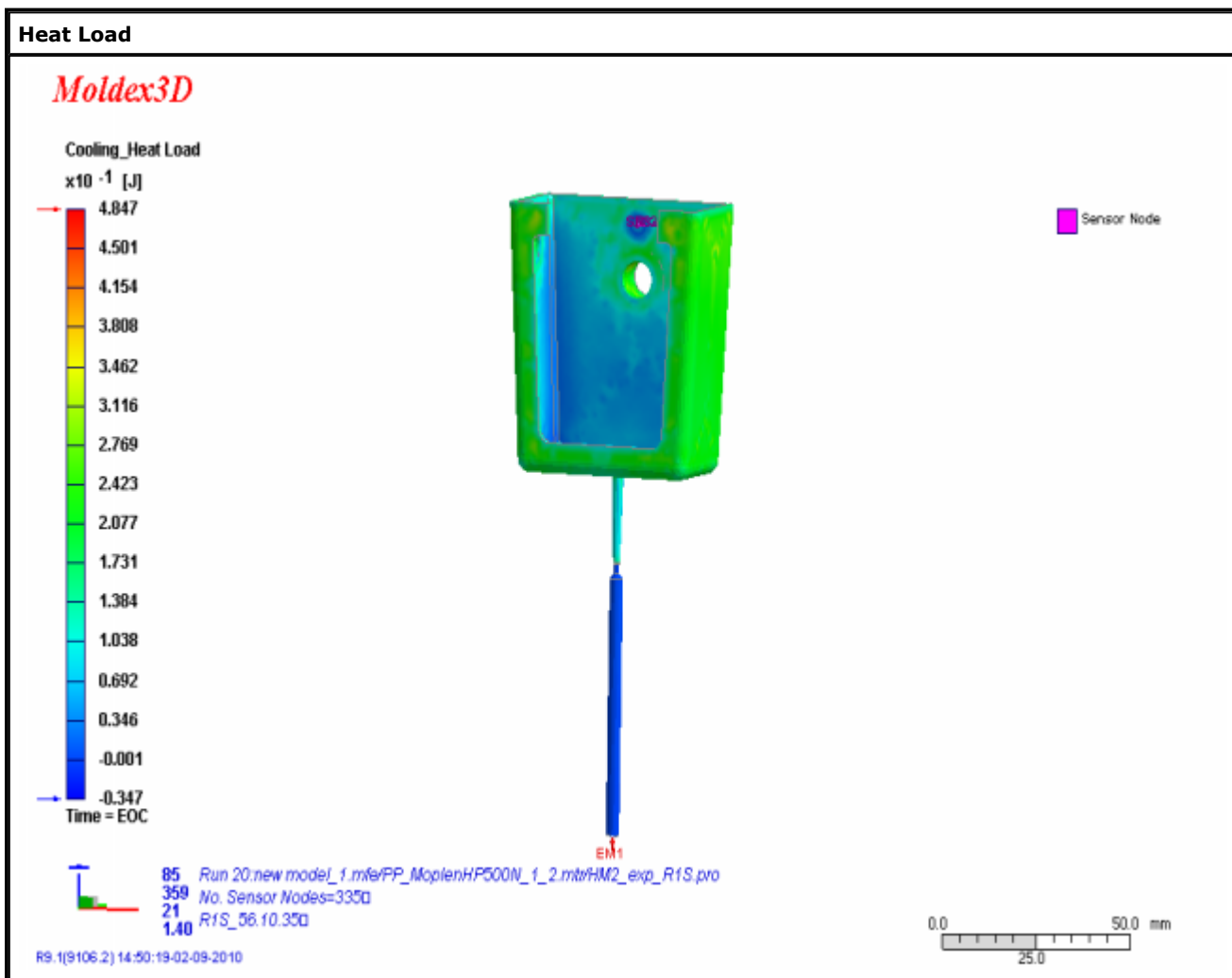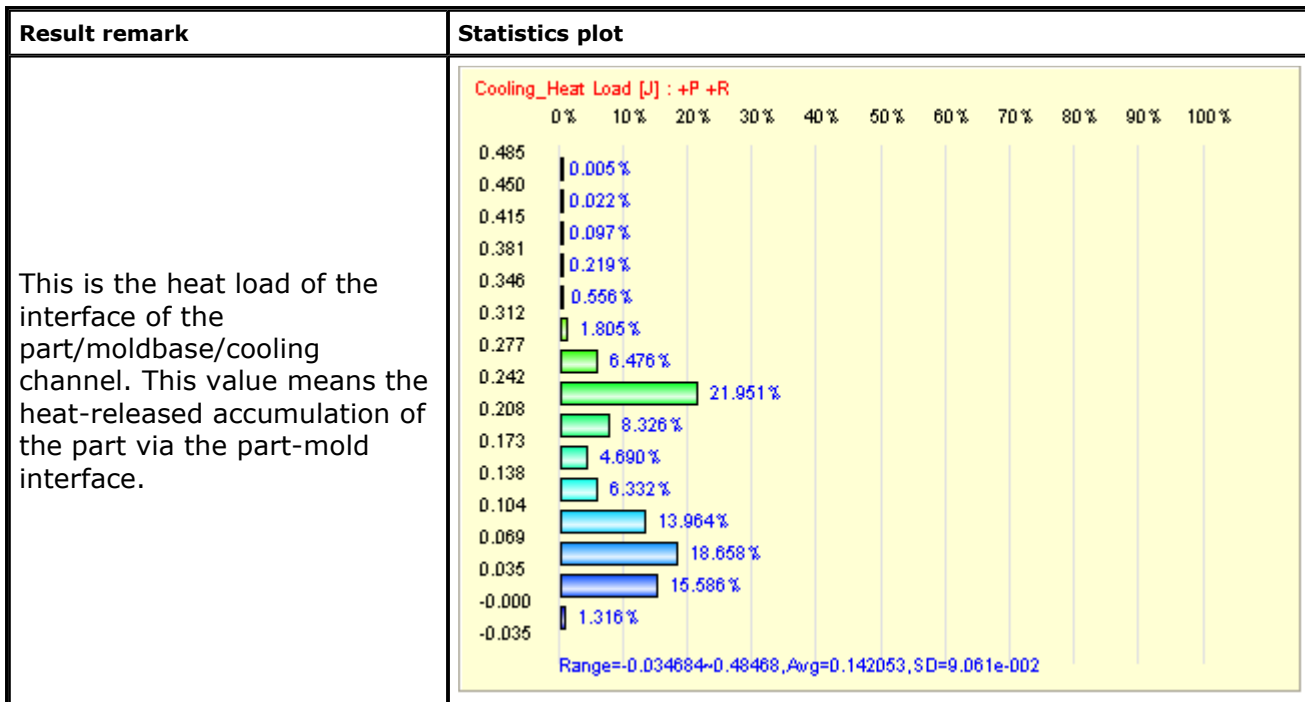
Back

7. Cooling Efficiency

Result remark	Statistics plot
This is the cooling efficiency of the cooling channel. If Q2 is the total absorbed heat through one cooling channel surface and Qm is the absorbed heat through mold surface via surroudings interface, the cooling efficiency of the cooling channel is defined as Q2/ (Q2+Qm) *100%. This data shows the percentage of heat withdrawn by the cooling channel. Positive value means cooling efficiency. Negative value represents heating efficiency.	

Cooling Efficiency
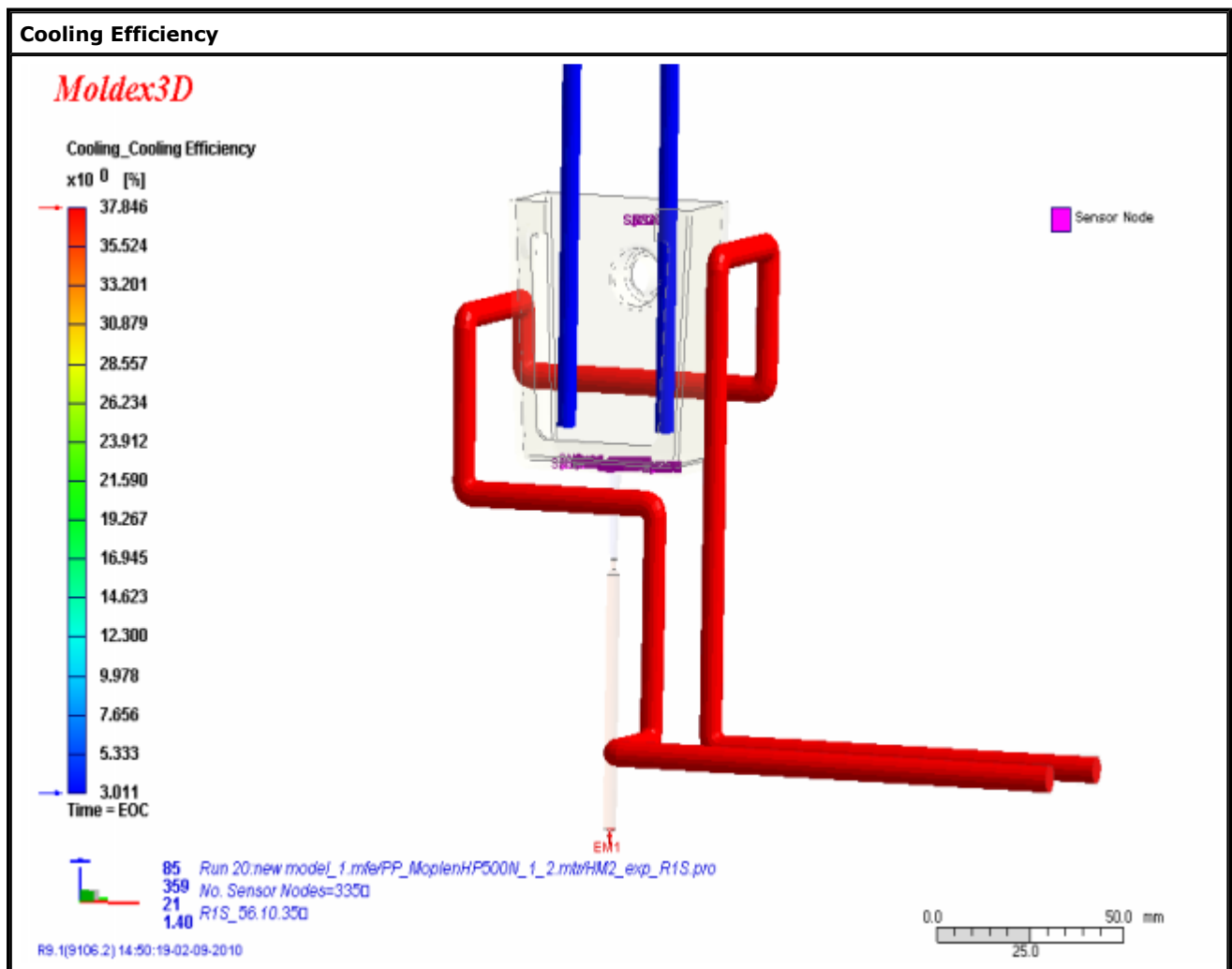
8. Melting Core

Result remark
This shows isosurface of plastic melt-zone. Region enclosed by the isosurface has temperature higher than freeze temperature specified in the process condition. This data can be used to check frozen layer thickness (region outside the melting core).

Melting Core
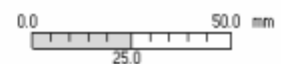
10. XY_Average Part Temperature History
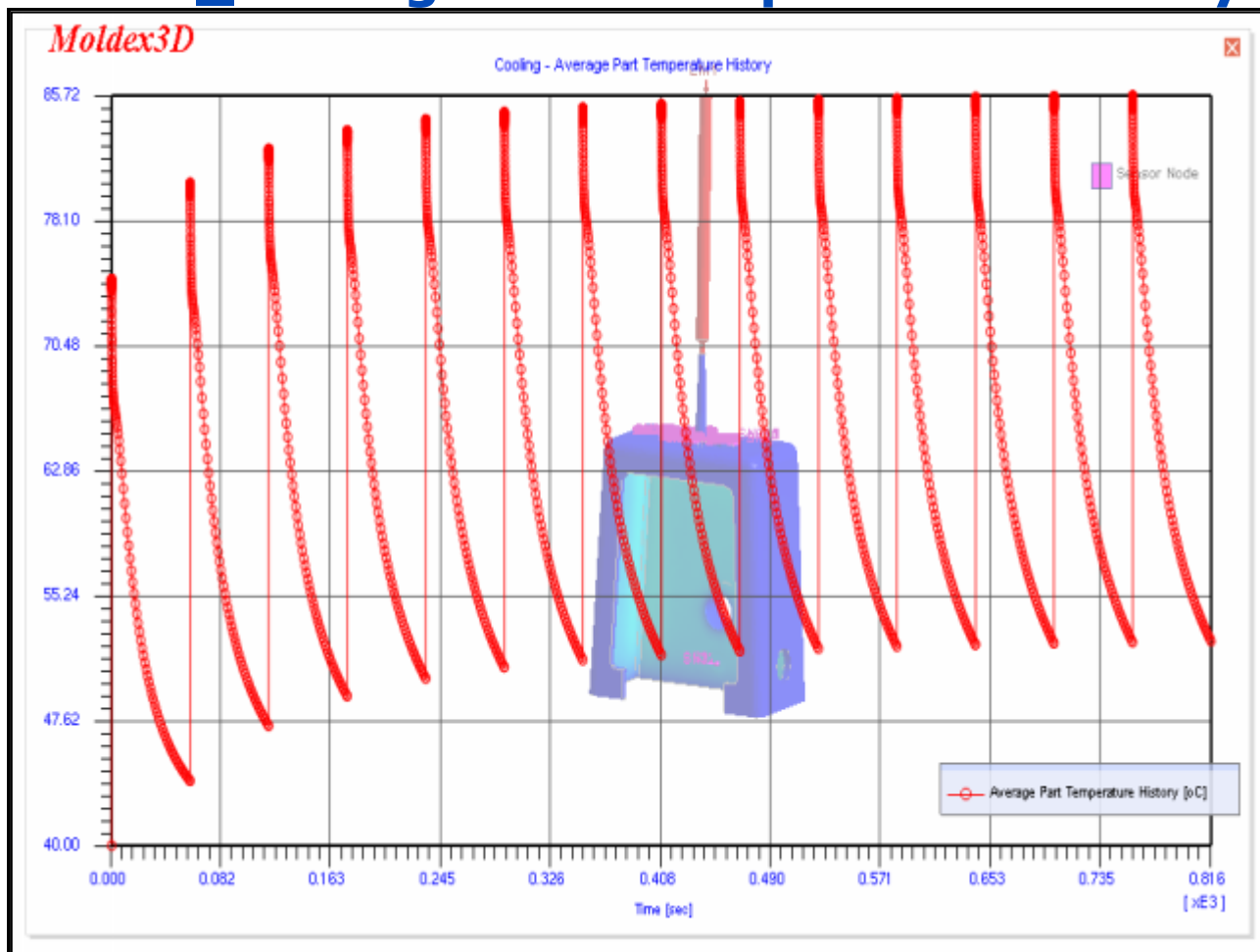
#

Appendix 6

ANSYS *Workbench* simulations

Project

First Saved	Sunday, March 09, 2008
Last Saved	Monday, January 25, 2010
Product Version	11.0 Release

Contents

Report Not Finalized

Not all objects described below are in a finalized state. As a result, data may be incomplete, obsolete or in error. View first state problem. To finalize this report, edit objects as needed and solve the analyses.

Units

TABLE 1

Unit System	Metric (mm, kg, N, °C, s, mV, mA)
Angle	Degrees
Rotational Velocity	rad/s

Model 3

Geometry

TABLE 2
Model 3 > Geometry

Object Name	*Geometry*
State	Fully Defined
Definition	
Source	HM1_Core_Plates.SLDASM
Type	SolidWorks
Length Unit	Meters
Element Control	Program Controlled
Display Style	Part Color
Bounding Box	

Length X	196.77 mm
Length Y	196.77 mm
Length Z	132. mm
Properties	
Volume	2.764e+006 mm³
Mass	20.414 kg
Statistics	
Bodies	4
Active Bodies	4
Nodes	86699
Elements	48559
Preferences	
Import Solid Bodies	Yes
Import Surface Bodies	Yes
Import Line Bodies	Yes
Parameter Processing	Yes
Personal Parameter Key	DS
CAD Attribute Transfer	No
Named Selection Processing	No
Material Properties Transfer	No
CAD Associativity	Yes
Import Coordinate Systems	No
Reader Save Part File	No
Import Using Instances	Yes
Do Smart Update	No
Attach File Via Temp File	No
Analysis Type	3-D
Mixed Import Resolution	None
Enclosure and Symmetry Processing	Yes

TABLE 3
Model 3 > Geometry > Parts

Object Name	Plate1-1	Plate2-1	0010 - M4-1	0010 - M3-1
State	Meshed			
Graphics Properties				
Visible	Yes			
Transparency	1			
Definition				
Suppressed	No			
Material	Steel_P20			BiresinL74_60Al
Stiffness Behavior	Flexible			
Nonlinear Material Effects	Yes			
Bounding Box				
Length X	196.77 mm		41.98 mm	78.721 mm
Length Y	196.77 mm		41.98 mm	79.95 mm
Length Z	36. mm	52. mm	104. mm	96. mm
Properties				
Volume	1.1899e+006 mm³	1.2869e+006 mm³	1.0094e+005 mm³	1.863e+005 mm³
Mass	9.2809 kg	10.038 kg	0.78732 kg	0.3074 kg
Centroid X	158.86 mm	159.44 mm	159.43 mm	159.44 mm
Centroid Y	-14.5 mm	-14.986 mm	-14.898 mm	-14.951 mm
Centroid Z	-5.7978 mm	35.003 mm	44.143 mm	57.633 mm
Moment of Inertia Ip1	29627 kg·mm²	40952 kg·mm²	797.03 kg·mm²	397.24 kg·mm²
Moment of Inertia Ip2	29686 kg·mm²	40543 kg·mm²	796.26 kg·mm²	397.07 kg·mm²
Moment of Inertia Ip3	57325 kg·mm²	77374 kg·mm²	185.34 kg·mm²	206.94 kg·mm²
Statistics				

Nodes	33902	38669	2593	11535
Elements	19009	21905	1271	6374

FIGURE 1
Model 3 > Geometry > Plate1-1 > Figure
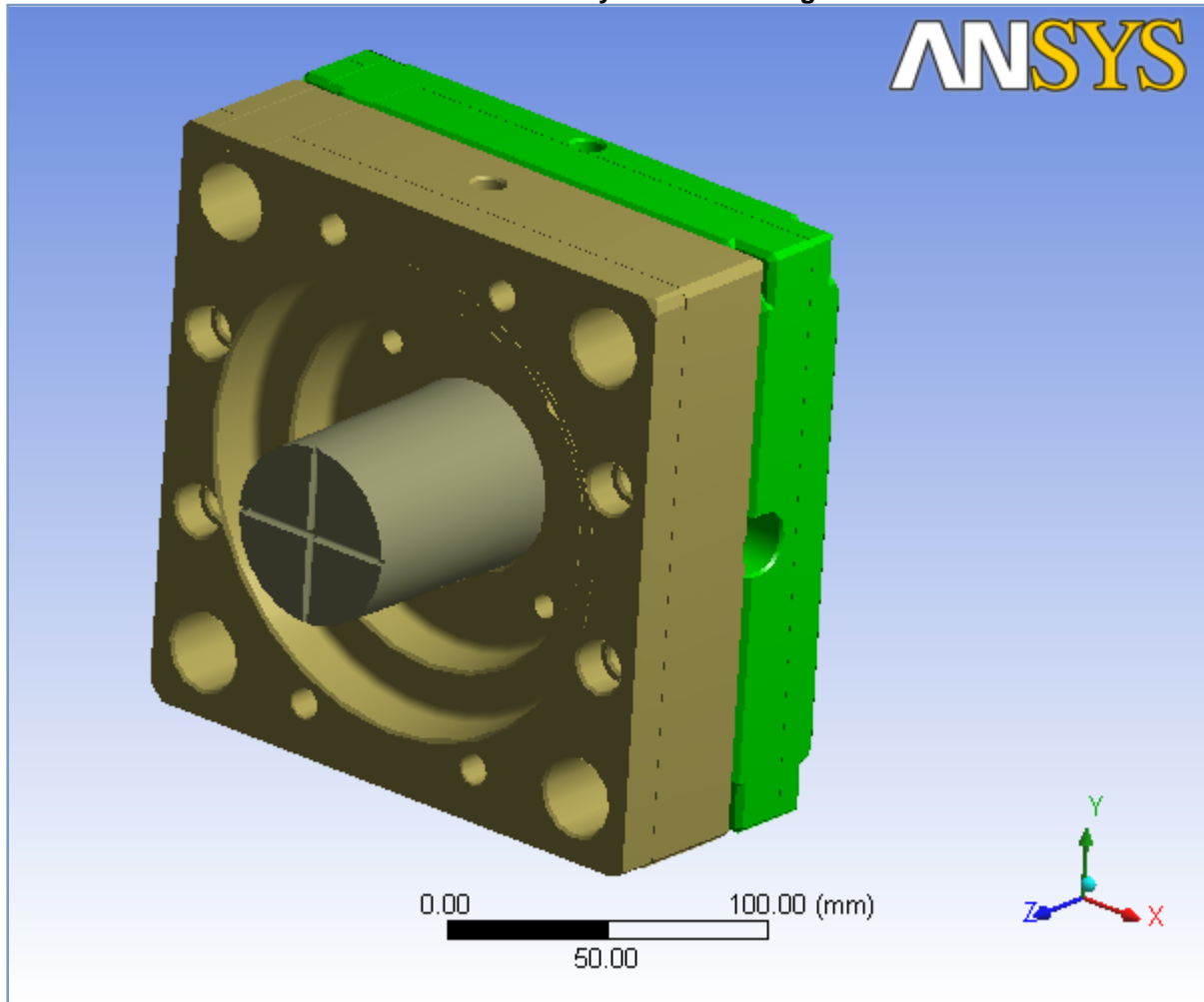
FIGURE 2
Model 3 > Geometry > Plate2-1 > Figure
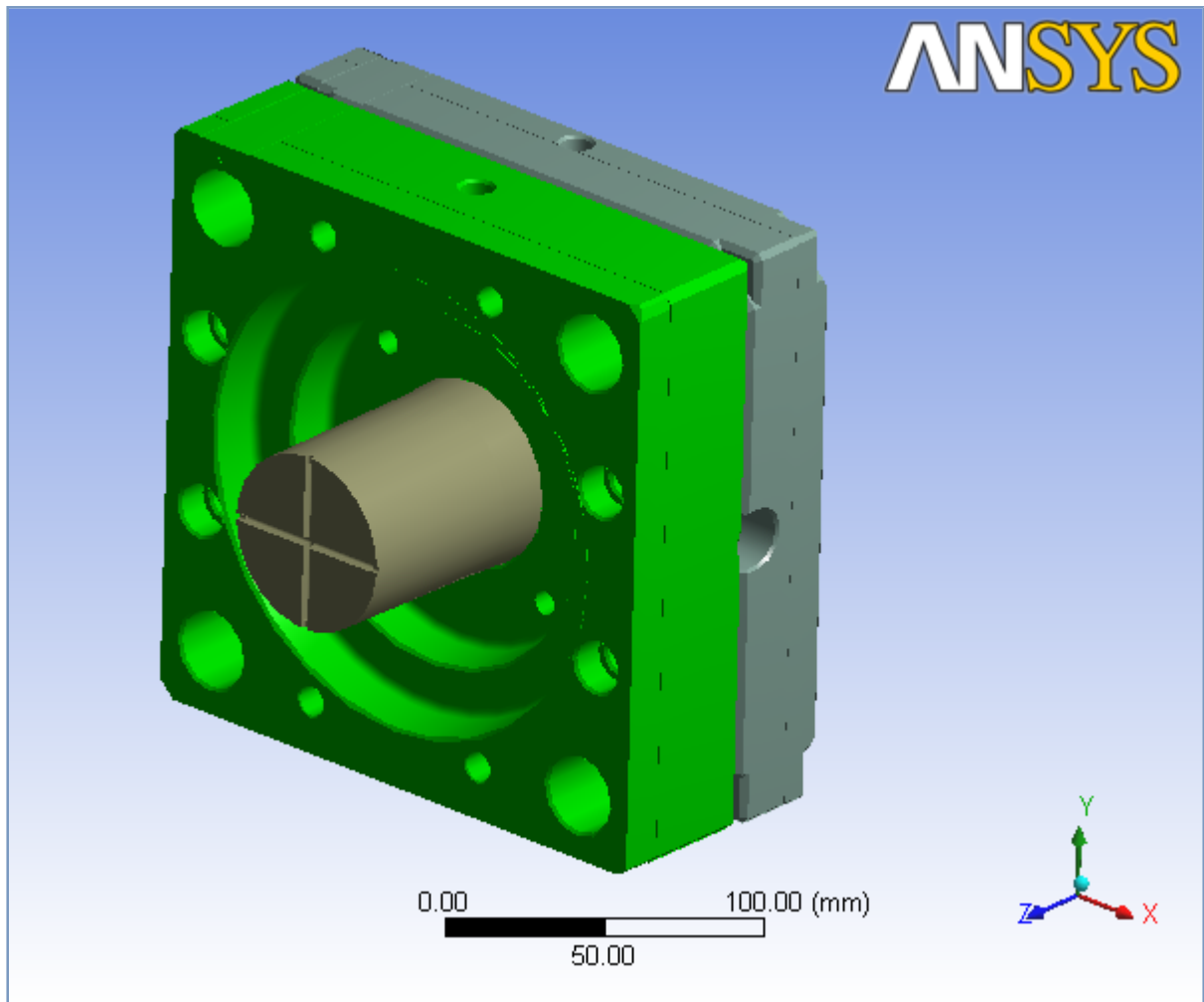
FIGURE 3
Model 3 > Geometry > 0010 - M4-1 > Figure
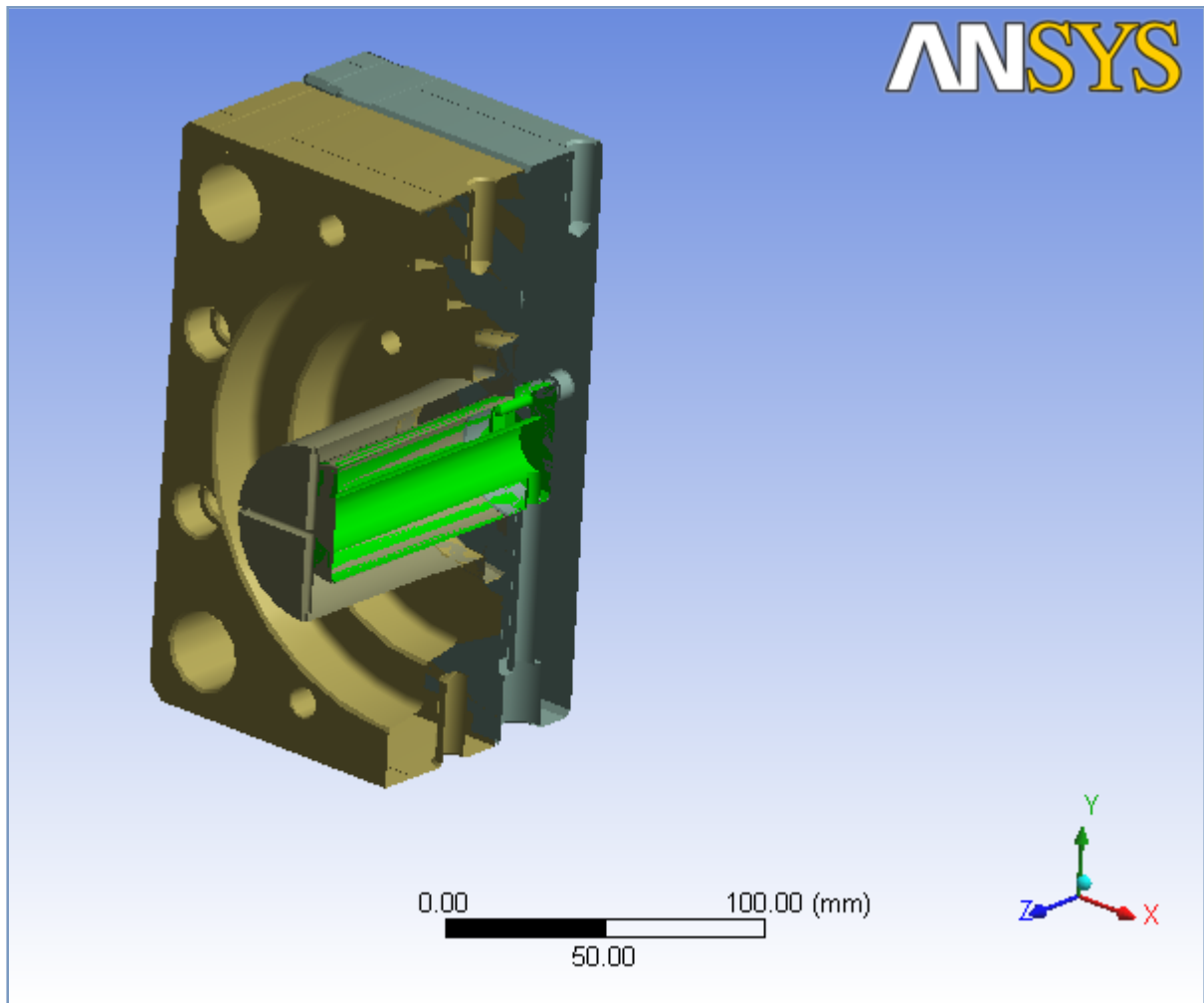
FIGURE 4
Model 3 > Geometry > 0010 - M3-1 > Figure
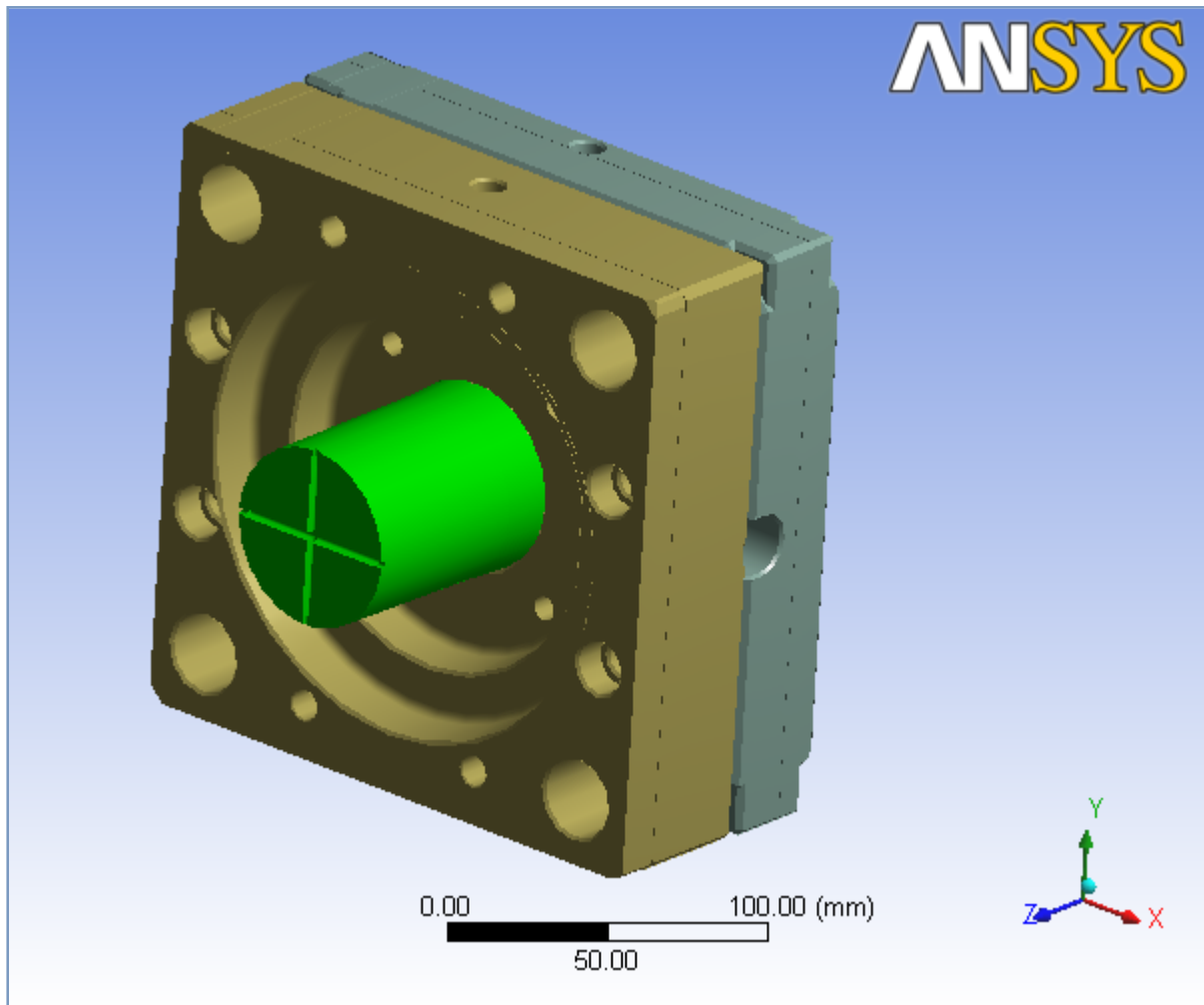
Connections

TABLE 4
Model 3 > Connections

Object Name	Connections
State	Fully Defined
Auto Detection	
Generate Contact On Update	Yes
Tolerance Type	Slider
Tolerance Slider	0.
Tolerance Value	0.76998 mm
Face/Face	Yes
Face/Edge	No
Edge/Edge	No
Priority	Include All
Same Body Grouping	Yes
Revolute Joints	Yes
Fixed Joints	Yes
Transparency	
Enabled	Yes

TABLE 5
Model 3 > Connections > Contact Regions

Object Name	Contact Region	Contact Region 2	Contact Region 3	Bonded - 0010 - M4-1 To 0010 - M3-1	Bonded - 0010 - M4-1 To Plate1-1
State	Fully Defined				

Scope				
Scoping Method	Geometry Selection			
Contact	1 Face	4 Faces	3 Faces	1 Face
Target	1 Face	7 Faces	3 Faces	1 Face
Contact Bodies	Plate1-1	Plate2-1	0010 - M4-1	
Target Bodies	Plate2-1	0010 - M3-1		Plate1-1
Definition				
Type	Bonded			
Scope Mode	Automatic			Manual
Behavior	Symmetric			
Suppressed	No			
Advanced				
Formulation	Pure Penalty			
Normal Stiffness	Program Controlled			
Update Stiffness	Never			
Thermal Conductance	Program Controlled			
Pinball Region	Program Controlled			

FIGURE 5
Model 3 > Connections > Contact Region > Figure
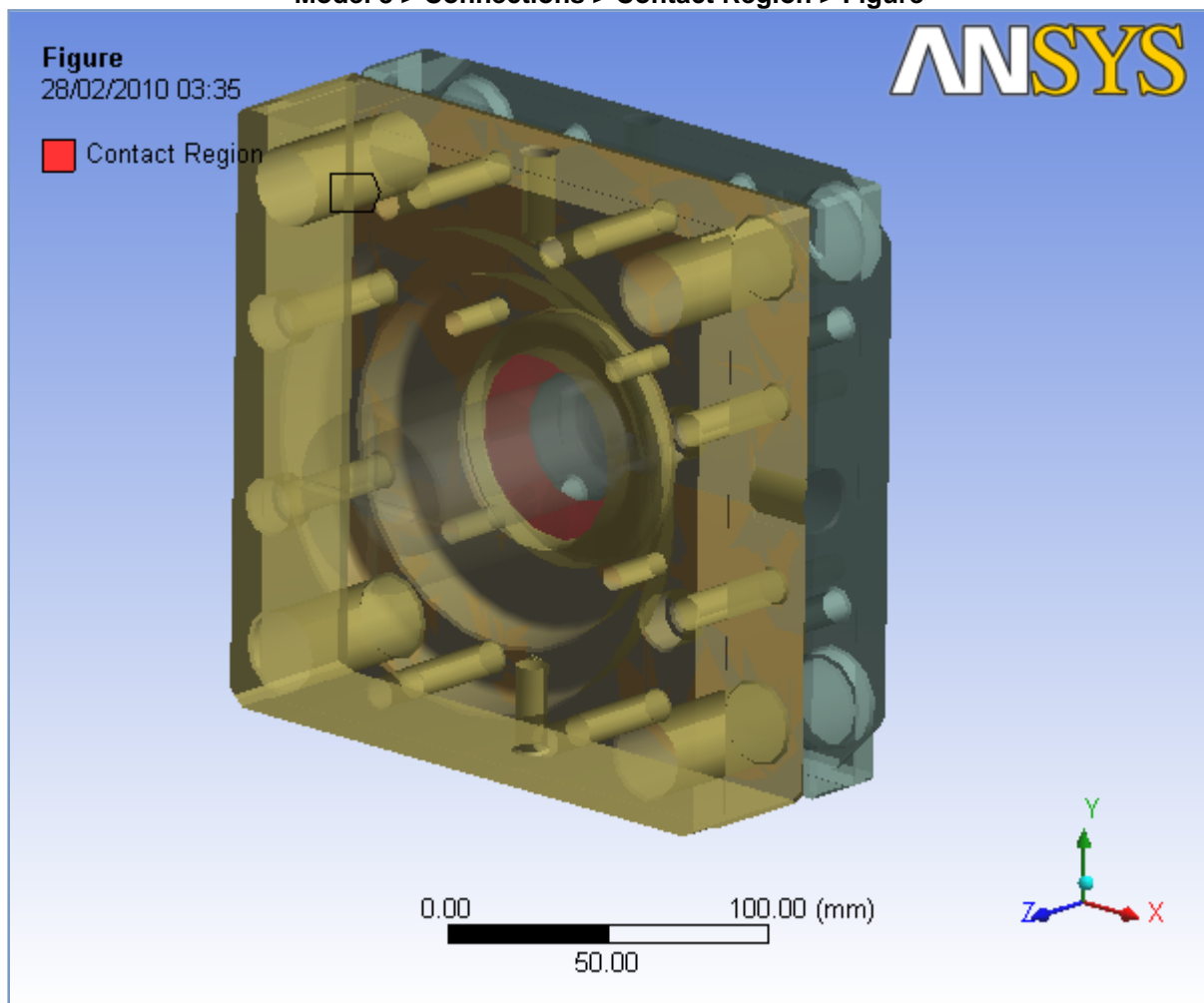
FIGURE 6
Model 3 > Connections > Contact Region 2 > Figure
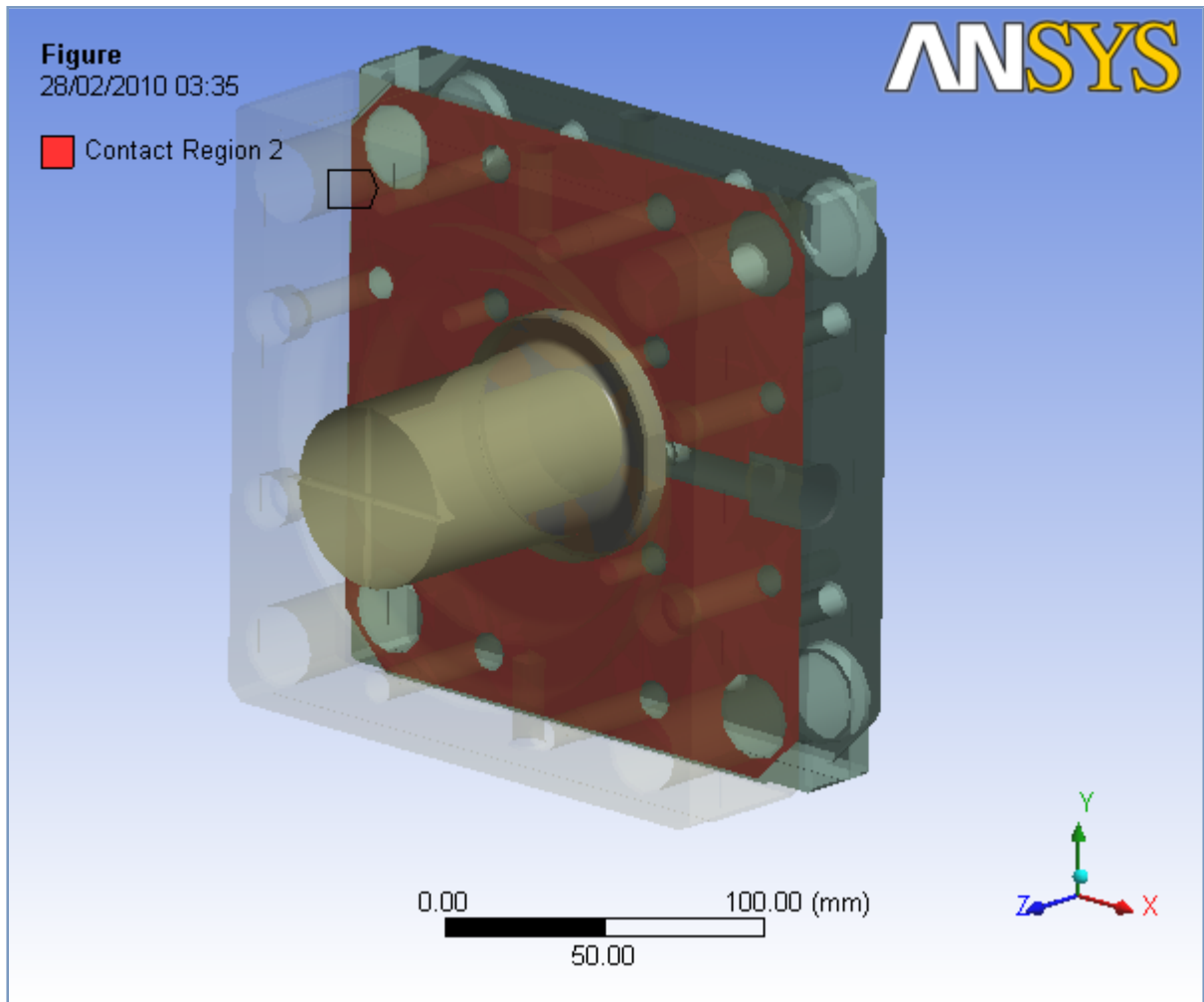
FIGURE 7
Model 3 > Connections > Contact Region 3 > Figure
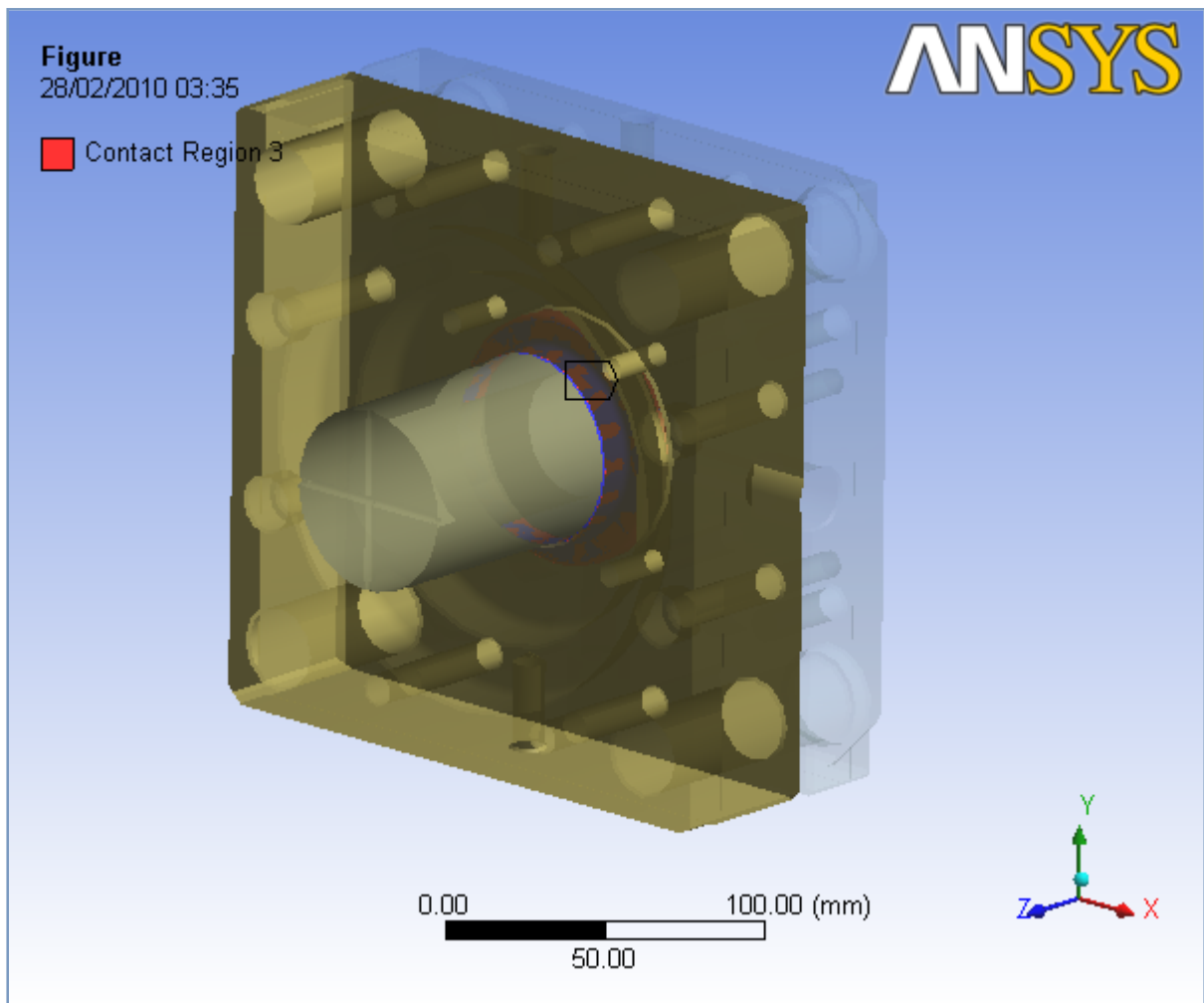
FIGURE 8
Model 3 > Connections > Bonded - 0010 - M4-1 To 0010 - M3-1 > Figure
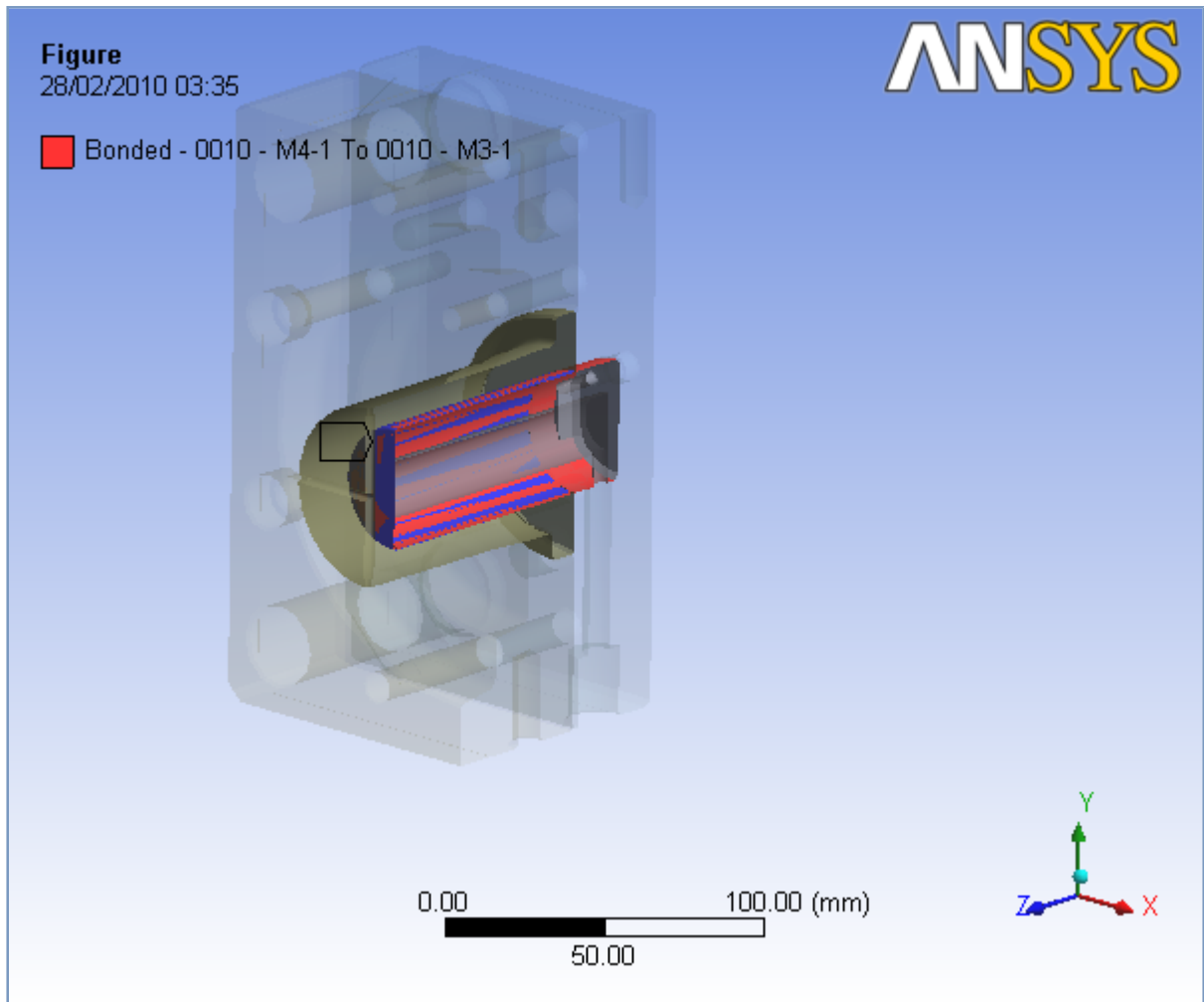
FIGURE 9
Model 3 > Connections > Bonded - 0010 - M4-1 To Plate1-1 > Figure
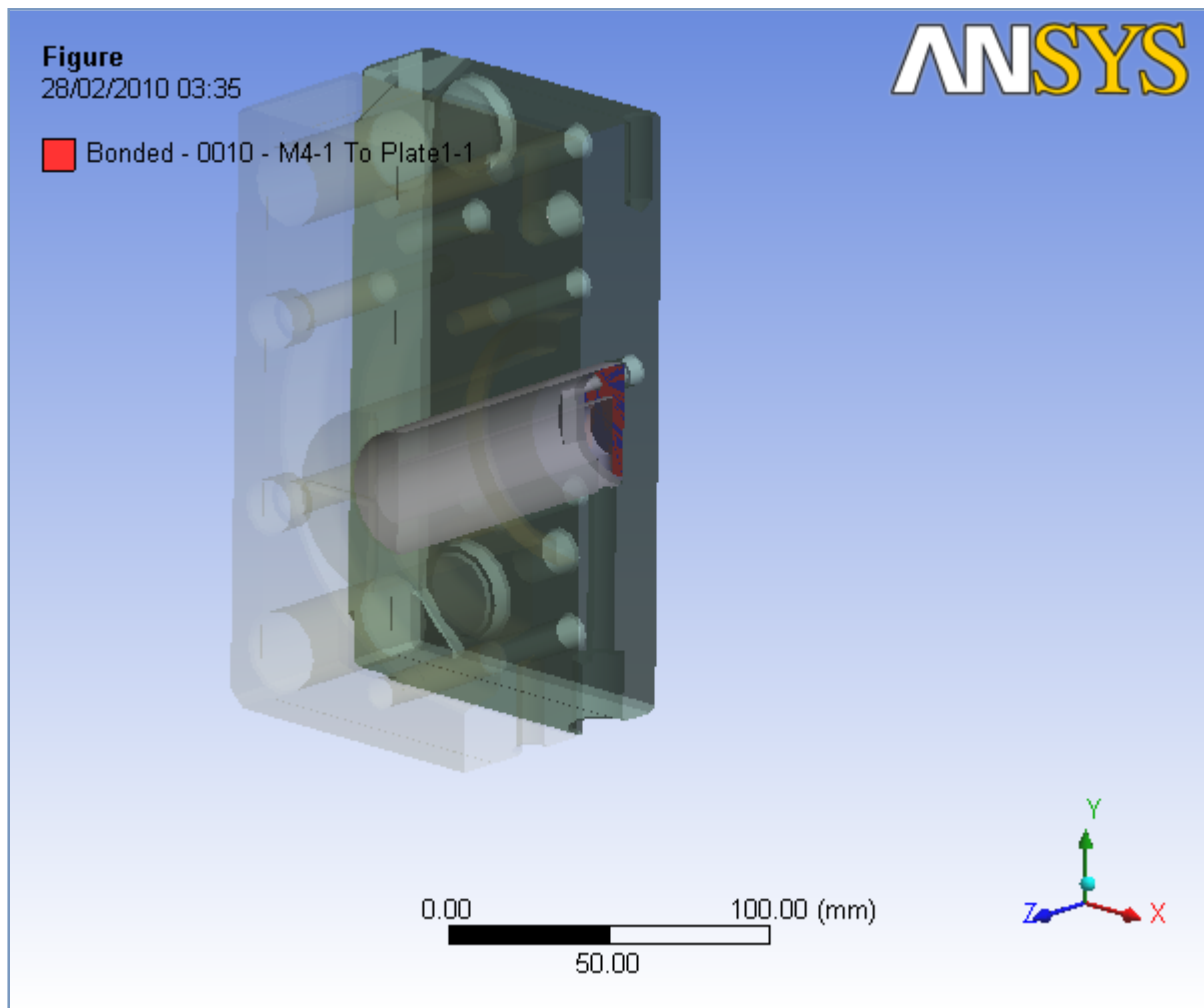
Mesh

TABLE 6
Model 3 > Mesh

Object Name	*Mesh*
State	Solved
Defaults	
Physics Preference	Mechanical
Relevance	0
Advanced	
Relevance Center	Coarse
Element Size	Default
Shape Checking	Standard Mechanical
Solid Element Midside Nodes	Program Controlled
Straight Sided Elements	No
Initial Size Seed	Active Assembly
Smoothing	Low
Transition	Fast
Statistics	
Nodes	86699
Elements	48559

Static Structural

TABLE 7
Model 3 > Analysis

Object Name	Static Structural
State	Fully Defined
Definition	
Physics Type	Structural
Analysis Type	Static Structural
Options	
Reference Temp	22. ℃

TABLE 8
Model 3 > Static Structural > Analysis Settings

Object Name	Analysis Settings
State	Fully Defined
Step Controls	
Number Of Steps	1.
Current Step Number	1.
Step End Time	600. s
Auto Time Stepping	Program Controlled
Solver Controls	
Solver Type	Program Controlled
Weak Springs	Program Controlled
Large Deflection	Off
Inertia Relief	Off
Nonlinear Controls	
Force Convergence	Program Controlled
Moment Convergence	Program Controlled
Displacement Convergence	Program Controlled
Rotation Convergence	Program Controlled
Line Search	Program Controlled
Output Controls	
Calculate Stress	Yes
Calculate Strain	Yes
Calculate Results At	All Time Points
Analysis Data Management	
Solver Files Directory	D:\DOUT\Experiments HM1\Structural Analysis\Sructural Analysis_ANSYS_CorePlates\HM1_Core_Plates Simulation Files\Static Structural (3)\
Future Analysis	None
Save ANSYS db	No
Delete Unneeded Files	Yes
Nonlinear Solution	No

TABLE 9
Model 3 > Static Structural > Loads

Object Name	Pressure	Pressure 2	Fixed Support	Displacement	Displacement 2
State	Fully Defined		Suppressed	Fully Defined	
Scope					
Scoping Method	Geometry Selection				
Geometry	1 Face	28 Faces	1 Face		8 Faces
Definition					
Define By	Normal To			Components	
Type	Pressure		Fixed Support	Displacement	

Magnitude	Tabular Data			
Suppressed	No	Yes	No	
X Component			Free	0. mm (ramped)
Y Component			Free	0. mm (ramped)
Z Component			0. mm (ramped)	Free

FIGURE 10
Model 3 > Static Structural > Pressure
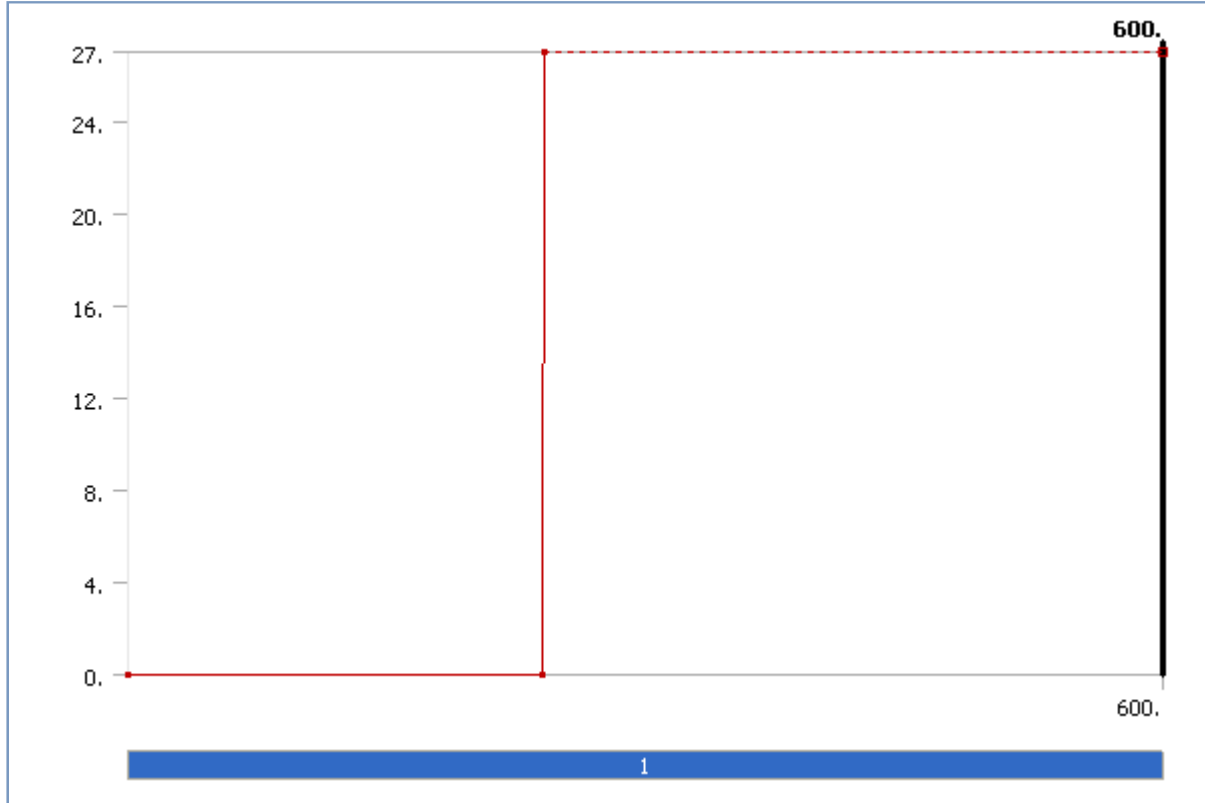
TABLE 10
Model 3 > Static Structural > Pressure

Steps	Time [s]	Pressure [MPa]
1	0.	0.
	240.	
	241.	27.
	600.	= 27.

FIGURE 11
Model 3 > Static Structural > Pressure > Figure
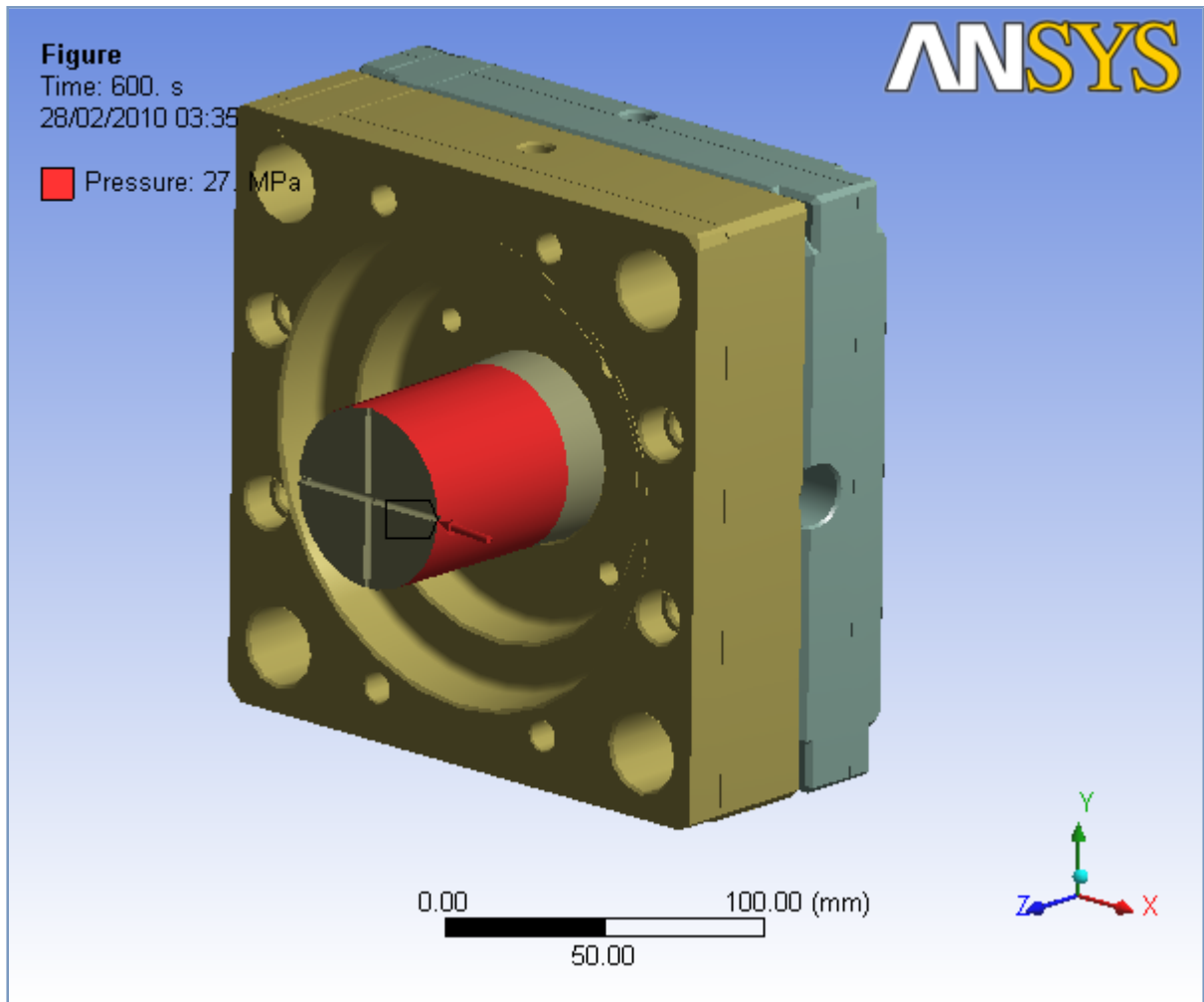
FIGURE 12
Model 3 > Static Structural > Pressure 2

TABLE 11
Model 3 > Static Structural > Pressure 2

Steps	Time [s]	Pressure [MPa]
1	0.	0.
	240.	
	241.	27.
	600.	= 27.

FIGURE 13
Model 3 > Static Structural > Pressure 2 > Figure
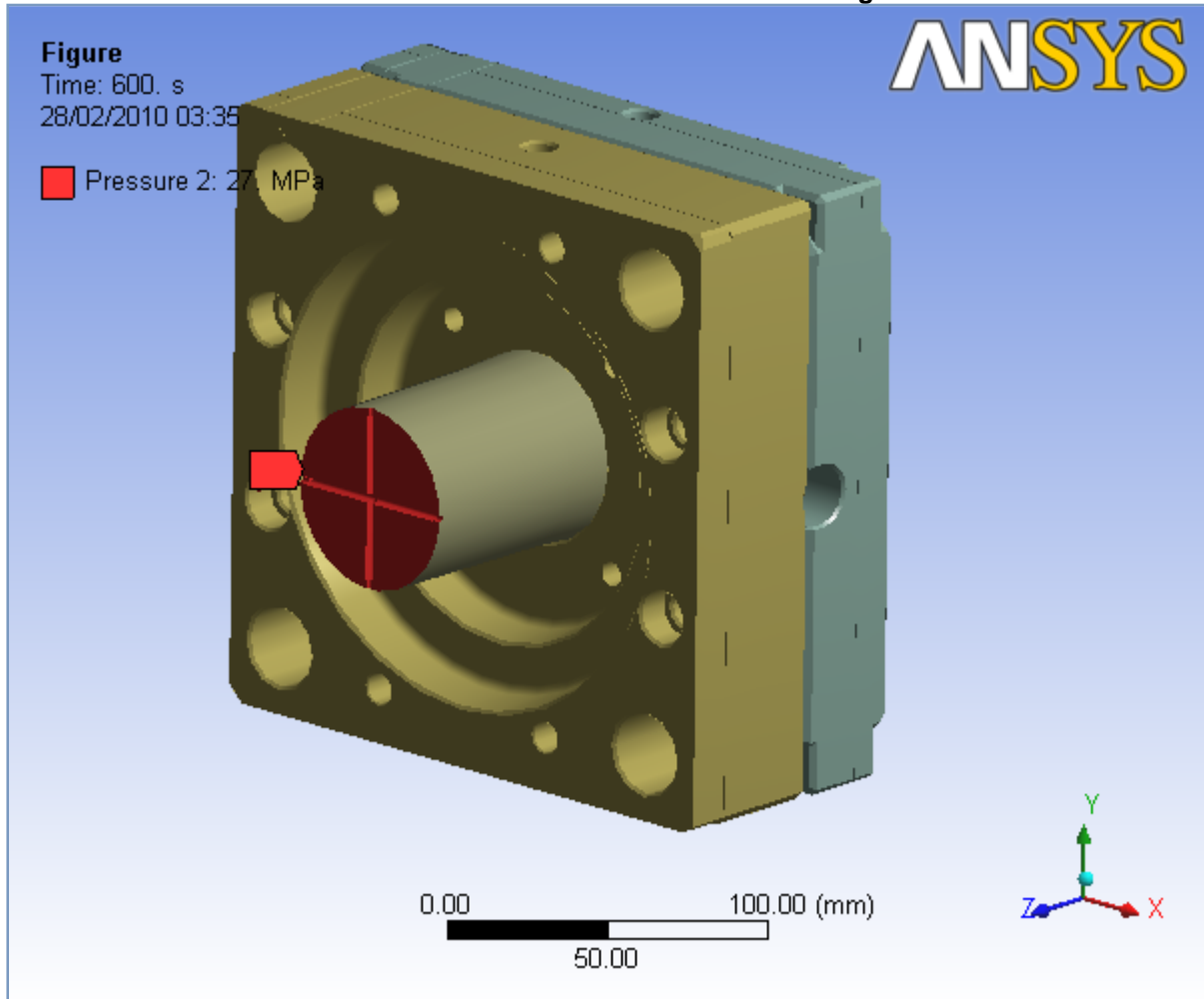
FIGURE 14
Model 3 > Static Structural > Displacement
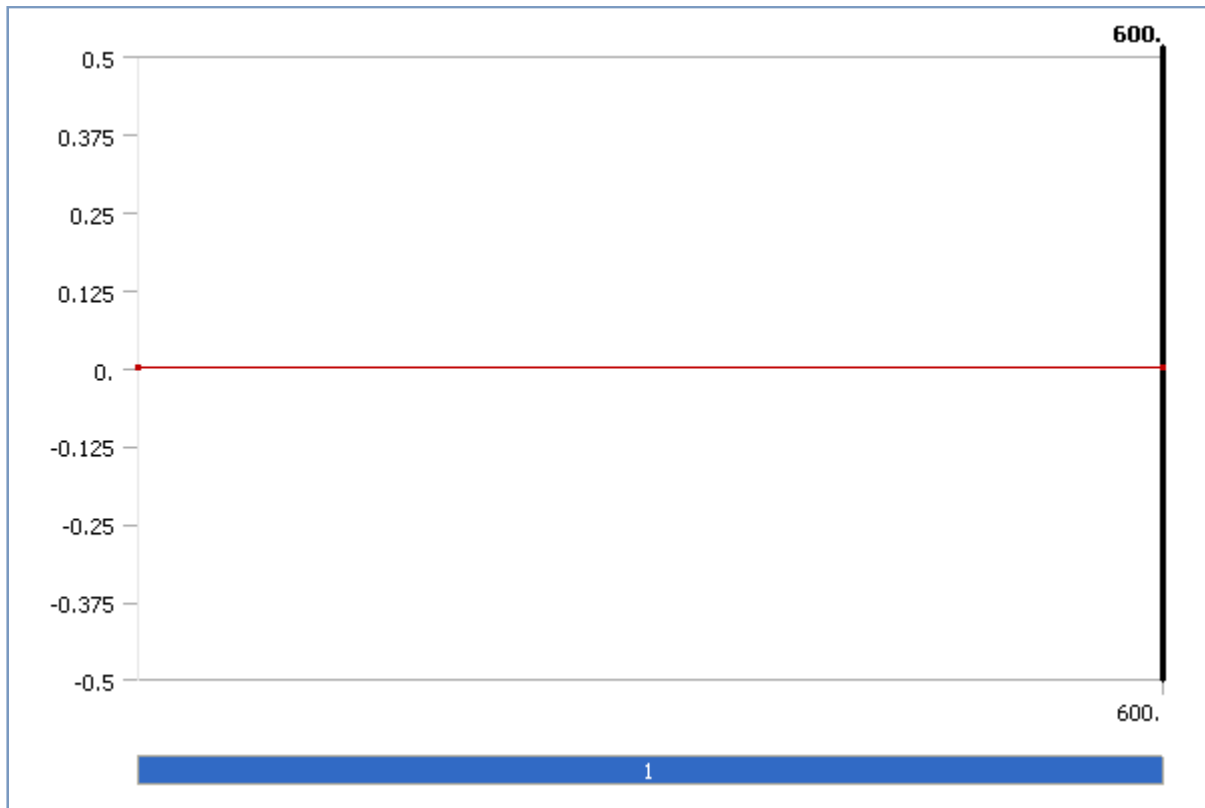
FIGURE 15
Model 3 > Static Structural > Displacement 2
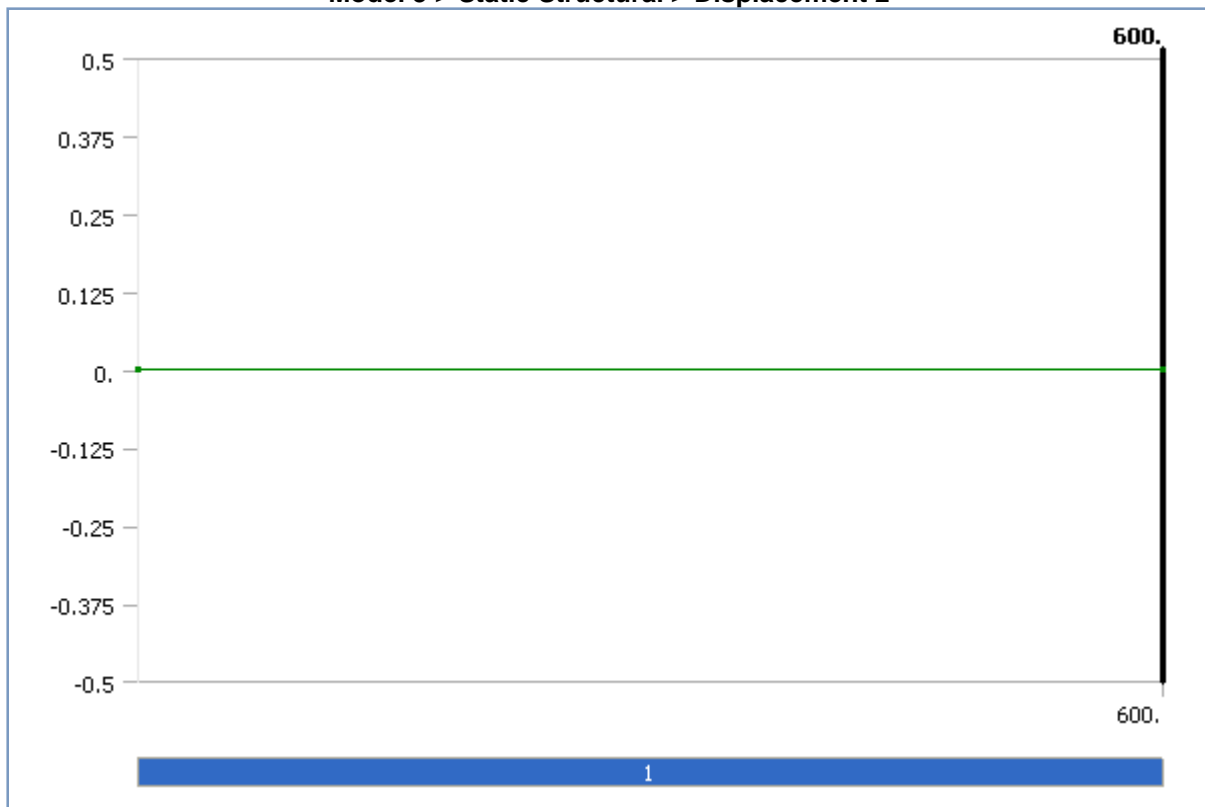
FIGURE 16
Model 3 > Static Structural > Displacement 2 > Figure
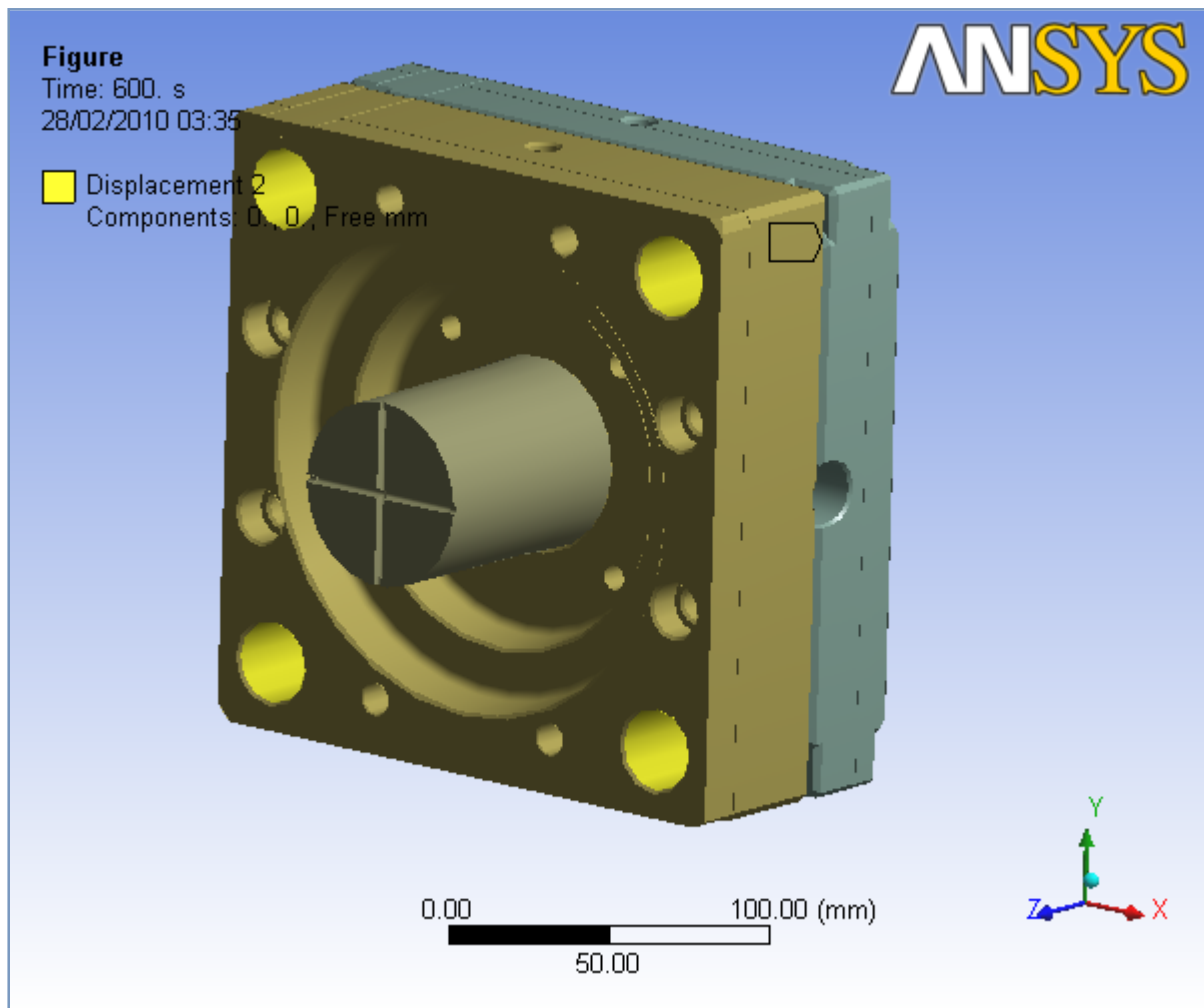
TABLE 12
Model 3 > Static Structural > Thermal Condition

Object Name	Thermal Condition
State	Fully Defined
Definition	
Condition	Non-Uniform Temperature
Thermal Environment	Steady-State Thermal
Time	End Time
Suppressed	No

Solution

TABLE 13
Model 3 > Static Structural > Solution

Object Name	Solution
State	Obsolete
Adaptive Mesh Refinement	
Max Refinement Loops	1.
Refinement Depth	2.

TABLE 14
Model 3 > Static Structural > Solution > Solution Information

Object Name	Solution Information
State	Not Solved
Solution Information	
Solution Output	Solver Output

Newton-Raphson Residuals	0
Update Interval	2.5 s
Display Points	All

TABLE 15
Model 3 > Static Structural > Solution > Results

Object Name	*Total Deformation*	*Directional DeformationX*	*Directional DeformationY*	*Directional DeformationZ*	*Equivalent Elastic Strain*
State	Obsolete				
Scope					
Geometry	All Bodies				
Definition					
Type	Total Deformation	Directional Deformation			Equivalent (von-Mises) Elastic Strain
Display Time	End Time				
Orientation		X Axis	Y Axis	Z Axis	
Results					
Minimum	1.3928e-004 mm	-3.9799e-002 mm	-4.1924e-002 mm	-3.2438e-002 mm	3.6403e-006 mm/mm
Maximum	5.4363e-002 mm	4.0296e-002 mm	3.9626e-002 mm	4.5787e-002 mm	8.1001e-003 mm/mm
Minimum Occurs On	Plate1-1	0010 - M3-1			Plate2-1
Maximum Occurs On	0010 - M3-1				
Information					
Time	600. s				
Load Step	1				
Substep	1				
Iteration Number	1				

TABLE 16
Model 3 > Static Structural > Solution > Results

Object Name	*Normal Elastic StrainX*	*Normal Elastic StrainY*	*Normal Elastic StrainZ*	*Equivalent Stress*
State	Obsolete			
Scope				
Geometry	All Bodies			
Definition				
Type	Normal Elastic Strain			Equivalent (von-Mises) Stress
Orientation	X Axis	Y Axis	Z Axis	
Display Time	209.68 s	End Time		
Results				
Minimum	-9.008e-003 mm/mm	-8.0318e-003 mm/mm	-3.9875e-003 mm/mm	0.54752 MPa
Maximum	3.3916e-003 mm/mm	3.3496e-003 mm/mm	3.6882e-003 mm/mm	225.81 MPa
Minimum Occurs On	0010 - M3-1			
Maximum Occurs On	0010 - M3-1			Plate1-1
Information				
Time	600. s			
Load Step	1			
Substep	1			

Iteration Number	1

FIGURE 17
Model 3 > Static Structural > Solution > Normal Elastic StrainY > Figure
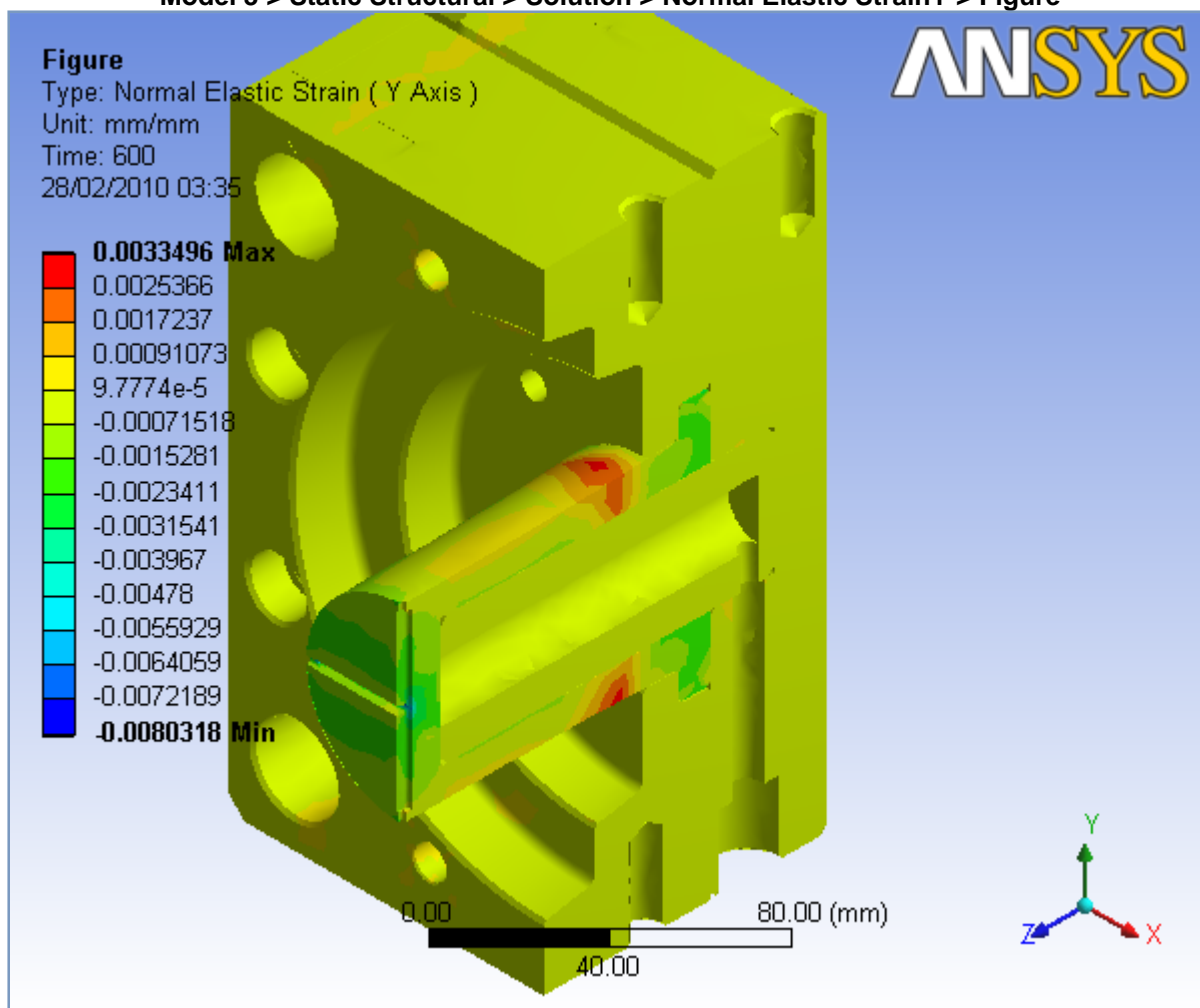
Steady-State Thermal

TABLE 17
Model 3 > Analysis

Object Name	Steady-State Thermal
State	Fully Defined
Definition	
Physics Type	Thermal
Analysis Type	Steady-State

TABLE 18
Model 3 > Steady-State Thermal > Initial Condition

Object Name	Initial Condition
State	Fully Defined
Definition	
Initial Temperature	Uniform Temperature
Initial Temperature Value	22. ℃

TABLE 19
Model 3 > Steady-State Thermal > Analysis Settings

Object Name	Analysis Settings
State	Fully Defined

Step Controls	
Number Of Steps	1.
Current Step Number	1.
Step End Time	600. s
Auto Time Stepping	Program Controlled
Solver Controls	
Solver Type	Program Controlled
Nonlinear Controls	
Heat Convergence	Program Controlled
Temperature Convergence	Program Controlled
Line Search	Program Controlled
Output Controls	
Calculate Thermal Flux	Yes
Calculate Results At	All Time Points
Analysis Data Management	
Solver Files Directory	D:\DOUT\Experiments HM1\Structural Analysis\Sructural Analysis_ANSYS_CorePlates\HM1_Core_Plates Simulation Files\Steady-State Thermal (3)\
Future Analysis	None
Save ANSYS db	No
Delete Unneeded Files	Yes
Nonlinear Solution	No

TABLE 20
Model 3 > Steady-State Thermal > Loads

Object Name	*Temperature*	*Temperature 2*	*Temperature 3*	*Temperature 4*	*Temperature 5*
State	Fully Defined				
Scope					
Scoping Method	Geometry Selection				
Geometry	1 Body			30 Faces	11 Faces
Definition					
Type	Temperature				
Magnitude	Tabular Data				
Suppressed	No				

FIGURE 18
Model 3 > Steady-State Thermal > Temperature
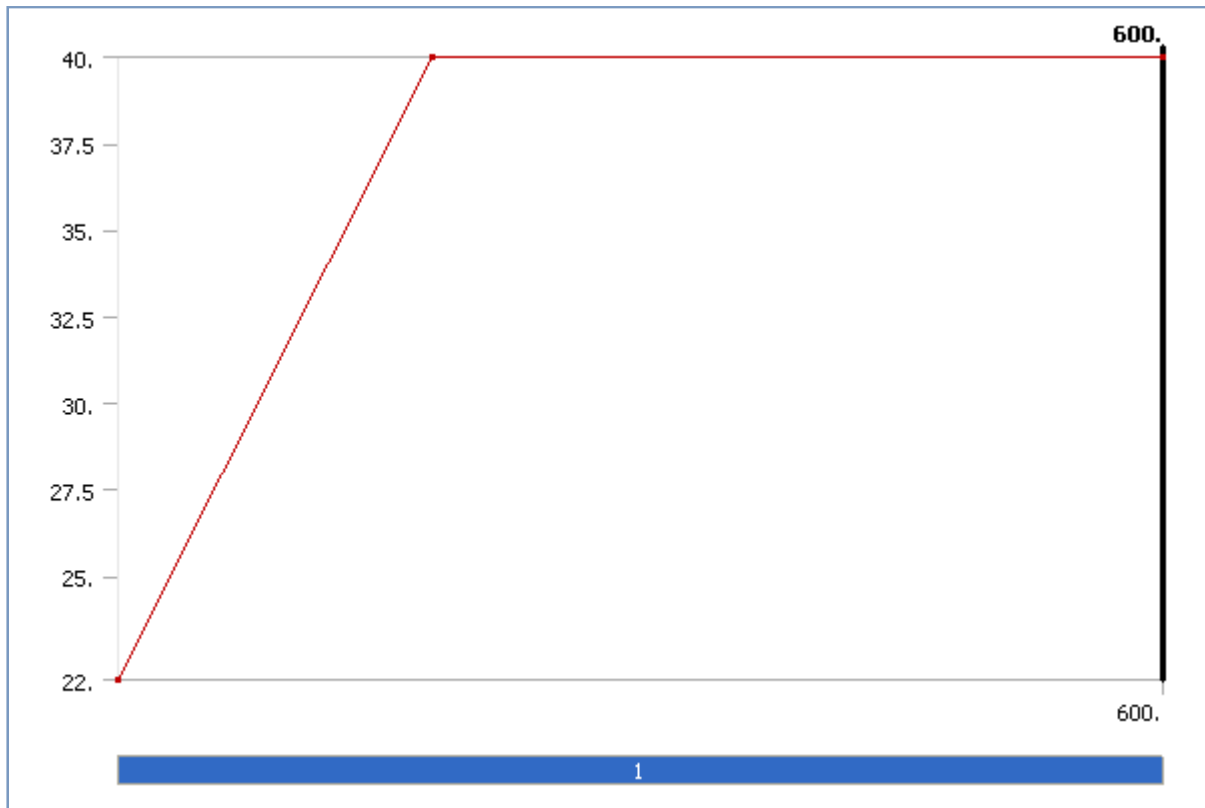
TABLE 21
Model 3 > Steady-State Thermal > Temperature

Steps	Time [s]	Temperature [℃]
1	0.	22.
	180.	40.
	600.	

FIGURE 19
Model 3 > Steady-State Thermal > Temperature > Figure
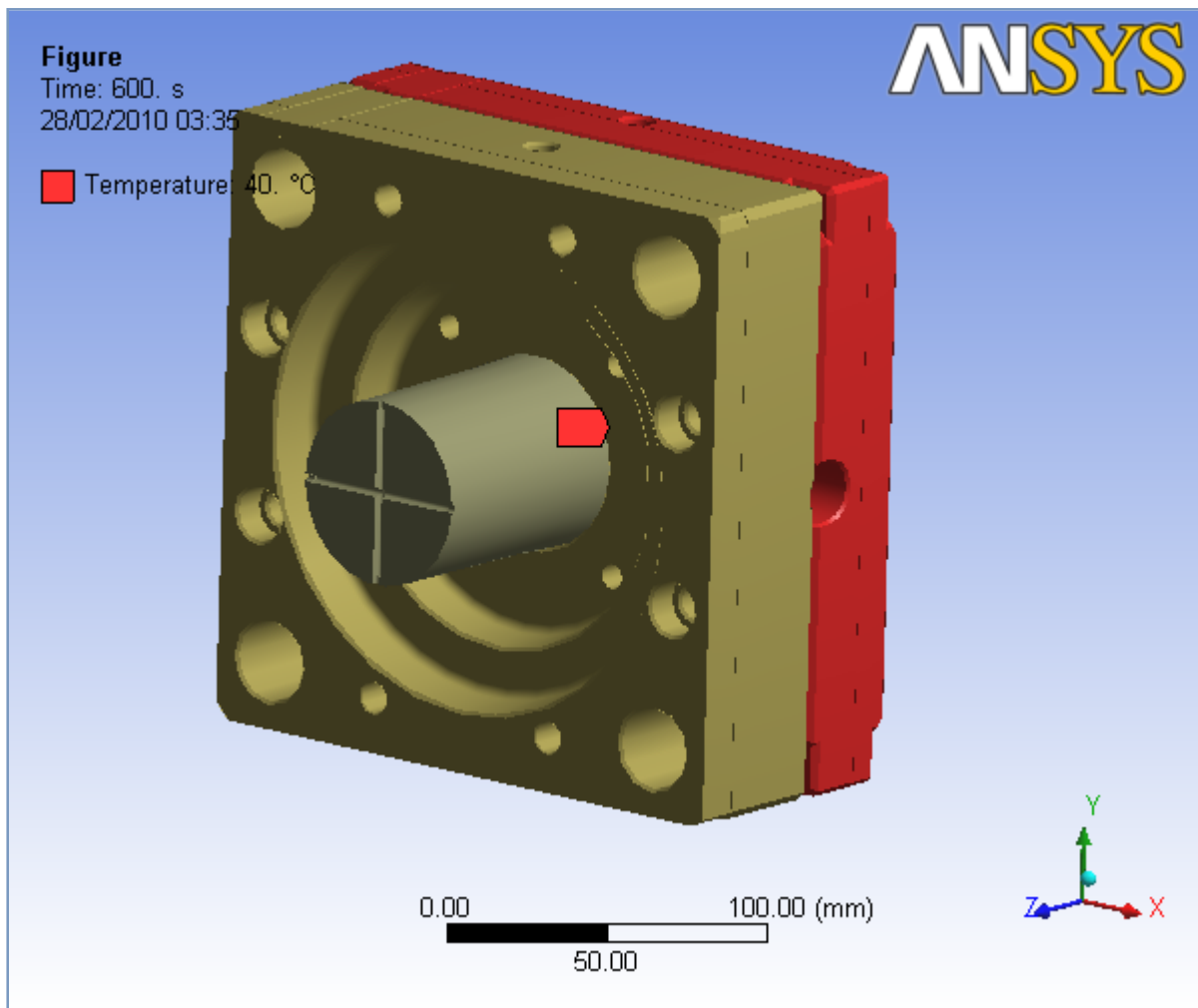
FIGURE 20
Model 3 > Steady-State Thermal > Temperature 2
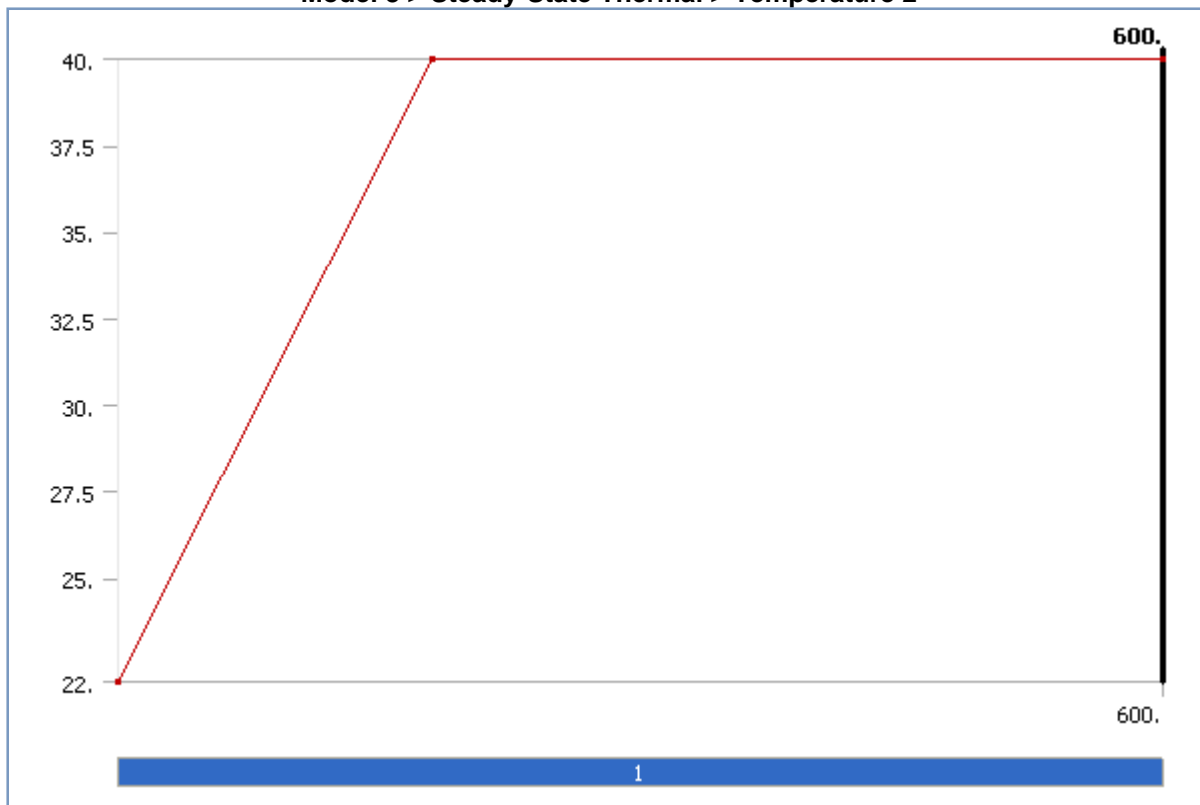
TABLE 22
Model 3 > Steady-State Thermal > Temperature 2

Steps	Time [s]	Temperature [°C]
1	0.	22.
	180.	40.
	600.	

FIGURE 21
Model 3 > Steady-State Thermal > Temperature 2 > Figure
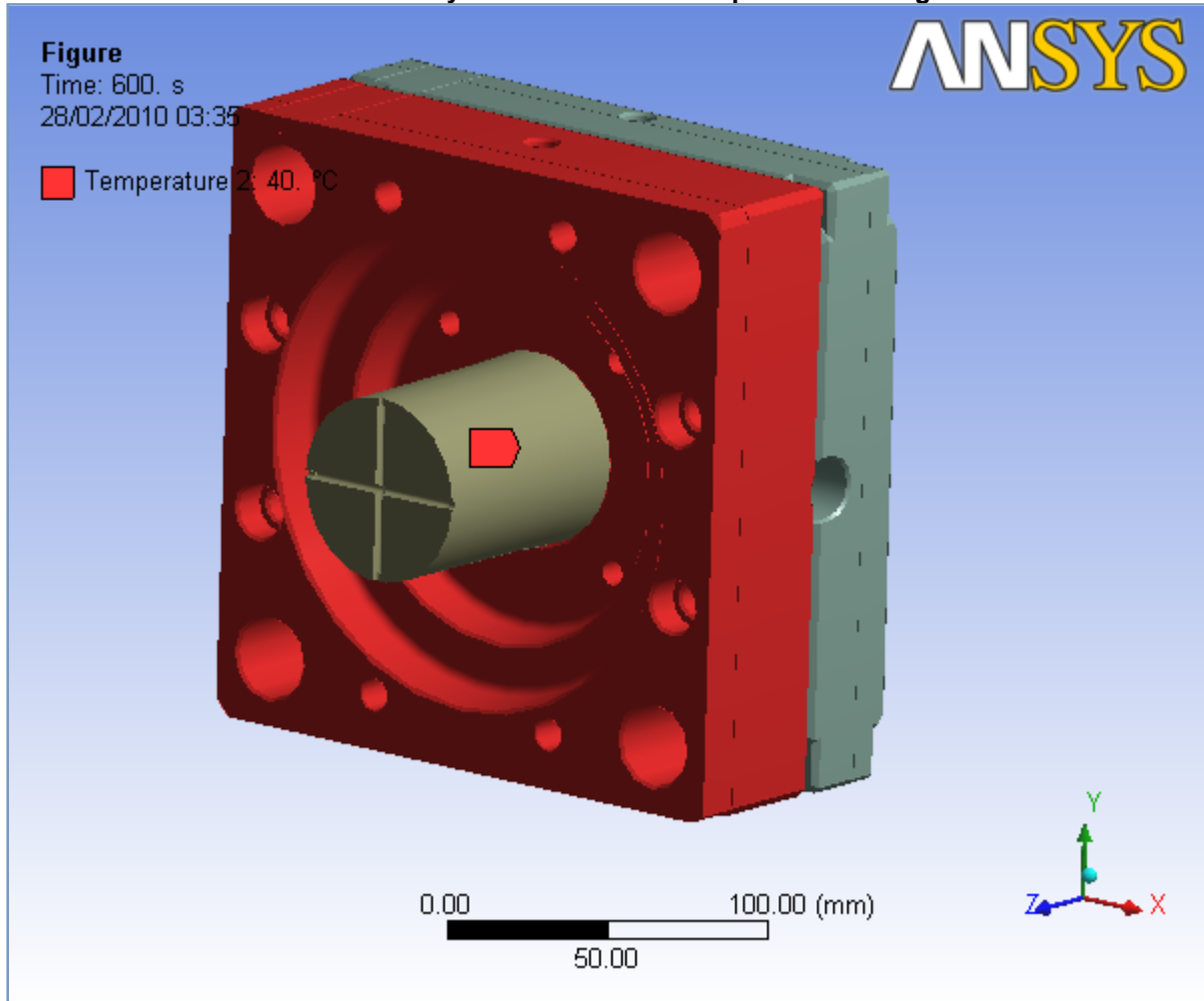
FIGURE 22
Model 3 > Steady-State Thermal > Temperature 3
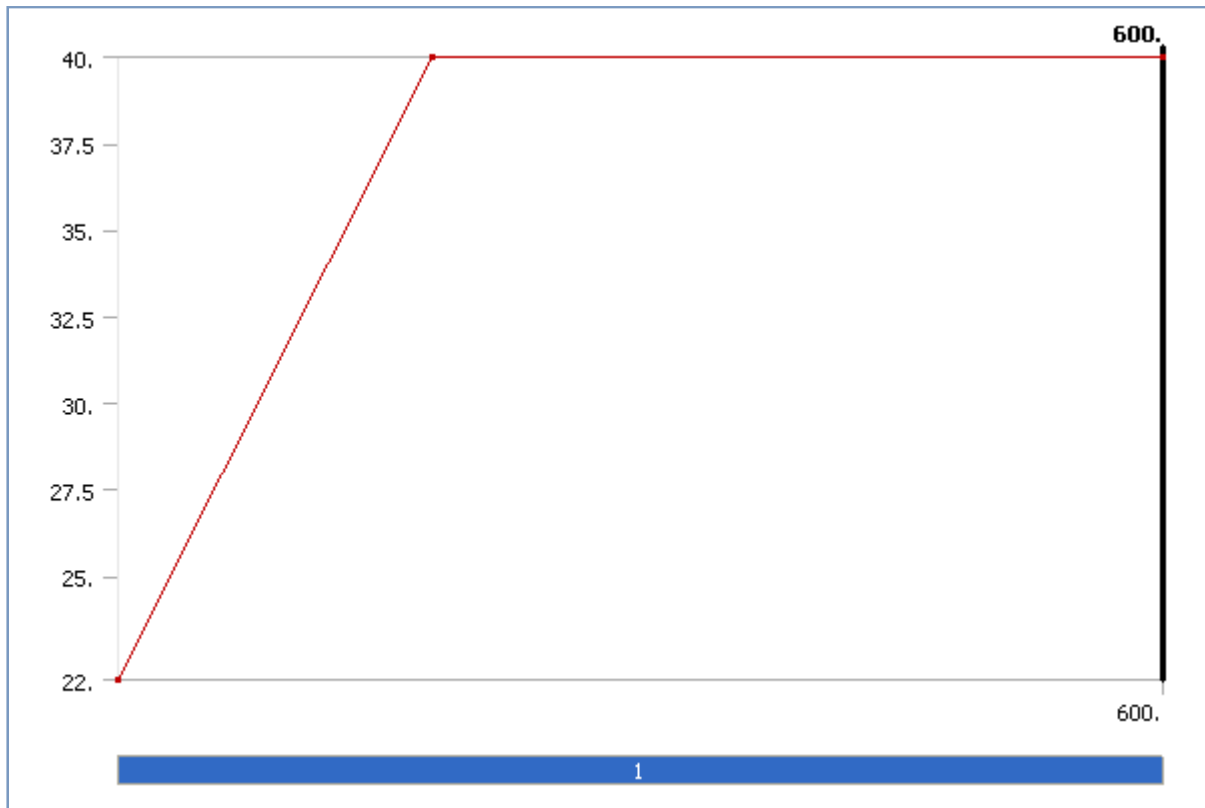
TABLE 23
Model 3 > Steady-State Thermal > Temperature 3

Steps	Time [s]	Temperature [°C]
1	0.	22.
	180.	40.
	600.	

FIGURE 23
Model 3 > Steady-State Thermal > Temperature 3 > Figure
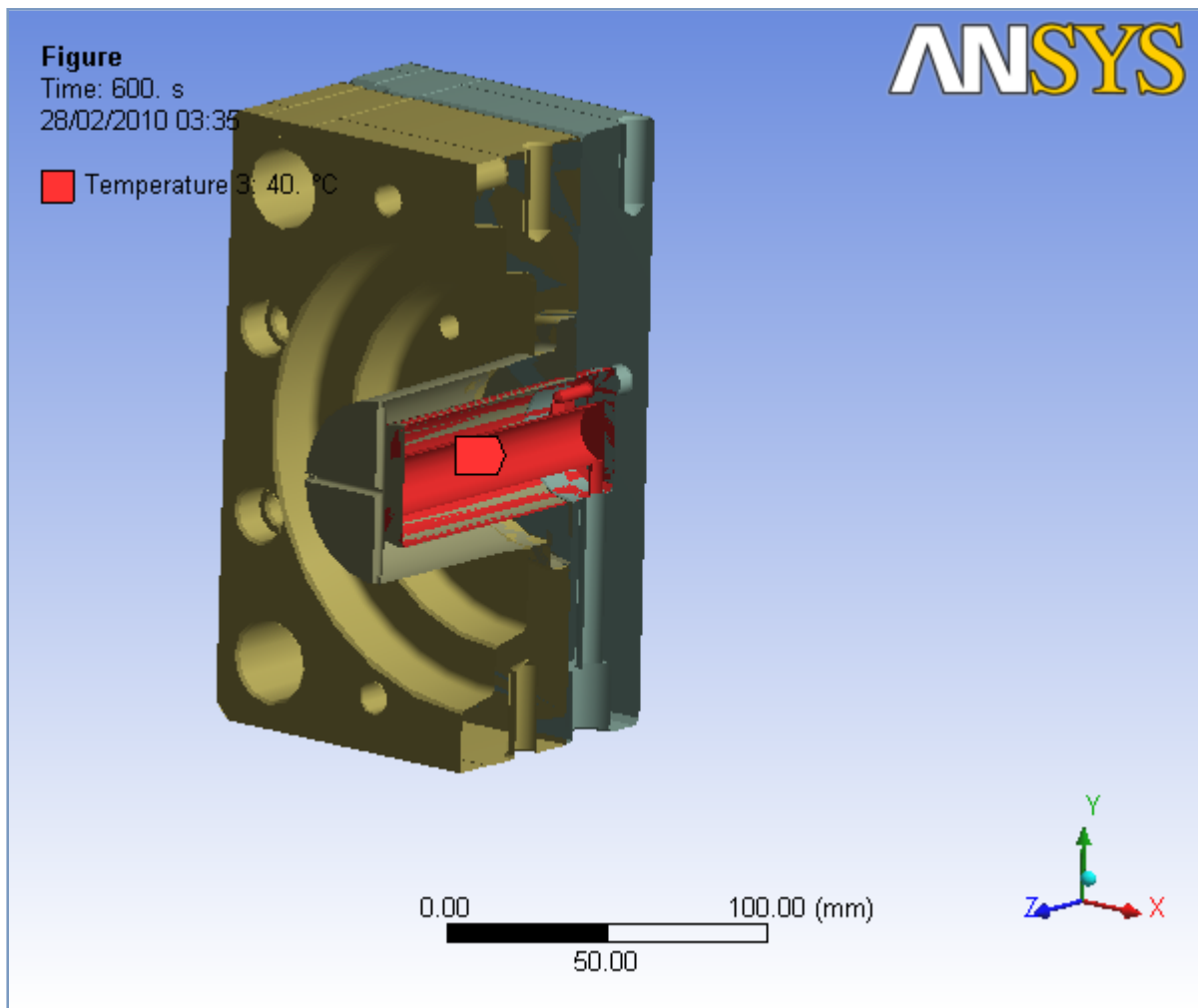
FIGURE 24
Model 3 > Steady-State Thermal > Temperature 4
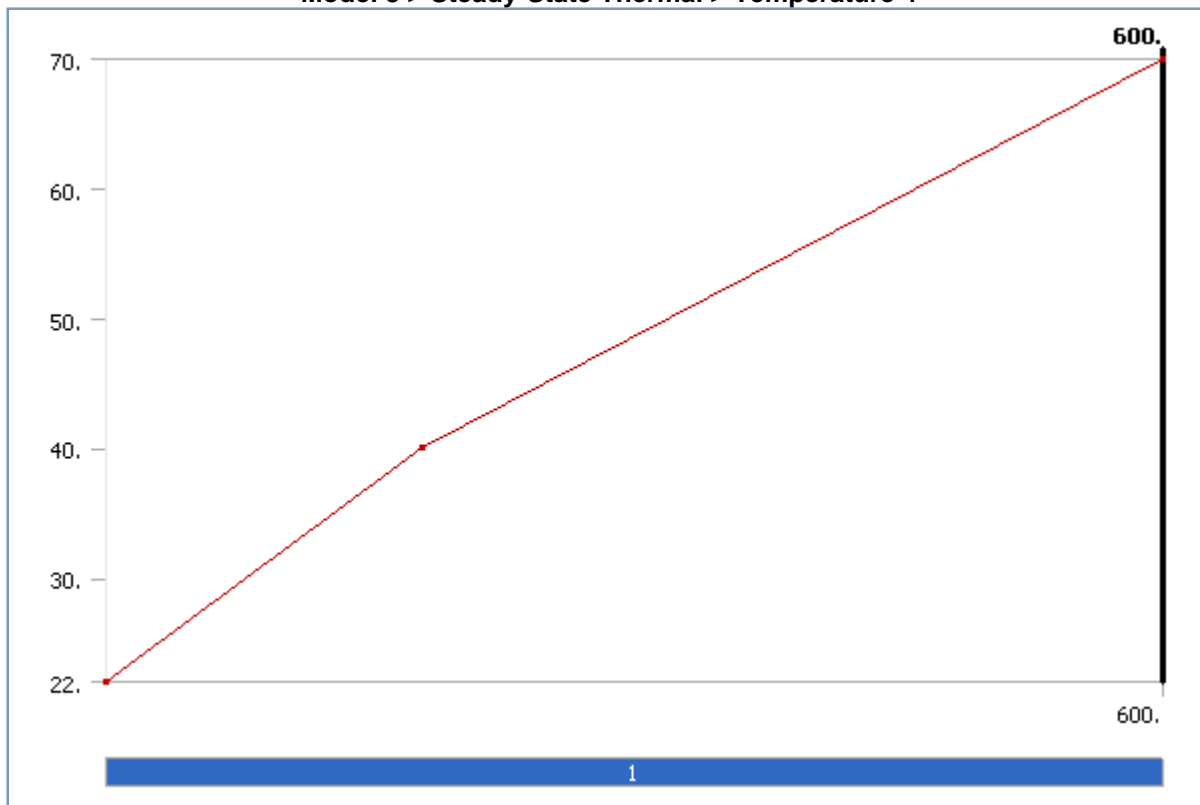
TABLE 24
Model 3 > Steady-State Thermal > Temperature 4

Steps	Time [s]	Temperature [°C]
	0.	22.
1	180.	40.
	600.	70.

FIGURE 25
Model 3 > Steady-State Thermal > Temperature 4 > Figure
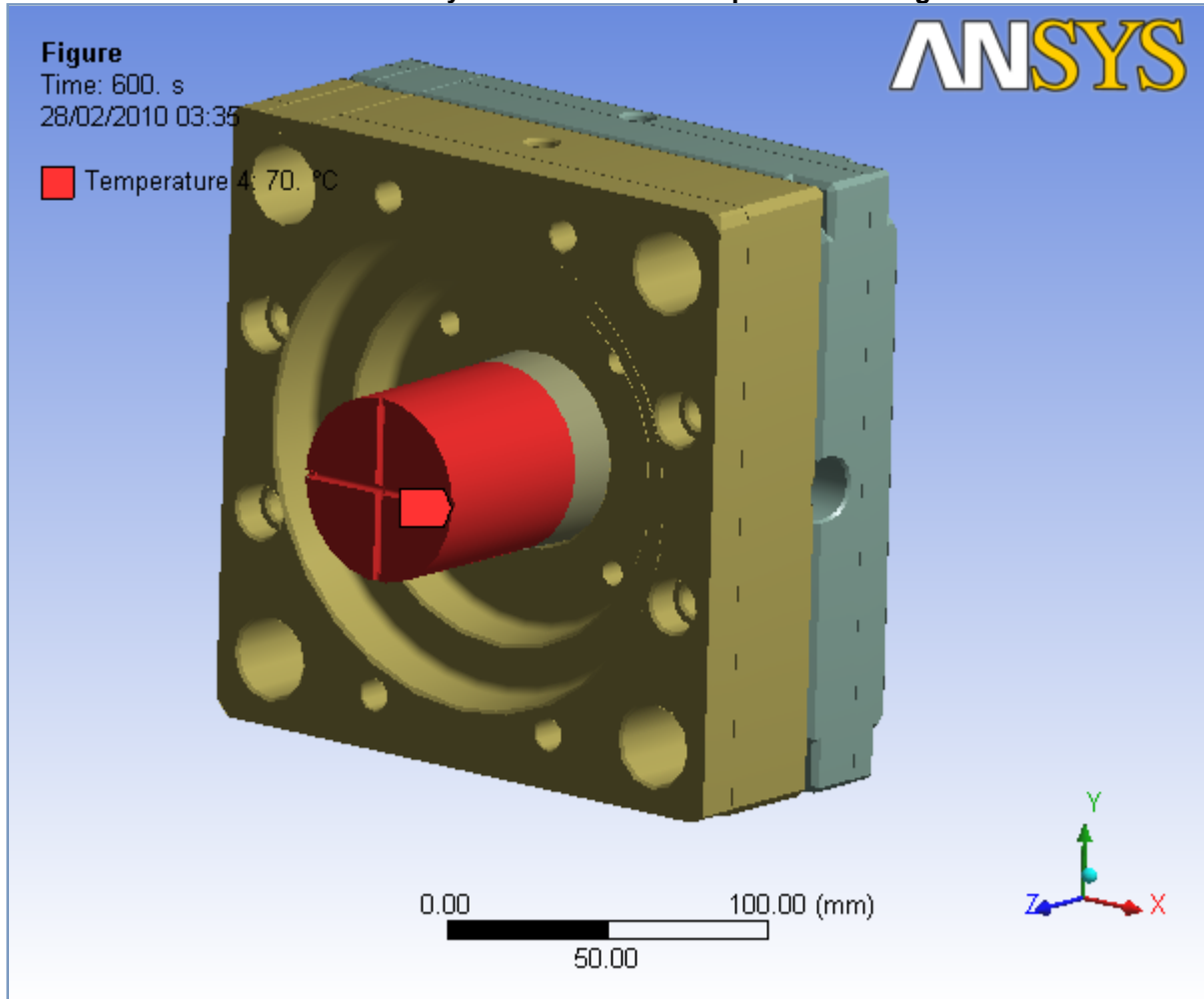
FIGURE 26
Model 3 > Steady-State Thermal > Temperature 5
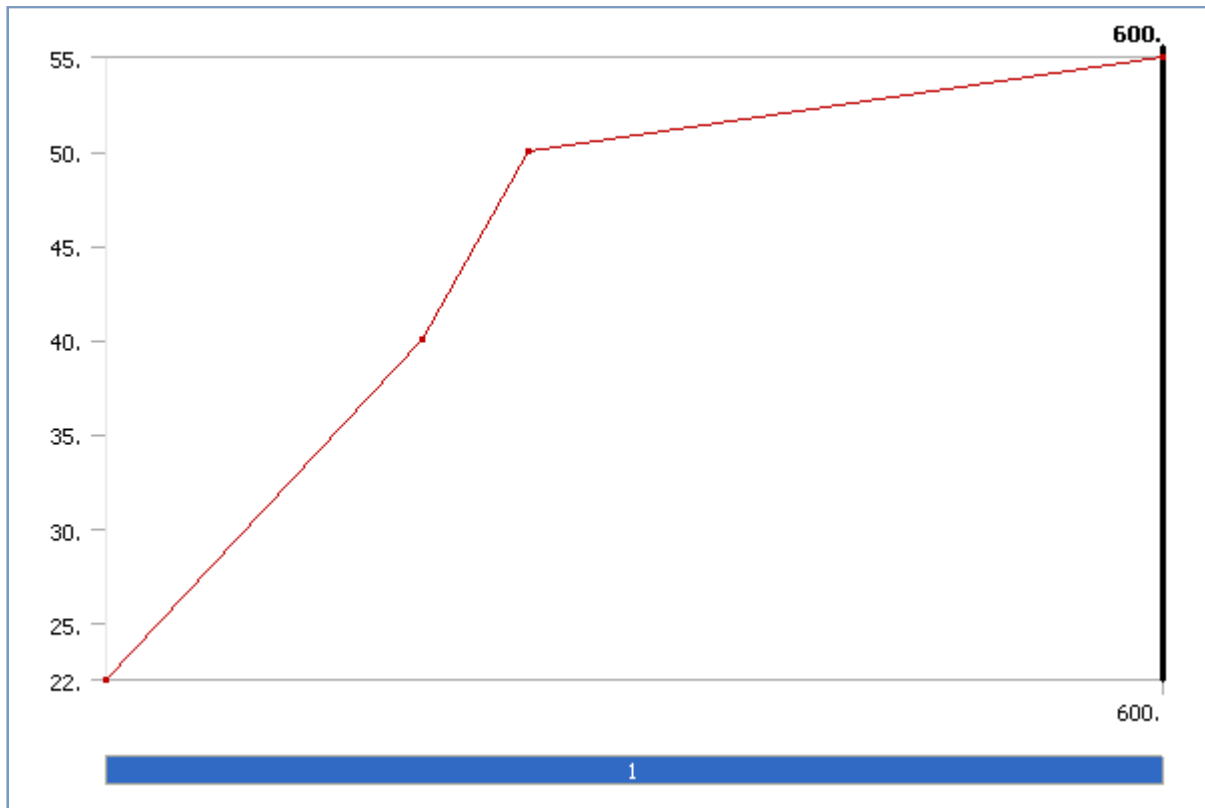
TABLE 25
Model 3 > Steady-State Thermal > Temperature 5

Steps	Time [s]	Temperature [°C]
1	0.	22.
	180.	40.
	240.	50.
	600.	55.

FIGURE 27
Model 3 > Steady-State Thermal > Temperature 5 > Figure
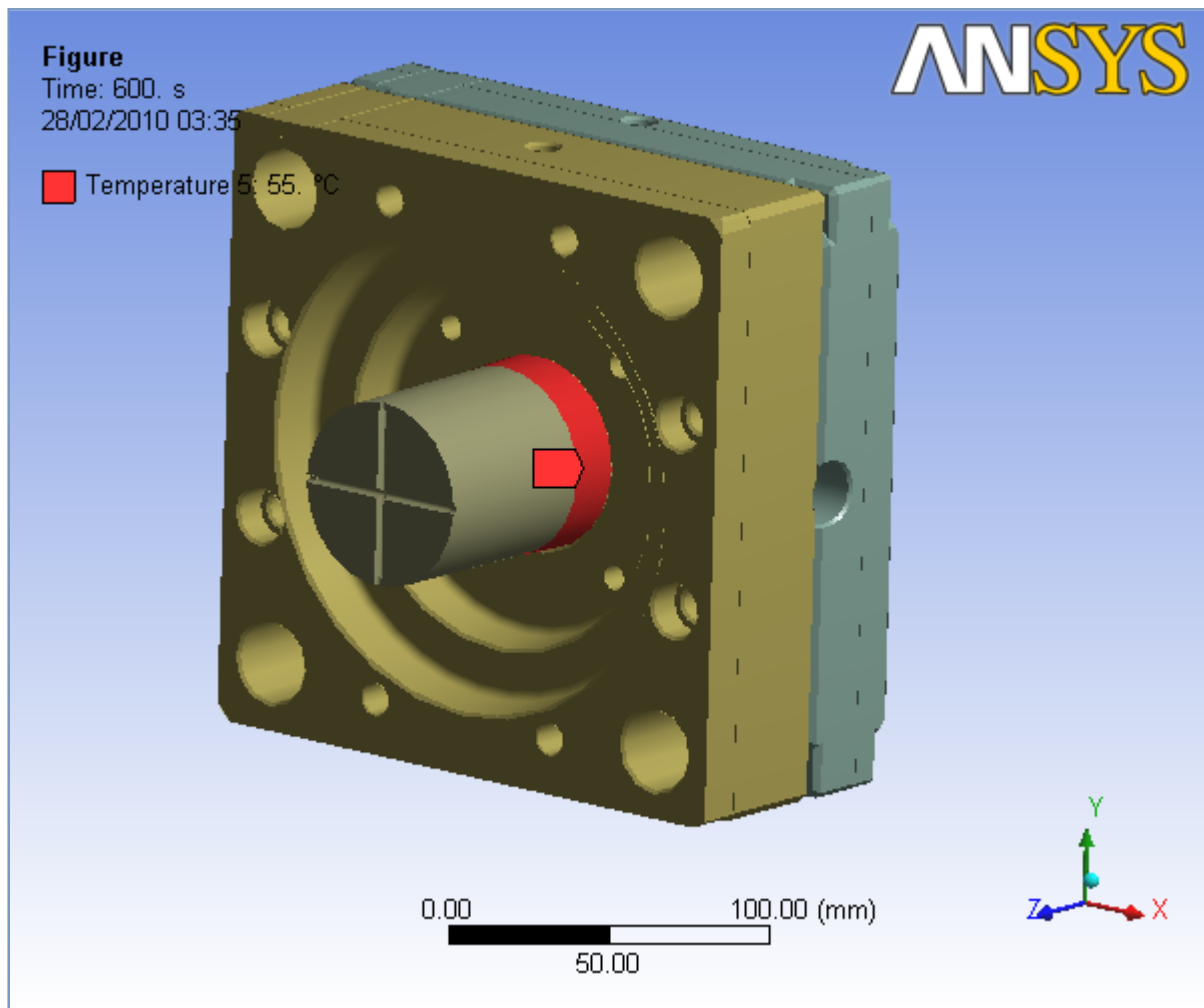
Solution

TABLE 26
Model 3 > Steady-State Thermal > Solution

Object Name	Solution
State	Solved
Adaptive Mesh Refinement	
Max Refinement Loops	1.
Refinement Depth	2.

TABLE 27
Model 3 > Steady-State Thermal > Solution > Solution Information

Object Name	Solution Information
State	Solved
Solution Information	
Solution Output	Solver Output
Update Interval	2.5 s
Display Points	All

TABLE 28
Model 3 > Steady-State Thermal > Solution > Results

Object Name	Temperature
State	Solved
Scope	
Geometry	All Bodies
Definition	

Type	Temperature
Display Time	End Time
Results	
Minimum	33.118 ℃
Maximum	70. ℃
Minimum Occurs On	0010 - M3-1
Maximum Occurs On	0010 - M3-1
Information	
Time	600. s
Load Step	1
Substep	1
Iteration Number	1

Material Data

Steel_P20

TABLE 29
Steel_P20 > Constants

Structural	
Young's Modulus	2.e+005 MPa
Poisson's Ratio	0.28
Density	7.8e-006 kg/mm³
Thermal Expansion	1.2e-005 1/℃
Tensile Yield Strength	250. MPa
Compressive Yield Strength	250. MPa
Tensile Ultimate Strength	460. MPa
Compressive Ultimate Strength	0. MPa
Thermal	
Thermal Conductivity	2.9e-002 W/mm·℃
Specific Heat	460. J/kg·℃
Electromagnetics	
Relative Permeability	10000
Resistivity	1.7e-004 Ohm·mm

FIGURE 28
Steel_P20 > Alternating Stress
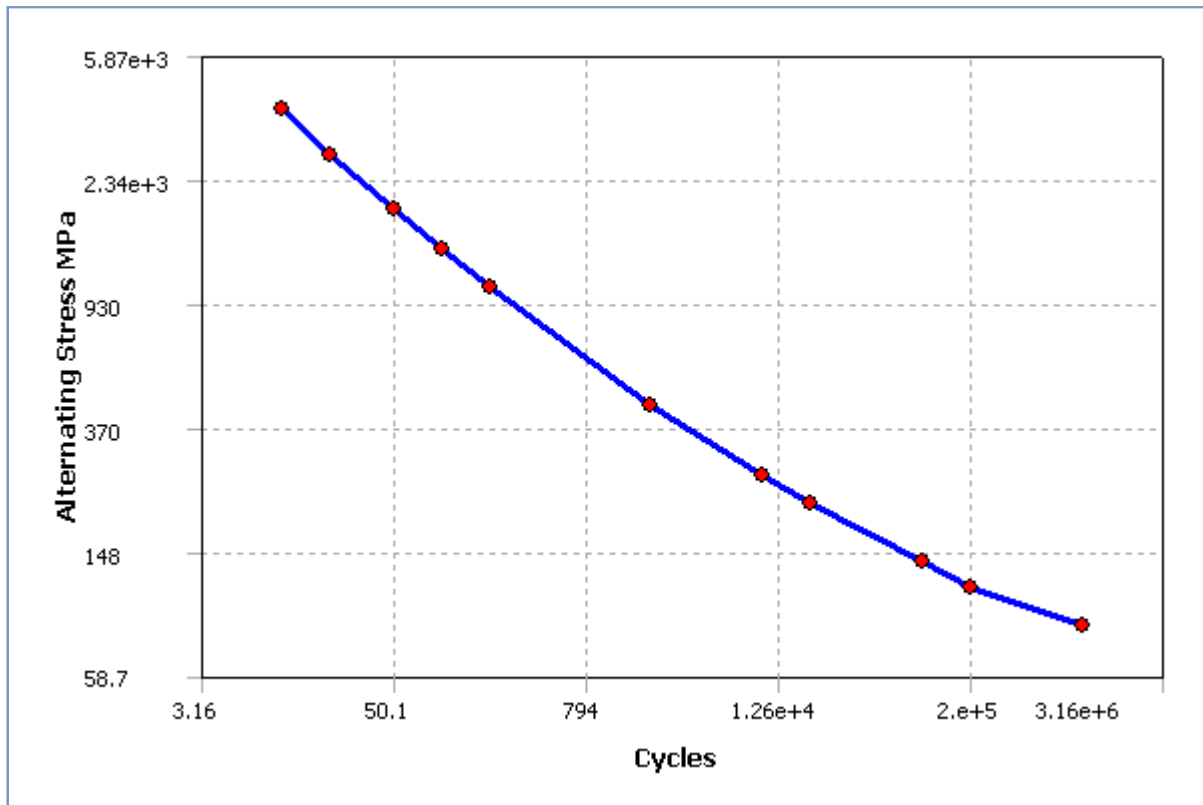
TABLE 30
Steel_P20 > Alternating Stress > Property Attributes

Interpolation	Log-Log
Mean Curve Type	Mean Stress

TABLE 31
Steel_P20 > Alternating Stress > Alternating Stress Curve Data

Mean Value MPa
0.

TABLE 32
Steel_P20 > Alternating Stress > Alternating Stress vs. Cycles

Cycles	Alternating Stress MPa
10.	3999.
20.	2827.
50.	1896.
100.	1413.
200.	1069.
2000.	441.
10000	262.
20000	214.
1.e+005	138.
2.e+005	114.
1.e+006	86.2

FIGURE 29
Steel_P20 > Strain-Life Parameters
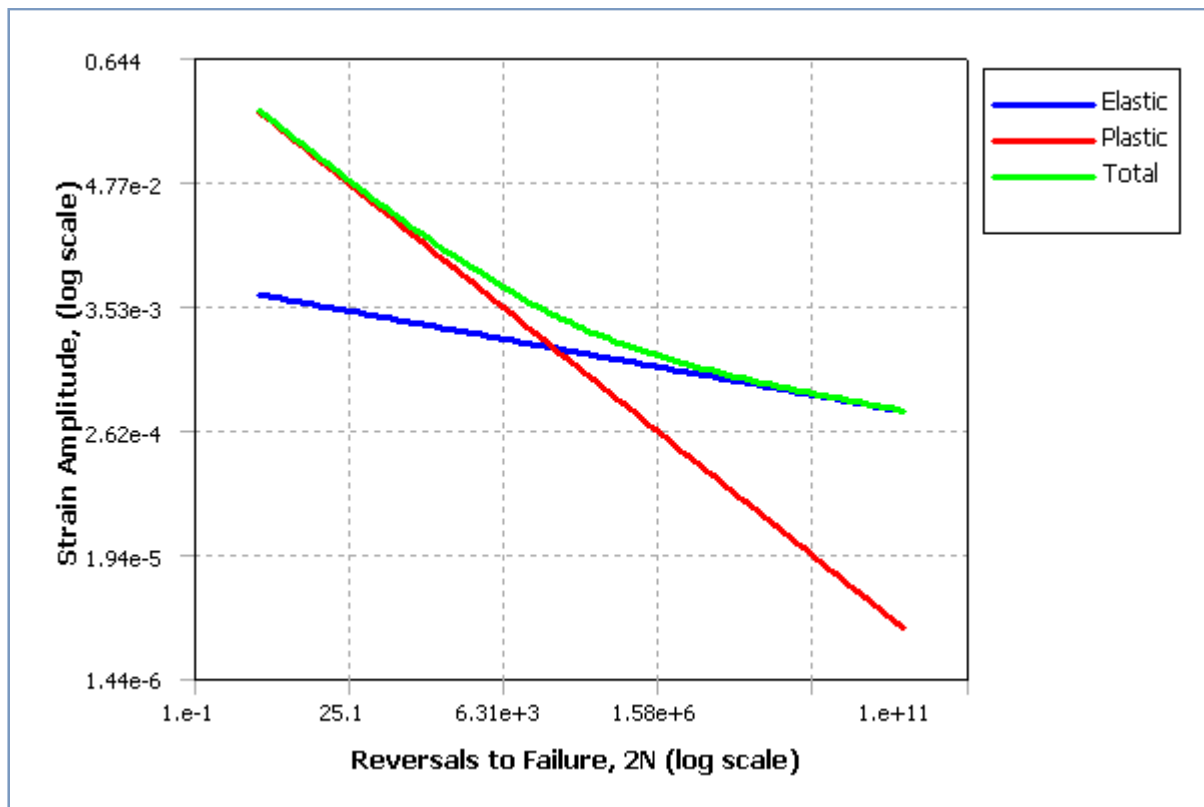
TABLE 33
Steel_P20 > Strain-Life Parameters > Property Attributes

Display Curve Type	Strain-Life

TABLE 34
Steel_P20 > Strain-Life Parameters > Strain-Life Parameters

Strength Coefficient MPa	920.
Strength Exponent	-0.106
Ductility Coefficient	0.213
Ductility Exponent	-0.47
Cyclic Strength Coefficient MPa	1000.
Cyclic Strain Hardening Exponent	0.2

BiresinL74_60AI

TABLE 35
BiresinL74_60AI > Constants

Structural	
Young's Modulus	5500. MPa
Poisson's Ratio	0.31
Density	1.65e-006 kg/mm³
Thermal Expansion	6.e-005 1/℃
Tensile Yield Strength	250. MPa
Compressive Yield Strength	250. MPa
Tensile Ultimate Strength	56. MPa
Compressive Ultimate Strength	0. MPa
Thermal	
Thermal Conductivity	6.06e-004 W/mm·℃
Specific Heat	1279.2 J/kg·℃
Electromagnetics	
Relative Permeability	10000
Resistivity	1.7e-004 Ohm·mm

FIGURE 30
BiresinL74_60Al > Alternating Stress
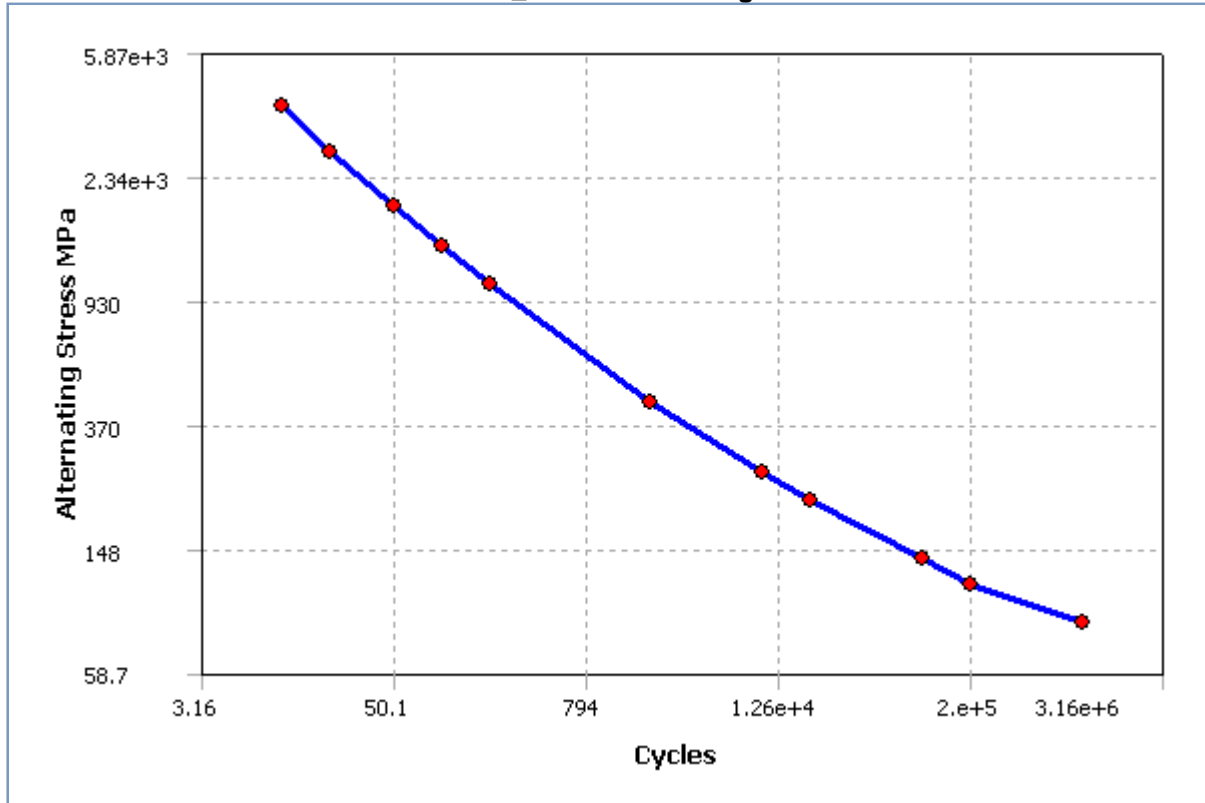
TABLE 36
BiresinL74_60Al > Alternating Stress > Property Attributes

Interpolation	Log-Log
Mean Curve Type	Mean Stress

TABLE 37
BiresinL74_60Al > Alternating Stress > Alternating Stress Curve Data

Mean Value MPa
0.

TABLE 38
BiresinL74_60Al > Alternating Stress > Alternating Stress vs. Cycles

Cycles	Alternating Stress MPa
10.	3999.
20.	2827.
50.	1896.
100.	1413.
200.	1069.
2000.	441.
10000	262.
20000	214.
1.e+005	138.
2.e+005	114.
1.e+006	86.2

FIGURE 31
BiresinL74_60Al > Strain-Life Parameters
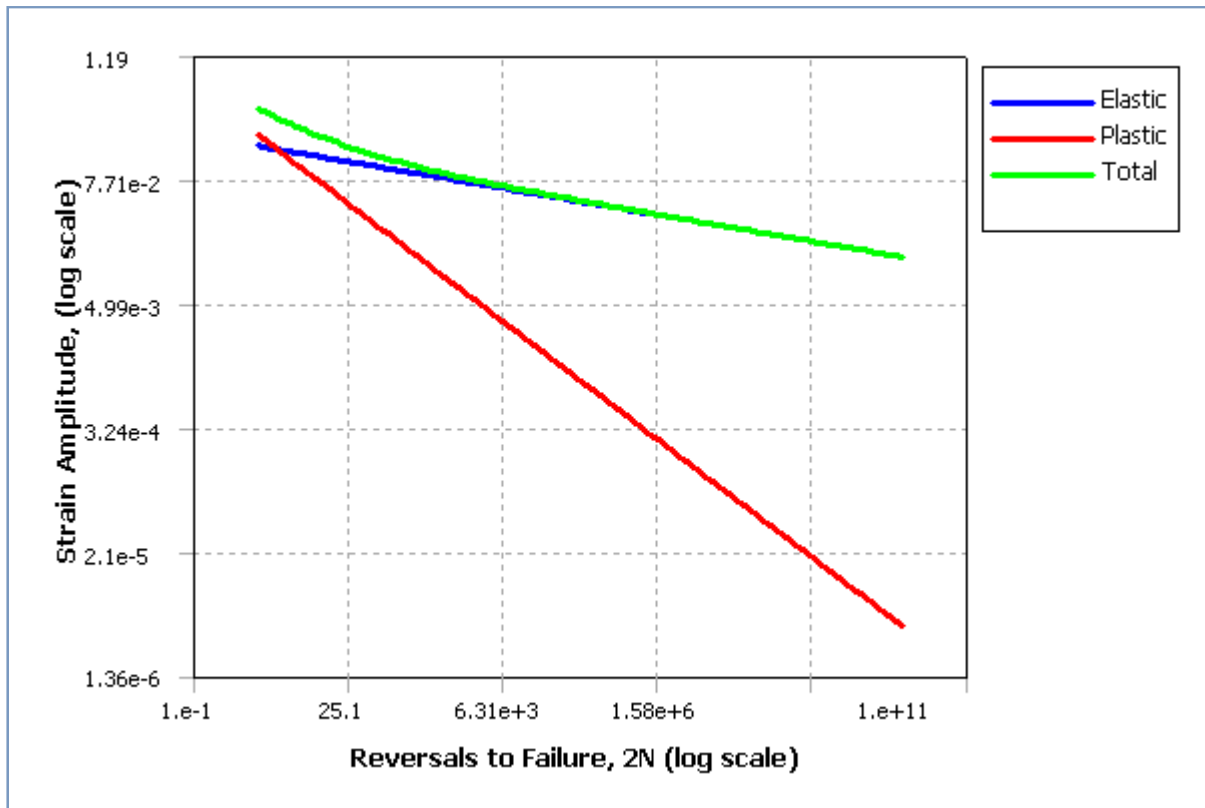
TABLE 39
BiresinL74_60AI > Strain-Life Parameters > Property Attributes
Display Curve Type | Strain-Life

TABLE 40
BiresinL74_60AI > Strain-Life Parameters > Strain-Life Parameters

Strength Coefficient MPa	920.
Strength Exponent	-0.106
Ductility Coefficient	0.213
Ductility Exponent	-0.47
Cyclic Strength Coefficient MPa	1000.
Cyclic Strain Hardening Exponent	0.2

Project

First Saved	Saturday, December 06, 2008
Last Saved	Tuesday, February 02, 2010
Product Version	11.0 Release

Contents

Report Not Finalized

Not all objects described below are in a finalized state. As a result, data may be incomplete, obsolete or in error. View first state problem. To finalize this report, edit objects as needed and solve the analyses.

Units

TABLE 1

Unit System	Metric (mm, kg, N, °C, s, mV, mA)
Angle	Degrees
Rotational Velocity	rad/s

Model_BirL74_60Al

Geometry

TABLE 2
Model_BirL74_60Al > Geometry

Object Name	*Geometry*
State	Fully Defined
Definition	
Source	D:\DOUT\Experiments HM2\Structural_Ansys_HM2_Pin\AssemFinalDim.SLDASM
Type	SolidWorks
Length Unit	Meters
Element Control	Program Controlled
Display Style	Part Color
Bounding Box	
Length X	12.33 mm
Length Y	12.306 mm
Length Z	10. mm
Properties	
Volume	900.75 mm³
Mass	1.0709e-003 kg
Statistics	
Bodies	2

Active Bodies	2
Nodes	107264
Elements	67799
Preferences	
Import Solid Bodies	Yes
Import Surface Bodies	Yes
Import Line Bodies	Yes
Parameter Processing	Yes
Personal Parameter Key	DS
CAD Attribute Transfer	No
Named Selection Processing	No
Material Properties Transfer	No
CAD Associativity	Yes
Import Coordinate Systems	No
Reader Save Part File	No
Import Using Instances	Yes
Do Smart Update	No
Attach File Via Temp File	No
Analysis Type	3-D
Mixed Import Resolution	None
Enclosure and Symmetry Processing	Yes

TABLE 3
Model_BirL74_60Al > Geometry > Parts

Object Name	MouldingPin_FinalDim-1	Plastic_Pin_FinalIDim-1
State	Meshed	Hidden
Graphics Properties		
Visible	Yes	No
Transparency	1	
Definition		
Suppressed	No	
Material	BiresinL74_60Al	Domo 1100N
Stiffness Behavior	Flexible	
Nonlinear Material Effects	Yes	
Bounding Box		
Length X	8.4776 mm	12.33 mm
Length Y	8.4823 mm	12.306 mm
Length Z	10. mm	9. mm
Properties		
Volume	339.54 mm³	561.21 mm³
Mass	5.6024e-004 kg	5.107e-004 kg
Centroid X	-5.0777e-008 mm	2.6913e-017 mm
Centroid Y	1.9251e-008 mm	-1.5667e-016 mm
Centroid Z	5.2344 mm	4.4388 mm
Moment of Inertia Ip1	7.0486e-003 kg·mm²	1.0455e-002 kg·mm²
Moment of Inertia Ip2	7.0486e-003 kg·mm²	1.0455e-002 kg·mm²
Moment of Inertia Ip3	6.3758e-003 kg·mm²	1.4031e-002 kg·mm²
Statistics		
Nodes	40077	67187
Elements	24891	42908

FIGURE 1
Model_BirL74_60Al > Geometry > MouldingPin_FinalDim-1 > Image
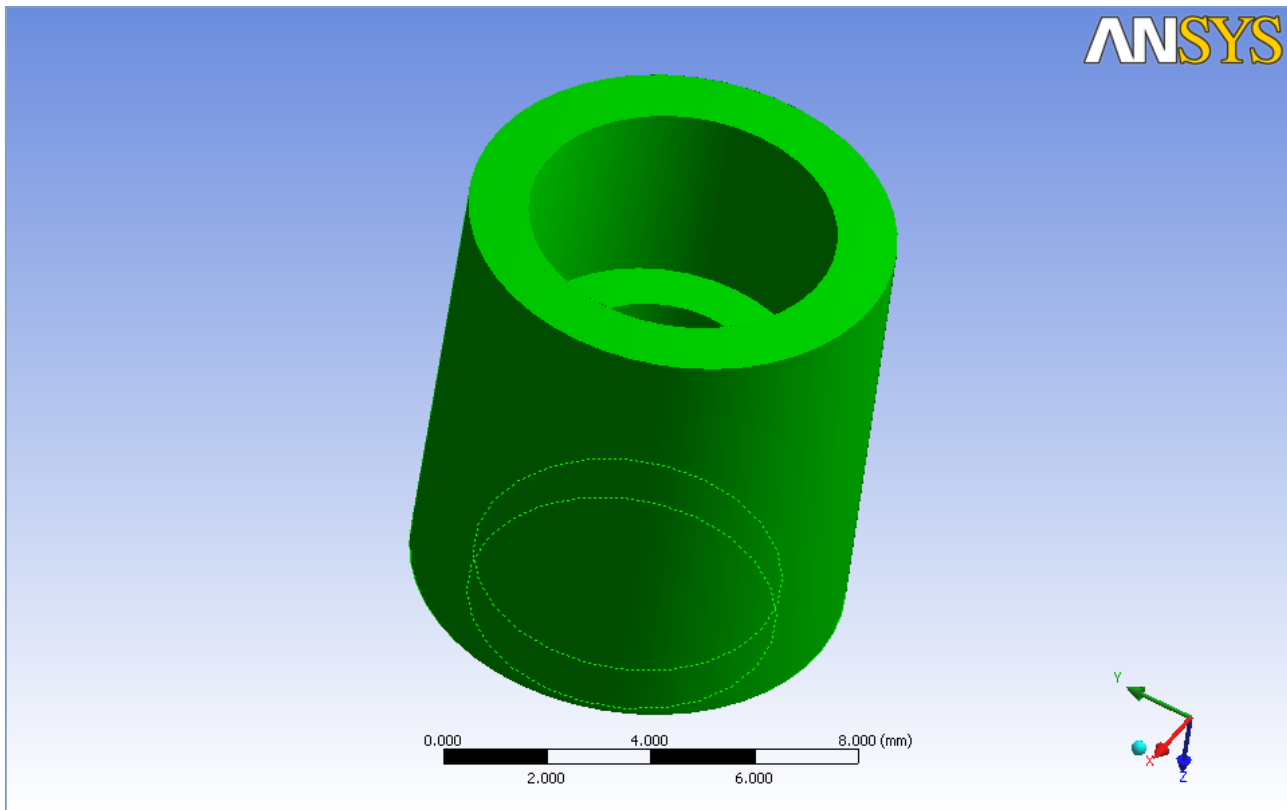
Connections

TABLE 4
Model_BirL74_60Al > Connections

Object Name	Connections
State	Fully Defined
Auto Detection	
Generate Contact On Update	Yes
Tolerance Type	Slider
Tolerance Slider	0.
Tolerance Value	5.0216e-002 mm
Face/Face	Yes
Face/Edge	No
Edge/Edge	No
Priority	Include All
Same Body Grouping	Yes
Revolute Joints	Yes
Fixed Joints	Yes
Transparency	
Enabled	Yes

TABLE 5
Model_BirL74_60Al > Connections > Contact Regions

Object Name	Frictional - MouldingPin_FinalDim-1 To Plastic_Pin_FinallDim-1
State	Fully Defined
Scope	
Scoping Method	Geometry Selection
Contact	1 Face
Target	1 Face
Contact Bodies	MouldingPin_FinalDim-1
Target Bodies	Plastic_Pin_FinallDim-1
Definition	
Type	Frictional
Friction Coefficient	0.332
Scope Mode	Automatic
Behavior	Symmetric
Suppressed	No
Advanced	
Formulation	Pure Penalty
Interface Treatment	Add Offset, Ramped Effects
Offset	0. mm
Normal Stiffness	Program Controlled
Update Stiffness	Never
Thermal Conductance	Program Controlled
Pinball Region	Program Controlled
Time Step Controls	None

FIGURE 2
Model_BirL74_60Al > Connections > Frictional - MouldingPin_FinalDim-1 To Plastic_Pin_FinallDim-1 > Figure 2
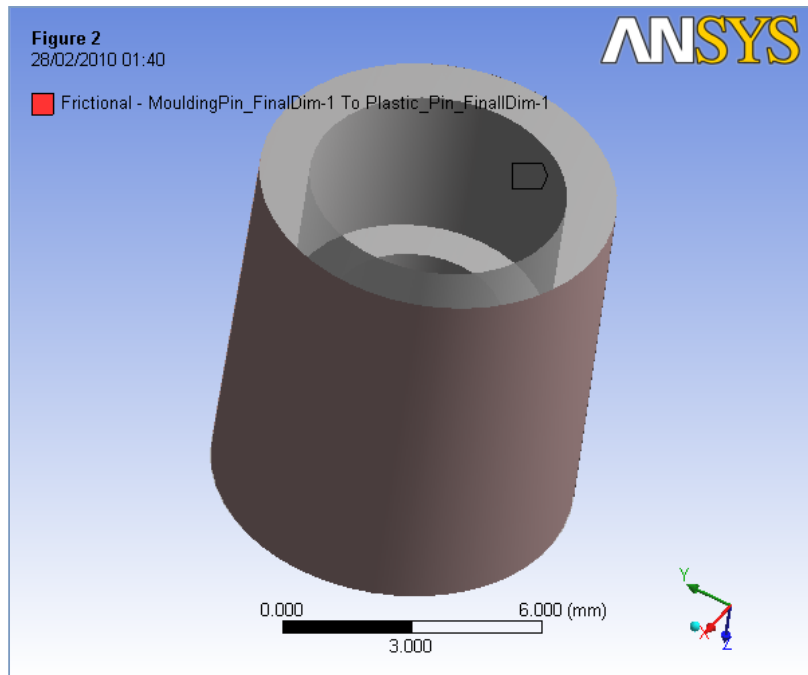
Mesh

TABLE 6
Model_BirL74_60Al > Mesh

Object Name	Mesh
State	Solved
Defaults	
Physics Preference	Mechanical
Relevance	0
Advanced	
Relevance Center	Coarse
Element Size	0.5 mm
Shape Checking	Standard Mechanical
Solid Element Midside Nodes	Program Controlled
Straight Sided Elements	No
Initial Size Seed	Active Assembly
Smoothing	Low
Transition	Fast
Statistics	
Nodes	107264
Elements	67799

TABLE 7
Model_BirL74_60Al > Mesh > Mesh Controls

Object Name	Body Sizing
State	Fully Defined
Scope	
Scoping Method	Geometry Selection
Geometry	2 Bodies
Definition	
Suppressed	No
Type	Element Size
Element Size	0.5 mm
Edge Behavior	Curv/Proximity Refinement

FIGURE 3
Model_BirL74_60Al > Mesh > Figure

0.000   6.000 (mm)
       3.000
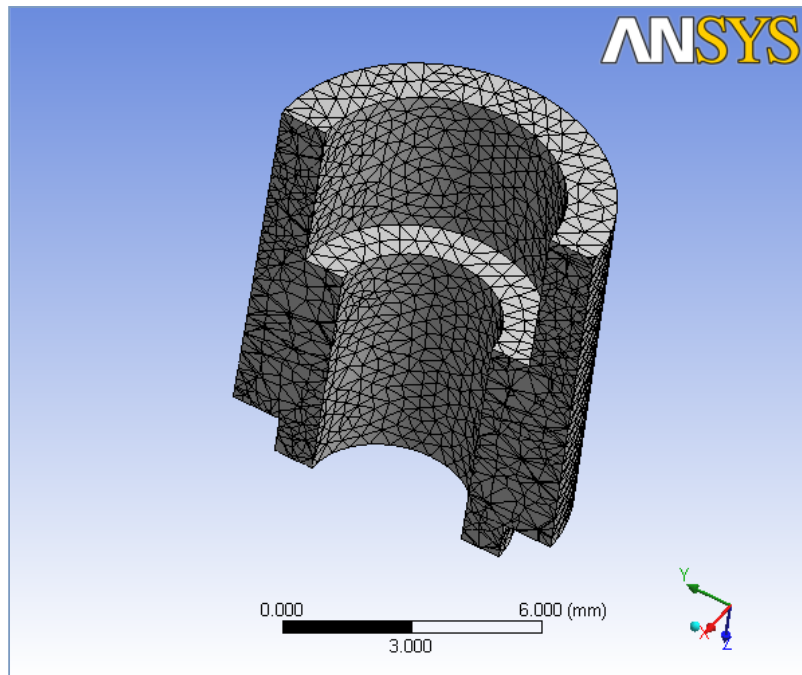
Static Structural

TABLE 8
Model_BirL74_60Al > Analysis

Object Name	Static Structural
State	Fully Defined
Definition	
Physics Type	Structural
Analysis Type	Static Structural
Options	
Reference Temp	22. ℃

TABLE 9
Model_BirL74_60Al > Static Structural > Analysis Settings

Object Name	Analysis Settings
State	Fully Defined
Step Controls	
Number Of Steps	1.
Current Step Number	1.
Step End Time	10. s
Auto Time Stepping	Program Controlled
Solver Controls	
Solver Type	Program Controlled
Weak Springs	Program Controlled
Large Deflection	Off
Inertia Relief	Off
Nonlinear Controls	
Force Convergence	Program Controlled
Moment Convergence	Program Controlled
Displacement Convergence	Program Controlled
Rotation Convergence	Program Controlled
Line Search	Program Controlled
Output Controls	
Calculate Stress	Yes
Calculate Strain	Yes
Calculate Results At	All Time Points
Analysis Data Management	
Solver Files Directory	D:\DOUT\Experiments HM2\Structural_Ansys_HM2_Pin\AssemFinalDim2 Simulation Files\Static Structural\
Future Analysis	None
Save ANSYS db	No
Delete Unneeded Files	Yes
Nonlinear Solution	Yes

TABLE 10
Model_BirL74_60Al > Static Structural > Loads

Object Name	Force	Pressure	Pressure 2
State	Fully Defined		Suppressed
Scope			
Scoping Method	Geometry Selection		
Geometry	1 Face		
Definition			
Define By	Components	Normal To	
Type	Force	Pressure	
X Component	0. N (ramped)		

Y Component	0. N (ramped)	
Z Component	Tabular Data	
Suppressed	No	Yes
Magnitude	Tabular Data	12. MPa (ramped)

FIGURE 4
Model_BirL74_60Al > Static Structural > Force
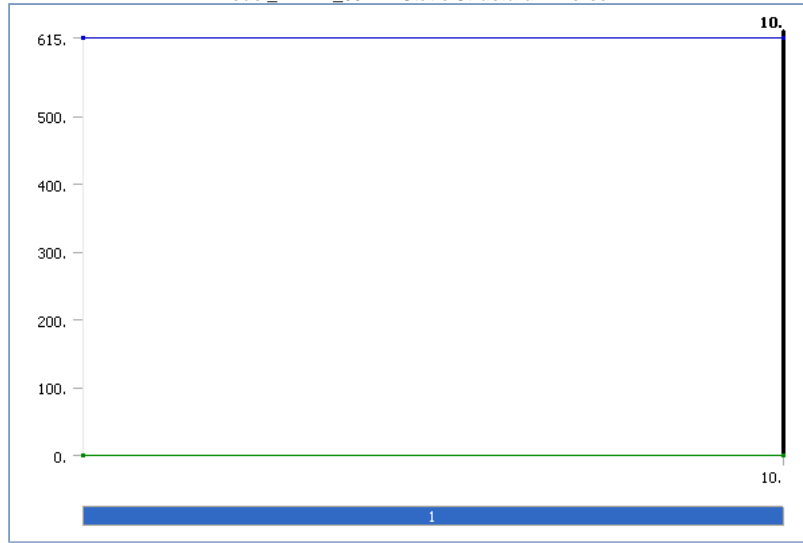
TABLE 11
Model_BirL74_60Al > Static Structural > Force

Steps	Time [s]	X [N]	Y [N]	Z [N]
1	0.	0.	0.	615.
	10.			

FIGURE 5
Model_BirL74_60Al > Static Structural > Force > Figure
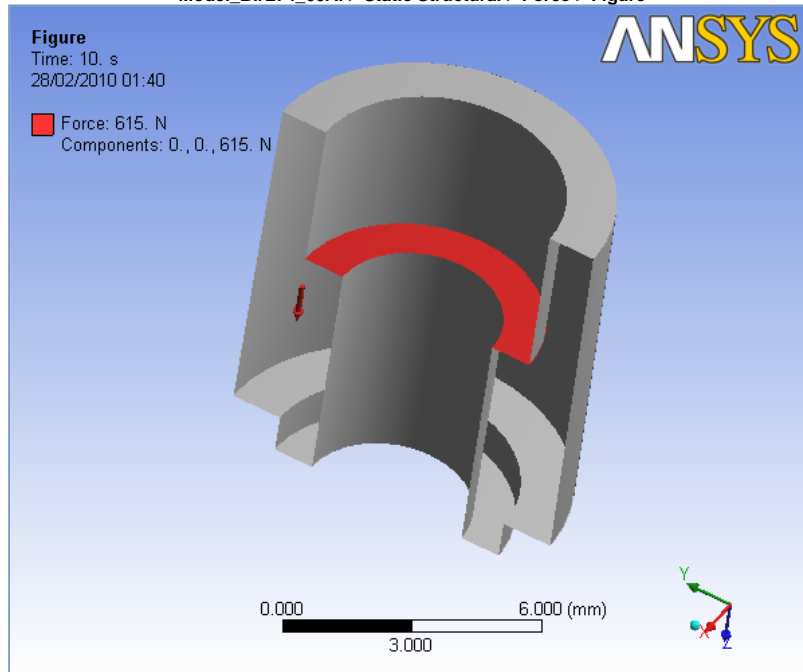
FIGURE 6
Model_BirL74_60Al > Static Structural > Pressure
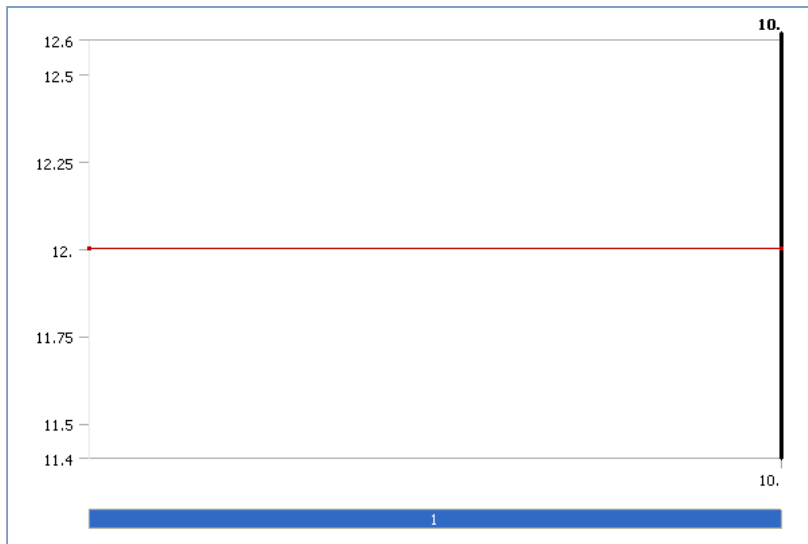
TABLE 12
Model_BirL74_60Al > Static Structural > Pressure

Steps	Time [s]	Pressure [MPa]
1	0.	12.
	10.	

FIGURE 7
Model_BirL74_60Al > Static Structural > Pressure 2
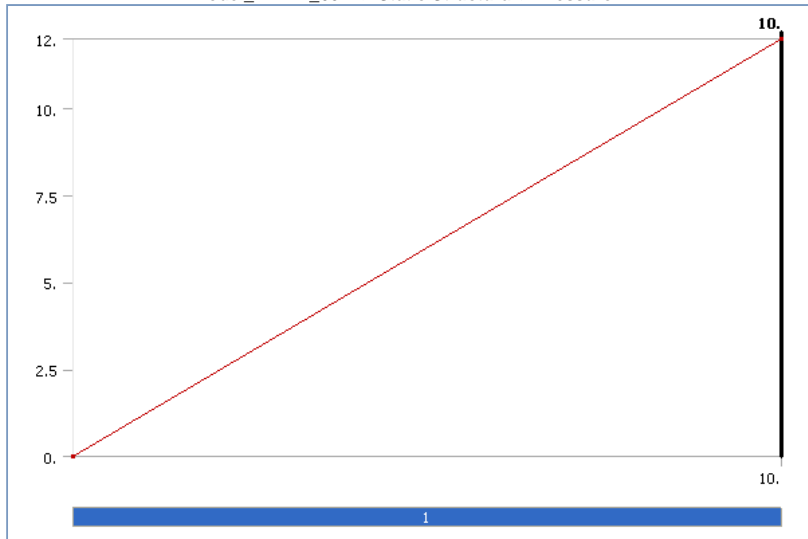
FIGURE 8
Model_BirL74_60Al > Static Structural > Pressure 2 > Figure

0.000   6.000 (mm)

3.000
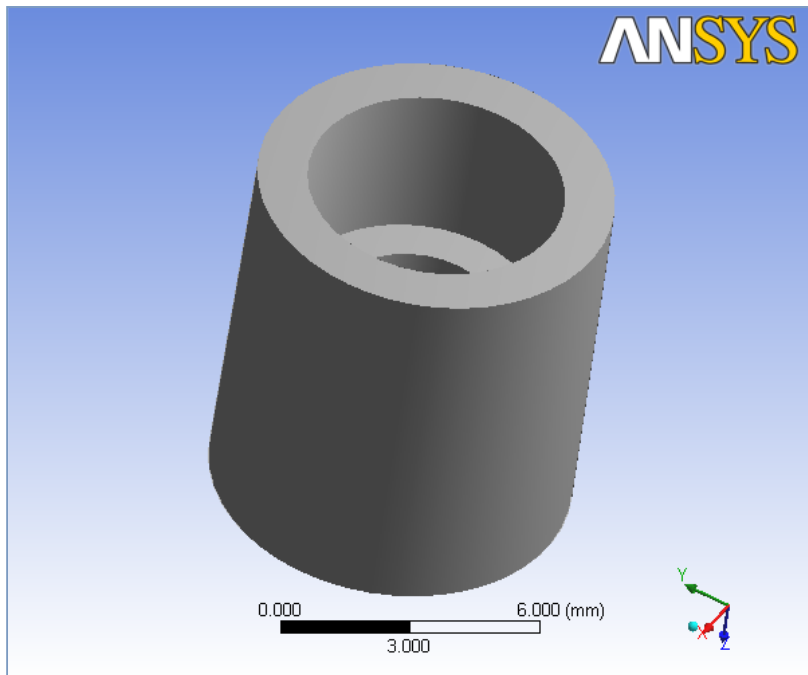
TABLE 13
Model_BirL74_60Al > Static Structural > Thermal Condition

Object Name	Thermal Condition
State	Fully Defined
Definition	
Condition	Uniform Temperature
Uniform Temp	70. ℃
Suppressed	No

TABLE 14
Model_BirL74_60Al > Static Structural > Loads

Object Name	Fixed Support
State	Fully Defined
Scope	
Scoping Method	Geometry Selection
Geometry	1 Face
Definition	
Type	Fixed Support
Suppressed	No

FIGURE 9
Model_BirL74_60Al > Static Structural > Fixed Support > Figure

0.000   6.000 (mm)

3.000
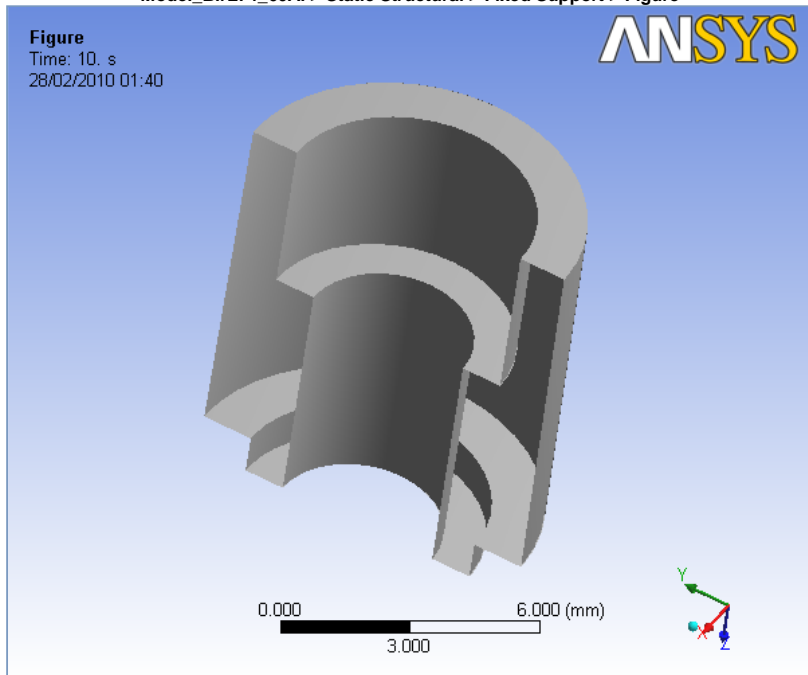
Solution

TABLE 15
Model_BirL74_60Al > Static Structural > Solution

Object Name	Solution
State	Obsolete
Adaptive Mesh Refinement	
Max Refinement Loops	1.
Refinement Depth	2.

TABLE 16
Model_BirL74_60Al > Static Structural > Solution > Solution Information

Object Name	Solution Information
State	Not Solved
Solution Information	
Solution Output	Solver Output
Newton-Raphson Residuals	0
Update Interval	2.5 s
Display Points	All

TABLE 17
Model_BirL74_60Al > Static Structural > Solution > Results

Object Name	Equivalent Elastic Strain	Equivalent Stress
State	Obsolete	
Scope		
Geometry	All Bodies	
Definition		
Type	Equivalent (von-Mises) Elastic Strain	Equivalent (von-Mises) Stress
Display Time	End Time	
Results		
Minimum	5.1257e-005 mm/mm	0.28192 MPa
Maximum	2.4059e-002 mm/mm	63.219 MPa
Minimum Occurs On	MouldingPin_FinalDim-1	
Maximum Occurs On	Plastic_Pin_FinallDim-1	MouldingPin_FinalDim-1
Information		
Time	10. s	
Load Step	1	
Substep	4	
Iteration Number	24	

FIGURE 10
Model_BirL74_60Al > Static Structural > Solution > Equivalent Elastic Strain

FIGURE 11
Model_BirL74_60Al > Static Structural > Solution > Equivalent Stress

TABLE 18
Model_BirL74_60AI > Static Structural > Solution > Stress Safety Tools

Object Name	Stress Tool
State	Not Solved
Definition	
Theory	Max Equivalent Stress
Stress Limit Type	Tensile Yield Per Material

TABLE 19
Model_BirL74_60AI > Static Structural > Solution > Stress Tool > Results

Object Name	Safety Factor
State	Obsolete
Scope	
Geometry	All Bodies
Definition	
Type	Safety Factor
Display Time	End Time
Results	
Minimum	0.83835
Minimum Occurs On	MouldingPin_FinalDim-1
Information	
Time	10. s
Load Step	1
Substep	4
Iteration Number	24

FIGURE 12
Model_BirL74_60AI > Static Structural > Solution > Stress Tool > Safety Factor
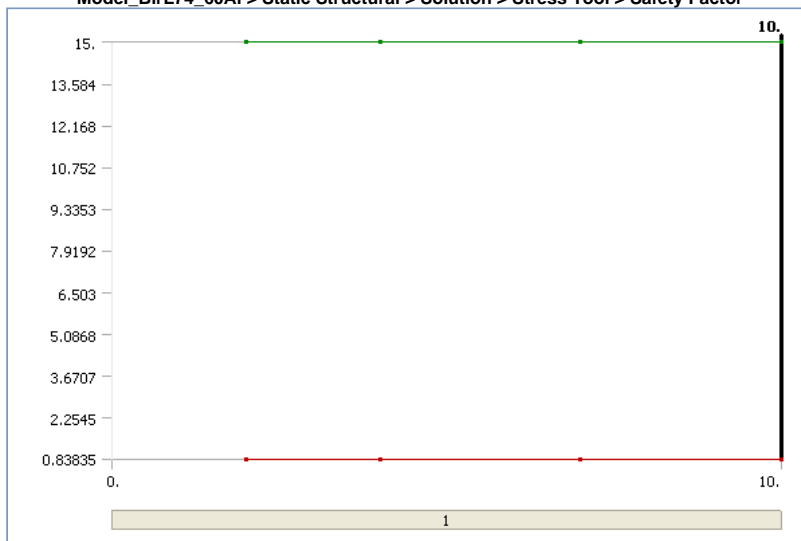
Steady-State Thermal

TABLE 20
Model_BirL74_60AI > Analysis

Object Name	Steady-State Thermal
State	Fully Defined
Definition	

Physics Type	Thermal
Analysis Type	Steady-State

TABLE 21
Model_BirL74_60Al > Steady-State Thermal > Initial Condition

Object Name	Initial Condition
State	Fully Defined
Definition	
Initial Temperature	Uniform Temperature
Initial Temperature Value	70. ℃

TABLE 22
Model_BirL74_60Al > Steady-State Thermal > Analysis Settings

Object Name	Analysis Settings
State	Fully Defined
Step Controls	
Number Of Steps	1.
Current Step Number	1.
Step End Time	10. s
Auto Time Stepping	Program Controlled
Solver Controls	
Solver Type	Program Controlled
Nonlinear Controls	
Heat Convergence	Program Controlled
Temperature Convergence	Program Controlled
Line Search	Program Controlled
Output Controls	
Calculate Thermal Flux	Yes
Calculate Results At	All Time Points
Analysis Data Management	
Solver Files Directory	D:\DOUT\Experiments HM2\Structural_Ansys_HM2_Pin\AssemFinalDim2 Simulation Files\Steady-State Thermal\
Future Analysis	None
Save ANSYS db	No
Delete Unneeded Files	Yes
Nonlinear Solution	Yes

TABLE 23
Model_BirL74_60Al > Steady-State Thermal > Loads

Object Name	Temperature
State	Fully Defined
Scope	
Scoping Method	Geometry Selection
Geometry	2 Bodies
Definition	
Type	Temperature
Magnitude	70. ℃ (ramped)
Suppressed	No

FIGURE 13
Model_BirL74_60Al > Steady-State Thermal > Temperature
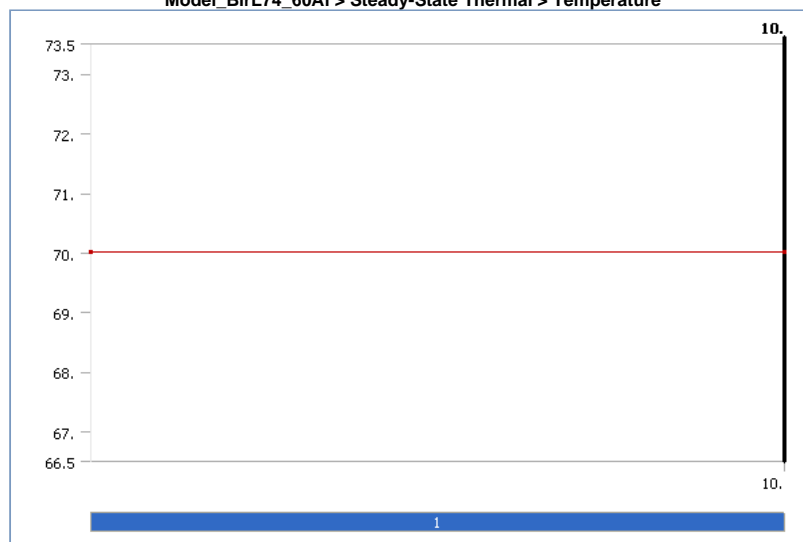
Solution

TABLE 24
Model_BirL74_60Al > Steady-State Thermal > Solution

Object Name	Solution
State	Solved
Adaptive Mesh Refinement	
Max Refinement Loops	1.
Refinement Depth	2.

TABLE 25
Model_BirL74_60AI > Steady-State Thermal > Solution > Solution Information

Object Name	Solution Information
State	Solved
Solution Information	
Solution Output	Solver Output
Update Interval	2.5 s
Display Points	All

TABLE 26
Model_BirL74_60AI > Steady-State Thermal > Solution > Results

Object Name	Temperature
State	Solved
Scope	
Geometry	All Bodies
Definition	
Type	Temperature
Display Time	End Time
Results	
Minimum	70. ℃
Maximum	70. ℃
Minimum Occurs On	MouldingPin_FinalDim-1
Maximum Occurs On	MouldingPin_FinalDim-1
Information	
Time	10. s
Load Step	1
Substep	1
Iteration Number	1

SSF

Geometry

TABLE 27
SSF > Geometry

Object Name	Geometry
State	Fully Defined
Definition	
Source	D:\DOUT\Experiments HM2\Structural_Ansys_HM2_Pin\AssemFinalDim.SLDASM
Type	SolidWorks
Length Unit	Meters
Element Control	Program Controlled
Display Style	Part Color
Bounding Box	
Length X	12.33 mm
Length Y	12.306 mm
Length Z	10. mm
Properties	
Volume	900.75 mm³
Mass	1.2237e-003 kg
Statistics	
Bodies	2
Active Bodies	2
Nodes	107264
Elements	67799
Preferences	
Import Solid Bodies	Yes
Import Surface Bodies	Yes
Import Line Bodies	Yes
Parameter Processing	Yes
Personal Parameter Key	DS
CAD Attribute Transfer	No
Named Selection Processing	No
Material Properties Transfer	No
CAD Associativity	Yes
Import Coordinate Systems	No
Reader Save Part File	No
Import Using Instances	Yes
Do Smart Update	No
Attach File Via Temp File	No
Analysis Type	3-D
Mixed Import Resolution	None
Enclosure and Symmetry Processing	Yes

TABLE 28
SSF > Geometry > Parts

Object Name	MouldingPin_FinalDim-1	Plastic_Pin_FinallDim-1
State	Meshed	Hidden
Graphics Properties		
Visible	Yes	No
Transparency	1	
Definition		
Suppressed	No	
Material	SSF	Domo 1100N

Stiffness Behavior	Flexible	
Nonlinear Material Effects	Yes	
Bounding Box		
Length X	8.4776 mm	12.33 mm
Length Y	8.4823 mm	12.306 mm
Length Z	10. mm	9. mm
Properties		
Volume	339.54 mm³	561.21 mm³
Mass	7.1304e-004 kg	5.107e-004 kg
Centroid X	-5.0777e-008 mm	2.6913e-017 mm
Centroid Y	1.9251e-008 mm	-1.5667e-016 mm
Centroid Z	5.2344 mm	4.4388 mm
Moment of Inertia Ip1	8.9709e-003 kg·mm²	1.0455e-002 kg·mm²
Moment of Inertia Ip2	8.9709e-003 kg·mm²	1.0455e-002 kg·mm²
Moment of Inertia Ip3	8.1146e-003 kg·mm²	1.4031e-002 kg·mm²
Statistics		
Nodes	40077	67187
Elements	24891	42908

Connections

TABLE 29
SSF > Connections

Object Name	*Connections*
State	Fully Defined
Auto Detection	
Generate Contact On Update	Yes
Tolerance Type	Slider
Tolerance Slider	0.
Tolerance Value	5.0216e-002 mm
Face/Face	Yes
Face/Edge	No
Edge/Edge	No
Priority	Include All
Same Body Grouping	Yes
Revolute Joints	Yes
Fixed Joints	Yes
Transparency	
Enabled	Yes

TABLE 30
SSF > Connections > Contact Regions

Object Name	*Frictional - MouldingPin_FinalDim-1 To Plastic_Pin_FinallDim-1*
State	Fully Defined
Scope	
Scoping Method	Geometry Selection
Contact	1 Face
Target	1 Face
Contact Bodies	MouldingPin_FinalDim-1
Target Bodies	Plastic_Pin_FinallDim-1
Definition	
Type	Frictional
Friction Coefficient	0.31
Scope Mode	Automatic
Behavior	Symmetric
Suppressed	No
Advanced	
Formulation	Pure Penalty
Interface Treatment	Add Offset, Ramped Effects
Offset	0. mm
Normal Stiffness	Program Controlled
Update Stiffness	Never
Thermal Conductance	Program Controlled
Pinball Region	Program Controlled
Time Step Controls	None

Mesh

TABLE 31
SSF > Mesh

Object Name	*Mesh*
State	Solved
Defaults	
Physics Preference	Mechanical
Relevance	0
Advanced	
Relevance Center	Coarse
Element Size	0.5 mm
Shape Checking	Standard Mechanical
Solid Element Midside Nodes	Program Controlled
Straight Sided Elements	No
Initial Size Seed	Active Assembly
Smoothing	Low
Transition	Fast

Statistics	
Nodes	107264
Elements	67799

TABLE 32
SSF > Mesh > Mesh Controls

Object Name	*Body Sizing*
State	Fully Defined
Scope	
Scoping Method	Geometry Selection
Geometry	2 Bodies
Definition	
Suppressed	No
Type	Element Size
Element Size	0.5 mm
Edge Behavior	Curv/Proximity Refinement

Static Structural

TABLE 33
SSF > Analysis

Object Name	*Static Structural*
State	Fully Defined
Definition	
Physics Type	Structural
Analysis Type	Static Structural
Options	
Reference Temp	22. °C

TABLE 34
SSF > Static Structural > Analysis Settings

Object Name	*Analysis Settings*
State	Fully Defined
Step Controls	
Number Of Steps	1.
Current Step Number	1.
Step End Time	10. s
Auto Time Stepping	Program Controlled
Solver Controls	
Solver Type	Program Controlled
Weak Springs	Program Controlled
Large Deflection	Off
Inertia Relief	Off
Nonlinear Controls	
Force Convergence	Program Controlled
Moment Convergence	Program Controlled
Displacement Convergence	Program Controlled
Rotation Convergence	Program Controlled
Line Search	Program Controlled
Output Controls	
Calculate Stress	Yes
Calculate Strain	Yes
Calculate Results At	All Time Points
Analysis Data Management	
Solver Files Directory	D:\DOUT\Experiments HM2\Structural_Ansys_HM2_Pin\AssemFinalDim2 Simulation Files\Static Structural (2)\
Future Analysis	None
Save ANSYS db	No
Delete Unneeded Files	Yes
Nonlinear Solution	Yes

TABLE 35
SSF > Static Structural > Loads

Object Name	Fixed Support	Force	Pressure
State	Fully Defined		
Scope			
Scoping Method	Geometry Selection		
Geometry	1 Face		
Definition			
Type	Fixed Support	Force	Pressure
Suppressed	No		
Define By		Components	Normal To
X Component		Tabular Data	
Y Component		Tabular Data	
Z Component		Tabular Data	
Magnitude			Tabular Data

FIGURE 14
SSF > Static Structural > Force
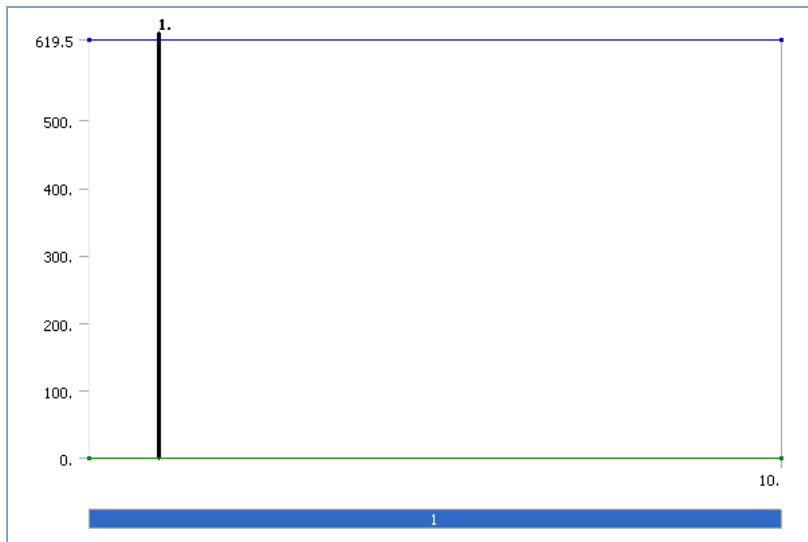
TABLE 36
SSF > Static Structural > Force

Steps	Time [s]	X [N]	Y [N]	Z [N]
1	0. / 10.	0.	0.	619.5

FIGURE 15
SSF > Static Structural > Force > Figure
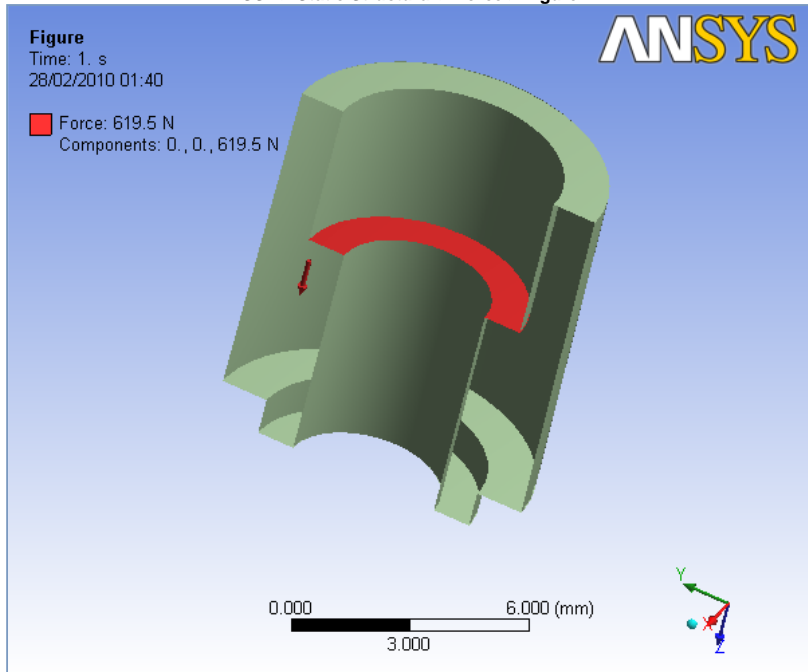
FIGURE 16
SSF > Static Structural > Pressure
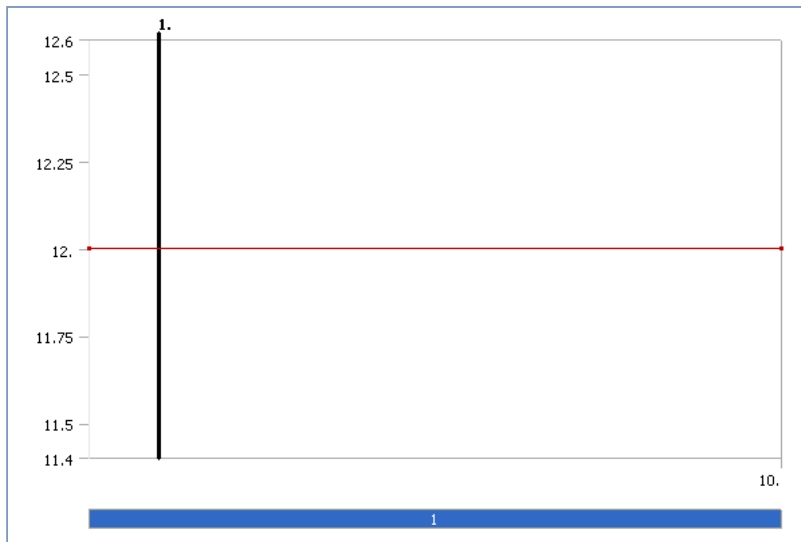
TABLE 37
SSF > Static Structural > Pressure

Steps	Time [s]	Pressure [MPa]
1	0. / 10.	12.

TABLE 38
SSF > Static Structural > Thermal Condition

Object Name	Thermal Condition
State	Fully Defined
Definition	
Condition	Uniform Temperature
Uniform Temp	70. ℃
Suppressed	No

TABLE 39
SSF > Static Structural > Loads

Object Name	Pressure 2
State	Suppressed
Scope	
Scoping Method	Geometry Selection
Geometry	1 Face
Definition	
Define By	Normal To
Type	Pressure
Magnitude	Tabular Data
Suppressed	Yes

FIGURE 17
SSF > Static Structural > Pressure 2
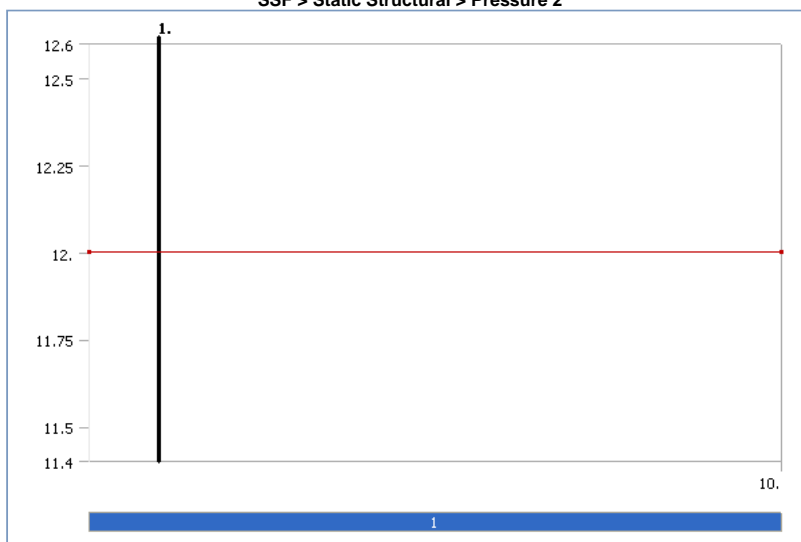
TABLE 40
SSF > Static Structural > Pressure 2

Steps	Time [s]	Pressure [MPa]
1	0. / 10.	12.

Solution

TABLE 41
SSF > Static Structural > Solution

Object Name	*Solution*
State	Solved
Adaptive Mesh Refinement	
Max Refinement Loops	1.
Refinement Depth	2.

TABLE 42
SSF > Static Structural > Solution > Solution Information

Object Name	*Solution Information*
State	Solved
Solution Information	
Solution Output	Solver Output
Newton-Raphson Residuals	0
Update Interval	2.5 s
Display Points	All

TABLE 43
SSF > Static Structural > Solution > Results

Object Name	*Equivalent Elastic Strain*	*Equivalent Stress*
State	Solved	
Scope		
Geometry	All Bodies	
Definition		
Type	Equivalent (von-Mises) Elastic Strain	Equivalent (von-Mises) Stress
Display Time	End Time	
Results		
Minimum	1.2964e-005 mm/mm	5.9632e-002 MPa
Maximum	2.4978e-002 mm/mm	62.533 MPa
Minimum Occurs On	MouldingPin_FinalDim-1	
Maximum Occurs On	Plastic_Pin_FinalIDim-1	MouldingPin_FinalDim-1
Information		
Time	10. s	
Load Step	1	
Substep	4	
Iteration Number	25	

FIGURE 18
SSF > Static Structural > Solution > Equivalent Elastic Strain
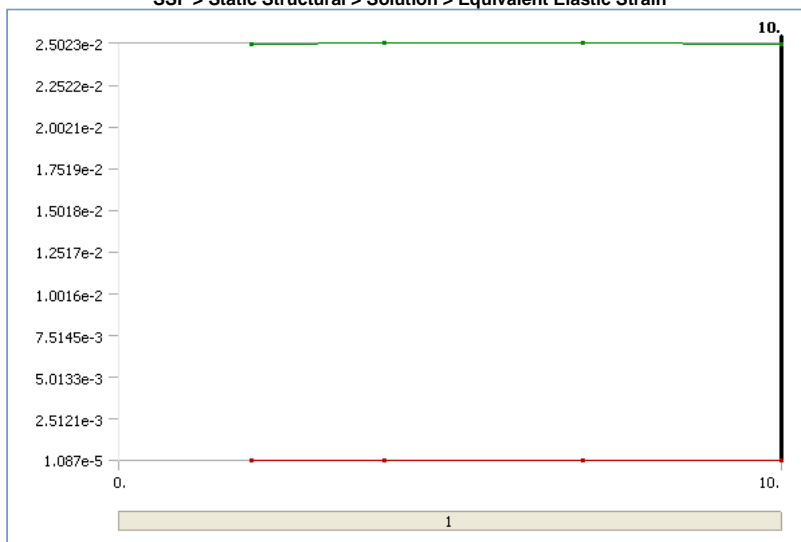
FIGURE 19
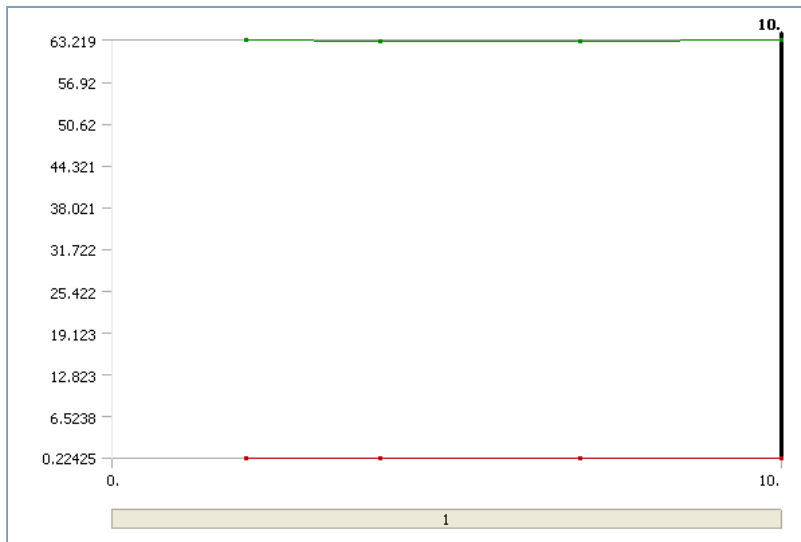**SSF > Static Structural > Solution > Equivalent Stress**

TABLE 44
SSF > Static Structural > Solution > Stress Safety Tools

Object Name	Stress Tool
State	Solved
Definition	
Theory	Max Equivalent Stress
Stress Limit Type	Tensile Yield Per Material

TABLE 45
SSF > Static Structural > Solution > Stress Tool > Results

Object Name	Safety Factor
State	Solved
Scope	
Geometry	All Bodies
Definition	
Type	Safety Factor
Display Time	End Time
Results	
Minimum	0.84755
Minimum Occurs On	MouldingPin_FinalDim-1
Information	
Time	10. s
Load Step	1
Substep	4
Iteration Number	25

FIGURE 20
SSF > Static Structural > Solution > Stress Tool > Safety Factor
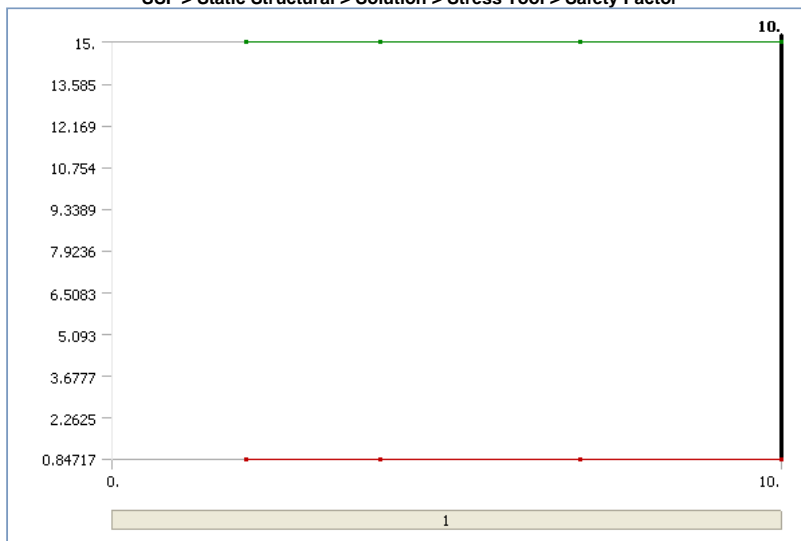
Steady-State Thermal

TABLE 46
SSF > Analysis

Object Name	Steady-State Thermal
State	Fully Defined
Definition	

Physics Type	Thermal
Analysis Type	Steady-State

TABLE 47
SSF > Steady-State Thermal > Initial Condition

Object Name	*Initial Condition*
State	Fully Defined
Definition	
Initial Temperature	Uniform Temperature
Initial Temperature Value	70. ℃

TABLE 48
SSF > Steady-State Thermal > Analysis Settings

Object Name	*Analysis Settings*
State	Fully Defined
Step Controls	
Number Of Steps	1.
Current Step Number	1.
Step End Time	10. s
Auto Time Stepping	Program Controlled
Solver Controls	
Solver Type	Program Controlled
Nonlinear Controls	
Heat Convergence	Program Controlled
Temperature Convergence	Program Controlled
Line Search	Program Controlled
Output Controls	
Calculate Thermal Flux	Yes
Calculate Results At	All Time Points
Analysis Data Management	
Solver Files Directory	D:\DOUT\Experiments HM2\Structural_Ansys_HM2_Pin\AssemFinalDim2 Simulation Files\Steady-State Thermal (2)\
Future Analysis	None
Save ANSYS db	No
Delete Unneeded Files	Yes
Nonlinear Solution	Yes

TABLE 49
SSF > Steady-State Thermal > Loads

Object Name	*Temperature*
State	Fully Defined
Scope	
Scoping Method	Geometry Selection
Geometry	2 Bodies
Definition	
Type	Temperature
Magnitude	80. ℃ (ramped)
Suppressed	No

FIGURE 21
SSF > Steady-State Thermal > Temperature
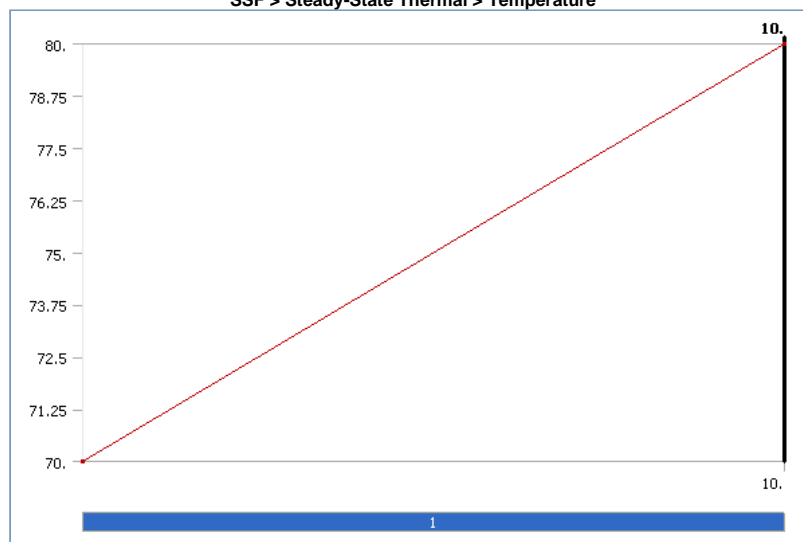
Solution

TABLE 50
SSF > Steady-State Thermal > Solution

Object Name	Solution
State	Solved
Adaptive Mesh Refinement	
Max Refinement Loops	1.
Refinement Depth	2.

TABLE 51
SSF > Steady-State Thermal > Solution > Solution Information

Object Name	Solution Information
State	Solved
Solution Information	
Solution Output	Solver Output
Update Interval	2.5 s
Display Points	All

TABLE 52
SSF > Steady-State Thermal > Solution > Results

Object Name	Temperature
State	Solved
Scope	
Geometry	All Bodies
Definition	
Type	Temperature
Display Time	End Time
Results	
Minimum	80. ℃
Maximum	80. ℃
Minimum Occurs On	MouldingPin_FinalDim-1
Maximum Occurs On	MouldingPin_FinalDim-1
Information	
Time	10. s
Load Step	1
Substep	1
Iteration Number	2

Somos11120

Geometry

TABLE 53
Somos11120 > Geometry

Object Name	Geometry
State	Fully Defined
Definition	
Source	D:\DOUT\Experiments HM2\Structural_Ansys_HM2_Pin\AssemFinalDim.SLDASM
Type	SolidWorks
Length Unit	Meters
Element Control	Program Controlled
Display Style	Part Color
Bounding Box	
Length X	12.33 mm
Length Y	12.306 mm
Length Z	10. mm
Properties	
Volume	900.75 mm³
Mass	8.9099e-004 kg
Statistics	
Bodies	2
Active Bodies	2
Nodes	107264
Elements	67799
Preferences	
Import Solid Bodies	Yes
Import Surface Bodies	Yes
Import Line Bodies	Yes
Parameter Processing	Yes
Personal Parameter Key	DS
CAD Attribute Transfer	No
Named Selection Processing	No
Material Properties Transfer	No
CAD Associativity	Yes
Import Coordinate Systems	No
Reader Save Part File	No
Import Using Instances	Yes
Do Smart Update	No
Attach File Via Temp File	No
Analysis Type	3-D
Mixed Import Resolution	None
Enclosure and Symmetry Processing	Yes

TABLE 54
Somos11120 > Geometry > Parts

Object Name	MouldingPin_FinalDim-1	Plastic_Pin_FinallDim-1
State	Meshed	Hidden
Graphics Properties		
Visible	Yes	No
Transparency	1	
Definition		
Suppressed	No	
Material	Somo11120	Domo 1100N

Stiffness Behavior	Flexible	
Nonlinear Material Effects	Yes	
Bounding Box		
Length X	8.4776 mm	12.33 mm
Length Y	8.4823 mm	12.306 mm
Length Z	10. mm	9. mm
Properties		
Volume	339.54 mm³	561.21 mm³
Mass	3.8029e-004 kg	5.107e-004 kg
Centroid X	-5.0777e-008 mm	2.6913e-017 mm
Centroid Y	1.9251e-008 mm	-1.5667e-016 mm
Centroid Z	5.2344 mm	4.4388 mm
Moment of Inertia Ip1	4.7845e-003 kg·mm²	1.0455e-002 kg·mm²
Moment of Inertia Ip2	4.7845e-003 kg·mm²	1.0455e-002 kg·mm²
Moment of Inertia Ip3	4.3278e-003 kg·mm²	1.4031e-002 kg·mm²
Statistics		
Nodes	40077	67187
Elements	24891	42908

Connections

TABLE 55
Somos11120 > Connections

Object Name	*Connections*
State	Fully Defined
Auto Detection	
Generate Contact On Update	Yes
Tolerance Type	Slider
Tolerance Slider	0.
Tolerance Value	5.0216e-002 mm
Face/Face	Yes
Face/Edge	No
Edge/Edge	No
Priority	Include All
Same Body Grouping	Yes
Revolute Joints	Yes
Fixed Joints	Yes
Transparency	
Enabled	Yes

TABLE 56
Somos11120 > Connections > Contact Regions

Object Name	*Frictional - MouldingPin_FinalDim-1 To Plastic_Pin_FinallDim-1*
State	Fully Defined
Scope	
Scoping Method	Geometry Selection
Contact	1 Face
Target	1 Face
Contact Bodies	MouldingPin_FinalDim-1
Target Bodies	Plastic_Pin_FinallDim-1
Definition	
Type	Frictional
Friction Coefficient	0.475
Scope Mode	Automatic
Behavior	Symmetric
Suppressed	No
Advanced	
Formulation	Pure Penalty
Interface Treatment	Add Offset, Ramped Effects
Offset	0. mm
Normal Stiffness	Program Controlled
Update Stiffness	Never
Thermal Conductance	Program Controlled
Pinball Region	Program Controlled
Time Step Controls	None

Mesh

TABLE 57
Somos11120 > Mesh

Object Name	*Mesh*
State	Solved
Defaults	
Physics Preference	Mechanical
Relevance	0
Advanced	
Relevance Center	Coarse
Element Size	0.5 mm
Shape Checking	Standard Mechanical
Solid Element Midside Nodes	Program Controlled
Straight Sided Elements	No
Initial Size Seed	Active Assembly
Smoothing	Low
Transition	Fast

Statistics	
Nodes	107264
Elements	67799

TABLE 58
Somos11120 > Mesh > Mesh Controls

Object Name	*Body Sizing*
State	Fully Defined
Scope	
Scoping Method	Geometry Selection
Geometry	2 Bodies
Definition	
Suppressed	No
Type	Element Size
Element Size	0.5 mm
Edge Behavior	Curv/Proximity Refinement

Static Structural

TABLE 59
Somos11120 > Analysis

Object Name	*Static Structural*
State	Fully Defined
Definition	
Physics Type	Structural
Analysis Type	Static Structural
Options	
Reference Temp	22. °C

TABLE 60
Somos11120 > Static Structural > Analysis Settings

Object Name	*Analysis Settings*
State	Fully Defined
Step Controls	
Number Of Steps	1.
Current Step Number	1.
Step End Time	10. s
Auto Time Stepping	Program Controlled
Solver Controls	
Solver Type	Program Controlled
Weak Springs	Program Controlled
Large Deflection	Off
Inertia Relief	Off
Nonlinear Controls	
Force Convergence	Program Controlled
Moment Convergence	Program Controlled
Displacement Convergence	Program Controlled
Rotation Convergence	Program Controlled
Line Search	Program Controlled
Output Controls	
Calculate Stress	Yes
Calculate Strain	Yes
Calculate Results At	All Time Points
Analysis Data Management	
Solver Files Directory	D:\DOUT\Experiments HM2\Structural_Ansys_HM2_Pin\AssemFinalDim2 Simulation Files\Static Structural (3)\
Future Analysis	None
Save ANSYS db	No
Delete Unneeded Files	Yes
Nonlinear Solution	Yes

TABLE 61
Somos11120 > Static Structural > Loads

Object Name	*Fixed Support*	*Force*	*Pressure*
State	Fully Defined		
Scope			
Scoping Method	Geometry Selection		
Geometry	1 Face		
Definition			
Type	Fixed Support	Force	Pressure
Suppressed	No		
Define By		Components	Normal To
X Component		Tabular Data	
Y Component		Tabular Data	
Z Component		Tabular Data	
Magnitude			Tabular Data

FIGURE 22
Somos11120 > Static Structural > Force
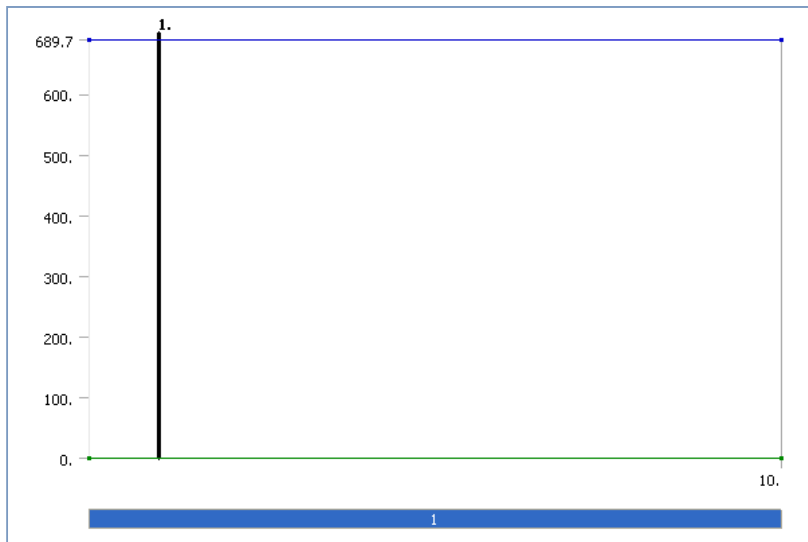
TABLE 62
Somos11120 > Static Structural > Force

Steps	Time [s]	X [N]	Y [N]	Z [N]
1	0. 10.	0.	0.	689.7

FIGURE 23
Somos11120 > Static Structural > Force > Figure
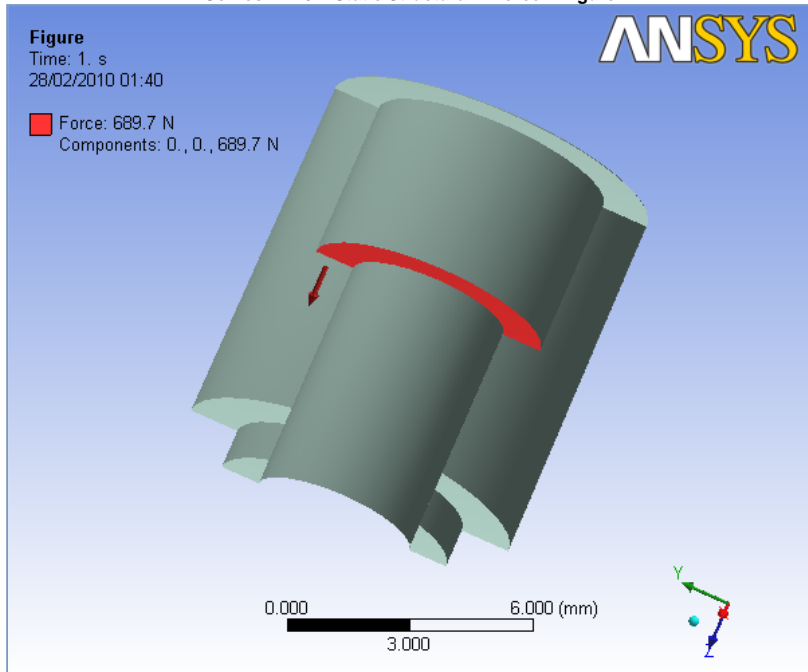
FIGURE 24
Somos11120 > Static Structural > Pressure
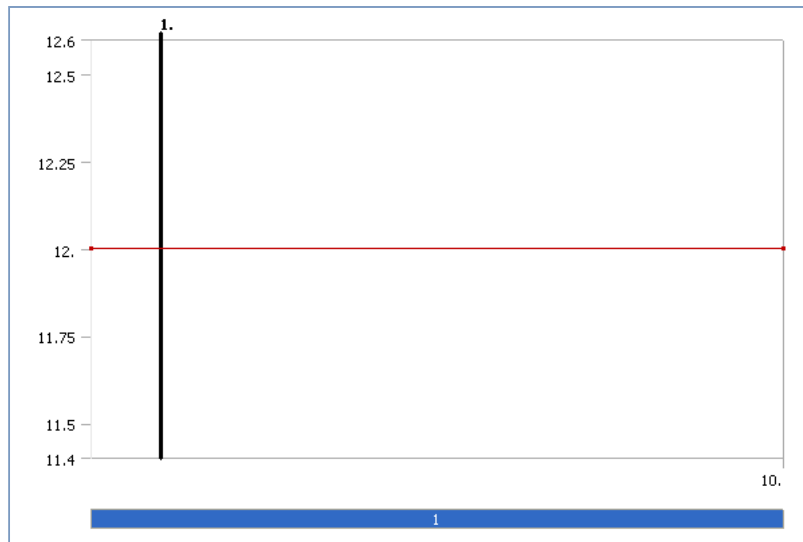
TABLE 63
Somos11120 > Static Structural > Pressure

Steps	Time [s]	Pressure [MPa]
1	0.	12.
	10.	

TABLE 64
Somos11120 > Static Structural > Thermal Condition

Object Name	Thermal Condition
State	Fully Defined
Definition	
Condition	Uniform Temperature
Uniform Temp	60. ℃
Suppressed	No

Solution

TABLE 65
Somos11120 > Static Structural > Solution

Object Name	Solution
State	Solved
Adaptive Mesh Refinement	
Max Refinement Loops	1.
Refinement Depth	2.

TABLE 66
Somos11120 > Static Structural > Solution > Solution Information

Object Name	Solution Information
State	Solved
Solution Information	
Solution Output	Solver Output
Newton-Raphson Residuals	0
Update Interval	2.5 s
Display Points	All

TABLE 67
Somos11120 > Static Structural > Solution > Results

Object Name	Equivalent Elastic Strain	Equivalent Stress
State	Solved	
Scope		
Geometry	All Bodies	
Definition		
Type	Equivalent (von-Mises) Elastic Strain	Equivalent (von-Mises) Stress
Display Time	End Time	
Results		
Minimum	2.0493e-004 mm/mm	0.55332 MPa
Maximum	2.4098e-002 mm/mm	65.066 MPa
Minimum Occurs On	MouldingPin_FinalDim-1	
Maximum Occurs On	MouldingPin_FinalDim-1	
Information		
Time	10. s	
Load Step	1	
Substep	4	
Iteration Number	25	

FIGURE 25
Somos11120 > Static Structural > Solution > Equivalent Elastic Strain

FIGURE 26
Somos11120 > Static Structural > Solution > Equivalent Stress

TABLE 68
Somos11120 > Static Structural > Solution > Stress Safety Tools

Object Name	Stress Tool
State	Solved
Definition	
Theory	Max Equivalent Stress
Stress Limit Type	Tensile Yield Per Material

TABLE 69
Somos11120 > Static Structural > Solution > Stress Tool > Results

Object Name	Safety Factor
State	Solved
Scope	
Geometry	All Bodies
Definition	
Type	Safety Factor
Display Time	End Time
Results	
Minimum	0.76845
Minimum Occurs On	MouldingPin_FinalDim-1
Information	
Time	10. s
Load Step	1
Substep	4
Iteration Number	25

FIGURE 27
Somos11120 > Static Structural > Solution > Stress Tool > Safety Factor

Steady-State Thermal

TABLE 70
Somos11120 > Analysis

Object Name	Steady-State Thermal
State	Fully Defined
Definition	
Physics Type	Thermal
Analysis Type	Steady-State

TABLE 71
Somos11120 > Steady-State Thermal > Initial Condition

Object Name	Initial Condition
State	Fully Defined
Definition	
Initial Temperature	Uniform Temperature
Initial Temperature Value	70. °C

TABLE 72
Somos11120 > Steady-State Thermal > Analysis Settings

Object Name	Analysis Settings
State	Fully Defined
Step Controls	
Number Of Steps	1.
Current Step Number	1.
Step End Time	10. s
Auto Time Stepping	Program Controlled
Solver Controls	
Solver Type	Program Controlled
Nonlinear Controls	
Heat Convergence	Program Controlled
Temperature Convergence	Program Controlled
Line Search	Program Controlled
Output Controls	
Calculate Thermal Flux	Yes
Calculate Results At	All Time Points
Analysis Data Management	
Solver Files Directory	D:\DOUT\Experiments HM2\Structural_Ansys_HM2_Pin\AssemFinalDim2 Simulation Files\Steady-State Thermal (3)\
Future Analysis	None
Save ANSYS db	No
Delete Unneeded Files	Yes
Nonlinear Solution	Yes

TABLE 73
Somos11120 > Steady-State Thermal > Loads

Object Name	Temperature
State	Fully Defined
Scope	
Scoping Method	Geometry Selection
Geometry	2 Bodies
Definition	
Type	Temperature
Magnitude	Tabular Data
Suppressed	No

FIGURE 28
Somos11120 > Steady-State Thermal > Temperature
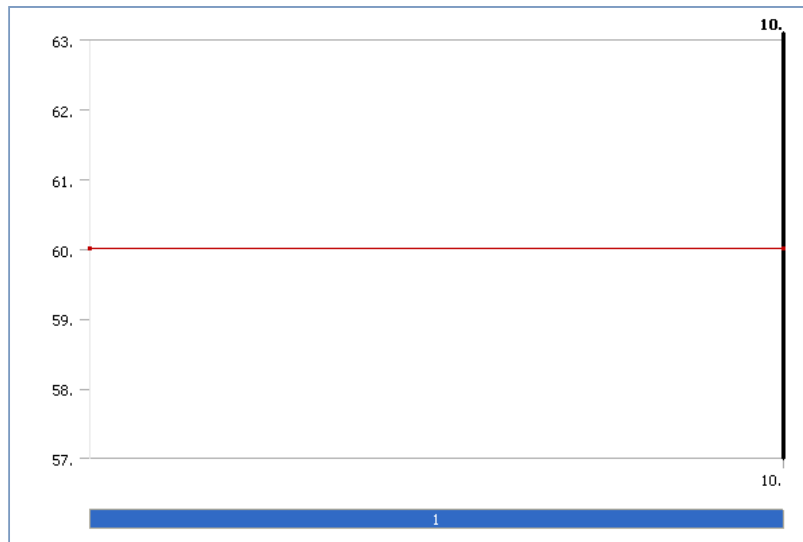
TABLE 74
Somos11120 > Steady-State Thermal > Temperature

Steps	Time [s]	Temperature [℃]
1	0.	60.
	10.	

Solution

TABLE 75
Somos11120 > Steady-State Thermal > Solution

Object Name	Solution
State	Solved
Adaptive Mesh Refinement	
Max Refinement Loops	1.
Refinement Depth	2.

TABLE 76
Somos11120 > Steady-State Thermal > Solution > Solution Information

Object Name	Solution Information
State	Solved
Solution Information	
Solution Output	Solver Output
Update Interval	2.5 s
Display Points	All

TABLE 77
Somos11120 > Steady-State Thermal > Solution > Results

Object Name	Temperature
State	Solved
Scope	
Geometry	All Bodies
Definition	
Type	Temperature
Display Time	End Time
Results	
Minimum	60. ℃
Maximum	60. ℃
Minimum Occurs On	MouldingPin_FinalDim-1
Maximum Occurs On	MouldingPin_FinalDim-1
Information	
Time	10. s
Load Step	1
Substep	1
Iteration Number	1

ProMetal

Geometry

TABLE 78
ProMetal > Geometry

Object Name	Geometry
State	Fully Defined
Definition	
Source	D:\DOUT\Experiments HM2\Structural_Ansys_HM2_Pin\AssemFinalDim.SLDASM
Type	SolidWorks
Length Unit	Meters
Element Control	Program Controlled
Display Style	Part Color

Bounding Box	
Length X	12.33 mm
Length Y	12.306 mm
Length Z	10. mm
Properties	
Volume	900.75 mm³
Mass	3.0573e-003 kg
Statistics	
Bodies	2
Active Bodies	2
Nodes	107264
Elements	67799
Preferences	
Import Solid Bodies	Yes
Import Surface Bodies	Yes
Import Line Bodies	Yes
Parameter Processing	Yes
Personal Parameter Key	DS
CAD Attribute Transfer	No
Named Selection Processing	No
Material Properties Transfer	No
CAD Associativity	Yes
Import Coordinate Systems	No
Reader Save Part File	No
Import Using Instances	Yes
Do Smart Update	No
Attach File Via Temp File	No
Analysis Type	3-D
Mixed Import Resolution	None
Enclosure and Symmetry Processing	Yes

TABLE 79
ProMetal > Geometry > Parts

Object Name	MouldingPin_FinalDim-1	Plastic_Pin_FinallDim-1
State	Meshed	Hidden
Graphics Properties		
Visible	Yes	No
Transparency	1	
Definition		
Suppressed	No	
Material	ProM	Domo 1100N
Stiffness Behavior	Flexible	
Nonlinear Material Effects	Yes	
Bounding Box		
Length X	8.4776 mm	12.33 mm
Length Y	8.4823 mm	12.306 mm
Length Z	10. mm	9. mm
Properties		
Volume	339.54 mm³	561.21 mm³
Mass	2.5466e-003 kg	5.107e-004 kg
Centroid X	-5.0777e-008 mm	2.6913e-017 mm
Centroid Y	1.9251e-008 mm	-1.5667e-016 mm
Centroid Z	5.2344 mm	4.4388 mm
Moment of Inertia Ip1	3.2039e-002 kg·mm²	1.0455e-002 kg·mm²
Moment of Inertia Ip2	3.2039e-002 kg·mm²	1.0455e-002 kg·mm²
Moment of Inertia Ip3	2.8981e-002 kg·mm²	1.4031e-002 kg·mm²
Statistics		
Nodes	40077	67187
Elements	24891	42908

Connections

TABLE 80
ProMetal > Connections

Object Name	Connections
State	Fully Defined
Auto Detection	
Generate Contact On Update	Yes
Tolerance Type	Slider
Tolerance Slider	0.
Tolerance Value	5.0216e-002 mm
Face/Face	Yes
Face/Edge	No
Edge/Edge	No
Priority	Include All
Same Body Grouping	Yes
Revolute Joints	Yes
Fixed Joints	Yes
Transparency	
Enabled	Yes

TABLE 81
ProMetal > Connections > Contact Regions

Object Name	Frictional - MouldingPin_FinalDim-1 To Plastic_Pin_FinallDim-1

State	Fully Defined
Scope	
Scoping Method	Geometry Selection
Contact	1 Face
Target	1 Face
Contact Bodies	MouldingPin_FinalDim-1
Target Bodies	Plastic_Pin_FinallDim-1
Definition	
Type	Frictional
Friction Coefficient	0.257
Scope Mode	Automatic
Behavior	Symmetric
Suppressed	No
Advanced	
Formulation	Pure Penalty
Interface Treatment	Add Offset, Ramped Effects
Offset	0. mm
Normal Stiffness	Program Controlled
Update Stiffness	Never
Thermal Conductance	Program Controlled
Pinball Region	Program Controlled
Time Step Controls	None

Mesh

TABLE 82
ProMetal > Mesh

Object Name	*Mesh*
State	Solved
Defaults	
Physics Preference	Mechanical
Relevance	0
Advanced	
Relevance Center	Coarse
Element Size	0.5 mm
Shape Checking	Standard Mechanical
Solid Element Midside Nodes	Program Controlled
Straight Sided Elements	No
Initial Size Seed	Active Assembly
Smoothing	Low
Transition	Fast
Statistics	
Nodes	107264
Elements	67799

TABLE 83
ProMetal > Mesh > Mesh Controls

Object Name	*Body Sizing*
State	Fully Defined
Scope	
Scoping Method	Geometry Selection
Geometry	2 Bodies
Definition	
Suppressed	No
Type	Element Size
Element Size	0.5 mm
Edge Behavior	Curv/Proximity Refinement

Static Structural

TABLE 84
ProMetal > Analysis

Object Name	*Static Structural*
State	Fully Defined
Definition	
Physics Type	Structural
Analysis Type	Static Structural
Options	
Reference Temp	22. ℃

TABLE 85
ProMetal > Static Structural > Analysis Settings

Object Name	*Analysis Settings*
State	Fully Defined
Step Controls	
Number Of Steps	1.
Current Step Number	1.
Step End Time	10. s
Auto Time Stepping	Program Controlled
Solver Controls	
Solver Type	Program Controlled
Weak Springs	Program Controlled
Large Deflection	Off
Inertia Relief	Off

Nonlinear Controls	
Force Convergence	Program Controlled
Moment Convergence	Program Controlled
Displacement Convergence	Program Controlled
Rotation Convergence	Program Controlled
Line Search	Program Controlled
Output Controls	
Calculate Stress	Yes
Calculate Strain	Yes
Calculate Results At	All Time Points
Analysis Data Management	
Solver Files Directory	D:\DOUT\Experiments HM2\Structural_Ansys_HM2_Pin\AssemFinalDim2 Simulation Files\Static Structural (4)\
Future Analysis	None
Save ANSYS db	No
Delete Unneeded Files	Yes
Nonlinear Solution	Yes

TABLE 86
ProMetal > Static Structural > Loads

Object Name	Fixed Support	Force	Pressure
State	Fully Defined		
Scope			
Scoping Method	Geometry Selection		
Geometry	1 Face		
Definition			
Type	Fixed Support	Force	Pressure
Suppressed	No		
Define By		Components	Normal To
X Component		Tabular Data	
Y Component		Tabular Data	
Z Component		Tabular Data	
Magnitude			Tabular Data

FIGURE 29
ProMetal > Static Structural > Force
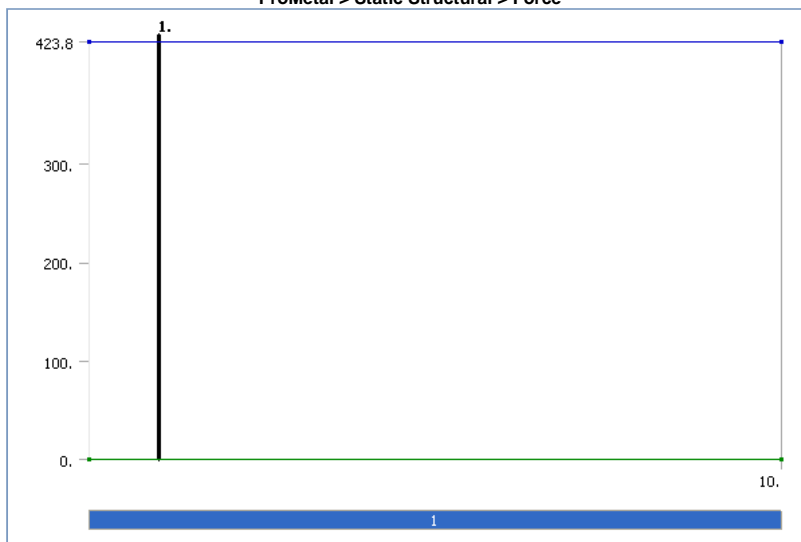
TABLE 87
ProMetal > Static Structural > Force

Steps	Time [s]	X [N]	Y [N]	Z [N]
1	0. / 10.	0.	0.	423.8

FIGURE 30
ProMetal > Static Structural > Force > Figure
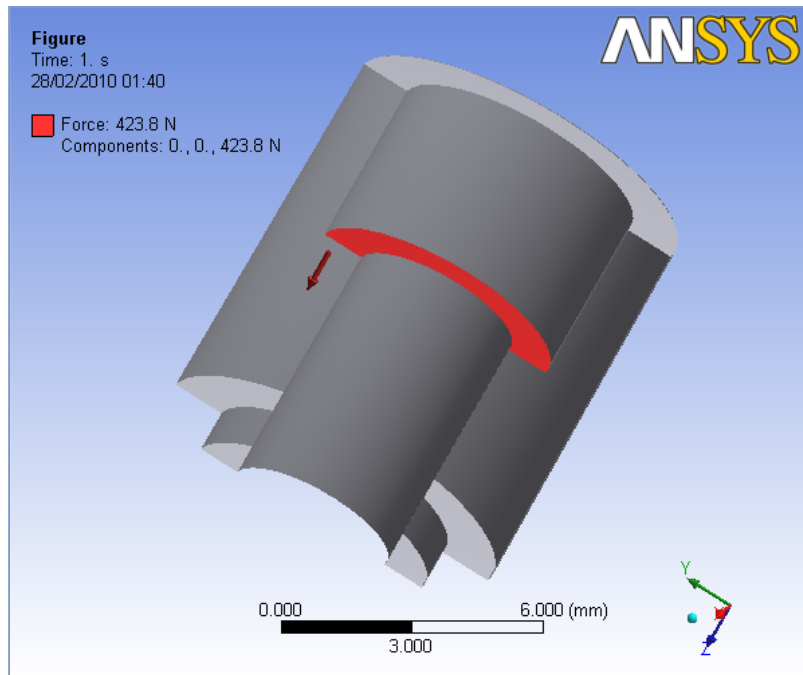
FIGURE 31
ProMetal > Static Structural > Pressure
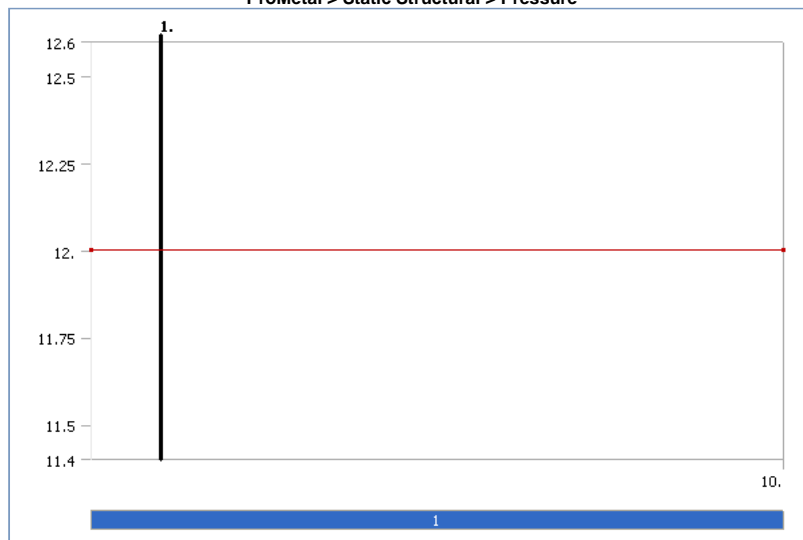
TABLE 88
ProMetal > Static Structural > Pressure

Steps	Time [s]	Pressure [MPa]
1	0.	12.
	10.	

TABLE 89
ProMetal > Static Structural > Thermal Condition

Object Name	Thermal Condition
State	Fully Defined
Definition	
Condition	Uniform Temperature
Uniform Temp	50. ℃
Suppressed	No

Solution

TABLE 90
ProMetal > Static Structural > Solution

Object Name	Solution
State	Obsolete
Adaptive Mesh Refinement	
Max Refinement Loops	1.
Refinement Depth	2.

TABLE 91
ProMetal > Static Structural > Solution > Solution Information

Object Name	Solution Information

State	Not Solved
Solution Information	
Solution Output	Solver Output
Newton-Raphson Residuals	0
Update Interval	2.5 s
Display Points	All

TABLE 92
ProMetal > Static Structural > Solution > Results

Object Name	*Equivalent Elastic Strain*	*Equivalent Stress*
State	Solved	
Scope		
Geometry	All Bodies	
Definition		
Type	Equivalent (von-Mises) Elastic Strain	Equivalent (von-Mises) Stress
Display Time	End Time	
Results		
Minimum	2.1542e-005 mm/mm	3.1666 MPa
Maximum	1.3455e-002 mm/mm	57.3 MPa
Minimum Occurs On	MouldingPin_FinalDim-1	
Maximum Occurs On	Plastic_Pin_FinalDim-1	MouldingPin_FinalDim-1
Information		
Time	10. s	
Load Step	1	
Substep	4	
Iteration Number	23	

FIGURE 32
ProMetal > Static Structural > Solution > Equivalent Elastic Strain
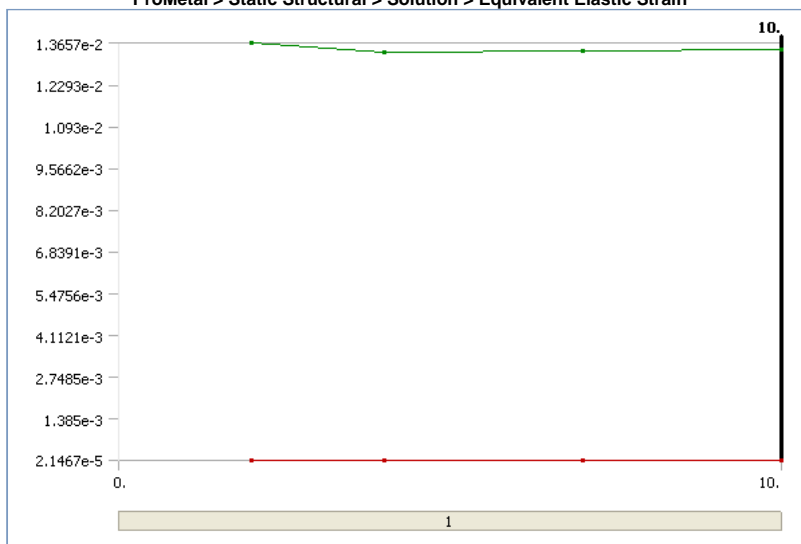
FIGURE 33
ProMetal > Static Structural > Solution > Equivalent Stress
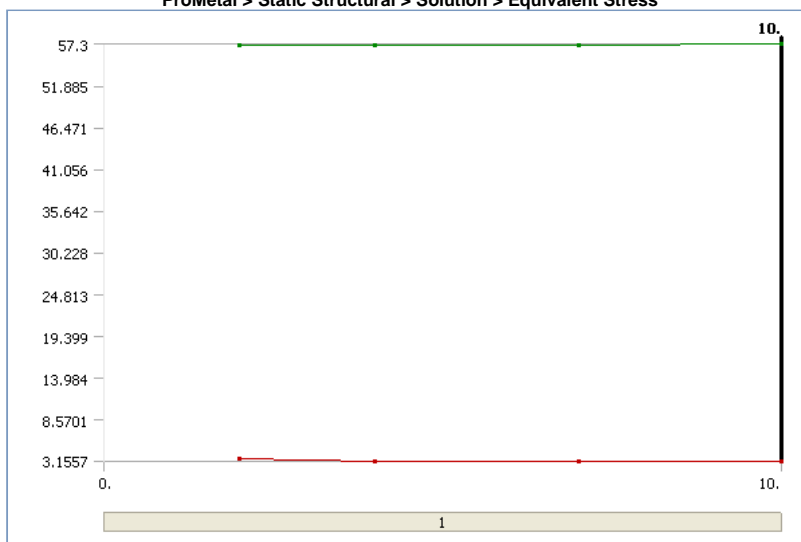
TABLE 93
ProMetal > Static Structural > Solution > Stress Safety Tools

Object Name	*Stress Tool*
State	Not Solved
Definition	

Theory	Max Equivalent Stress
Stress Limit Type	Tensile Yield Per Material

TABLE 94
ProMetal > Static Structural > Solution > Stress Tool > Results

Object Name	Safety Factor
State	Obsolete
Scope	
Geometry	All Bodies
Definition	
Type	Safety Factor
Display Time	End Time
Results	
Minimum	1.6783
Minimum Occurs On	Plastic_Pin_FinallDim-1
Information	
Time	10. s
Load Step	1
Substep	4
Iteration Number	23

FIGURE 34
ProMetal > Static Structural > Solution > Stress Tool > Safety Factor
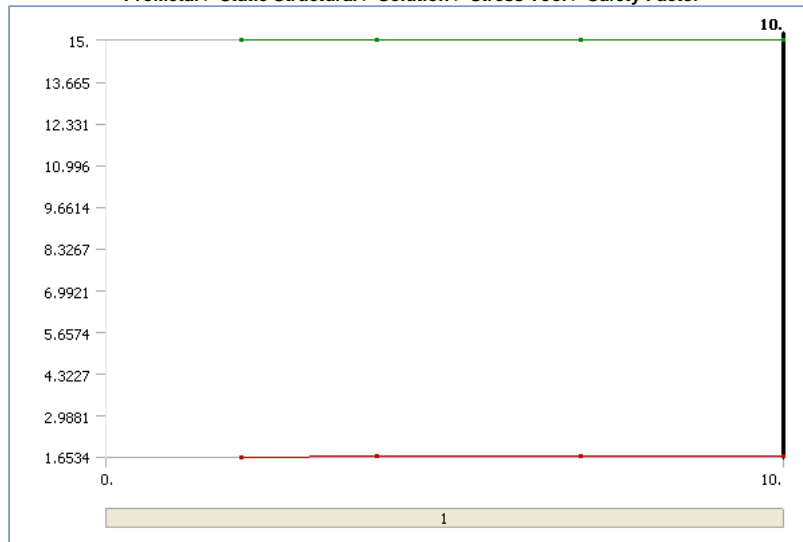
Steady-State Thermal

TABLE 95
ProMetal > Analysis

Object Name	Steady-State Thermal
State	Fully Defined
Definition	
Physics Type	Thermal
Analysis Type	Steady-State

TABLE 96
ProMetal > Steady-State Thermal > Initial Condition

Object Name	Initial Condition
State	Fully Defined
Definition	
Initial Temperature	Uniform Temperature
Initial Temperature Value	70. °C

TABLE 97
ProMetal > Steady-State Thermal > Analysis Settings

Object Name	Analysis Settings
State	Fully Defined
Step Controls	
Number Of Steps	1.
Current Step Number	1.
Step End Time	10. s
Auto Time Stepping	Program Controlled
Solver Controls	
Solver Type	Program Controlled
Nonlinear Controls	
Heat Convergence	Program Controlled
Temperature Convergence	Program Controlled
Line Search	Program Controlled
Output Controls	
Calculate Thermal Flux	Yes
Calculate Results At	All Time Points
Analysis Data Management	

Solver Files Directory	D:\DOUT\Experiments HM2\Structural_Ansys_HM2_Pin\AssemFinalDim2 Simulation Files\Steady-State Thermal (4)\
Future Analysis	None
Save ANSYS db	No
Delete Unneeded Files	Yes
Nonlinear Solution	Yes

TABLE 98
ProMetal > Steady-State Thermal > Loads

Object Name	Temperature
State	Fully Defined
Scope	
Scoping Method	Geometry Selection
Geometry	2 Bodies
Definition	
Type	Temperature
Magnitude	Tabular Data
Suppressed	No

FIGURE 35
ProMetal > Steady-State Thermal > Temperature
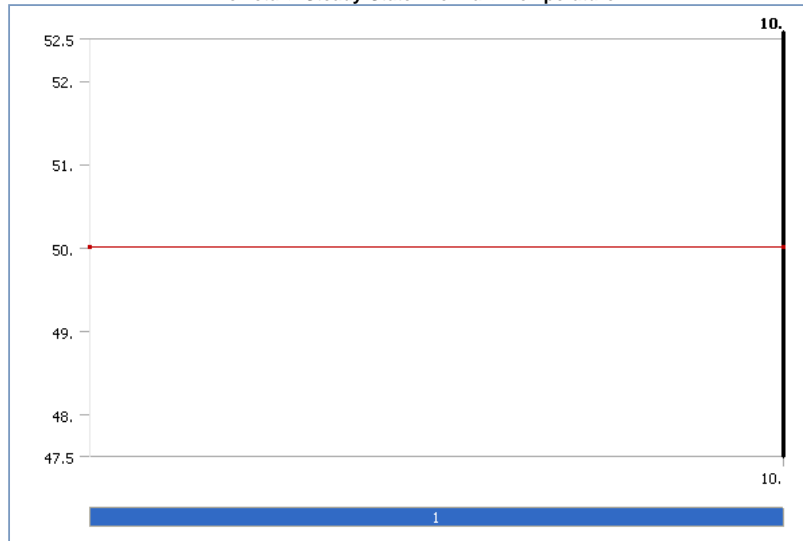
TABLE 99
ProMetal > Steady-State Thermal > Temperature

Steps	Time [s]	Temperature [°C]
1	0.	50.
	10.	

Solution

TABLE 100
ProMetal > Steady-State Thermal > Solution

Object Name	Solution
State	Solved
Adaptive Mesh Refinement	
Max Refinement Loops	1.
Refinement Depth	2.

TABLE 101
ProMetal > Steady-State Thermal > Solution > Solution Information

Object Name	Solution Information
State	Solved
Solution Information	
Solution Output	Solver Output
Update Interval	2.5 s
Display Points	All

TABLE 102
ProMetal > Steady-State Thermal > Solution > Results

Object Name	Temperature
State	Solved
Scope	
Geometry	All Bodies
Definition	
Type	Temperature
Display Time	End Time
Results	
Minimum	50. °C
Maximum	50. °C
Minimum Occurs On	MouldingPin_FinalDim-1
Maximum Occurs On	MouldingPin_FinalDim-1
Information	

Time	10. s
Load Step	1
Substep	1
Iteration Number	2

Steel_P20

Geometry

TABLE 103
Steel_P20 > Geometry

Object Name	Geometry
State	Fully Defined
Definition	
Source	D:\DOUT\Experiments HM2\Structural_Ansys_HM2_Pin\AssemFinalDim.SLDASM
Type	SolidWorks
Length Unit	Meters
Element Control	Program Controlled
Display Style	Part Color
Bounding Box	
Length X	12.33 mm
Length Y	12.306 mm
Length Z	10. mm
Properties	
Volume	900.75 mm³
Mass	3.1591e-003 kg
Statistics	
Bodies	2
Active Bodies	2
Nodes	107264
Elements	67799
Preferences	
Import Solid Bodies	Yes
Import Surface Bodies	Yes
Import Line Bodies	Yes
Parameter Processing	Yes
Personal Parameter Key	DS
CAD Attribute Transfer	No
Named Selection Processing	No
Material Properties Transfer	No
CAD Associativity	Yes
Import Coordinate Systems	No
Reader Save Part File	No
Import Using Instances	Yes
Do Smart Update	No
Attach File Via Temp File	No
Analysis Type	3-D
Mixed Import Resolution	None
Enclosure and Symmetry Processing	Yes

TABLE 104
Steel_P20 > Geometry > Parts

Object Name	MouldingPin_FinalDim-1	Plastic_Pin_FinallDim-1
State	Meshed	Hidden
Graphics Properties		
Visible	Yes	No
Transparency	1	
Definition		
Suppressed	No	
Material	Steel_P20	Domo 1100N
Stiffness Behavior	Flexible	
Nonlinear Material Effects	Yes	
Bounding Box		
Length X	8.4776 mm	12.33 mm
Length Y	8.4823 mm	12.306 mm
Length Z	10. mm	9. mm
Properties		
Volume	339.54 mm³	561.21 mm³
Mass	2.6484e-003 kg	5.107e-004 kg
Centroid X	-5.0777e-008 mm	2.6913e-017 mm
Centroid Y	1.9251e-008 mm	-1.5667e-016 mm
Centroid Z	5.2344 mm	4.4388 mm
Moment of Inertia Ip1	3.3321e-002 kg·mm²	1.0455e-002 kg·mm²
Moment of Inertia Ip2	3.3321e-002 kg·mm²	1.0455e-002 kg·mm²
Moment of Inertia Ip3	3.014e-002 kg·mm²	1.4031e-002 kg·mm²
Statistics		
Nodes	40077	67187
Elements	24891	42908

Connections

TABLE 105
Steel_P20 > Connections

Object Name	Connections
State	Fully Defined
Auto Detection	
Generate Contact On Update	Yes
Tolerance Type	Slider
Tolerance Slider	0.
Tolerance Value	5.0216e-002 mm
Face/Face	Yes
Face/Edge	No
Edge/Edge	No
Priority	Include All
Same Body Grouping	Yes
Revolute Joints	Yes
Fixed Joints	Yes
Transparency	
Enabled	Yes

TABLE 106
Steel_P20 > Connections > Contact Regions

Object Name	Frictional - MouldingPin_FinalDim-1 To Plastic_Pin_FinallDim-1
State	Fully Defined
Scope	
Scoping Method	Geometry Selection
Contact	1 Face
Target	1 Face
Contact Bodies	MouldingPin_FinalDim-1
Target Bodies	Plastic_Pin_FinallDim-1
Definition	
Type	Frictional
Friction Coefficient	0.258
Scope Mode	Automatic
Behavior	Symmetric
Suppressed	No
Advanced	
Formulation	Pure Penalty
Interface Treatment	Add Offset, Ramped Effects
Offset	0. mm
Normal Stiffness	Program Controlled
Update Stiffness	Never
Thermal Conductance	Program Controlled
Pinball Region	Program Controlled
Time Step Controls	None

Mesh

TABLE 107
Steel_P20 > Mesh

Object Name	Mesh
State	Solved
Defaults	
Physics Preference	Mechanical
Relevance	0
Advanced	
Relevance Center	Coarse
Element Size	0.5 mm
Shape Checking	Standard Mechanical
Solid Element Midside Nodes	Program Controlled
Straight Sided Elements	No
Initial Size Seed	Active Assembly
Smoothing	Low
Transition	Fast
Statistics	
Nodes	107264
Elements	67799

TABLE 108
Steel_P20 > Mesh > Mesh Controls

Object Name	Body Sizing
State	Fully Defined
Scope	
Scoping Method	Geometry Selection
Geometry	2 Bodies
Definition	
Suppressed	No
Type	Element Size
Element Size	0.5 mm
Edge Behavior	Curv/Proximity Refinement

Static Structural

TABLE 109
Steel_P20 > Analysis

Object Name	Static Structural
State	Fully Defined

Definition	
Physics Type	Structural
Analysis Type	Static Structural
Options	
Reference Temp	22. ℃

TABLE 110
Steel_P20 > Static Structural > Analysis Settings

Object Name	*Analysis Settings*
State	Fully Defined
Step Controls	
Number Of Steps	1.
Current Step Number	1.
Step End Time	10. s
Auto Time Stepping	Program Controlled
Solver Controls	
Solver Type	Program Controlled
Weak Springs	Program Controlled
Large Deflection	Off
Inertia Relief	Off
Nonlinear Controls	
Force Convergence	Program Controlled
Moment Convergence	Program Controlled
Displacement Convergence	Program Controlled
Rotation Convergence	Program Controlled
Line Search	Program Controlled
Output Controls	
Calculate Stress	Yes
Calculate Strain	Yes
Calculate Results At	All Time Points
Analysis Data Management	
Solver Files Directory	D:\DOUT\Experiments HM2\Structural_Ansys_HM2_Pin\AssemFinalDim2 Simulation Files\Static Structural (5)\
Future Analysis	None
Save ANSYS db	No
Delete Unneeded Files	Yes
Nonlinear Solution	Yes

TABLE 111
Steel_P20 > Static Structural > Loads

Object Name	Fixed Support	Force	Pressure
State		Fully Defined	
Scope			
Scoping Method		Geometry Selection	
Geometry		1 Face	
Definition			
Type	Fixed Support	Force	Pressure
Suppressed		No	
Define By		Components	Normal To
X Component		Tabular Data	
Y Component		Tabular Data	
Z Component		Tabular Data	
Magnitude			Tabular Data

FIGURE 36
Steel_P20 > Static Structural > Force
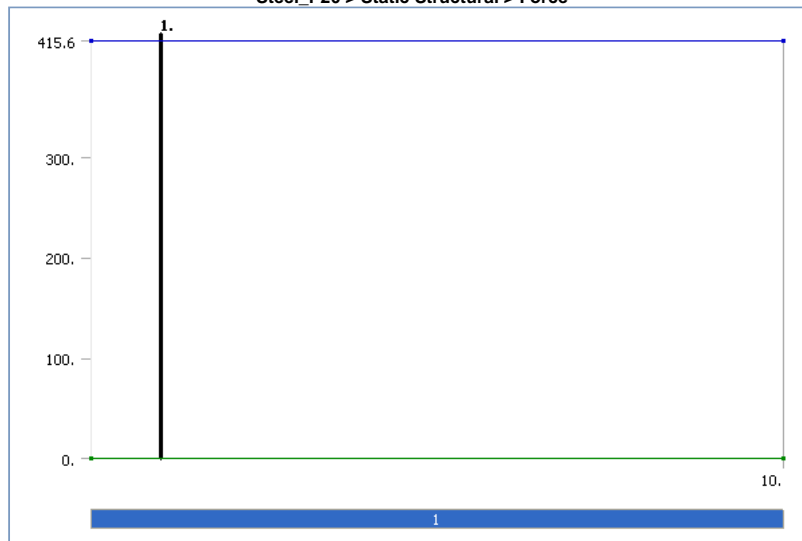
TABLE 112
Steel_P20 > Static Structural > Force

Steps	Time [s]	X [N]	Y [N]	Z [N]
1	0. 10.	0.	0.	415.6

FIGURE 37
Steel_P20 > Static Structural > Pressure

TABLE 113
Steel_P20 > Static Structural > Pressure

Steps	Time [s]	Pressure [MPa]
1	0.	12.
	10.	

TABLE 114
Steel_P20 > Static Structural > Thermal Condition

Object Name	Thermal Condition
State	Fully Defined
Definition	
Condition	Uniform Temperature
Uniform Temp	50. ℃
Suppressed	No

Solution

TABLE 115
Steel_P20 > Static Structural > Solution

Object Name	Solution
State	Obsolete
Adaptive Mesh Refinement	
Max Refinement Loops	1.
Refinement Depth	2.

TABLE 116
Steel_P20 > Static Structural > Solution > Solution Information

Object Name	Solution Information
State	Not Solved
Solution Information	
Solution Output	Solver Output
Newton-Raphson Residuals	0
Update Interval	2.5 s
Display Points	All

TABLE 117
Steel_P20 > Static Structural > Solution > Results

Object Name	Equivalent Elastic Strain	Equivalent Stress
State	Solved	
Scope		
Geometry	All Bodies	
Definition		
Type	Equivalent (von-Mises) Elastic Strain	Equivalent (von-Mises) Stress
Display Time	End Time	
Results		
Minimum	1.7073e-005 mm/mm	3.4145 MPa
Maximum	1.3469e-002 mm/mm	56.837 MPa
Minimum Occurs On	MouldingPin_FinalDim-1	
Maximum Occurs On	Plastic_Pin_FinallDim-1	MouldingPin_FinalDim-1
Information		
Time	10. s	
Load Step	1	
Substep	4	
Iteration Number	22	

FIGURE 38
Steel_P20 > Static Structural > Solution > Equivalent Elastic Strain
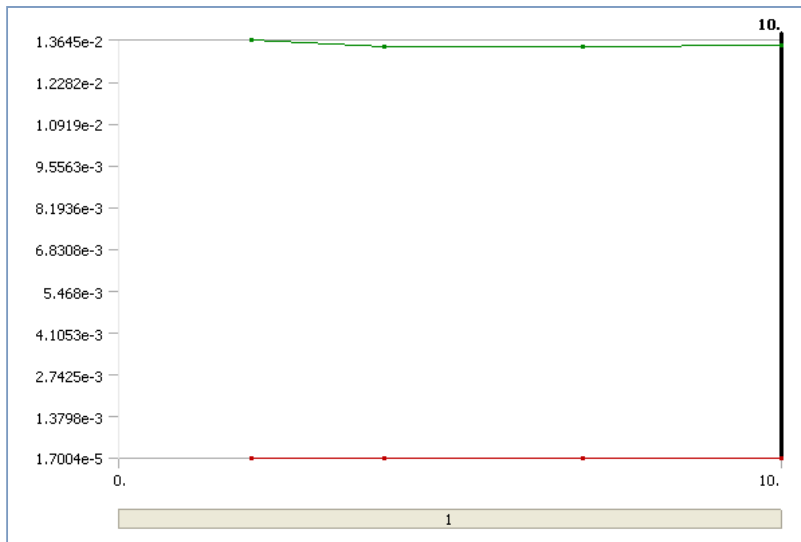
FIGURE 39
Steel_P20 > Static Structural > Solution > Equivalent Stress
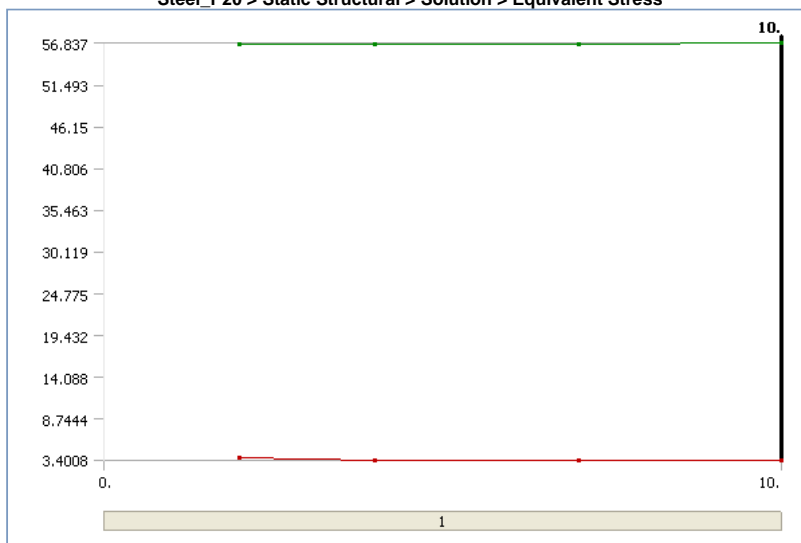
TABLE 118
Steel_P20 > Static Structural > Solution > Stress Safety Tools

Object Name	Stress Tool
State	Not Solved
Definition	
Theory	Max Equivalent Stress
Stress Limit Type	Tensile Yield Per Material

TABLE 119
Steel_P20 > Static Structural > Solution > Stress Tool > Results

Object Name	Safety Factor
State	Obsolete
Scope	
Geometry	All Bodies
Definition	
Type	Safety Factor
Display Time	End Time
Results	
Minimum	1.6765
Minimum Occurs On	Plastic_Pin_FinallDim-1
Information	
Time	10. s
Load Step	1
Substep	4
Iteration Number	22

FIGURE 40
Steel_P20 > Static Structural > Solution > Stress Tool > Safety Factor

Steady-State Thermal

TABLE 120
Steel_P20 > Analysis

Object Name	Steady-State Thermal
State	Fully Defined
Definition	
Physics Type	Thermal
Analysis Type	Steady-State

TABLE 121
Steel_P20 > Steady-State Thermal > Initial Condition

Object Name	Initial Condition
State	Fully Defined
Definition	
Initial Temperature	Uniform Temperature
Initial Temperature Value	70. °C

TABLE 122
Steel_P20 > Steady-State Thermal > Analysis Settings

Object Name	Analysis Settings
State	Fully Defined
Step Controls	
Number Of Steps	1.
Current Step Number	1.
Step End Time	10. s
Auto Time Stepping	Program Controlled
Solver Controls	
Solver Type	Program Controlled
Nonlinear Controls	
Heat Convergence	Program Controlled
Temperature Convergence	Program Controlled
Line Search	Program Controlled
Output Controls	
Calculate Thermal Flux	Yes
Calculate Results At	All Time Points
Analysis Data Management	
Solver Files Directory	D:\DOUT\Experiments HM2\Structural_Ansys_HM2_Pin\AssemFinalDim2 Simulation Files\Steady-State Thermal (5)\
Future Analysis	None
Save ANSYS db	No
Delete Unneeded Files	Yes
Nonlinear Solution	Yes

TABLE 123
Steel_P20 > Steady-State Thermal > Loads

Object Name	Temperature
State	Fully Defined
Scope	
Scoping Method	Geometry Selection
Geometry	2 Bodies
Definition	
Type	Temperature
Magnitude	Tabular Data
Suppressed	No

FIGURE 41
Steel_P20 > Steady-State Thermal > Temperature
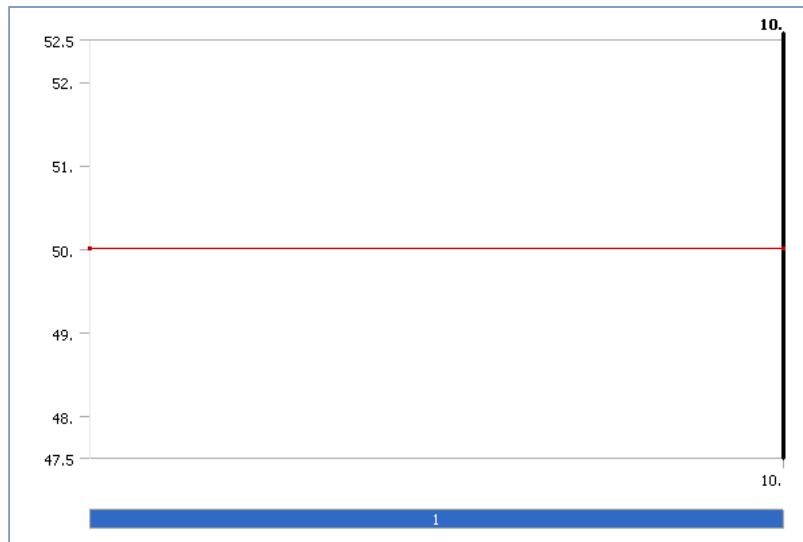
TABLE 124
Steel_P20 > Steady-State Thermal > Temperature

Steps	Time [s]	Temperature [℃]
1	0.	50.
	10.	

Solution

TABLE 125
Steel_P20 > Steady-State Thermal > Solution

Object Name	Solution
State	Solved
Adaptive Mesh Refinement	
Max Refinement Loops	1.
Refinement Depth	2.

TABLE 126
Steel_P20 > Steady-State Thermal > Solution > Solution Information

Object Name	Solution Information
State	Solved
Solution Information	
Solution Output	Solver Output
Update Interval	2.5 s
Display Points	All

TABLE 127
Steel_P20 > Steady-State Thermal > Solution > Results

Object Name	Temperature
State	Solved
Scope	
Geometry	All Bodies
Definition	
Type	Temperature
Display Time	End Time
Results	
Minimum	50. ℃
Maximum	50. ℃
Minimum Occurs On	MouldingPin_FinalDim-1
Maximum Occurs On	MouldingPin_FinalDim-1
Information	
Time	10. s
Load Step	1
Substep	1
Iteration Number	2

Material Data

BiresinL74_60Al

TABLE 128
BiresinL74_60Al > Constants

Structural	
Young's Modulus	5500. MPa
Poisson's Ratio	0.36
Density	1.65e-006 kg/mm³
Thermal Expansion	6.e-005 1/℃
Tensile Yield Strength	53. MPa
Compressive Yield Strength	137. MPa
Tensile Ultimate Strength	53. MPa

Thermal	
Thermal Conductivity	6.06e-004 W/mm·℃
Specific Heat	1279.2 J/kg·℃
Electromagnetics	
Relative Permeability	10000
Resistivity	1.7e-004 Ohm·mm

Domo 1100N

TABLE 129
Domo 1100N > Constants

Structural	
Young's Modulus	1550. MPa
Poisson's Ratio	0.42
Density	9.1e-007 kg/mm³
Thermal Expansion	1.8e-004 1/℃
Tensile Yield Strength	35. MPa
Tensile Ultimate Strength	50. MPa
Thermal	
Thermal Conductivity	2.8e-004 W/mm·℃
Specific Heat	296. J/kg·℃

SSF

TABLE 130
SSF > Constants

Structural	
Young's Modulus	4600. MPa
Poisson's Ratio	0.36
Density	2.1e-006 kg/mm³
Thermal Expansion	6.e-005 1/℃
Tensile Yield Strength	53. MPa
Compressive Yield Strength	137. MPa
Tensile Ultimate Strength	53. MPa
Thermal	
Thermal Conductivity	3.92e-004 W/mm·℃
Specific Heat	1279.2 J/kg·℃
Electromagnetics	
Relative Permeability	10000
Resistivity	1.7e-004 Ohm·mm

Somo11120

TABLE 131
Somo11120 > Constants

Structural	
Young's Modulus	2700. MPa
Poisson's Ratio	0.36
Density	1.12e-006 kg/mm³
Thermal Expansion	9.e-005 1/℃
Tensile Yield Strength	50. MPa
Compressive Yield Strength	50. MPa
Tensile Ultimate Strength	56. MPa
Thermal	
Thermal Conductivity	1.664e-005 W/mm·℃
Specific Heat	286.26 J/kg·℃
Electromagnetics	
Relative Permeability	10000
Resistivity	1.7e-004 Ohm·mm

ProM

TABLE 132
ProM > Constants

Structural	
Young's Modulus	1.47e+005 MPa
Poisson's Ratio	0.28
Density	7.5e-006 kg/mm³
Thermal Expansion	1.2e-005 1/℃
Tensile Yield Strength	250. MPa
Compressive Yield Strength	250. MPa
Tensile Ultimate Strength	460. MPa
Thermal	
Thermal Conductivity	2.26e-002 W/mm·℃
Specific Heat	418. J/kg·℃
Electromagnetics	
Relative Permeability	10000
Resistivity	1.7e-004 Ohm·mm

Steel_P20

TABLE 133
Steel_P20 > Constants

Structural	

Young's Modulus	2.e+005 MPa
Poisson's Ratio	0.28
Density	7.8e-006 kg/mm³
Thermal Expansion	1.2e-005 1/℃
Tensile Yield Strength	250. MPa
Compressive Yield Strength	250. MPa
Tensile Ultimate Strength	460. MPa
Thermal	
Thermal Conductivity	2.9e-002 W/mm·℃
Specific Heat	460. J/kg·℃
Electromagnetics	
Relative Permeability	10000
Resistivity	1.7e-004 Ohm·mm